

Arthritis & Rheumatology

An Official Journal of the American College of Rheumatology
www.arthritisrheum.org and wileyonlinelibrary.com

Editor

Richard J. Bucala, MD, PhD
Yale University School of Medicine, New Haven

Deputy Editor

Daniel H. Solomon, MD, MPH, *Boston*

Co-Editors

Joseph E. Craft, MD, *New Haven*
David T. Felson, MD, MPH, *Boston*
Richard F. Loeser Jr., MD, *Chapel Hill*
Peter A. Nigrovic, MD, *Boston*
Christopher T. Ritchlin, MD, MPH, *Rochester*
John Varga, MD, *Chicago*

Co-Editor and Review Article Editor

Robert Terkeltaub, MD, *San Diego*

Clinical Trials Advisor

Michael E. Weinblatt, MD, *Boston*

Journal Publications Committee

Nora G. Singer, MD, *Chair, Cleveland*
Kelli D. Allen, PhD, *Chapel Hill*
Shervin Assassi, MD, MS, *Houston*
Cecilia P. Chung, MD, MPH, *Nashville*
Eric J. Gapud, MD, PhD, *Baltimore*
Kim D. Jones, RN, PhD, FNP, *Portland*
Brian L. Kotzin, MD, *Los Angeles*
Linda C. Li, PT, MSc, PhD, *Vancouver*

Editorial Staff

Jane S. Diamond, MPH, *Managing Editor, Atlanta*
Patricia K. Reichert, *Assistant Managing Editor, Atlanta*
Lesley W. Allen, *Senior Manuscript Editor, Atlanta*
Patricia L. Mabley, *Manuscript Editor, Atlanta*
Kristin W. Mitchell, *Manuscript Editor, Atlanta*
Emily W. Wehby, MA, *Manuscript Editor, Atlanta*
Michael Weinberg, MA, *Manuscript Editor, Atlanta*
Joshua J. Reynolds, *Editorial Coordinator, Atlanta*
Brittany Swett, *Editorial Assistant, New Haven*
Carolyn Roth, *Senior Production Editor, Boston*

Associate Editors

Daniel Aletaha, MD, MS, *Vienna*
Heather G. Allore, PhD, *New Haven*
Lenore M. Buckley, MD, MPH, *New Haven*
Daniel J. Clauw, MD, *Ann Arbor*
Robert A. Colbert, MD, PhD, *Bethesda*
Karen H. Costenbader, MD, MPH, *Boston*
Nicola Dalbeth, MD, FRACP, *Auckland*
Kevin D. Deane, MD, *Denver*
Patrick M. Gaffney, MD, *Oklahoma City*

Mark C. Genovese, MD, *Palo Alto*
Andrew H. Haims, MD, *New Haven*
Insoo Kang, MD, *New Haven*
Arthur Kavanaugh, MD, *La Jolla*
Wan-Uk Kim, MD, PhD, *Seoul*
S. Sam Lim, MD, MPH, *Atlanta*
Anne-Marie Malfait, MD, PhD, *Chicago*
Paul A. Monach, MD, PhD, *Boston*
Chester V. Oddis, MD, *Pittsburgh*
Andras Perl, MD, PhD, *Syracuse*

Janet E. Pope, MD, MPH, FRCPC, *London, Ontario*
Timothy R. D. J. Radstake, MD, PhD, *Utrecht*
William Robinson, MD, PhD, *Palo Alto*
Georg Schett, MD, *Erlangen*
Nan Shen, MD, *Shanghai*
Betty P. Tsao, PhD, *Charleston*
Ronald van Vollenhoven, MD, PhD, *Amsterdam*
Fredrick M. Wigley, MD, *Baltimore*

Advisory Editors

Tatsuya Atsumi, MD, PhD, *Sapporo*
Charles Auffray, PhD, *Lyon*
Dominique Baeten, MD, PhD, *Amsterdam*
Loré Ballesteros-Tato, PhD, *Birmingham*
Lorenzo Beretta, MD, *Milan*
Bryce A. Binstadt, MD, PhD, *Minneapolis*
Jaime Calvo-Alen, MD, *Vitoria*
Scott Canna, MD, *Pittsburgh*

Andrew P. Cope, MD, PhD, *London*
Niek de Vries, MD, PhD, *Amsterdam*
Jörg H. W. Distler, MD, *Erlangen*
Liana Fraenkel, MD, MPH, *New Haven*
Erica Herzog, MD, PhD, *New Haven*
Hui-Chen Hsu, PhD, *Birmingham*
Mariana J. Kaplan, MD, *Bethesda*
Jonathan Kay, MD, *Worcester*
Dwight H. Kono, MD, *La Jolla*

Martin A. Kriegel, MD, PhD, *New Haven*
Francis Lee, MD, PhD, *New Haven*
Sang-II Lee, MD, PhD, *Jinju*
Bing Lu, PhD, *Boston*
Tony R. Merriman, PhD, *Otago*
Yukinori Okada, MD, PhD, *Osaka*
Raghunatha Yammani, PhD, *Winston-Salem*
Kazuki Yoshida, MD, MPH, MS, *Boston*

AMERICAN COLLEGE OF RHEUMATOLOGY

David I. Daikh, MD, PhD, *San Francisco*, **President**
Paula Marchetta, MD, MBA, *New York*, **President-Elect**

Charles M. King, MD, *Tupelo*, **Treasurer**
Ellen M. Gravallese, MD, *Worcester*, **Secretary**
Mark Andrejeski, *Atlanta*, **Executive Vice-President**

© 2018 American College of Rheumatology. All rights reserved. No part of this publication may be reproduced, stored or transmitted in any form or by any means without the prior permission in writing from the copyright holder. Authorization to copy items for internal and personal use is granted by the copyright holder for libraries and other users registered with their local Reproduction Rights Organization (RRO), e.g. Copyright Clearance Center (CCC), 222 Rosewood Drive, Danvers, MA 01923, USA (www.copyright.com), provided the appropriate fee is paid directly to the RRO. This consent does not extend to other kinds of copying such as copying for general distribution, for advertising or promotional purposes, for creating new collective works or for resale. Special requests should be addressed to: permissions@wiley.com

Access Policy: Subject to restrictions on certain backfiles, access to the online version of this issue is available to all registered Wiley Online Library users 12 months after publication. Subscribers and eligible users at subscribing institutions have immediate access in accordance with the relevant subscription type. Please go to onlinelibrary.wiley.com for details.

The views and recommendations expressed in articles, letters, and other communications published in *Arthritis & Rheumatology* are those of the authors and do not necessarily reflect the opinions of the editors, publisher, or American College of Rheumatology. The publisher and the American College of Rheumatology do not investigate the information contained in the classified advertisements in this journal and assume no responsibility concerning them. Further, the publisher and the American College of Rheumatology do not guarantee, warrant, or endorse any product or service advertised in this journal.

Cover design: Todd Machen

⊗ This journal is printed on acid-free paper.

Arthritis & Rheumatology

An Official Journal of the American College of Rheumatology
www.arthritisrheum.org and wileyonlinelibrary.com

VOLUME 70

FEBRUARY 2018

NO. 2

In This Issue	A15
Clinical Connections	A17
Special Articles	
Editorial: Prevalence of Arthritis Revisited <i>Jeffrey N. Katz</i>	153
Editorial: Bench to Bedside—and Back Again: Finding the Goldilocks Zone Within the Scleroderma Universe <i>Janet E. Pope, Jason J. Lee, and Christopher P. Denton</i>	155
Editorial: Wnt Signaling Related to Subchondral Bone Density and Cartilage Degradation in Osteoarthritis <i>David B. Burr and Achint Utreja</i>	157
Review: Defining a Unified Vascular Phenotype in Systemic Sclerosis <i>Yannick Allanore, Oliver Distler, Marco Matucci-Cerinic, and Christopher P. Denton</i>	162
Nomenclature of Cutaneous Vasculitis: Dermatologic Addendum to the 2012 Revised International Chapel Hill Consensus Conference Nomenclature of Vasculitides <i>Cord H. Sunderkötter, Bernhard Zelger, Ko-Ron Chen, Luis Requena, Warren Piette, J. Andrew Carlson, Jan Dutz, Peter Lamprecht, Alfred Mahr, Elisabeth Aberer, Victoria P. Werth, David A. Wetter, Seiji Kawana, Raashid Lugmani, Camille Frances, Joseph Jorizzo, J. Richard Watts, Dieter Metze, Marzia Caproni, Erkan Alpsoy, Jeffrey P. Callen, David Fiorentino, Peter A. Merkel, Ronald J. Falk, and J. Charles Jennette</i>	171
Rheumatoid Arthritis	
Updated Estimates Suggest a Much Higher Prevalence of Arthritis in United States Adults Than Previous Ones <i>S. Reza Jafarzadeh and David T. Felson</i>	185
Germinal Center B Cells Are Essential for Collagen-Induced Arthritis <i>Albert Dahdah, Katrin Habir, Kutty Selva Nandakumar, Amit Saxena, Bingze Xu, Rikard Holmdahl, and Stephen Malin</i>	193
Osteoarthritis	
Brief Report: A Phase IIb Trial of a Novel Extended-Release Microsphere Formulation of Triamcinolone Acetonide for Intraarticular Injection in Knee Osteoarthritis <i>Philip G. Conaghan, Stanley B. Cohen, Francis Berenbaum, Joelle Lufkin, James R. Johnson, and Neil Bodick</i>	204
Knee Alignment Is Quantitatively Related to Periarticular Bone Morphometry and Density, Especially in Patients With Osteoarthritis <i>Grace H. Lo, Mehveen G. Merchant, Jeffrey B. Driban, Jeffrey Duryea, Lori Lyn Price, Charles B. Eaton, and Timothy E. McAlindon</i>	212
Brief Report: Loss of Muscle Strength Prior to Knee Replacement: A Question of Anatomic Cross-Sectional Area or Specific Strength? <i>Adam G. Culvenor, Felix C. Hamler, Jana Kemnitz, Wolfgang Wirth, and Felix Eckstein</i>	222
Loading-Induced Reduction in Sclerostin as a Mechanism of Subchondral Bone Plate Sclerosis in Mouse Knee Joints During Late-Stage Osteoarthritis <i>Haoruo Jia, Xiaoyuan Ma, Yulong Wei, Wei Tong, Robert J. Tower, Abhishek Chandra, Luqiang Wang, Zeyang Sun, Zhaochun Yang, Farid Badar, Kairui Zhang, Wei-Ju Tseng, Ina Kramer, Michaela Kneissel, Yang Xia, X. Sherry Liu, James H. C. Wang, Lin Han, Motomi Enomoto-Iwamoto, and Ling Qin</i>	230
Spondyloarthritis	
Gut Microbiota Perturbations in Reactive Arthritis and Postinfectious Spondyloarthritis <i>Julia Manasson, Nan Shen, Helga R. Garcia Ferrer, Carles Ubeda, Isa Iraheta, Adriana Heguy, Joan M. Von Feldt, Luis R. Espinoza, Abraham Garcia Kutzbach, Leopoldo N. Segal, Alexis Ogdie, Jose C. Clemente, and Jose U. Scher</i>	242

Genetic Variants in <i>ERAP1</i> and <i>ERAP2</i> Associated With Immune-Mediated Diseases Influence Protein Expression and the Isoform Profile <i>Aimee L. Hanson, Thomas Cuddihy, Katelin Haynes, Dorothy Loo, Craig J. Morton, Udo Oppermann, Paul Leo, Gethin P. Thomas, Kim-Anh Lê Cao, Tony J. Kenna, and Matthew A. Brown</i>	255
Systemic Lupus Erythematosus	
Efficacy and Safety of Atacicept in Patients With Systemic Lupus Erythematosus: Results of a Twenty-Four-Week, Multicenter, Randomized, Double-Blind, Placebo-Controlled, Parallel-Arm, Phase IIb Study <i>Joan T. Merrill, Daniel J. Wallace, Stephen Wax, Amy Kao, Patricia A. Fraser, Peter Chang, and David Isenberg, on behalf of the ADDRESS II Investigators</i>	266
Understanding the Antibody Repertoire in Neuropsychiatric Systemic Lupus Erythematosus and Neuromyelitis Optica Spectrum Disorders: Do They Share Common Targets? <i>Simone Mader, Venkatesh Jeganathan, Yoshiyuki Arinuma, Yuichiro Fujieda, Irena Dujmovic, Jelena Drulovic, Yuka Shimizu, Yuko Sakuma, Joel N. H. Stern, Cynthia Aranow, Meggan Mackay, Shinsuke Yasuda, Tatsuya Atsumi, Shunsei Hirohata, and Betty Diamond</i>	277
A Rare Variant (rs933717) at <i>FBXO31-MAP1LC3B</i> in Chinese Is Associated With Systemic Lupus Erythematosus <i>Yuan-yuan Qi, Xu-jie Zhou, Swapan K. Nath, Celi Sun, Yan-na Wang, Ping Hou, Rong Mu, Chun Li, Jian-ping Guo, Zhan-guo Li, Geng Wang, Hu-ji Xu, Yan-jie Hao, Zhuo-li Zhang, Wei-hua Yue, Huoru Zhang, Ming-hui Zhao, and Hong Zhang</i>	287
Clinical Images	
Unilateral Plantar Erythema Nodosum in Sarcoidosis <i>Axel J. Hueber, Georg Schett, and Bernhard Manger</i>	297
Sjögren's Syndrome	
Accumulation of Antigen-Driven Lymphoproliferations in Complement Receptor 2/CD21 ^{low} B Cells From Patients With Sjögren's Syndrome <i>Salomé Glauzy, Marco Boccitto, Jason M. Bannock, Fabien R. Delmotte, David Saadoun, Patrice Cacoub, John A. Ice, Kathy L. Sivils, Judith A. James, Sandra L. Wolin, and Eric Meffre</i>	298
Systemic Sclerosis	
Belimumab for the Treatment of Early Diffuse Systemic Sclerosis: Results of a Randomized, Double-Blind, Placebo-Controlled, Pilot Trial <i>Jessica K. Gordon, Viktor Martynov, Jennifer M. Franks, Elana J. Bernstein, Jackie Szymonifka, Cynthia Magro, Horatio F. Wildman, Tammara A. Wood, Michael L. Whitfield, and Robert F. Spiera</i>	308
Letters	
Implications of Elevated C-Reactive Protein and Serum Amyloid A Levels in IgG4-Related Disease: Comment on the Article by Perugino et al <i>A. Faiz Karim, Laura E. M. Eurelings, P. Martin van Hagen, and Jan A. M. van Laar</i>	317
Reply <i>Cory A. Perugino and John H. Stone</i>	318
Varicella Zoster Virus-Specific T Cell Responses in Untreated Giant Cell Arteritis: Comment on the Article by England et al <i>Marc B. Bigler, Julia R. Hirsiger, Mike Recher, Matthias Mehling, Thomas Daikeler, and Christoph T. Berger</i>	318
Reply <i>Bryant R. England, Ted R. Mikuls, and Jeffrey R. Curtis</i>	320
Single-Strain Versus Multistrain Probiotic Supplementation Treatment Strategy for Rheumatoid Arthritis: Comment on the Article by Marietta et al <i>Giancarlo Ceccarelli, Vincenzo Vullo, and Gabriella d'Ettorre</i>	320
Reply <i>Eric Marietta, Ashutosh Mangalam, Joseph Murray, and Veena Taneja</i>	321
Clinical Images	
Aneurysm Formation After Stent Grafting in Vascular Behçet's Disease <i>Suguru Honda, Fumio Hirano, Mariko Mouri, Hisanori Hasegawa, and Hitoshi Kohsaka</i>	322
ACR Announcements	A24

Cover image: The figure on the cover (from Qi et al, page 291) illustrates the worldwide geographic allele frequency distribution of rs933717, as determined using the Human Genome Diversity Project Selection Browser. Blue represents the ancestral (T) allele and orange the derived (C) allele. A rare variant in the Chinese population as seen, rs933717 was shown to be associated with systemic lupus erythematosus and to regulate expression of *LC3B*, an established marker of autophagy.

In this Issue

Highlights from this issue of *A&R* | By Lara C. Pullen, PhD

Antibody Repertoire in Neuropsychiatric SLE and Neuromyelitis Optica Spectrum Disorder

In this issue, Mader et al (p. 277) report the results of their analysis of the frequency of brain-reactive antibodies in patients with neuropsychiatric systemic lupus erythematosus (NPSLE) and compare that to the frequency of antibodies found in patients with systemic lupus erythematosus (SLE) without neuropsychiatric manifestations. They found that sera from 82% of patients with neuromyelitis optica spectrum disorder (NMOSD) and 27% of patients with demyelinating NPSLE were positive for IgG anti-aquaporin 4 (AQP-4) antibodies. In contrast, all sera from patients with non-demyelinating NPSLE, patients with SLE, and healthy controls were negative for IgG anti-AQP-4.

The investigators detected IgG anti-myelin oligodendrocyte glycoprotein (anti-MOG) at high titers in 50% of the patients with NMOSD who were negative for IgG anti-AQP-4, and at low titers in 18% of patients with demyelinating NPSLE and 1% of patients with non-demyelinating NPSLE. Although they found IgG antibodies to double-stranded DNA (anti-dsDNA) in 33% of

NMOSD patients, only 12% of NMOSD patients were positive for IgG anti-DWEYS, compared to 29% of SLE patients and 55% of NPSLE patients. They found IgG anti-DWEYS antibodies in 58% of patients with non-demyelinating NPSLE and 27% of patients with demyelinating NPSLE. Serum IgG brain-reactive antibodies were also found at a similar frequency in patients with non-demyelinating NPSLE, demyelinating NPSLE, and SLE, but these antibodies were less frequent in patients with NMOSD.

The authors conclude that patients with demyelinating NPSLE should be tested for antibodies to AQP-4, MOG, and DWEYS. While IgG anti-AQP-4 may be diagnostic of NMOSD, none of the tested antibodies appear to be diagnostic of demyelinating NPSLE. The investigators also note that while IgG anti-dsDNA antibodies are present in patients with NMOSD, the antibodies are not cross-reactive with IgG anti-DWEYS. This discrepancy suggests that demyelinating NPSLE and NMOSD may result from different antigenic stimuli and mechanisms of tissue damage.

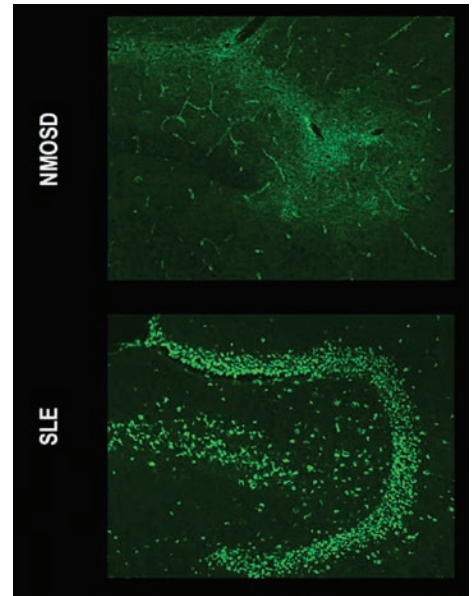


Figure 1. Staining patterns of serum IgG anti-brain antibodies. Representative results show immunostaining for serum IgG anti-brain antibodies in mouse brain tissue from the hippocampus region incubated with serum from a patient with neuromyelitis optica spectrum disorder (NMOSD) and serum from a patient with systemic lupus erythematosus (SLE). Original magnification $\times 40$.

Novel Formulation of Triamcinolone Acetonide Helps Knee Osteoarthritis

In this issue, Conaghan et al (p. 204) describe a prolonged reduction in symptoms of knee osteoarthritis (OA) in patients following intraarticular (IA) injection with FX006, a novel, microsphere-based, extended-release formulation of triamcinolone acetonide for IA injection. The formulation was designed to maintain drug concentration in the joint and provide prolonged analgesic benefits in patients with OA of the knee. This phase IIb study compared the analgesic benefits of 2 doses of FX006 (16 mg and 32 mg) with saline placebo injection.

The primary end point of the clinical trial was significant improvement in average daily pain (ADP) intensity at week 12 of treatment. While the primary end point was not met, the investigators found an obvious dose response and a safety profile similar to that of placebo. Specifically, there

were significant improvements in ADP intensity in patients treated with 32 mg of FX006 as compared to saline placebo at weeks 1–11 and week 13. Post hoc analysis of the standardized effect size for 32 mg of FX006 compared with saline placebo showed an effect size based on the Western Ontario and McMaster Universities Osteoarthritis Index (WOMAC) pain subscale above 0.30 at weeks 4 and 8 and approaching 0.30 at week 12.

The improvements in ADP intensity were also significantly greater with FX006 16 mg versus saline placebo at weeks 1–9. Although FX006 16 mg and 32 mg had comparable median times to onset of analgesia (day 4) and provided similar and significant maximal analgesic effects from approximately week 5, the maximal effect persisted longer with the 32-mg dose. Thus, FX006 32 mg provided increased therapeutic benefit relative to FX006 16 mg.

Rare Variant of Autophagy Protein Associated With SLE in Chinese Subjects

Recent evidence from genetic, cell biology, and animal model studies have suggested that autophagy plays a role in mediating systemic lupus erythematosus (SLE).

p. 287 Despite this connection between autophagy and SLE, the genetic basis for pathophysiology has not been thoroughly examined. In this issue, Qi et al (p. 287) report on their efforts to identify SLE susceptibility variants in autophagy-related genes and investigate the functional significance of the association. Their study included a gene family-based genetic association analysis that involved 26 autophagy-related genes.

The investigators used ImmunoChip arrays and selected the most strongly

associated polymorphisms for replication in additional cohorts. They next analyzed publicly available blood expression quantitative trait locus data and Encyclopedia of DNA Elements data on transcription factor binding sites and cell type-specific differential expression. They found a likely genetic association between light chain 3B (LC3B) and susceptibility to SLE. LC3B is a central protein in autophagy as well as a widely used marker of autophagy.

The investigators evaluated 14,474 samples from Chinese subjects and observed that the rare Chinese variant (rs933717T) of *MAP1LC3B*, which encodes microtubule-associated protein LC3B, was associated with genome-wide significance with susceptibility to

SLE (odds ratio 0.13, $P = 2.36 \times 10^{-10}$). They found that the rs933717 risk allele C correlated with increased *MAP1LC3B* expression; moreover, increased *MAP1LC3B* messenger RNA was noted in SLE patients as well as lupus-prone mice. When they tested the functional effects of *MAP1LC3B* using luciferase reporter assays, electrophoretic mobility shift assays, and differential gene expression assays, they found that the risk allele increased luciferase activity by 2.7–3.8-fold in both HEK 293T and Jurkat cell lines. Moreover, nuclear extracts of HEK 293T and Jurkat cells had increased binding to the risk allele. These findings thus confirm a likely association between LC3B and susceptibility to SLE.

Gut Microbiota in Reactive Arthritis and Postinfectious Spondyloarthritis

In this issue, Manasson et al (p. 242) report the results of the first culture-independent study designed to characterize the gut microbial community in postinfectious arthritis. They found that while subjects with reactive arthritis (ReA) were like control subjects with preceding infections but without arthritis in terms of gut bacterial richness or diversity, individuals with ReA and postinfectious peripheral spondyloarthritis (SpA) had an increased prevalence of enteropathogens. These patients also had a significantly higher abundance of *Erwinia* and *Pseudomonas*.

p. 242 When the investigators focused their attention on subjects who had ultrasound evidence of enthesitis, they found that these individuals were enriched in *Campylobacter*. In contrast, subjects with uveitis were enriched in *Erwinia* and *Dialister*, and subjects with radiographic sacroiliitis were enriched in unclassified Ruminococcaceae and *Dialister*. In addition, the researchers noted that while bacterial factors correlated with disease presence and clinical features of ReA, host genetics also appeared to be an independent driver of the composition of the intestinal community. HLA-A24 was associated with differences in gut microbiota diversity irrespective of disease status, such that they were able to identify several co-occurring taxa that were predictive of HLA-A24 status. The authors conclude that an understanding of the gut microbiota–host genetic relationships may help to further clarify the pathogenesis of postinfectious spondyloarthritis.

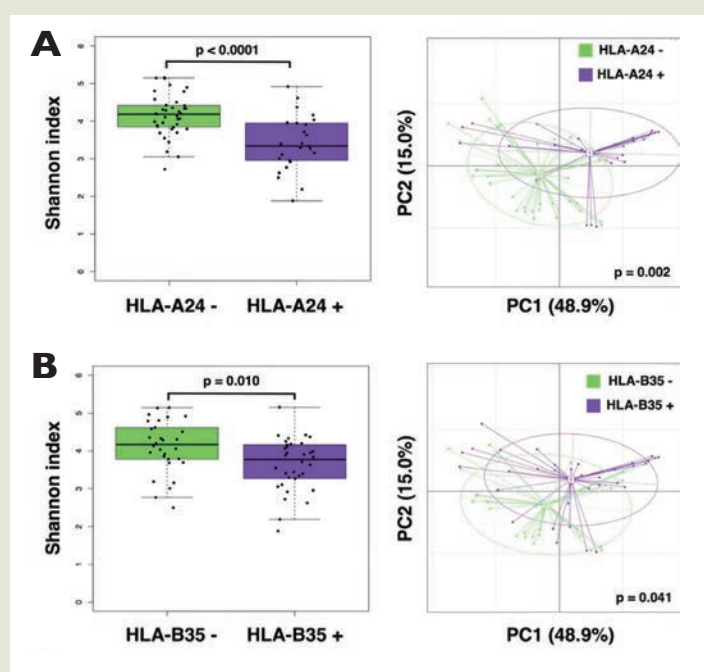


Figure 1. Alpha diversity (left) and beta diversity (right) for subjects grouped by HLA alleles. A and B. Alpha diversity was significantly lower in subjects carrying the HLA-A24 allele (A) and the HLA-B35 allele (B). Correspondingly, differences in beta diversity were also seen in subjects with HLA-A24 (A) and subjects with HLA-B35 (B).

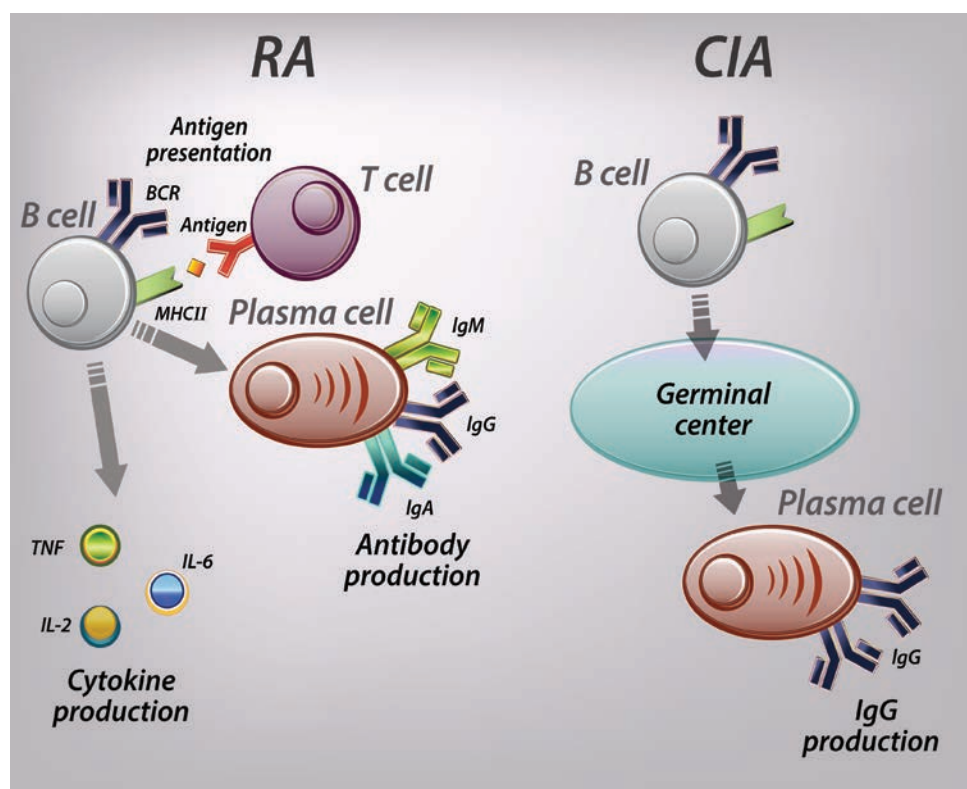
Clinical Connections

Germinal Center B Cells Are Essential for Collagen-Induced Arthritis

Dahdah et al, *Arthritis Rheumatol* 2018;70:193–203.

CORRESPONDENCE

Stephen Malin, PhD: stephen.malin@ki.se



KEY POINTS

- CIA induces the formation of GCs in secondary lymph nodes.
- Mice lacking either B2 cells or GC B cells are fully protected against CIA.
- Anticollagen antibodies are largely derived from the GCs.
- Arthritis induction through injection of anticollagen antibodies bypasses the need for GCs.

SUMMARY

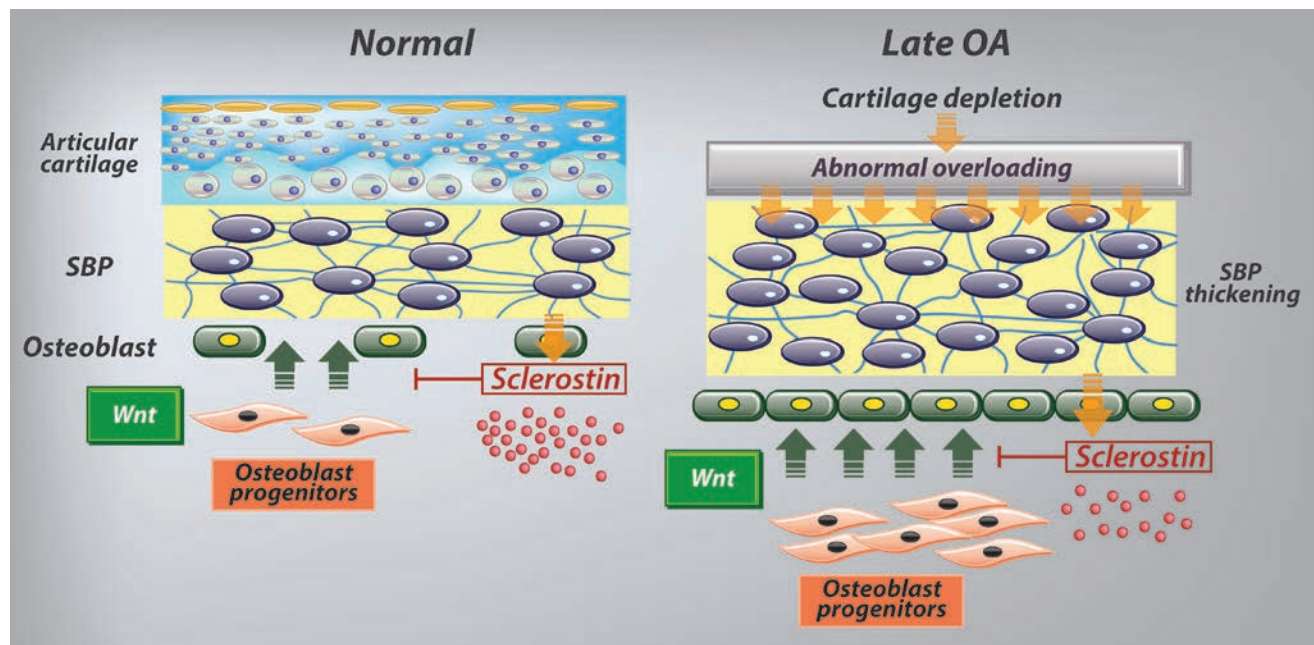
B lymphocytes provide the humoral arm of adaptive immunity due to their unique ability to terminally differentiate into antibody-producing plasma cells. These antibodies can be both protective and pathogenic, and recognition of cartilage by autoantibodies is thought to be a critical component of the progression to rheumatoid arthritis (RA). The relative importance of other B cell functions, such as antigen presentation and cytokine secretion (tumor necrosis factor [TNF], interleukin-6 [IL-6], etc.), in promoting experimental collagen-induced arthritis (CIA) was not previously known. Dahdah and colleagues found that mice lacking most functional mature B cells are protected against CIA. The germinal center (GC) response, which can develop with the help of T cells to improve the quality and type of antibodies produced, is critical for producing anticollagen antibodies. However, mice lacking GCs were susceptible to experimental arthritis induced by injection of pathologic antibodies. This indicates that the critical pathologic mechanism of B cells in CIA is autoantibody production. While B cells likely have a much more complex function in RA, targeting the GC response could be of potential therapeutic benefit.

Loading-Induced Reduction in Sclerostin as a Mechanism of Subchondral Bone Plate Sclerosis in Mouse Knee Joints During Late-Stage Osteoarthritis

Jia et al, *Arthritis Rheumatol* 2018;70:230–241.

CORRESPONDENCE

Ling Qin, PhD: qinling@pennmedicine.upenn.edu



SUMMARY

Thickening of the subchondral bone plate (SBP), the layer of bone underneath the articular cartilage, is a hallmark of late-stage osteoarthritis (OA). To better understand this process, Jia and colleagues devised a 3-dimensional approach for measuring the thickness of the entire SBP in mouse femurs and then studied 4 distinct mouse models that develop severe knee joint OA: a genetically modified, cartilage-damaged mouse model with or without OA-inducing surgery, and normal mice with 2 different OA-inducing surgical procedures. In each model, abnormal overloading of the SBP caused by depletion of the overlying cartilage was associated with decreased levels of the osteocyte glycoprotein sclerostin. Sclerostin inhibits Wnt signaling, a pathway that strongly promotes bone formation. This decreased sclerostin content led to an increase in the formation and activity of osteoblasts at the bone marrow side of the SBP and its subsequent expansion. These data reveal a novel mechanism of pathologic subchondral bone changes associated with late-stage OA and offer a new approach for experimental OA research.

KEY POINTS

- A new micro-computed tomography protocol was developed to measure the thickness of the SBP in mouse distal femurs.
- Four mouse models with severe knee joint OA were generated to characterize SBP changes of late-stage OA.
- SBP thickening under damaged cartilage is due to elevated bone formation at the bone marrow side of the SBP and a reduction of sclerostin levels in osteocytes within the SBP.
- These studies reveal the intimate relationship among mechanical loading, osteocytic sclerostin, and SBP sclerosis in late-stage OA.

Arthritis & Rheumatology

An Official Journal of the American College of Rheumatology
www.arthritisrheum.org and wileyonlinelibrary.com

EDITORIAL

Prevalence of Arthritis Revisited

Jeffrey N. Katz

Estimates of disease prevalence have far-reaching consequences. By providing a baseline understanding of the impact of a disease, these estimates are used to justify investment in research, prevention, and treatment. For years, estimates of arthritis prevalence have been derived from a single screening question on the National Health Interview Survey (NHIS): “Have you ever been told by a doctor or other health professional that you have some form of arthritis, rheumatoid arthritis, gout, lupus, or fibromyalgia?” (1) This question alone grounds the prevailing estimates of ~54 million US adults living with arthritis (2).

What do we know about the accuracy of this question on doctor-diagnosed arthritis? In a validation study performed at the Fallon Clinic in central Massachusetts, Sacks and colleagues compared responses to this specific NHIS item to a determination based on a medical record review, a standardized physical examination, and a physician’s interpretation of these data (3). The study documented sensitivity of the doctor-diagnosed arthritis question of 53% in persons ages 45–64 years and 69% in those ages ≥65 years. Thus, the NHIS question misses 47% and 31% of arthritis cases, respectively, in the two age groups. Specificity of the question was ~80% in both age groups. These modest sensitivities and specificities suggest that prevalence estimates based on this question risk substantial misclassification. In particular, the low sensitivity points to underestimation of arthritis prevalence, especially in persons younger than 65 years of age.

Surely, we *can* and *should* do better, given that estimates of prevalence can translate into investment into research, prevention, and management.

In this issue of *Arthritis & Rheumatology*, Drs. Jafarzadeh and Felson (4) bring to the field of arthritis epidemiology a Bayesian method of estimating arthritis prevalence that may be considerably more accurate than prior estimates using the single NHIS item on doctor-diagnosed arthritis. Their method incorporates two additional NHIS items pertaining to arthritis: one asks about joint pain, aching, or stiffness in the last 30 days, and the other asks if symptoms have lasted for more than 90 days. In their validation study, Sacks and colleagues also examined the sensitivity and specificity of these items in addition to the question on doctor-diagnosed arthritis. They found that chronic joint symptoms (joint aching, pain, or stiffness lasting longer than 90 days) had a sensitivity of 69% for both age groups (45–64 years and ≥65 years) and specificities of 67% and 89% in the younger and older groups, respectively. Using the sensitivities and specificities of each of these arthritis screening questions, Jafarzadeh and Felson used Bayesian methods to estimate the prevalence of arthritis in adults ages 45–65 years and ≥65 years. The authors’ updated prevalence estimate was 91 million Americans, 68% higher than the original estimate. The findings suggest that prior survey estimates based on the single doctor-diagnosed arthritis question may have underestimated arthritis prevalence substantially.

Limitations inherent in the data used to derive these new prevalence estimates urge some caution in interpreting the findings. The work relies upon a single validation study performed at the Fallon Clinic with a population that was 97% white. Although it is not known whether the performance characteristics of the 3 arthritis screening questions varies among persons of different racial or ethnic backgrounds, the sample homogeneity

Jeffrey N. Katz, MD, MSc: Brigham and Women’s Hospital, Harvard Medical School, Boston, Massachusetts.

Address correspondence to Jeffrey N. Katz, MD, MSc, Orthopedic and Arthritis Center for Outcomes Research, Brigham and Women’s Hospital, 75 Francis Street, BTM-5016, Boston, MA 02115. E-mail: jnkatz@partners.org.

Submitted for publication October 7, 2017; accepted in revised form October 17, 2017.

may limit the generalizability of the results. Also, while the gold standard—consisting of a standardized examination by a trained nurse, a medical record review, and a physician's judgement—was executed using rigorous protocols, the findings are nonetheless subject to observer variability. Furthermore, the Fallon validation study had a limited sample size (389 subjects) to begin with, and sensitivities and specificities were calculated on subgroups of this sample. Consequently, the estimated sensitivities and specificities of each survey item have limited precision. These limitations in the Fallon data, and therefore in the estimates of Jafarzadeh and Felson, can be overcome with more research to improve the accuracy of screening questions. Development of such items is an important research agenda.

Discussion of arthritis prevalence invites broader consideration of what “arthritis” means in this context. Doctor-diagnosed “arthritis” is defined in the NHIS survey item to include rheumatoid arthritis, fibromyalgia, lupus, and other problems. As these disorders vary considerably in prevalence, mechanism, impact on productivity and quality of life, and direct medical costs (5–8), separate estimates of the prevalence of the individual disorders would be more informative for many policy-making applications. That said, surveys must be reasonably brief, creating a trade-off between specificity of the items and robustness of the response rate.

Dollars (for research, prevention, and treatment) generally follow burden. In particular, investment by the National Institutes of Health (NIH) in disease-specific research is associated with prevalence and even more so with measures that combine both prevalence and impact, such as disability-adjusted life years lost. Indeed, Gillum and colleagues showed that disability-adjusted life years lost explained 33% of the variance in NIH disease-specific funding in 2006; prevalence explained 6% (9). Thus, while there are exceptions (for example, systemic lupus erythematosus is among the least prevalent rheumatic disorders but among the most generously supported by NIH research dollars [10]), highly prevalent disorders, especially those that are disabling, tend to command more resources than less widespread conditions. Consequently, systematic underestimates of prevalence could lead to underinvestment in research, prevention, and therapy.

The work of Drs. Jafarzadeh and Felson moves our field a large step forward, both by introducing a set

of techniques that permits more nuanced use of existing survey data and by highlighting the limits of the specific questions deployed at present in national prevalence surveys. While additional research will continue to refine the estimates of Jafarzadeh and Felson, the adjusted prevalence estimates these authors present are sufficiently robust and concerning to justify a policy agenda encouraging greater investment of scarce resources into research on the pathogenesis, prevention, and treatment of arthritis conditions.

ACKNOWLEDGMENT

The author acknowledges the editorial assistance of Angela Chen, BA.

AUTHOR CONTRIBUTIONS

Dr. Katz drafted the article, revised it critically for important intellectual content, and approved the final version to be published.

REFERENCES

- Centers for Disease Control and Prevention. National Center for Health Statistics. National Health Interview Survey. URL: <https://www.cdc.gov/nchs/nhis/data-questionnaires-documentation.htm>.
- Hootman JM, Helmick CG, Barbour KE, Theis KA, Boring MA. Updated projected prevalence of self-reported doctor-diagnosed arthritis and arthritis-attributable activity limitation among US adults, 2015–2040. *Arthritis Rheumatol* 2016;68:1582–7.
- Sacks JJ, Harrold LR, Helmick CG, Gurwitz JH, Emani S, Yood RA. Validation of a surveillance case definition for arthritis. *J Rheumatol* 2005;32:340–7.
- Jafarzadeh SR, Felson DT. Updated estimates suggest a much higher prevalence of arthritis in US adults than previous ones. *Arthritis Rheumatol* 2018;70:185–92.
- Boonen A, Severens JL. The burden of illness of rheumatoid arthritis. *Clin Rheumatol* 2011;30 Suppl 1:S3–8.
- Xie F, Kovic B, Jin X, He X, Wang M, Silvestre C. Economic and humanistic burden of osteoarthritis: a systematic review of large sample studies. *Pharmacoeconomics* 2016;34:1087–100.
- Chandran A, Schaefer C, Ryan K, Baik R, McNett M, Zlateva G. The comparative economic burden of mild, moderate, and severe fibromyalgia: results from a retrospective chart review and cross-sectional survey of working-age U.S. adults. *J Manag Care Pharm* 2012;18:415–26.
- Narayanan S, Wilson K, Ogelsby A, Juneau P, Durden E. Economic burden of systemic lupus erythematosus flares and comorbidities in a commercially insured population in the United States. *J Occup Environ Med* 2013;55:1262–70.
- Gillum LA, Gouveia C, Dorsey ER, Pletcher M, Mathers CD, McCulloch CE, et al. NIH disease funding levels and burden of disease. *PLoS One* 2011;6:e16837.
- National Institutes of Health. Estimates of funding for various research, condition, and disease categories (RDCDC). July 3, 2017. URL: https://report.nih.gov/categorical_spending.aspx.

EDITORIAL

Bench to Bedside—and Back Again: Finding the Goldilocks Zone Within the Scleroderma Universe

Janet E. Pope,¹ Jason J. Lee,² and Christopher P. Denton³

Systemic sclerosis (SSc) is a complex inflammatory connective tissue disease characterized by skin thickening, organ fibrosis, and vasculopathy (1,2). The underlying disease mechanisms and pathophysiology are not fully understood. However, it appears to be, at least in part, driven by autoimmunity and inflammation associated with microvascular dysfunction, ultimately resulting in excess extracellular matrix deposition in target organs (2–4). Clinical heterogeneity coupled with our lack of understanding of the disease pathogenesis means that current treatment strategies are mostly organ-based therapies using antirheumatic drugs that were originally approved for other indications (5). Of course, this clinical diversity not only provides challenges to discovery of disease mechanisms, it also complicates often underpowered clinical trials that aim to find the right drugs for the right patient at the right time.

One approach to discovery of the “Goldilocks Zone” of disease-modifying therapy for all patients with SSc is to start at a point of known commonality. For example, SSc is often characterized by the presence of autoantibodies (6,7). More specifically, there has been recent interest in B cell biology and modulation, including data derived from animal models of disease, human tissue analyses, and even small randomized clinical trials of B cell depletion in patients with SSc (6,8,9). In addition to their role in autoantibody formation, B cells have been shown to be elevated in blood and tissue samples from patients with SSc, with abnormal chronic activation while demonstrating secretion of important disease cytokines such as interleukin-6 and transforming growth factor β (6).

In this issue of *Arthritis & Rheumatology*, Gordon et al present their experience with belimumab in a randomized, placebo-controlled trial (10). Belimumab is a human monoclonal antibody directed against BAFF, also known as B lymphocyte stimulator. Their study assessed the potential benefit of adding belimumab to standard treatment of early diffuse cutaneous SSc (dcSSc) with mycophenolate mofetil (MMF). The authors evaluated safety and looked for signals of efficacy. The results showed improvement in the modified Rodnan skin thickness score (11) during the treatment period, with a numerically greater decrease in patients randomized to receive belimumab than in those randomized to receive placebo (median change of –10 versus –3), although the difference was not statistically significant. Interestingly, the authors investigated differential gene expression for patients who received belimumab, which clearly identified the clinical improvers compared to the nonresponders.

While the trends toward benefit with use of belimumab are promising for patients with SSc, this modern study design also highlights an important innovative paradigm shift in the approach to research of heterogeneous autoimmune connective tissue diseases. Specifically, in this study, the research design incorporated clinical data along with differential gene expression data, which allowed for a deeper, more intelligent interpretation of the end point results. Although the study was underpowered to show statistical significance for overall clinical outcomes, we are encouraged by the biologic data that demonstrated expected drug target modulation along with identification of a subset of patients who derived substantial benefit. This is important since one can envision a truly translational research loop that not only allows bench data to drive clinical trials, but also allows clinical trial experiences to guide further biologic research.

Therefore, another approach to discovery of our elusive Goldilocks Zone may be to translate traditional clinical trials data into modern basic and clinical research that unravels the heterogeneity of SSc. Using novel techniques, studies by Milano et al (12) and others (13) have shown that disease stratification and personalization are

¹Janet E. Pope, MD, MPH, FRCPC: St. Joseph's Health Care, University of Western Ontario, London, Ontario, Canada; ²Jason J. Lee, MD, FRCPC: University of Western Ontario, London, Ontario, Canada; ³Christopher P. Denton, PhD, FRCP: Royal Free Hospital and University College London Medical School, London, UK.

Address correspondence to Janet E. Pope, MD, MPH, FRCPC, Division of Rheumatology, St. Joseph's Health Care, 268 Grosvenor Street, London, Ontario N6A 4V2, Canada. E-mail: janet.pope@sjhc.london.on.ca.

Submitted for publication September 29, 2017; accepted in revised form November 3, 2017.

within reach. Going forward, biologic precision will allow clinicians and researchers to reveal more powerful truths within small trials of uncommon and rare diseases. For instance, a very small study of imatinib in active dcSSc used changes in levels of cytokines from skin biopsy samples and serum to determine if there were changes correlating with treatment response (14).

Change to SSc trial design should take into consideration various factors such as ethical considerations including background immune suppression (Good Clinical Practice) and weighing this against gaining insight about how a treatment works compared to placebo (for example, as monotherapy and not combined with other standard of care treatment). Interpretation of pilot studies in general, use of genomics or other parameters to help to understand early trial results, and overall interpretation of pathophysiology of early SSc and role of B cell signaling are all important in this particular trial design.

The strengths of the study by Gordon et al include randomization, blinding, a placebo control, and the addition of study drug to a standardized background treatment (MMF). Limitations include the small number of patients, the single-center design with potential bias (or center effect), and the confounding effect of concurrent immunosuppression with MMF. This cotherapy makes it impossible to attribute any treatment effect solely to belimumab and may have blunted the difference in treatment response between the 2 groups. However, it allowed for all patients to receive standard of care, which enhances recruitment and allows for Good Clinical Practice. Future studies may need to determine whether MMF is needed and also whether other immunosuppressive drugs could be used. This study provides data for a power calculation of a larger trial.

The gene expression analysis may be difficult to interpret due to small numbers, and the MMF response and natural history may confound the effect of belimumab. However, the authors showed modulation of B cell receptor activation and profibrotic signaling in the belimumab group and not in clinical improvers in the placebo group.

In conclusion, the study by Gordon et al sets some important precedents. Their novel trial in early dcSSc, which incorporated standard of care treatment and gene expression analysis, constitutes a template for future SSc trials.

AUTHOR CONTRIBUTIONS

All authors drafted the article, revised it critically for important intellectual content, and approved the final version to be published.

REFERENCES

1. Gabrielli A, Avvedimento EV, Krieg T. Scleroderma. *N Engl J Med* 2009;360:1989–2003.
2. Denton CP, Black CM, Abraham DJ. Mechanisms and consequences of fibrosis in systemic sclerosis. *Nat Clin Pract Rheumatol* 2006;2:134–44.
3. Bhattacharyya S, Wei J, Tourtellotte WG, Hinchcliff M, Gottardi CG, Varga J. Fibrosis in systemic sclerosis: common and unique pathobiology. *Fibrogenesis Tissue Repair* 2012;5 Suppl 1: S18.
4. Beyer C, Schett G, Distler O, Distler JH. Animal models of systemic sclerosis: prospects and limitations [review]. *Arthritis Rheum* 2010;62:2831–44.
5. Lee JJ, Pope JE. Diagnosis and management of systemic sclerosis: a practical approach. *Drugs* 2016;76:203–13.
6. Sato S, Fujimoto M, Hasegawa M, Takehara K, Tedder TF. Altered B lymphocyte function induces systemic autoimmunity in systemic sclerosis. *Mol Immunol* 2004;41:1123–33.
7. Bhattacharyya S, Wei J, Varga J. Understanding fibrosis in systemic sclerosis: shifting paradigms, emerging opportunities. *Nat Rev Rheumatol* 2012;8:42–54.
8. Daoussis D, Melissaropoulos K, Sakellaropoulos G, Antonopoulos I, Markatseli TE, Simopoulou T, et al. A multicenter, open-label, comparative study of B-cell depletion therapy with rituximab for systemic sclerosis-associated interstitial lung disease. *Semin Arthritis Rheum* 2017;46:625–31.
9. Leask A. Emerging targets for the treatment of scleroderma. *Expert Opin Emerg Drugs* 2012;17:173–9.
10. Gordon JK, Martyanov V, Franks JM, Bernstein EJ, Szymonifka J, Magro C, et al. Belimumab for the treatment of early diffuse systemic sclerosis: results of a randomized, double-blind, placebo-controlled, pilot trial. *Arthritis Rheumatol* 2018;70:308–16.
11. Clements P, Lachenbruch P, Seibold J, White B, Weiner S, Martin R, et al. Inter and intraobserver variability of total skin thickness score (modified Rodnan TSS) in systemic sclerosis. *J Rheumatol* 1995;22:1281–5.
12. Milano A, Pendergrass SA, Sargent JL, George LK, McCalmont TH, Connolly MK, et al. Molecular subsets in the gene expression signatures of scleroderma skin. *PloS One* 2008;3: e2696.
13. Derrett-Smith EC, Martyanov V, Chighizola CB, Moynadeh P, Campochiaro C, Khan K, et al. Limited cutaneous systemic sclerosis skin demonstrates distinct molecular subsets separated by a cardiovascular development gene expression signature. *Arthritis Res Ther* 2017;19:156.
14. Pope J, Walker KM, de Leon F, Vanderhoek L, Seney S, Summers KL. Correlations between changes in cytokines and clinical outcomes for early phase (proof of concept) trials in active diffuse systemic sclerosis using data from an imatinib study. *Rheumatology (Oxford)* 2014;53:1830–4.

EDITORIAL

Wnt Signaling Related to Subchondral Bone Density and Cartilage Degradation in Osteoarthritis

David B. Burr¹ and Achint Utreja²

The role of subchondral bone in the progression of osteoarthritis (OA) has been a controversial topic for nearly 50 years (1,2). The observation that subchondral sclerosis is nearly always present in end-stage disease led to the conclusion that the increased stiffness caused by a thicker subchondral bone plate detracted from the bone's ability to attenuate the loads imposed on the joint cartilage, increasing cartilage stresses and initiating the process of joint deterioration. Because cartilage damage does not always progress to full-thickness cartilage loss and OA, Radin and Rose (3) proposed that the initiation and the progression of cartilage deterioration were separate processes. They suggested that it was steep stiffness gradients at the joint margins, primarily regions of high tensile and shear stresses, that tend to create inhomogeneities in the subchondral plate–cartilage complex. They hypothesized that these changes can lead to differential deformation between more compliant and denser regions of the subchondral bone, tearing the cartilage attached to it and initiating fibrillation. They further proposed that progression of cartilage loss, a separate process, ensues when continued loading occurs on an already dense and stiff subchondral plate. Findings from several animal models support this progression of events. In a model of spontaneous age-related OA in cynomolgus macaques, an animal model of aging-related OA much like that in humans, Carlson et al (4,5) clearly demonstrated that cartilage damage occurs subsequent to subchondral bone densification.

In the study by Jia et al in this issue of *Arthritis & Rheumatology*, the investigators examined the mechanisms of subchondral densification, and whether increased

subchondral plate density is a sine qua non of progressive disease (6). Jia and colleagues employed several different mouse models for the study, and induced OA with 2 different surgical approaches.

They first developed a cartilage-specific knock-out of the epidermal growth factor receptor (*Egfr*-CKO), which they had previously shown regulates chondrocyte number and joint lubrication (7,8). They surgically destabilized the medial meniscus (DMM), and in some cases hemisected the meniscus (DMMH), in *Egfr*-CKO or wild-type (WT) mice, and subsequently observed changes in the meniscus after 2–3 months. To simulate the effects of aging, the study investigators performed DMM on WT mice, and observed cartilage changes 10 months after surgery. They also examined the spontaneous initiation and progression of OA in *Egfr*-CKO mice over a 12-month period. To determine the effect of preexisting bone densification on the process of cartilage degeneration, they also subjected mice with knockout of the sclerostin gene (*Sost*-KO mice) to DMMH. This directly tests the Radin and Rose hypothesis that increased density and stiffness of the subchondral bone are a necessary precondition for the progression of OA. If they do in fact represent a precondition for disease progression, then one might expect an accelerated onset of OA or cartilage degeneration that is more severe than that in WT mice. If they are not a precondition, then the expectation is that cartilage degeneration will be similarly severe and OA will develop in a similar manner in mice with and those without preexisting subchondral densification, or may not occur at all.

In addition, Jia et al utilized a novel microfocal computed tomography (micro-CT) approach that allowed them to visualize bone and cartilage changes 3-dimensionally (3-D) (6), rather than by 2-D histologic serial sectioning. Given the focal nature of cartilage degeneration in OA, 2-D histologic approaches can provide an imperfect view of the relationship between cartilage and bone in the regions where cartilage fibrillation occurs. This new 3-D micro-CT method allowed the investigators in this study

¹David B. Burr, PhD, FAAA: Indiana University School of Medicine and Indiana University–Purdue University–Indianapolis, Indianapolis, Indiana; ²Achint Utreja, BDS, MS, PhD: Indiana University School of Dentistry, Indianapolis.

Address correspondence to David B. Burr, PhD, FAAA, Department of Anatomy and Cell Biology, MS 5035, Indiana University School of Medicine, 635 Barnhill Drive, Indianapolis, IN 46202. E-mail: dburr@iupui.edu.

Submitted for publication October 26, 2017; accepted in revised form November 14, 2017.

to localize subchondral bone changes to the areas in which cartilage was either healthy or degenerating.

What Jia and colleagues observed in the OA models in which mouse knees were subjected to DMM surgery was a location-specific increase in subchondral plate thickness, occurring from the marrow side of the subchondral plate, but only at sites of cartilage deterioration and not at sites where the overlying cartilage was healthy. This was associated with a localized reduction in sclerostin in subchondral bone, increased vessel ingrowth, and more osteoblasts, but only at those sites associated with increased thickness and cartilage damage. These areas were in load-bearing sites of the joints; non-loading-bearing sites did not show similar changes in cartilage or bone. This implicates mechanical loading as complicit in the degenerative process. In situations in which there was not cartilage damage, and in non-load-bearing sites, these subchondral plate changes did not occur. Interestingly, spontaneous age-related development of cartilage damage in the *Egfr*-CKO mice was not localized to the medial weight-bearing sites, but was also found laterally in association with reduced sclerostin. As has been observed in other models in which subchondral plate sclerosis occurs in association with cartilage loss (9), the trabecular bone adjacent to the subchondral plate becomes osteopenic and its microarchitecture deteriorates, which is likely attributable to the effects of stress shielding.

The authors conclude that subchondral bone sclerosis occurs through a down-regulation of sclerostin that is fueled by mechanical loading in those regions of the joint in which cartilage is breaking down (6). This is consistent with what we know about the role of sclerostin in mechanically induced bone formation from animal models involving in vivo mechanical loading of the joints (10). In the Jia study, in mice at 2 months after DMM surgery, changes in proteoglycan and cartilage fibrillation can be seen, at a time when the investigators were unable to identify any changes in the subchondral bone. Based on this, Jia et al conclude that subchondral sclerosis is secondary to the cartilage change, and is driven by the mechanically mediated down-regulation of sclerostin.

As further evidence of this, they note that *Sost*-KO mice do not develop spontaneous cartilage deterioration, even in mature 14-month-old mice (6), despite the fact that down-regulation of *Sost* results in a significant increase in bone volume and density (11). This is consistent with observations in human subjects, in individuals who have a gain-of-function mutation of the lipoprotein receptor-related protein 5 gene (*LRP5*), which leads to high bone mass (12). However, there is no evidence of increased incidence of OA in individuals with this mutation as compared to normal healthy subjects, suggesting

that sclerotic subchondral bone alone does not lead to cartilage disease.

Animal models also have shown that the existence of elevated subchondral density alone does not lead to cartilage deterioration and OA, unless preceded by a period of increased subchondral remodeling and vascularization. In the Dunkin-Hartley guinea pig model of OA, animals exhibit a high rate of subchondral bone turnover within the first 2 months of life, and develop severe OA progressively over 12 months (13). In a second guinea pig strain (Strain 13), the animals, at 2 months of age, have a subchondral plate thickness that is 6–7 times higher than that of Dunkin-Hartley guinea pigs, do not have a high rate of subchondral bone turnover, and do not develop OA. All of these lines of evidence show that subchondral plate densification by itself does not initiate joint disease. In fact, Jia and colleagues make this clear when they state that subchondral bone plate thickening alone is “not sufficient to affect cartilage degeneration” and also conclude that subchondral bone plate thickening “cannot be an initiator of cartilage and joint damage in OA” (6).

When DMMH is performed on *Sost*-KO mice, the resulting cartilage deterioration is no worse than that in WT mice, suggesting that subchondral sclerosis is not driving the progression of joint degeneration either, but rather reacting to it. The fact that preexisting subchondral sclerosis neither accelerates the process of joint degeneration nor makes the OA worse may detract from the thesis of Radin and Rose that subchondral sclerosis is required for progression of disease once cartilage deterioration has initiated. However, conclusive evidence that subchondral sclerosis either exists (in *Sost*-KO mice) or develops (in WT mice) during the process of joint destruction is lacking. Evidence that subchondral sclerosis does not contribute to joint deterioration would only be conclusive if it could be shown that OA develops even in the absence of subchondral sclerosis. Therefore, an experiment like the ones conducted in the Jia study, in which subchondral bone is prevented from becoming sclerotic (perhaps by performing DMMH in a *Sost*-overexpressing mouse, or by preventing increased subchondral plate thickness), would provide the negative control needed to conclusively reject the hypothesis that subchondral sclerosis is a necessary component of progressive disease.

Sclerostin is also expressed by chondrocytes (14), and therefore changes in Wnt signaling may also be important to cartilage health either independent of or concurrent with changes that occur in subchondral bone. A comparison of the expression of Wnt genes in bone samples from patients with hip fractures or hip/knee OA showed up-regulation of 7 genes, including *LRP5*, in the OA samples (15). This led the authors to conclude that

Wnt pathway genes not only affect the subchondral bone but also regulate cartilage degradation in OA. This is supported by earlier observations in a mouse model of OA with β -catenin overexpression induced by conditional activation, in which increased β -catenin signaling was associated with an OA phenotype (16). Wnt signaling can be induced by proinflammatory cytokines (17,18), and can generate cartilage matrix degradation by stimulating the expression of matrix metalloproteinases (MMPs) and ADAMTS motifs (19). Shin et al compared the expression of *LRP5*, type II collagen, and MMPs in human and mouse OA cartilage, and found a relationship between increased *LRP5* expression and cartilage destruction in OA (20). Conversely, *LRP5* deficiency decreased Wnt-mediated cartilage destruction. Similar findings were reported in a study that investigated Wnt signaling and *LRP5* expression in human OA chondrocytes (21). Increased *LRP5* expression was consistent with greater severity of cartilage destruction, whereas decreased levels reduced the extent of cartilage damage.

Joint instability (induced by DMM) in *Sost*-KO mice leads to higher scores for the severity of OA cartilage degeneration, pointing to the significance of sclerostin in the maintenance of cartilage integrity during mechanical loading (22). Similarly, selective inhibition of the Wnt pathway by Dkk-1 decreases the severity of OA in mice (23). However, in both sheep and mouse models of surgically induced OA, the levels of *Sost* were increased in cartilage, but only focally, in regions of cartilage damage, while being focally decreased in the subchondral bone associated with the cartilage damage (14). The up-regulation of *Sost* in these cases seems somewhat contradictory to the idea that increased Wnt signaling promotes cartilage degradation. However, this could be a secondary response to the increased inflammation associated with the initiation of cartilage degeneration (17,18), and therefore temporal relationships in the regulation of sclerostin expression and Wnt signaling are important to study. Preventing expression of sclerostin and allowing Wnt signaling will increase subchondral bone density and may permit the initiation of cartilage degradation, but later-stage inflammatory processes could stimulate sclerostin production, leading to full-thickness cartilage loss.

The observation that increased plate thickness occurs subsequent to the initiation of cartilage deterioration does not address whether other changes to subchondral bone that occur prior to overt cartilage deterioration contribute to the disease. Although the findings in the study by Jia et al do not support the hypothesis of Radin and Rose, since they provide no evidence that increased subchondral density drives progression of disease, this

leaves open the question of what initiates the process in the first place. There is now accumulating evidence that increased remodeling in the early phases of joint disease may be required for progression of disease. This was noted many years ago by Li and Aspden (24), who showed that bone in patients with OA was significantly less stiff for a given apparent density than normal or osteoporotic bone. This does not mean that the subchondral plate is less stiff at a structural level, and it may not be. However, the tissue modulus is lower because of the high turnover and mineralization lag period prior to full maturation and mineralization of the tissue. Day et al (25) showed that subjects who were in the early phases of cartilage loss but had not yet developed arthritis had lower subchondral bone tissue modulus, confirming the earlier work of Li and Aspden. The increase in remodeling rate in the early phases of OA has been verified using animal models.

When this early remodeling reaction is suppressed using bisphosphonates (26–29) or RANKL inhibitors (30,31), which prevent the early increase in remodeling but eventually lead to increased subchondral plate thickness, cartilage is protected from progressive deterioration. The protective effect may be both dose- and time-related. More potent bisphosphonates appear to have a greater effect (29), as does treatment earlier in the degenerative process (32–34). Although suppression of remodeling is not effective at preventing all cartilage damage, early suppression is associated with prevention of progressive joint disease. These studies clearly demonstrate that increased bone remodeling is a precursor to OA, and that suppression of remodeling in early phases of the disease can prevent OA, even if it leads to subchondral densification.

The work by Jia et al is instructive in showing that mechanically induced down-regulation of sclerostin provides a mechanism for focally increased subchondral bone density. Lower sclerostin expression in bone biopsy tissue has been observed in OA patients as compared to healthy controls (35), but this may not reflect processes involving Wnt signaling in cartilage (36,37). In the OA models used by Jia et al, it would be fascinating to understand the temporal expression of the *Sost* gene in cartilage and the associated changes in Wnt signaling. The data suggest that an early decrease in sclerostin expression leads to increased bone density but also can create permissive conditions for the acceleration of cartilage degradation, with a subsequent inflammation-related increase in cartilage *Sost* expression. This Wnt signaling link makes the relationship between cartilage loss and subchondral bone densification more complex.

Evidence that cartilage loss occurs prior to sclerostin down-regulation and the subsequent densification of subchondral bone has not been conclusive, and such

a conclusion would require a more thorough temporal analysis of both cartilage and bone changes in the models that have been employed. The argument over whether OA initiates in the bone or in the cartilage has not been resolved fully, as evidenced by a scheduled debate on the topic at the 2018 meeting of the Orthopaedic Research Society. One difficulty in resolving this question is that OA is a condition that takes a long time to develop. Therefore, it is difficult to know if and when early joint changes will progress to OA in humans. It is also difficult to determine, in individuals with OA, when the process began, or what the initiating factor might have been. In this regard, there is a movement toward increasing studies of posttraumatic OA (PTOA), in which the time of disease initiation can be identified precisely. As PTOA progresses in a way that is consistent with age-related OA (at least macro- and microscopically), this is an appropriate way to develop new therapies, even though we do not really know whether PTOA and age-related OA are equivalent mechanistically.

It has been suggested that OA represents a common final outcome for a multitietologic set of joint diseases and conditions that all lead to the same joint degenerative changes, involving both elevated subchondral density and augmented cartilage deterioration and eventual loss. It is possible that the common mechanistic pathway ultimately recognized for OA might be through Wnt signaling, which both accelerates cartilage deterioration and underlies increased subchondral density. This may be the long-sought link between bone and cartilage changes that Radin and his colleagues attempted to identify nearly 50 years ago. Based on the data presented in the current study by Jia et al (6), Radin and colleagues appear to have been correct about the role of mechanical loading (2). However, at that time, it was not possible to identify the molecular link for these events, which only became apparent more recently with the discovery of the role of the Wnt pathway and its inhibitors, such as sclerostin and Dkk. The role of subchondral bone in the progression of OA thus deserves more study, both in animal models and in humans.

AUTHOR CONTRIBUTIONS

Drs. Burr and Utreja drafted the article, revised it critically for important intellectual content, and approved the final version to be published.

REFERENCES

1. Radin EL, Paul IL, Tolkoﬀ MJ. Subchondral bone changes in patients with early degenerative joint disease. *Arthritis Rheum* 1970;13:400–5.
2. Radin EL, Paul IL, Rose RM. Role of mechanical factors in pathogenesis of primary osteoarthritis. *Lancet* 1972;1:519–22.
3. Radin EL, Rose RM. Role of subchondral bone in the initiation and progression of cartilage damage. *Clin Orthop Rel Res* 1986;213:34–40.
4. Carlson CS, Loeser RF, Jayo MJ, Weaver DS, Adams MR, Jerome CP. Osteoarthritis in cynomolgus macaques: a primate model of naturally occurring disease. *J Orthop Res* 1994;12:331–9.
5. Carlson CS, Loeser RF, Purser CB, Gardin JF, Jerome CP. Osteoarthritis in cynomolgus macaques III: effects of age, gender, and subchondral bone thickness on the severity of disease. *J Bone Miner Res* 1996;11:1209–17.
6. Jia H, Ma X, Wei Y, Tong W, Tower RJ, Chandra A, et al. Loading-induced reduction in sclerostin as a mechanism of subchondral bone plate sclerosis in mouse knee joints during late-stage osteoarthritis. *Arthritis Rheumatol* 2018;70:230–41.
7. Zhang X, Zhu J, Li Y, Lin T, Siclari VA, Chandra A, et al. Epidermal growth factor receptor (EGFR) signaling regulates epiphyseal cartilage development through β -catenin-dependent and -independent pathways. *J Biol Chem* 2013;288:32229–40.
8. Jia H, Ma X, Tong W, Doyran B, Sun Z, Wang L, et al. EGFR signaling is critical for maintaining the superficial layer of articular cartilage and preventing osteoarthritis initiation. *Proc Natl Acad Sci U S A* 2016;113:14360–5.
9. Dedrick DK, Goldstein SA, Brandt KD, O'Connor BL, Goulet RW, Albrecht M. A longitudinal study of subchondral plate and trabecular bone in cruciate-deficient dogs with osteoarthritis followed up for 54 months. *Arthritis Rheum* 1993;36:1460–7.
10. Robling AG, Niziolek PJ, Baldridge LA, Condon KW, Allen MR, Alam I, et al. Mechanical stimulation of bone in vivo reduces osteocyte expression of Sost/sclerostin. *J Biol Chem* 2008;283:5866–75.
11. Roudier M, Li X, Niu QT, Pacheco E, Pretorius JK, Graham K, et al. Sclerostin is expressed in articular cartilage but loss or inhibition does not affect cartilage remodeling during aging or following mechanical injury. *Arthritis Rheum* 2013;65:721–31.
12. Johnson ML, Gong G, Kimberling W, Recker SM, Kimmel DB, Recker RR. Linkage of a gene causing high bone mass to human chromosome 11 (11q12-13). *Am J Hum Genet* 1997;60:1326–32.
13. Huebner JL, Hanes MA, Beckman B, TeKoppele JM, Kraus VB. A comparative analysis of bone and cartilage metabolism in two strains of guinea-pig with varying degrees of naturally occurring osteoarthritis. *Osteoarthritis Cartilage* 2002;10:758–67.
14. Chan BY, Fuller ES, Russell A, Smith SS, Smith MM, Jackson MT, et al. Increased chondrocyte sclerostin may protect against cartilage degradation in osteoarthritis. *Osteoarthritis Cartilage* 2011;19:874–85.
15. Velasco J, Zarrabeitia MT, Prieto JR, Perez-Castrillon JL, Perez-Aguilar MD, Perez-Nunez MI, et al. Wnt pathway genes in osteoporosis and osteoarthritis: differential expression and genetic association study. *Osteoporos Int* 2010;21:109–18.
16. Zhu M, Tang D, Wu Q, Hao S, Chen M, Xie C, et al. Activation of β -catenin signaling in articular chondrocytes leads to osteoarthritis-like phenotype in adult β -catenin conditional activation mice. *J Bone Miner Res* 2009;23:12–21.
17. Vincent C, Findlay DM, Welldon KJ, Wijenayaka AR, Zheng TS, Haynes DR, et al. Proinflammatory cytokines TNF-related weak inducer of apoptosis (TWEAK) and TNF α induce the mitogen-activated protein kinase (MAPK)-dependent expression of sclerostin in human osteoblasts. *J Bone Miner Res* 2009;24:1434–49.
18. Heiland GR, Swerina K, Baum W, Kireva T, Distler JH, Brisanti M, et al. Neutralisation of Dkk-1 protects from systemic bone loss during inflammation and reduces sclerostin expression. *Ann Rheum Dis* 2010;69:2152–9.
19. Yuasa T, Otani T, Koike T, Iwamoto M, Enomoto-Iwamoto M. Wnt/ β -catenin signaling stimulates matrix catabolic genes and activity in articular chondrocytes: its possible role in joint degeneration. *Lab Invest* 2008;88:264–74.

20. Shin Y, Huh YH, Kim K, Kim S, Park KH, Koh JT, et al. Low-density lipoprotein receptor-related protein 5 governs Wnt-mediated osteoarthritic cartilage destruction. *Arthritis Res Ther* 2014; 16:R37.
21. Papathanasiou I, Malizos KN, Tsezou A. Low-density lipoprotein receptor-related protein 5 (LRP5) expression in human osteoarthritic chondrocytes. *J Orthop Res* 2010;28:348–53.
22. Bouaziz W, Funck-Brentano T, Lin H, Marty C, Ea HK, Hay E, et al. Loss of sclerostin promotes osteoarthritis in mice via β -catenin-dependent and -independent Wnt pathways. *Arthritis Res Ther* 2015;17:24.
23. Funck-Brentano T, Bouaziz W, Marty C, Geoffroy V, Hay E, Cohen-Solal M. Dkk-1-mediated inhibition of Wnt signaling in bone ameliorates osteoarthritis in mice. *Arthritis Rheumatol* 2014;66:3028–39.
24. Li B, Aspden RM. Composition and mechanical properties of cancellous bone from the femoral head of patients with osteoporosis and osteoarthritis. *J Bone Miner Res* 1997;12:641–51.
25. Day JS, Ding M, van der Linden JC, Hvid I, Sumner DR, Weinans H. A decreased subchondral trabecular bone tissue elastic modulus is associated with pre-arthritis cartilage damage. *J Orthop Res* 2001;19:914–8.
26. Hayami T, Pickarski M, Wesolowski GA, Mclane J, Bone A, Destefano J, et al. The role of subchondral bone remodeling in osteoarthritis: reduction of cartilage degeneration and prevention of osteophytes formation by alendronate in the rat anterior cruciate ligament transection model. *Arthritis Rheum* 2004;50:1193–206.
27. Shirai T, Kobayashi M, Nishitani K, Satake T, Kuroki H, Nakagawa Y, et al. Chondroprotective effects of alendronate in a rabbit model of osteoarthritis. *J Orthop Res* 2011;29:1572–7.
28. Pelletier JP, Troncy E, Bertaim T, Thibaud D, Goulet AC, Abram F, et al. Treatment with tiludronic acid helps reduce the development of experimental osteoarthritis lesions in dogs with anterior cruciate ligament transection followed by reconstructive surgery: a 1-year study with quantitative magnetic resonance imaging. *J Rheumatol* 2011;38:118–28.
29. Lampropoulou-Adamidou K, Dontas I, Stathopoulos IP, Khaldi L, Lelovas P, Vlamis J, et al. Chondroprotective effect of high-dose zoledronic acid: an experimental study in a rabbit model of osteoarthritis. *J Orthop Res* 2014;32:1646–51.
30. Kadri A, Ea HK, Bazille C, Hannouche D, Lioté F, Cohen-Solal ME. Osteoprotegerin inhibits cartilage degradation through an effect on trabecular bone in murine experimental osteoarthritis. *Arthritis Rheum* 2008;58:2379–86.
31. Kadri A, Funck-Brentano T, Lin H, Ea HK, Hannouche D, Marty C, et al. Inhibition of bone resorption blunts osteoarthritis in mice with high bone remodeling. *Ann Rheum Dis* 2010;69:1533–48.
32. Yu DG, Yu B, Mao YQ, Zhao X, Wang XQ, Ding HF, et al. Efficacy of zoledronic acid in treatment of teoarthritis [sic] is dependent on the disease progression stage in rat medial meniscal tear model. *Acta Pharmacol Sin* 2012;33:924–34.
33. Mohan G, Perilli E, Parkinson IH, Humphries JM, Fazzalari NL, Kuliwaba JS. Pre-emptive, early, and delayed alendronate treatment in a rat model of knee osteoarthritis: effect on subchondral trabecular bone microarchitecture and cartilage degradation of the tibia, bone/cartilage turnover, and joint discomfort. *Osteoarthritis Cartilage* 2013;21:1595–604.
34. Zhu S, Chen K, Lan Y, Zhang N, Jiang R, Hu J. Alendronate protects against articular cartilage erosion by inhibiting subchondral bone loss in ovariectomized rats. *Bone* 2013;53:340–9.
35. Appel H, Ruiz-Heiland G, Listing J, Zwerina J, Hermann M, Mueller R, et al. Altered skeletal expression of sclerostin and its link to radiographic progression in ankylosing spondylitis. *Arthritis Rheum* 2009;60:3257–62.
36. Luyten FP, Tylzanowski P, Lories RJ. Wnt signaling and osteoarthritis. *Bone* 2009;44:522–7.
37. Lories RJ, Luyten FP. The bone-cartilage unit in osteoarthritis. *Nature Rev Rheum* 2011;7:43–9.

REVIEW

Defining a Unified Vascular Phenotype in Systemic Sclerosis

Yannick Allanore,¹ Oliver Distler,² Marco Matucci-Cerinic,³ and Christopher P. Denton⁴

Microcirculation impairment and related vasculopathy are hallmarks of systemic sclerosis (SSc). Digital ulceration is second only to Raynaud's phenomenon as a vascular complication occurring in patients with SSc. Digital ulcers are painful and generate disability. Furthermore, patients may develop recurrent digital ulcers, and it is reasonable to question whether the outcomes of such patients might be different from those of patients who are not affected. Recently, several registries have provided relevant information about digital ulcers. Male sex and severe skin disease appear to be the main associated factors observed in several registries. However, limitations of those studies are the differences in the definitions of digital ulcers and organ involvement. Few longitudinal studies are available, and the more robust data from the European League Against Rheumatism Scleroderma Trial and Research cohort suggested worse outcomes in patients with a history of digital ulcers but could not demonstrate that a history of digital ulcers can predict additional vascular complications such as pulmonary arterial hypertension, heart failure, or renal crisis. Nevertheless, the autopsy studies published many years ago and the more recent longitudinal biomarker studies

support the concept of generalized vasculopathy and a potential association between various cardiovascular complications. It is expected that with the availability of several structured registries, identification of a vascular profile or vascular phenotype will be addressed using more robust data in the near future.

Introduction

Systemic sclerosis (SSc) is an autoimmune connective tissue disorder that is characterized by a complex interplay of vascular abnormalities, immune system activation, and an uncontrolled fibrotic response. The vascular component is often referred to as vasculopathy and is thought to have a key role in the early pathogenesis of SSc. Patients with SSc develop a broad spectrum of vascular manifestations, including Raynaud's phenomenon (RP) (distal vasospasm), which is almost universal, digital ulcers, which are common, and critical digital ischemia, which is rare. In parallel, within this very heterogeneous disease, some patients will develop vascular disease-related organ damage leading to heart or kidney failure (1–3). It is still unclear whether there is a continuum between peripheral vasculopathy promoting digital ulceration, or critical ischemia, and some other vascular disease-related complications (4,5). The objective of this review is to address this question by analyzing whether severe digital vasculopathy could be a surrogate for vasculopathy elsewhere. The various sources of information used to answer this research question are shown in Figure 1.

Generalized microvascular damage, from RP to obliterated small vessels

SSc vasculopathy depends on the complex interaction of various pathologic processes including autoimmunity,

¹Yannick Allanore, MD, PhD: Cochin Hospital, INSERM U1016, Paris Descartes University, Paris, France; ²Oliver Distler, MD, PhD: University Hospital Zurich, Zurich, Switzerland; ³Marco Matucci-Cerinic, MD, PhD: Azienda Ospedaliera Universitaria Careggi, University of Florence, Florence, Italy; ⁴Christopher P. Denton, MD, PhD: University College London and Royal Free Hospital, London, UK.

Dr. Allanore has received consulting fees from Actelion, Bayer, Boehringer Ingelheim, ChemomAb, Genentech/Roche, Inventiva, Pfizer, Sanofi, and Servier and research funding from those companies (less than \$10,000 each). Dr. Distler has received consulting fees from Actelion, Bayer, Boehringer Ingelheim, ChemomAb, EspeRare Foundation, Genentech/Roche, GlaxoSmithKline, Inventiva, Eli Lilly, Medac, MedImmune, Mitsubishi Tanabe Pharma, Novartis, Pfizer, Sanofi, Sinoxa, and UCB Pharma and research funding from those companies (less than \$10,000 each); he also has a patent (microRNA-29) for the treatment of systemic sclerosis. Dr. Matucci-Cerinic has received consulting fees from Bristol-Myers Squibb, Pfizer, Eli Lilly, Celgene, Actelion, ChemomAb, and CSL Behring and research funding from those companies (less than \$10,000 each). Dr. Denton has received consulting fees from Genentech/Roche, Actelion, Glaxo-SmithKline, Sanofi-Aventis, Inventiva, Boehringer Ingelheim, CSL Behring, EMD Serono, and UCB Pharma and research funding from those companies (less than \$10,000 each).

Address correspondence to Yannick Allanore, MD, PhD, Service de Rhumatologie A, Hôpital Cochin, Université Paris Descartes, 27 Rue du Faubourg St. Jacques, 75014 Paris, France. E-mail: yannick.allanore@aphp.fr.

Submitted for publication September 14, 2017; accepted in revised form November 10, 2017.

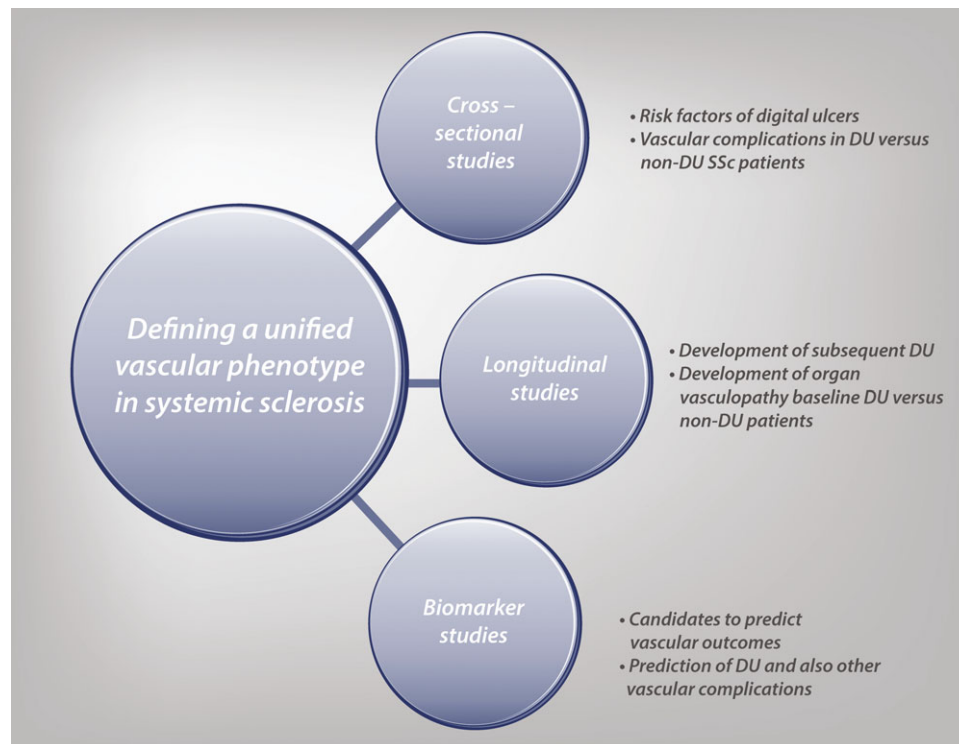


Figure 1. Sources of information used to answer the research question about the relationship between digital ulcers (DUs) and other systemic sclerosis (SSc)-related vascular complications.

impaired compensatory vasculogenesis and angiogenesis, endothelial-mesenchymal transition, endothelial dysfunction, and an impaired coagulation/fibrinolysis system. SSc vasculopathy is characterized by a variety of such changes that affect primarily the microcirculation and small arterioles (4,5). Disease in larger vessels can occur in SSc (6), although there are still some debates about the risk of atherosclerosis in SSc (7). That topic is beyond the scope of this review, which focuses primarily on the potential risk of generalized microangiopathy and a potential continuum between digital ulcers and organ-based vasculopathy.

The hallmark of functional abnormalities related to SSc vasculopathy is RP. It is characterized by exaggerated but reversible vasospasm in response to cold exposure, stress, or emotional upset. Vascular tone dysfunction is mainly attributable to impaired endothelial function. Several studies have shown reduced flow-mediated dilation values, supporting the notion of impaired nitric oxide production (8). It must be pointed out that although impaired endothelial function is mainly recognized at the digital level, it is well established that all microcirculatory systems can be affected (4,5). For example, cardiac imaging showed abnormal perfusion related to small coronary artery disturbances after cold stress (7).

With the progression of structural vascular changes, functional alteration of vascular cells includes

endothelial cell apoptosis, impaired coagulation/fibrinolysis system, aberrant expression of soluble factors and cell adhesion molecules, leading to the pathologic inflammation. During this phase, perivascular infiltrates are evident, endothelial cells, pericytes, and vascular smooth muscle cells proliferate, endothelial-mesenchymal transition takes place, and myofibroblasts are activated in the dermal tissue (9). The next steps include altered neovascularization and vascular remodeling due to impairment of compensatory vasculogenesis and exaggerated angiogenesis (10–16). Circulating levels of various angiogenic/angiostatic factors are largely altered and, so far, most studies have shown that proangiogenic factor levels are increased throughout the disease course, especially during the active stage (17,18). The progression of these events leads to intima and media fibroproliferation, which will provoke microvessel obliteration. Consequently, chronic hypoxia may further promote fibrosis of the surrounding tissue (16). Early damage to the endothelium, together with the vascular instability and the chronic hypoxia generating reactive oxygen species, thus have a downstream deleterious effect on capillaries (17). This leads eventually to aberrant angiogenesis and progressively to a loss of capillaries. The vessel obliteration will further progress to tissue anoxia,

which will have a devastating effect on the extremities, with tissue necrosis and gangrene (17).

Taken together, these findings support the notion of generalized microvascular impairment in SSc. It is reasonable to ask why the digits might be primarily affected, but exposure to cold in this area could result in more important and/or earlier damage, which could explain the high risk for the development of digital ischemia and ulceration. Nevertheless, the pathogenesis of the vasculopathy, the findings of abnormal circulating markers as previously highlighted, such as the inverse correlation between flow-mediated dilation values and pulmonary artery pressure (PAP) and the association of decreased flow-mediated dilation values with the presence of pulmonary arterial hypertension (PAH) and digital ulcers, indicate the presence of a generalized vascular abnormality (19,20). Therefore, the natural course of the disease should be evaluated more deeply to determine whether the proliferative and obliterative vasculopathy may gradually and sometimes subclinically progress along with disease duration, eventually becoming clinically evident, with variable tonality of severe vessel involvement. This may thus lead to periodic or recurrent digital ulcers, PAH, heart failure, and renal function decline or renal crisis.

Data from cross-sectional studies of risk factors and vascular complications in SSc patients with digital ulcers

To investigate the clinical vascular manifestations occurring in SSc patients with digital ulcers, the characteristics of patients with digital ulcers versus those without digital ulcers (extracted from publications of large cross-sectional series) were analyzed.

In a French multicenter study, a cross-sectional analysis of 599 patients with SSc (the Itin  AIR-Scl  rodermie cohort) showed that 53% of these patients had prior or current digital ulcers (21). When associated variables were considered, digital ulceration appeared to occur more frequently in male patients, patients with a higher modified Rodnan skin thickness score (MRSS) (22), patients with early onset of disease, patients with a diffusing capacity for carbon monoxide (DLco) of <60% predicted, and patients with anti-topoisomerase I antibodies. It must be highlighted that sex and skin disease were the variables with the strongest associations. The frequency of PAH was not higher in patients with prior or current digital ulcers than in those who were never affected (21). DLco measures gas exchanges through the alveolar membrane and can be influenced by the thickness of the alveolar membrane and lung capillary

volume. Therefore, a reduced DLco in the absence of impairment in pulmonary function (forced vital capacity [% predicted]) may represent a surrogate marker of vasculopathy. The associations with DLco impairment, worsening of RP, and recurrent digital ulcers indicate the pathophysiologic link between the involvement of 2 different endothelial systems, the lungs and the digits. However, no relationship between prior or current digital ulcers and PAH was observed in the French study (21).

The German Network for Systemic Scleroderma (23) has provided data for 1,880 patients, among whom 1,690 were evaluable for digital ulcers. Among these patients, 408 (24%) had digital ulcers at the time of entry into the registry. In multivariate analyses, data sets for 1,164 patients were used and revealed that male sex was the most powerful independent predictor of the presence of digital ulcers, and that PAH, anti-Scl-70 antibodies (but not anticentromere antibodies [ACAs]), involvement of the mouth or esophagus, an elevated erythrocyte sedimentation rate, and onset of RP at a young age were all risk factors for the presence of digital ulcers. Diffuse skin sclerosis in combination with PAH was the most powerful predictor for the occurrence of digital ulcers.

In a Spanish study, a total of 19 referral centers participated in the recruitment of 1,326 SSc patients (24). Among these patients, 552 had prior or current digital ulcers. Multivariate analysis showed that the presence of prior/current digital ulcers was independently associated with younger age at SSc diagnosis, diffuse cutaneous SSc (dcSSc), and the presence of peripheral vascular manifestations such as RP, telangiectasia, and acroosteolysis. However, a history of digital ulcers was not associated with any visceral vasculopathy such as PAH or scleroderma renal crisis.

The Canadian Scleroderma Research Group (25) investigated the features associated with digital ulcers and their complications and sought to determine whether digital ulceration was associated with PAH and scleroderma renal crisis. Among 938 SSc patients, 8% had a current digital ulcer, 44% had a digital ulcer ever, and 53% had digital pitting scars. In the multivariate analysis, the most important variables predictive of digital ulcers were younger age at disease onset, interstitial lung disease, higher hand and finger skin scores, and a higher Health Assessment Questionnaire (26) score. There was no significant association between a history of digital ulcers and any definition of PAH (prevalence 9%) or with renal crisis (prevalence 5%).

If microcirculation impairment is fundamental in SSc vasculopathy, large vessel disease may overlap and contribute to tissue damage, although the potential role of atherosclerosis in SSc-related vascular damage is still being debated. In a Japanese cross-sectional study (27),

the association of carotid artery atherosclerosis with digital ulcers was examined by comparing SSc patients with digital ulcers ($n = 48$ [29.5%]) and those without digital ulcers ($n = 206$ [70.5%]). No multivariable analysis was performed, but it is of interest to point out that carotid atherosclerosis was not more common in SSc patients with digital ulcers than in those without digital ulcers. Regarding SSc characteristics, digital ulcers were more common in male patients and in those with dcSSc, and the MRSS was higher in patients with a history of digital ulcers, confirming previously reported findings in patient populations in other geographic regions (28). An evaluation of heart disease showed that the incidence of PAH was not higher in SSc patients with digital ulcers than in those without digital ulcers (9% and 10%, respectively). After exclusion of the patients with PAH, those with digital ulcers more commonly had elevated levels of natriuretic peptide or milder cardiac abnormalities such as electrocardiographic changes or coronary artery disease.

Cutaneous telangiectasias are common in SSc and are part of the American College of Rheumatology/European League Against Rheumatism (EULAR) 2010 classification criteria for rheumatoid arthritis (29). A previous cross-sectional study (30) was performed to determine whether the number and size of cutaneous telangiectasias were associated with the pattern of microvascular lesions assessed by nailfold videocapillaroscopy and markers reflecting the severity of SSc-related vasculopathy.

Among 87 patients, both profuse and pseudotumoral cutaneous telangiectasias were associated with capillary loss and severe dysangiogenesis on nailfold videocapillaroscopy. In a multivariate analysis, profuse pseudotumoral cutaneous telangiectasias were independently associated with past or current digital ulcers, whereas pseudotumoral cutaneous telangiectasias were independently associated with the late nailfold videocapillaroscopy pattern and PAH (31). Of most interest, a previous study showed some association between telangiectasias and PAH; the adjusted relative odds of PAH was 12.4 for patients with a 10-point increase in the telangiectasia score (30). These 2 studies emphasized telangiectasia as being a potential clinical marker of more widespread aberrant microvascular disease in SSc. Regarding renal crisis, another vascular organ complication, few studies address the risk factors for renal crisis; however, none of these studies suggested that digital ulcers or PAH may be a risk factor for such an event (31).

The results of the main studies described above are summarized in Table 1; the associations observed in multivariable analyses are highlighted. Overall, even with the limitation of cross-sectional designs, these studies showed that digital ulcers were more common in patients with early-onset SSc, in male patients, in those with dcSSc, and in association with a high MRSS, but they did not consistently show a higher risk of PAH, heart failure, or renal crisis in patients with digital ulcers compared with those without digital ulcers.

Table 1. Associations of SSc with digital ulcers as determined by multivariable analyses in large multicenter cross-sectional studies*

Variable	French ItinérAIR-Sclérodémie registry (2009) (n = 599)	German Network for Systemic Scleroderma registry (2009) (n = 1,690)	Canadian Scleroderma Research Group registry (2011) (n = 938)	Spanish registry on SSc (2016) (n = 1,326)
Digital ulceration status	Prior or current†	Active at inclusion‡	Prior or current§	Prior or current¶
Age	+	—	+	+
Male sex	+	+	—	—
Smoking	—	Not studied	—	—
Disease duration	+	—	—	—
Severe skin involvement	+	NA	+ (finger MRSS)	—
Diffuse cutaneous SSc	—	—	—	+
Anti-topo antibodies	—	+	—	—
ESR	Not studied	+	—	Not studied
Esophageal involvement	Not studied	+	+ #	Not studied
DLco <60% predicted	+	NA	—	—
Interstitial lung disease	Exclusion criterion if severe	—	+	+
Pulmonary hypertension	Exclusion criterion	+	—	—
Renal crisis	—	—	—	—
HAQ score	Not studied	Not studied	+	Not studied

* NA = not available; MRSS = modified Rodnan skin thickness score; anti-topo = antitopoisomerase; ESR = erythrocyte sedimentation rate; DLco = diffusing capacity for carbon monoxide; HAQ = Health Assessment Questionnaire.

† Prevalence 53%.

‡ Prevalence 24%.

§ Prevalence 44%.

¶ Prevalence 42%.

Only diffuse cutaneous systemic sclerosis (SSc).

Data from longitudinal studies of vascular complications in SSc patients with digital ulcers

Another way to investigate whether digital ulcers may be a surrogate for generalized vasculopathy is to examine prospective data to determine whether SSc patients with digital ulcers at baseline develop more organ vasculopathy compared with patients who are not affected.

A study looking at the natural history of SSc-related digital ulcers was based on 103 patients, among whom 46 had a history of digital ulcers (32). The mean duration of follow-up after the first non-RP symptom of SSc was ~12 years. The first digital ulcer occurred within 1 year following the first non-RP symptom in 43% of patients and within 5 years in 73% of patients. A multivariable analysis showed that in SSc patients who were younger when the first non-RP symptom occurred and in patients with a higher MRSS (21) (e.g., those classified as being in the dcSSc subset), digital ulcers occurred earlier. It must also be pointed out that the first digital ulcer manifestation was delayed when vasodilator therapy was given (mainly calcium-channel blockers or angiotensin-converting enzyme inhibitors). PAH occurred in 11 patients (11%) during the course of the disease, and its prevalence was comparable between the SSc patients in the subgroup with PAH and the subgroup with no digital ulcers (14% and 9%, respectively; $P = 0.53$) (31).

One of the main studies that highlighted the link between DLco and vasculopathy used the Pittsburgh Scleroderma Databank to match 106 patients who had a diagnosis of PAH with 106 subjects according to SSc skin subtype, age, sex, race, disease duration, and mean time to the diagnosis of PAH after the initial visit. If a decline in DLco occurred before a diagnosis of PAH, patients with PAH and controls had a similar frequency of RP, digital tip ulcers, and digital gangrene. However, visual analog scales showed that patients had significantly higher values for both the severity of RP and the severity of digital tip ulcers (33).

In the EULAR Scleroderma Trials and Research (EUSTAR) cohort, it was shown that at presentation, 1,092 of 3,196 patients (34%) had a history of digital ulcers. Follow-up of 3 years was the cutoff time for determining the occurrence of complications (34). In multivariable analyses adjusting for age, sex, and other parameters that were considered to be potentially significant, a history of digital ulcers was strongly predictive for the presence of digital ulcers at prospective visits but also for an elevated systolic PAP on heart ultrasound, for any cardiovascular event (new digital ulcers, elevated systolic PAP by echocardiography, left ventricular failure, and death). Overt PAH could not be

analyzed, and there was no prediction for renal crisis (34).

In the Australian Scleroderma Interest Group PAH registry, among 1,636 patients with SSc, 194 (12%) had PAH proven by right-sided heart catheterization; among these patients, 160 were detected prospectively by screening (35). The study primarily reviewed the outcomes of patients according to the screening programs, but the characteristics of SSc-related PAH were detailed and analyzed using univariate analyses. The data showed that SSc patients with PAH were older, had a longer disease duration from the first non-RP clinical manifestation, were more likely to be positive for ACAs, and to have telangiectasia, calcinosis, and joint contractures. Furthermore, digital ulcers were more frequent in patients with PAH (53% in patients with SSc-related PAH and 42% in SSc patients without PAH), but the strength of association was not very great, and only multivariable analyses could clarify whether the various variables associated in univariate analyses are independently associated if they are still associated in the multivariable model. Therefore, their independence can be demonstrated only by multivariate analyses.

The German investigators also reviewed prospective data regarding digital ulcers and showed various degrees of progression according to SSc characteristics (36). Unfortunately, no details were provided for other outcomes, with the exception of a statement that the weak or lack of association of digital ulcers with PAH or heart and renal involvement indicates that vasculopathy in digital arteries and the renal and pulmonary vasculature seems to be affected by different pathophysiologic pathways.

As opposed to the cross-sectional analyses, the available longitudinal data appeared to support some links between baseline digital ulcers and the subsequent risk of more severe vasculopathy defined by recurrent digital ulcers but also the risk of PAH. The low frequency of renal crisis and heart failure limits the possibility of identifying such links, but the large EUSTAR registry supports a predictive value of baseline digital ulcers for overall cardiovascular complications. Confirmation will have to be investigated in the future using new database extracts that may contain more patients with a longer follow-up.

Vascular biomarker studies

In recent years, many studies have investigated candidate vascular biomarkers. Although some of these studies were mainly descriptive, using cross-sectional designs, others were based on longitudinal data, allowing prediction of overall vascular risk (37).

The pentraxins are a highly conserved family of proteins with a unique architecture. In humans, the 2 main

members of this family are C-reactive protein and serum amyloid P. Pentraxin 3 (PTX3) is expressed predominantly in atherosclerotic lesions that involve various cells such as macrophages, neutrophils, dendritic cells, or smooth muscle cells. Interestingly, PTX3 has been examined as a novel biomarker for inflammatory cardiovascular disease. In SSc, circulating levels of PTX3, but also fibroblast growth factor 2 (FGF-2), have been shown to be significantly higher in SSc patients than in healthy control subjects (38). Of most interest is the observation that the PTX3 level was elevated in SSc patients who had digital ulcers or PAH, while the level of FGF-2 was reduced in SSc patients with PAH. Multivariate analysis identified an elevated PTX3 level as an independent parameter associated with the presence of digital ulcers and PAH. Furthermore, PTX3 levels were a useful predictor of future occurrences of digital ulcers, and reduced FGF-2 levels were independently associated with the presence of PAH.

Chemokine CXCL4 levels have been demonstrated to be correlated with skin and lung fibrosis and also with PAH (39). No data regarding digital ulcers were provided, but among chemokines, only CXCL4 predicted the risk and progression of SSc.

In a prospective cohort of 100 SSc patients who were followed up for 3 years, vascular biomarkers of new events were investigated, primarily to predict the development of new digital ulcers, which occurred in 17 SSc patients. Both angiogenic and vasculogenic markers were measured. Based on various multivariable models, a history of digital ulcers, but also placenta growth factor (PlGF) levels and the endothelial progenitor cell count, were independent predictors of the development of digital ulcers (40). The prediction of other cardiovascular end points was studied, suggesting stimulating clues with these markers, but the number of events was low, which limited statistical power. Interestingly, another study confirmed the promise of PlGF as well as Flit-1 as measures of pulmonary hypertension in SSc (41).

Functional autoantibodies are directed against the vascular receptors angiotensin II receptor type 1 (AT₁) and endothelin 1 type A receptor (ETAR). A majority of SSc patients have increased levels of anti-ETAR and anti-AT₁ antibodies compared with those in healthy donors. Moreover, in SSc patients, the autoantibodies are associated with various vascular symptoms of the disease, such as PAH, digital ulcers, and renal crisis. Nevertheless, the antibodies are also associated with dcSSc as well as lung fibrosis. Taken together, these data suggest a possible role of these antibodies in disease mechanisms, but their use in clinical practice for predicting damage remains to be established. In the context of digital ulcers, it has been shown that anti-ETAR autoantibodies can be used, together with

the current or past presence of digital ulcers, to identify patients with SSc who are at risk for the development of subsequent digital ulcers (42,43).

Imaging may also provide some tools to predict digital ulcers and vascular outcomes. Although few studies have been performed so far, capillaroscopy has been shown to be an interesting candidate, and a prospective study with a 6-month duration showed that the mean number of capillaries per millimeter in the middle finger of the dominant hand, the number of digital ulcers at enrollment, and the presence of critical digital ischemia at enrollment were risk factors for the development of new digital ulcers. Other cardiovascular outcomes were not measured for a duration of 6 months (44).

The carotid-femoral pulse wave velocity (PWV) is a marker of aortic stiffness that holds prognostic significance in various vascular conditions, including systemic hypertension, renal failure, and heart failure. The augmentation index standardized to a heart rate of 75/minute (Aix₇₅), defined as the amplitude of the reflected wave from the periphery to the heart, can be measured by applanation tonometry and depends on several factors, including large artery (but also medium and small artery) stiffness. Radial applanation tonometry was performed in a group of 63 SSc patients to investigate an association of PWV or the Aix₇₅ with digital ulcers in 10 SSc patients. At baseline, there were no differences between SSc patients with digital ulcers and those without digital ulcers with regard to the cutaneous subset of SSc, disease duration, renal and pulmonary function, cardiovascular risk factors, heart function, and PAP (45). SSc patients with digital ulcers had an increased Aix₇₅ compared with patients without digital ulcers, while there was no difference in PWV. The results of the multivariate logistic regression revealed that age, sex, erythrocyte sedimentation rate, aortic pulse pressure, and digital ulcers were independently associated with the Aix₇₅ (45).

Collectively, these results suggest the existence of increased stiffness of small and medium arteries in SSc patients with digital ulcers, without significantly increased aortic stiffness when compared with SSc patients without digital ulcers. The predictive value of such a tool on broader cardiovascular outcomes and in a larger population would be of interest.

Conclusions

Vascular injury and subsequent vascular dysfunction are among the earliest alterations in SSc and are considered to act within the initiating steps in SSc pathogenesis. Microcirculation impairment, the hallmark of the disease, may also spread to larger vessels, even if

the reality of an increased prevalence of atherosclerosis in SSc remains controversial. The disease process is undoubtedly generalized, and all microvascular territories are affected. This notion is strongly supported by autopsy studies that showed lung and kidney vessel involvement despite the lack of any evidence of organ involvement (46). It is well known that among all vascular complications, digital ulcers are the most common clinical expression of advanced vasculopathy. It remains unclear why the digits are affected most, although permanent exposure to external stress might contribute to the severity. Some investigators have speculated that digital ulcers could be a clinical marker of tissue damage (vascular and fibrotic changes), but epidemiologic studies do not clearly and reproducibly demonstrate a strong link between digital ulcers and other vascular complications. Indeed, cross-sectional studies show that SSc patients with digital ulcers have more severe disease, but a higher frequency of PAH or renal crisis has not been observed. Longitudinal studies further support poorer outcomes in SSc patients with digital ulcers, and some of these studies suggest a predictive value of baseline digital ulcers for subsequent digital ulcers or even PAH or overall cardiovascular complications. Currently, however, several methodologic issues preclude firm conclusions. Indeed, the definition of the events differs between studies, the time of observation is usually not very long for PAH (which is usually a late complication), and because of the scarcity of major cardiovascular events, the sample size may be an issue.

Biomarker studies highlight the systemic component of vasculopathy and suggest some links between digital ulcers and PAH, although it appears that additional further and potential regional factors might contribute to more severe remodeling in the finger, lungs, or kidneys. Autoantibodies might contribute to these specificities, and it is of interest to observe that digital ulcers are more common in patients with dcSSc and probably those who are positive for antitopoisomerase antibodies, whereas ACAs are reproducibly found in patients with SSc-related PAH, and that anti-RNA polymerase III antibodies are strong markers for renal crisis. The roles of other autoantibodies that could be functional autoantibodies are interesting clues in this context.

Regarding therapy for vascular SSc, several PAH drugs are available for the treatment of SSc-related PAH, but the drugs are given to patients who have already developed histologically very advanced vasculopathy. At a less severe stage of vasculopathy, calcium-channel blockers and iloprost are licensed for the treatment of severe RP and bosentan is licensed for prevention of digital ulcers. Clinical trials have shown the respective beneficial effects of these agents, but the

duration of the trials was short, with a relatively small number of selected patients. Therefore, the effects on other vascular outcomes could not be reliably measured. Scarce data are available from long-term observational studies, but the results of several studies suggested that long-term iloprost treatment may reduce the progression of vascular complications (47,48), and that long-term use of calcium-channel blockers could reduce heart or kidney disease progression (49,50). Although such results could support the notion of a continuum in vasculopathy, because these data are very preliminary, no definite conclusion can be drawn.

One might add that the natural course of vasculopathy and its complications has changed. Indeed, in recent years, the clinical trials of digital ulcer recurrence showing both faster healing and fewer relapses of digital ulcers in SSc patients are encouraging new research to better understand SSc-related vascular outcomes and update its management (51–53). Therefore, SSc patients with digital ulcers have worse outcomes compared with patients without digital ulcers, and patients with digital ulcers should be managed as having a severe form of the disease (54). However, the reason why vasculopathy may be mainly expressed in digital arteries in some patients and in pulmonary or kidney arteries in others remains unclear. Improving knowledge in the field would distress this part of the disease, which is a huge contributor to excessive morbidity and mortality.

AUTHOR CONTRIBUTIONS

All authors were involved in drafting the article or revising it critically for important intellectual content, and all authors approved the final version to be published.

REFERENCES

1. Elhai M, Avouac J, Kahan A, Allanore Y. Systemic sclerosis: recent insights. *Joint Bone Spine* 2015;82:148–53.
2. Denton CP, Khanna D. Systemic sclerosis. *Lancet* 2017. E-pub ahead of print.
3. Elhai M, Meune C, Boubaya M, Avouac J, Hachulla E, Balbir-Gurman A. Mapping and predicting mortality from systemic sclerosis. *Ann Rheum Dis* 2017;76:1897–905.
4. Matucci-Cerinic M, Kahaleh B, Wigley FM. Evidence that systemic sclerosis is a vascular disease [review]. *Arthritis Rheum* 2013;65:1953–62.
5. Asano Y, Sato S. Vasculopathy in scleroderma. *Semin Immunopathol* 2015;37:489–500.
6. Au K, Singh MK, Bodukam V, Bae S, Maranian P, Ogawa R, et al. Atherosclerosis in systemic sclerosis: a systematic review and meta-analysis. *Arthritis Rheum* 2011;63:2078–90.
7. Allanore Y, Meune C. Primary myocardial involvement in systemic sclerosis: evidence for a microvascular origin. *Clin Exp Rheumatol* 2010;28 Suppl 62:S48–53.
8. Silva I, Loureiro T, Teixeira A, Almeida I, Mansilha A, Vasconcelos C, et al. Digital ulcers in systemic sclerosis: role of flow-mediated dilatation and capillaroscopy as risk assessment tools. *Eur J Dermatol* 2015;25:444–51.


9. Manetti M, Romano E, Rosa I, Guiducci S, Bellando-Randone S, de Paulis A, et al. Endothelial-to-mesenchymal transition contributes to endothelial dysfunction and dermal fibrosis in systemic sclerosis. *Ann Rheum Dis* 2017;76:924–34.
10. Avouac J, Vallucci M, Smith V, Senet P, Ruiz B, Sulli A, et al. Correlations between angiogenic factors and capillaroscopic patterns in systemic sclerosis. *Arthritis Res Ther* 2013;15:R55.
11. Manetti M, Guiducci S, Romano E, Avouac J, Rosa I, Ruiz B, et al. Decreased expression of the endothelial cell-derived factor EGFL7 in systemic sclerosis: potential contribution to impaired angiogenesis and vasculogenesis. *Arthritis Res Ther* 2013;15:R165.
12. Bellando-Randone S, George J, Mazzotta C, Guiducci S, Furst DE, Mor A, et al. Angiostatic and angiogenic chemokines in systemic sclerosis: an overview. *J Scleroderma Relat Disord* 2017; 2:1–10.
13. Maurer B, Distler A, Suliman YA, Gay RE, Michel BA, Gay S, et al. Vascular endothelial growth factor aggravates fibrosis and vasculopathy in experimental models of systemic sclerosis. *Ann Rheum Dis* 2014;73:1880–7.
14. Derrett-Smith EC, Dooley A, Gilbane AJ, Trinder SL, Khan K, Baliga R, et al. Endothelial injury in a transforming growth factor β -dependent mouse model of scleroderma induces pulmonary arterial hypertension. *Arthritis Rheum* 2013;65:2928–39.
15. Avouac J, Wipff J, Goldman O, Ruiz B, Couraud PO, Chiochia G, et al. Angiogenesis in systemic sclerosis: impaired expression of vascular endothelial growth factor receptor 1 in endothelial progenitor-derived cells under hypoxic conditions. *Arthritis Rheum* 2008;58:3550–61.
16. Matucci-Cerinic M, Pietrini U, Marabini S. Local venomotor response to intravenous infusion of substance P and glyceryl trinitrate in systemic sclerosis. *Clin Exp Rheumatol* 1990;8:561–5.
17. Suliman YA, Distler O. Novel aspects in the pathophysiology of peripheral vasculopathy in systemic sclerosis. *Curr Rheumatol Rev* 2013;9:237–44.
18. Chora I, Romano E, Manetti M, Mazzotta C, Costa R, Machado V, et al. Evidence for a derangement of the microvascular system in patients with a very early diagnosis of systemic sclerosis. *J Rheumatol* 2017;44:1190–7.
19. Hofstee HM, Voskuyl AE, Vonk Noordegraaf A, Smulders YM, Postmus PE, Dijkmans BA, et al. Pulmonary arterial hypertension in systemic sclerosis is associated with profound impairment of microvascular endothelium-dependent vasodilatation. *J Rheumatol* 2012;39:100–5.
20. Takahashi T, Asano Y, Amiya E, Hatano M, Tamaki Z, Takata M, et al. Clinical correlation of brachial artery flow-mediated dilation in patients with systemic sclerosis. *Mod Rheumatol* 2014;24:106–11.
21. Tiev KP, Diot E, Clerson P, Dupuis-Siméon F, Hachulla E, Hatron PY, et al. Clinical features of scleroderma patients with or without prior or current ischemic digital ulcers: post-hoc analysis of a nationwide multicenter cohort (ItinAIR-Sclérodémie). *J Rheumatol* 2009;36:1470–6.
22. Clements P, Lachenbruch P, Seibold J, White B, Weiner S, Martin R, et al. Inter and intraobserver variability of total skin thickness score (modified Rodnan TSS) in systemic sclerosis. *J Rheumatol* 1995;22:1281–5.
23. Sunderkötter C, Herrgott I, Brückner C, Moynadeh P, Pfeiffer C, Gerss J, et al. Comparison of patients with and without digital ulcers in systemic sclerosis: detection of possible risk factors. *Br J Dermatol* 2009;160:835–43.
24. Tolosa-Vilella C, Morera-Morales ML, Simeón-Aznar CP, Mari-Alfonso B, Colunga-Argüelles D, Callejas Rubio JL, et al. Digital ulcers and cutaneous subsets of systemic sclerosis: clinical, immunological, nailfold capillaroscopy, and survival differences in the Spanish RESCLE Registry. *Semin Arthritis Rheum* 2016;46: 200–8.
25. Khimdas S, Harding S, Bonner A, Zummer B, Baron M, Pope J, and the Canadian Scleroderma Research Group. Associations with digital ulcers in a large cohort of systemic sclerosis: results from the Canadian Scleroderma Research Group registry. *Arthritis Care Res (Hoboken)* 2011;63:142–9.
26. Fries JF, Spitz P, Kraines RG, Holman HR. Measurement of patient outcome in arthritis. *Arthritis Rheum* 1980;23:137–45.
27. Motegi S, Toki S, Hattori T, Yamada K, Uchiyama A, Ishikawa O. No association of atherosclerosis with digital ulcers in Japanese patients with systemic sclerosis: evaluation of carotid intima-media thickness and plaque characteristics. *J Dermatol* 2014;41:604–8.
28. Hurabielle C, Avouac J, Lepri G, de Risi T, Kahan A, Allanore Y. Skin telangiectasia and the identification of a subset of systemic sclerosis patients with severe vascular disease. *Arthritis Care Res (Hoboken)* 2016;68:1021–7.
29. Aletaha D, Neogi T, Silman AJ, Funovits J, Felson DT, Bingham CO III, et al. 2010 rheumatoid arthritis classification criteria: an American College of Rheumatology/European League Against Rheumatism collaborative initiative. *Arthritis Rheum* 2010;62:2569–81.
30. Shah AA, Wigley FM, Hummers LK. Telangiectases in scleroderma: a potential clinical marker of pulmonary arterial hypertension. *J Rheumatol* 2010;37:98–104.
31. Woodworth TG, Suliman YA, Furst DE, Clements P. Scleroderma renal crisis and renal involvement in systemic sclerosis. *Nat Rev Nephrol* 2016;12:678–91.
32. Hachulla E, Clerson P, Launay D, Lambert M, Morell-Dubois S, Queyrel V, et al. Natural history of ischemic digital ulcers in systemic sclerosis: single-center retrospective longitudinal study. *J Rheumatol* 2007;34:2423–30.
33. Steen V, Medsger TA Jr. Predictors of isolated pulmonary hypertension in patients with systemic sclerosis and limited cutaneous involvement. *Arthritis Rheum* 2003;48:516–22.
34. Mihai C, Landewé R, van der Heijde D, Walker UA, Constantin PI, Gherghe AM, et al, and EUSTAR co-authors. Digital ulcers predict a worse disease course in patients with systemic sclerosis. *Ann Rheum Dis* 2016;75:681–6.
35. Morrisroe K, Stevens W, Sahhar J, Rabusa C, Nikpour M, Proudman S, et al. Epidemiology and disease characteristics of systemic sclerosis-related pulmonary arterial hypertension: results from a real-life screening programme. *Arthritis Res Ther* 2017;19:42.
36. Hunzelmann N, Riemekasten G, Becker MO, Moynadeh P, Kreuter A, Melchers I, et al. The Predict Study: low risk for digital ulcer development in patients with systemic sclerosis with increasing disease duration and lack of topoisomerase-1 antibodies. *Br J Dermatol* 2016;174:1384–7.
37. Chora I, Guiducci S, Manetti M, Romano E, Mazzotta C, Bellando-Randone S, et al. Vascular biomarkers and correlation with peripheral vasculopathy in systemic sclerosis. *Autoimmun Rev* 2015;14:314–22.
38. Shirai Y, Okazaki Y, Inoue Y, Tamura Y, Yasuoka H, Takeuchi T, et al. Elevated levels of pentraxin 3 in systemic sclerosis: associations with vascular manifestations and defective vasculogenesis. *Arthritis Rheumatol* 2015;67:498–507.
39. Van Bon L, Affandi AJ, Broen J, Christmann RB, Marijnissen RJ, Stawski L, et al. Proteome-wide analysis and CXCL4 as a biomarker in systemic sclerosis. *N Engl J Med* 2014;370:433–43.
40. Avouac J, Meune C, Ruiz B, Couraud PO, Uzan G, Boileau C, et al. Angiogenic biomarkers predict the occurrence of digital ulcers in systemic sclerosis. *Ann Rheum Dis* 2012;71:394–9.
41. McMahan Z, Schoenhoff F, van Eyk JE, Wigley FM, Hummers LK. Biomarkers of pulmonary hypertension in patients with scleroderma: a case-control study. *Arthritis Res Ther* 2015;17:201.
42. Cabral-Marques O, Riemekasten G. Vascular hypoxia revisited: role of stimulating antibodies against angiotensin and endothelin receptors in the pathogenesis of systemic sclerosis. *Autoimmun Rev* 2016;15:690–4.
43. Avouac J, Riemekasten G, Meune C, Ruiz B, Kahan A, Allanore Y. Autoantibodies against endothelin 1 type A receptor are strong predictors of digital ulcers in systemic sclerosis. *J Rheumatol* 2015;42:1801–7.
44. Cutolo M, Herrick AL, Distler O, Becker MO, Beltran E, Carpentier P, et al, on behalf of the CAP Study Investigators.

- Nailfold videocapillaroscopic features and other clinical risk factors for digital ulcers in systemic sclerosis: a multicenter, prospective cohort study. *Arthritis Rheumatol* 2016;68:2527–39.
45. Aïssou L, Meune C, Avouac J, Meunier M, Elhaï M, Sorbets E, et al. Small, medium but not large arteries are involved in digital ulcers associated with systemic sclerosis. *Joint Bone Spine* 2016;83:444–7.
 46. D'Angelo WA, Fries JF, Masi AT, Shulman LE. Pathologic observations in systemic sclerosis (scleroderma): a study of fifty-eight autopsy cases and fifty-eight matched controls. *Am J Med* 1969;46:428–40.
 47. Airò P, Rossi M, Scarsi M, Danieli E, Grottole A, Zambruni A, et al. Disease-modifying effects of long-term cyclic iloprost therapy in systemic sclerosis: a retrospective analysis and comparison with a control group. *Clin Exp Rheumatol* 2007;25:722–7.
 48. Caramaschi P, Dalla Gassa A, Prati D, Barausse G, Tinazzi I, Ravagnani V, et al. Severe vascular complications in patients affected by systemic sclerosis cyclically treated with iloprost. *Rheumatol Int* 2012;32:1933–8.
 49. Allanore Y, Meune C, Vonk MC, Airo P, Hachulla E, Caramaschi P, et al. Prevalence and factors associated with left ventricular dysfunction in the EULAR Scleroderma Trial and Research group (EUSTAR) database of patients with systemic sclerosis. *Ann Rheum Dis* 2010;69:218–21.
 50. Montanelli G, Beretta L, Santaniello A, Scorza R. Effect of dihydropyridine calcium channel blockers and glucocorticoids on the prevention and development of scleroderma renal crisis in an Italian case series. *Clin Exp Rheumatol* 2013;31 Suppl 76:135–9.
 51. Khanna D, Denton CP, Merkel PA, Krieg T, Le Brun FO, Marr A, et al. Effect of macitentan on the development of new ischemic digital ulcers in patients with systemic sclerosis: DUAL-1 and DUAL-2 randomized clinical trials. *JAMA* 2016;315:1975–88.
 52. Hachulla E, Hatron PY, Carpentier P, Agard C, Chatelus E, Jegou P, et al. Efficacy of sildenafil on ischaemic digital ulcer healing in systemic sclerosis: the placebo-controlled SEDUCE study. *Ann Rheum Dis* 2016;75:1009–15.
 53. Suliman YA, Bruni C, Johnson SR, Praino E, Alemam M, Borazan N, et al. Defining skin ulcers in systemic sclerosis: systematic literature review and proposed World Scleroderma Foundation (WSF) definition. *J Scleroderma Relat Disord* 2017;2:115–120.
 54. Hughes M, Ong VH, Anderson ME, Hall F, Moinzadeh P, Griffiths B, et al. Consensus best practice pathway of the UK Scleroderma Study Group: digital vasculopathy in systemic sclerosis. *Rheumatology (Oxford)* 2015;54:2015–24.

SPECIAL ARTICLE

Nomenclature of Cutaneous Vasculitis

Dermatologic Addendum to the 2012 Revised International Chapel Hill Consensus Conference Nomenclature of Vasculitides

Cord H. Sunderkötter,¹ Bernhard Zelger,² Ko-Ron Chen,³ Luis Requena,⁴ Warren Piette,⁵ J. Andrew Carlson,⁶ Jan Dutz,⁷ Peter Lamprecht,⁸ Alfred Mahr ,⁹ Elisabeth Aberer,¹⁰ Victoria P. Werth,¹¹ David A. Wetter,¹² Seiji Kawana,¹³ Raashid Luqmani,¹⁴ Camille Frances,¹⁵ Joseph Jorizzo,¹⁶ J. Richard Watts,¹⁷ Dieter Metze,¹⁸ Marzia Caproni,¹⁹ Erkan Alpsoy,²⁰ Jeffrey P. Callen,²¹ David Fiorentino,²² Peter A. Merkel,²³ Ronald J. Falk,²⁴ and J. Charles Jennette²⁴

Objective. To prepare a dermatologic addendum to the 2012 revised International Chapel Hill Consensus Conference Nomenclature of Vasculitides (CHCC2012) to address vasculitides affecting the skin (D-CHCC). The goal was to standardize the names and definitions for cutaneous vasculitis.

Methods. A nominal group technique with a facilitator was used to reach consensus on the D-CHCC nomenclature, using multiple face-to-face meetings, e-mail discussions, and teleconferences.

Results. Standardized names, definitions, and descriptions were adopted for cutaneous components of systemic vasculitides (e.g., cutaneous IgA vasculitis as a component of systemic IgA vasculitis), skin-limited variants of systemic vasculitides (e.g., skin-limited IgA vasculitis,

drug-induced skin-limited antineutrophil cytoplasmic antibody-associated vasculitis), and cutaneous single-organ vasculitides that have no systemic counterparts (e.g., nodular vasculitis). Cutaneous vasculitides that were not included in the CHCC2012 nomenclature were introduced.

Conclusion. Standardized names and definitions are a prerequisite for developing validated classification and diagnostic criteria for cutaneous vasculitis. Accurate identification of specifically defined variants of systemic and skin-limited vasculitides requires knowledgeable integration of data from clinical, laboratory, and pathologic studies. This proposed nomenclature of vasculitides affecting the skin, the D-CHCC, provides a standard framework both for clinicians and for investigators.

Supported in part by the European Academy of Dermatology and Venereology (grant 2014-028; Project on Nomenclature and Diagnostic Criteria of Cutaneous Vasculitis).

¹Cord H. Sunderkötter, MD: University Hospital of Halle, Halle (Saale), Germany, and University of Münster, Münster, Germany; ²Bernhard Zelger, MD: Medical University Innsbruck, Innsbruck, Austria; ³Ko-Ron Chen, MD, PhD: Meguro Chen Dermatology Clinic, Tokyo, Japan; ⁴Luis Requena, MD: Universidad Autónoma, Madrid, Spain; ⁵Warren Piette, MD: John H. Stroger Jr. Hospital of Cook County and Rush University Medical Center, Chicago, Illinois; ⁶J. Andrew Carlson, MD: Albany Medical College, Albany, New York; ⁷Jan Dutz, MD, FRCPC: University of British Columbia, Vancouver, British Columbia, Canada; ⁸Peter Lamprecht, MD: University of Lübeck, Lübeck, Germany; ⁹Alfred Mahr, MD, PhD: Hospital Saint-Louis, University Paris 7, Paris, France; ¹⁰Elisabeth Aberer, MD: Medical University of Graz, Graz, Austria; ¹¹Victoria P. Werth, MD: University of Pennsylvania and Corporal Michael J. Crescenz Veterans Affairs Medical Center, Philadelphia, Pennsylvania; ¹²David A. Wetter, MD: Mayo Clinic, Rochester, Minnesota; ¹³Seiji Kawana, MD, PhD: Nippon Medical School, Tokyo, Japan; ¹⁴Raashid Luqmani, DM: University of Oxford, Oxford, UK; ¹⁵Camille Frances, MD: University Paris 6, Hôpital Tenon, Paris, France; ¹⁶Joseph Jorizzo, MD: Wake Forest School of Medicine, Winston Salem, North Carolina; ¹⁷J. Richard

Watts, MD: Ipswich Hospital NHS Trust, Ipswich, UK, and Norwich Medical School University of East Anglia, Norwich, UK; ¹⁸Dieter Metze, MD: University of Münster, Münster, Germany; ¹⁹Marzia Caproni, MD: University of Florence, Florence, Italy; ²⁰Erkan Alpsoy, MD: Akdeniz University School of Medicine, Antalya, Turkey; ²¹Jeffrey P. Callen, MD: University of Louisville, Louisville, Kentucky; ²²David Fiorentino, MD, PhD: Stanford University School of Medicine, Stanford, California; ²³Peter A. Merkel, MD, MPH: University of Pennsylvania, Philadelphia; ²⁴Ronald J. Falk, MD, J. Charles Jennette, MD: University of North Carolina at Chapel Hill.

Dr. Sunderkötter has received consulting fees and/or speaking fees from Pfizer, Actelion, Janssen, and Novartis (less than \$10,000 each). Dr. Jorizzo has received consulting fees from Amgen (less than \$10,000). Dr. Jennette has received consulting fees, speaking fees, and/or honoraria from Genentech (more than \$10,000).

Address correspondence to Cord H. Sunderkötter, MD, Department of Translational Dermatoinfectiology, University of Münster and Department of Dermatology, University Hospital of Halle, Ernst-Grube-Strasse 40, 06120 Halle (Saale), Germany. E-mail: cord.sunderkoetter@uk-halle.de.

Submitted for publication June 24, 2017; accepted in revised form November 8, 2017.

Introduction

The 2012 revised International Chapel Hill Consensus Conference Nomenclature of Vasculitides (CHCC2012) (1) reflects advances in the understanding of vasculitis since the first CHCC nomenclature introduced in 1994. One of the most frequently affected organs in vasculitis is the skin. CHCC2012 did not deal with the special features of cutaneous vasculitis and did not explicitly discuss the presence of skin-limited or skin-dominant forms of vasculitis. Therefore, a consensus group was formed to propose an addendum to the CHCC2012 that focuses on cutaneous vasculitis (Table 1). The goal was to standardize the names and definitions for cutaneous vasculitis, but not to establish diagnostic criteria. The group consisted of dermatologists with expertise in vasculitis, drawn from the European Academy of Dermatology and Venereology International Vasculitis Task Force and the American Rheumatologic Dermatology Society. In addition, dermatology experts from Japan were included to provide an Asian perspective. Seven of the participants were from the CHCC2012 work group.

The work group that convened to devise the dermatologic addendum to the CHCC2012 (D-CHCC) used

a nominal group technique that was similar to that used in formulating the CHCC2012 (1). This process was led by a facilitator (CHS) and included multiple face-to-face meetings, e-mail discussions, and teleconferences to reach consensus.

Cutaneous vasculitis

Vasculitis of the skin (cutaneous vasculitis) can present in several forms: 1) a cutaneous component of systemic vasculitides (e.g., cutaneous manifestations of IgA vasculitis); 2) a skin-limited or skin-dominant expression or variant of a systemic vasculitis (e.g., skin-limited IgA vasculitis); or 3) a single-organ vasculitis (SOV) of the skin that differs from recognized systemic vasculitides with regard to clinical, laboratory, and pathologic features (e.g., nodular vasculitis). The latter does not develop into a full systemic vasculitis, while skin-dominant forms may. Systemic vasculitis is a vasculitis that is present in at least one organ in addition to skin. Nonspecific signs or symptoms of systemic inflammatory reactions, such as leukocytosis, a raised C-reactive protein level, or arthralgia, are not sufficient evidence of a systemic vasculitis.

Table 1. Skin involvement status by vasculitis category and disease*

CHCC2012 vasculitis category, name	Skin involvement status	
	Cutaneous component of systemic vasculitis	Skin-limited or skin-dominant variant
Large vessel vasculitis		
Takayasu arteritis	No	No
Giant cell arteritis	Rare	No
Medium vessel vasculitis		
Polyarteritis nodosa	Yes	Yes
Kawasaki disease	No	No
Small vessel vasculitis		
Microscopic polyangiitis	Yes	Yes
Granulomatosis with polyangiitis	Yes	Yes
Eosinophilic granulomatosis with polyangiitis	Yes	Yes
Anti-glomerular basement membrane disease	No	No
Cryoglobulinemic vasculitis	Yes	Yes
IgA vasculitis (Henoch-Schönlein)	Yes	Yes
Hypocomplementemic urticarial vasculitis (anti-C1q vasculitis)	Yes	Yes
Variable vessel vasculitis		
Behçet's disease	Yes	Yes
Cogan's syndrome	Rare	No
Vasculitis associated with systemic disease		
SLE, rheumatoid arthritis, sarcoidosis, etc.	Yes	Yes
Vasculitis associated with probable etiology		
Drugs, infections, sepsis, autoimmune diseases, etc.	Yes	Yes
Cutaneous SOV (not included in CHCC2012)		
IgM/IgG vasculitis	No (not observed yet)	Yes (as SOV)
Nodular vasculitis (erythema induratum of Bazin)	No	Yes (as SOV)
Erythema elevatum et diutinum	No	Yes (as SOV)
Hypergammaglobulinemic macular vasculitis	No	Yes (as SOV)
Normocomplementemic urticarial vasculitis	No	Yes (as SOV)

* CHCC2012 = 2012 revised International Chapel Hill Consensus Conference Nomenclature of Vasculitides; SLE = systemic lupus erythematosus; SOV = single-organ vasculitis.

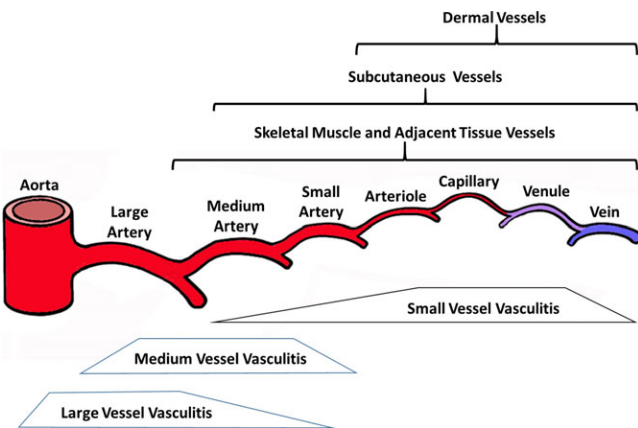


Figure 1. Distribution of vessel involvement in large vessel vasculitis (LVV), medium vessel vasculitis (MVV), and small vessel vasculitis (SVV). The heights of the trapezoids indicate the predilections of the different categories of vasculitis for different types of vessels. The brackets delineate the types of vessels in the dermis, subcutis, and adjacent tissues. Not shown is variable vessel vasculitis, which can affect any type of vessel, from aorta to veins. Note that LVV, MVV, and SVV are not confined to large, medium, or small vessels. Vasculitis in the dermis is most likely to be SVV, and LVV and MVV are more often seen in the subcutaneous tissue and adjacent soft tissue than in the dermis.

The cutaneous component of systemic vasculitides, as well as skin-limited variants of systemic vasculitides and SOV of the skin, are defined and described in Tables 2–5. To conclude that a patient fulfills the definition of skin-limited vasculitis or cutaneous SOV in a clinical setting, there must be no detectable involvement of another, non-cutaneous organ by vasculitis.

The CHCC work group’s definition of skin includes the panniculus (subcutis) and mucosa, although most vasculitides that are restricted to the skin do not affect the mucosa. The skin has small arteries, arterioles, capillaries, venules, and small veins (Figure 1). CHCC2012 distinguishes small vessels from medium vessels based on structure and function, rather than diameter. Small vessels

are intraparenchymal arteries, arterioles, capillaries, venules, and veins, while medium vessels comprise main visceral arteries and veins and their initial branches. The largest arteries and veins in the septae of the panniculus are medium vessels. The histopathologic features of cutaneous vasculitis are influenced by treatment and duration of time since onset. Demonstration of, e.g., leukocytoclastic immune complex vasculitis (LCV) in a biopsy specimen is best achieved by selecting a lesion that is between 24 and 48 hours old. Immunofluorescence analysis for demonstration of immunoreactants in dermal vessels ideally requires biopsy of an early or histamine-induced lesion, because immunoglobulins may disappear over time (2,3).

Large vessel vasculitis

Large vessel vasculitis (LVV) affects large arteries more often than other vasculitides (Table 2). Large arteries are defined as the aorta and its major branches, although arteries of any size may be affected. There are no large arteries in the dermis or subcutaneous tissues; however, as illustrated in Figure 1, LVV can involve medium vessels, and even small vessels. The 2 major forms of LVV are Takayasu arteritis (TAK) and giant cell arteritis (GCA). No cutaneous vasculitis has been reported in TAK, although nonvasculitic dermatoses may occur.

In most cases of GCA, vessels of the skin are not affected; however, occlusion of inflamed extracutaneous arteries that feed the skin or the mucosa results in necrosis of supplied tissue, e.g., tongue necrosis due to arteritis of the lingual artery (4). There are single case reports of GCA affecting small arteries in the panniculus (5).

Medium vessel vasculitis

Medium vessel vasculitis (MVV) predominantly affects medium arteries, although arteries of any size may be affected (Table 3 and Figure 1). Since both some small

Table 2. Systemic and cutaneous variants of large vessel vasculitis*

CHCC2012 vasculitis name	Abbreviated CHCC2012 definition	Cutaneous component of systemic vasculitis	Skin-limited or skin-dominant variant
Takayasu arteritis	Arteritis, often granulomatous, predominantly affecting the aorta and/or its major branches; onset at age <50 years	No definite vasculitic lesions in the skin	None
Giant cell arteritis	Arteritis, often granulomatous, usually affecting the aorta and/or its major branches, with a predilection for the branches of the carotid and vertebral arteries; onset at age >50 years	Occlusive vasculitis of extracutaneous arteries, possibly leading to cutaneous infarction; very rare involvement of small arteries in subcutis or submucosa	None

* Large vessel vasculitis affects large arteries more often than other vasculitides. Large arteries are the aorta and its major branches. Any size artery may be affected. The 2012 revised International Chapel Hill Consensus Conference Nomenclature of Vasculitides (CHCC2012) definitions are detailed in ref. 1.

Table 3. Systemic and cutaneous variants of medium vessel vasculitis*

CHCC2012 vasculitis name	Abbreviated CHCC2012 definition	Cutaneous component of systemic vasculitis	Skin-limited or skin-dominant variant
Polyarteritis nodosa	Necrotizing arteritis of medium or small arteries, without glomerulonephritis or vasculitis in arterioles, capillaries, or venules; not associated with ANCA	Acute arteritis of small arteries or arterioles, manifesting as digital arteritis, purpura, and/or skin nodules with ulcers; in a subgroup, postcapillary venules may be involved in the skin	Cutaneous arteritis (cutaneous polyarteritis nodosa); arteritis affecting small arteries in the panniculus extending to arterioles at the dermosubcutaneous junction, but not to postcapillary venules
Kawasaki disease	Arteritis associated with mucocutaneous lymph node syndrome, predominantly affecting medium and small arteries; usually occurs in infants and young children	Cutaneous vasculitis is not a characteristic feature; nonvasculitic mucocutaneous lesions are common	None

* Medium vessel vasculitis predominantly affects medium arteries, defined as the main visceral arteries and their branches. Any size artery may be affected. The 2012 revised International Chapel Hill Consensus Conference Nomenclature of Vasculitides (CHCC2012) definitions are detailed in ref. 1. ANCA = antineutrophil cytoplasmic antibodies.

and medium vessel vasculitides may involve small arteries in the skin, the presence of cutaneous arteritis alone does not distinguish these.

The 2 major forms of MVV are polyarteritis nodosa (PAN) and Kawasaki disease (KD) (Table 3). PAN may have cutaneous vasculitis, while KD has characteristic nonvasculitic skin involvement (so-called mucocutaneous lymph node syndrome) (1).

PAN, as defined in the CHCC2012 nomenclature (1), is rare. Various forms of cutaneous involvement in PAN have been reported. Manifestations consistent with involvement of medium vessels are skin infarction, livedo reticularis, intradermal nodules, and deep ulcers. Yet, purpura, hemorrhagic macules, erythema, and hemorrhagic blisters have also been reported in some patients (6); these findings suggest that PAN has a component of SVV (likely with involvement of venules). These cases may constitute a subgroup of PAN that is an exception to the CHCC group's strict definition of PAN, with vasculitis confined to arteries. Of note, use of vasculitis associated with hepatitis B or hepatitis C as a model for idiopathic PAN is problematic, because hepatitis B- and hepatitis C-associated vasculitis has a spectrum of cutaneous manifestations, ranging from arteritis to SVV without artery involvement, e.g., in the context of cryoglobulinemic vasculitis (CV) or immune complex-mediated vasculitis (7).

Cutaneous arteritis (also called cutaneous PAN) is a chronic, relapsing vasculitis that affects small arteries and arterioles in the panniculus and dermal-subcutaneous junction (8). It does not directly involve veins (9). In some case series, arteritis in adjacent skeletal muscle or involvement of peripheral nerves have been reported, although it is not certain whether this represents nerve damage that

can be attributed to severe vessel inflammation in the vicinity or to true mononeuritis multiplex; there is no agreement as to whether the occurrence of mononeuritis multiplex or arteritis in adjacent skeletal muscle would justify a diagnosis of systemic PAN (10,11).

Most cases of cutaneous arteritis are confined to the extremities (12). The clinical picture encompasses livedo and macules or subcutaneous nodules, with or without ulceration. The macular form has given rise to new terms, such as macular arteritis, that have not been sufficiently defined to clearly distinguish them from PAN.

In contrast to microscopic polyangiitis (MPA), PAN, strictly defined, always affects arteries but not postcapillary venules. In contrast to the lesions of nodular vasculitis, inflammation in cutaneous PAN does not extend past the adventitia of the arterial vessel, and thus does not significantly involve subcutaneous lobules (13).

Cutaneous PAN (even with inclusion of those cases with distinct noncutaneous involvement of the nerves and muscles underlying the involved dermis) is different from systemic PAN, because it is more chronic and more uniform (9,14). In most studies, no evolution of cutaneous arteritis into systemic vasculitis has been observed (10,15), while reports of cutaneous PAN developing into systemic PAN several years later are so rare that one cannot exclude the possibility of accidental occurrence of 2 different vasculitides (16) or the presence of another etiologic factor, such as CV (17).

A recently identified, genetically determined form of PAN has a broad spectrum of disease. Loss-of-function mutation in the adenosine deaminase type 2 gene (known as ADA2 deficiency) is linked to autosomal, recessive, childhood-onset disease with features similar to those of classic PAN, shows considerable variability in severity, and

ranges from cutaneous to systemic vasculopathy (18,19). These observations demonstrate that in this rare form of PAN-like disease, the same etiology can lead to both cutaneous and systemic forms of arteritis.

Small vessel vasculitis

Small vessel vasculitis (SVV) predominantly affects small vessels, defined as small intraparenchymal arteries, arterioles, capillaries, and venules. Medium arteries and veins may also be affected. The 2 major immunopathologic categories of SVV are antineutrophil cytoplasmic antibody (ANCA)-associated vasculitis (AAV) and immune complex vasculitis (1), both of which often affect vessels in the skin (20).

ANCA-associated vasculitis. AAV has a spectrum of systemic and organ-limited manifestations that can be classified on the basis of specific pathologic and clinical features as MPA, granulomatosis with polyangiitis (GPA), or eosinophilic granulomatosis with polyangiitis (EGPA) (1). In addition, AAV can be classified further by serology, as serum positive for ANCAs specific for proteinase 3 (PR3-ANCAs) or ANCAs specific for myeloperoxidase (MPO-ANCAs), or as an ANCA-negative AAV. Both the clinico-pathologic variant and the ANCA serotype have value for predicting outcomes.

The cutaneous component of systemic AAV may have one of the following presentations: 1) LCV of dermal postcapillary venules, sometimes extending into arterioles or small veins, and clinically manifesting as hemorrhagic papules or macules, sometimes nodules; 2) vasculitis of small arteries or arterioles, clinically manifesting as inflammatory retiform purpura or livedo and nodules, or sometimes as noninflammatory retiform purpura or digital infarcts; 3) extravascular non-vasculitic granulomatous inflammation (in GPA and EGPA) (21); or 4) other nonvasculitic (muco)cutaneous lesions (hyperplastic gingivitis, especially in GPA) (22).

There are reports of AAVs that are limited to the skin. Most of them are drug-induced cutaneous AAVs (see more details below). However, there are single case reports of AAV limited to the skin with no linkage to disease-eliciting drugs or other causal factors (23,24) (Table 4).

The presence of ANCAs is mandatory for a definition of skin-limited AAV, because the variety of skin lesions in AAV and the type of SVV alone are not specific enough to be used as the defining feature. As there are case reports of skin-limited vasculitis with granuloma, typical of GPA or EGPA (24), skin-limited AAV may be further defined as skin-limited MPA, GPA, or EGPA, in

concordance with the CHCC2012 criteria (except for those criteria referring to a systemic vasculitis). Organ-limited forms of AAV also occur in organs other than the skin, including GPA or EGPA limited to the respiratory tract or renal-limited disease with glomerulonephritis (the latter being the most common form of nongranulomatous organ-limited AAV). Skin-limited AAV may be followed by systemic AAV up to 10 years later (25).

ANCAs are sometimes absent in organ-limited or early forms of AAV. An ANCA-negative skin-limited AAV is difficult to define (and would be difficult to diagnose). Further evaluations are therefore needed.

MPA. MPA encompasses vasculitis of small vessels in the skin, with few or no immune deposits. It is associated with ANCAs, but has no granulomatous inflammation in any organ. There is often involvement of subcutaneous vessels, including arteries.

GPA. GPA involves cutaneous vasculitis that is indistinguishable from that in MPA, but additionally encompasses dermal granulomas outside the walls of cutaneous vessels, with palisades of epithelioid macrophages and giant cells. Smaller lesions may present as interstitial granulomatous dermatitis. Microabscesses contain few eosinophils, and the central zone of necrosis is usually more basophilic than eosinophilic. There is no history of asthma and no eosinophilia in GPA, in contrast to that in EGPA.

EGPA. EGPA exhibits cutaneous vasculitis and granulomatous inflammation, as in GPA, but is also characterized by prominent eosinophils and a history of asthma. The spectrum of vasculitides in EGPA ranges from neutrophilic LCV to eosinophil-rich vasculitis (without much leukocytoclasia) to vasculitis of arterioles, small arteries, or small veins (22). The extravascular dermal changes encompass diffuse interstitial infiltrates containing eosinophils and flame figures (a clinical and histologic reaction pattern also referred to as Wells syndrome), dermal granulomatous inflammation of palisading macrophages admixed with eosinophils around variable eosinophilic necrotic lesions (Churg-Strauss granuloma), and urticarial lesions (20).

Drug-induced skin-limited AAV. Drug-induced skin-limited AAV predominantly affects small vessels in the dermis, and is more often associated with MPO-ANCAs than with PR3-ANCAs. A criterion for drug-induced AAV is the temporal association between drug intake and disease onset, and its common reversibility following discontinuation of the etiologic drug (e.g., propylthiouracil, minocycline, hydralazine, or levamisole-adulterated cocaine). Drug-induced AAV can also be a systemic vasculitis, with renal and pulmonary involvement (26).

Immune complex vasculitis. Of the systemic immune complex vasculitides defined in the CHCC2012 nomenclature, all except anti-glomerular basement

Table 4. Systemic and cutaneous variants of small vessel vasculitis*

CHCC12 vasculitis category, name	Abbreviated CHCC2012 definition	Cutaneous component of systemic vasculitis	Skin-limited or skin-dominant variant
ANCA-associated vasculitis	Necrotizing vasculitis with few or no immune deposits, predominantly affecting small vessels (i.e., capillaries, venules, arterioles, and small arteries); associated with ANCA	Vasculitis of cutaneous postcapillary venules, small veins, arterioles, and small arteries; associated with ANCA	ANCA-associated vasculitis limited to the skin (not further specified)
MPA	Necrotizing vasculitis with few or no immune deposits, predominantly affecting small vessels (i.e., capillaries, venules, or arterioles)	Vasculitis of small-to-medium vessels in the skin (postcapillary venules, arterioles, venules, or small arteries), often with leukocytoclasia and without granulomatous inflammation	Skin-limited MPA (including drug-induced skin-limited MPA); vasculitis of small vessels in the skin (postcapillary venules, arterioles, venules, or small arteries), without cutaneous granulomatous inflammation and without systemic vasculitis; associated with ANCA
GPA	Necrotizing granulomatous inflammation usually involving the upper and lower respiratory tracts, and necrotizing vasculitis affecting predominantly small-to-medium vessels (e.g., capillaries, venules, arterioles, arteries, and veins)	Vasculitis of small-to-medium vessels in the skin (postcapillary venules, arterioles, small veins, or small arteries), often with leukocytoclasia and nonvasculitic extravascular dermal granulomatous inflammation	Skin-limited GPA (including drug-induced skin-limited GPA); vasculitis of small vessels in the skin (spectrum as in MPA), with nonvasculitic extravascular dermal granulomatous inflammation but without eosinophilia, without a history of asthma, and without systemic vasculitis; associated with ANCA
EGPA	Eosinophil-rich and necrotizing granulomatous inflammation often involving the respiratory tract, and necrotizing vasculitis predominantly affecting small-to-medium vessels and associated with a history of asthma and eosinophilia	Eosinophil-rich vasculitis of small-to-medium vessels in the skin (postcapillary venules, arterioles, small venules, or small arteries), sometimes with leukocytoclasia and, e.g., nonvasculitic extravascular dermal granulomatous inflammation	Skin-limited EGPA (including drug-induced skin-limited EGPA); eosinophil-rich vasculitis of small vessels in the skin (spectrum as in MPA), with, e.g., nonvasculitic extravascular dermal granulomatous inflammation, and with a history of asthma, but without systemic vasculitis; associated with ANCA
Immune complex vasculitis	Vasculitis with moderate-to-marked vessel wall deposits of immunoglobulin and/or complement components, predominantly affecting small vessels (i.e., capillaries, venules, arterioles, and small arteries)	Leukocytoclastic immune complex vasculitis of small vessels (mostly postcapillary venules, occasionally small veins or arterioles)	Skin-limited immune complex vasculitis
Anti-GBM disease	Vasculitis affecting glomerular capillaries, pulmonary capillaries, or both, with GBM deposition of anti-GBM autoantibodies	None	None
CV	Vasculitis with cryoglobulin immune deposits affecting small vessels (predominantly capillaries, venules, or arterioles); associated with serum cryoglobulins	Leukocytoclastic vasculitis of small vessels (postcapillary venules, small veins, or arterioles); associated with serum cryoglobulins (usually type II and type III)	Skin-limited CV, without systemic vasculitis
IgA vasculitis (Henoch-Schönlein)	Vasculitis with IgA1-dominant immune deposits, affecting small vessels (predominantly capillaries, venules, or arterioles)	Leukocytoclastic IgA1-dominant vasculitis of mostly postcapillary venules and also veins or arterioles in the skin, with vascular IgA deposits	Skin-limited IgA vasculitis, without systemic vasculitis

Table 4. (Cont'd)

CHCC12 vasculitis category, name	Abbreviated CHCC2012 definition	Cutaneous component of systemic vasculitis	Skin-limited or skin-dominant variant
HUV (anti-C1q vasculitis)	Vasculitis accompanied by urticaria and hypocomplementemia, affecting small vessels (i.e., capillaries, venules, or arterioles) and associated with anti-C1q antibodies; common forms include glomerulonephritis, arthritis, obstructive pulmonary disease, and ocular inflammation	Cutaneous leukocytoclastic vasculitis of mostly postcapillary venules with vascular deposits of immunoglobulins, and manifesting with lasting urticarial lesions; anti-C1q antibodies may be present	Skin-limited HUV, without systemic vasculitis (but often associated with other systemic diseases, e.g., SLE)

* Small vessel vasculitis predominantly affects small vessels, defined as small intraparenchymal arteries, arterioles, capillaries, and venules. Medium arteries and veins may be affected as well. The 2012 revised International Chapel Hill Consensus Conference Nomenclature of Vasculitides (CHCC2012) definitions are detailed in ref. 1. ANCA = antineutrophil cytoplasmic antibody; MPA = microscopic polyangiitis; GPA = granulomatosis with polyangiitis; EGPA = eosinophilic granulomatosis with polyangiitis; anti-GBM = anti-glomerular basement membrane; CV = cryoglobulinemic vasculitis; HUV = hypocomplementemic urticarial vasculitis; SLE = systemic lupus erythematosus.

membrane disease have cutaneous features of vasculitis (Table 4). Palpable purpura with predilection for the legs (or dependent parts) is a constant feature of IgA vasculitis or genuine IgM/IgG vasculitis, as is the inducibility of lesions by vasodilatory stimuli during acute phases. Extensive involvement of vessels beyond the postcapillary venules and a lack of predilection for the lower legs is more likely associated with other forms of vasculitis, such as CV, rheumatoid vasculitis, and lupus vasculitis.

Cryoglobulinemic vasculitis. CV involves the skin in the systemic form, but there is also a skin-limited form. CV often is associated with hepatitis C infection. Vasculitis in the skin involves mostly postcapillary venules, but also arterioles and medium vessels (systemically rare in large vessels as well [7]). CV is seen most often in type II, and sometimes type III, cryoglobulinemia. It has also been described in cases of type I monoclonal cryoglobulinemia (27,28); however, high titers of type I monoclonal cryoglobulinemia more often result in occlusive vasculopathy (27), with intraluminal aggregates of cryoglobulins in small blood vessels of the dermis as well as in capillaries of subcutaneous fat lobules (29), and an absence of primary inflammation.

IgA vasculitis (Henoch-Schönlein). IgA vasculitis (Henoch-Schönlein) regularly presents with cutaneous vasculitis predominantly of postcapillary venules, sometimes extending to the small veins and perhaps to arterioles, and with primarily IgA1 deposits (30). This leads to round and, when extending to larger vessels, retiform palpable purpura (31), with a predilection for the lower legs.

There is a skin-limited form of IgA vasculitis that, in adults, is more frequent than the systemic form (meaning, there is no clinically detectable involvement of systemic organs; e.g., repeated absence of erythrocyte casts or of dysmorphic erythrocytes in urine analysis indicates the absence of glomerular involvement).

Cutaneous IgM or IgG immune complex vasculitis.

Cutaneous IgM or IgG immune complex vasculitis is a provisional category of vasculitis not included in the CHCC2012. It is an LCV of postcapillary venules that, in skin, is clinically almost indistinguishable from IgA vasculitis (palpable purpura with predilection for the legs, elicitable by vasodilation); however, findings on repeated immunofluorescence microscopy revealed that IgM and/or IgG, rather than IgA, predominates in early or histamine-induced lesions (2,3,32–34). This category had been described in reviews of cutaneous vasculitis, and has been subsumed in groups called IgA-negative immune complex vasculitis, hypersensitivity vasculitis, or idiopathic cutaneous LCV (32,35,36). The term “cutaneous IgG/IgM vasculitis” as used herein is meant for those cases of LCV with IgG/IgM deposits that do not belong to one of the other defined immune (complex) vasculitides, such as vasculitis in cryoglobulinemia, monoclonal gammopathy, systemic lupus erythematosus (SLE), rheumatoid arthritis (33), or dermatomyositis. Similarly, LCV with, for example, IgA cryoglobulins would be CV, and not IgA vasculitis.

Ongoing studies will reveal the prevalence of IgG/IgM LCV and whether it could be associated with systemic vasculitis. Of note, the term “leukocytoclastic vasculitis” should not be used as a synonym for IgA or IgG/IgM immune complex vasculitis and does not represent a distinct type of vasculitis. It is a descriptive term for a pattern of injury that is found in pathogenetically distinct small vessel vasculitides (20) and also as part of diseases that are not primary vasculitides (e.g., in tissue reactions around ulcers or infected vessels).

Hypocomplementemic urticarial vasculitis (anti-C1q vasculitis). Hypocomplementemic urticarial vasculitis (HUV) (anti-C1q vasculitis), as defined in the CHCC2012, is a rare systemic vasculitis. Importantly, although more than

Table 5. Systemic and cutaneous variants of variable vessel vasculitis, vasculitis associated with probable etiology, and cutaneous single-organ vasculitides not included in the CHCC2012*

CHCC2012 vasculitis category, name	Abbreviated CHCC2012 definition	Cutaneous component of systemic vasculitis	Skin-limited or skin-dominant variant
Variable vessel vasculitis	Vasculitis with no predominant type of vessel involved; can affect vessels of any size and type		
Behçet's disease	Vasculitis that can affect arteries or veins, characterized by recurrent oral and/or genital aphthous ulcers and accompanied by cutaneous, ocular, articular, gastrointestinal, and/or central nervous system inflammatory lesions; small vessel vasculitis, thromboangiitis, thrombosis, arteritis, and arterial aneurysms may occur	A vessel-based neutrophilic reaction with leukocytoclasia and (muco)cutaneous small vessel vasculitis of mostly venules and/or thrombophlebitis; associated with vasculitis in other organs	Skin-limited (muco)cutaneous vasculitis in absence of systemic vasculitis (Behçet's disease with skin-limited vasculitis)
Cogan's syndrome	Vasculitis with manifestations that may include arteritis, aortitis, aortic aneurysms, and aortic and mitral valvulitis	Vasculitis of small arteries in the panniculus and dermosubcutaneous junction, and small vessels in the dermis (rare)	None
Vasculitis associated with systemic disease	Vasculitis that is associated with and maybe secondary to (caused by) a systemic disease (e.g., rheumatoid vasculitis, SLE, sarcoid vasculitis, etc.); the name (diagnosis) should have a prefix term specifying the systemic disease (e.g., rheumatoid vasculitis, lupus vasculitis, etc.)	Cutaneous vasculitis as a component of systemic vasculitis; the type of cutaneous vasculitis (small vessel or medium vessel vasculitis) varies depending on the underlying systemic disease	Cutaneous vasculitis, without systemic vasculitis (the name should be, e.g., skin-limited rheumatoid vasculitis, etc.)
Vasculitis associated with probable etiology	Vasculitis that is associated with a probable specific etiology, e.g., drug, infection, sepsis, neoplasm, etc.	Cutaneous vasculitis as a component of systemic vasculitis that is associated with a probable specific etiology, e.g., drug, sepsis, etc.	Cutaneous vasculitis, without systemic vasculitis (e.g., septic vasculitis of the skin)
Single-organ vasculitis	Vasculitis in a single organ that has no features that indicate that it is a limited expression of a systemic vasculitis		
Cutaneous IgM/IgG immune complex vasculitis	Not in CHCC2012; D-CHCC definition is vasculitis, with IgM- and/or IgG-dominant or codominant immune deposits, affecting small vessels (predominantly postcapillary venules) in the skin	None (not described yet)	Cutaneous IgM- or IgG-dominant/codominant leukocytoclastic vasculitis of mostly postcapillary venules, without systemic involvement or cryoglobulins
Nodular cutaneous vasculitis (erythema induratum of Bazin)	Not in CHCC2012; D-CHCC definition is lobular panniculitis with varying combinations of vasculitis of venules in fat lobules and/or of veins or arteries of the connective tissue septa; sometimes accompanied by pannicular coagulative and caseous necrosis; presence of lymphocytic, neutrophilic, or granulomatous inflammation	None	Vasculitis with lobular panniculitis of mostly small blood vessels of the fat lobule (postcapillary venules) and rarely of small or medium vessels in the panniculus or septae, with varying combinations of vasculitis of fat lobule venules and/or veins or arteries of the connective tissue septa
Erythema elevatum et diutinum	Not in CHCC2012; D-CHCC definition is neutrophilic dermatosis and chronic fibrosing leukocytoclastic vasculitis, mostly of postcapillary venules, often with vascular immunoglobulin deposits; inflammation may include eosinophils and plasma cells; fibrosis is angiocentric and storiform	None	A neutrophilic dermatosis and chronic localized fibrosing leukocytoclastic vasculitis (associated with monoclonal gammopathy, hematologic disease, or HIV infection)

Table 5. (Cont'd)

CHCC2012 vasculitis category, name	Abbreviated CHCC2012 definition	Cutaneous component of systemic vasculitis	Skin-limited or skin-dominant variant
Recurrent macular vasculitis in hypergamma- globulinemia (hypergamma- globulinemic purpura of Waldenström)	Not in CHCC2012; D-CHCC definition is cutaneous small vessel vasculitis with recurring macules and purpura associated with hypergammaglobulinemia and vascular immunoglobulin deposits	None	Relapsing, short-lasting macular vasculitis of small blood vessels with perivascular deposits of immunoglobulins (usually associated with polyclonal hypergammaglobulinemia)
Normocomplementemic urticarial vasculitis (NUV) (non-anti-C1q vasculitis)	Not in CHCC2012; D-CHCC definition is cutaneous small vessel vasculitis, accompanied by lasting urticarial lesions and associated with normocomplementemia and absence of anti-C1q antibodies	None (not observed yet)	Cutaneous small vessel vasculitis, accompanied by lasting urticarial lesions and associated with normocomplementemia and absence of anti-C1q antibodies; may be part of a spectrum with neutrophilic urticarial dermatosis

* The 2012 revised International Chapel Hill Consensus Conference Nomenclature of Vasculitides (CHCC2012) definitions are detailed in ref. 1. For those with a vasculitis defined by the dermatologic addendum to the CHCC2012 nomenclature (D-CHCC), the definition was for a category of cutaneous vasculitis that was not included in the CHCC2012. SLE = systemic lupus erythematosus.

one-half of patients with HUV have anti-C1q antibodies, patients can have HUV without these antibodies.

Cutaneous vasculitis in HUV is characterized pathologically by LCV of mostly postcapillary venules, often with subepidermal edema (urticaria) and vascular immune deposits. Clinically, it is characterized by persistent urticarial lesions that may have petechiae or postinflammatory hyperpigmentation. It does not show a strong predilection for the lower legs, thereby distinguishing it from, e.g., IgA or IgG/IgM immune complex vasculitis. It needs to be discriminated from neutrophilic urticarial dermatosis (NUD), a reaction pattern recently described in auto-inflammatory syndromes and in SLE. Clinically, NUD shows pale reddish macules, papules, or slightly raised plaques, but not the persistent erythematous wheals of HUV. Histologically, NUD lacks the presence of fibrinoid vessel necrosis and of perivascular leukocytoclasia, and instead presents a typical neutrophilic epitheliotropism (i.e., a perivascular and more diffuse interstitial neutrophilic infiltrate focally extending into the epithelia of the epidermis, hair follicles, and sebaceous and sweat glands) (37).

Urticarial vasculitis (HUV or normocomplementemic urticarial vasculitis [NUV] [as described below and in Table 5]) and NUD may yet be recognized as part of a spectrum of neutrophilic dermatoses. Skin-limited HUV without systemic vasculitis is often, but not always, associated with systemic diseases, such as LE, serum sickness, and hepatitis B (38,39). In contrast to vasculitis in LE or in rheumatoid vasculitis, HUV or NUV are limited to mostly postcapillary venules, while those other forms of vasculitis often involve deeper and larger vessels.

Normocomplementemic urticarial vasculitis. NUV usually is not accompanied by evidence of systemic vasculitis, and thus is considered to be a skin-limited SOV (38,39). It also needs to be distinguished from NUD on the basis of the above-mentioned criteria. While NUV has been diagnosed occasionally in the past, its prevalence based on the D-CHCC definition needs to be clarified in the future.

Variable vessel vasculitis

Behçet's disease (BD) and Cogan's syndrome are forms of variable vessel vasculitis, according to the CHCC2012 nomenclature (1) (Table 5).

BD has many different manifestations in the skin. Recurrent oral aphthous ulcers are an almost universal feature, while genital aphthous ulcers, erythema nodosum-like lesions, superficial thrombophlebitis, positive reaction on the skin pathergy test, and nonfollicular papulopustular lesions occur less regularly. The consensus among experts in BD is that, except for the (acneiform) follicular pustules, the early stages of cutaneous lesions are vessel-based neutrophilic reactions with leukocytoclasia and endothelial swelling, and sometimes vasculitis with fibrinoid necrosis. Larger vessels with thrombosis often present with vasculitis of the vasa vasorum. Erythema nodosum-like lesions in BD are chronic, macrophage-rich lesions that initially may show LCV within septa (40). LCV, lobular infiltrates, and lack of Miescher's granulomas distinguish BD from classic erythema nodosum. Arterial lesions are rare in BD, and on the lower leg, these lesions may have been sometimes misdiagnosed due to the difficulty in distinguishing arterioles

from altered venules (40). Biopsies of older lesions in BD or obtained during systemic therapy have revealed lymphocytic infiltration in and around vessel walls and have led to controversies about whether BD is a vasculopathy or a lymphocytic vasculitis.

MAGIC syndrome (mouth and genital ulcers with inflamed cartilage) encompasses cutaneous features of BD in patients with relapsing polychondritis and vasculitis (41). Some patients with BD have skin-limited vasculitis and erythema nodosum-like lesions but have no clinical evidence of a systemic vasculitis such as clinically detectable central nervous system vasculitis (particularly, parenchymal and brain stem), gastrointestinal vasculitis, or large vessel vasculitis (of, e.g., the pulmonary artery), the latter often being described in BD. Similarly, some patients diagnosed as having BD according to the presence of oral ulcers, genital ulcers, papulopustular lesions, and/or a positive skin pathergy test reaction may not develop systemic involvement of BD, as manifested by eye disease, oligoarthritis, or other (e.g., neurologic) manifestations (42,43), regardless of whether the disease manifestations are vasculitic or non-vasculitic in origin.

Cutaneous single-organ vasculitis

Skin-limited vasculitis that does not share sufficient clinical, laboratory, and/or pathologic features with a systemic vasculitis qualifies as a cutaneous SOV, in accordance with the CHCC2012 definitions (Table 5).

IgM/IgG immune complex vasculitis. IgM/IgG immune complex vasculitis (as described above) is not known to be associated with systemic vasculitis, and thus qualifies as an SOV.

Nodular vasculitis (erythema induratum of Bazin). Nodular vasculitis (erythema induratum of Bazin) is a lobular panniculitis with vasculitis of vessels in the panniculus. In the presence of tuberculosis (usually with hyperergic reaction), it has been referred to as erythema induratum of Bazin (44). Affected vessels, in order of frequency, are as follows: 1) small venules of fat lobules; 2) both veins of connective tissue septae and venules of fat lobules; 3) only veins of connective tissue septae; 4) veins and arteries of connective tissue septae and venules of fat lobules; and 5) veins and arteries of connective tissue septae. In some cases, vasculitis could not be demonstrated within serial sections throughout the specimen (44). Nodular vasculitis with lobular panniculitis can be associated with coagulative and caseous necrosis, and with (extravascular) granulomatous inflammation. Depending on the stage of disease, vasculitis is associated with neutrophilic, granulomatous, or lymphocytic inflammation (13).

Lobular panniculitis distinguishes nodular vasculitis from cutaneous PAN, and the primary localization of vasculitis in the panniculus distinguishes it from GPA and EGPA.

Erythema elevatum et diutinum. Erythema elevatum et diutinum (EED) is a neutrophilic dermatosis and chronic localized fibrosing LCV, initially presenting with LCV of mostly postcapillary venules, often with vascular immune deposits and the presence of plasma cells and, variably, eosinophils, followed typically by storiform and angiocentric fibrosis. EED can be associated with monoclonal gammopathy (in ~15% of individuals), autoimmune disease, or infection (45). Granuloma faciale has been referred to as EED localized to the face. Recently, it was suggested that both belong to a spectrum of IgG4-related disease (46).

Recurrent macular vasculitis in hypergammaglobulinemia (hypergammaglobulinemic purpura of Waldenström). Recurrent macular vasculitis in hypergammaglobulinemia (hypergammaglobulinemic purpura of Waldenström) is a relapsing episodic vasculitis of the small blood vessels, with vascular deposits of immunoglobulins. It is associated with hypergammaglobulinemia (usually polyclonal, but sometimes also monoclonal), an elevated sedimentation rate, often with non-IgM rheumatoid factor (IgG or IgA), and relapsing sudden occurrence of many small, short-lived hemorrhagic macules on the lower legs (47,48). It is sometimes associated with other (auto-immune) diseases, e.g., Sjögren's syndrome (47), but not with systemic vasculitis.

Normocomplementemic urticarial vasculitis. NUV is a cutaneous SOV described in more detail above in the context of hypocomplementemic urticarial vasculitis.

Vasculitis associated with systemic disease

Cutaneous vasculitis that is associated with, and may be secondary to, a systemic disease often coincides with other cutaneous features of the associated disease, in addition to the other criteria of the respective systemic disease.

Rheumatoid vasculitis. Rheumatoid vasculitis occurs in patients with positive titers of rheumatoid factor who have longstanding disease, and who often have erosive rheumatoid arthritis. In the skin, it ranges from (often IgG/IgM-positive, but also IgA-positive) LCV of postcapillary venules (33) to arteritis at the dermal-subcutaneous junction or in the panniculus (49). A more frequent involvement of vessels larger than postcapillary venules distinguishes it from genuine IgA or IgG/IgM vasculitis and results in a more varied clinical presentation,

including cutaneous ulcers, digital gangrene, or nailfold infarction. Involvement of the vasa nervorum may be an etiologic factor in neuropathy. Rheumatoid vasculitis affecting muscular arteries (MVV) is distinguished from cutaneous or systemic PAN by the additional involvement of postcapillary venules as well as by the presence of rheumatoid factor and arthritis.

A similarly heterogeneous presentation of vasculitides may occur in LE (mostly cutaneous SVV, or MVV often involving peripheral nerves) (50), and more rarely in dermatomyositis or systemic sclerosis. Cutaneous vasculitis in patients with LE may also present as HUV or as an immune complex vasculitis, both of which are restricted primarily to postcapillary venules. HUV in LE is defined by the features of urticaria and LCV without predilection for the lower legs, while immune complex vasculitis is defined by predilection for the lower legs and absence of urticaria.

Sjögren's syndrome vasculitis. Sjögren's syndrome vasculitis is often either recurrent macular vasculitis in hypergammaglobulinemia (see above) or cryoglobulinemic vasculitis (51).

Sarcoidosis. Sarcoidosis may have cutaneous LCV or granulomatous vasculitis, though this is rare. Cutaneous LCV is more often associated with acute sarcoidosis and/or systemic symptoms (fever, arthralgia) and is usually self-limited. Sarcoid granulomatous vasculitis is more often associated with chronic sarcoidosis and systemic vasculitis. The symptoms may resemble GCA, except that small vessels are also involved, and small vessels are more often affected than medium or large vessels (52).

Vasculitis associated with probable etiology

Identifiable probable etiologies for vasculitis include drugs, infections (e.g., hepatitis B and C), sepsis, and neoplasms. Syphilis-associated aortitis should not be included in this category, because it is the result of direct invasion of *Treponema pallidum* in the vessel wall, and because the CHCC2012 does not include these forms of infectious vasculitides in its nomenclature (1).

Drug-induced vasculitis. Drug-induced vasculitis may be systemic or skin-limited. Minocycline-associated arteritis may present with features similar to cutaneous or systemic PAN. Drug-associated AAV may present as a skin-limited variant of AAV (see more detailed discussions above), but also as a systemic disease featuring, e.g., glomerulonephritis or pulmonary involvement (26). Levamisole-adulterated cocaine can cause a thrombotic vasculopathy and development of ANCA (53). Drug-induced immune complex vasculitides also come in skin-limited and

systemic forms, clinically indistinguishable from immune complex vasculitides arising from other causes.

A relevant criterion for skin-limited, drug-induced vasculitis is the temporal association of onset with intake and the eventual reversibility with discontinuation of the likely etiologic drug. Therefore, whenever it applies, "drug-induced" should be added as a modifier, because this term indicates a case is a drug-induced vasculitis that will usually remit when the drug is discontinued and will not recur unless the drug is reintroduced.

Septic vasculitis. Septic vasculitis is not contained in the original CHCC2012. Purpuric lesions in sepsis often are attributable to either disseminated intravascular coagulation (DIC), septic emboli containing pathogens, or infection of endothelial cells by pathogens (the latter is not included in the CHCC system). However, some patients with bacteremia have cutaneous SVV without detection of microbes in the vessel wall or in thrombi (54). This involves vessels of different sizes, from capillaries to medium vessels, which distinguishes it from any other SVV, such as immune complex vasculitis (55). In rare cases, it may occur without DIC, e.g., as in smoldering vasculitis in gonococcal bacteremia.

More often, septic vasculitis occurs in conjunction with thrombotic occlusions of capillaries and larger vessels, due to coagulopathy. Clinically, septic SVV manifests as single, randomly distributed small purpuric papules. They may develop into retiform purpura and necrotic ulcers when, additionally, occlusive mechanisms (e.g., DIC) come into effect. Septic vasculitis without DIC must not be confused with ANCA-associated or immune complex vasculitis. It is also important to recognize that infections can induce immune complex vasculitis and AAV, and that bacteremia may be associated with development of ANCA (mostly, PR3-ANCA) without development of AAV (56).

Diseases not recognized by consensus as a primary vasculitis

Superficial thrombophlebitis. Superficial thrombophlebitis (except thrombophlebitis in BD) was not recognized by full CHCC consensus as a primary vasculitis. This is partly because of the controversy regarding whether small veins and arteries (and thus PAN and thrombophlebitis) are always distinguishable in the lower legs, given the stasis-induced changes of venular walls. The majority of investigators have considered thrombophlebitis to be a sequela of degenerative or anatomic alterations of the vessel walls, slowed blood flow, and/or hypercoagulable conditions, which then secondarily lead to inflammatory infiltration.

Vasculitis in monoclonal gammopathy. Vasculitis occurs rarely in cases of monoclonal gammopathy (type I cryoglobulinemia being a special case of monoclonal gammopathy) and is associated with, but distinct from, the more frequent occlusive vasculopathy in gammopathy. It has been described explicitly in a case of systemic IgA vasculitis (57). This cutaneous vasculitis presents clinically with purpuric macules or papules, in addition to livedo or retiform purpura from vasculopathy. In contrast to genuine IgA or IgG/IgM vasculitis, vasculitic lesions do not regularly present with a typical predilection for the lower legs. Immunofluorescence analysis reveals vascular deposits of the same immunoglobulin class as the monoclonal immunoglobulin. Similarly, as with vasculitis in type I cryoglobulinemia, it is not known whether these cases are due to aggregates of monoclonal immunoglobulin that can activate complement, whether the monoclonal immunoglobulin becomes directly fixed to structures of the vascular wall and induces vasculitis, or whether vessel damage and inflammation are secondary to vascular occlusion. The latter cannot be excluded at this point, and therefore this entity requires further studies in cohorts to reach a full consensus as to whether this is an original vasculitis.

Monoclonal gammopathy also is associated with EED and several nonvasculitic dermatoses.

Exercise-induced vasculitis. Exercise-induced vasculitis ("golfer's vasculitis") is described as palpable purpura or short-lived hemorrhagic macules on the lower legs that occur after prolonged exercise or standing upright for long periods. It is probably a form of cutaneous immune complex vasculitis or recurrent macular vasculitis in hypergammaglobulinemia (58).

Lymphocytic vasculitis. Lymphocytic vasculitis is, by strict definition, a vasculitis in which the primary event is infiltration and damage (fibrinoid necrosis) of the vessel walls by primarily lymphocytes (13). It is not clear if such a vasculitis exists. Candidates are pityriasis lichenoides et varioliformis acuta or (noninfected) arteritis in the context of Epstein-Barr virus infection. The term has also been used for later stages of other vasculitides in which lymphocytes have followed the initially infiltrating neutrophils and monocytes (e.g., in BD, LE, or PAN).

The term "lymphocytic vasculitis" has also been used for a reaction pattern in which lymphocytes infiltrate the vessel walls without constituting a specific form of vasculitis.

Lesions not fulfilling sufficient criteria as distinct vasculitides

Lymphocytic arteritis/macular arteritis. Lymphocytic arteritis/macular arteritis is mostly considered an early or indolent or reparative stage of cutaneous PAN (59).

Eosinophilic vasculitis. Eosinophilic vasculitis is a term that has been used not only for eosinophil-rich LCV in EGPA, but also for eosinophil-rich arteritis observed in GCA, for vasculitis associated with connective tissue disease, EGPA, or hypereosinophilic syndrome, or for vasculitic reactions associated with blood eosinophilia. The term therefore refers to a pattern of injury, but does not define a specific form of vasculitis.

Granulomatous vasculitis. Granulomatous vasculitis similarly refers to a pattern of injury that occurs in, e.g., GCA, TAK, GPA, EGPA, and sarcoid vasculitis.

Erythema (nodosum) leprosum. Erythema (nodosum) leprosum is an immune-mediated systemic disease in multibacillary leprosy, characterized by erythematous tender subcutaneous nodules or plaques, and histologically by initial neutrophilic infiltrates in the deep dermis and lobular panniculitis, and/or sometimes vasculitis of the small blood vessels (primarily venules, rarely arterioles) on the background of macrophage-rich leprosy lesions. It has been considered to be an immune complex vasculitis (60); however, vasculitis is not a constant feature in skin biopsy specimens (61,62), and skin lesions show no predilection for the lower legs and are not inducible by intracutaneous histamine.

Summary

The primary goals of this dermatologic addendum to the CHHC2012 are to clarify the CHCC2012 categories that are applicable to skin vasculitis, and to add definitions of cutaneous vasculitis that are not included in the CHCC2012. The D-CHCC does not provide diagnostic criteria, but rather provides standard terminology and definitions for many, but not all, forms of cutaneous vasculitis. This review and commentary clearly show that, in most patients, a precise diagnosis that is most likely to lead to optimum patient management can only be made by knowledgeably integrating data from clinical, laboratory, and pathologic studies.

The authors encourage careful confirmation of the validity of the definitions, further improvements, and documentation of the clinical and pathologic features in cohorts of patients, and also encourage thorough identification of examples of cutaneous vasculitis that cannot be allocated to these D-CHCC categories. Future adjustments and additions will result from advances in the understanding of cutaneous vasculitis.

AUTHOR CONTRIBUTIONS

All authors were involved in drafting the article or revising it critically for important intellectual content, and all authors approved the final version to be published.

REFERENCES

- Jennette JC, Falk RJ, Bacon PA, Basu N, Cid MC, Ferrario F, et al. 2012 revised International Chapel Hill Consensus Conference Nomenclature of Vasculitides. *Arthritis Rheum* 2013;65:1–11.
- Braverman IM, Yen A. Demonstration of immune complexes in spontaneous and histamine-induced lesions and in normal skin of patients with leukocytoclastic angitis. *J Invest Dermatol* 1975;64:105–12.
- Gower RG, Sams WM Jr, Thorne EG, Kohler PF, Claman HN. Leukocytoclastic vasculitis: sequential appearance of immunoreactants and cellular changes in serial biopsies. *J Invest Dermatol* 1977;69:477–84.
- Obermoser G, Posch L, Zelger B. Spitting out the tongue. *Br J Dermatol* 2004;151:721–2.
- Cuvelier C, Kremer B, Kawski H, Guichard JF, Maurier F. Subcutaneous nodules of the head and neck heralding giant cell arteritis. *Ann Dermatol Venerol* 2014;141:518–22. In French.
- Kluger N, Pagnoux C, Guillemin L, Frances C. Comparison of cutaneous manifestations in systemic polyarteritis nodosa and microscopic polyangiitis. *Br J Dermatol* 2008;159:615–20.
- Au WY, Kwok JS, Chu KM, Ma ES. Life-threatening cryoglobulinemia in HCV-negative Southern Chinese and a novel association with structural aortic abnormalities. *Ann Hematol* 2005;84:95–8.
- Requena L, Yus ES. Panniculitis. Part I. Mostly septal panniculitis. *J Am Acad Dermatol* 2001;45:163–83; quiz 84–6.
- Yus ES, Simon RS, Requena L. Vein, artery, or arteriole? A decisive question in hypodermal pathology. *Am J Dermatopathol* 2012;34:229–32.
- Daoud MS, Hutton KP, Gibson LE. Cutaneous periarteritis nodosa: a clinicopathological study of 79 cases. *Br J Dermatol* 1997;136:706–13.
- Mimouni D, Ng PP, Rencic A, Nikolskaia OV, Bernstein BD, Nousari HC. Cutaneous polyarteritis nodosa in patients presenting with atrophie blanche. *Br J Dermatol* 2003;148:789–94.
- Criado PR, Marques GF, Morita TC, de Carvalho JF. Epidemiological, clinical and laboratory profiles of cutaneous polyarteritis nodosa patients: report of 22 cases and literature review. *Autoimmun Rev* 2016;15:558–63.
- Carlson JA, Chen KR. Cutaneous vasculitis update: neutrophilic muscular vessel and eosinophilic, granulomatous, and lymphocytic vasculitis syndromes. *Am J Dermatopathol* 2007;29:32–43.
- Alibaz-Oner F, Koster MJ, Crowson CS, Makol A, Ytterberg SR, Salvarani C, et al. Clinical spectrum of medium-sized vessel vasculitis. *Arthritis Care Res (Hoboken)* 2017;69:884–91.
- Chen KR. Cutaneous polyarteritis nodosa: a clinical and histopathological study of 20 cases. *J Dermatol* 1989;16:429–42.
- Dewar CL, Bellamy N. Necrotizing mesenteric vasculitis after longstanding cutaneous polyarteritis nodosa. *J Rheumatol* 1992;19:1308–11.
- Minkowitz G, Smoller BR, McNutt NS. Benign cutaneous polyarteritis nodosa: relationship to systemic polyarteritis nodosa and to hepatitis B infection. *Arch Dermatol* 1991;127:1520–3.
- Navon Elkan P, Pierce SB, Segel R, Walsh T, Barash J, Padeh S, et al. Mutant adenosine deaminase 2 in a polyarteritis nodosa vasculopathy. *N Engl J Med* 2014;370:921–31.
- Nanthapaisal S, Murphy C, Omoyinmi E, Hong Y, Standing A, Berg S, et al. Deficiency of adenosine deaminase type 2: a description of phenotype and genotype in fifteen cases. *Arthritis Rheumatol* 2016;68:2314–22.
- Ratzinger G, Zelger BG, Carlson JA, Burgdorf W, Zelger B. Vasculitic wheel: an algorithmic approach to cutaneous vasculitides. *J Dtsch Dermatol Ges* 2015;13:1092–117.
- Cottin V, Bel E, Bottero P, Dalhoff K, Humbert M, Lazor R, et al. Revisiting the systemic vasculitis in eosinophilic granulomatosis with polyangiitis (Churg-Strauss): a study of 157 patients by the Groupe d'Etudes et de Recherche sur les Maladies Orphelines Pulmonaires and the European Respiratory Society Taskforce on eosinophilic granulomatosis with polyangiitis (Churg-Strauss). *Autoimmun Rev* 2017;16:1–9.
- Chen KR. Skin involvement in ANCA-associated vasculitis. *Clin Exp Nephrol* 2013;17:676–82.
- Irvine AD, Bruce IN, Walsh MY, Bingham EA. Microscopic polyangiitis: delineation of a cutaneous-limited variant associated with antimyeloperoxidase autoantibody. *Arch Dermatol* 1997;133:474–7.
- Newell EL, Mallipeddi R, Murdoch ME, Groves R, Black MM, Robson A. A case of cutaneous extravascular necrotizing granuloma without systemic manifestations. *Clin Exp Dermatol* 2007;32:509–12.
- Figarella I, Bazarbachi T, Marie B, Scheid P, Martinet Y, Schmutz JL. Cutaneous nodules recurring in the legs ten years before the diagnosis of Wegener's granulomatosis. *Rev Med Interne* 2000;21:693–7. In French.
- Pendergraft WF III, Niles JL. Trojan horses: drug culprits associated with antineutrophil cytoplasmic autoantibody (ANCA) vasculitis. *Curr Opin Rheumatol* 2014;26:42–9.
- Ramos-Casals M, Stone JH, Cid MC, Bosch X. The cryoglobulinemias. *Lancet* 2012;379:348–60.
- Terrier B, Karras A, Kahn JE, le Guenno G, Marie I, Benarous L, et al. The spectrum of type I cryoglobulinemia vasculitis: new insights based on 64 cases. *Medicine (Baltimore)* 2013;92:61–8.
- Requena L, Kutzner H, Angulo J, Renedo G. Generalized livedo reticularis associated with monoclonal cryoglobulinemia and multiple myeloma. *J Cutan Pathol* 2007;34:198–202.
- Egan CA, Taylor TB, Meyer LJ, Petersen MJ, Zone JJ. IgA1 is the major IgA subclass in cutaneous blood vessels in Henoch-Schönlein purpura. *Br J Dermatol* 1999;141:859–62.
- Piette WW, Stone MS. A cutaneous sign of IgA-associated small dermal vessel leukocytoclastic vasculitis in adults (Henoch-Schönlein purpura). *Arch Dermatol* 1989;125:53–6.
- Boom BW, Mommaas AM, Vermeer BJ. Presence and interpretation of vascular immune deposits in human skin: the value of direct immunofluorescence. *J Dermatol Sci* 1992;3:26–34.
- Schroeter AL, Conn DL, Jordon RE. Immunoglobulin and complement deposition in skin of rheumatoid arthritis and systemic lupus erythematosus patients. *Ann Rheum Dis* 1976;35:321–6.
- Sanchez NP, van Hale HM, Su WP. Clinical and histopathologic spectrum of necrotizing vasculitis: report of findings in 101 cases. *Arch Dermatol* 1985;121:220–4.
- Arora A, Wetter DA, Gonzalez-Santiago TM, Davis MD, Lohse CM. Incidence of leukocytoclastic vasculitis, 1996 to 2010: a population-based study in Olmsted County, Minnesota. *Mayo Clin Proc* 2014;89:1515–24.
- Garcia-Porrúa C, Gonzalez-Gay MA. Comparative clinical and epidemiological study of hypersensitivity vasculitis versus Henoch-Schönlein purpura in adults. *Semin Arthritis Rheum* 1999;28:404–12.
- Broekaert SM, Boer-Auer A, Kerl K, Herrgott I, Schulz X, Bonsmann G, et al. Neutrophilic epitheliotropism is a histopathological clue to neutrophilic urticarial dermatosis. *Am J Dermatopathol* 2016;38:39–49.
- Davis MD, Daoud MS, Kirby B, Gibson LE, Rogers RS III. Clinicopathologic correlation of hypocomplementemic and normocomplementemic urticarial vasculitis. *J Am Acad Dermatol* 1998;38:899–905.
- Loricera J, Calvo-Rio V, Mata C, Ortiz-Sanjuan F, Gonzalez-Lopez MA, Alvarez L, et al. Urticarial vasculitis in northern Spain: clinical study of 21 cases. *Medicine (Baltimore)* 2014;93:53–60.
- Kim B, LeBoit PE. Histopathologic features of erythema nodosum-like lesions in Behçet disease: a comparison with erythema nodosum focusing on the role of vasculitis. *Am J Dermatopathol* 2000;22:379–90.
- Firestein GS, Gruber HE, Weisman MH, Zvaifler NJ, Barber J, O'Duffy JD. Mouth and genital ulcers with inflamed cartilage: MAGIC syndrome. Five patients with features of relapsing poly-chondritis and Behçet's disease. *Am J Med* 1985;79:65–72.

42. Hamuryudan V, Hatemi G, Tascilar K, Sut N, Ozyazgan Y, Seyahi E, et al. Prognosis of Behçet's syndrome among men with mucocutaneous involvement at disease onset: long-term outcome of patients enrolled in a controlled trial. *Rheumatology (Oxford)* 2010;49:173–7.
43. Ugurlu N, Bozkurt S, Bacanlı A, Akman-Karakas A, Uzun S, Alpsoy E. The natural course and factors affecting severity of Behçet's disease: a single-center cohort of 368 patients. *Rheumatol Int* 2015;35:2103–7.
44. Segura S, Pujol RM, Trindade F, Requena L. Vasculitis in erythema induratum of Bazin: a histopathologic study of 101 biopsy specimens from 86 patients. *J Am Acad Dermatol* 2008;59:839–51.
45. Wahl CE, Bouldin MB, Gibson LE. Erythema elevatum diutinum: clinical, histopathologic, and immunohistochemical characteristics of six patients. *Am J Dermatopathol* 2005;27:397–400.
46. Kavand S, Lehman JS, Gibson LE. Granuloma faciale and erythema elevatum diutinum in relation to immunoglobulin G4-related disease: an appraisal of 32 cases. *Am J Clin Pathol* 2016;145:401–6.
47. Malaviya AN, Kaushik P, Budhiraja S, al-Mutairi M, Nampoory MR, Hussein A, et al. Hypergammaglobulinemic purpura of Waldenström: report of 3 cases with a short review. *Clin Exp Rheumatol* 2000;18:518–22.
48. Capra JD, Winchester RJ, Kunkel HG. Hypergammaglobulinemic purpura: studies on the unusual anti-globulins characteristic of the sera of these patients. *Medicine (Baltimore)* 1971;50:125–38.
49. Chen KR, Toyohara A, Suzuki A, Miyakawa S. Clinical and histopathological spectrum of cutaneous vasculitis in rheumatoid arthritis. *Br J Dermatol* 2002;147:905–13.
50. Ramos-Casals M, Nardi N, Lagrutta M, Brito-Zeron P, Bove A, Delgado G, et al. Vasculitis in systemic lupus erythematosus: prevalence and clinical characteristics in 670 patients. *Medicine (Baltimore)* 2006;85:95–104.
51. Quartuccio L, Isola M, Baldini C, Priori R, Bartoloni E, Carubbi F, et al. Clinical and biological differences between cryoglobulinaemic and hypergammaglobulinaemic purpura in primary Sjögren's syndrome: results of a large multicentre study. *Scand J Rheumatol* 2015;44:36–41.
52. Fernandes SR, Singsen BH, Hoffman GS. Sarcoidosis and systemic vasculitis. *Semin Arthritis Rheum* 2000;30:33–46.
53. Jenkins J, Babu K, Hsu-Hung E, Robinson-Bostom L, Kroumpouzos G. ANCA-positive necrotizing vasculitis and thrombotic vasculopathy induced by levamisole-adulterated cocaine: a distinctive clinicopathologic presentation. *J Am Acad Dermatol* 2011;65:e14–6.
54. Drolet BA, Baselga E, Esterly NB. Painful, purpuric plaques in a child with fever. *Arch Dermatol* 1997;133:1500–1.
55. Shapiro L, Teisch JA, Brownstein MH. Dermatohistopathology of chronic gonococcal sepsis. *Arch Dermatol* 1973;107:403–6.
56. Mahr A, Batteux F, Tubiana S, Goulvestre C, Wolff M, Papo T, et al. Prevalence of antineutrophil cytoplasmic antibodies in infective endocarditis. *Arthritis Rheumatol* 2014;66:1672–7.
57. Boumediene A, Oblet C, Oruc Z, Duchez S, Morelle W, Huynh A, et al. Gammopathy with IgA mesangial deposition provides a monoclonal model of IgA nephritogenicity and offers new insights into its molecular mechanisms. *Nephrol Dial Transplant* 2011;26:3930–7.
58. Kelly RI, Opie J, Nixon R. Golfer's vasculitis. *Australas J Dermatol* 2005;46:11–4.
59. Buffiere-Morgado A, Battistella M, Vignon-Pennamen MD, de Masson A, Rybojad M, Petit A, et al. Relationship between cutaneous polyarteritis nodosa (cPAN) and macular lymphocytic arteritis (MLA): blinded histologic assessment of 35 cPAN cases. *J Am Acad Dermatol* 2015;73:1013–20.
60. Wemambu SN, Turk JL, Waters MF, Rees RJ. Erythema nodosum leprosum: a clinical manifestation of the arthus phenomenon. *Lancet* 1969;2:933–5.
61. Massone C, Belachew WA, Schettini A. Histopathology of the lepromatous skin biopsy. *Clin Dermatol* 2015;33:38–45.
62. Ridley MJ, Ridley DS. The immunopathology of erythema nodosum leprosum: the role of extravascular complexes. *Lepr Rev* 1983;54:95–107.

Updated Estimates Suggest a Much Higher Prevalence of Arthritis in United States Adults Than Previous Ones

S. Reza Jafarzadeh¹ and David T. Felson²

Objective. National estimates of arthritis prevalence rely on a single survey question about doctor-diagnosed arthritis without using survey information on joint symptoms, even though some subjects with only the latter have been shown to have arthritis. The sensitivity of the current surveillance definition is only 53% and 69% in subjects ages 45–64 years and ages ≥65 years, respectively, resulting in misclassification of nearly one-half and one-third of subjects in those age groups. This study was undertaken to estimate arthritis prevalence based on an expansive surveillance definition that is adjusted for the measurement errors in the current definition.

Methods. Using the 2015 National Health Interview Survey, we developed a Bayesian multinomial latent class model for arthritis surveillance based on doctor-diagnosed arthritis, joint symptoms, and whether symptom duration exceeded 3 months.

Results. Of 33,672 participants, 19.3% of men and 16.7% of women ages 18–64 years and 15.7% of men and 13.5% of women ages ≥65 years affirmed joint symptoms without doctor-diagnosed arthritis. The measurement error-adjusted prevalence of arthritis was 29.9% (95% Bayesian probability interval [95% PI] 23.4–42.3) in men ages 18–64 years, 31.2% (95% PI 25.8–44.1) in women ages 18–64 years, 55.8% (95% PI 49.9–70.4) in men ages ≥65 years, and 68.7% (95% PI 62.1–79.9) in women ages ≥65 years. Arthritis affected 91.2 million adults (of 247.7 million; 36.8%) in the US in 2015, which included 61.1 million persons between 18 and 64 years of age (of 199.9 million; 30.6%). Our arthritis prevalence estimate was 68% higher than the previously reported national estimate.

Conclusion. Arthritis prevalence in the US population has been substantially underestimated, especially among adults younger than 65 years of age.

Arthritis is a highly prevalent condition in the US and a leading cause of disability. The economic burden of arthritis is estimated to be at least \$128 billion annually in the US (1). Effective surveillance of arthritis on a national scale is challenging and requires a screening strategy that goes beyond recognizing symptoms reported in a clinical setting.

National surveillance efforts for arthritis rely on self-report surveys as a practical tool to estimate the burden of disease. The Centers for Disease Control and Prevention (CDC) routinely publishes estimates of the prevalence of arthritis in the US (2–4). One source of data used for arthritis surveillance is the National Health Interview Survey (NHIS), administered by the US Census Bureau, which includes questions that are used to identify cases of arthritis. Although identifying subjects with arthritis from these health surveys is a reasonable method for national surveillance efforts, the accuracy of estimates depends on the validity of the surveillance definition used to identify cases of arthritis. The main item from the NHIS used to identify cases of arthritis has been a single question asking subjects if they ever had doctor-diagnosed arthritis.

In a validation study in which they actually verified clinical cases of arthritis, Sacks et al (5) documented the diagnostic sensitivity and specificity of arthritis-related survey questions. Survey validation has shown reassuring but imperfect accuracy. While a survey approach using a report of doctor-diagnosed arthritis had a higher sensitivity (68.8%) among those ages ≥65 years, the sensitivity of this surveillance definition was lower (52.5%) for persons ages 45–64 years. Such a low sensitivity, especially in a younger population, where almost half of true arthritis cases are missed, results in substantial misclassification and underestimation of prevalence and would have a detrimental effect on planning and needs assessment (3,4).

Subsequent studies that have relied on the assurance of the Sacks et al (5) validation study have produced

Supported by the NIH (grant AR-47785).

¹S. Reza Jafarzadeh, DVM, MPVM, PhD: Boston University School of Medicine, Boston, Massachusetts; ²David T. Felson, MD, MPH: Boston University School of Medicine, Boston, Massachusetts, and University of Manchester and Central Manchester NHS Foundation Trust, Manchester, UK.

Address correspondence to S. Reza Jafarzadeh, DVM, MPVM, PhD, Clinical Epidemiology Research and Training Unit, Boston University School of Medicine, 650 Albany Street, Suite X200, Boston, MA 02118. E-mail: srjafarz@bu.edu.

Submitted for publication May 23, 2017; accepted in revised form October 17, 2017.

a national estimate of the prevalence of arthritis or of doctor-diagnosed arthritis of 54.4 million adults (22.7%) in the US in 2015 (3,4). No data have been released that correct these estimates for the measurement errors caused by the imperfect sensitivity and specificity of surveillance definitions (3,4,6). Further, this likely underestimation of arthritis prevalence, especially in subjects ages 45–64 years, has suggested that prevalence in this age group is low at a time when other studies noted a marked increase in the rates of knee and hip replacement in this age group (7).

Strategies exist to increase the accuracy of surveillance criteria, such as combining the results of multiple individual diagnostic criteria. For example, one diagnostic criterion could be based on a self-reported diagnosis of arthritis from a health professional. Another diagnostic criterion could be self-reported symptoms that are consistent with arthritis. Questions about chronic joint symptoms are in fact included in the NHIS, and the Sacks et al (5) validation study reported that some subjects with chronic joint symptoms who did not report having doctor-diagnosed arthritis had a clinical diagnosis of arthritis. Nonetheless, chronic joint symptoms have not been used in combination with doctor-diagnosed arthritis to derive national estimates of arthritis prevalence. While self-reported doctor-diagnosed arthritis has an acceptable specificity (i.e., 81.1%) for arthritis in adults ages ≥ 65 years (5), many persons younger than 65 years of age did not report receiving a diagnosis from a health professional despite reporting chronic joint symptoms.

In this study, we developed a Bayesian model to estimate the prevalence of arthritis among adults in the US in 2015, that is, an estimate adjusted for the measurement errors due to the imperfect accuracy of surveillance criteria based on both the report of chronic joint symptoms and doctor-diagnosed arthritis. We used the term “adjusted prevalence,” in contrast to “unadjusted prevalence,” for our measurement error–corrected prevalence estimates (8–13). We note that an adjusted prevalence estimate obtained using a survey is not equivalent to the exact number of rheumatologist-verified arthritis cases, even though the survey questions were actually validated against such cases, but we use the word “adjusted” to suggest that we are correcting estimates for the systematic underestimation of prevalence that occurs when surveillance instruments with imperfect sensitivity are used.

PATIENTS AND METHODS

Study setting and data. We obtained the most recent publicly available Sample Adult Core from the 2015 NHIS data release, which contains data for individuals ages 18 years and older. The NHIS, which is routinely used to derive national

estimates of arthritis prevalence, is one of the most prominent population health surveys that covers the noninstitutionalized population in the US; it excludes those in long-term care facilities, active duty armed forces personnel, and US nationals living in a foreign country.

As noted in the study by Sacks et al (5), the National Arthritis Data Workgroup suggested that “arthritis” be broadly defined as a condition with clinical significance that is either symptomatic or requires attention from a health professional for treatment. The purpose of the definition, which excluded injuries, was to have a practical method to estimate the burden and impact of arthritis. For example, a case of asymptomatic radiographic osteoarthritis resulting from a previous injury was not considered clinically significant, nor were asymptomatic Heberden’s nodes.

In our study, identical to the definition used by the CDC, a case of doctor-diagnosed arthritis was defined as a positive response to the NHIS survey question, “Have you ever been told by a doctor or other health professional that you have some form of arthritis, rheumatoid arthritis, gout, lupus, or fibromyalgia?” In addition to doctor-diagnosed arthritis, the NHIS included a separate set of questions designed to identify those with chronic joint symptoms, defined as participants who gave a positive response to the question, “The next questions refer to your joints. Please do not include the back or neck. During the past 30 days, have you had any symptoms of pain, aching, or stiffness in or around a joint?” Moreover, if the person reported recent chronic joint symptoms, they were asked the follow-up question, “Did your joint symptoms first begin more than 3 months ago?” We developed surveillance criteria based on the 3 questions that were used to define doctor-diagnosed arthritis, chronic joint symptoms, and whether the duration of symptoms exceeded 3 months.

Surveillance criteria. We considered each of the 3 questions described in the previous section as a diagnostic test with imperfect accuracy for arthritis. The answer to the third question regarding the duration of symptoms was only available (i.e., positive or negative) if the person reported the existence of recent chronic joint symptoms. Therefore, the data consisted of frequencies corresponding to one of the 6 possible realizations of test outcomes (yes/yes/yes, yes/no/null, yes/yes/no, no/yes/yes, no/no/null, or no/yes/no) for doctor-diagnosed arthritis, chronic joint symptoms, and duration of symptoms, respectively. The null value indicates that the value for the duration of symptoms was not available due to a negative response to the recent chronic joint symptoms criterion. We further stratified the results of the surveillance criteria into 4 subpopulations based on sex and the age groups 18–64 years and ≥ 65 years (Table 1).

Model. We developed a Bayesian multinomial latent class model for the 6 realizations of test outcomes in the 4 subpopulations presented in Table 1. Bayesian latent class models have previously been used in a variety of models for diagnostic test outcomes when a perfect reference standard is not available (8–21). Latent class models do not require the true disease status of each subject to be known (i.e., observed) in order to estimate prevalence and measures of diagnostic accuracy (12,13). The multinomial probabilities corresponding to the observed frequencies of surveillance criteria were defined as functions of true prevalence and the sensitivity and specificity of each criterion, as described by Branscum et al (9) and others (10). For example, the probability of observing (yes/yes/yes) frequency is a product of the true arthritis prevalence and the sensitivities of the 3 criteria in the surveillance definition, which is the

Table 1. Cross-classified outcomes of arthritis surveillance criteria based on doctor-diagnosed arthritis, chronic joint symptoms, and symptom duration*

	No. (%)	Doctor's diagnosis, no. (%)	Chronic joint symptoms without doctor's diagnosis, no. (%)	Total, no. (%) (n = 33,672)
Ages 18–64 years				
Men		1,740 (15.0)	2,242 (19.3)	11,597 (34.4)
DDx/CJS/S-3M				
yes/yes/yes	1,260 (3.7)	–	–	–
yes/no/null	405 (1.2)	–	–	–
yes/yes/no	75 (0.2)	–	–	–
no/yes/yes	1,849 (5.5)	–	–	–
no/no/null	7,615 (22.6)	–	–	–
no/yes/no	393 (1.2)	–	–	–
Women		2,734 (20.0)	2,294 (16.7)	13,697 (40.7)
DDx/CJS/S-3M				
yes/yes/yes	2,002 (5.9)	–	–	–
yes/no/null	608 (1.8)	–	–	–
yes/yes/no	124 (0.4)	–	–	–
no/yes/yes	1,856 (5.5)	–	–	–
no/no/null	8,669 (25.7)	–	–	–
no/yes/no	438 (1.3)	–	–	–
Ages ≥65 years				
Men		1,511 (43.5)	545 (15.7)	3,474 (10.3)
DDx/CJS/S-3M				
yes/yes/yes	980 (2.9)	–	–	–
yes/no/null	469 (1.4)	–	–	–
yes/yes/no	62 (0.2)	–	–	–
no/yes/yes	477 (1.4)	–	–	–
no/no/null	1,418 (4.2)	–	–	–
no/yes/no	68 (0.2)	–	–	–
Women		2,704 (55.1)	660 (13.5)	4,904 (14.6)
DDx/CJS/S-3M				
yes/yes/yes	1,958 (5.8)	–	–	–
yes/no/null	608 (1.8)	–	–	–
yes/yes/no	138 (0.4)	–	–	–
no/yes/yes	581 (1.7)	–	–	–
no/no/null	1,540 (4.6)	–	–	–
no/yes/no	79 (0.2)	–	–	–

* The null value indicates that the criterion symptom duration longer than 3 months (S-3M) was not applicable due to a negative response to the question regarding recent chronic joint symptoms (CJS). DDx = doctor-diagnosed arthritis.

true-positive fraction plus the product of the prevalence of true nonarthritis (i.e., $1 -$ the prevalence of true arthritis) and the false-positive fraction ($1 -$ the specificity of each criterion). All multinomial probabilities corresponding to observed frequencies are enumerated in the Supplementary Materials, available on the *Arthritis & Rheumatology* web site at <http://onlinelibrary.wiley.com/doi/10.1002/art.40355/abstract>.

As shown in the validation study by Sacks et al (5) and in other studies (17,22), the sensitivity of a diagnostic test is often higher when it is applied to a population with higher prevalence (in this case, this would be true of older versus younger subjects). This occurs in part because there tends to be more severe disease in a high-prevalence population (17,23). In general, the diagnostic specificity, the probability of a negative outcome in a truly healthy (i.e., non-diseased) population, where the prevalence remains constant at 0, is less variable across non-diseased populations. To obtain a more robust estimate for arthritis prevalence (15,17), we allowed the sensitivity of the surveillance criteria to differ across the 4 subpopulations of men ages 18–64 years, women ages 18–64 years, men ages ≥65 years, and women ages ≥65 years. In an alternative parameterization

for the purpose of sensitivity analysis, we assumed the sensitivity of the surveillance criteria to be the same among men and women, per estimates by Sacks et al (5), but to be different only by age (i.e., higher sensitivity for the older population). The alternative parameterization involves fewer parameters to be estimated with the same degrees of freedom (i.e., 2 sensitivities for each criterion instead of 4 sensitivities for each criterion in the primary model). The number of parameters and degrees of freedom affect model identifiability, as discussed below.

The diagnostic specificity of criteria can be increased by serial interpretation of individual criteria results, that is, considering criteria positive when all individual components are positive. On the other hand, parallel interpretation of diagnostic criteria, that is, considering criteria positive when any individual component is positive, results in increased diagnostic sensitivity at the expense of reduced specificity. Similarly, sequential interpretation of criteria, where an individual criterion result is available only if another criterion is positive or negative, could result in improved sensitivity or specificity. Since subjects with symptoms such as pain are more likely to seek a health professional and receive a diagnosis of arthritis, we included conditional covariances, as described

by Dendukuri and Joseph (24), to account for the potential dependence between the outcomes for doctor-diagnosed arthritis and chronic joint symptoms. Conditional dependence affects the joint-testing sensitivity and specificity because the sensitivity (or specificity) of a test would not be independent of the outcome of another test (25). A positive dependence between the sensitivities of the 2 tests occurs when the sensitivity of one test is lower among truly diseased subjects who have negative results on the other test and vice versa. Consequently, a positive or negative dependence between the sensitivities of 2 diagnostic criteria increases or decreases, respectively, serial joint-testing sensitivity. Similarly, a dependence between test specificities affects joint-testing accuracy (25).

Bayesian inference and priors. We used a Bayesian approach (26) to estimate the parameters of the multinomial latent class model for cross-classified outcomes of the arthritis surveillance criteria. In this approach, probability distributions are specified for model parameters, which consisted of the arthritis prevalences for the 4 subpopulations, the sensitivities and specificities of the surveillance criteria, and the conditional covariances between the outcomes of the doctor-diagnosed arthritis and chronic joint symptoms criteria. These probability distributions are referred to as priors and are elicited from past knowledge or expert opinion, or specified to be noninformative when every possible value of the parameter is defined to have an equal probability of occurring. The prior distributions are updated with the observed data to obtain posterior distributions for the parameters of the model using Markov chain Monte Carlo techniques (26). The Monte Carlo-based posterior distributions are then summarized as the mean, median, or mode and the 2.5th and 97.5th percentiles of the Monte Carlo samples as Bayesian 95% probability intervals (95% PIs). For a description of prior elicitation and all the priors specified for the parameters of the multinomial model, see the Supplementary Materials, including Supplementary Table 1, available on the *Arthritis & Rheumatology* web site at <http://onlinelibrary.wiley.com/doi/10.1002/art.40355/abstract>.

In latent class models, non-identifiability occurs when the model cannot guarantee a unique set of parameter estimates, often due to insufficient degrees of freedom (27). Non-identifiability can be mitigated with proper informative priors or by putting constraints on priors in Bayesian analysis (15,27,28). Hence, we ordered priors on prevalences and sensitivities in the subpopulations such that the prior distribution mean was higher in the older population than the younger population and higher in women than in men.

Bayesian analysis was performed using JAGS software (29) version 4.2.0 through rjags package (30) version 4-6 in R software (31) version 3.3.3. Beta priors were elicited using epiR package (32) version 0.9-79 in R. The program code for running Bayesian computations was adapted from the study by Branscum et al (9).

RESULTS

Table 1 presents the cross-classified outcomes of the arthritis surveillance criteria for 33,672 participants in the 2015 NHIS. In subjects ages 18–64 years, 19.3% of men (2,242 of 11,597) and 16.7% of women (2,294 of 13,697) responded “yes” to the question on chronic joint symptoms, regardless of whether symptom duration

exceeded 3 months, but responded “no” to the question of whether they had ever received a diagnosis of arthritis from a doctor (Table 1). Among those ages ≥ 65 years, 15.7% of men (545 of 3,474) and 13.5% of women (660 of 4,904) responded “yes” to the question on chronic joint symptoms, regardless of symptom duration, without a concurrent report of doctor-diagnosed arthritis (Table 1).

The proportion who responded “yes” to having doctor-diagnosed arthritis, with or without a concurrent report of chronic joint symptoms or symptom duration longer than 3 months if applicable, was 15.0% of men ages 18–64 years (1,740 of 11,597), 20.0% of women ages 18–64 years (2,734 of 13,697), 43.5% of men ages ≥ 65 years (1,511 of 3,474), and 55.1% of women ages ≥ 65 years (2,704 of 4,904) (Table 1).

Posterior probability estimates and the corresponding 95% PIs for the measurement error–adjusted prevalences in the 4 subpopulations stratified by age and sex are presented in Table 2. The posterior median for the adjusted prevalence of arthritis based on the primary model was 29.9% (95% PI 23.4–42.3) in men ages 18–64 years, 31.2% (95% PI 25.8–44.1) in women ages 18–64 years, 55.8% (95% PI 49.9–70.4) in men ages ≥ 65 years, and 68.7% (95% PI 62.1–79.9) in women ages ≥ 65 years. The results of the sensitivity analysis that used identical values for sensitivity of the criteria in men and women suggested estimates similar to the results of the primary analysis (i.e., with overlapping 95% PIs) (Table 2).

The accuracy of the surveillance criteria is provided in Table 3. The results suggested that the doctor-diagnosed arthritis criterion had very low sensitivity in subjects ages 18–64 years, and that the symptom duration criterion had the highest sensitivity across all age and sex strata, despite having the lowest specificity. Thus, a substantial fraction of the population with arthritis, who are between 18 and 64 years of age, but are misclassified as

Table 2. Posterior probability estimates for the measurement error–adjusted prevalence of arthritis among US adults in 2015*

	Model with distinct sensitivity for 4 subpopulations stratified by age and sex	Model with identical sensitivity for men and women, and distinct sensitivity by age
Ages 18–64 years		
Men	29.9 (23.4–42.3)	24.3 (18.3–32.3)
Women	31.2 (25.8–44.1)	34.0 (25.8–44.5)
Ages ≥ 65 years		
Men	55.8 (49.9–70.4)	57.9 (50.6–65.3)
Women	68.7 (62.1–79.9)	75.8 (66.6–84.6)

* Values are the posterior median probability (%) (95% probability interval). Adjusted prevalence, in contrast to unadjusted prevalence, is the estimate that is corrected for the measurement errors as a result of imperfect sensitivity and specificity of the surveillance criteria.

Table 3. Accuracy measures for the arthritis surveillance criteria*

Criterion	Model with distinct sensitivity for 4 subpopulations stratified by age and sex	Model with identical sensitivity for men and women, and distinct sensitivity by age
Doctor-diagnosed arthritis		
Sensitivity		
Ages 18–64 years		
Men	22.0 (11.1–48.3)	50.0 (39.0–64.2)
Women	34.1 (24.3–62.3)	50.0 (39.0–64.2)
Ages ≥65 years		
Men	67.9 (59.4–76.1)	71.5 (64.5–80.5)
Women	74.9 (67.4–82.0)	71.5 (64.5–80.5)
Specificity	87.2 (82.5–96.1)	95.8 (94.2–97.2)
Chronic joint symptoms		
Sensitivity		
Ages 18–64 years		
Men	62.7 (43.6–72.5)	46.8 (38.2–60.3)
Women	64.9 (46.1–73.9)	46.8 (38.2–60.3)
Ages ≥65 years		
Men	69.1 (55.5–75.4)	64.2 (59.7–70.2)
Women	74.1 (64.9–80.5)	64.2 (59.7–70.2)
Specificity	83.3 (75.1–91.8)	74.8 (72.1–77.3)
Symptom duration >3 months		
Sensitivity		
Ages 18–64 years		
Men	87.4 (79.5–94.4)	94.1 (93.3–94.9)
Women	88.8 (80.4–94.7)	94.1 (93.3–94.9)
Ages ≥65 years		
Men	93.1 (89.1–94.9)	94.3 (93.6–95.1)
Women	93.4 (90.8–95.1)	94.3 (93.6–95.1)
Specificity	15.2 (1.6–51.3)	18.8 (17.5–20.7)

* Values are the posterior median probability (%) (95% probability interval).

healthy by the doctor-diagnosed arthritis criterion due to low sensitivity, are captured by the 2 remaining questions on joint pain, aching, or stiffness.

Finally, the estimated number of adults with arthritis in the US, based on the 2015 National Population Projections provided by the US Census Bureau (33), was 91.2 million individuals (of the 247.7 million total projected population; 36.8%), which included 29.8 million men ages 18–64 years, 11.8 million men ages ≥65 years, 31.3 million women ages 18–64 years, and 18.3 million women ages ≥65 years.

DISCUSSION

Using NHIS data, we developed an arthritis surveillance definition by which to estimate the measurement error-adjusted prevalence of arthritis in the US, based on 3 criteria with imperfect accuracy, i.e., doctor-diagnosed arthritis, chronic joint symptoms, and symptom duration longer than 3 months. Our estimate suggested that 91.2 million adults in the US (36.8%) were affected by arthritis in 2015. Our results suggested that the adjusted prevalence of arthritis, doctor-diagnosed or otherwise, is substantially higher than a previously reported uncorrected estimate of the prevalence of doctor-diagnosed arthritis of 54.4 million

adults in the US (22.7%) (4) and also higher than the estimate of the adjusted prevalence of doctor-diagnosed arthritis of 52.9 million adults (21.4%) (34). Further, we estimated that 61.1 million adults between the ages of 18 and 64 years (of 199.9 million total adults ages 18–64 years; 30.6%) in the US had arthritis in 2015.

The higher prevalence that we report is due in large part to the previous underestimate of arthritis in adults ages 18–64 years. Recent reports have suggested a marked increase in total knee replacement utilization, especially in the population 45–64 years of age, that has outpaced the increasing rate of obesity in the same age group (7). Another study demonstrated higher arthritis prevalence in more recent birth cohorts, compared to previous generations of the same age, partly due to changing patterns of obesity in relatively younger populations (35). Individuals younger than 65 years of age may perceive arthritis as a condition affecting only the elderly and thus may visit a health professional less often or may ignore occasional joint symptoms. Moreover, arthritis may not be reported on electronic health records or insurance claims data if arthritis is not the primary reason for a referral to a health care provider. A previous study noted that of the total of 13.7% of adults (6,064 of 44,326) in the 2005 NHIS data who had chronic joint symptoms but

no indication of doctor-diagnosed arthritis, 89.1% were younger than 65 years of age (36), compared to 79.0% (4,536 of 5,741) in our study population in 2015 (Table 1).

Previous studies that either supported (37,38) or opposed (36) the addition of chronic joint symptoms to an arthritis surveillance definition, through creating a pseudo-gold standard based on other criteria such as functional or activity-limiting factors or any other indication of arthritis, are subject to the same flaws and limitations of relying on an imperfect surveillance definition. In contrast, our latent class analytic approach did not rely on the assumption of having a perfect reference standard (i.e., a gold standard) and did not require us to identify the true arthritis status of each individual in the population in order to estimate the measurement error-adjusted prevalence (8,39).

The question on doctor-diagnosed arthritis in the NHIS includes fibromyalgia among the conditions under the arthritis rubric. While fibromyalgia can cause joint pain and lead to a diagnosis by a health professional, it is not a form of arthritis. Consequently, inclusion of fibromyalgia resulted in an imperfect specificity for the doctor-diagnosed arthritis criterion, which affected the uncorrected estimates for the prevalence reported in previous studies (2–4); however, this inclusion did not affect our estimates for the adjusted prevalence because we had already corrected our estimate for the imperfect specificity of the doctor-diagnosed arthritis criterion. Conversely, absence of osteoarthritis, the most prevalent form of arthritis, from the NHIS question on doctor-diagnosed arthritis results in an imperfect sensitivity for the doctor-diagnosed arthritis criterion and subsequently affected uncorrected estimates for the prevalence in previous reports (2–4).

In addition to problems with measurement errors, there are shortcomings in the reliance of the previously published (3,4) national estimates of arthritis prevalence on a single survey question regarding doctor-diagnosed arthritis. Implicit in the question on doctor-diagnosed arthritis, when the response is positive, is that the surveyed individual sought or had access to medical care from a health professional. However, a negative response to the doctor-diagnosed arthritis question could be the result of either lack of medical attention to joint symptoms or a truly negative diagnosis with regard to arthritis. Moreover, an individual who is diagnosed as having arthritis by a health professional may never be explicitly informed of the diagnosis.

The chronic joint symptoms question does not require pain on more than half of days and could represent mild or moderate joint pain. We note that the validation study by Sacks et al (5) reported the sensitivity and specificity of these questions for subjects who were ages 45–64 years. We generalized these estimates to those ages

18–64 years, and it is conceivable that our arthritis prevalence estimates for persons ages 18–44 years are off if these estimates of sensitivity and specificity are imprecise. However, our Bayesian approach mitigated this potential inaccuracy by specifying diffuse prior distributions that covered a wide range of sensitivity and specificity values, in contrast to a frequentist approach, in which these values are assumed to be fixed.

The NHIS has a complex survey sample design, and our approach did not use a weighting scheme to estimate prevalence. There are conceptually competing and fundamentally distinct approaches to making “inferences” from complex surveys, which include the classical design-based (randomization-based) approach that uses a weighting scheme, as described by Neyman (40), and our model-based approach that relies on developing statistical models to infer population parameters. While weights are useful for “designing” a cost-effective survey sample, their use in inference after survey data are collected is debated in statistical literature because relying on weighting alone may fail to sufficiently account for other factors that influence the accuracy of estimation, such as misclassification. Weights are not attributes of the individuals or a particular disease under study, but are constructed as a product of probability calculations to correct for the perceived differences between a sample and a target population based on “design” variables such as age, sex, or location (41).

There is a large body of statistical literature on the philosophical and fundamental differences between the design-based and the model-based approaches (see, for example, refs. 41–43). Some argue that reliance on a general framework to calculate weights, which requires many arbitrary choices on weighting factor, pooling, or truncation of weights, does not provide much benefit over using a model-based approach to directly estimate parameters of interest, especially when auxiliary data are available (i.e., accuracy of survey questions) or when faced with biases unrelated to sampling weights, such as measurement error. While the federal agencies have historically produced statistical summaries using the design-based approach (44), the US Census Bureau recently formed a Research and Methodology Directorate to more effectively utilize model-based approaches for inference in official statistics by federal agencies (43). Our approach was based on a model to adjust for the sensitivities and specificities of the test’s performance in the 4 subpopulations identified by sex and age. We acknowledge that the inability to directly apply weighting in our model-based approach may have introduced inaccuracy with regard to the precision of our estimates (i.e., wider PIs for the probability of true population parameters), but the gain in

accuracy with regard to misclassification bias is so substantial that we believe it justifies our choice.

The validity of our Bayesian inference relies on the correct specification and estimation of the underlying probability distributions that generated the observed frequencies of the NHIS questions' outcomes in the 4 sub-populations shown in Table 1. Our modeling approach does not specify distinct priors on the diagnostic sensitivity and specificity of the NHIS questions across states, because the validation study by Sacks et al (5) did not provide evidence that the accuracy of NHIS questions varied by state. Therefore, regardless of the sampling unit from which an individual was selected, for example, Massachusetts versus New York, the probability of observing a specific realization of outcomes for the NHIS questions for an individual relies only on whether the individual has arthritis, and the sensitivities and specificities of the questions.

Our model-based approach provides several advantages over previous studies that did not correct for measurement errors (2–4). In addition to directly applying the sensitivity and specificity of NHIS survey questions to our estimates, we allowed the correlation (i.e., conditional dependence) between responses to survey questions to be formally incorporated to get corrected estimates. Further, the Bayesian approach provided a coherent framework for model-based re-validation (i.e., that does not rely on a gold standard) of the findings of the Sacks et al (5) study, through updating the sensitivities and specificities of the survey questions from the validation study with the 2015 NHIS data, to obtain posterior probabilities (i.e., re-validated estimates), which we presented in Table 3.

The underlying rheumatic diseases resulting in arthritis are diverse. While our inference was limited to aggregate-level population surveillance on the burden of arthritis, further studies are needed to evaluate potential changes in the specific causes of arthritis, especially among adults younger than 65 years of age. Arthritis causes enormous economic and public health implications. Direct health care costs and long-term indirect costs resulting from loss of productivity and disability attributable to arthritis need be revised to account for the corrected prevalence of arthritis affecting individuals at younger ages than previously perceived (1,45).

AUTHOR CONTRIBUTIONS

All authors were involved in drafting the article or revising it critically for important intellectual content, and all authors approved the final version to be published. Dr. Jafarzadeh had full access to all of the data in the study and takes responsibility for the integrity of the data and the accuracy of the data analysis.

Study conception and design. Jafarzadeh, Felson.

Acquisition of data. Jafarzadeh.

Analysis and interpretation of data. Jafarzadeh, Felson.

REFERENCES

1. Cisternas MG, Murphy LB, Yelin EH, Foreman AJ, Pasta DJ, Helmick CG. Trends in medical care expenditures of US adults with arthritis and other rheumatic conditions 1997 to 2005. *J Rheumatol* 2009;36:2531–38.
2. Hootman JM, Helmick CG. Projections of US prevalence of arthritis and associated activity limitations. *Arthritis Rheum* 2006; 54:226–9.
3. Hootman JM, Helmick CG, Barbour KE, Theis KA, Boring MA. Updated projected prevalence of self-reported doctor-diagnosed arthritis and arthritis-attributable activity limitation among US adults, 2015–2040. *Arthritis Rheumatol* 2016;68:1582–7.
4. Barbour KE, Helmick CG, Boring M, Brady TJ. Vital signs: prevalence of doctor-diagnosed arthritis and arthritis-attributable activity limitation: United States, 2013–2015. *MMWR Morb Mortal Wkly Rep* 2017;66:246–53.
5. Sacks JJ, Harrold LR, Helmick CG, Gurwitz JH, Emani S, Yood RA. Validation of a surveillance case definition for arthritis. *J Rheumatol* 2005;32:340–7.
6. Murphy LB, Cisternas MG, Greenlund KJ, Giles W, Hannan C, Helmick CG. Defining arthritis for public health surveillance: methods and estimates in four US population health surveys. *Arthritis Care Res (Hoboken)* 2017;69:356–67.
7. Losina E, Thornhill TS, Rome BN, Wright J, Katz JN. The dramatic increase in total knee replacement utilization rates in the United States cannot be fully explained by growth in population size and the obesity epidemic. *J Bone Joint Surg Am* 2012;94: 201–7.
8. Branscum AJ, Gardner IA, Johnson WO. Bayesian modeling of animal- and herd-level prevalences. *Prev Vet Med* 2004;66:101–12.
9. Branscum AJ, Gardner IA, Johnson WO. Estimation of diagnostic-test sensitivity and specificity through Bayesian modeling. *Prev Vet Med* 2005;68:145–63.
10. Ladouceur M, Rahme E, Pineau CA, Joseph L. Robustness of prevalence estimates derived from misclassified data from administrative databases. *Biometrics* 2007;63:272–9.
11. Messam LL, Branscum AJ, Collins MT, Gardner IA. Frequentist and Bayesian approaches to prevalence estimation using examples from John's disease. *Anim Health Res Rev* 2008;9:1–23.
12. Collins J, Huynh M. Estimation of diagnostic test accuracy without full verification: a review of latent class methods. *Stat Med* 2014;33:4141–69.
13. Kostoulas P, Nielsen SS, Branscum AJ, Johnson WO, Dendukuri N, Dhand NK, et al. STARD-BLCM: standards for the reporting of diagnostic accuracy studies that use Bayesian latent class models. *Prev Vet Med* 2017;138:37–47.
14. Joseph L, Gyorkos TW, Coupal L. Bayesian estimation of disease prevalence and the parameters of diagnostic tests in the absence of a gold standard. *Am J Epidemiol* 1995;141:263–72.
15. Johnson WO, Gastwirth JL, Pearson LM. Screening without a "gold standard": the Hui-Walter paradigm revisited. *Am J Epidemiol* 2001;153:921–4.
16. Berkvens D, Speybroeck N, Praet N, Adel A, Lesaffre E. Estimating disease prevalence in a Bayesian framework using probabilistic constraints. *Epidemiology* 2006;17:145–53.
17. Johnson WO, Gardner IA, Metoyer CN, Branscum AJ. On the interpretation of test sensitivity in the two-test two-population problem: assumptions matter. *Prev Vet Med* 2009;91:116–21.
18. Jafarzadeh SR, Johnson WO, Utts JM, Gardner IA. Bayesian estimation of the receiver operating characteristic curve for a diagnostic test with a limit of detection in the absence of a gold standard. *Stat Med* 2010;29:2090–106.

19. Jafarzadeh SR, Warren DK, Nickel KB, Wallace AE, Mines D, Fraser VJ, et al. Bayesian estimation of the accuracy of ICD-9-CM- and CPT-4-based algorithms to identify cholecystectomy procedures in administrative data without a reference standard. *Ann Epidemiol* 2013;23:592.
20. Jafarzadeh SR, Johnson WO, Gardner IA. Bayesian modeling and inference for diagnostic accuracy and probability of disease based on multiple diagnostic biomarkers with and without a perfect reference standard. *Stat Med* 2016;35:859–76.
21. Jafarzadeh SR, Thomas BS, Gill J, Fraser VJ, Marschall J, Warren DK. Sepsis surveillance from administrative data in the absence of a perfect verification. *Ann Epidemiol* 2016;26:717–22.e1.
22. Jafarzadeh SR. Bayesian methods for evaluation of diagnostic accuracy of quantitative tests and disease diagnosis in the absence of a perfect reference standard with examples from John's disease [dissertation]. Davis (CA): University of California; 2012.
23. Greiner M, Gardner IA. Epidemiologic issues in the validation of veterinary diagnostic tests. *Prev Vet Med* 2000;45:3–22.
24. Dendukuri N, Joseph L. Bayesian approaches to modeling the conditional dependence between multiple diagnostic tests. *Biometrics* 2001;57:158–67.
25. Gardner IA, Stryhn H, Lind P, Collins MT. Conditional dependence between tests affects the diagnosis and surveillance of animal diseases. *Prev Vet Med* 2000;45:107–22.
26. Christensen R, Johnson WO, Branscum AJ, Hanson TE. Bayesian ideas and data analysis: an introduction for scientists and statisticians. 1st ed. CRC Press; 2010.
27. Jones G, Johnson WO, Hanson TE, Christensen R. Identifiability of models for multiple diagnostic testing in the absence of a gold standard. *Biometrics* 2010;66:855–63.
28. Georgiadis MP, Johnson WO, Gardner IA, Singh R. Correlation-adjusted estimation of sensitivity and specificity of two diagnostic tests. *J R Stat Soc Ser C Appl Stat* 2003;52:63–76.
29. Plummer M. JAGS version 4.2.0 user manual. Lyon, France: International Agency for Research on Cancer; 2016.
30. Plummer M, Stukalov A, Denwood M. rjags: Bayesian graphical models using MCMC. 2016. URL: <https://cran.r-project.org/web/packages/rjags/index.html>.
31. R Core Team. R: a language and environment for statistical computing. Vienna, Austria: R Foundation for Statistical Computing. 2017. URL: <http://www.r-project.org>.
32. Stevenson M, Nunes T, Heuer C, Marshall J, Sanchez J, Thornton R, et al. epiR: tools for the analysis of epidemiological data. 2016. URL: <https://cran.r-project.org/web/packages/epiR/index.html>.
33. Colby SL, Ortman JM, for the US Census Bureau. Projections of the size and composition of the U.S. population: 2014 to 2060. March 3, 2015. URL: <https://www.census.gov/library/publications/2015/demo/p25-1143.html>.
34. Jafarzadeh SR, Felson DT. Corrected estimates for the prevalence of self-reported doctor-diagnosed arthritis among US adults [letter]. *Arthritis Rheumatol* 2017;69:1701–2.
35. Badley EM, Canizares M, Perruccio AV. A population-based study of changes in arthritis prevalence and arthritis risk factors over time: generational differences and the role of obesity. *Arthritis Care Res (Hoboken)* 2017. E-pub ahead of print.
36. Bolen J, Helmick CG, Sacks JJ, Gizlice Z, Potter C. Should people who have joint symptoms, but no diagnosis of arthritis from a doctor, be included in surveillance efforts? *Arthritis Care Res (Hoboken)* 2011;63:150–4.
37. Feinglass J, Nelson C, Lawther T, Chang RW. Chronic joint symptoms and prior arthritis diagnosis in community surveys: implications for arthritis prevalence estimates. *Public Health Rep* 2003;118:230–9.
38. Busija L, Buchbinder R, Osborne RH. Quantifying the impact of transient joint symptoms, chronic joint symptoms, and arthritis: a population-based approach. *Arthritis Rheum* 2009;61:1312–21.
39. Suess EA, Gardner IA, Johnson WO. Hierarchical Bayesian model for prevalence inferences and determination of a country's status for an animal pathogen. *Prev Vet Med* 2002;55:155–71.
40. Neyman J. On the two different aspects of the representative method: the method of stratified sampling and the method of purposive selection. *J R Stat Soc* 1934;97:558–625.
41. Gelman A. Struggles with survey weighting and regression modeling. *Stat Sci* 2007;22:153–64.
42. Rao JN. Impact of frequentist and Bayesian methods on survey sampling practice: a selective appraisal. *Stat Sci* 2011;26:240–56.
43. Little RJ. Calibrated Bayes, an alternative inferential paradigm for official statistics. *J Off Stat* 2012;28:309.
44. Bell RM, Cohen ML. Struggles with survey weighting and regression modeling. *Stat Sci* 2007;22:165–7.
45. Yelin E, Murphy L, Cisternas MG, Foreman AJ, Pasta DJ, Helmick CG. Medical care expenditures and earnings losses among persons with arthritis and other rheumatic conditions in 2003, and comparisons with 1997. *Arthritis Rheum* 2007;56:1397–407.

Germinal Center B Cells Are Essential for Collagen-Induced Arthritis

Albert Dahdah,¹ Katrin Habir,¹ Kutty Selva Nandakumar,² Amit Saxena,¹ Bingze Xu,¹
Rikard Holmdahl,¹ and Stephen Malin¹

Objective. Rheumatoid arthritis (RA) is considered to be a prototypical autoimmune disorder. Several mechanisms have been proposed for the known pathologic function of B cells in RA, including antigen presentation, cytokine secretion, and humoral immunity. The aim of this study was to address the function of B lymphocytes in experimental arthritis.

Methods. We mapped the adaptive immune response following collagen-induced arthritis (CIA). We subsequently monitored these responses and disease outcomes in genetically modified mouse strains that lack mature B cell or germinal center (GC) functionality in a B cell–intrinsic manner.

Results. Following primary immunization, the draining lymph nodes broadly reacted against type II collagen (CII) with the formation of GCs and T cell activation. Mice that lacked mature B cell function were fully protected against CIA and had a severely attenuated ability to mount isotype-switched humoral immune responses against CII. Almost identical results were observed in mice that were selectively deficient in GC responses. Importantly, GC-deficient mice were fully susceptible to collagen antibody–induced arthritis.

Conclusion. We identified GC formation and anticollagen antibody production as the key pathogenic functions of B cells in CIA. The role of B cells in RA is likely to be more complex. However, targeting the GC reaction could allow for therapeutic interventions that are more refined than general B cell depletion.

Rheumatoid arthritis (RA) is a common autoimmune disease that leads to chronic destruction of the joints. Similar to what is observed in other autoimmune disorders, self-reactivity begins years before the clinical onset of RA, with the presence of circulating autoantibodies. In otherwise healthy individuals destined to develop RA, the first antibodies to appear are rheumatoid factors (RFs) (1), followed by antibodies to citrullinated proteins (2). Around the time of disease onset, a complex pattern of different antibodies is detectable, including antibodies to joint proteins such as type II collagen (CII) (3). Because these increased autoantibody levels are genetically associated with major histocompatibility complex (MHC) class II genes, it is likely that activation of autoreactive B cells is T cell dependent. The mechanisms of activation and the function of different B cell subsets remain unknown.

The use of animal models has provided important insight into the pathogenesis of RA, in particular the use of the collagen-induced arthritis (CIA) model (4). CIA invokes T cell– and B cell–mediated immune responses against CII. Antibodies recognizing CII are considered to be a central pathogenic factor in CIA, because they can bind and destabilize cartilage, forming local immune complexes that can trigger synovial cell activation and later neutrophil infiltration of the joints (5,6). Similar antibody specificities that occur in CIA can also be observed in clinical subsets of RA (7). Notably, mice that are genetically deficient in B cells and hence lack antibodies are protected against CIA (8), and B cell–depleting anti-CD20 therapy can also prevent CIA (9). The efficacy of anti-CD20 therapy in RA patients has made identifying the B

Supported by the Swedish Medical Research Council (grant to the Linné Center, Center of Excellence for Research on Inflammation and Cardiovascular Disease), the European Union Seventh Framework Programme (Health-2013-Innovation-1 Programme; project Athero-B-Cell), the Alex and Eva Wallströms Foundation, the Knut and Alice Wallenberg Foundation, the Swedish Strategic Science Foundation, and the European Union Innovative Medicine Initiative (BeTheCure grant).

¹Albert Dahdah, PhD, Katrin Habir, PhD, Amit Saxena, PhD, Bingze Xu, Rikard Holmdahl, MD, PhD, Stephen Malin, PhD: Karolinska University Hospital, Karolinska Institutet, Stockholm, Sweden; ²Kutty Selva Nandakumar, PhD: Karolinska University Hospital, Karolinska Institutet, Stockholm, Sweden, and Southern Medical University, Guangzhou, China.

Address correspondence to Stephen Malin, PhD, Karolinska Institutet, Department of Medicine, Center for Molecular Medicine, L8:03, Karolinska University Hospital, S-171 76 Stockholm, Sweden. E-mail: Stephen.malin@ki.se.

Submitted for publication June 29, 2017; accepted in revised form October 12, 2017.

cell subset(s) that mediate the disease to be of potential therapeutic interest.

A long-recognized histologic feature of RA is the presence of germinal centers (GCs) in inflamed joint tissue (10,11). GCs also form in rodents following the induction of CIA, in both the limbs and secondary lymphoid tissue (12,13). GCs are a major source of somatically mutated and class-switched antibodies, and the GC reaction generates memory B cells and plasma cells, thereby increasing the overall titers of antibodies. It has therefore been proposed that the GC reaction is an important contributor to RA (14).

Although B cells are clearly important for the development of experimental arthritis, it is currently unknown whether the formation of GCs and subsequent autoantibody production represent crucial pathogenic B cell functions. It is possible that other B cell functions in addition to humoral responses, such as antigen presentation or cytokine secretion, could be critical, as has been shown in other autoimmune diseases (15). Additionally, spleens that develop in genetically B cell-deficient mouse strains display several defects in splenic dendritic cell populations (16) that can alter T helper cell responses. Interestingly, isolated pathogenic antibodies recognizing CII have a germline configuration (17), and anti-CII antibodies with somatic mutations can be reverted to germline configuration without loss of antigen recognition (18). Furthermore, *Cd4*^{-/-} mice, which have attenuated GC responses, are still susceptible to CIA (19,20) or are only partially protected (21), whereas *Tcrb*^{-/-} (α/β T cell-deficient) mice are completely protected (22). Hence, although functional T cells are required for CIA, the requirement of B cells through GC-derived pathogenic antibody production is not known.

In this report, we present evidence that the GC reaction is absolutely required for CIA. We created novel mice that are genetically susceptible to CIA but are unable to form GCs or alternatively have largely lost mature B cell function. These mice were completely protected against CIA. Furthermore, resistance to arthritis could be bypassed through injection of pathogenic anti-CII antibodies. Thus, our findings support the proposal that B cells have a causal function in CIA via the formation of GCs, which subsequently leads to the production of pathogenic antibodies.

MATERIALS AND METHODS

Animals. All animals were housed, bred, and maintained under specific pathogen-free conditions at the animal housing facility at the Karolinska Institutet Medical Inflammation Research Unit. All mice were genetically controlled

and backcrossed onto the B6NQ mouse strain expressing the H-2^q haplotype.

The *Pax5*^{-/-} (23), *Pax5*^{fl/fl} (24), *Aicda-Cre*, and *Cd23-Cre* (25) lines have been previously described and were a kind gift from Dr. Meinrad Busslinger (Research Institute of Molecular Pathology, Vienna Biocenter, Vienna, Austria). The *Pax5*^{fl/fl}, *Pax5*^{+/-} *Aicda-Cre*, and *Pax5*^{+/-} *Cd23-Cre* mouse lines were bred and maintained independently and intercrossed together to generate experimental and control littermates. All animal experiments were performed according to valid ethics permits approved by the Stockholm Board for Animal Ethics (permit nos. N35 and N16).

CIA. CIA was initiated by injection of 100 μ g of rat CII purified from Swarm rat chondrosarcoma as previously described (26), emulsified in Freund's complete adjuvant (catalog no. 263810, lot no. 6005687; Becton Dickinson) intradermally at the base of the tail on day 0. Mice were given a second injection 35 days later with 50 μ g of CII emulsified in Freund's incomplete adjuvant. For CIA experiments, 10–12-week-old male mice were used.

Collagen antibody-induced arthritis (CAIA). CAIA was induced in 10–12-week-old male mice by intravenous injection of a 4-mg cocktail consisting of 4 monoclonal antibodies directed against different epitopes of CII (CIIC1 [an IgG2a antibody binding the C1 epitope], M1239 [an IgG2b antibody binding the J1 epitope], C2 [an IgG2b antibody binding the collagen D3 epitope], and UL1 [an IgG2b antibody binding the U1 epitope]) together with 100 μ g of lipopolysaccharide (LPS) administered intraperitoneally. On day 2 after the initial immunization, the mice received a secondary (booster) injection of LPS (100 μ g intraperitoneally).

Clinical evaluation of arthritis. After induction of arthritis, scoring of CIA was performed in a blinded manner every day or twice daily. CAIA was scored every day. Arthritis development was scored using a macroscopic scoring system. A score of 1 was given for each inflamed toe or knuckle, and a score of 5 was given for an inflamed wrist or ankle, resulting in a maximum possible score of 15 per limb and a total possible score of 60 per mouse.

Confocal microscopy preparation. Inguinal lymph node (LN) sections (10 mm thick) were fixed in ice-cold acetone and blocked with Fc Block (CD16/CD32) in phosphate buffered saline (PBS) and 0.1% bovine serum albumin prior to incubation with Alexa Fluor 488-conjugated antibody, GL7, and PerCP-conjugated IgD (11-26c.2a), and counterstaining with DAPI. Confocal images were obtained using a Leica TCS inverted microscope.

Flow cytometric analysis. Spleens and lymph nodes were fractionated to a single-cell suspension. Erythrocytes were lysed for 5 minutes at room temperature followed by an additional 5 minutes on ice with 1 ml of ACK Lysing Buffer. The following antibodies were used: CD3 ϵ (Pacific Blue-conjugated 500A2 or PerCP-conjugated 145-2C11), CD4 (allophycocyanin [APC]-H7-conjugated GK1.5), CD8 (fluorescein isothiocyanate [FITC]-conjugated 53-6.7), CD44 (phycoerythrin [PE]-conjugated IM7), CD62L (APC-conjugated MEL-14), B220 (APC-Cy7-conjugated RA3-6B2), CD19 (APC-conjugated 1D3), GL7 (APC-conjugated GL7), CD95 (PE-Cy7-conjugated Jo2), IgD (PerCP-conjugated 11-26c.2a), CD21 (FITC-conjugated 7G6), and CD23 (PE-Cy7-conjugated B3B4).

For intracellular staining, following staining for the extracellular markers, splenocytes were treated using a FoxP3/

Transcription Factor Staining Buffer Set kit (eBioscience) according to the manufacturer's protocol and stained with the intracellular antibodies FoxP3 (PE-conjugated FJK-16s) and retinoic acid receptor-related orphan nuclear receptor γ t (ROR γ t) (Brilliant Violet 421-conjugated 4B10) for 30 minutes on ice. Immune cell populations were defined as follows: B-1 cells (CD19+B220^{low}), B-2 cells (CD19+B220+), GC B cells (CD19+B220+IgD⁺GL7+CD95+ or B220+Lin[GR1+IgM+IgD+CD138+][IgG1+CII+CD19+CD38-), follicular B cells (CD19+B220+CD21^{low}CD23+), marginal zone cells (CD19+B220+CD21+CD23^{low}), memory B cells (B220+Lin-IgG1+CII+CD19+CD38+), CD4 T cells (CD3+CD4+CD8-), CD8 T cells (CD3+CD4+CD8+), naive CD4 T cells (CD3+CD4+CD8-CD44-CD62L+), activated CD4 T cells (CD3+CD4+CD8-CD44+CD62L-), FoxP3+ T cells (CD3+CD4+FoxP3+), and ROR γ t T cells (CD3+CD4+ROR γ t+). MHC class II-loaded CII peptide GalHyK264 tetramers were synthesized as previously described (27). Samples were acquired with a Dako CyAn flow cytometer (Beckman Coulter) and analyzed using FlowJo software.

Serum and immunoglobulin measurements. Plates were coated overnight with IgG heavy and light chains (2.5 μ g/ml) or CII (10 μ g/ml) in PBS at 4°C. The plates were then blocked with 1% bovine serum albumin (Sigma) in PBS for 1 hour at room temperature. Total IgG, IgM, and CII-specific antibody responses were determined by adding sample sera (diluted 1:1,000 1:5,000, 1:25,000, 1:125,000, and 1:625,000) in PBS to the various coated plates for 2 hours at room temperature.

Antibody binding was detected with alkaline phosphatase-conjugated goat anti-mouse total IgG, IgG1, or IgM and phosphatase substrate dissolved in 1M diethanolamine. Absorbance at 405 nm was measured in duplicate samples. CII-positive mouse serum (2.0–0.062 μ g/ml) was used as a standard for the CII-specific autoantibodies. SoftmaxPro software was used to determine sample concentrations, using a 4-parameter logistic regression curve.

Statistical analysis. GraphPad Prism was used for statistical analysis.

RESULTS

Kinetics of the adaptive immune response to CIA. To determine the contribution of the GC reaction to the development of CIA, we first monitored the kinetics of GC formation following immunization. We monitored the clinical scores and incidence of CIA in C57/B6N mice that express MHC class II H-2^q. The MHC class II allele A^q is required for antigen presentation of the immunodominant CII^{260–270} peptide (28). Mice received primary immunization with heterologous rat CII in complete Freund's adjuvant and secondary immunization with CII in incomplete Freund's adjuvant 35 days later (see Supplementary Figure 1, available on the *Arthritis & Rheumatology* web site at <http://onlinelibrary.wiley.com/doi/10.1002/art.40354/abstract>). Both disease incidence and disease severity were moderate prior to administration of the booster injection, with a maximum of 7 of 20 mice exhibiting arthritis symptoms. However, after secondary immunization, di-

sease severity rapidly increased, and all mice eventually developed arthritis (Figure 1A).

We next correlated the incidence and severity of disease progression with lymphocyte activation in draining inguinal LNs and spleen following primary and secondary immunizations. We observed large increases in T cell and B cell populations in the inguinal LNs following the first (primary) immunization with CII, ranging from 2.3-fold (for FoxP⁺ Treg cells) to 8.9-fold for B-2 cells. These increases were greater than those in the spleen (maximum 2.9-fold), and cell expansion in the inguinal LNs largely dissipated following secondary immunization, with subsequent 1.8-fold to 6.2-fold decreases (Figure 1B). A notable exception to this pattern was that the spleen maintained durable expansion of the B-2 cell population (~3-fold) even after secondary immunization.

To determine whether GCs contribute to the B cell expansion following CIA, the B220+CD19+IgD⁺CD95+GL7+ cell population was quantified in the spleen and inguinal LNs following primary and secondary immunizations (Figure 1C). Notably, using this definition, the only major site of GC formation was the inguinal LNs following primary the immunization. As a second approach, we quantified the number of IgG1 B cells recognizing a triple-helix epitope at position 358–369 of CII (C1 epitope) and designated them as CD19+CD38+ (memory) or CD19+CD38- (GC). Using this criterion, we confirmed that inguinal LNs are a prominent site of anti-CII GC production following primary immunization; however, the spleen also contributed to CII-reactive GC populations following immunization (Figure 1D). In summary, CII immunization induced GC formation in inguinal LNs and to a lesser extent in spleen.

Novel mouse models of B cell-intrinsic loss of GC formation. Because CII immunization promoted multiple immune responses, we next sought to determine the contribution of GC formation to disease progression. To achieve this, we constructed 2 strains in which the B cell-specific transcription factor PAX-5 is conditionally deleted. Loss of PAX-5 within the B cell lineage leads to loss of B cell identity and function (29–31). The first strain employed *Cd23-Cre*, which is expressed in transitional B cells (25) and efficiently deletes follicular and marginal zone B cells (32), as well as memory B cells, following immunization (33). The second strain is *Aicda-Cre*, which effectively deletes floxed alleles in the GC and has previously been utilized to abolish GC function (25,34). These 2 strains were additionally crossed onto a B6N.Q background to render them susceptible to CIA, and we thus generated *Pax5^{fl/-} Cd23-Cre* H-2^q and *Pax5^{fl/-} Aicda-Cre* H-2^q strains as well as relevant controls.

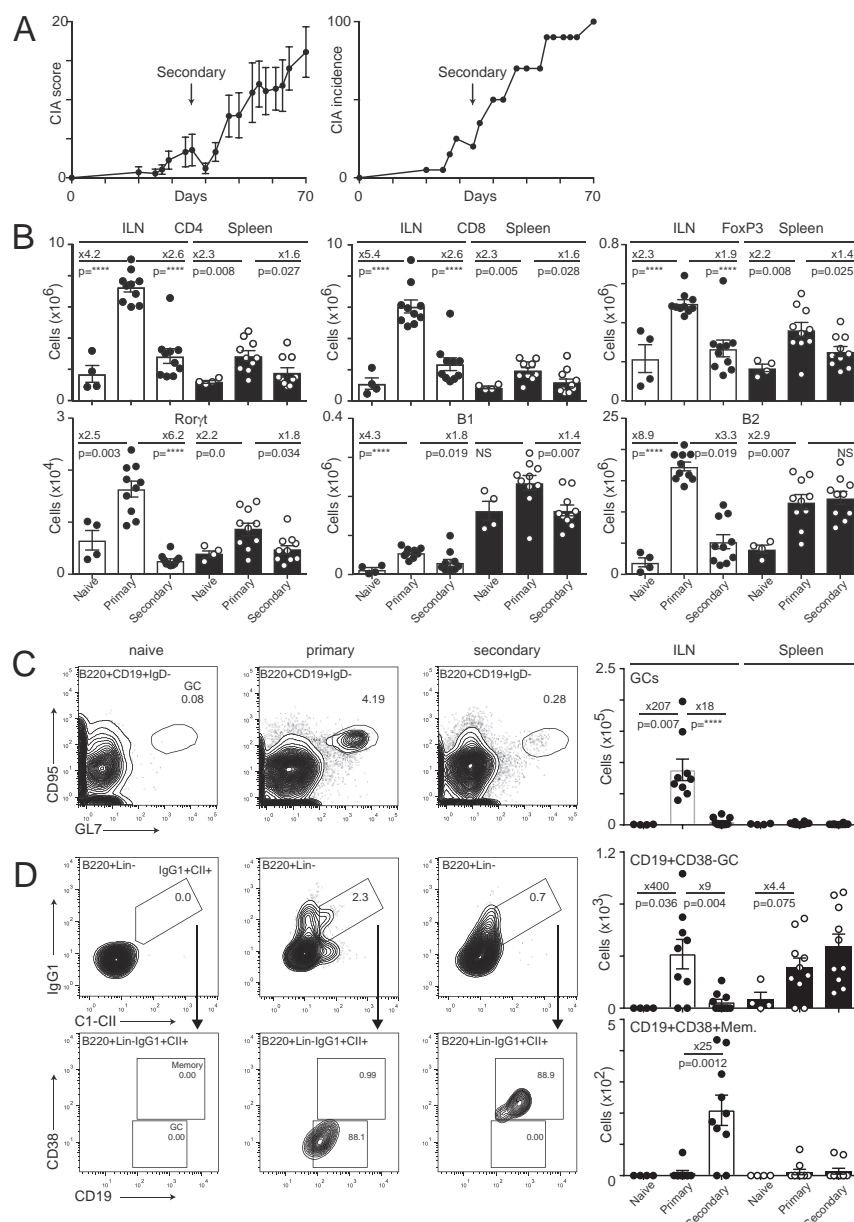


Figure 1. Adaptive immune response to collagen-induced arthritis (CIA). **A**, Clinical scores and disease incidence in B6NQ mice (n = 20) following immunization with rat type II collagen (CII) on day 0 and after secondary immunization on day 35. **B**, Absolute cell counts in the inguinal lymph nodes (ILNs) (open bars) and spleens (solid bars) of naive mice (n = 4), mice 35 days after primary immunization (n = 10), and mice 35 days after secondary immunization (n = 10). **C**, Quantification of germinal center (GC) B cells (defined as CD19+B220+IgD-GL7+CD95+). Left, Representative flow cytometry plots. Right, Absolute cell counts. Percentages are indicated for the relative gates. **D**, Quantification of collagen-binding GCs (defined as B220+Lin-IgG1+CII+CD19+CD38+) and memory (Mem.) B cells (defined as B220+Lin-IgG1+CII+CD19+CD38+). Left, Representative flow cytometry plots of inguinal LNs. Right, Absolute cell counts in inguinal LNs and spleens. In **A** (left), **B**, **C** (right), and **D** (right), bars show the mean ± SEM. The numbers above the horizontal lines are the fold change. P values were determined by t-test. **** = <0.0001. RORγt = retinoic acid receptor-related orphan nuclear receptor γt; NS = not significant.

We examined inguinal LNs and spleen on day 14 after primary immunization and on day 35 following secondary immunization with CII. This latter time point occurred during fulminant arthritis. On day 35

after administration of a booster injection, the numbers of B-1 cells were similarly increased in the *Pax5^{fl/-}* *Aicda-Cre* and *Pax5^{fl/-}* *Cd23-Cre* mice compared with controls. In the inguinal LNs, however, there was an

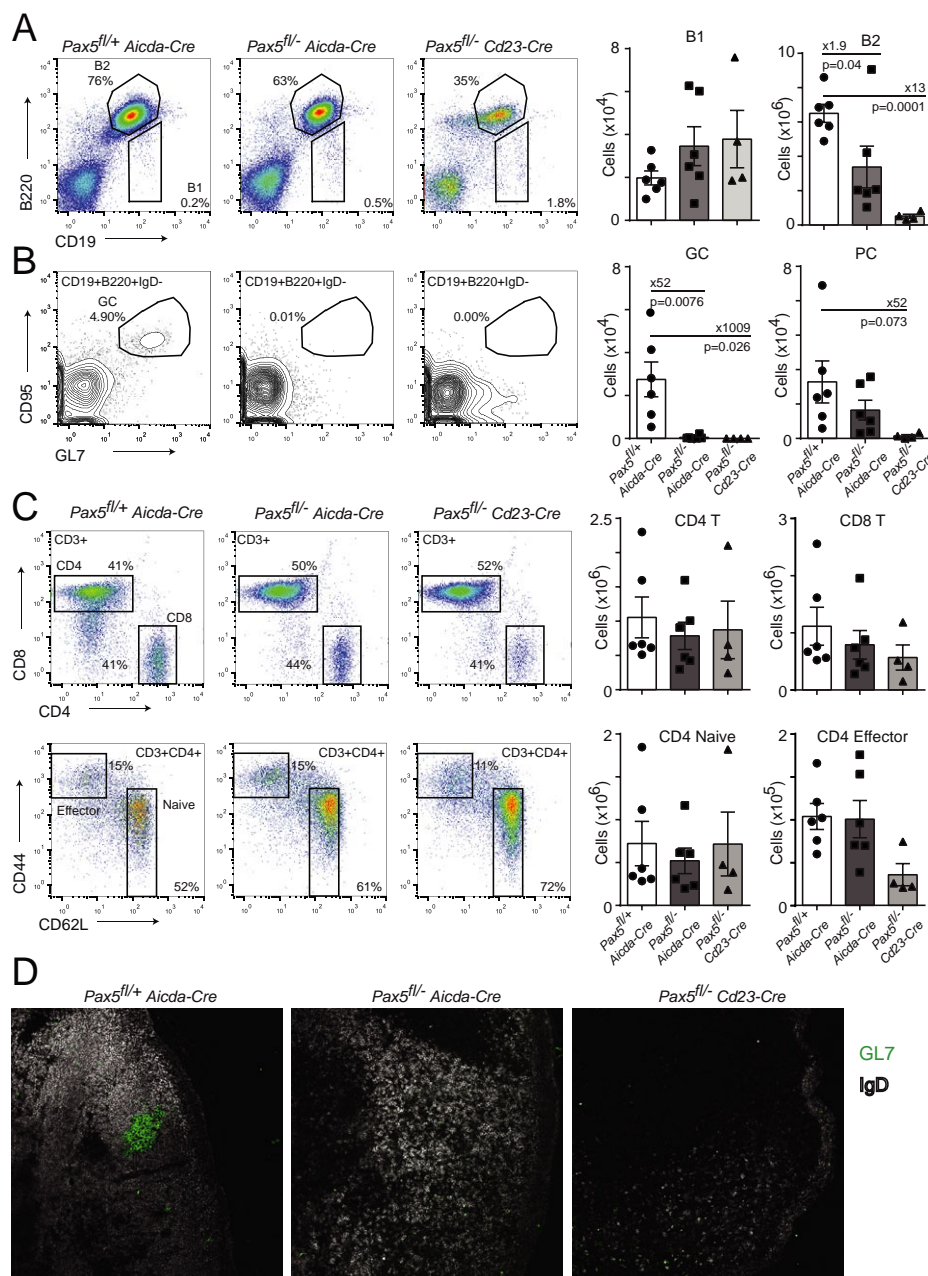


Figure 2. Characterization of GC- and B-2 cell-deleted mouse strains. **A**, Analysis of inguinal LN B cell subsets in *Pax5^{fl/+} Aicda-Cre* mice ($n = 6$), *Pax5^{fl/-} Aicda-Cre* mice ($n = 6$), and *Pax5^{fl/-} Cd23-Cre* mice ($n = 4$) 35 days after secondary immunization. Left, Representative flow cytometry plots. Right, Absolute cell counts. **B**, Flow cytometric analysis of GC B cells (defined as CD19+B220+IgD-GL7+CD95+) from the inguinal LNs of mice 35 days after secondary immunization. Left, Representative flow cytometry plots. Right, Absolute cell counts. **C**, T cell subsets in the inguinal LNs analyzed on day 35 after secondary immunization. In **A–C** (right), bars show the mean \pm SEM. The numbers above the horizontal lines in **A** and **B** are the fold change. P values were determined by t -test. **D**, Immunohistochemical analysis of inguinal LNs after secondary immunization, for detection of GCs. GL7- and B220-stained. Original magnification $\times 10$. PC = plasma cell (see Figure 1 for other definitions).

~2-fold decrease in the number of B-2 cells in *Pax5^{fl/-} Aicda-Cre* mice and a 13-fold decrease in the *Pax5^{fl/-} Cd23-Cre* strain (Figure 2A). This substantial decrease in the number of B-2 cells in the *Pax5^{fl/-} Cd23-Cre* mice was due to a loss of follicular B cells in the

inguinal LNs and a combination of follicular and marginal zone B cells in the spleen (see Supplementary Figure 2A, available on the *Arthritis & Rheumatology* web site at <http://onlinelibrary.wiley.com/doi/10.1002/art.40354/abstract>).

Strikingly, both $Pax5^{fl/-} Aicda-Cre$ and $Pax5^{fl/-} CD23-Cre$ strains completely lacked GC responses (Figure 2B) and showed reduced numbers of plasma cells (PCs) in response to CIA. In contrast to these defined B cell defects, the $Pax5^{fl/-} Aicda-Cre$ mice had normal numbers of T cells, whereas the $Pax5^{fl/-} Cd23-Cre$ mice had small decreases in the number of CD4 central effector memory cells in the inguinal LNs relative to controls (Figure 2C). In both strains, the spleen showed no T cell defects (see Supplementary Figure 2B). The selective loss of B cell function was also observed in the spleen and inguinal LNs on day 14 following primary immunization (see Supplementary Figure 3, available on the *Arthritis & Rheumatology* web site at <http://onlinelibrary.wiley.com/doi/10.1002/art.40354/abstract>).

Finally, we directly confirmed the GC defect through immunohistochemical analysis of the inguinal LNs. GL7+IgD⁺ GCs could be detected in control mice

but were absent in both $Pax5^{fl/-} Aicda-Cre$ and $Pax5^{fl/-} Cd23-Cre$ strains (Figure 2D). In summary, the $Pax5^{fl/-} Aicda-Cre$ H-2^q and $Pax5^{fl/-} Cd23-Cre$ H-2^q strains showed defective GC or B-2 cell responses, respectively, in response to CIA.

Requirement of the GC reaction for CIA. We next determined how loss of B-2 or GC subsets would impact CIA. We first compared $Pax5^{fl/+} Cd23-Cre$ with $Pax5^{fl/-} Aicda-Cre$ mice over an extended time period. $Pax5^{fl/+} Cd23-Cre$ mice developed widespread, sustained, and severe arthritis up to 94 days following administration of a secondary immunization, as previously observed in H-2^q-bearing mice (28). In contrast, $Pax5^{fl/-} Cd23-Cre$ mice were completely protected against arthritis throughout this period (Figure 3A). We next sought to determine whether this protection was attributable to a failure in GC formation. We therefore repeated the experiment and included the $Pax5^{fl/-} Aicda-Cre$ strain. Similar to the $Pax5^{fl/-} Cd23-Cre$ mice, the $Pax5^{fl/-} Aicda-Cre$ mice were

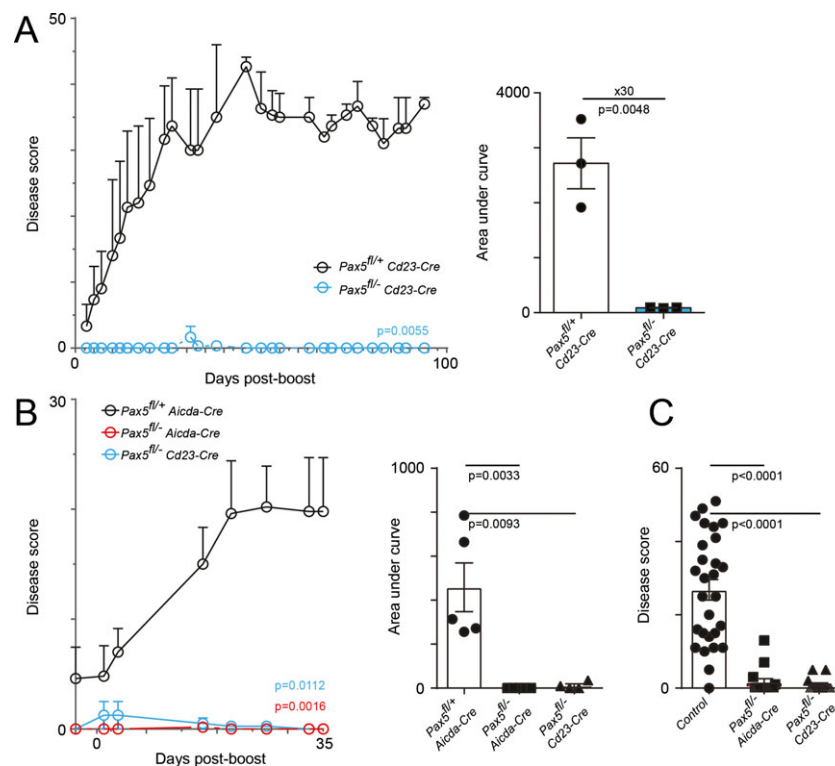


Figure 3. Absolute requirement for GCs in CIA. **A**, Left, Disease scoring was initiated following subcutaneous administration of 100 μ g of rat CII in Freund's complete adjuvant on day 0. Right, Extent of disease, as measured by the area under the curve. A second injection (50 μ g of rat CII emulsified in Freund's incomplete adjuvant) was administered 35 days later. The incidence was determined by the presence of inflammation in any of the paws or ankle. The number above the horizontal line is the fold change. **B**, Induction of arthritis in $Pax5^{fl/+} Aicda-Cre$ mice (n = 5), $Pax5^{fl/-} Aicda-Cre$ mice (n = 6), and $Pax5^{fl/-} Cd23-Cre$ mice (n = 4). **C**, Collated results from multiple experiments indicating the maximum arthritis scores in control mice (n = 28), $Pax5^{fl/-} Aicda-Cre$ mice (n = 15), and $Pax5^{fl/-} Cd23-Cre$ mice (n = 13). $Pax5^{fl/+} Aicda-Cre$, $Pax5^{fl/+} Cd23-Cre$, and B6NQ mice were used as controls. Bars show the mean \pm SEM. P values shown in the line graphs were determined by two-way analysis of variance, and P values shown in the bar graphs were determined by t-test. See Figure 1 for definitions. Color figure can be viewed in the online issue, which is available at <http://onlinelibrary.wiley.com/doi/10.1002/art.40354/abstract>.

also completely protected against CIA (Figure 3B). Finally, pooling of all control, *Pax5^{fl/-} Aicda-Cre*, and *Pax5^{fl/-} Cd23-Cre* mice from multiple experiments again showed highly significant ($P < 0.0001$) decreases in arthritis severity in experimental mice (Figure 3C). In summary, CIA was critically dependent on the formation of GCs.

Kinetics of humoral immune responses to CII.

Because GC B cells are a source of increases in specific antibody responses, we next quantified the appearance of PCs in the spleen and inguinal LNs. Similar to the B cell responses, we observed an 11-fold increase in the number of PCs (defined as B220^{low}CD19^{low}CD138⁺CD28⁺) in the inguinal LNs after primary immunization and a decrease in these numbers 35 days after secondary immunization (Figure 4A). The spleen also showed a 2-fold increase in PC numbers that, in contrast to the inguinal LNs, was maintained after administration of the booster injection. To correlate humoral responses with this PC expansion, we performed enzyme-linked immunosorbent assay (ELISA) to measure and quantify total IgG antibody levels as well as specific humoral immune responses against CII. Large increases in both total IgG and IgG anti-CII antibody titers were observed after the primary injection, and these titers did not increase significantly after administration of a booster injection (Figures 4B and C).

We next assessed how loss of B-2 or GC lymphocytes in our mouse models would affect specific immunoglobulin responses. Total IgM levels were similar across all genotypes, and no specific IgM anti-CII responses could be detected, as previously reported (35) (Figure 5A). In contrast, total IgG titers were strongly reduced (3.2- to 16-fold) in both *Pax5^{fl/-} Aicda-Cre* and *Pax5^{fl/-} Cd23-Cre* mouse strains when measured on day 5 and day 14 following primary immunization and day 35 after secondary immunization (day 70 after primary immunization). Additionally, anti-CII antibody responses were almost completely absent in both of the experimental strains (Figure 5B). On day 14 after primary immunization, we observed a 4.6-fold reduction in anti-CII responses in *Pax5^{fl/-} Aicda-Cre* mice relative to controls, with the residual anti-CII titers in the *Pax5^{fl/-} Aicda-Cre* strain probably corresponding to extrafollicular responses. In summary, anti-CII antibody responses were largely dependent on formation of the GC.

Reintroduction of arthritis through the exogenous supply of pathogenic antibodies. The requirement of GCs for arthritis induction indicated that GC-derived antibodies are critical for CIA. However, it remained possible that antigen presentation by cells within the GC may have a pathologic function distinct from B cell clonal selection (e.g., to facilitate T cell activation). We therefore subjected *Pax5^{fl/+} Aicda-Cre* and *Pax5^{fl/-} Aicda-Cre* mice to CAIA.

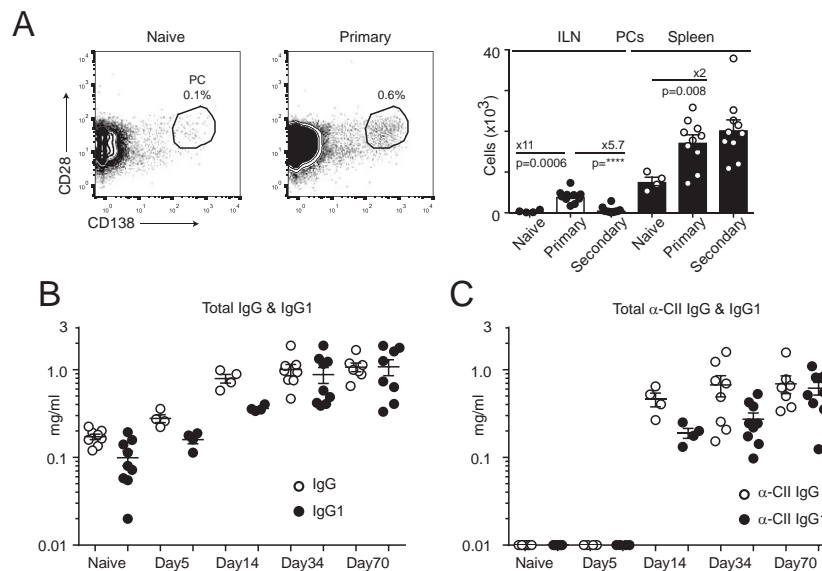


Figure 4. Humoral immunity following immunization with CII. **A**, Left, Flow cytometry plots indicating gating of plasma cells (PCs). Right, Absolute numbers of PCs (defined as B220^{low}CD19^{low}CD138⁺CD28⁺) in the inguinal LNs and spleens of naive mice ($n = 4$), mice on day 35 following primary immunization ($n = 10$), and mice on day 35 following secondary immunization ($n = 10$). The numbers above the horizontal lines are the fold change. P values were determined by t -test. **** = <0.0001 . **B**, Enzyme-linked immunosorbent assay (ELISA)-derived measurements of total IgG and IgG1 in plasma. Plasma was collected from naive mice and on days 5, 14, 34, and 70 following primary immunization. Secondary immunization was performed on day 35. **C**, ELISA-derived measurements of collagen-specific IgG and IgG1. Reactivity was measured against rat collagen. Bars show the mean \pm SEM. See Figure 1 for other definitions.

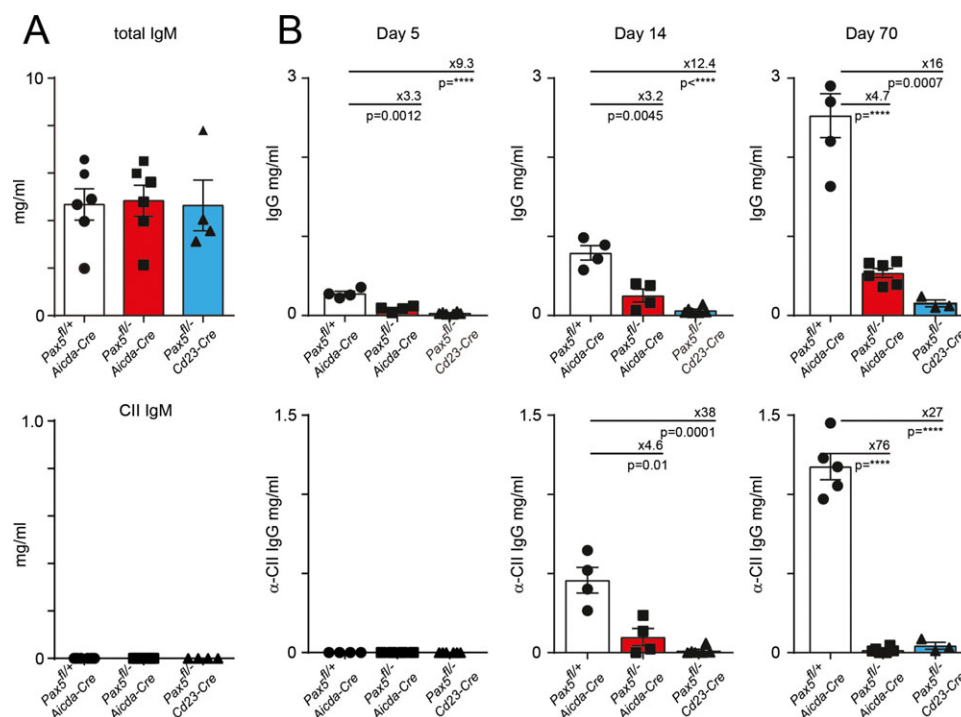


Figure 5. Anti-type II collagen (anti-CII) antibodies are germinal center derived. **A**, Enzyme-linked immunosorbent assay (ELISA)-derived measurements of total IgM and CII-specific IgM in plasma from *Pax5^{fl/+} Aicda-Cre* mice ($n = 6$), *Pax5^{fl/-} Aicda-Cre* mice ($n = 6$), and *Pax5^{fl/-} Cd23-Cre* mice ($n = 4$) 35 days after secondary immunization (day 70 after primary immunization). **B**, ELISA-derived measurements of total IgG and CII-specific IgG in plasma from *Pax5^{fl/+} Aicda-Cre* mice ($n = 4-5$), *Pax5^{fl/-} Aicda-Cre* mice ($n = 4-6$), and *Pax5^{fl/-} Cd23-Cre* mice ($n = 3-6$) on day 5, day 14, and day 70 after primary immunization. The numbers above the horizontal lines are the fold change. Bars show the mean \pm SEM. P values were determined by t -test. **** = <0.0001 . Color figure can be viewed in the online issue, which is available at <http://onlinelibrary.wiley.com/doi/10.1002/art.40354/abstract>.

According to this protocol, 4 separate IgG antibodies recognizing CII are injected into the mice, and arthritis is induced (6). Following performance of this procedure, both *Pax5^{fl/+} Aicda-Cre* and *Pax5^{fl/-} Aicda-Cre* mice were fully susceptible to development of CAIA (Figure 6A), indicating that the requirement for GC formation in the pathology of CIA can be bypassed by the exogenous supply of disease-causing antibodies. There was, however, a trend toward a significant reduction in the frequency of CAIA (16% reduction) in *Pax5^{fl/-} Aicda-Cre* mice, indicating that GC B cells may have additional minor functions other than antibody secretion. Finally, by subsequently immunizing the mice with CII and quantifying antigen-specific T cells using specific tetramer staining, we confirmed that T cells reactive against CII could be produced in these GC-deficient mice. The CII peptide GalHyK264 is the galactosylated form of the CII²⁵⁹⁻²⁷¹ peptide, which is the major epitope recognized by T cells after CII immunization in MHC class A^q-expressing. The *Pax5^{fl/-} Aicda-Cre* GC-deficient strain produced normal numbers of CII-specific CD4⁺ T cells recognizing the MHC class II A^q-loaded CII peptide GalHyK264 compared with *Pax5^{fl/+} Aicda-Cre* controls (Figure 6B).

DISCUSSION

The B lymphocyte is a well-established mediator of arthritis, although the relative contribution of different B cell subtypes to disease pathogenesis is not currently known. In the present study, we obtained in vivo evidence that GC B cells are a major driver of CIA through the production of anti-CII antibodies.

It has been recognized that CII immunization induces the formation of GCs (36), but a comprehensive analysis of the kinetics and localization of this response has been lacking. We now show that both the draining inguinal LNs and the spleen responded to CII by forming GCs. Notably, although the inguinal LNs appeared to respond more vigorously, equal amounts of CII-specific GCs were present in both inguinal LNs and spleen after secondary immunization, although memory cell responses appeared to be preferentially located in the inguinal LNs. There was also an increase in the titers of IgG and IgG1 against CII following secondary immunization, which correlated with increased disease severity and incidence. It was previously suggested that IgG2a anti-CII is the arthritogenic IgG isotype (37), but later

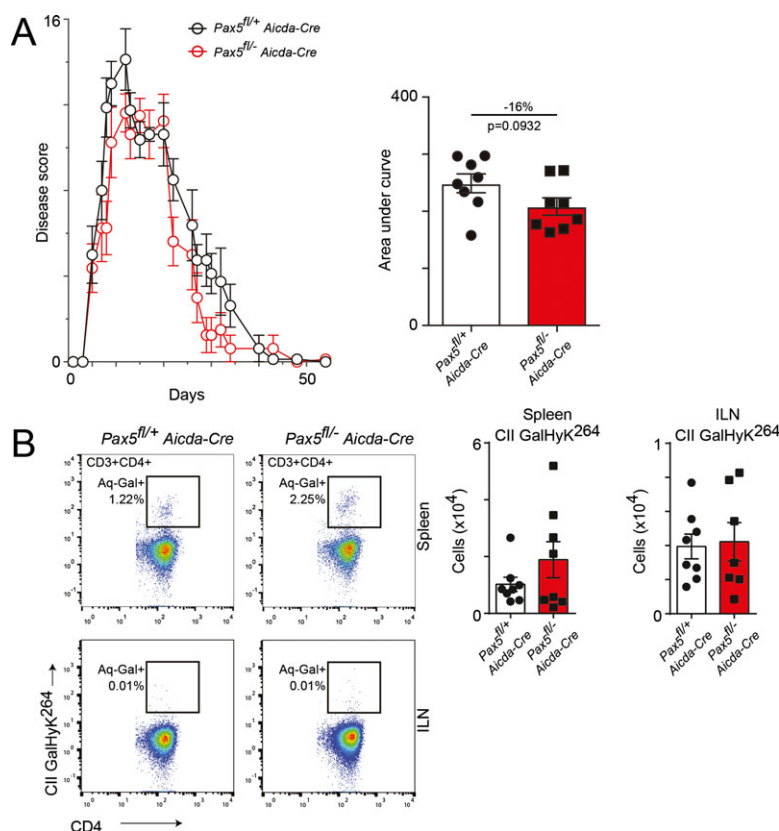


Figure 6. Ability of pathogenic antibodies to circumvent the requirement for the germinal center reaction. **A**, Left, Severity of collagen antibody-induced arthritis (CAIA) in $Pax5^{fl/+} Aicda-Cre$ mice and $Pax5^{fl/-} Aicda-Cre$ mice. Right, Extent of disease, as measured by the area under the curve. Mice were immunized with 4 mg of 4 monoclonal antibodies recognizing type II collagen (CII) and 100 μ g of lipopolysaccharide (LPS). LPS was administered again on day 2. Disease scoring for CAIA was performed in a manner identical to that for collagen-induced arthritis (CIA). The number above the horizontal line is the fold change. The P value was determined by t -test. **B**, Left, Representative flow cytometry plots. Right, Absolute cell counts. CD4+CD3+ cells recognizing the major histocompatibility complex class II-loaded CII peptide GalHyK264 in the inguinal LNs (ILNs) and spleens of mice with CIA were quantified on day 35. In **A** and **B** (right), bars show the mean \pm SEM. Color figure can be viewed in the online issue, which is available at <http://onlinelibrary.wiley.com/doi/10.1002/art.40354/abstract>.

studies showed that IgG1 and IgG2b are also arthritogenic (38).

Studies using $\mu MT^{-/-}$ mice, which are genetically deficient in B cells, have indicated that B cells are important for the pathologic response to heterologous CII injection. We also showed that disease can be induced in $\mu MT^{-/-}$ mice through CAIA (39). The interpretation of these results is complicated by additional defects in the organization of the spleen observed in this strain due to the important function of mature B cells in secreting lymphotoxin α (40). Additionally, because $\mu MT^{-/-}$ mice lack all mature B cells, it has not been possible to identify the subset or subsets that are pathogenic in CIA.

In addition to secreting antibodies, B cells can also function as antigen-presenting cells (41). The relative contribution of B cells versus other professional antigen-presenting cells is a matter of debate. GC B

cells clearly function as antigen-presenting cells to follicular helper T cells within the GC itself, and clonal competition for T cell help is a key affinity-based selection mechanism for affinity maturation (42). Although we could efficiently induce arthritis in our $Pax5^{fl/-} Aicda-Cre$ mouse strain by injecting previously cloned pathogenic antibodies, the extent of disease was marginally lower in this GC-deficient strain. This could be interpreted as GC B cells having other functions relevant to disease development. Clearly, however, a critical function of GC B cells in CIA is the production of anti-CII antibodies. This is further supported by studies showing that mice that lack GCs and additionally have broader immune defects also have reduced responses to CII (43,44), albeit on an MHC H-2^b background. Importantly, however, the B6 mouse model of CIA does not involve CII-reactive T cells, because the

immune response is more likely to be triggered by heterologous proteins contaminating the CII preparations and will therefore be different from classic CIA in A^g-expressing mice (28).

The contribution of GCs to clinical RA is not known. In RA, anti-citrullinated protein antibodies (ACPAs) and RFs (autoantibodies recognizing the Fc portion of immunoglobulins) are used routinely in the clinic for early classification of patients with RA. A mechanistic link between the GC and the pathogenesis of RA was postulated more than 55 years ago, with the observation that RFs can be located within structures resembling GCs (45). These autoantibodies also appear to have a germline configuration (46). ACPAs have been suggested to be somatically mutated (47,48) and are clearly isotype-switched to IgG. This would imply that GCs in humans are also relevant for disease. However, whether ACPAs or RFs are pathogenic or in fact protect against the disease has not been clarified.

It is not known whether RA patients also develop systemic GCs in secondary lymphoid tissue. Interestingly, antibodies reacting to CII (AC2A) also arise in a subset of RA patients and are in particular produced in affected joints (49). Although present in a minor subset of patients, it is important to note that the only antibodies that have so far been shown to induce arthritis are reactive with joint cartilage, including ACPAs that cross-react with CII (50). The AC2A antibodies in RA are isotype-switched, but there is currently no evidence that they are extensively somatically mutated, similar to the mouse model of CIA (3). Alternatively, the GC reaction increases the absolute titers of antibodies and allows for class-switch recombination, both of which have critical effects in disease progression in addition to the affinity maturation process. Additional mechanisms, such as Th17 cells regulating the glycosylation pattern of anti-CII antibodies through interactions with plasmablasts emerging from the GC, could also be important (13). Consistent with this, anti-CD20 therapy in RA patients can reduce autoantibody titers and the disease burden over an extended time period (51), although the function of B cells in RA is likely to be complex and to involve functions in addition to antibody production.

In conclusion, we have demonstrated an indispensable role of GCs in CIA. Targeting the formation of B cell subtypes in clinical arthritis may help to further refine B cell-depleting therapies.

ACKNOWLEDGMENTS

We thank Carlos and Kristina Palestro for providing excellent care of the experimental animals.

AUTHOR CONTRIBUTIONS

All authors were involved in drafting the article or revising it critically for important intellectual content, and all authors approved the final version to be published. Dr. Malin had full access to all of the data in the study and takes responsibility for the integrity of the data and the accuracy of the data analysis.

Study conception and design. Dahdah, Nandakumar, Holmdahl, Malin.

Acquisition of data. Dahdah, Habir, Saxena, Xu.

Analysis and interpretation of data. Dahdah, Habir, Nandakumar, Saxena, Xu, Holmdahl, Malin.

REFERENCES

1. Aho K, Palosuo T, Raunio V, Puska P, Aromaa A, Salonen JT. When does rheumatoid disease start? *Arthritis Rheum* 1985;28:485–9.
2. Aho K, Palosuo T, Heliövaara M, Knekt P, Alha P, von Essen R. Antifilaggrin antibodies within “normal” range predict rheumatoid arthritis in a linear fashion. *J Rheumatol* 2000;27:2743–6.
3. Holmdahl R, Malmström V, Burkhardt H. Autoimmune priming, tissue attack and chronic inflammation: the three stages of rheumatoid arthritis. *Eur J Immunol* 2014;44:1593–9.
4. Bevaart L, Vervoordeldonk MJ, Tak PP. Collagen-induced arthritis in mice. *Methods Mol Biol* 2009;602:181–92.
5. Banda NK, Hyatt S, Antonioli AH, White JT, Glogowska M, Takahashi K, et al. Role of C3a receptors, C5a receptors, and complement protein C6 deficiency in collagen antibody-induced arthritis in mice. *J Immunol* 2011;188:1469–78.
6. Nandakumar KS, Holmdahl R. Antibody-induced arthritis: disease mechanisms and genes involved at the effector phase of arthritis. *Arthritis Res Ther* 2007;8:223.
7. Burkhardt H, Koller T, Engström Å, Nandakumar KS, Turnay J, Kraetsch HG, et al. Epitope-specific recognition of type II collagen by rheumatoid arthritis antibodies is shared with recognition by antibodies that are arthritogenic in collagen-induced arthritis in the mouse. *Arthritis Rheum* 2002;46:2339–48.
8. Svensson L, Jirholt J, Holmdahl R, Jansson L. B cell-deficient mice do not develop type II collagen-induced arthritis (CIA). *Clin Exp Immunol* 1998;111:521–6.
9. Yanaba K, Hamaguchi Y, Venturi GM, Steeber DA, St Clair EW, Tedder TF. B cell depletion delays collagen-induced arthritis in mice: arthritis induction requires synergy between humoral and cell-mediated immunity. *J Immunol* 2007;179:1369–80.
10. Takemura S, Braun A, Crowson C. Lymphoid neogenesis in rheumatoid synovitis. *J Immunol* 2001;167:1072.
11. Greiner A, Seyfert C, Berek C. Differentiation of B cells in the nonlymphoid tissue of the synovial membrane of patients with rheumatoid arthritis. *Proc Natl Acad Sci U S A* 1996;93:221–5.
12. Han S, Cao S, Bheekha-Escura R, Zheng B. Germinal center reaction in the joints of mice with collagen-induced arthritis: an animal model of lymphocyte activation and differentiation in arthritis joints. *Arthritis Rheum* 2001;44:1438–43.
13. Koeleman CA, Toes R, Winkler TH, Holmdahl R. Regulation of autoantibody activity by the IL-23-TH17 axis determines the onset of autoimmune disease. *Nat Immunol* 2017;18:104–13.
14. Vinuesa CG, Sanz I, Cook MC. Dysregulation of germinal centres in autoimmune disease. *Nat Rev Immunol* 2009;9:845–57.
15. Barr TA, Shen P, Brown S, Lampropoulou V, Roch T, Lawrie S, et al. B cell depletion therapy ameliorates autoimmune disease through ablation of IL-6-producing B cells. *J Exp Med* 2012;209:1001–10.
16. Crowley MT, Reilly CR, Lo D. Influence of lymphocytes on the presence and organization of dendritic cell subsets in the spleen. *J Immunol* 1999;163:4894–900.
17. Mo JA, Holmdahl R. The B cell response to autologous type II collagen: biased V gene repertoire with V gene sharing and epitope shift. *Int Immunol* 1996;157:2440–8.

18. Böiers U, Lanig H, Sehnert B, Holmdahl R, Burkhardt H. Collagen type II is recognized by a pathogenic antibody through germline encoded structures. *Eur J Immunol* 2008;38:2784–95.
19. Tada Y, Ho A, Koh DR, Mak TW. Collagen-induced arthritis in CD4- or CD8-deficient mice: CD8+ T cells play a role in initiation and regulate recovery phase of collagen-induced arthritis. *J Immunol* 1996;156:4520–6.
20. Zheng B, Ozen ZZ, Cao S, Zhang Y. CD4-deficient T helper cells are capable of supporting somatic hypermutation and affinity maturation of germinal center B cells. *Eur J Immunol* 2002;32:3315–25.
21. Ehinger M, Vestberg M, Johansson AC, Johannesson M, Svensson A, Holmdahl R. Influence of CD4 or CD8 deficiency on collagen-induced arthritis. *Immunology* 2001;103:291–300.
22. Johansson A, Vestberg M, Holmdahl R. Collagen-induced arthritis development requires $\alpha\beta$ T cells but not $\gamma\delta$ T cells: studies with T cell-deficient (TCR mutant) mice. *Int Immunol* 1999;11:1065.
23. Urbánek P, Wang ZQ, Fetka I, Wagner EF, Busslinger M. Complete block of early B cell differentiation and altered patterning of the posterior midbrain in mice lacking Pax5/BSAP. *Cell* 1994;79:901–12.
24. Horcher M, Souabni A, Busslinger M. Pax5/BSAP maintains the identity of B cells in late B lymphopoiesis. *Immunity* 2001;14:779–90.
25. Kwon K, Hutter C, Sun Q, Bilic I, Cobaleda C, Malin S, et al. Instructive role of the transcription factor E2A in early B lymphopoiesis and germinal center B cell development. *Immunity* 2008;28:751–62.
26. Holmdahl R, Carlsen S, Mikulowska A, Vestburg M, Brunsberg U, Hansson A-S, et al. Genetic analysis of mouse models for rheumatoid arthritis. In: Adolpho KW, editor. *Human genetics methods*. New York (NY): CRC Press; 1998:215–238.
27. Sareila O, Hagert C, Kelkka T, Linja M, Xu B, Kihlberg J, et al. Reactive oxygen species regulate both priming and established arthritis, but with different mechanisms. *Antioxid Redox Signal* 2017. E-pub ahead of print.
28. Bäcklund J, Li C, Jansson E, Carlsen S, Merky P, Haag S, et al. C57BL/6 mice need MHC class II Aq to develop collagen-induced arthritis dependent on autoreactive T cells. *Ann Rheum Dis* 2012;72:1225–32.
29. Cobaleda C, Schebesta A, Delogu A, Busslinger M. Pax5: the guardian of B cell identity and function. *Nat Immunol* 2007;8:463.
30. Schebesta A, McManus S, Salvagiotto G, Delogu A, Busslinger GA, Busslinger M. Transcription factor Pax5 activates the chromatin of key genes involved in B cell signaling, adhesion, migration, and immune function. *Immunity* 2007;27:49–63.
31. Delogu A, Schebesta A, Sun Q, Aschenbrenner K, Perlot T, Busslinger M. Gene repression by Pax5 in B cells is essential for blood cell homeostasis and is reversed in plasma cells. *Immunity* 2006;24:269–81.
32. Wöhner M, Tagoh H, Bilic I, Jaritz M, Poliakov DK, Fischer M, et al. Molecular functions of the transcription factors E2A and E2-2 in controlling germinal center B cell and plasma cell development. *J Exp Med* 2016;213:1201–21.
33. Malin S, McManus S, Cobaleda C, Novatchkova M, Delogu A, Bouillet P, et al. Role of STAT5 in controlling cell survival and immunoglobulin gene recombination during pro-B cell development. *Nat Immunol* 2009;11:171–9.
34. Vikstrom I, Carotta S, Lühje K, Peperzak V, Jost PJ, Glaser S, et al. Mcl-1 is essential for germinal center formation and B cell memory. *Science* 2010;330:1095–9.
35. Holmdahl R, Bailey C, Enander I, Mayer R, Klareskog L, Moran T, et al. Origin of the autoreactive anti-type II collagen response. Part II. Specificities, antibody isotypes and usage of V gene families of anti-type II collagen B cells. *J Immunol* 1989;142:1881–6.
36. Del Nagro CJ, Kolla RV, Rickert RC. A critical role for complement C3d and the B cell coreceptor (CD19/CD21) complex in the initiation of inflammatory arthritis. *J Immunol* 2005;175:5379–89.
37. Watson WC, Townes AS. Genetic susceptibility to murine collagen II autoimmune arthritis: proposed relationship to the IgG2 autoantibody subclass response, complement C5, major histocompatibility complex (MHC) and non-MHC loci. *J Exp Med* 1985;162:1878–91.
38. Nandakumar KS, Andrén M, Martinsson P, Bajtner E, Hellström S, Holmdahl R, et al. Induction of arthritis by single monoclonal IgG anti-collagen type II antibodies and enhancement of arthritis in mice lacking inhibitory Fc γ RIIB. *Eur J Immunol* 2003;33:2269–77.
39. Nandakumar KS, Bäcklund J, Vestberg M, Holmdahl R. Collagen type II (CII)-specific antibodies induce arthritis in the absence of T or B cells but the arthritis progression is enhanced by CII-reactive T cells. *Arthritis Res Ther* 2004;6:R544–50.
40. Tumanov A, Kuprash D, Lagarkova M, Grivennikov S, Abe K, Shakhov A, et al. Distinct role of surface lymphotoxin expressed by B cells in the organization of secondary lymphoid tissues. *Immunity* 2002;17:239–50.
41. Crawford A, Macleod M, Schumacher T, Corlett L, Gray D. Primary T cell expansion and differentiation in vivo requires antigen presentation by B cells. *J Immunol* 2006;176:3498–506.
42. Victora GD, Nussenzweig MC. Germinal centers. *Annu Rev Immunol* 2012;30:429–57.
43. Van Nieuwenhuijze A, Dooley J, Humblet-Baron S, Sreenivasan J, Koenders M, Schlenner SM, et al. Defective germinal center B cell response and reduced arthritic pathology in microRNA-29a-deficient mice. *Cell Mol Life Sci* 2017;74:2095–106.
44. Sakuraba K, Oyamada A, Fujimura K, Spolski R, Iwamoto Y, Leonard WJ, et al. Interleukin-21 signaling in B cells, but not in T cells, is indispensable for the development of collagen-induced arthritis in mice. *Arthritis Res Ther* 2016;18:188.
45. Mellors RC, Heimer R, Corcos J, Korngold L. Cellular origin of rheumatoid factor. *J Exp Med* 1959;110:875–86.
46. Thompson KM, Børretzen M, Randen I, Førre O, Natvig JB. V-gene repertoire and hypermutation of rheumatoid factors produced in rheumatoid synovial inflammation and immunized healthy donors. *Ann N Y Acad Sci* 1995;764:440–9.
47. Amara K, Steen J, Murray F, Morbach H, Fernandez-Rodriguez BM, Joshua V, et al. Monoclonal IgG antibodies generated from joint-derived B cells of RA patients have a strong bias toward citrullinated autoantigen recognition. *J Exp Med* 2013;210:445–55.
48. Kerkman PF, Fabre E, van der Voort EI, Zaldumbide A, Rombouts Y, Rispen T, et al. Identification and characterisation of citrullinated antigen-specific B cells in peripheral blood of patients with rheumatoid arthritis. *Ann Rheum Dis* 2015;75:1170–6.
49. Lindh I, Snir O, Lönnblom E, Uysal H, Andersson I, Nandakumar KS, et al. Type II collagen antibody response is enriched in the synovial fluid of rheumatoid joints and directed to the same major epitopes as in collagen induced arthritis in primates and mice. *Arthritis Res Ther* 2014;16:R143.
50. Ge C, Tong D, Liang B, Lönnblom E, Schneider N, Hagert C, et al. Anti-citrullinated protein antibodies cause arthritis by cross-reactivity to joint cartilage. *JCI Insight* 2017;2:93688.
51. Thurlings RM, Vos K, Wijnbrandts CA, Zwiderman AH, Gerlag DM, Tak PP. Synovial tissue response to rituximab: mechanism of action and identification of biomarkers of response. *Ann Rheum Dis* 2007;67:917–25.

BRIEF REPORT

A Phase IIB Trial of a Novel Extended-Release Microsphere Formulation of Triamcinolone Acetonide for Intraarticular Injection in Knee Osteoarthritis

Philip G. Conaghan,¹ Stanley B. Cohen,² Francis Berenbaum,³ Joelle Lufkin,⁴ James R. Johnson,⁴ and Neil Bodick⁴

Objective. FX006 is a novel, microsphere-based, extended-release formulation of triamcinolone acetonide for intraarticular (IA) injection designed to maintain treatment concentration in the joint and provide prolonged analgesic benefits in patients with osteoarthritis (OA) of the knee. This study was undertaken to compare the analgesic benefits of 2 FX006 doses with saline placebo injection.

Methods. In this phase IIB study, participants with knee OA (Kellgren/Lawrence grade 2–3) and average daily pain (ADP) intensity ≥ 5 to ≤ 9 (on a 0–10 Numerical Rating Scale) were randomized (1:1:1) to receive single IA injections of FX006 32 mg (n = 104) or 16 mg (n = 102) or saline placebo (n = 100). The primary end point was the least squares mean (LSM) change from baseline to week 12 in weekly mean ADP intensity scores for FX006 32 mg versus saline placebo.

Results. The primary end point was not met (LSM change at week 12 -3.1 with FX006 32 mg versus -2.5 with saline placebo; LSM difference [95% confidence interval] -0.58 [-1.22 , 0.07]) ($P = 0.08$). However, improvements in ADP intensity were significantly greater with FX006 32 mg than saline placebo at weeks 1–11 and

week 13. Improvements in ADP intensity were significantly greater with FX006 16 mg versus saline placebo at weeks 1–9. A dose-response effect in duration of maximal analgesic effect was evident (13 weeks with 32 mg versus 9 weeks with 16 mg), with FX006 32 mg providing increased therapeutic benefit relative to FX006 16 mg. All treatments were well tolerated.

Conclusion. Although the primary end point was not met, our findings indicate a prolonged reduction in symptoms with FX006 with an evident dose response and a safety profile similar to saline placebo.

Osteoarthritis (OA) of the knee is characterized by pain, progressive cartilage destruction, subchondral bone changes, and joint inflammation (1). Treatment guidelines recommend intraarticular (IA) corticosteroids (2). Standard IA corticosteroids provide moderate improvements in pain, but the magnitude of benefit rapidly wanes after injection (3). FX006, an extended-release formulation of triamcinolone acetonide in 75:25 poly(lactic-co-glycolic acid) microspheres, was designed to maintain prolonged concentrations of triamcinolone acetonide in the joint, with the intent to improve analgesic effect and reduce systemic

ClinicalTrials.gov identifier: NCT02116972.

The views expressed herein are those of the authors and do not necessarily reflect those of the NHS, the NIHR, or the Department of Health.

Supported by Flexion Therapeutics. Dr. Conaghan's work is supported in part by the NIHR Leeds Biomedical Research Centre.

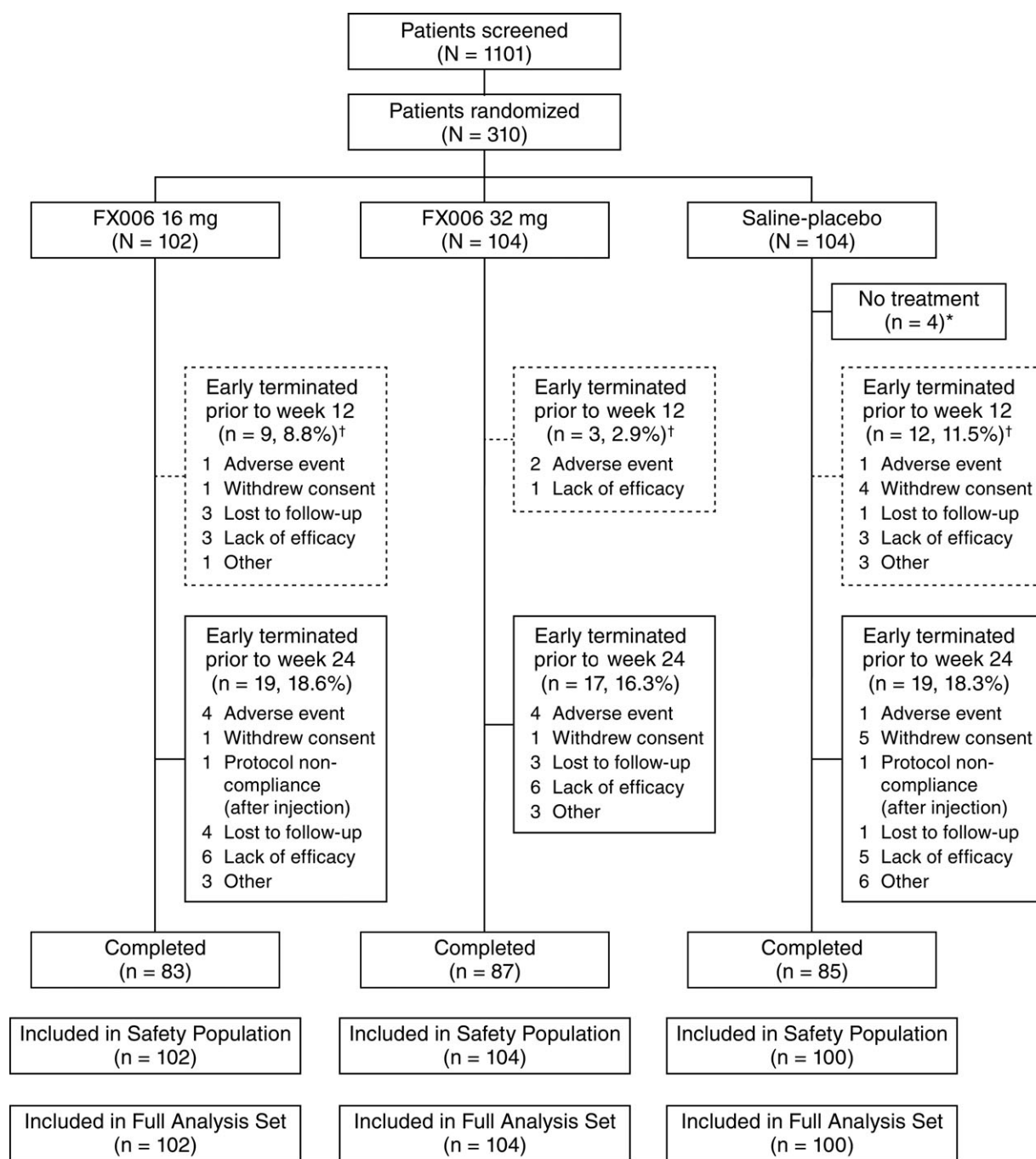
¹Philip G. Conaghan, MBBS, PhD, FRACP, FRCP: University of Leeds and NIHR Leeds Biomedical Research Centre, Leeds, UK; ²Stanley B. Cohen, MD: University of Texas Southwestern Medical School, Dallas; ³Francis Berenbaum, MD, PhD: Pierre and Marie Curie University, Paris, France; ⁴Joelle Lufkin, MPH, James R. Johnson, PhD (current address: Summit Analytical, Cary, North Carolina), Neil Bodick, MD, PhD: Flexion Therapeutics, Burlington, Massachusetts.

Dr. Conaghan has received consulting fees from AbbVie, Flexion Therapeutics, Infirst, Medivir, Merck Serono, Novartis, and Ono Pharmaceutical (less than \$10,000 each). Dr. Cohen has received consulting fees from Flexion Therapeutics (less than \$10,000). Dr. Berenbaum has received consulting fees, speaking fees, and/or honoraria from AbbVie, Biogaran, Biogen, Expanscience, Flexion Therapeutics, IBSA, Janssen, Merck Serono, Novartis, Pfizer, Sanofi,

Servier, TRB Chemedica, and UCB (less than \$10,000 each). Ms Lufkin owns stock or stock options in Flexion Therapeutics. Dr. Johnson has received consulting fees from Acura Pharmaceuticals, Flexion Therapeutics, Iroko Pharmaceuticals, iX Biopharma, and Tolmar (more than \$10,000 each). Dr. Bodick owns stock or stock options in Flexion Therapeutics, holds a patent for corticosteroids for the treatment of joint pain, and has patent applications pending related to corticosteroid formulations for maintaining corticosteroid synovial fluid formulations, corticosteroid formulations and methods for the treatment of joint pain in patients with type 2 diabetes mellitus, and corticosteroid formulations and methods for the treatment of joint pain in patients with diabetes.

Address correspondence to Philip G. Conaghan, MBBS, PhD, FRACP, FRCP, Leeds Institute of Rheumatic and Musculoskeletal Medicine, University of Leeds and NIHR Leeds Biomedical Research Centre, 2nd Floor, Chapel Allerton Hospital, Chapeltown Road, Leeds LS7 4SA, UK. E-mail: p.conaghan@leeds.ac.uk.

Submitted for publication May 8, 2017; accepted in revised form October 24, 2017.



* After randomization but prior to administration of study drug, two patients withdrew consent to participate, one patient did not return to the study center for administration of study drug, and one patient was unwilling to discontinue a prohibited medication during study participation and was discontinued.

[†] Early terminations prior to week 12 are included in the total early terminations through week 24.

Figure 1. Disposition of the patients.

exposure versus commercially available triamcinolone acetonide crystalline suspension. In a pharmacokinetic study (ClinicalTrials.gov identifier: NCT02637323), FX006 demonstrated prolonged residency in synovial fluid and reduced systemic exposure following IA injection versus triamcinolone acetonide crystalline suspension in people with knee OA (4).

In the first clinical study of efficacy following a single IA injection of FX006 (target low, mid, and high doses of 10 mg, 40 mg, and 60 mg, respectively) in patients with knee OA (ClinicalTrials.gov identifier: NCT01487161) (5), the mid dose of FX006 yielded pain relief superior to triamcinolone acetonide crystalline suspension 40 mg with treatment differences achieving statistical significance at weeks 5–10 (all $P < 0.05$) and numerical improvement at each of weeks 2–12. Pain relief with the high dose of FX006 compared with triamcinolone acetonide crystalline suspension was similar to that for the mid dose through week 6, but diminished from weeks 7 to 12. Pain relief was numerically improved with the low dose of FX006 compared with triamcinolone acetonide crystalline suspension at each of weeks 2–12, but the effect did not achieve

statistical significance. Hence, the mid dose of FX006 was concluded to be the most efficacious tested in that trial (5) and further evaluation was deemed appropriate.

The present study (ClinicalTrials.gov identifier: NCT02116972) was conducted to confirm the appropriate target dose of FX006 and further assess FX006 efficacy and safety. Two notable differences exist between the previous dose-ranging study (5) and the present one with regard to administration and dosing of FX006. First, the injection volume increased from 3 ml in the previous study to 5 ml in the present study following adjustment of the diluent volume to enhance microsphere dispersion and reduce aggregation. Second, the FX006 doses reported here (16 mg and 32 mg) reflect the amount of drug received by patients following an ~20% reduction during reconstitution, as determined by dose-delivery studies.

PATIENTS AND METHODS

In this phase IIb, double-blind, parallel-group, dose-ranging, single-injection study, participants were randomized (1:1:1, block of 6; by a centralized interactive web randomization system) to receive a single 5-ml IA injection of FX006 16 mg, FX006 32

Table 1. Baseline demographic and disease characteristics of the patients with OA (full analysis set)*

	FX006 16 mg (n = 102)	FX006 32 mg (n = 104)	Saline placebo (n = 100)	Total (n = 306)
Male, no. (%)	40 (39.2)	53 (51.0)	39 (39.0)	132 (43.1)
White, no. (%)	81 (79.4)	85 (81.7)	82 (82.0)	248 (81.0)
Age at consent, mean \pm SD years	58.2 \pm 8.34	58.7 \pm 8.06	59.7 \pm 8.23	58.8 \pm 8.20
BMI, mean \pm SD kg/m ²	30.6 \pm 4.86	31.0 \pm 4.55	31.2 \pm 5.11	30.9 \pm 4.84
Weight category, no. (%)				
Underweight (BMI <18.5)	2 (2.0)	0 (0.0)	0 (0.0)	2 (0.7)
Normal weight (BMI 18.5–24.9)	12 (11.8)	10 (9.6)	10 (10.0)	32 (10.5)
Overweight (BMI 25.0–29.9)	32 (31.4)	35 (33.7)	33 (33.0)	100 (32.7)
Obesity class I (BMI 30.0–34.9)	37 (36.3)	39 (37.5)	29 (29.0)	105 (34.3)
Obesity class II (BMI 35.0–39.9)	19 (18.6)	18 (17.3)	27 (27.0)	64 (20.9)
Morbid obesity (BMI \geq 40.0)	0 (0.0)	2 (1.9)	1 (1.0)	3 (1.0)
Type of knee OA, no. (%)				
Unilateral	45 (44.1)	46 (44.2)	38 (38.0)	129 (42.2)
Bilateral	57 (55.9)	58 (55.8)	62 (62.0)	177 (57.8)
Years since diagnosis, mean \pm SD	6.7 \pm 6.66	7.2 \pm 7.27	6.4 \pm 5.79	6.8 \pm 6.60
Kellgren/Lawrence grade, no. (%)				
2	33 (32.4)	28 (26.9)	37 (37.0)	98 (32.0)
3	69 (67.6)	76 (73.1)	63 (63.0)	208 (68.0)
Prior index knee surgeries/interventions, no. (%)				
Surgery or procedure	20 (19.6)	17 (16.3)	15 (15.0)	52 (17.0)
IA steroid injection	32 (31.4)	35 (33.7)	24 (24.0)	91 (29.7)
IA hyaluronic acid injection	6 (5.9)	11 (10.6)	19 (19.0)	36 (11.8)
ADP intensity, mean \pm SD (0–10 scale)	6.6 \pm 0.97	6.5 \pm 1.01	6.7 \pm 1.08	6.6 \pm 1.02
WOMAC pain subscale, mean \pm SD (0–4 scale)	2.3 \pm 0.62	2.1 \pm 0.58	2.3 \pm 0.65	2.2 \pm 0.62
WOMAC stiffness subscale, mean \pm SD (0–4 scale)	2.5 \pm 0.74	2.4 \pm 0.71	2.4 \pm 0.68	2.4 \pm 0.71
WOMAC physical function subscale, mean \pm SD (0–4 scale)	2.3 \pm 0.68	2.1 \pm 0.57	2.3 \pm 0.65	2.2 \pm 0.63

* The Patient Global Impression of Change (PGIC) is the patient's report of change since baseline; thus, there is no PGIC assessment at baseline. OA = osteoarthritis; BMI = body mass index; IA = intraarticular; ADP = average daily pain; WOMAC = Western Ontario and McMaster Universities Osteoarthritis Index.

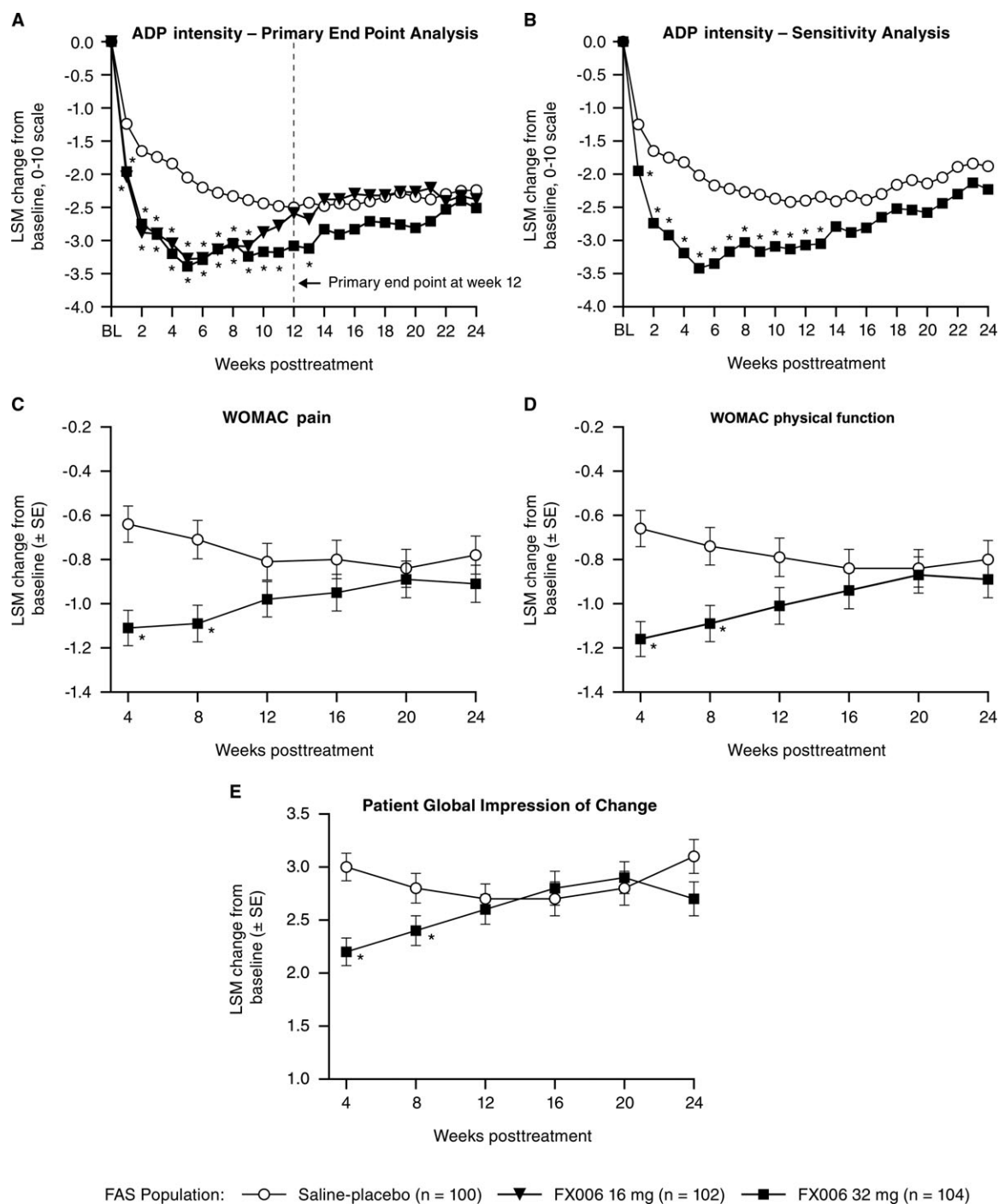


Figure 2. A, Least squares mean (LSM) change from baseline (BL) in weekly mean average daily pain (ADP) intensity scores at the primary end point at week 12 and key secondary end points at weeks 16, 20, and 24 (observed data; mixed model for repeated measures). B, Sensitivity analysis of ADP intensity (imputed data; last observation carried forward/baseline observation carried forward). C, Western Ontario and McMaster Universities Osteoarthritis Index (WOMAC) pain subscale. D, WOMAC physical function subscale (key secondary end point at week 12). E, Patient Global Impression of Change score (key secondary end point at week 12) through week 24. FAS = full analysis set. Values are the LSM \pm SEM. * = $P < 0.05$.

Table 2. Summary of AEs among all treated patients*

	FX006 16 mg (n = 102)	FX006 32 mg (n = 104)	Saline placebo (n = 100)
Patients with ≥ 1 AE	43 (42.2)	46 (44.2)	43 (43.0)
AEs occurring in $>2.0\%$ of patients in any treatment group†			
Arthralgia (any joint)	10 (9.8)	8 (7.7)	16 (16.0)
Back pain	3 (2.9)	2 (1.9)	2 (2.0)
Bronchitis	3 (2.9)	2 (1.9)	2 (2.0)
Headache	3 (2.9)	4 (3.8)	2 (2.0)
Joint swelling	4 (3.9)	5 (4.8)	5 (5.0)
Ligament sprain	4 (3.9)	4 (3.8)	2 (2.0)
Nasopharyngitis	2 (2.0)	2 (1.9)	4 (4.0)
Neck pain	0 (0.0)	3 (2.9)	0 (0.0)
Sinusitis	3 (2.9)	2 (1.9)	1 (1.0)
Toothache	0 (0.0)	3 (2.9)	1 (1.0)
Patients with ≥ 1 serious AE	1 (1.0)	3 (2.9)	0 (0.0)
Patients with ≥ 1 AE leading to study discontinuation	4 (3.9)‡	4 (3.8)§	1 (1.0)¶
Drug-related	1 (1.0)#	0 (0.0)	1 (1.0)#
Due to serious AE	0 (0.0)	1 (1.0)**	0 (0.0)
Patients with ≥ 1 index knee-related AE	15 (14.7)	14 (13.5)	17 (17.0)
Index knee-related AEs occurring in $>2.0\%$ of patients in any treatment group†			
Arthralgia	8 (7.8)	7 (6.7)	14 (14.0)
Joint swelling	4 (3.9)	4 (3.8)	3 (3.0)
Ligament sprain	3 (2.9)	1 (1.0)	0 (0.0)
Patients with ≥ 1 index knee-related serious AE	1 (1.0)	1 (1.0)	0 (0.0)
Patients with ≥ 1 index knee-related AE leading to study discontinuation	4 (3.9)‡	3 (2.9)§	1 (1.0)¶
Drug-related	1 (1.0)#	0 (0.0)	1 (1.0)#
Due to serious AE	0 (0.0)	0 (0.0)	0 (0.0)

* Values are the number (%).

† Listed in alphabetical order.

‡ Joint effusion (day 131, grade 1, not related to study drug), arthralgia (day 57, grade 2, definitely related to study drug), and joint swelling (day 57, grade 3, not related to study drug) in 1 patient each, and arthralgia, arthritis, joint swelling, and synovial cyst all in 1 patient (day 88, all grade 2 and either not related or unlikely related to study drug). All adverse events (AEs) were index knee related.

§ Joint swelling (day 84, grade 1, not related to study drug), worsening ankle osteoarthritis (OA) (day 37, grade 2, not related to study drug, serious), positive *Klebsiella* test (day 21, subsequently considered to be a false-positive finding by the investigator, grade 3, not related to study drug), and synovitis (day 112, grade 3, unlikely related to study drug). All AEs were index knee related except ankle OA.

¶ Arthralgia (day 41, grade 3, probably related to study drug); index knee related.

Arthralgia.

** Ankle OA.

mg, or saline placebo. Participants and assessors were blinded with regard to treatment administered by a nonblinded injector. Details related to randomization, blinding, and the injection procedure are provided in the Supplementary text, available on the *Arthritis & Rheumatology* web site at <http://onlinelibrary.wiley.com/doi/10.1002/art.40364/abstract>. After screening, participants were seen on day 1 (baseline) and at weeks 4, 8, 12, 16, 20, and 24.

Eligible participants (ages ≥ 40 years, body mass index ≤ 40 kg/m²) had knee OA according to the American College of Rheumatology clinical and radiologic criteria (6) for ≥ 6 months before screening, a Kellgren/Lawrence grade of 2 or 3 on a centrally read screening radiograph (7), pain in the index knee (defined as the most painful knee in participants with bilateral disease) on >15 days of the previous month, and a mean average daily pain (ADP) intensity score ≥ 5 and ≤ 9 (on an 11-point Numerical Rating Scale [NRS]). Patients were excluded if they had ipsilateral hip OA, other arthritic/immune-mediated inflammatory disorders, or unstable knee joints (e.g., torn anterior cruciate ligament) within 12 months of screening or received prior IA

corticosteroids within 3 months of screening, prior IA hyaluronic acid injections in the index knee within 6 months of screening, prior FX006 at any time, or intramuscular, oral, inhaled, intranasal, or topical corticosteroids within 2 weeks of screening.

From screening through week 24, participants logged daily ADP intensity scores via an interactive voice response system, using a 0–10 NRS (where 0 = “no pain” and 10 = “pain as bad as you can imagine”). Participants completed the Western Ontario and McMaster Universities Osteoarthritis Index (WOMAC) (8) on day 1 prior to randomization and at weeks 4, 8, 12, 16, 20, and 24, and the Patient Global Impression of Change (PGIC) (9) at weeks 4, 8, 12, 16, 20, and 24.

Safety was evaluated via adverse events (AEs) spontaneously reported or discovered by the investigator from information obtained via patient electronic diaries, routine physical/laboratory evaluations, and assessments of the index knee by an investigator who was blinded with regard to treatment group. After informed consent was obtained, and for ≥ 7 days pretreatment, analgesic medications for index knee pain

were not to be taken or used during the study with the exception of study-issued acetaminophen ($\leq 3,000$ mg/day in sponsor-provided 500-mg tablets) as rescue pain treatment.

The primary efficacy end point, change from baseline to week 12 in weekly mean ADP intensity scores for FX006 32 mg versus saline placebo in the full analysis set (all randomized and treated participants), was analyzed using longitudinal mixed model for repeated measures (MMRM) methodology on observed data with no imputation for missing data (see the Supplementary text, available on the *Arthritis & Rheumatology* web site at <http://onlinelibrary.wiley.com/doi/10.1002/art.40364/abstract>). A sample size of ~300 participants (100 per treatment arm) was estimated to provide 80% power (2-sided alpha level of 0.05) if the true underlying primary end point treatment effect was 1.0 on the 0–10 NRS.

All secondary efficacy end points were first compared between FX006 32 mg and saline placebo, followed by FX006 16 mg versus saline placebo. Predefined key secondary end points (in order of step-down testing) were change from baseline to week 12 in WOMAC physical function and PGIC scores, and changes in weekly mean ADP intensity scores from baseline to weeks 16, 20, and 24. Additional secondary outcomes included percent of responders according to Outcome Measures in Rheumatology (OMERACT)–Osteoarthritis Research Society International (OARSI) “strict” criteria (defined as $\geq 50\%$ improvement and an absolute improvement of ≥ 20 points from baseline in either ADP intensity or the WOMAC physical function subscale) (10) at weeks 4, 8, 12, 16, 20, and 24; change from baseline to each week (except weeks 12, 16, 20, and 24 as outlined above, which are specified as the primary and secondary end points) in weekly mean ADP intensity score; change from baseline to each of weeks 4, 8, 12, 16, 20, and 24 in the WOMAC pain subscale; change from baseline to each of weeks 4, 8, 16, 20, and 24 in the WOMAC physical function subscale and PGIC; and time to onset of pain relief (time to first ADP intensity assessment showing $>30\%$ improvement from baseline).

To quantify the magnitude of difference between FX006 16 mg and 32 mg and saline placebo, standardized effect sizes were determined post hoc using methods described previously (11) (see the Supplementary text, available on the *Arthritis & Rheumatology* web site at <http://onlinelibrary.wiley.com/doi/10.1002/art.40364/abstract>). Safety summaries included treated patients.

This trial was conducted according to Good Clinical Practice guidelines. Each site’s governing ethics body approved the protocol, and participants provided written informed consent.

RESULTS

Patient disposition and baseline characteristics.

The trial was conducted from April 29, 2014 to August 8, 2015. Participants were screened at 48 sites (43 in the US and 5 in Canada) and enrolled at 44 sites (40 in the US and 4 in Canada). Among 310 randomized participants, 306 were treated (4 randomized to saline placebo were not treated). Approximately 8% and 18% of participants prematurely discontinued participation through week 12 (primary end point) and week 24 (study completion), respectively (Figure 1). Ultrasound guidance during IA injection was used in 4 patients.

All baseline characteristics, except sex, were generally well-balanced across arms. A higher proportion of men comprised the FX006 32 mg group (51%) compared with the 16 mg group (39%) or saline placebo group (39%). Baseline ADP intensity scores (mean 6.6) indicated substantial daily pain at a moderate level of intensity (Table 1).

Efficacy. The primary end point was not met. The least squares mean (LSM) change in ADP intensity at week 12 was -3.1 with FX006 32 mg versus -2.5 with saline placebo. The LSM difference in ADP intensity (95% confidence interval [95% CI]) for FX006 32 mg versus saline placebo at week 12 was -0.58 ($-1.22, 0.07$) ($P = 0.08$). However, FX006 32 mg resulted in significant improvements in ADP intensity versus saline placebo at each of weeks 1–11 ($P \leq 0.036$) and week 13 ($P \leq 0.039$) and numerical improvements at week 12 and each of weeks 14–24 (Figure 2A). Patients receiving FX006 16 mg had significant improvements in ADP at weeks 1–9; thereafter, the difference in pain scores between FX006 16 mg and saline placebo was small and not statistically significant (Figure 2A). As such, a dose-response effect was evident in the duration of maximal effect. FX006 16 mg and 32 mg had similar median time to onset of analgesic effect (day 4), which was more rapid than saline placebo (day 8). The maximum magnitude of analgesic effect was similar for FX006 16 mg and 32 mg (achieved at weeks 4–5; LSM difference -1.22 for FX006 16 mg at week 4, -1.23 for FX006 16 mg at week 5, -1.36 for FX006 32 mg at week 4, and -1.34 for FX006 32 mg at week 5) (Figure 2A).

Sensitivity analyses of the primary end point (last observation carried forward [LOCF]/baseline observation carried forward [BLOCF]) addressing patient discontinuations prior to week 12 showed that ADP intensity was significantly improved with FX006 32 mg versus saline placebo at each visit from weeks 1 to 13 (all $P < 0.05$), including week 12 (LSM difference [95% CI] -0.67 [$-1.32, -0.02$]; $P = 0.042$) (Figure 2B). Results of a multiple imputation sensitivity analysis of the primary end point demonstrated consistent differences between FX006 32 mg and saline placebo in ADP intensity changes from baseline to week 12 (LSM difference [95% CI] -0.65 [$-1.30, 0.01$]; $P = 0.053$) (data not shown). Consistent results were observed from a post hoc exploratory primary end point analysis performed with site added to the MMRM as a covariate (week 12 LSM difference [95% CI] -0.72 [$-1.39, -0.05$]; $P = 0.034$) (data not shown). Inclusion of the 4 patients who were randomized and not treated (i.e., the intent-to-treat population) yielded results identical to those of the analysis based on the full analysis set population, because none of these 4 patients had efficacy data after their screening visit.

Results from secondary analyses also favored FX006 32 mg compared with saline placebo. FX006 32 mg was associated with significantly improved WOMAC pain (Figure 2C), WOMAC physical function (Figure 2D), and PGIC (Figure 2E) scores, and resulted in a higher proportion of patients who achieved OMERACT-OARSI “strict” responder criteria versus saline placebo at week 4 and week 8 (Supplementary Table 1, available on the *Arthritis & Rheumatology* web site at <http://onlinelibrary.wiley.com/doi/10.1002/art.40364/abstract>). Numerical advantage was maintained at week 12 for all of these end points except OMERACT-OARSI “strict” responders. Secondary end point findings for FX006 16 mg versus saline placebo showed a similar pattern, with a reduced duration of effect, no trend favoring FX006 16 mg over saline placebo for improvements in ADP intensity at week 12, and lower OMERACT-OARSI “strict” response rates at week 8 (Figure 2A and Supplementary Table 1).

Results from post hoc standardized effect size size determinations indicated that the effect sizes based on ADP were consistently lower than those for the WOMAC pain subscale. The ADP effect sizes for FX006 32 mg at weeks 4, 8, and 12 were 0.27, 0.13, and 0.12, respectively, and the effect sizes for the WOMAC pain subscale were 0.72, 0.54, and 0.27, respectively. For each instrument, the effect sizes for FX006 16 mg were similar to those of FX006 32 mg at weeks 4 and 8. Consistent with prespecified secondary end points, effect sizes for both ADP and the WOMAC pain subscale were markedly lower for FX006 16 mg versus FX006 32 mg at week 12 (Supplementary Table 2, available on the *Arthritis & Rheumatology* web site at <http://onlinelibrary.wiley.com/doi/10.1002/art.40364/abstract>).

Safety. Similar proportions of participants reported AEs through week 24 across treatment arms (Table 2). Most AEs were grade 1 or 2, nonserious, and considered unrelated to the study drug by investigators who were blinded with regard to treatment group. No deaths occurred. Serious AEs occurred in 4 (1.9%) of the FX006-treated patients (left distal femur fracture in the 16 mg group and worsening left ankle OA, myocardial infarction, and rheumatoid arthritis in the 32 mg group). All were unrelated to study drug. No AE was consistent with postinjection flare. AEs causing study discontinuation occurred in 8 (3.9%) of the FX006-treated patients and 1 (1.0%) of the saline placebo-treated patients (Table 2). The onset of such events was not temporally associated with study drug administration. All of these events were considered unrelated to study drug except for 1 grade 2 AE (in the FX006 16 mg group) and 1 grade 3 AE (in the saline placebo group). The incidence of index knee-related AEs was relatively low given the study population. AEs related to the injection procedure were observed in 2.0%, 0%, and 6.0%

of FX006 16 mg-, FX006 32 mg-, and saline placebo-treated patients, respectively.

DISCUSSION

The primary end point of this study, significant improvement in ADP intensity at week 12 with FX006 32 mg versus placebo, was not achieved ($P = 0.08$); however, significant improvement with FX006 32 mg was seen at all time points from week 1 to week 11 ($P \leq 0.036$) and at week 13 ($P = 0.039$). The placebo response at week 12 (LSM reduction of -2.5) was the largest reported over the 24-week study. Studies show that placebo effects may confound the interpretation of clinical data (12) and are more pronounced with IA versus other routes of administration (13). Differences in saline placebo response across study sites were noted; a post hoc exploratory analysis with a site covariate included in the MMRM accounted for the variability in site responses, and the model demonstrated statistical significance for the primary end point at week 12 ($P = 0.034$). Sensitivity analyses (LOCF/BLOCF) that addressed patient discontinuations prior to week 12 indicated that FX006 32 mg was significantly superior to saline placebo at weeks 1–13 ($P \leq 0.042$). Results of a multiple imputation analysis demonstrated consistent differences between FX006 32 mg and saline placebo in ADP intensity changes from baseline to week 12.

Although FX006 16 mg and 32 mg had comparable median times to onset of analgesia (day 4) and provided similar and significant maximal analgesic effects (beginning at approximately week 5) versus saline placebo, maximal effect persisted longer with FX006 32 mg (to approximately week 13) than 16 mg (to approximately week 9). Numerically larger pain relief, as measured by ADP intensity, was maintained with FX006 32 mg versus saline placebo at all time points through week 24. Other measures of OA signs/symptoms (WOMAC physical function subscale, PGIC, WOMAC pain subscale, and OMERACT-OARSI “strict” response) were significantly improved with FX006 32 mg through week 8 with strong trends remaining at week 12; results for FX006 16 mg versus saline placebo showed a similar pattern but were not as robust or long lasting. A previous clinical study of FX006 in patients with OA demonstrated a dose-dependent increase in synovial fluid concentrations of triamcinolone acetonide at week 6 following IA injection (14). It is postulated that there is a critical synovial fluid concentration required to maintain an analgesic effect and that the loss of analgesic effect after week 9 with FX006 16 mg is attributable to synovial fluid triamcinolone acetonide levels dropping below that critical concentration.

The clinical relevance of these findings was assessed with post hoc analysis of standardized effect size (11), a measure used to quantify the magnitude of difference between 2 treatment groups. An effect size >0.3 is considered an important change for a patient-reported outcome (15). For FX006 32 mg compared with saline placebo, effect size for the WOMAC pain instrument exceeded 0.30 at weeks 4 and 8 and approached 0.30 at week 12. Effect size with the 16-mg dose was comparable to that of the 32-mg dose at week 4 but was notably lower at week 8, and no active treatment effect was seen at week 12. Effect sizes assessed with ADP were consistently lower than those for the WOMAC pain subscale for both FX006 doses at each of these time points. Across a large number of trials, the multi-item, knee OA-specific WOMAC pain instrument has proved to be a more sensitive measure of treatment effect than the single-item, general purpose ADP intensity 0–10 NRS (11). Overall, both FX006 doses demonstrated systemic and local safety profiles similar to saline placebo. No FX006 dose relationship in AEs was apparent.

In conclusion, although the study's primary end point was not met, the dose effect on duration of analgesic efficacy observed in this phase IIb study of people with knee OA confirms that FX006 32 mg confers increased therapeutic benefit relative to FX006 16 mg with similar safety, and that improvements in pain afforded by FX006 32 mg were of a magnitude that would be important to patients.

ACKNOWLEDGMENTS

The authors thank the FX006-2014-006 study participants and their enrolling investigators.

AUTHOR CONTRIBUTIONS

All authors were involved in drafting the article or revising it critically for important intellectual content, and all authors approved the final version to be published. Dr. Conaghan had full access to all of the data in the study and takes responsibility for the integrity of the data and the accuracy of the data analysis.

Study conception and design. Conaghan, Lufkin, Johnson, Bodick.

Acquisition of data. Lufkin, Bodick.

Analysis and interpretation of data. Conaghan, Cohen, Berenbaum, Lufkin, Johnson, Bodick.

ROLE OF THE STUDY SPONSOR

Flexion Therapeutics sponsored and funded this study. Together with guidance from regulatory authorities, a subset of the authors (including the corresponding author) worked with the sponsor to develop the study design, study protocol, and statistical analysis plan, and subsequently to interpret study data. Site management and monitoring were provided by contract research organizations (CROs). Data collection and database maintenance were performed by a CRO. A full audit trail was maintained from the time of data entry to database lock. The database was then securely transferred to a

separate CRO for the conduct of statistical analyses (by Karen Ozer and Teresa Curto, Cytel, Waltham, MA). All authors participated in data interpretation and manuscript development in collaboration with a professional medical writer/editor (Michelle L. Perate, MS) funded by the sponsor. All authors had full access to the study data, and the corresponding author takes final responsibility for the decision to submit for publication. No author external to the sponsor received financial compensation to write the manuscript. Publication of this article was not contingent upon approval by Flexion Therapeutics.

REFERENCES

1. Goldring SR, Goldring MB. Clinical aspects, pathology and pathophysiology of osteoarthritis. *J Musculoskelet Neuronal Interact* 2006;6:376–8.
2. McAlindon TE, Bannuru RR, Sullivan MC, Arden NK, Berenbaum F, Bierma-Zeinstra SM, et al. OARSI guidelines for the non-surgical management of knee osteoarthritis. *Osteoarthritis Cartilage* 2014;22:363–88.
3. Da Costa BR, Hari R, Juni P. Intra-articular corticosteroids for osteoarthritis of the knee. *JAMA* 2016;316:2671–2.
4. Kraus VB, Conaghan PG, Aazami HA, Mehra P, Kivitz AJ, Lufkin J, et al. Synovial and systemic pharmacokinetics of triamcinolone acetonide following intra-articular injection of an extended-release microsphere-based formulation (FX006) or standard crystalline suspension in patients with knee osteoarthritis. *Osteoarthritis Cartilage* 2017. E-pub ahead of print.
5. Bodick N, Lufkin J, Willwerth C, Kumar A, Bolognese J, Schoonmaker C, et al. An intra-articular, extended-release formulation of triamcinolone acetonide prolongs and amplifies analgesic effect in patients with osteoarthritis of the knee: a randomized clinical trial. *J Bone Joint Surg Am* 2015;97:877–88.
6. Altman R, Asch E, Bloch D, Bole G, Borenstein D, Brandt K, et al. Development of criteria for the classification and reporting of osteoarthritis: classification of osteoarthritis of the knee. *Arthritis Rheum* 1986;29:1039–49.
7. Kellgren JH, Lawrence JS. Radiological assessment of osteoarthritis. *Ann Rheum Dis* 1957;16:494–502.
8. WOMAC Osteoarthritis Index. WOMAC 3.1 Index: knee and hip osteoarthritis index. URL: <http://www.womac.org/womac/index.htm>.
9. Dworkin RH, Turk DC, Farrar JT, Haythornthwaite JA, Jensen MP, Katz NP, et al. Core outcome measures for chronic pain clinical trials: IMMPACT recommendations. *Pain* 2005;113:9–19.
10. Pham T, van der Heijde D, Altman RD, Anderson JJ, Bellamy N, Hochberg M, et al. OMERACT–OARSI initiative: Osteoarthritis Research Society International set of responder criteria for osteoarthritis clinical trials revisited. *Osteoarthritis Cartilage* 2004;12:389–99.
11. Dworkin RH, Peirce-Sandner S, Turk DC, McDermott MP, Gibofsky A, Simon L, et al. Outcome measures in placebo-controlled trials of osteoarthritis: responsiveness to treatment effects in the REPORT database. *Osteoarthritis Cartilage* 2011;19:483–92.
12. Abhishek A, Doherty M. Mechanisms of the placebo response in pain in osteoarthritis. *Osteoarthritis Cartilage* 2013;21:1229–35.
13. Bannuru RR, McAlindon TE, Sullivan MC, Wong JB, Kent DM, Schmid CH. Effectiveness and implications of alternative placebo treatments: a systematic review and network meta-analysis of osteoarthritis trials. *Ann Intern Med* 2015;163:365–72.
14. Bodick N, Lufkin J, Willwerth C, Hauben J, Kumar A, Boen P, et al. Prolonged joint residency of triamcinolone acetonide after an intra-articular injection of FX006, a sustained release formulation for the treatment of osteoarthritis [abstract]. *Osteoarthritis Cartilage* 2015;23 Suppl:A360–1.
15. Zhang W, Nuki G, Moskowitz RW, Abramson S, Altman RD, Arden NK, et al. OARSI recommendations for the management of hip and knee osteoarthritis. Part III. Changes in evidence following systematic cumulative update of research published through January 2009. *Osteoarthritis Cartilage* 2010;18:476–99.

Knee Alignment Is Quantitatively Related to Periarticular Bone Morphometry and Density, Especially in Patients With Osteoarthritis

Grace H. Lo,¹ Mehveen G. Merchant,² Jeffrey B. Driban,³ Jeffrey Duryea,⁴
Lori Lyn Price,⁵ Charles B. Eaton,⁶ and Timothy E. McAlindon³

Objective. Static alignment influences knee loading and predicts osteoarthritis (OA) progression. Periarticular bone is important in dispersing forces across the knee, and there is substantial evidence for molecular crosstalk between cartilage and subchondral bone. The aim of this study was to evaluate the relationship between periarticular trabecular bone morphology and bone mineral density (BMD) and knee alignment in OA.

Methods. This was a cross-sectional analysis of participants in the Osteoarthritis Initiative Bone Ancillary Study. Dual x-ray absorptiometry (DXA) was performed to measure tibial periarticular bone mineral density (paBMD). Magnetic resonance imaging of knee trabecular bone was performed to calculate the apparent bone volume fraction (aBVF), apparent trabecular number (aTbN), apparent trabecular spacing (aTbSp), and apparent trabecular thickness (aTbTh). Static alignment was assessed by measuring the hip–knee–ankle (HKA) angle on long-limb films.

Results. The study group comprised 436 participants (mean \pm SD age 65.4 ± 9.2 years, 46% female, mean \pm SD body mass index 29.6 ± 4.6 kg/m²), 71% of

whom had OA. Correlations between the HKA angle and medial:lateral paBMD, medial paBMD, aBVF, aTbN, aTbTh, and aTbSp were -0.63 , -0.34 , -0.29 , -0.32 , -0.22 , and 0.30 , respectively. More varus alignment was associated with higher medial:lateral paBMD, medial paBMD, aBVF, aTbN, aTbTh, and lower aTbSp. In OA knees, the results were more pronounced. In non-OA knees, the most consistent association was with medial:lateral paBMD.

Conclusion. Static alignment was associated with medial:lateral paBMD in all knees and with medial paBMD and trabecular morphometry in OA knees only. Aberrant knee loading may lead to increased relative subchondral bone density, which is partly related to a higher aBVF and a greater number of thicker trabeculae with smaller intertrabecular spacing. Knee DXA may be a useful early biomarker of knee OA.

Knee osteoarthritis (OA) is a substantial public health problem, affecting an estimated 30.8 million people in the US (1). OA is the most common type of arthritis, is a common chronic symptom in the outpatient setting (2), and is the source of substantial disability (2). Currently, there are only a few effective treatments for this condition, including nonsteroidal antiinflammatory medications, physical therapy, and ultimately total knee

This article was prepared using an Osteoarthritis Initiative (OAI) public-use data set, and its contents do not necessarily reflect the opinions or views of the OAI investigators, the NIH, or the private funding partners of the OAI. The OAI is a public–private partnership between the NIH (contracts N01-AR-2-2258, N01-AR-2-2259, N01-AR-2-2260, N01-AR-2-2261, and N01-AR-2-2262) and private funding partners (Merck Research Laboratories, Novartis Pharmaceuticals, GlaxoSmithKline, and Pfizer, Inc.) and is conducted by the OAI investigators. Private sector funding for the OAI is managed by the Foundation for the NIH. The authors of this article are not part of the OAI investigative team.

Supported in part by the VA Health Services Research & Development Center for Innovations in Quality, Effectiveness and Safety, Michael E. DeBakey VA Medical Center (grant CIN 13-413) and the NIH (National Institute of Arthritis and Musculoskeletal and Skin Diseases [NIAMS] grant R01-AR-060718 to Dr. McAlindon). Dr. Lo's work was supported by the NIH (NIAMS grant K23-AR-062127).

¹Grace H. Lo, MD, MSc: Baylor College of Medicine and Houston VA Health Services Research & Development Center for

Innovations in Quality, Effectiveness and Safety, Michael E. DeBakey Medical Center, Houston, Texas; ²Mehveen G. Merchant, MD: Nova Scotia Health Authority, Dalhousie University, Halifax, Nova Scotia, Canada; ³Jeffrey B. Driban, PhD, Timothy E. McAlindon, DM: Tufts Medical Center, Boston, Massachusetts; ⁴Jeffrey Duryea, PhD: Brigham and Women's Hospital, Boston, Massachusetts; ⁵Lori Lyn Price, MAS, MLA: Tufts Medical Center and Tufts University, Boston, Massachusetts; ⁶Charles B. Eaton, MD, MS: Memorial Hospital of Rhode Island and Alpert Medical School of Brown University, Pawtucket, Rhode Island.

Address correspondence to Grace H. Lo, MD, MSc, Baylor College of Medicine, 1 Baylor Plaza, BCM-285, Houston, TX 77030. E-mail: ghlo@bcm.edu.

Submitted for publication March 31, 2017; accepted in revised form September 13, 2017.

replacement in patients with the most severe disease. A better understanding of the natural history of this disease may play a critical role in identifying novel effective therapies.

There is substantial evidence for crosstalk between cartilage and subchondral bone at a molecular level (3,4). Although OA is often characterized as a disorder of articular cartilage, the presence of malalignment and changes in periarticular bone are prominent among the protean pathophysiologic manifestations of knee OA. Furthermore, biomechanical studies have shown that much of the load dispersion across a knee occurs within the periarticular bone as compared to the hyaline cartilage (up to 50% compared with only ~3%) (5). Static alignment influences load distribution in the knee joint and is predictive of disease progression in the compartment in which the load is increased (6,7).

Measures of periarticular bone in OA can be obtained using dual x-ray absorptiometry (DXA) of periarticular bone mineral density (paBMD) and magnetic resonance imaging (MRI)-based trabecular morphometry (8–20). These measures are also strongly associated with the presence of knee OA. Knee OA is associated with higher DXA-measured tibial paBMD, bone volume fraction (BVF), trabecular number (TbN), and trabecular thickness (TbTh) but lower trabecular spacing (TbSp) (12–14,17,21).

Because static alignment affects load distribution and is a potent predictor of knee OA progression and aberrations in periarticular bone are prominent in knee OA, we hypothesized that static alignment is associated with periarticular bone measured by DXA (paBMD) and MRI (trabecular BVF, TbN, TbTh, and TbSp). Furthermore, we expected this relationship to be present in persons with and those without radiographic evidence of knee OA, because we anticipated that static alignment influences periarticular bone changes antedating the development of radiographic OA. To address this question, we performed a knee-based cross-sectional study of participants in the Osteoarthritis Initiative (OAI) for whom periarticular bone and static alignment measures were available.

PATIENTS AND METHODS

Overall study design. This was a knee-based cross-sectional study nested within 2 studies ancillary to the OAI, including only members of the progression subcohort who had static alignment measures in addition to DXA measures of paBMD and MRI-assessed trabecular morphometry.

Parent study design. The OAI is a multicenter observational study focused on identifying biomarkers of knee OA (22). Four clinical centers participated in this study: the University of Maryland School of Medicine, Ohio State University, University

of Pittsburgh, and Memorial Hospital of Rhode Island. The coordinating center was the University of California San Francisco. Both male and female OAI participants were included; subjects were ages 45–79 years and were from all ethnic groups. The progression subcohort included those with at least one knee with symptomatic tibiofemoral OA in a native knee joint.

Because the OAI was designed to address multiple scientific questions, standard knee radiographs were obtained annually as part of the parent study. Static alignment and periarticular bone measures were not part of the original protocol and were not obtained for all participants at the same visits. Long-limb films, funded by one ancillary study, were used to measure mechanical alignment and were obtained mostly at the 12-month visit (86%). However, if time did not permit, these films were obtained at the subsequent 24-month or 36-month visit. In a separate ancillary study, knee DXA scans and trabecular MRIs were obtained only from participants in the OAI progression subcohort who were seen from August 8, 2007 to April 3, 2009, attending their 30-month or 36-month visit and willing to have additional knee DXA and trabecular MRI sequences. Subjects with contraindications to MRI and/or bilateral knee replacements at the time of the OAI 30-month or 36-month visit were excluded. Those who had knee DXA scans and trabecular knee MRIs at their 30-month or 36-month visit additionally had 48-month follow-up examinations with knee DXA scans and MRIs.

To align the time points at which data were evaluated, only participants with OAI 48-month visit data, including knee DXA, trabecular morphometry, and standard radiography, were included in these analyses. Additionally, at least one measure of mechanical alignment obtained from long-limb films at any time point was also required.

Standing long-limb films. The gold standard for evaluating static alignment is measurement of the hip-knee-ankle (HKA) angle on standing long-limb films. These films included the hip and tibiotalar joints. Participants were instructed to stand with the tibial tubercle facing forward. The distance between the x-ray beam and the participant was 2.4 meters. Settings of 100–300 mA/second and 80–90 kilovolts were used to optimize the film for limb size and tissue characteristics. These films were taken of bilateral lower extremities. HKA measurements represent the angle at the intersection of 2 lines: the line connecting the femoral head and intercondylar notch centers, and the line connecting the ankle talar surface center and the tibial inter-spinous sulcus base. We used publicly released centralized readings, supervised by Dr. Derek Cooke (OAISYS, Inc., Tempe, Arizona). Interreader reproducibility was high (intraclass correlation coefficient [ICC] 0.99) (23). By convention, negative values represented varus alignment, and positive values represented valgus alignment (23).

Knee radiographs. Weight-bearing, bilateral, fixed-flexion, posteroanterior radiographs of the knees were obtained at the OAI 48-month visit. These images were measured for anatomic axis alignment, the femorotibial angle (FTA), using proprietary software, supervised by Dr. Jeff Duryea; these measures were downloaded from a publicly released data set (24). Based on recommendations by Iranpour-Boroujeni et al, we applied a sex-specific adjustment to the FTA to more closely reflect the HKA angle (24). Additionally, these images were centrally scored for overall radiographic severity using Kellgren/Lawrence (K/L) grades (range 0–4) (25) and medial joint space narrowing grades (range 0–3) using the Osteoarthritis Research Society

International atlas (26), readings that were funded by the parent OAI study and publicly released. The reliability of these readings (read–reread) was good (weighted kappa value [intrarater reliability] 0.70–0.78) (27).

MRI acquisition. A Siemens 3T Trio MRI scanner was used at the OAI 48-month visit to acquire trabecular sequences in one knee (the right knee), unless there was a contraindication; this decision was made based on convenience for the participants in the parent study. For these sequences, the parameters were as follows: oblique coronal 3-dimensional fast imaging with steady-state precession, 72 slices, 1-mm slice thickness, with in-plane spatial resolution of $0.23 \text{ mm} \times 0.23 \text{ mm}$, 12-cm field of view, a 512×512 matrix, an echo time of 4.92 msec (fat/water in-phase), repetition time of 20 msec, flip angle of 50° (phase right-left), and no partial Fourier transformation option (28).

Measurement of trabecular morphometry with MRI.

Full details for measuring trabecular morphometry using proprietary software have been published previously (28–30). One reader analyzed all of the images. A standardized signal intensity threshold was applied to create a bone mask. A signal threshold was selected after application of 20 0.7-mm-diameter circular regions of interest (ROIs) in the cortical bone of the medial and lateral femoral condyles. A rectangular ROI was then placed on 20 consecutive coronal slices, central to the medial tibia. The standardized rectangular ROI had a height of 3.75 mm and a width of 14–17 mm, varying with the size of the tibial plateau. The ROI was placed adjacent to the articular cartilage (Figure 1A). The 20 ROIs were then analyzed, providing measurements of apparent BVF (aBVF), apparent TbTh (aTbTh), apparent TbN (aTbN), and apparent TbSp (aTbSp). The aBVF (apparent bone volume/total volume) was calculated as the percentage of pixels comprising the void in the bone signal over the total number of pixels in the ROI. Apparent TbTh was calculated by obtaining the mean of the intercept length of all angles through a given image, in millimeters. The aTbN was calculated by dividing aBVF by aTbTh. The aTbSp was calculated as $(1/\text{aTbN}) - \text{aTbTh}$. For each trabecular morphometry parameter, an average of the 20 ROIs for each knee was obtained. The ICCs for intrarater (measurement–remeasurement) reliability were 0.97 (95% confidence interval [95% CI] 0.91, 0.99) for aBVF, 0.98 (95% CI 0.92, 0.99) for aTbTh, 0.92 (95% CI 0.73, 0.98) for TbN, and 0.77 (95% CI 0.38, 0.93) for aTbSp (31).

DXA acquisition. At the OAI 48-month visit, bilateral knee imaging was performed unless contraindicated. Each of the 4 clinical sites had identical DXA scanners (GE Lunar Prodigy Advance scanner). Details about obtaining the tibial DXA scans have been published previously (13). Briefly, the lower extremity was placed with the tibia perpendicular to the x-ray beam in a neutral position and with the knee slightly flexed, using knee and foot positioners.

DXA analysis. Full details of the tibial plateau paBMD measurements have been published previously (13). The tibial ROIs had a height of 10 mm, and the width of the medial and lateral ROIs each were half the width of the tibial plateau (Figure 1B). The superior portion of the rectangle was aligned parallel to the superior aspect of the medial joint surface of the tibia. We calculated the medial:lateral paBMD by dividing the medial tibial paBMD by the lateral measure. In a subset of 10 persons, the scan–rescan ICC was 0.997 (95% CI 0.992, 0.999) (31).

Clinical variables collected. Date of birth and date of the 48-month visit were used to calculate the ages of the participants. Body mass index (BMI) was calculated using body weight at the 48-month visit and height at the 36-month visit, the closest time point to the 48-month visit that height was measured. All publicly available data were accessed from the OAI web site (<http://oai.epi-ucsf.org/datarelease/>).

Statistical analysis. Because trabecular morphometry MRIs were obtained for only one knee (usually the right knee), only one knee per participant was included in all analyses. Furthermore, only knees with concordant standard radiographs and DXA at the 48-month visit were included. Because measurement of the HKA angle was funded to be obtained only once during the OAI, and because that measure was obtained at different time points for different participants, measurements of the HKA angle from any time point were included. We used Pearson's correlations to evaluate associations between the HKA angle and knee trabecular morphometry measures and knee paBMD. We also performed correlations of the HKA angle with age and BMI, because these are traditional risk factors for OA (32). We performed stratified analyses based on radiographic OA status (K/L grade ≥ 2). Additionally, we stratified analyses based on sex.

Although the HKA angle, or mechanical alignment, is the gold standard for assessing static alignment, these measures were not obtained at the OAI 48-month visit, when all of the periarticular bone measures were available. Instead, the FTA,

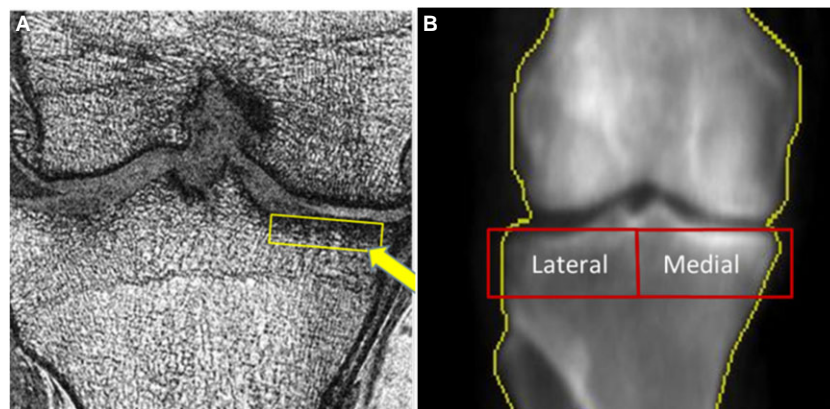


Figure 1. A, Representative trabecular bone sequence–acquired coronal slide. Arrow indicates a region of interest (ROI). B, Representative dual x-ray absorptiometry image of the same knee. Medial and lateral ROIs are shown in red.

or anatomic alignment, which is closely associated with the HKA angle, was available at the OAI 48-month visit. Therefore, we performed sensitivity analyses using the adjusted FTA measures instead of the HKA angle.

To evaluate the contribution of variability in the HKA angle by various combinations of the periarticular bone measures, we assessed the square of the correlation coefficient (R^2) in linear regression models.

RESULTS

As shown in Figure 2, with an a priori plan to enroll 600 participants in the study, the Bone Ancillary Study recruited 629 of the 1,390 participants in the progression subcohort. Of these 629 participants, 503 had sufficient-quality knee DXAs and trabecular MRIs that could be read at the OAI 48-month visit. Of those participants, 451 had HKA readings at any of the time points. Among those participants, 436 had plain radiographs that were read for FTA at the OAI 48-month visit, which was our final sample.

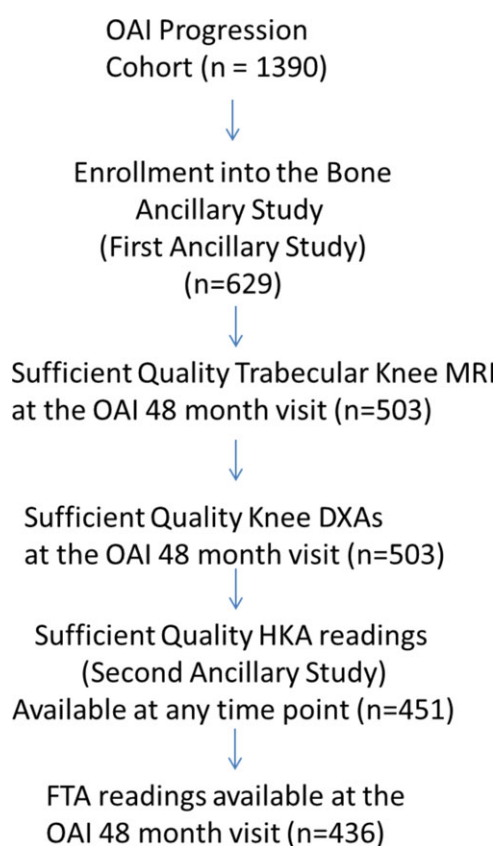


Figure 2. Flow diagram illustrating which participants were included in the study. OAI = Osteoarthritis Initiative; MRI = magnetic resonance imaging; DXA = dual x-ray absorptiometry; HKA = hip-knee-ankle; FTA = femorotibial angle. Color figure can be viewed in the online issue, which is available at <http://onlinelibrary.wiley.com/doi/10.1002/art.40325/abstract>.

Table 1. Characteristics of the subjects and knees that were included or not included in analyses at the 48-month visit*

	Included (n = 436) [†]	Not included (n = 954) [‡]
Subjects		
Female sex, %	46	57
Age, years	65.4 ± 9.2	65.7 ± 8.8§
Body mass index, kg/m ²	29.6 ± 4.6	30.0 ± 5.0¶
Race, %		
White	78	73
Black	20	24
Other	2	3
Knees		
K/L score, %		
0	14	12
1	15	12
2	33	33
3	27	29
4	11	14
HKA angle, degrees#	−1.32 ± 3.65	—
Medial:lateral paBMD, gm/cm ²	1.12 ± 0.15	—
Medial paBMD, gm/cm ²	1.13 ± 0.22	—
Medial tibial aBVF	0.11 ± 0.07	—
Medial tibial aTbN, 1/mm	0.78 ± 0.38	—
Medial tibial aTbTh, mm	0.13 ± 0.02	—
Medial tibial aTbSp, mm	1.75 ± 1.33	—

* Except where indicated otherwise, values are the mean ± SD. K/L = Kellgren/Lawrence; HKA = hip-knee-ankle; paBMD = periarticular bone mineral density; aBVF = apparent bone volume fraction; aTbN = apparent trabecular number; aTbTh = apparent trabecular thickness; aTbSp = apparent trabecular spacing.

[†] Right knees, n = 420; left knees, n = 16.

[‡] All right knees.

§ Obtained in 818 subjects.

¶ Obtained in 725 subjects.

Negative values represent varus alignment.

The demographic features of the participants are shown in Table 1 (see also Supplementary Table A, available on the *Arthritis & Rheumatology* web site at <http://onlinelibrary.wiley.com/doi/10.1002/art.40325/abstract>). The mean ± SD age of the 436 included participants (420 right knees and 16 left knees) was 65.4 ± 9.2 years, 46% were female, and the mean ± SD BMI was 29.6 ± 4.6 kg/m². The characteristics of subjects who were in the progression subcohort (n = 954) but were not included in this study were similar, except the percentage of female subjects was higher (57%), and 32% of the subjects (306 of 954) had missing radiographs at the 48-month visit. Negative HKA values represented varus alignment, and positive values represented valgus alignment. The correlation between the OAI 48-month visit adjusted FTA measures and the OAI 12–36-month visit HKA measures was 0.70 (95% CI 0.65, 0.7). The HKA angle was associated with sex; men had a lower mean HKA compared with women (−2.3 versus −0.2; $P < 0.0001$), which is consistent with more varus alignment. The HKA angle was not associated with age or BMI.

Table 2. Correlations between periarticular bone measures and mechanical alignment (hip–knee–ankle angle), stratified by study group*

	r (95% CI) in all subjects (n = 436)	r (95% CI) in subjects with no radiographic OA (n = 123)	r (95% CI) in subjects with radiographic OA (n = 313)
Medial:lateral paBMD	−0.63 (−0.69, −0.57)	−0.33 (−0.48, −0.16)	−0.68 (−0.74, −0.62)
Medial paBMD	−0.34 (−0.42, −0.26)	−0.09 (−0.26, 0.09)	−0.40 (−0.49, −0.30)
Medial tibial aBVF	−0.29 (−0.37, −0.20)	−0.15 (−0.31, 0.03)	−0.32 (−0.41, −0.21)
Medial tibial aTbN	−0.32 (−0.40, −0.23)	−0.18 (−0.34, 0)	−0.35 (−0.44, −0.25)
Medial tibial aTbTh	−0.22 (−0.31, −0.13)	−0.08 (−0.25, 0.10)	−0.25 (−0.35, −0.15)
Medial tibial aTbSp	0.30 (0.21, 0.38)	0.19 (0.02, 0.37)	0.32 (0.22, 0.42)
Age	0.01 (−0.08, 0.10)	0.06 (−0.12, 0.24)	0 (−0.11, 0.11)
Body mass index	−0.05 (−0.14, 0.05)	0.02 (−0.16, 0.20)	−0.06 (−0.17, 0.05)

* Negative values represent varus alignment. OA = osteoarthritis; 95% CI = 95% confidence interval; paBMD = periarticular bone mineral density; aBVF = apparent bone volume fraction; aTbN = apparent trabecular number; aTbTh = apparent trabecular thickness; aTbSp = apparent trabecular spacing.

The correlation coefficient for the relationship between HKA and medial:lateral paBMD, the only periarticular bone measure that was a ratio, was larger than that for any other bone measure (Table 2). Subjects with a more varus alignment had a higher medial: lateral paBMD, aBVF, aTbN, and aTbTh and a lower aTbSp. Sensitivity analysis using adjusted FTA values from the OAI 48-month follow-up visit yielded similar findings, except that the point estimates were slightly greater in magnitude (see Supplementary Table B, available on the *Arthritis & Rheumatology* web site at <http://onlinelibrary.wiley.com/doi/10.1002/art.40325/abstract>).

In subjects with and those without radiographic OA, medial:lateral paBMD was associated with mechanical alignment, but the strength of the association was greater in those with radiographic OA (Table 2). Similarly, all of the absolute measures of bone had a significant association with mechanical alignment in subjects with radiographic OA, but these correlations were substantially attenuated in those without radiographic OA (Table 2). As with the whole group (those with and those without radiographic OA), male subjects tended to have a more varus alignment (−2.6 versus −0.7 [$P < 0.0001$] and −1.7 versus −0.4 [$P < 0.01$], respectively).

In the sex-specific analyses, there were slightly more men than women, but the correlation coefficients for the relationship between periarticular bone and mechanical alignment were similar, and all correlation coefficients except aTbTh thickness in women were statistically significant (Table 3). In both men and women, age and BMI were not significantly associated with mechanical alignment. Similar to what was seen in the analysis for the whole group (Table 2), when stratified by radiographic OA status (Table 3), the medial:lateral paBMD was associated with HKA angle in those without radiographic OA, but much more so in those with

radiographic OA. Additionally, the absolute measures of periarticular bone were associated with HKA only in those with radiographic OA.

Table 4 shows the contribution of periarticular bone measures to the variation in the HKA angle. The medial:lateral paBMD accounted for 40% of the variation in the HKA angle in the whole cohort. When restricting the analyses to only those knees with radiographic OA, medial:lateral paBMD accounted for 47% of variation in the HKA angle. However, when limiting the analyses to those knees without radiographic OA, it accounted for only 11% of variation in the HKA angle. For all of these analyses, the addition of all the absolute measures of periarticular bone, including medial paBMD, aBVF, aTbN, aTbTh, and aTbSp only marginally increased the percentage of variation in the HKA angle that could be explained. The absolute value for medial paBMD accounted for only 12% of variability in the HKA angle in the whole sample, 16% in subjects with radiographic OA, and 0% in those without radiographic OA. All 4 trabecular morphometry measures combined performed worse than the medial paBMD alone. When paBMD was combined with the 4 trabecular morphometry measures, the additional variability in the HKA angle was only marginally improved over that using paBMD alone.

DISCUSSION

This study confirms a relationship between knee joint alignment and structural measures of the subchondral bone. This relationship was strongest for medial: lateral paBMD and static alignment. This association was present in individuals with and those without radiographic OA but was more pronounced in those with OA. Additionally, we observed that absolute measures of periarticular bone, including medial paBMD, aBVF,

Table 3. Correlations of periarticular bone measures as they relate to mechanical alignment (HKA angle), stratified by sex*

	r (95% CI) in men (n = 234)	r (95% CI) in women (n = 202)	r (95% CI) in men		r (95% CI) in women	
			No radiographic OA (n = 74)	Radiographic OA (n = 160)	No radiographic OA (n = 49)	Radiographic OA (n = 153)
Medial:lateral paBMD	-0.58 (-0.66, -0.48)	-0.66 (-0.73, -0.57)	-0.25 (-0.45, -0.02)	-0.64 (-0.72, -0.53)	-0.34 (-0.56, -0.06)	-0.71 (-0.78, -0.62)
Medial paBMD	-0.25 (-0.37, -0.12)	-0.30 (-0.42, -0.17)	0.09 (-0.15, 0.31)	-0.31 (-0.45, -0.17)	-0.19 (-0.45, 0.09)	-0.33 (-0.47, -0.18)
Medial tibial aBVF	-0.25 (-0.3, -0.12)	-0.16 (-0.3, -0.03)	-0.07 (-0.29, 0.16)	-0.27 (-0.41, -0.12)	-0.13 (-0.4, 0.16)	-0.17 (-0.32, -0.01)
Medial tibial aTbN	-0.25 (-0.37, -0.13)	-0.20 (-0.33, -0.06)	-0.06 (-0.28, 0.17)	-0.29 (-0.42, -0.14)	-0.2 (-0.45, 0.09)	-0.20 (-0.35, -0.04)
Medial tibial aTbTh	-0.23 (-0.35, -0.10)	-0.11 (-0.24, 0.03)	-0.08 (-0.31, 0.14)	-0.25 (-0.39, -0.10)	-0.03 (-0.4, 0.16)	-0.13 (-0.29, 0.03)
Medial tibial aTbSp	0.21 (0.08, 0.33)	0.24 (0.10, 0.37)	0.07 (-0.16, 0.29)	0.23 (0.08, 0.37)	0.16 (-0.12, 0.43)	0.26 (0.10, 0.4)
Age	0.02 (-0.11, 0.15)	-0.04 (-0.18, 0.10)	0.15 (-0.08, 0.37)	-0.02 (-0.17, 0.14)	-0.07 (-0.35, 0.21)	-0.04 (-0.20, 0.12)
BMI	-0.04 (-0.17, 0.09)	-0.09 (-0.22, 0.05)	0.15 (-0.09, 0.36)	-0.10 (-0.26, 0.05)	-0.08 (-0.35, 0.21)	-0.10 (-0.25, 0.07)

* Negative values represent varus alignment, and positive values represent valgus alignment. HKA = hip-knee-ankle; OA = osteoarthritis; 95% CI = 95% confidence interval; paBMD = periarticular bone mineral density; aBVF = apparent bone volume fraction; aTbN = apparent trabecular number; aTbTh = apparent trabecular thickness; aTbSp = apparent trabecular spacing; BMI = body mass index.

Table 4. Contribution of periarticular bone measures to variation in the HKA angle*

Independent variables	Whole cohort	Subjects with radiographic OA	Subjects without radiographic OA
Medial:lateral paBMD	0.40	0.47	0.11
Medial:lateral paBMD, medial paBMD, aBVF, aTbN, aTbTh, aTbSp	0.41	0.49	0.13
Medial paBMD	0.12	0.16	0†
aBVF, aTbN, aTbTh, aTbSp	0.11	0.13	0.05†
Medial paBMD, aBVF, aTbN, aTbTh, aTbSp	0.14	0.19	0.05†

* Values are the square of the correlation coefficients for the association between the hip–knee–ankle (HKA) angle and the variable(s). OA = osteoarthritis; paBMD = periarticular bone mineral density; aBVF = apparent bone volume fraction; aTbN = apparent trabecular number; aTbTh = apparent trabecular thickness; aTbSp = apparent trabecular spacing.

† *P* value for the model is not statistically significant at a level of ≤ 0.05 .

aTbN, aTbTh, and aTbSp, were associated with static alignment, but this was generally present only in those with radiographic OA. Finally, little additional variation in the HKA angle is explained by the addition of absolute measures of periarticular bone after the ratio of medial:lateral paBMD is included as an independent variable. These observations persisted in analyses restricted by sex.

The relationship between static alignment and medial:lateral paBMD has previously been reported in 2 smaller studies of fewer than 100 subjects. In those studies, participants were preselected to have medial tibiofemoral knee OA; the observed correlations were 0.44 and 0.53, respectively (15,17), which are similar to the correlation observed in our study (0.63). Important differences between prior studies and the current study include the fact that our study sample was larger (>400 participants were evaluated), the locations of the ROIs we used on the DXA scanner were more proximal, we included both knees with and those without OA, and we did not preselect for those with medial tibiofemoral OA. Additionally, neither of the prior studies had measures of trabecular morphometry or included additional analyses focusing on the subgroups of those without OA, men only, or women only.

The observations from our study provide potentially important insights into the natural history of knee OA. We had anticipated that periarticular bone measures would be associated with static alignment in individuals with and those without knee OA. The one bone measure that performed in this manner was the medial:lateral paBMD ratio, a relative measure of periarticular bone that compares the medial compartment with the lateral compartment. This finding supports the idea that static alignment is associated with relative loading in the medial and lateral compartments, even in a pre-OA setting. Because of the cross-sectional design of our study, we cannot assign directionality of causation. It is possible that changes in periarticular bone could predispose to the

development of static alignment. Perhaps trauma to the bone, which causes an increase in BMD, might lead to changes in static alignment. However, it is our conjecture that it is more likely that static alignment dictates periarticular bone measures, where changes in static alignment then cause damage to periarticular bone.

A finding that was somewhat surprising was that the absolute measures of periarticular bone were associated with static alignment primarily in those knees with OA and not in those without OA. This may indicate that the absolute measures of periarticular bone are identifying a construct that is present in the periarticular bone, only as OA develops or after the development of OA. For example, in a prior study, we observed that in regions where bone marrow lesions are visualized on T2-weighted, fat-suppressed images, there is a higher aBVF, aTbN, and aTbTh, and lower aTbSp (33), similar to the pattern seen with increased varus alignment. Thus, there may be bone marrow lesions in the regions of bone indicated by higher absolute measures of periarticular bone. An alternative explanation could be that the changes observed in the periarticular bone are a consequence of bone attempting to remodel and repair after incurring damage.

A prior study showed that medial:lateral paBMD is associated with subchondral sclerosis (10), which usually is a feature of more severe OA, occurring in the region where tibial paBMD is assessed. We observed that in knees without OA, only 11% of the variability of static alignment is explained by the medial:lateral paBMD ratio, while in knees with OA, 47% of the variability of static alignment is explained by the medial:lateral paBMD ratio. The association between static alignment and medial:lateral paBMD is stronger in persons with OA, perhaps because in the situation in which OA exists, the relative measure of medial:lateral paBMD is increased for 2 reasons: 1) *physiologic relative changes* and 2), *pathologic changes*. The physiologic relative changes in periarticular bone may occur because of loading differences in the medial and lateral tibiofemoral compartments because of

static alignment. The pathologic changes may occur after or when OA occurs as identified by those with a higher aBVF, aTbN, and aTbTh, and lower aTbSp. In further support of this possibility, we expected and observed that the range of periarticular bone and static alignment measures was broader in subjects with OA compared with those without OA (see Supplementary Table A, available on the *Arthritis & Rheumatology* web site at <http://online.library.wiley.com/doi/10.1002/art.40325/abstract>).

The medial-to-lateral ratio of paBMD is a relative measure of periarticular bone that allows for an internal control within the knee. We were able to create this ratio only for paBMD because we did not have measurements for periarticular trabecular morphometry in the lateral compartment due to financial constraints. If we did have trabecular morphometry measures in the lateral compartment, we suspect they would perform similarly to paBMD, as a higher absolute paBMD is associated with greater tibial aBVF, aTbN, tibial aTbTh, and lower tibial aTbSp (32). In future studies of trabecular morphometry, ratios of the measures that would also allow for internal controls may also prove to be more powerful than the absolute measures, as is the case with DXA-assessed paBMD (Table 4). A greater understanding of the relationship between static alignment and periarticular bone changes could have important implications regarding treatment targets in knee OA.

In the current study, DXA-assessed paBMD performed similarly to the trabecular morphometry measures, but it is much easier to acquire and measure DXA-assessed trabecular morphometry compared with MRI-assessed trabecular morphometry. Additionally, DXA scanners are almost ubiquitous in a clinical setting because they are widely used to assess for osteoporosis. Therefore, there is an opportunity to consider its use to measure paBMD as an early biomarker for OA. However, in order to understand paBMD in OA, it is critical to understand that DXA-assessed paBMD is a measure of apparent density, not material density.

Apparent density is bone mass/total volume of bone (includes volume occupied by bone marrow), whereas material density is bone mass/bone volume (excludes volume occupied by bone marrow) (33). Based on histologic finding, OA bone has a lower material bone density but a higher apparent density compared with non-OA periarticular bone (34). Although it might seem intuitive to expect that material density would be more informative than apparent density in OA, because it provides a more precise measure of bone mineralization, in OA, apparent density is associated with bone stiffness, whereas material density is not (34). Stiffness is a measure of resistance offered by a body against

deformation, or a measure of the amount of force required to cause a displacement in the direction of the force applied. Bone that is stiffer is less able to absorb energy in the setting of mechanical impact. In OA, persons with a higher apparent density have greater periarticular bone stiffness, meaning that bone with higher paBMD requires more force to compress a given amount than bone with lower paBMD. Perhaps the pathologic changes detectable with trabecular morphometry contribute to a higher paBMD and confer greater stiffness to bone.

Existing evidence supports the possibility that modifying static alignment can influence periarticular bone. In a study by Akamatsu et al, a group of participants with medial knee OA ($n = 20$) identified for high tibial osteotomy, an extreme method of modifying static alignment, had their periarticular bone density assessed prior to the surgical intervention and subsequent to the procedure (12). The medial:lateral paBMD ratios were high preoperatively and decreased postoperatively, suggesting that an effort to alter static alignment might confer changes in periarticular bone, although we must point out that there was no comparator arm in this study. Additionally, less-extreme interventions may also modify static alignment, such as knee bracing. In a study by Katsuragawa et al, all participants ($n = 14$) had a knee with varus alignment, upon which a valgus brace was applied; after 3 months of follow-up, the braced knees had statistically significant improvement in the tibial paBMD ratio, which was not seen in the unbraced knees (35). However, similar to the study by Akamatsu et al, the current study was small and had no comparator arm. Larger randomized controlled studies of tibial osteotomy and knee bracing are needed to confirm whether these interventions targeting static alignment can modify paBMD.

The current study has several limitations. First, MRI provides only indirect measurements of the parameters of bone morphology. Only direct histology, which requires a bone biopsy and is difficult to acquire in subjects with milder disease and those without disease, would allow direct periarticular bone measurements; however, in the absence of such information, surrogate measures must be used to extrapolate measurements such as TbTh and TbSp. An additional limitation of this study is that the HKA angle, the gold standard for assessment of static alignment, and periarticular bone measures were generally not assessed at the same visit, because inclusion of the HKA angle and trabecular morphometry measures were funded by separate ancillary projects to the OAI and were included when convenient, taking into consideration the entire study schedule. To address this limitation, we performed sensitivity analyses using adjusted FTA measures that were all contemporaneous with the periarticular

bone measures instead of the HKA angle and observed results (see Supplementary Table B, available on the *Arthritis & Rheumatology* web site at <http://onlinelibrary.wiley.com/doi/10.1002/art.40325/abstract>) similar to those in the main study using the HKA angle (Table 2). An additional limitation is that a longitudinal study would be needed to assess causation in the relationship between static alignment and periarticular bone abnormalities. Because the HKA angle was determined at only one time point in our study, we were unable to test this relationship.

In summary, static knee alignment is associated with relative paBMD, as measured by DXA, in individuals with and those without OA. Absolute measures of periarticular bone are associated with static alignment only in individuals with OA. The variation in static alignment explained by trabecular morphometry is mostly captured with the relative paBMD measure. Understanding the underlying pathophysiology driving the aberrations in trabecular morphometry could provide important insights into identifying new targets for OA therapies, some of which may be biomechanically based. Longitudinal studies are needed to elucidate whether biomechanical changes may alter periarticular bone in knee OA and ultimately prevent, slow, and maybe even reverse the progression of OA. Additionally, our findings indicate the potential utility of DXA and MRI-based measures to evaluate the effects of biomechanical or bone-targeted interventions in knee OA.

AUTHOR CONTRIBUTIONS

All authors were involved in drafting the article or revising it critically for important intellectual content, and all authors approved the final version to be published. Dr. Lo had full access to all of the data in the study and takes responsibility for the integrity of the data and the accuracy of the data analysis.

Study conception and design. Lo.

Acquisition of data. Lo, McAlindon.

Analysis and interpretation of data. Lo, Merchant, Driban, Duryea, Price, Eaton, McAlindon.

REFERENCES

1. Cisternas MG, Murphy L, Sacks JJ, Solomon DH, Pasta DJ, Helmick CG. Alternative methods for defining osteoarthritis and the impact on estimating prevalence in a US population-based survey. *Arthritis Care Res (Hoboken)* 2016;68:574–80.
2. Lawrence RC, Felson DT, Helmick CG, Arnold LM, Choi H, Deyo RA, et al. Estimates of the prevalence of arthritis and other rheumatic conditions in the United States. Part II. *Arthritis Rheum* 2008;58:26–35.
3. Findlay DM, Atkins GJ. Osteoblast-chondrocyte interactions in osteoarthritis. *Curr Osteoporos Rep* 2014;12:127–34.
4. Yuan XL, Meng HY, Wang YC, Peng J, Guo QY, Wang AY, et al. Bone-cartilage interface crosstalk in osteoarthritis: potential pathways and future therapeutic strategies. *Osteoarthritis Cartilage* 2014;22:1077–89.
5. Radin EL, Paul IL, Lowy M. A comparison of the dynamic force transmitting properties of subchondral bone and articular cartilage. *J Bone Joint Surg Am* 1970;52:444–56.
6. Sharma L, Song J, Dunlop D, Felson D, Lewis CE, Segal N, et al. Varus and valgus alignment and incident and progressive knee osteoarthritis. *Ann Rheum Dis* 2010;69:1940–5.
7. Sharma L, Chmiel JS, Almagor O, Felson D, Guermazi A, Roemer F, et al. The role of varus and valgus alignment in the initial development of knee cartilage damage by MRI: the MOST study. *Ann Rheum Dis* 2013;72:235–40.
8. Felson DT, McLaughlin S, Goggins J, LaValley MP, Gale ME, Totterman S, et al. Bone marrow edema and its relation to progression of knee osteoarthritis. *Ann Intern Med* 2003;139:330–6.
9. Lo GH, Zhang Y, McLennan C, Niu J, Kiel DP, McLean RR, et al. The ratio of medial to lateral tibial plateau bone mineral density and compartment-specific tibiofemoral osteoarthritis. *Osteoarthritis Cartilage* 2006;14:984–90.
10. Lo GH, Hunter DJ, Zhang Y, McLennan CE, LaValley MP, Kiel DP, et al. Bone marrow lesions in the knee are associated with increased local bone density. *Arthritis Rheum* 2005;52:2814–21.
11. Lo GH, Schneider E, Price L, Driban J, Tassinari A, Nevitt M, et al. Periarticular bone density and trabecular morphology predict knee OA structural progression. *Osteoarthritis Cartilage* 2012;20 Suppl 1:S76–7.
12. Akamatsu Y, Koshino T, Saito T, Wada J. Changes in osteosclerosis of the osteoarthritic knee after high tibial osteotomy. *Clin Orthop Relat Res* 1997;207–14.
13. Dore D, Quinn S, Ding C, Winzenberg T, Jones G. Correlates of subchondral BMD: a cross-sectional study. *J Bone Miner Res* 2009;24:2007–15.
14. Thorp LE, Wimmer MA, Block JA, Moio KC, Shott S, Goker B, et al. Bone mineral density in the proximal tibia varies as a function of static alignment and knee adduction angular momentum in individuals with medial knee osteoarthritis. *Bone* 2006;39:1116–22.
15. Sepriano A, Roman-Blas JA, Little RD, Pimentel-Santos F, Arribas JM, Largo R, et al. DXA in the assessment of subchondral bone mineral density in knee osteoarthritis: a semi-standardized protocol after systematic review. *Semin Arthritis Rheum* 2015;45:275–83.
16. Wada M, Maezawa Y, Baba H, Shimada S, Sasaki S, Nose Y. Relationships among bone mineral densities, static alignment and dynamic load in patients with medial compartment knee osteoarthritis. *Rheumatology (Oxford)* 2001;40:499–505.
17. Beuf O, Ghosh S, Newitt DC, Link TM, Steinbach L, Ries M, et al. Magnetic resonance imaging of normal and osteoarthritic trabecular bone structure in the human knee. *Arthritis Rheum* 2002;46:385–93.
18. Majumdar S, Kothari M, Augat P, Newitt DC, Link TM, Lin JC, et al. High-resolution magnetic resonance imaging: three-dimensional trabecular bone architecture and biomechanical properties. *Bone* 1998;22:445–54.
19. Lo GH, Tassinari AM, Driban JB, Price LL, Schneider E, Majumdar S, et al. Cross-sectional DXA and MR measures of tibial periarticular bone associate with radiographic knee osteoarthritis severity. *Osteoarthritis Cartilage* 2012;20:686–93.
20. Driban JB, Barbe MF, Amin M, Kalariya NS, Zhang M, Lo GH, et al. Validation of quantitative magnetic resonance imaging-based apparent bone volume fraction in peri-articular tibial bone of cadaveric knees. *BMC Musculoskelet Disord* 2014;15:143.
21. The osteoarthritis initiative: protocol for the cohort study. URL: <https://oai.epi-ucsf.org/datarelease/docs/studydesignprotocol.pdf>.
22. Central assessment of full-limb x-rays for frontal plane lower limb alignment. URL: https://oai.epi-ucsf.org/datarelease/SASDocs/fIXR_KneeAlign_Descrip.pdf.
23. Central assessment of longitudinal knee x-rays for femoral-tibial angle (anatomic alignment). URL: https://oai.epi-ucsf.org/datarelease/SASDocs/kXR_FTA_Duryea_descrip.pdf.
24. Iranpour-Boroujeni T, Li J, Lynch JA, Nevitt M, Duryea J, for the OAI Investigators. A new method to measure anatomic knee alignment for large studies of OA: data from the osteoarthritis initiative. *Osteoarthritis Cartilage* 2014;22:1668–74.
25. Kellgren JH, Lawrence JS. Radiological assessment of osteoarthritis. *Ann Rheum Dis* 1957;16:494–502.

26. Altman RD, Gold GE. Atlas of individual radiographic features in osteoarthritis, revised. *Osteoarthritis Cartilage* 2007;15 Suppl A:A1–56.
27. Project 15 test-retest reliability of semi-quantitative readings from knee radiographs. URL: https://oai.epi-ucsf.org/datarelease/SASDocs/kXR_SQ_Rel_BU_descrip.pdf.
28. Schneider E, Lo GH, Sloane G, Fanella L, Hunter DJ, Eaton CB, et al. Magnetic resonance imaging evaluation of weight-bearing subchondral trabecular bone in the knee. *Skeletal Radiol* 2011;40:95–103.
29. Majumdar S, Kothari M, Augat P, Newitt DC, Link TM, Lin JC, et al. High-resolution magnetic resonance imaging: three-dimensional trabecular bone architecture and biomechanical properties. *Bone* 1998;22:445–54.
30. Felson DT. The epidemiology of knee osteoarthritis: results from the Framingham Osteoarthritis Study. *Semin Arthritis Rheum* 1990;20:42–50.
31. Drihan JB, Tassinari A, Lo GH, Price LL, Schneider E, Lynch JA, et al. Bone marrow lesions are associated with altered trabecular morphometry. *Osteoarthritis Cartilage* 2012;20:1519–26.
32. Burr DB. The importance of subchondral bone in the progression of osteoarthritis. *J Rheumatol Suppl* 2004;70:77–80.
33. Li B, Aspden RM. Composition and mechanical properties of cancellous bone from the femoral head of patients with osteoporosis or osteoarthritis. *J Bone Miner Res* 1997;12:641–51.
34. Malekipour F, Whitton C, Oetomo D, Lee PV. Shock absorbing ability of articular cartilage and subchondral bone under impact compression. *J Mech Behav Biomed Mater* 2013; 26:127–35.
35. Katsuragawa Y, Fukui N, Nakamura K. Change of bone mineral density with valgus knee bracing. *Int Orthop* 1999;23:164–7.

BRIEF REPORT

Loss of Muscle Strength Prior to Knee Replacement: A Question of Anatomic Cross-Sectional Area or Specific Strength?

Adam G. Culvenor,¹ Felix C. Hamler,² Jana Kemnitz,² Wolfgang Wirth,³ and Felix Eckstein³

Objective. To determine whether loss in thigh muscle strength prior to knee replacement is caused by reductions of muscle strength in the anatomic cross-sectional area or by reductions of specific strength.

Methods. All 100 of the participants in the Osteoarthritis Initiative who underwent knee replacement and whose medical records included data on thigh isometric muscle strength and magnetic resonance imaging (MRI) (58 women, and 42 men, mean \pm SD age 65 ± 8 years, mean \pm SD body mass index [BMI] 29 ± 5 kg/m²) were matched with a control (no knee replacement) for age, sex, height, BMI, and radiographic severity. Thigh muscle anatomic cross-sectional area was determined by MRI at the research visit before knee replacement (time 0) and 2 years before time 0 (time –2). Specific strength (strength/anatomic cross-sectional area) was calculated, and the measures were compared by conditional logistic regression (i.e., odds ratio [OR] per standard deviation). ORs adjusted for pain (OR_{adj}) and 95% confidence intervals (95% CIs) were also calculated.

Results. Knee replacement cases had significantly smaller extensor (but not flexor) anatomic cross-sectional areas than controls at time 0 (women, OR_{adj} 1.89 [95% CI 1.05–3.90]; men, OR_{adj} 2.22 [95% CI 1.04–4.76]), whereas no significant differences were found at time –2. Women who had knee replacement showed

lower levels of extensor specific strength than controls at time 0 (OR 1.59 [95% CI 1.02–2.50]), although this difference was not observed in men and did not maintain significance after adjustment for pain (OR_{adj} 1.22 [95% CI 0.71–2.08]). Female cases lost significantly more extensor specific strength between time –2 and time 0 than controls (OR_{adj} 3.76 [95% CI 1.04–13.60]), whereas no significant differences were noted at time –2, or in men.

Conclusion. Prior to knee replacement, a significant reduction in knee extensor strength appears to occur in women through 2 mechanisms: one driven by pain (loss of specific strength) and one independent of pain (loss of muscle anatomic cross-sectional area). Men who underwent knee replacement showed significantly reduced levels of extensor anatomic cross-sectional area, but not significantly lower strength or specific strength.

In an effort to improve pain and function associated with end-stage knee osteoarthritis (OA), >600,000 total knee replacements are performed annually in the US (1). This number is expected to increase to 3.5 million per year by 2030, resulting in significant increases in the health and economic burden caused by OA (1). These increases reinforce the urgency of identifying strategies for modifying the risk of knee replacement surgery due to progressive knee OA.

This article was prepared using an Osteoarthritis Initiative (OAI) public-use data set, and its contents do not necessarily reflect the opinions or views of the OAI Study Investigators, the NIH, or the private funding partners of the OAI. The OAI is a public-private partnership between the NIH (contracts N01-AR-2-2258, N01-AR-2-2259, N01-AR-2-2260, N01-AR-2-2261, and N01-AR-2-2262) and private funding partners (Merck Research Laboratories, Novartis Pharmaceuticals, GlaxoSmithKline, and Pfizer, Inc.) and is conducted by the OAI Study Investigators. Private sector funding for the OAI is managed by the Foundation for the NIH. The authors of this article are not part of the OAI investigative team.

Supported by the European Union under the Seventh Framework Programme (project KNEEMO; FP7-PEOPLE-2013-ITN; grant 607510). Dr. Culvenor is recipient of a National Health and Medical Research Council of Australia Early Career Fellowship (Neil Hamilton Fairley Clinical Fellowship 1121173).

¹Adam G. Culvenor, PhD: Paracelsus Medical University, Salzburg, Austria, and La Trobe University, Bundoora, Victoria, Australia;

²Felix C. Hamler, MD, Jana Kemnitz, MSc: Paracelsus Medical University, Salzburg, Austria; ³Wolfgang Wirth, PhD, Felix Eckstein, MD: Paracelsus Medical University, Salzburg, Austria, and Chondrometrics, Ainring, Germany.

Dr. Wirth is employed part-time by, and is co-owner of, Chondrometrics GmbH, in which he owns stock or stock options. Dr. Eckstein has received consulting fees, speaking fees, and/or honoraria from Merck Serono, Samumed, BioClinica/Synarc, and Medtronic (less than \$10,000 each) and research support from Pfizer, Eli Lilly, Merck Serono, Novartis, Stryker, AbbVie, Kolon, Synarc, Ampio, BICL, OrthoTrophix, and TissueGene; he is chief executive officer and co-owner of Chondrometrics GmbH, in which he owns stock or stock options.

Address correspondence to Adam G. Culvenor, PhD, Institute of Anatomy, Paracelsus Medical University, Strubergasse 21, A5020 Salzburg, Austria. E-mail: adam.culvenor@pmu.ac.at.

Submitted for publication May 29, 2017; accepted in revised form September 29, 2017.

Thigh muscle weakness has been identified as a determinant of radiographic and symptomatic knee OA incidence and progression (2,3). In a recent matched case-control study of adults with knee OA from the Osteoarthritis Initiative (OAI), we identified thigh muscle weakness as a predictor of knee replacement in women, independent of disease severity and pain (4). However, this relationship was not observed in men (4).

Given the modifiable nature of muscle strength, these findings identify a potential therapeutic strategy to modify the risk of knee replacement in women. However, the mechanisms driving the sex-specific relationship between muscle weakness and knee replacement (and other knee OA outcomes) are unknown, but are important in directing individualized treatment strategies to counteract deficits in muscle strength. For example, deficits in the muscle anatomic cross-sectional area have been reported in symptomatic knee OA (5) and may be responsible for loss of muscle strength prior to knee replacement. Conversely, loss in muscle specific strength (e.g., strength per anatomic cross-sectional area) has recently been identified to play a role in onset of knee OA in women (6) and would require different therapeutic approaches (e.g., interventions targeting muscle activation impairments, such as muscle biofeedback or neuromuscular electrical stimulation) as compared with a situation in which reduction in muscle anatomic cross-sectional area is the only mechanism that is responsible for muscle strength deficits. In order to establish the mechanisms behind thigh muscle weakness and knee replacement risk observed in women (4), we undertook the present study to determine how thigh muscle anatomic cross-sectional area and/or specific strength, or longitudinal changes in these measures, independently impact risk of subsequent knee replacement in men and women.

PATIENTS AND METHODS

Participants. All OAI participants who were included in our recent analysis of muscle strength prior to knee replacement (4) were eligible for inclusion in the current analysis. Briefly, all OAI participants who reported having had knee replacement at any annual OAI visit between 12- and 60-month follow-up, and who had thigh muscle strength assessed within the 2 years prior to knee replacement, were eligible as cases ($n = 136$) (4). Only cases with T1-weighted axial spin-echo magnetic resonance imaging (MRI) acquisitions of the thigh at the same time points could be included in the current analysis (1 knee per person; $n = 100$). In the OAI, thigh isometric muscle strength measurements and thigh MRIs were obtained biennially (i.e., baseline, 24-month, and 48-month visits). In some participants, muscle strength measurements and thigh MRIs were obtained at 12-month and/or 36-month visits instead of baseline and/or 24-month visits. The time point at which muscle strength and MRI examinations were analyzed as preceding knee replacement

(time 0) was within a window of 2 years prior to knee replacement (e.g., for a knee replacement detected at the 36-month visit, time 0 was the 12- or 24-month measurement, whichever was available, and for a 48-month knee replacement, time 0 was the 36- or 24-month measurement). The time point 2 years prior to time 0 was termed time -2 (4).

Controls (1 knee per person) were selected from OAI participants who had not received a knee replacement in either knee between baseline and 60-month follow-up and had muscle strength and MRI assessments at the same time points as knee replacement cases. Cases and controls were matched 1:1 by sex, age (± 5 years), height (± 5 cm), body mass index (BMI) (± 3 kg/m²), knee replacement limb (dominant [preferred kicking leg] versus nondominant), baseline Kellgren/Lawrence (K/L) score (7) (grades 0–4) from the central readings, as well as presence and location (i.e., medial/lateral joint space narrowing [JSN]) of baseline compartmental involvement. Due to a lack of thigh MRIs at time 0 in 3 controls from our recent analysis of this cohort (4), we rematched these ineligible controls with new eligible OAI controls with thigh MRIs. The OAI was approved by local ethics committees and participants gave informed consent for OAI public database inclusion.

Evaluation of muscle strength and anatomic cross-sectional areas. Maximal isometric knee extensor and flexor strength had been measured with the Good Strength Chair (Metitur), at 60° of knee flexion, as previously described (4). Muscle anatomic cross-sectional areas of the quadriceps and hamstrings were measured from axial MRI at anatomically consistent locations (33% femoral length; distal-to-proximal) (6) using custom semi automated software developed at our institution (8). This method has been shown to display reliability and validity in longitudinal studies (8). To account for remaining differences in body size (despite the matching procedure), anatomic cross-sectional areas were normalized to femoral size (femur anatomic cross-sectional area from same MRI slice). Specific strength was calculated as strength per unit anatomic cross-sectional area (N/cm²) (6). We used strength measurements directly (not muscle torque) to estimate muscle strength, because both the lever arm between the load cell and joint center and that between the muscle tendons and joint center depend on body size and are roughly proportional (9).

Statistical analysis. After confirming normality, paired *t*-tests between sex-specific case-control pairs were conducted for extensor and flexor anatomic cross-sectional area and specific strength at time 0 and time -2 , and for change between time -2 and time 0. Further, sex-specific case-control conditional logistic regression (case-control odds ratios [ORs] per standard deviation) was performed, for extensor and flexor anatomic cross-sectional area and specific strength at time 0 and time -2 , and for longitudinal change between time -2 and time 0. The case-control ORs were additionally adjusted for the effect of pain (4), using standard categories of no pain, infrequent pain, and frequent pain (based on most days of a month in past 12 months). Analysis was performed using SPSS version 23.0 software. *P* values less than 0.05 were considered significant.

RESULTS

Of the 136 OAI participants who had a confirmed knee replacement up to the 60-month visit (4), 36 cases could not be included in the current analysis because

Table 1. Baseline characteristics of the KR cases and the non-KR controls*

Characteristic	Women		Men	
	Cases (n = 58)	Controls (n = 58)	Cases (n = 42)	Controls (n = 42)
Age, mean \pm SD years	64 \pm 8	65 \pm 8	66 \pm 9	66 \pm 9
Body mass index, mean \pm SD kg/m ²	28.8 \pm 4.6	28.5 \pm 4.4	29.1 \pm 3.8	29.0 \pm 3.2
Height, mean \pm SD meters	1.61 \pm 0.05	1.61 \pm 0.05	1.77 \pm 0.05	1.77 \pm 0.05
Weight, mean \pm SD kg	74.6 \pm 13.3	74.2 \pm 12.5	91.3 \pm 13.3	90.1 \pm 11.5
KR in dominant leg†	34 (59)	NA	16 (38)	NA
Kellgren/Lawrence grade				
0	5 (9)	5 (9)	2 (5)	2 (5)
1	0 (0)	0 (0)	2 (5)	2 (5)
2	11 (19)	11 (19)	4 (10)	4 (10)
3–4	42 (72)	42 (72)	34 (81)	34 (81)
Medial joint space narrowing	41 (71)	41 (71)	37 (88)	37 (88)
Lateral joint space narrowing	9 (15)	9 (15)	4 (10)	4 (10)
Duration from time 0 to KR, mean \pm SD months‡	12 \pm 6	NA	11 \pm 7	NA
Time 0 knee extensor strength, mean \pm SD newtons	215 \pm 75	260 \pm 80	384 \pm 130	383 \pm 94
Time 0 knee flexor strength, mean \pm SD newtons	87 \pm 35	101 \pm 42	163 \pm 70	147 \pm 52

* If a case participant had a knee replacement (KR) at time 0 in both knees, the one that had been replaced earlier was included. However, if both had been replaced at the same time point, the knee with the lower Kellgren/Lawrence grade at baseline was analyzed. Except where indicated otherwise, values are the number (%) of participants. NA = not applicable.

† The dominant leg is the leg participants would use to kick a ball.

‡ Time 0 was the examination prior to knee replacement (≤ 2 years).

thigh MRI was not available at time 0. Baseline age, sex, BMI, K/L grade, or distribution of JSN of the 36 cases who did not have thigh MRI available at time 0 did not differ from that of the 100 cases included in the current analysis ($P > 0.05$). MRI and strength data were available for 58 female pairs at time 0, and also for 30 at time -2 , while these data were available for 42 male case/control pairs at time 0, and for 25 at time -2 (Table 1). Thigh muscle strength differences between cases and controls were of similar magnitude in the current 100 matched pairs to those observed in the larger sample of 136 matched pairs previously reported (4) (Table 1).

Extensor and flexor anatomic cross-sectional area and specific strength in women. Female cases displayed less extensor anatomic cross-sectional area at time 0 compared with matched controls ($P = 0.041$ by paired t -test, unadjusted $P [P_{\text{unadj}}] = 0.049$, adjusted $P [P_{\text{adj}}] = 0.033$), but not at time -2 (Table 2). No differences in flexor anatomic cross-sectional area were observed between cases and controls at time 0 or time -2 . Differences in the 2-year longitudinal change of extensor anatomic cross-sectional area from time -2 to time 0 between cases and controls did not reach statistical significance.

Knee extensor specific strength was significantly lower in cases than in controls at time 0 ($P = 0.032$ by paired t -test) in unadjusted analyses, although the difference did not maintain statistical significance after adjustment for pain ($P = 0.471$). No significant differences in any of the above measures were observed at time -2 . Female knee replacement cases lost significantly more extensor

specific strength between time -2 and time 0 (mean \pm SD -1.1 ± 1.5 N/cm² versus 0.3 ± 1.8 N/cm²; $P = 0.002$ by paired t -test, $P_{\text{unadj}} = 0.011$, $P_{\text{adj}} = 0.043$) than their matched non-knee replacement controls. Flexor specific strength and its longitudinal change, in contrast, were not significantly associated with knee replacement. Similar results were observed in sensitivity analyses using muscle torque (Nm/cm²) (see Supplementary Table 1, available on the *Arthritis & Rheumatology* web site at <http://onlinelibrary.wiley.com/doi/10.1002/art.40343/abstract>).

Extensor and flexor anatomic cross-sectional area and specific strength in men. Similar to female cases, male cases displayed less extensor anatomic cross-sectional area at time 0 compared with their matched controls ($P = 0.011$ by paired t -test, $P_{\text{unadj}} = 0.020$, $P_{\text{adj}} = 0.039$), but not at time -2 (Table 3). No statistically significant differences in knee flexor anatomic cross-sectional area or specific strength were, however, observed at any time point between male cases and controls, or for the change in knee extensor or flexor anatomic cross-sectional area and specific strength. There was a trend toward male knee replacement cases displaying somewhat greater (rather than reduced) specific strength compared with their matched controls at time 0 and time -2 .

DISCUSSION

To elucidate mechanisms behind thigh muscle weakness and clinical progression of knee OA, we explored whether loss in thigh muscle anatomic cross-sectional areas

Table 2. ACSA and specific strength in female knee replacement cases and matched non-knee replacement controls*

	No. of matched pairs analyzed	ACSA		Specific strength			
		Mean \pm SD cm ²		Mean \pm SD N/cm ²			
		Cases	Controls	Cases	Controls	Case-control OR (95% CI)	Case-control OR _{adj} (95% CI)†
Knee extensors							
Time 0	58	6.5 \pm 1.4	7.1 \pm 1.7	6.2 \pm 2.1	6.9 \pm 2.3	1.59 (1.00-2.51)‡	1.22 (0.71-2.08)‡
Time -2	30	6.8 \pm 1.5	7.3 \pm 1.6	6.9 \pm 2.2	6.8 \pm 2.2	1.55 (0.85-2.82)	0.81 (0.41-1.64)
Knee flexors							
Time 0	57§	4.9 \pm 1.1	5.0 \pm 1.0	4.0 \pm 1.3	3.8 \pm 1.6	1.07 (0.64-1.79)	1.23 (0.75-2.04)
Time -2	29§	5.1 \pm 1.2	5.0 \pm 1.0	4.0 \pm 1.4	3.7 \pm 1.7	0.98 (0.58-1.66)	1.01 (0.39-2.63)
Knee extensors, change from time -2 to time 0	30	-0.2 \pm 0.9	-0.2 \pm 1.0	-1.1 \pm 1.5	0.3 \pm 1.8	1.17 (0.62-2.20)	3.76 (1.04-13.60)‡
Knee flexors, change from time -2 to time 0	29§	0.0 \pm 0.5	-0.1 \pm 0.6	-0.7 \pm 1.3	0.0 \pm 1.3	0.95 (0.53-1.72)	1.75 (0.73-4.23)

* A case-control conditional logistic regression odds ratio (OR) of >1 represents greater odds of a knee replacement in the presence of less anatomic cross-sectional area (ACSA) or specific strength, or greater loss of these parameters over time. ORs are based on standardized measures (per SD of ACSA and specific strength at each interval). ACSA is adjusted for individual femur size. 95% CI = 95% confidence interval; time 0 = examination prior to occurrence of knee replacement (≤ 2 years); time -2 = examination 2 years prior to time 0.

† Case-control OR after adjustment for the effects of pain at the start of each interval.

‡ $P < 0.05$ versus controls by paired t -test.

§ One participant had flexor strength values of <10 N at time 0 and time -2, with extensor strength within normal range, suggesting that the measurement of flexor strength was inaccurate (not included in this analysis).

Table 3. ASCA and specific strength in male knee replacement cases and matched non-knee replacement controls*

	No. of matched pairs analyzed	ASCA				Specific strength			
		Mean \pm SD cm ²		Case-control OR (95% CI)	Case-control OR _{adj} (95% CI)†	Mean \pm SD N/cm ²		Case-control OR (95% CI)	Case-control OR _{adj} (95% CI)†
		Cases	Controls			Cases	Controls		
Knee extensors									
Time 0	42	7.2 \pm 1.5	8.1 \pm 1.8	2.06 (1.12–3.77)‡	2.22 (1.04–4.76)‡	7.1 \pm 1.8	6.7 \pm 1.7	0.79 (0.51–1.25)	0.59 (0.30–1.15)
Time -2	25	7.6 \pm 1.6	8.1 \pm 1.8	1.59 (0.75–3.40)	1.24 (0.52–2.93)	7.2 \pm 1.6	6.7 \pm 1.6	0.71 (0.40–1.27)	0.64 (0.29–1.41)
Knee flexors									
Time 0	42	5.1 \pm 1.0	5.4 \pm 1.2	1.35 (0.83–2.18)	1.33 (0.74–2.38)	4.3 \pm 1.5	3.8 \pm 1.4	0.78 (0.51–1.18)	0.75 (0.44–1.25)
Time -2	25	5.4 \pm 1.1	5.5 \pm 0.9	1.20 (0.56–2.56)	1.18 (0.45–3.07)	4.5 \pm 1.6	3.7 \pm 1.6	0.68 (0.38–1.20)	0.63 (0.30–1.30)
Knee extensors, change from time -2 to time 0	25	-0.2 \pm 0.7	-0.1 \pm 0.8	1.12 (0.63–2.00)	1.33 (0.64–2.78)	-0.1 \pm 1.4	-0.2 \pm 1.3	0.94 (0.45–1.96)	0.66 (0.26–1.72)
Knee flexors, change from time -2 to time 0	25	-0.2 \pm 0.5	-0.1 \pm 0.7	1.26 (0.66–2.39)	1.37 (0.62–3.02)	-0.1 \pm 1.4	-0.1 \pm 1.2	0.95 (0.46–1.95)	0.87 (0.36–2.12)

* A case-control conditional logistic regression odds ratio (OR) of >1 represents greater odds of a knee replacement in the presence of less anatomic cross-sectional area (ASCA) or specific strength, or greater loss of these parameters over time. ORs are based on standardized measures (per SD of ASCA and specific strength at each interval). 95% CI = 95% confidence interval; time 0 = examination prior to occurrence of knee replacement (≤ 2 years); time -2 = examination 2 years prior to time 0. ASCA is adjusted for individual femur size.

† Case-control OR after adjustment for the effects of pain at the start of each interval.

‡ $P < 0.05$ versus controls by paired t -test.

or specific strength increase knee replacement risk. In this study, we found that significant deficits in knee extensor anatomic cross-sectional area preceded knee replacement in both men and women, independent of age, BMI, disease severity, and pain, when measured at a time point within 2 years prior to surgery (i.e., time 0).

Moreover, female knee replacement cases displayed 10% lower knee extensor specific strength than controls at time 0, but these differences did not remain statistically significant after adjustment for pain. Male knee replacement cases, in contrast, displayed slightly higher muscle specific strength (5%) than matched controls without knee replacement. Interestingly, over a 2-year observational period prior to knee replacement, female knee replacement cases displayed a significantly greater longitudinal loss of knee extensor specific strength than female controls; this loss exceeded that in male knee replacement cases by a factor of 10. Hence, this study is the first to suggest that muscle weakness preceding clinical progression of knee OA to knee replacement in women is caused by both deficits in muscle anatomic cross-sectional area (independent of pain) and specific strength (dependent on pain), whereas no deficits in muscle specific strength were apparent in men prior to knee replacement.

The results of the current study help to clarify the sex-specific mechanisms behind the recently observed relationship between clinical measures of muscle strength and OA incidence and progression (4,6). Specifically, there appear to be 2 mechanisms contributing to the strength deficits that increase knee replacement risk in women (4)—one that is driven by pain (specific strength deficit) and one that is independent of pain (anatomic cross-sectional area deficit). Specific strength reflects the availability of contractile tissue per unit area of muscle and/or the ability to activate existing muscle fibers, with the latter potentially being affected by pain through either a reduction in neural activation or a reluctance of individuals with pain to maximally contract (10). Muscle anatomic cross-sectional area, in contrast, is a structural feature that is potentially less influenced by pain.

In contrast to women, deficits in muscle anatomic cross-sectional area in male knee replacement cases were accompanied by a somewhat greater specific strength than in their matched controls. Although this apparent compensatory mechanism may be a chance finding given the relatively small number of men in our study, it does potentially help to explain the lack of significant differences in muscle strength between male knee replacement cases and controls that we observed previously (4). Similar sex-specific responses of muscle specific strength have

also recently been observed in those at risk of incident knee OA, with thigh muscle specific strength maintained in men with greater BMI, but not in women (6).

The presence, persistence, and particularly the worsening of disabling pain are key criteria for patient decisions to undergo knee replacement. The loss of a significant relationship between knee extensor specific strength in women at risk of knee replacement (at time 0) after adjustment for pain suggests that the mechanism through which muscle weakness impacts knee replacement risk in women is dependent on pain. Our previous study showed that muscle weakness in women was associated with subsequent knee replacement risk independent of pain (4), likely through a mechanism involving greater loss of anatomic cross-sectional area prior to knee replacement compared with non-knee replacement controls.

Consistent with these findings, anatomic cross-sectional area has been shown to be an important driver of muscle deficits that cause incident knee OA in older women (11). In the Multicenter Osteoarthritis Study (MOST), knee extensor specific strength in women was predictive of worsening JSN whereas muscle mass was not, while neither was predictive of worsening JSN in men (12). Importantly, analyses in the MOST study were not adjusted for pain, which would likely attenuate the predictive capacity of specific strength as we observed in the current study. Additionally, muscle mass was assessed as total thigh lean mass by dual x-ray absorptiometry rather than in isolated muscle groups (as possible by MRI). Our finding that male knee replacement cases appear to compensate for a significant loss of muscle anatomic cross-sectional area by somewhat increased specific strength explains why we did not previously observe a relationship between muscle strength and knee replacement risk in men. The somewhat greater specific strength in male knee replacement cases may also help to explain why in some reports of radiographic knee OA progression, male cases displayed increased knee extensor strength prior to progression (13).

Interestingly, muscle anatomic cross-sectional area and specific strength in male knee replacement cases and controls were relatively stable over the 2–4-year period prior to knee replacement (<3% loss), whereas female knee replacement cases displayed a significantly greater longitudinal loss of knee extensor specific strength over the same period (up to 18%) compared with female control knees. This longitudinal loss of specific strength remained a significant predictor of knee replacement, even after adjustment for pain. Importantly, the reports of pain at the start of the

observational period (i.e., time -2) were used to adjust case-control ORs, consistent with our previous analyses, which may have resulted in lower pain levels being included in the model compared with time 0.

These findings suggest that women have a more dramatic loss of muscle specific strength prior to knee replacement than men and highlight the importance of addressing muscle specific strength deficits (i.e., an inability to activate existing muscle tissue or increase noncontractile tissue) in those with or at risk of knee OA. Such interventions may need to have a greater focus on addressing fear and confidence, which can influence muscle activation capacity, or on maintaining contractile tissue per muscle unit area. While eccentric strength training may more effectively increase muscle anatomic cross-sectional area and neural adaptations than concentric approaches (14), any heavy resistance training is likely to improve neural activation through increasing motor unit firing frequency and recruitment (15). The utility of specific muscle activation interventions (such as muscle biofeedback and neuromuscular electrical stimulation) as well as interventions addressing confidence, fear, and motivation should be a focus of future research.

We evaluated only a limited period of time prior to knee replacement, and it is possible that changes in thigh muscles prior to this window are also important in predicting future progression to knee replacement. However, the lack of significant findings earlier than 2–4 years prior to knee replacement (4) suggests that muscle characteristics in the immediate years prior to knee replacement are most strongly implicated in progression risk. The relatively few eligible participants within the total OAI cohort with a knee replacement limited the number of included cases to 100. The strict matching approach used to select the 100 controls ensured that the potential confounding effects of radiographic severity, BMI, age, and sex were addressed. Although we analyzed measures of muscle strength, morphology (anatomic cross-sectional area), and quality (specific strength), the OAI did not include measures of voluntary muscle activation (e.g., electromyography), which may provide additional information on knee replacement risk.

In conclusion, the current study is the first to suggest that muscle strength deficits preceding clinical progression of knee OA to knee replacement in women appear to occur through 2 mechanisms: one driven by pain (loss in specific strength) and one independent of pain (loss in anatomic cross-sectional area), whereas men with knee replacement displayed lower extensor anatomic cross-sectional area, but not strength or specific strength.

These findings reveal potential specific targets for treatment of muscle impairments in men, and particularly in women, with knee OA.

ACKNOWLEDGMENTS

We would like to thank the OAI participants, OAI investigators, and OAI Clinical Center staff for generating this publicly available image data set. The study and image acquisition were supported by the OAI.

AUTHOR CONTRIBUTIONS

All authors were involved in drafting the article or revising it critically for important intellectual content, and all authors approved the final version to be published. Dr. Culvenor had full access to all of the data in the study and takes responsibility for the integrity of the data and the accuracy of the data analysis.

Study conception and design. Culvenor, Wirth, Eckstein.

Acquisition of data. Hamler, Kemnitz, Wirth.

Analysis and interpretation of data. Culvenor, Hamler, Eckstein.

REFERENCES

1. Kurtz S, Ong K, Lau E, Mowat F, Halpern M. Projections of primary and revision hip and knee arthroplasty in the United States from 2005 to 2030. *J Bone Joint Surg* 2007;89A:780–5.
2. Culvenor AG, Ruhdorfer A, Juhl C, Eckstein F, Oiestad BE. Knee extensor strength and risk of structural, symptomatic and functional decline in knee osteoarthritis: a systematic review and meta-analysis. *Arthritis Care Res (Hoboken)* 2017;69:649–58.
3. Oiestad BE, Juhl CB, Eitzen I, Thorlund JB. Knee extensor muscle weakness increases the risk of knee osteoarthritis: a systematic review and meta-analysis. *Osteoarthritis Cartilage* 2015;23:171–7.
4. Culvenor AG, Wirth W, Ruhdorfer A, Eckstein F. Thigh muscle strength predicts knee replacement risk independent of radiographic disease and pain in women: data from the Osteoarthritis Initiative. *Arthritis Rheumatol* 2016;68:1145–55.
5. Sattler M, Dannhauer T, Hudelmaier M, Wirth W, Sanger AM, Kwok CK, et al. Side differences of thigh muscle cross-sectional areas and maximal isometric muscle force in bilateral knees with the same radiographic disease stage, but unilateral frequent pain: data from the osteoarthritis initiative. *Osteoarthritis Cartilage* 2012;20:532–40.
6. Culvenor AG, Felson DT, Niu J, Wirth W, Sattler M, Dannhauer T, et al. Thigh muscle specific strength and the risk of incident knee osteoarthritis: the influence of sex and greater body mass index. *Arthritis Care Res (Hoboken)* 2017;69:1266–70.
7. Kellgren JH, Lawrence JS. Radiological assessment of osteoarthritis. *Ann Rheum Dis* 1957;16:494–501.
8. Kemnitz J, Eckstein F, Culvenor AG, Ruhdorfer A, Dannhauer T, Ring-Dimitriou S, et al. Validation of an active shape model-based semi-automated segmentation algorithm for the analysis of thigh muscle and adipose tissue cross-sectional areas. *MAGMA* 2017;30:489–503.
9. Tsaopoulos DE, Maganaris CN, Baltzopoulos V. Can the patellar tendon moment arm be predicted from anthropometric measures? *J Biomech* 2007;40:645–51.
10. Salomoni S, Tucker K, Hug F, McPhee M, Hodges P. Reduced maximal force during acute anterior knee pain is associated with deficits in voluntary muscle activation. *PLoS One* 2016;11:e0161487.
11. Ikeda S, Tsumura H, Torisu T. Age-related quadriceps-dominant muscle atrophy and incident radiographic knee osteoarthritis. *J Orthop Sci* 2005;10:121–6.

12. Segal NA, Findlay C, Wang K, Torner JC, Nevitt MC. The longitudinal relationship between thigh muscle mass and the development of knee osteoarthritis. *Osteoarthritis Cartilage* 2012;20:1534–40.
13. Culvenor AG, Wirth W, Roth M, Hunter DJ, Eckstein F. Predictive capacity of thigh muscle strength in symptomatic and/or radiographic knee osteoarthritis progression: data from the Foundation for the National Institutes of Health osteoarthritis biomarkers consortium. *Am J Phys Med Rehab* 2016;95:931–8.
14. Higby EJ, Cureton KJ, Warren GL, Prior BM. Effects of concentric and eccentric training on muscle strength, cross-sectional area, and neural activation. *J App Physiol* 1996;81:2173–81.
15. Sale DG. Neural adaptation to resistance training. *Med Sci Sports Exerc* 1988;20:S135–45.

Loading-Induced Reduction in Sclerostin as a Mechanism of Subchondral Bone Plate Sclerosis in Mouse Knee Joints During Late-Stage Osteoarthritis

Haoruo Jia,¹ Xiaoyuan Ma,² Yulong Wei,³ Wei Tong,³ Robert J. Tower,⁴ Abhishek Chandra,⁴ Luqiang Wang,² Zeyang Sun,⁴ Zhaochun Yang,⁵ Farid Badar,⁶ Kairui Zhang,⁷ Wei-Ju Tseng,⁴ Ina Kramer,⁸ Michaela Kneissel,⁸ Yang Xia,⁶ X. Sherry Liu,⁴ James H. C. Wang,⁵ Lin Han,⁹ Motomi Enomoto-Iwamoto,¹⁰ and Ling Qin⁴

Objective. To establish an unbiased, 3-dimensional (3-D) approach that quantifies subchondral bone plate (SBP) changes in mouse joints, and to investigate the mechanism that mediates SBP sclerosis at a late stage of osteoarthritis (OA).

Methods. A new micro-computed tomography (micro-CT) protocol was developed to characterize the entire thickness of the SBP in the distal femur of a normal mouse knee. Four mouse models of severe joint OA were generated: cartilage-specific *Egfr*-knockout (*Egfr*-CKO) mice at 2 months after surgical destabilization of the medial meniscus (DMM), *Egfr*-CKO mice with aging-related spontaneous OA, wild-type (WT) mice at 10 months after DMM, and WT mice at 14 weeks after DMM plus hemisectomy of the meniscus (DMMH) surgery. As an additional model, mice with knockout of the sclerostin gene (*Sost*-KO) were subjected to DMMH surgery. Knee joints were examined by micro-CT, histology, and immunohistochemical analyses.

Results. Examination of the mouse distal femur by 3-D micro-CT revealed a positive correlation between

SBP thickness and the loading status in normal knees. In all 4 mouse models of late-stage OA, SBP sclerosis was restricted to the areas under severely eroded articular cartilage. This was accompanied by elevated bone formation at the bone marrow side of the SBP and a drastic reduction in the levels of sclerostin in osteocytes within the SBP. Unlike in WT mice, no further increase in the thickness of the SBP was observed in response to DMMH in *Sost*-KO mice.

Conclusion. Since focal stress on the SBP underlying sites of cartilage damage increases during late stages of OA, these findings establish mechanical loading-induced attenuation of sclerostin expression and elevation of bone formation along the SBP surface as the major mechanisms characterizing subchondral bone phenotypes associated with severe late-stage OA in mice.

As the most common type of arthritis in the aging population, osteoarthritis (OA) is primarily characterized by progressive degeneration of knee articular cartilage. To date, most of the research seeking treatments for this disease has focused on prevention or repair of the degenerated cartilage. However, clinical observations

Supported by the American Society for Bone and Mineral Research (Research Career Enhancement Award to Dr. Qin), and the NIH (National Institute of Arthritis and Musculoskeletal and Skin Diseases grants AR-060991 and AR-062908 [to Dr. Enomoto-Iwamoto], AR-069047 [to Dr. Xia], AR-065949 [to Dr. J. H. C. Wang], AR-066824 [to Dr. Han], AR-066743 [to Dr. Liu], and P30-AR-06919 [to Penn Center for Musculoskeletal Disorders], and National Institute of Diabetes and Digestive and Kidney Diseases grant DK-095803 [to Dr. Qin]).

¹Haoruo Jia, MD: University of Pennsylvania, Philadelphia, and The First Affiliated Hospital of the Medical College, Shihezi University, Shihezi, China; ²Xiaoyuan Ma, MD, PhD, Luqiang Wang, MD: Shandong University Qilu Hospital, Jinan, China, and University of Pennsylvania, Philadelphia; ³Yulong Wei, MD, Wei Tong, MD, PhD: University of Pennsylvania, Philadelphia, and Union Hospital, Huazhong University of Science and Technology, Wuhan, China; ⁴Robert J. Tower, PhD, Abhishek Chandra, PhD, Zeyang Sun, MS, Wei-Ju Tseng, MS, MSE, X. Sherry Liu, PhD, Ling Qin, PhD: University of Pennsylvania, Philadelphia; ⁵Zhaochun Yang, PhD,

James H. C. Wang, PhD: University of Pittsburgh School of Medicine, Pittsburgh, Pennsylvania; ⁶Farid Badar, BS, Yang Xia, PhD: Oakland University, Rochester, Michigan; ⁷Kairui Zhang, MD: Nanfang Hospital, Southern Medical University, Guangzhou, China; ⁸Ina Kramer, PhD, Michaela Kneissel, PhD: Novartis Institutes for BioMedical Research, Basel, Switzerland; ⁹Lin Han, PhD: Drexel University, Philadelphia, Pennsylvania; ¹⁰Motomi Enomoto-Iwamoto, DDS, PhD: The Children's Hospital of Philadelphia, Philadelphia, Pennsylvania, and University of Maryland, Baltimore.

Drs. Jia and Ma contributed equally to this work.

Address correspondence to Ling Qin, PhD, Department of Orthopaedic Surgery, University of Pennsylvania, G14A Stemmler Hall, 36th Street and Hamilton Walk, Philadelphia, PA 19104. E-mail: qinling@pennmedicine.upenn.edu.

Submitted for publication March 14, 2017; accepted in revised form October 6, 2017.

and animal studies over the past several decades have accumulated sufficient evidence to support the concept that OA is a disease of the whole joint, involving changes not only in articular cartilage but also in its neighboring tissue, such as subchondral bone, ligaments, menisci, periarticular muscles, peripheral nerves, and synovium (1). Indeed, the first radiographic criteria for the diagnosis of OA, developed in the 1950s, included subchondral sclerosis as a hallmark of this disease (2).

Anatomically, subchondral bone consists of 2 parts: a layer of corticalized subchondral bone plate (SBP) and the underlying subchondral trabecular bone (STB). It is important to distinguish these 2 subchondral bone components in OA research, not only because they have intrinsic architectural and mechanical differences, but also because different pathologic changes can occur in each component during OA development (3). Thickening of the SBP is considered an indisputable sign of late-stage OA (4). However, the underlying mechanisms responsible for such thickening are still largely unknown. In the STB, the bone remodeling rate is consistently increased during the progression of OA, leading to undermineralized bone tissue and reduced mechanical strength of the trabecular bone (5–7). Several mechanisms to explain this phenomenon have been proposed, such as cellular signaling for microdamage repair, stimulation of vascular invasion, and bone–cartilage cross-talk occurring via channels in the SBP (8). Interestingly, results of recent studies have shown that modifying osteoblastic gene expression or inhibiting osteoclastic bone resorption could prevent the progression of OA in mice (9), suggesting that subchondral bone activity may control articular cartilage degeneration. Currently, it is still largely under debate whether subchondral bone sclerosis is the initiator of cartilage damage or the consequence of such damage.

Research on subchondral bone has been performed mostly in human OA joints as well as in non-rodent animal models with subchondral bone sizes larger than that of rodents. To elucidate the molecular mechanisms regulating the SBP and STB in OA, genetically modified mice are powerful tools. Micro-computed tomography (micro-CT) is commonly used to characterize subchondral bone changes in mice. Generally, the proximal tibia is scanned at a relatively low resolution (10–20 μm) and then contoured for 3-dimensional (3-D) analysis of the STB. Because the proximal tibia of mice is relatively small in size, the results might not be accurate. Measuring the thickness of the SBP is particularly troublesome, because it is usually performed on longitudinally sectioned, 2-D images of the tibia. The results could be highly variable, due to the inconsistency of sectioning angle and location. Furthermore, since it is based on 2-D images, this approach does not capture

changes in the entire SBP. Thus, there is an urgent need to design an unbiased, 3-D approach to accurately quantify the bone parameters of the SBP and STB in mouse joints.

In this study, we designed a protocol that is capable of measuring SBP thickness at any location within the mouse femoral condyle, allowing comparisons among different anatomic sites (anterior versus posterior, medial versus lateral). Utilizing this 3-D analytic tool, we examined SBP changes in several mouse models of severe late-stage OA, either surgery-induced or spontaneously developing in aging mice, with the use of genetically modified and unmodified mice. Biomechanical factors, such as those seen in obesity, trauma, and joint injury, play central roles in the development and progression of OA (10). Sclerostin (gene form *Sost*), a canonical, anti-osteogenic Wnt inhibitor whose expression is largely restricted to osteocytes (11,12), is an important mediator of mechanical loading-induced new bone formation (13). Targeting this protein with a neutralizing antibody is a novel therapeutic strategy that is currently being developed for patients with osteoporosis (14). In the present study, we explored potential relationships among mechanical loading, sclerostin levels, and SBP thickness under either normal or pathologic conditions in several mouse models of OA. The results of our studies reveal a novel mechanism to explain how cartilage degeneration can lead to the development of SBP sclerosis specifically underlying the sites of cartilage damage.

MATERIALS AND METHODS

Animals. Mice with cartilage-specific knockout of the endothelial growth factor receptor (EGFR) gene (*Egfr*-CKO; *Col2-Cre Egfr^{Wa5/f}*) were generated as previously described (15). Briefly, we first bred *Col2a1-Cre* with *Egfr^{Wa5/+}* mice, to obtain *Col2-Cre Egfr^{Wa5/+}* mice, which were then crossed with *Egfr^{fl/f}* to generate *Egfr*-CKO mice and their *Wa5* (*Egfr^{Wa5/f}*) and wild-type (WT) (*Col2-Cre Egfr^{fl/+}* and *Egfr^{fl/+}*) siblings. *Wa5* is a dominant-negative allele of *Egfr* (16) and is required in order to reduce the activity of EGFR to a very low level in *Egfr*-CKO mice (15). We previously reported that *Wa5* mice are morphologically and functionally closer to WT mice than to *Egfr*-CKO mice, which can be attributed to the fact that EGFR activity is only modestly decreased in *Wa5* mouse cells but drastically reduced in *Egfr*-CKO mouse cells (15,17–19). We made similar observations in the present study, and therefore all data on *Wa5* mice were omitted.

Rosa-Tomato mice were purchased from The Jackson Laboratory. To construct *Egfr*-CKO *Rosa-Tomato* mice, we first obtained *Egfr^{fl/f}* *Rosa-Tomato* homozygous mice, and then used these mice to breed with *Col2-Cre Egfr^{Wa5/+}* mice. As an additional model, *Sost*-knockout (*Sost*-KO) mice were used (kindly provided by Novartis Pharma AG).

To induce OA, destabilization of the medial meniscus (DMM) or DMM plus hemisection of the meniscus (DMMH) surgery was performed on the right knees of 2-month-old male mice (for DMMH) (20) or 3-month-old male mice (for DMM)

(21). Sham surgery was performed on the left knees. In accordance with the standards for animal housing, mice were group-housed in an atmosphere of 23–25°C with a 12-hour light/dark cycle, and allowed free access to water and standard laboratory pellets. All work performed on animals was approved by the Institutional Animal Care and Use Committee at the University of Pennsylvania.

Micro-CT analysis. After the mice were euthanized, the knee joints were harvested, fixed in 4% paraformaldehyde for 2 days, rinsed with running water, and stored in 1× phosphate buffered saline. A 3-mm region from the distal femur and 3-mm region from the proximal tibia were each scanned with a Scanco Medical MicroCT 35 scanner at a 6-μm isotropic voxel size. All images were smoothened using a Gaussian filter (sigma 1.2, support 2.0).

For analysis of the STB, sagittal images were thresholded, corresponding to 472.1 mg HA/cm³, and contoured between the SBP and growth plate. The bone parameters of bone volume fraction/total volume (BV/TV), trabecular thickness, trabecular separation, trabecular number, and structure model index were each calculated using 3-D standard microstructural analysis (22). For analysis of the SBP, sagittal images were contoured for the SBP, followed by generation of a 3-D color map of thickness for the entire SBP. This map was converted to a gray-scale thickness map, whose histogram was then used for quantification of the average SBP thickness at any defined area.

Histology. After the mouse knee joints were scanned by micro-CT, they were decalcified in 0.5M EDTA (pH 7.4) for 4 weeks prior to paraffin embedding. A series of 6-μm-thick sagittal sections were cut across the entire medial and lateral compartments of the joint. Mankin scores for the severity of OA cartilage degeneration (scale of 0–14, where 0 = normal intact cartilage, 1–5 = mild-to-moderate OA, 6–14 = moderate-to-severe late-stage OA) were calculated as previously described (23). Briefly, 2 sections within every 6 consecutive sections in the entire section set for each knee were stained with Safranin O-fast green; the stained sections were then scored by 2 blinded observers (HJ and XM). Each knee compartment received a single Mankin score, representing the maximal score of its section.

Additional paraffin-embedded knee joint sections, derived from the middle of the medial or lateral parts of the knee joints, were used for immunohistochemical analyses. After antigen retrieval, slides were incubated at 4°C overnight with primary antibodies, such as rabbit anti-osteocalcin (m173; Takara ClonTech) and goat anti-sclerostin (AF1589; R&D Systems), followed by binding with biotinylated secondary antibodies and color development with diaminobenzidine. The images of each section under the same conditions were captured using a Nikon Eclipse 90i microscope.

For quantification of osteoblasts, we counted all osteocalcein-positive cells along the SBP surface at the bone marrow side, underneath the articular cartilage within the femoral-tibial contact region; osteoblast numbers were normalized against the length of the SBP surface. For quantification of the staining intensity of sclerostin expression in osteocytes, the entire SBP region underneath the articular cartilage was contoured, and its staining intensity was quantified by the mean gray value after thresholding to remove background staining. Frozen sections were used for immunofluorescence staining. Frontal sections (90 μm in thickness) at the center of the posterior region were incubated with endomucin antibody (sc-65495; Santa Cruz Biotechnology) at 4°C overnight, followed by Alexa Fluor

488-conjugated donkey anti-rabbit IgG secondary antibody (A-21206; Thermo Scientific). The samples were scanned using an LSM710 confocal microscope, and images were processed and analyzed using Velocity software. The length of the SBP surface at the bone marrow side that was aligned with blood vessels was measured and normalized against the total length of the SBP surface. In all analyses, the SBP regions or surfaces that did not have overlying articular cartilage were excluded.

Statistical analysis. Data are expressed as the mean ± SD. Two-way analysis of variance was performed when 2 independent variables (sham versus DMM surgery, WT versus *Egfr*-CKO genotype) were compared. When there was a significant interaction effect between treatment and genotype, Mann-Whitney U test with Bonferroni adjustment for multiple comparisons was performed to test the difference between surgery groups within each genotype, as well as differences between genotypes within each group. In a scenario in which a single independent variable was considered for comparisons, Mann-Whitney U test was performed. Specifically, paired U tests were performed for comparisons between surgery groups (sham versus DMM) and between anatomic locations (anterior versus posterior, medial versus lateral), while unpaired U tests were performed for comparisons between mouse genotypes (WT versus either *Egfr*-CKO or *Sost*-KO mice). Two-sided *P* values less than 0.05 were considered significant.

RESULTS

Positive correlation of SBP thickness with loading status in a normal mouse knee, as revealed by micro-CT. Examination of the 3-D-reconstructed micro-CT images of an adult mouse knee joint, in a series of evenly divided frontal sections of the joint, indicated that the distal femoral subchondral region was much larger and thicker than the proximal tibial subchondral region (Figures 1A and B). On average, the height of the tibial STB was 180 μm across the entire plateau. This limited height prevents precise segregation of the SBP and STB in most images, even when the bone is scanned at the highest resolution. In contrast, structural analysis of subchondral bone is better performed in the femur (with an average height of ~600 μm) despite sectioning of the bone into sagittal, frontal, and transverse planes.

Unlike human knee joints, mouse knee joints are unable to fully extend. As shown in Figure 1C, their bending angle is between ~30° and ~150°. This results in the posterior part, but not the anterior part, of the distal femoral condyle being in direct contact with the tibial plateau, and therefore the posterior part is the area that undergoes load bearing and energy dissipation during joint motion. Interestingly, in sagittal images of the normal mouse knee joint, the posterior region appeared to have a thicker SBP relative to the anterior region (Figure 1D).

To quantify SBP thickness at any given area, we designed a new protocol to convert the micro-CT images

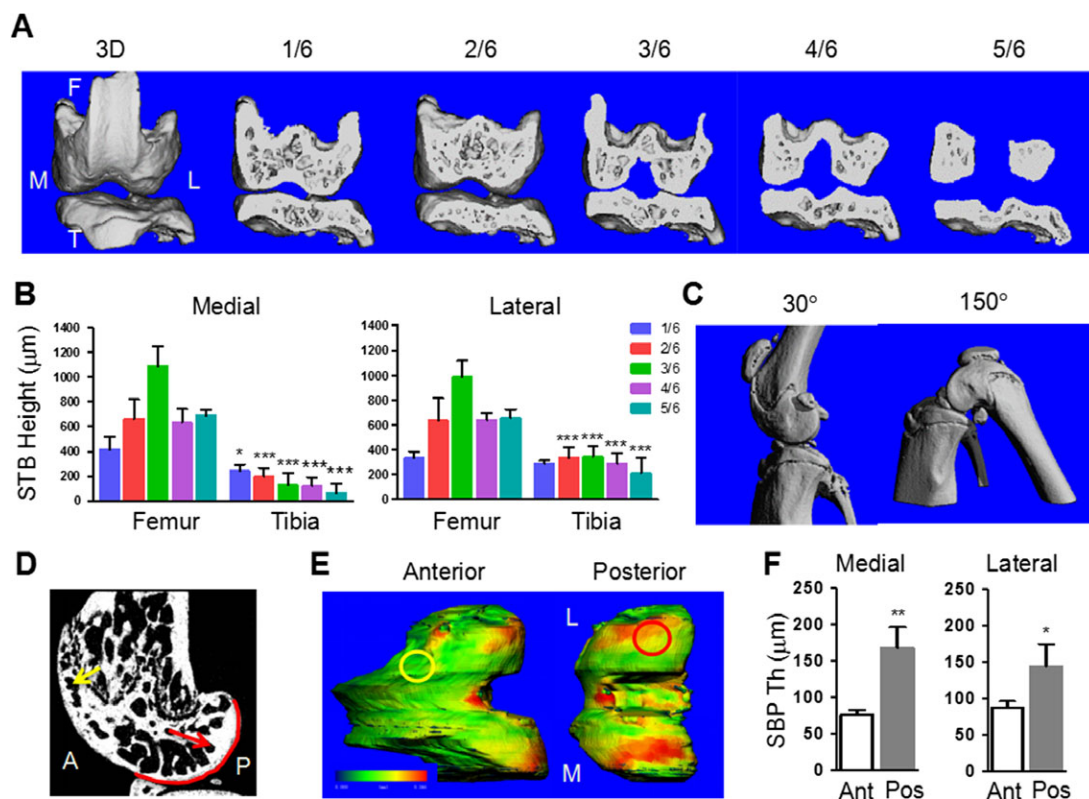


Figure 1. Characterization of mouse subchondral bone using a new micro-computed tomography protocol. **A**, Three-dimensional (3-D)-reconstructed images of the femur (F) and tibia (T) (medial [M] and lateral [L] sites) of a 4-month-old wild-type (WT) mouse. The images were completely sectioned along the frontal plane, with sections corresponding to positions 1/6, 2/6, 3/6, 4/6, and 5/6 from the most anterior part (0) to the most posterior part (1). **B**, Height of the subchondral trabecular bone (STB) at the middle of the medial and lateral regions of 1/6 to 5/6 positions in WT mouse femurs and tibiae. Results are the mean \pm SD ($n = 6$ mice). * = $P < 0.05$; *** = $P < 0.001$, versus the corresponding position in the femur. **C**, Bending angle between the tibia and femur of a WT mouse (between 30° and 150°). **D**, Sagittal image of the epiphyseal region of a WT mouse femur. The image reveals that only the posterior (P) site of the subchondral bone plate (SBP) is the load-transducing site (outlined in red), and the SBP is thicker at the posterior site (red arrow) than at the anterior (A) site (yellow arrow). **E**, Anterior and posterior views of a WT mouse femur on 3-D color maps of SBP thickness. Yellow and red circles indicate the regions for thickness calculation at the lateral anterior and lateral posterior sites, respectively. Color ranges from 0 (blue) to 246 μm (red). **F**, SBP thickness (Th) at 4 distinct sites (medial anterior [Ant], medial posterior [Pos], lateral anterior, and lateral posterior) in the femoral condyle. Results are the mean \pm SD ($n = 5$ mice). * = $P < 0.05$; ** = $P < 0.01$.

into a 3-D color map, in which the color at any position linearly corresponds to its SBP thickness. Using this method, we can manually define the region of interest within the SBP and calculate the average thickness within this region (Figure 1E). Quantification of the SBP thickness in a normal mouse knee joint confirmed that the posterior SBP of the femoral condyle at the medial and lateral sites was 2.2-fold and 1.6-fold thicker, respectively, compared to the anterior medial and lateral SBP sites (Figure 1F). These results provide the first line of evidence that SBP thickness is positively correlated with loading status. Since tibial SBP is very close to the growth plate, it is difficult to apply this approach to the tibia. Therefore, we focused on the distal femur for analyses of the STB and SBP in our studies.

Development of SBP sclerosis at the medial posterior site in *Egfr*-CKO mice after DMM. We previously reported that the activity of EGFR is critical for maintaining the number of superficial chondrocytes, promoting cartilage surface lubrication, and retaining cartilage mechanical functions (17). Strikingly, *Egfr*-CKO (*Col2-Cre Egfr^{Wt5lf}*) mice developed a severe OA phenotype at 2–3 months after DMM surgery, with a complete depletion of the articular cartilage layer at the medial posterior site (see Supplementary Figure 1A, available on the *Arthritis & Rheumatology* web site at <http://onlinelibrary.wiley.com/doi/10.1002/art.40351/abstract>). The cartilage remained intact at the medial anterior site in both WT and *Egfr*-CKO mice after DMM (see Supplementary Figure 1B).

Micro-CT analysis of the femoral STB detected a modest but significant decrease in the BV/TV, accompanied by reduced trabecular thickness, in the knee sections from *Egfr*-CKO mice, but not in those from WT mice, after DMM (see Supplementary Figure 2, <http://onlinelibrary.wiley.com/doi/10.1002/art.40351/abstract>). Interestingly, progression of OA induced a drastic increase in the structure model index of the STB in *Egfr*-CKO mice, indicating that a deterioration of the trabecular structure occurs in late-stage OA.

Examination of the 2-D micro-CT images of frontal knee sections indicated that the SBP at the medial site of the femurs of *Egfr*-CKO mice was substantially thickened after DMM (Figure 2A). By applying our new protocol, we calculated the SBP thickness at 4 locations within the femoral condyle (medial posterior, lateral posterior, medial anterior, and lateral anterior). Interestingly, in *Egfr*-CKO mice after DMM, we observed a significant increase in SBP thickness (increase of 31%) only at the medial posterior site, an area where cartilage degradation was the most severe (see Supplementary Figure 1). This thickening of the SBP was absent from

the other 3 sites of the femoral condyles of *Egfr*-CKO mice after DMM, and was absent from all 4 sites in WT mice (Figures 2B and C), implying that this localized SBP response can likely be attributed to depletion of the overlying articular cartilage.

SBP thickening in *Egfr*-CKO mice after DMM coinciding with increased bone formation at the bone marrow side of the SBP and reduced sclerostin levels in the SBP. To elucidate the mechanism of SBP thickening, we first investigated the sites of new bone formation. In *Egfr*-CKO mice after DMM surgery, osteocalcin staining revealed that the number of osteoblasts lining the SBP at the bone marrow side was increased 8.6-fold at the medial side of the femur as compared to the lateral side. Moreover, the number of osteoblasts lining the SBP at the bone marrow side was increased 9.7-fold in DMM-operated femurs compared to sham-operated femurs (Figures 3A and B). This enhanced bone formation was accompanied by an increased length of blood vessels lining the SBP surface (Figures 3C and D), likely providing more oxygen and nutrients needed for active bone formation.

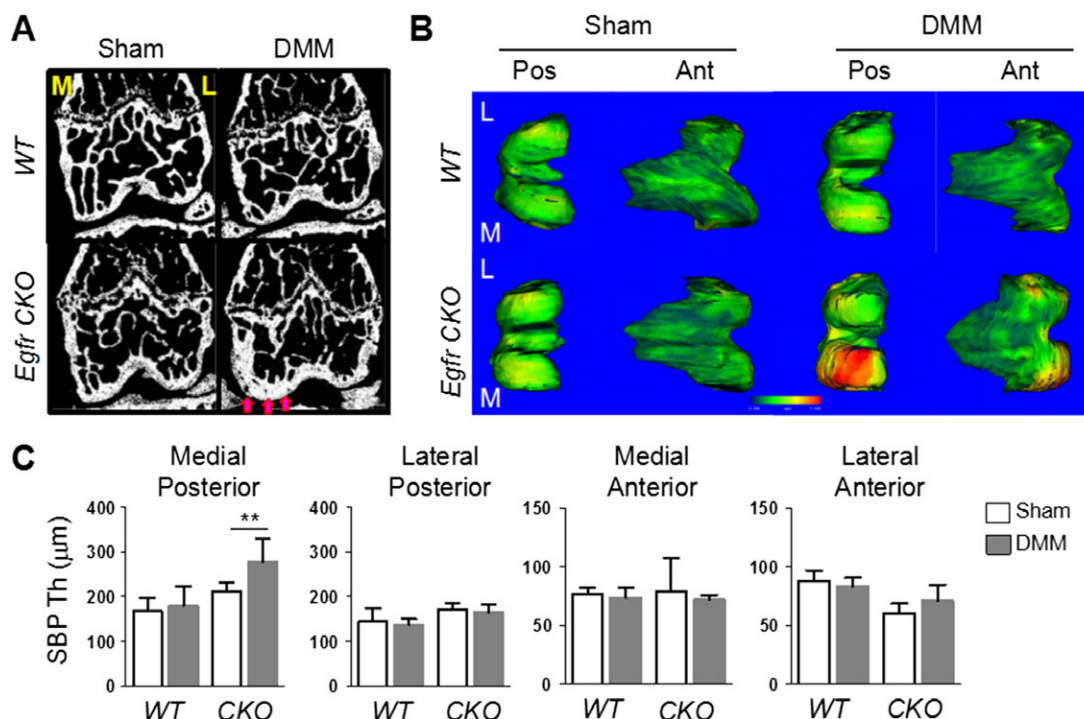


Figure 2. Evidence of local subchondral bone plate (SBP) sclerosis underneath areas of severely damaged cartilage in the femurs of cartilage-specific *Egfr*-knockout (*Egfr*-CKO) mice after destabilization of the medial meniscus (DMM) surgery. **A**, Representative micro-computed tomography frontal images of the femoral epiphyseal region in wild-type (WT) and *Egfr*-CKO mice at 2 months after DMM or sham surgery. **Arrows** indicate thickened SBP at the medial (M) site. **B**, Representative 3-dimensional color maps of SBP thickness (Th) in the femurs of WT and *Egfr*-CKO mice after sham or DMM surgery (posterior [Pos] and anterior [Ant] angles, lateral [L] and medial sites). Color ranges from 0 (blue) to 430 μm (red). **C**, SBP thickness at 4 distinct sites in the femurs. Results are the mean ± SD (n = 5 mice per genotype). A significant interaction between surgery and genotype ($P < 0.05$ by 2-way analysis of variance) was seen at the medial posterior site in *Egfr*-CKO mice. ** = $P < 0.01$. Color figure can be viewed in the online issue, which is available at <http://onlinelibrary.wiley.com/doi/10.1002/art.40351/abstract>.

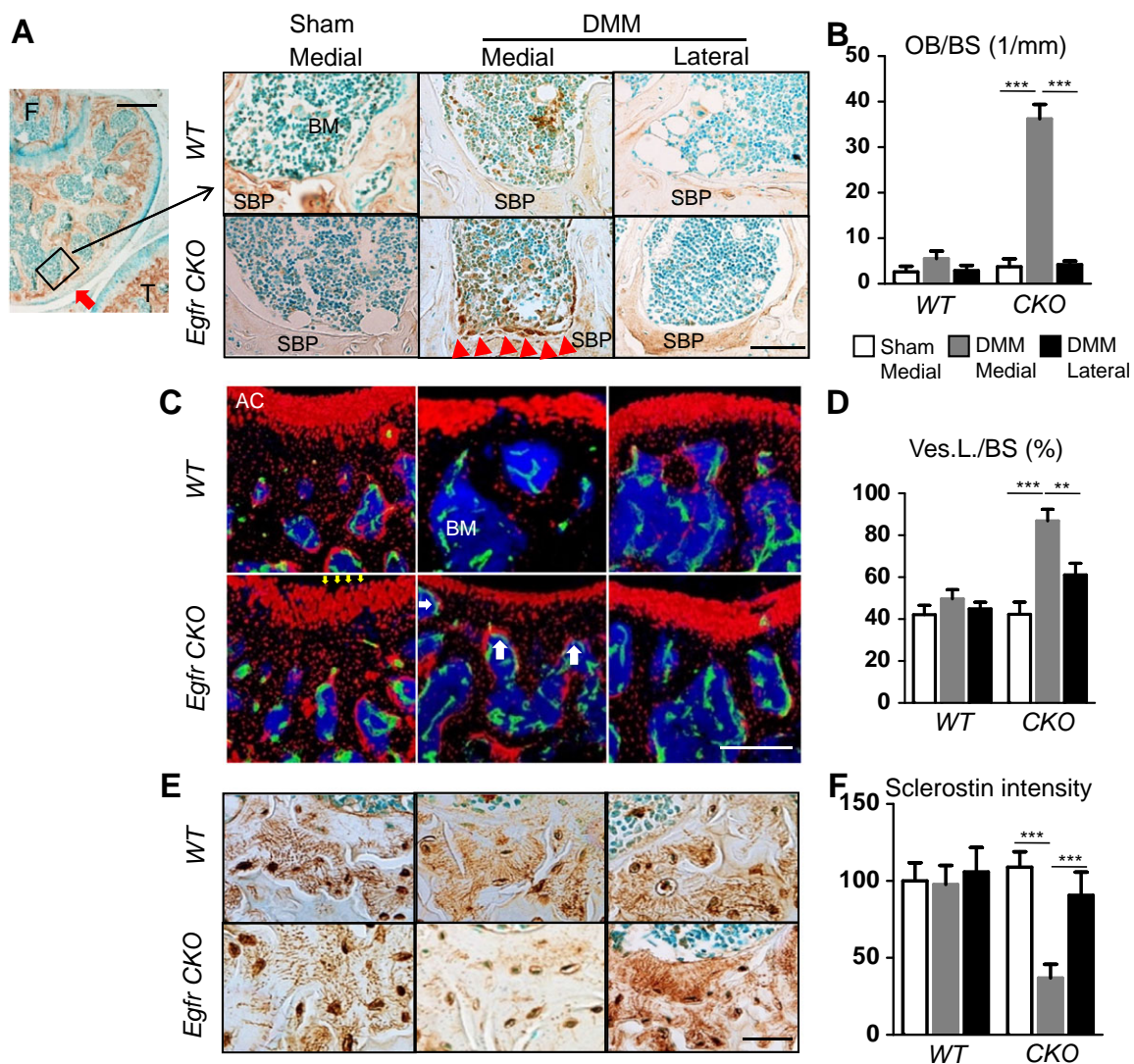


Figure 3. Escalated bone formation activity beneath the thickened SBP and reduced sclerostin levels in the SBP in DMM-operated knees of *Egfr*-CKO mice. **A**, Immunohistochemical analyses of osteocalcin were used to identify osteoblasts beneath the SBP (medial or lateral compartments of the femur [F]) in WT and *Egfr*-CKO mice at 2 months after sham or DMM surgery. **Arrowheads** indicate increased numbers of osteoblasts along the SBP. Boxed area with **red arrow** on the left (bar = 400 μ m) is shown at higher magnification on the right (bar = 100 μ m). **B**, The number of osteoblasts lining the SBP was quantified. Results are the mean \pm SD osteoblasts per bone surface area (OB/BS) ($n = 4$ mice per genotype). *** = $P < 0.001$. **C**, Representative confocal images of endomucin staining (green) to label bone marrow (BM) vasculature in WT and *Egfr*-CKO mouse joints are shown (images counterstained with DAPI [blue]; bar = 150 μ m). These mice also had the *Rosa-Tomato* transgene, and therefore all bone marrow mesenchymal lineage cells, including bone lining osteoblasts, osteocytes, bone marrow mesenchymal progenitors, and articular chondrocytes, are *Rosa-Tomato*-positive cells (red). **White arrows** indicate vessels aligned along with the SBP surface (**yellow arrows**). **D**, The percentage of SBP bone surface aligned with blood vessels (Ves.L./BS) was determined. Results are the mean \pm SD ($n = 4$ mice per genotype). ** = $P < 0.01$; *** = $P < 0.001$. **E**, Immunohistochemical analyses were performed to determine the level of sclerostin staining intensity in the SBP. Bar = 30 μ m. **F**, Sclerostin staining intensity was quantified. Results are the mean \pm SD ($n = 4$ mice per genotype). *** = $P < 0.001$. T = tibia; AC = articular cartilage (see Figure 2 for other definitions). Color figure can be viewed in the online issue, which is available at <http://onlinelibrary.wiley.com/doi/10.1002/art.40351/abstract>.

Wnt proteins are potent signals for osteoblastic bone formation. Sclerostin is a Wnt pathway antagonist that is almost exclusively secreted by osteocytes (12). Interestingly, its expression is mainly regulated by mechanical stimulation on bone (13). It is commonly accepted that in

normal joints, the meniscus plays a key role in reducing the contact stresses on articular cartilage (24), and that a loss of cartilage in the later stages of OA results in greatly amplified focal stresses on the underlying subchondral bone (25). Therefore, we hypothesized that expression of sclerostin is

specifically down-regulated in the SBP under the damaged cartilage of mice after DMM, due to abnormal overloading. Similar to the findings in the cortical bone, osteocytes in the SBP expressed high amounts of sclerostin within cell bodies and throughout dendritic processes (Figure 3E), indicating that sclerostin may have a possible role in maintaining the SBP. In WT mice, DMM surgery did not alter the levels of sclerostin at either the medial or the lateral sites (Figures 3E and F). Strikingly, in *Egfr*-CKO mice, the amount of sclerostin was markedly attenuated within the SBP at the medial site, but not the lateral site, of the femurs after DMM surgery (Figures 3E and F). These results suggest that a loss of sclerostin in the SBP underneath the damaged cartilage during late-stage OA may play a role in new bone formation at the bone marrow side of the SBP.

Similar mechanisms of SBP thickening in DMM-operated *Egfr*-CKO mouse knees and knees of older *Egfr*-CKO mice with spontaneous OA. *Egfr*-CKO mice were previously observed to develop spontaneous OA with no SBP phenotype at 6 months of age (17). In the present study, in mice at age 12 months, while typical OA

phenotypes in the articular cartilage continued (Figures 4A and B), the STB displayed significant bone loss accompanied by deterioration in structure (see Supplementary Figure 3, <http://onlinelibrary.wiley.com/doi/10.1002/art.40351/abstract>).

Unlike surgery-induced OA in mice, age-related spontaneous OA in 12-month-old mice was characterized by cartilage damage at both the medial and lateral regions. This was associated with a similar level of SBP sclerosis at the posterior site, across the entire distal femur, in *Egfr*-CKO mice (Figures 4C and D). WT mouse knees remained healthy at this age. We found that the number of osteoblasts was elevated by 4.3- and 5.4-fold at the medial and lateral sites, respectively, in *Egfr*-CKO mice compared to WT mice (Figures 4E and F).

Analysis of sections of the mouse knee joints by dynamic histomorphometry revealed that newly formed bone surfaces were observed only at the bone marrow side of the SBP, and not at the cartilage side (see Supplementary Figure 4A, <http://onlinelibrary.wiley.com/doi/10.1002/art.40351/abstract>). Moreover, the bone formation

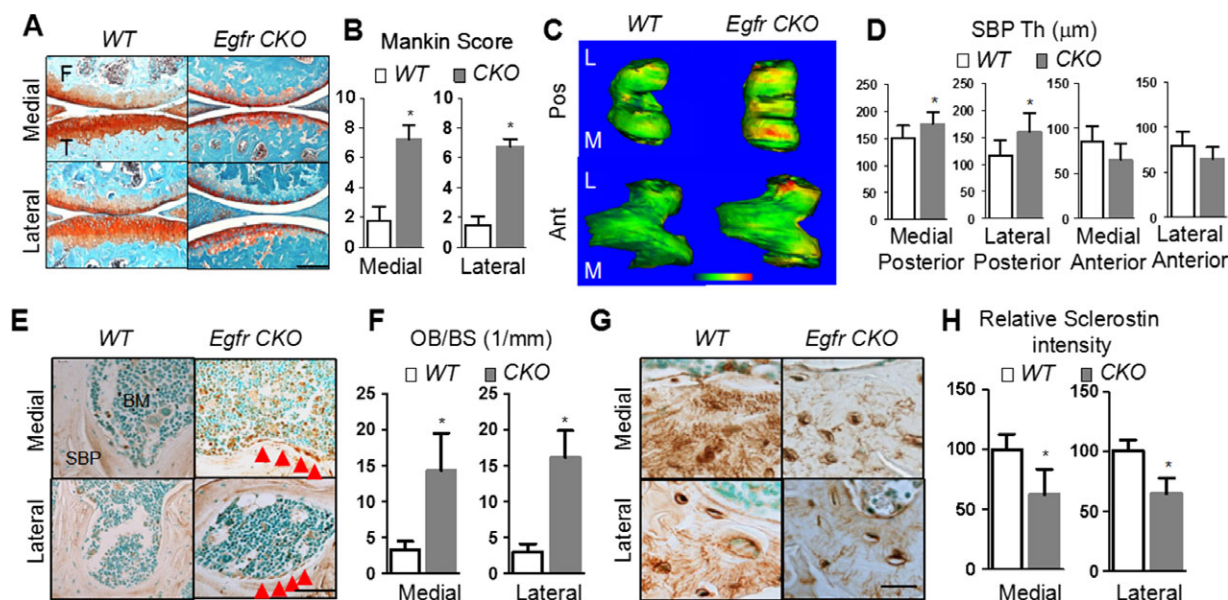


Figure 4. Increased bone formation along the SBP surface and suppressed sclerostin levels in the SBP upon SBP thickening in the knees of older *Egfr*-CKO mice. **A**, Safranin O staining was used to evaluate cartilage damage in the epiphyseal regions of the femur (F) and tibia (T) (medial and lateral sites) of 1-year-old WT and *Egfr*-CKO mice. Bar = 200 μm. **B**, Severity of osteoarthritis was measured using the Mankin score (scale 0–14). Results are the mean ± SD (n = 5 mice per genotype). * = $P < 0.05$. **C**, Representative 3-dimensional color maps show SBP thickness in WT and *Egfr*-CKO mouse femurs. Color ranges from 0 (blue) to 300 μm (red). **D**, SBP thickness at 4 distinct femoral sites is shown. Results are the mean ± SD (n = 9–11 mice per genotype). * = $P < 0.05$. **E**, Immunohistochemical analyses of osteocalcin were performed to identify osteoblasts beneath the SBP in WT and *Egfr*-CKO mice. **Arrowheads** indicate increased numbers of osteoblasts along the SBP surface. Bar = 100 μm. **F**, The number of osteoblasts lining the SBP surface was quantified. Results are the mean ± SD osteoblasts per bone surface area (OB/BS) (n = 4 mice per genotype). * = $P < 0.05$. **G**, Immunohistochemical analyses were performed to determine the level of sclerostin staining intensity in the SBP of the femurs in aging WT and *Egfr*-CKO mice. Bar = 30 μm. **H**, Sclerostin staining intensity was quantified in the medial and lateral sites of the femurs of aging WT and *Egfr*-CKO mice. Results are the mean ± SD (n = 4 mice per genotype). * = $P < 0.05$. **BM** = bone marrow (see Figure 2 for other definitions). Color figure can be viewed in the online issue, which is available at <http://onlinelibrary.wiley.com/doi/10.1002/art.40351/abstract>.

rate (BFR) was elevated 3.5-fold at both the medial and lateral sites of the femurs of *Egfr*-CKO mice compared to WT mice (see Supplementary Figures 4B and C). Furthermore, the levels of sclerostin expression by osteocytes in the SBP were significantly decreased at both the medial and lateral sites of the femurs of *Egfr*-CKO mice compared to WT mice (Figures 4G and H).

SBP sclerosis in other models of late-stage OA.

To confirm that our findings were not restricted to *Egfr*-CKO mice, we tested 2 other late-stage OA models in WT mice. At 10 months after DMM surgery, WT mice exhibited severe OA phenotypes, including a complete depletion of articular cartilage (Figures 5A and B) and a trend toward bone loss in the STB (see Supplementary Figure 5, <http://onlinelibrary.wiley.com/doi/10.1002/art.40351/abstract>). Consistent with the findings in our *Egfr*-CKO mouse model of DMM-induced OA, the DMM-operated femurs of WT mice at 10 months after surgery displayed thickening of the SBP only at the medial posterior site, and not at the other 3 sites of the femoral condyle (Figures 5C and D). Staining of osteocytes in the SBP confirmed that osteocytic

sclerostin levels were reduced within the thickened SBP at 10 months after DMM surgery (Figures 5E and F).

Compared to DMM, which produces only moderate OA, DMMH induces more severe OA (20). At 14 weeks post-DMMH surgery, WT mouse knee joints had already developed late-stage OA phenotypes, with severe cartilage degeneration at the medial posterior site (Figures 6A and B). No significant signs of cartilage degeneration were observed in the sham-operated joints. Thus, SBP thickening was evident only at the medial posterior site, and not at the lateral posterior site, of the femurs of WT mice at 14 weeks after DMMH (Figures 6C and D). Moreover, we observed a significant decrease in the levels of sclerostin only at the medial site, and not at the lateral site, of DMMH-operated mouse knees (Figure 6F).

To determine whether inhibition of sclerostin mediates SBP sclerosis, we performed DMMH surgery on the knee joints of *Sost*-KO mice. Consistent with the findings reported previously (26), the sham-operated joints of *Sost*-KO mice had much more subchondral bone compared to the sham-operated joints of WT mice. Strikingly, although the medial posterior site of

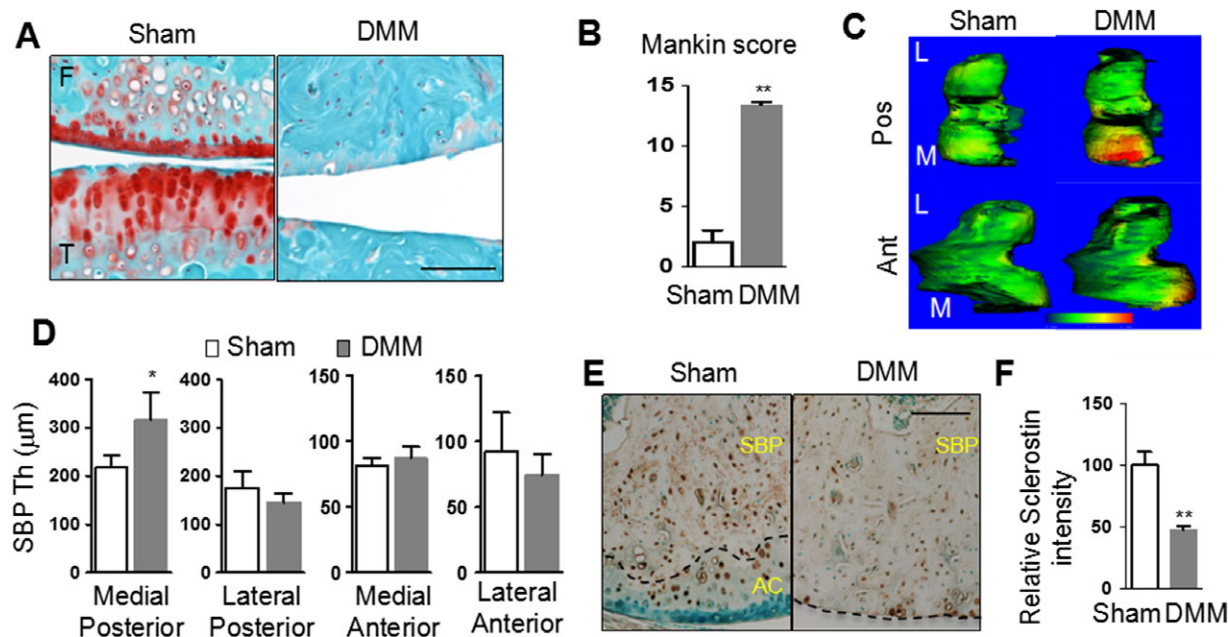


Figure 5. Severe cartilage degeneration accompanied by substantial SBP thickening and suppression of sclerostin within the SBP in the knees of WT mice at 10 months after DMM surgery. **A**, Safranin O staining was used to evaluate cartilage damage in the femur (F) and tibia (T) of WT mice at 10 months after sham or DMM surgery. Bar = 100 μm. **B**, Severity of osteoarthritis was measured using the Mankin score (scale 0–14). Results are the mean ± SD (n = 3 mice per group). ** = $P < 0.01$. **C**, Representative 3-dimensional color maps show SBP thickness in the sham- and DMM-operated femurs of WT mice. Color ranges from 0 (blue) to 420 μm (red). **D**, SBP thickness at 4 distinct femoral sites is shown. Results are the mean ± SD (n = 3 mice per group). * = $P < 0.05$. **E**, Immunohistochemical analyses were performed to determine the level of sclerostin staining intensity at the medial posterior site of the SBP. The broken line indicates the chondral–osseous junction. Bar = 100 μm. **F**, Sclerostin staining intensity was quantified. Results are the mean ± SD (n = 3 mice per group). ** = $P < 0.01$. AC = articular cartilage (see Figure 2 for other definitions). Color figure can be viewed in the online issue, which is available at <http://onlinelibrary.wiley.com/doi/10.1002/art.40351/abstract>.

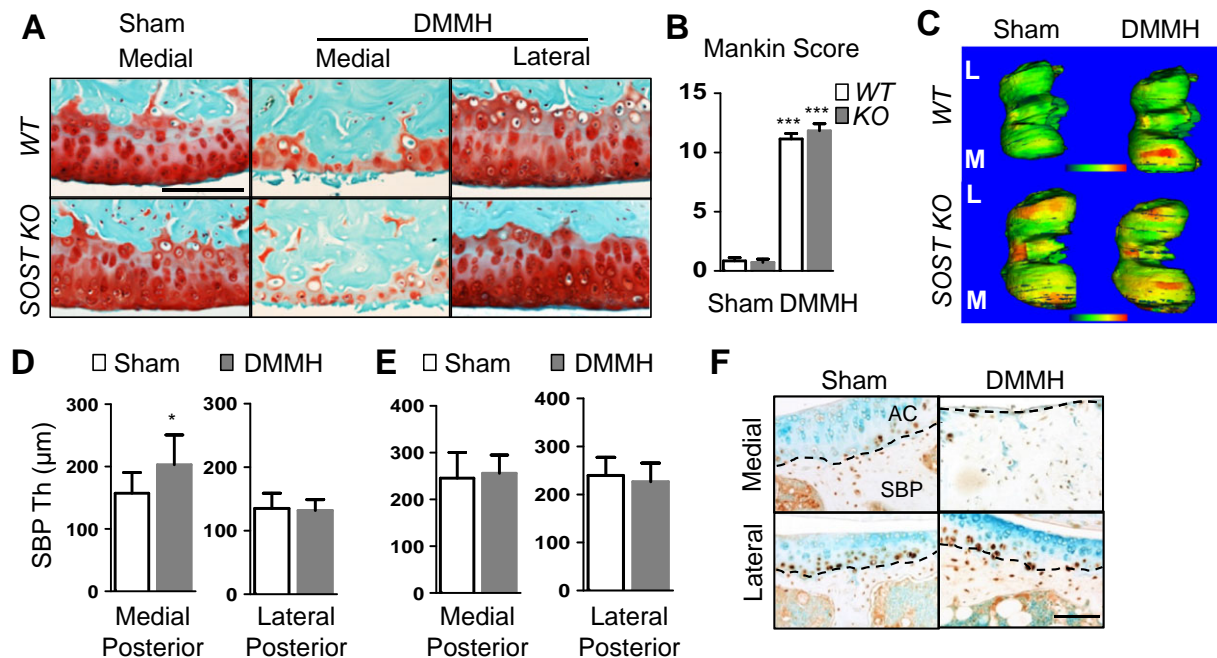


Figure 6. DMM plus hemisection of the meniscus (DMMH) surgery results in a thickened SBP at late stages of osteoarthritis (OA) in WT mice but not in mice with knockout of the sclerostin gene (*Sost*-KO). **A**, Safranin O staining was used to evaluate SBP thickening in the femurs of WT and *Sost*-KO mice at 14 weeks after sham or DMMH surgery. Bar = 100 μ m. **B**, Severity of OA at the medial posterior site was measured using the Mankin score (scale 0–14). Results are the mean \pm SD ($n = 6$ –7 mice per group). *** = $P < 0.001$ versus the corresponding mouse group that underwent sham surgery. **C**, Representative 3-dimensional color maps show SBP thickness in the femurs of WT and *Sost*-KO mice after sham or DMMH surgery. Color ranges from 0 (blue) to 282 μ m (red) for WT mice, and from 0 (blue) to 354 μ m (red) for *Sost*-KO mice. **D**, SBP thickness was determined at the medial posterior and lateral posterior sites of the femurs of WT mice. Results are the mean \pm SD ($n = 8$ mice per group). * = $P < 0.05$. **E**, SBP thickness was determined at the medial posterior and lateral posterior sites of the femurs of *Sost*-KO mice. Results are the mean \pm SD ($n = 7$ mice per group). **F**, Osteocytes were stained for sclerostin expression in the SBP (medial and lateral sites) of the femurs of WT mice. The broken line indicates the chondral–osseous junction. Bar = 100 μ m. AC = articular cartilage (see Figure 2 for other definitions). Color figure can be viewed in the online issue, which is available at <http://onlinelibrary.wiley.com/doi/10.1002/art.40351/abstract>.

the DMMH-operated joints developed a level of cartilage degeneration that was similar to that in WT mice (Figures 6A and B), the SBP thickness in the DMMH-operated joints was the same as that in the sham-operated joints (Figures 6C and E). Taken together, our data from these OA models support the notion that SBP sclerosis is likely the result of reduced osteocyte expression of sclerostin in the SBP during the progression of OA.

DISCUSSION

Abnormal mechanical loading plays a pivotal role in the development of OA (27). The major risk factors for knee OA that have been identified to date include older age, female sex, obesity, knee injury, and occupational overuse of the knee joints (28,29). While the first 2 factors are indicative of the vulnerability of the knee to injury, the latter 3 represent the presence of either chronic stress, excessive loading, or focally increased stress on the knee. Most previous studies focused on the mechanobiology of

chondrocytes and cartilage tissue in their attempt to understand the role of overloading in the initiation and progression of OA (30). In patients with OA, it has been long observed that subchondral bone becomes abnormal with increased bone resorption (31). In this study, we took advantage of 4 models of severe late-stage OA both in genetically modified mice and in WT mice, and we demonstrated that abnormal overloading, as a result of depletion of the overlying cartilage, attenuates osteocytic sclerostin expression within the SBP, and subsequently increases bone formation at the bone marrow side of the SBP, presumably via the activation of Wnt signaling. Thus, our findings elucidate the intimate relationship among mechanical loading, osteocytic sclerostin, and SBP sclerosis during late-stage OA. This conclusion is further supported by the results of a recent study in which sclerostin levels within the SBP in patients with OA were found to be negatively correlated with OA severity (32).

A prerequisite to reaching our conclusions was the use of a novel micro-CT protocol in which we calculated SBP thickness in a 3-D manner across the

entire femoral epiphyseal area. This method eliminates bias arising from sectioning angle and location. Moreover, this approach allows us to compare the same region among different bones and different anatomic sites within the same bone, thus decreasing sample variations. Because of the small size of mouse joints, we have found that the distal femur is a better site than the proximal tibia for analysis of mouse subchondral bone under normal conditions. After mouse knee joints are subjected to DMM, SBP thickening in the tibia often results in fusion of the SBP with the growth plate, making it impossible to analyze bone structure.

Several lines of evidence support our conclusion. First, our analysis of the distal femoral epiphyseal bone revealed that the load-bearing posterior site is thicker than the non-load-bearing anterior site of the same bone, regardless of whether this was observed in the medial location or lateral location. These findings indicate that SBP thickness is positively correlated with the loading applied to it.

Second, we tested 4 distinct mouse models of either severe OA or long-term chronic OA symptoms. In all models, we observed a substantial decrease in sclerostin levels expressed by osteocytes within the thickened SBP underlying damaged articular cartilage. This phenomenon is location specific. In surgery models (*Egfr*-CKO mice at 2 months after DMM, WT mice at 10 months after DMM, and WT mice at 14 weeks after DMMH), the SBP was expanded and the amount of sclerostin was attenuated only at the medial posterior site, an area where cartilage damage was the most concentrated. The SBP responses were not detected at the lateral posterior site, where cartilage damage was modest at best. In contrast, since we observed that OA-induced cartilage degeneration developed chronically at both the medial and lateral sites of the femoral condyles of 12-month-old *Egfr*-CKO mice with spontaneous, aging-related OA, alterations in the SBP were correspondingly observed at both the lateral and medial posterior sites.

Third, despite the occurrence of changes in the posterior region, the thickness of the anterior SBP, regardless of whether it was located in the medial site or the posterior site, remained the same in all of our OA models.

Finally, our findings in *Sost*-KO mice after DMMH surgery support the idea that sclerostin mediates SBP thickening underneath the eroded cartilage at the late stages of OA. Repetitive mechanical loading on diaphyseal cortical bone reduces sclerostin expression to achieve anabolic bone formation (33). Indeed, the SBP is structurally similar to cortical bone and has higher sclerostin levels when compared to trabecular

bone (data not shown). It is very likely that the suppressed expression of sclerostin that was observed in the SBP underneath the damaged cartilage could be attributed to the increased focal stress on the SBP. Therefore, our data provide another piece of evidence supporting the role of sclerostin in the bone responses toward mechanical loading. Taken together, our findings demonstrate a critical role of mechanics in shaping the SBP after the development of OA, and elucidate the underlying molecular mechanism.

Interestingly, in the *Egfr*-CKO mouse models of OA, in addition to thickening of the SBP, the STB became modestly osteopenic. Our previous study demonstrated that metaphyseal trabecular bone and serum bone markers are not affected in *Egfr*-CKO mice (17), indicating that overall, bone remodeling is not altered as a consequence of the genetic modification of *Egfr* in cartilage. This result is consistent with a previous finding indicating that OA-induced bone damage is restricted to the subchondral bone region (34). We believe that defects in articular cartilage are sufficient to induce subchondral bone abnormalities under enhanced mechanical loads.

Whether subchondral bone sclerosis is a driving force for cartilage degeneration or a consequence of cartilage degeneration has been disputed for many years. Since the DMM surgery used in our current model led to the development of moderately severe OA in WT mice, we only detected significant changes in the SBP and STB at 10 months after surgery. At 2 months after surgery, while DMM had already generated changes in the articular cartilage, such as partial loss of proteoglycan and surface fibrillation, it had no detectable effect on subchondral bone structure in these mice. All subchondral bone responses in our models require either a substantial period of time after OA initiation or a CKO mouse model that is predisposed to OA development. Moreover, our previous findings revealed that the cartilage surface modulus at future sites of OA is substantially reduced at 1 week after DMM surgery, owing to increased catabolic activities (35). This time point is much earlier than any detectable emergence of cartilage morphologic changes, let alone subchondral bone alterations. Hence, our data strongly support the idea that subchondral bone sclerosis is secondary to cartilage degeneration.

We were also interested in exploring whether changes in the subchondral bone could exaggerate overlying cartilage degeneration. *Sost*-KO mice have substantially more trabecular and cortical bone than WT mice (36). In 1-year-old *Sost*-KO mice, the STB robustly expands, resulting in a solid bone between articular cartilage and the growth plate (data not shown). Consistent with the results of a previous study (37), we did not detect

any cartilage degeneration in *Sost*-KO mice from ages 3 months up to 14 months (data not shown). Four weeks of sclerostin antibody injections in WT mice also did not alter the articular cartilage, whereas it drastically increased BV/TV in the STB and thickened the SBP (data not shown).

In contrast to previous findings showing that OA was accelerated in *Sost*-KO mice after DMM surgery (26), we found that DMMH surgery resulted in symptoms of OA that were similarly severe between WT and *Sost*-KO mice. Furthermore, a strategy of intermittent injections of parathyroid hormone (PTH) 1–34 peptide, a potent anabolic agent for stimulating bone formation and bone turnover, has been shown to either attenuate OA progression (38) or have no effect in surgery-induced OA models (39). In our experiments, PTH injections quickly enlarged the SBP within 2–3 weeks but did not accelerate OA progression after DMM (data not shown). More importantly, no clinical study has shown a positive correlation between PTH treatment and incidence of OA in patients with osteoporosis. From a mechanical point of view, thickening of the SBP from the bone marrow side, as we have demonstrated to be the major site of new bone formation during OA, is unlikely to affect the load distribution at the surface of overlying cartilage. We believe that SBP thickening alone is not sufficient to affect cartilage degeneration, and therefore it cannot be an initiator of cartilage and joint damage in OA development. Whether bone alterations in the STB, predicated by enhanced bone turnover, contribute to the progression of OA is still not clear from our studies.

Our studies have several limitations. First, our sham surgery was performed in the contralateral joint rather than in a separate group of mice. Though we did not detect any obvious OA changes in the sham-operated joints, animals may still have altered loading patterns and gaits. Second, DMMH was performed on mice with immature skeletons. We chose this age (8 weeks old) because the SBP in *Sost*-KO mice continuously thickens throughout their life, thereby making it difficult to accurately measure its thickness in older mice. Third, it is possible that the BFR at the bone marrow side of the SBP of *Sost*-KO mice has already reached its maximum, and so cannot be further enhanced by the increased loading after cartilage depletion. However, PTH injections have been shown to increase the high basal levels of periosteal and endosteal BFR in the femoral midshaft of *Sost*-KO mice (40), suggesting that the BFR in the SBP of *Sost*-KO mice can be further elevated. Finally, all of our data were derived from mouse models. While mouse models have many advantages in cartilage research, particularly in discovering novel cellular and molecular mechanisms,

studies of OA in larger animals are required before we can translate our findings into workable designs for future clinical applications.

In summary, the results of our study establish mechanical loading-induced attenuation of sclerostin expression and elevation of bone formation along the SBP as the major mechanisms responsible for subchondral bone sclerosis associated with late-stage OA. Thus, correcting abnormal loading of the knee joint might be an effective approach for attenuating subchondral bone damage in patients with OA.

AUTHOR CONTRIBUTIONS

All authors were involved in drafting the article or revising it critically for important intellectual content, and all authors approved the final version to be published. Dr. Qin had full access to all of the data in the study and takes responsibility for the integrity of the data and the accuracy of the data analysis.

Study conception and design. Jia, Ma, Enomoto-Iwamoto, Qin.

Acquisition of data. Jia, Ma, Wei, Tong, Chandra, L. Wang, Sun, Yang, Badar, Zhang, Tseng.

Analysis and interpretation of data. Jia, Ma, Wei, Tong, Tower, Kramer, Kneissel, Xia, Liu, J. H. C. Wang, Han, Enomoto-Iwamoto, Qin.

ADDITIONAL DISCLOSURES

Authors Kramer and Kneissel are employees of Novartis Institutes for BioMedical Research.

REFERENCES

1. Lane NE, Brandt K, Hawker G, Peeva E, Schreyer E, Tsuji W, et al. OARSI-FDA initiative: defining the disease state of osteoarthritis. *Osteoarthritis Cartilage* 2011;19:478–82.
2. Kellgren JH, Lawrence JS. Radiological assessment of osteoarthritis. *Ann Rheum Dis* 1957;16:494–502.
3. Dedrick DK, Goldstein SA, Brandt KD, O'Connor BL, Goulet RW, Albrecht M. A longitudinal study of subchondral plate and trabecular bone in cruciate-deficient dogs with osteoarthritis followed up for 54 months. *Arthritis Rheum* 1993;36:1460–7.
4. Goldring SR, Goldring MB. Changes in the osteochondral unit during osteoarthritis: structure, function and cartilage-bone cross-talk. *Nat Rev Rheumatol* 2016;12:632–44.
5. Bailey AJ, Mansell JP, Sims TJ, Banse X. Biochemical and mechanical properties of subchondral bone in osteoarthritis. *Biorheology* 2004;41:349–58.
6. Bettica P, Cline G, Hart DJ, Meyer J, Spector TD. Evidence for increased bone resorption in patients with progressive knee osteoarthritis: longitudinal results from the Chingford study. *Arthritis Rheum* 2002;46:3178–84.
7. Funck-Brentano T, Cohen-Solal M. Crosstalk between cartilage and bone: when bone cytokines matter. *Cytokine Growth Factor Rev* 2011;22:91–7.
8. Burr DB, Gallant MA. Bone remodelling in osteoarthritis. *Nat Rev Rheumatol* 2012;8:665–73.
9. Findlay DM, Kuliwaba JS. Bone-cartilage crosstalk: a conversation for understanding osteoarthritis. *Bone Res* 2016;4:16028.
10. Arden N, Nevitt MC. Osteoarthritis: epidemiology. *Best Pract Res Clin Rheumatol* 2006;20:3–25.
11. Poole KE, van Bezooijen RL, Loveridge N, Hamersma H, Papapoulos SE, Löwik CW, et al. Sclerostin is a delayed secreted

- product of osteocytes that inhibits bone formation. *Faseb J* 2005; 19:1842–4.
12. Van Bezooijen RL, Roelen BA, Visser A, van der Wee-Pals L, de Wilt E, Karperien M, et al. Sclerostin is an osteocyte-expressed negative regulator of bone formation, but not a classical BMP antagonist. *J Exp Med* 2004;199:805–14.
 13. Galea GL, Lanyon LE, Price JS. Sclerostin's role in bone's adaptive response to mechanical loading. *Bone* 2017;96:38–44.
 14. McClung MR, Grauer A, Boonen S, Bolognese MA, Brown JP, Diez-Perez A, et al. Romosozumab in postmenopausal women with low bone mineral density. *N Engl J Med* 2014;370:412–20.
 15. Zhang X, Zhu J, Li Y, Lin T, Siclari VA, Chandra A, et al. Epidermal growth factor receptor (EGFR) signaling regulates epiphyseal cartilage development through β -catenin-dependent and -independent pathways. *J Biol Chem* 2013;288:32229–40.
 16. Lee D, Cross SH, Strunk KE, Morgan JE, Bailey CL, Jackson IJ, et al. Wa5 is a novel ENU-induced antimorphic allele of the epidermal growth factor receptor. *Mamm Genome* 2004;15:525–36.
 17. Jia H, Ma X, Tong W, Doyran B, Sun Z, Wang L, et al. EGFR signaling is critical for maintaining the superficial layer of articular cartilage and preventing osteoarthritis initiation. *Proc Natl Acad Sci U S A* 2016;113:14360–5.
 18. Zhang X, Siclari VA, Lan S, Zhu J, Koyama E, Dupuis HL, et al. The critical role of the epidermal growth factor receptor in endochondral ossification. *J Bone Miner Res* 2011;26:2622–33.
 19. Zhang X, Tamasi J, Lu X, Zhu J, Chen H, Tian X, et al. Epidermal growth factor receptor plays an anabolic role in bone metabolism in vivo. *J Bone Miner Res* 2011;26:1022–34.
 20. Kamekura S, Hoshi K, Shimoaka T, Chung U, Chikuda H, Yamada T, et al. Osteoarthritis development in novel experimental mouse models induced by knee joint instability. *Osteoarthritis Cartilage* 2005;13:632–41.
 21. Zhang X, Zhu J, Liu F, Li Y, Chandra A, Levin LS, et al. Reduced EGFR signaling enhances cartilage destruction in a mouse osteoarthritis model. *Bone Res* 2014;2:14015.
 22. Boussein ML, Boyd SK, Christiansen BA, Guldberg RE, Jepsen KJ, Muller R. Guidelines for assessment of bone microstructure in rodents using micro-computed tomography. *J Bone Miner Res* 2010;25:1468–86.
 23. Aigner T, Cook JL, Gerwin N, Glasson SS, Lavery S, Little CB, et al. Histopathology atlas of animal model systems: overview of guiding principles. *Osteoarthritis Cartilage* 2010;18 Suppl 3:S2–6.
 24. Walker PS, Erkman MJ. The role of the menisci in force transmission across the knee. *Clin Orthop Relat Res* 1975;109:184–92.
 25. Eberhardt AW, Keer LM, Lewis JL, Vithoontien V. An analytical model of joint contact. *J Biomech Eng* 1990;112:407–13.
 26. Bouaziz W, Funck-Brentano T, Lin H, Marty C, Ea HK, Hay E, et al. Loss of sclerostin promotes osteoarthritis in mice via β -catenin-dependent and -independent Wnt pathways. *Arthritis Res Ther* 2015;17:24.
 27. Felson DT. Osteoarthritis as a disease of mechanics. *Osteoarthritis Cartilage* 2013;21:10–5.
 28. Blagojevic M, Jinks C, Jeffery A, Jordan KP. Risk factors for onset of osteoarthritis of the knee in older adults: a systematic review and meta-analysis. *Osteoarthritis Cartilage* 2010;18:24–33.
 29. Felson DT. Obesity and vocational and avocational overload of the joint as risk factors for osteoarthritis. *J Rheumatol Suppl* 2004;70:2–5.
 30. Sanchez-Adams J, Leddy HA, McNulty AL, O'Connor CJ, Guilak F. The mechanobiology of articular cartilage: bearing the burden of osteoarthritis. *Curr Rheumatol Rep* 2014;16:451.
 31. Hunter DJ, Hart D, Snieder H, Bettica P, Swaminathan R, Spector TD. Evidence of altered bone turnover, vitamin D and calcium regulation with knee osteoarthritis in female twins. *Rheumatology (Oxford)* 2003;42:1311–6.
 32. Wu L, Guo H, Sun K, Zhao X, Ma T, Jin Q. Sclerostin expression in the subchondral bone of patients with knee osteoarthritis. *Int J Mol Med* 2016;38:1395–402.
 33. Robling AG, Niziolek PJ, Baldridge LA, Condon KW, Allen MR, Alam I, et al. Mechanical stimulation of bone in vivo reduces osteocyte expression of Sost/sclerostin. *J Biol Chem* 2008;283:5866–75.
 34. Brown TD, Radin EL, Martin RB, Burr DB. Finite element studies of some juxtaarticular stress changes due to localized subchondral stiffening. *J Biomech* 1984;17:11–24.
 35. Doyran B, Tong W, Li Q, Jia H, Zhang X, Chen C, et al. Nanoindentation modulus of murine cartilage: a sensitive indicator of the initiation and progression of post-traumatic osteoarthritis. *Osteoarthritis Cartilage* 2017;25:108–17.
 36. Chandra A, Lin T, Young T, Tong W, Ma X, Tseng WJ, et al. Suppression of sclerostin alleviates radiation-induced bone loss by protecting bone-forming cells and their progenitors through distinct mechanisms. *J Bone Miner Res* 2017;32:360–72.
 37. Roudier M, Li X, Niu QT, Pacheco E, Pretorius JK, Graham K, et al. Sclerostin is expressed in articular cartilage but loss or inhibition does not affect cartilage remodeling during aging or following mechanical injury. *Arthritis Rheum* 2013;65:721–31.
 38. Sampson ER, Hilton MJ, Tian Y, Chen D, Schwarz EM, Mooney RA, et al. Teriparatide as a chondroregenerative therapy for injury-induced osteoarthritis. *Sci Transl Med* 2011;3:101ra93.
 39. Bagi CM, Berryman E, Zakur DE, Wilkie D, Andresen CJ. Effect of antiresorptive and anabolic bone therapy on development of osteoarthritis in a posttraumatic rat model of OA. *Arthritis Res Ther* 2015;17:315.
 40. Robling AG, Kedlaya R, Ellis SN, Childress PJ, Bidwell JP, Bellido T, et al. Anabolic and catabolic regimens of human parathyroid hormone 1–34 elicit bone- and envelope-specific attenuation of skeletal effects in Sost-deficient mice. *Endocrinology* 2011;152:2963–75.

Gut Microbiota Perturbations in Reactive Arthritis and Postinfectious Spondyloarthritis

Julia Manasson,¹ Nan Shen,² Helga R. Garcia Ferrer,³ Carles Ubeda,⁴ Isa Iraheta,³ Adriana Heguy,⁵ Joan M. Von Feldt,⁶ Luis R. Espinoza,⁷ Abraham Garcia Kutzbach,³ Leopoldo N. Segal,⁵ Alexis Ogdie,⁶ Jose C. Clemente,² and Jose U. Scher¹

Objective. Reactive arthritis (ReA) is an inflammatory disorder occurring several weeks after gastrointestinal or genitourinary tract infections. HLA-B27 positivity is considered a risk factor, although it is not necessarily predictive of disease incidence. Among non-genetic factors, the intestinal microbiome may play a role in disease susceptibility. The objective of this study was to characterize the gut microbiota and host gene interactions in ReA and postinfectious spondyloarthritis.

Supported by the Guatemala-Penn Partners Program and the Fogarty International Center (NIH grant D43-TW-008317), the National Psoriasis Foundation (Early Career Research grant to Dr. Manasson), the NIH (National Institute of Arthritis and Musculoskeletal and Skin Diseases [NIAMS] T32 grant T32-AR-069515 to Dr. Manasson, NIAMS grant K23-AR-063764 to Dr. Ogdie, and NIAMS grants K23-AR-064318 and R03-AR-072182 to Dr. Scher), the Spanish Ministerio de Economía y Competitividad (grant SAF2014-60234-R to Dr. Ubeda), the Rheumatology Research Foundation (grant to Dr. Ogdie), the Colton Center for Autoimmunity, the Riley Family Foundation, and the Snyder Family Foundation.

¹Julia Manasson, MD, Jose U. Scher, MD: New York University School of Medicine and Hospital for Joint Diseases, New York, New York; ²Nan Shen, MS, Jose C. Clemente, PhD: Icahn School of Medicine at Mount Sinai, New York, New York; ³Helga R. Garcia Ferrer, MD, Isa Iraheta, MD, Abraham Garcia Kutzbach, MD: Guatemalan Association Against Rheumatic Diseases and Universidad Francisco Marroquin, Guatemala City, Guatemala; ⁴Carles Ubeda, PhD: Fundación para el Fomento de la Investigación Sanitaria y Biomédica de la Comunitat Valenciana, Valencia, Spain, and CIBER en Epidemiología y Salud Pública, Madrid, Spain; ⁵Adriana Heguy, PhD, Leopoldo N. Segal, MD: New York University School of Medicine, New York, New York; ⁶Joan M. Von Feldt, MD, Alexis Ogdie, MD, MSCE: University of Pennsylvania, Philadelphia; ⁷Luis R. Espinoza, MD: Louisiana State University Health Science Center, New Orleans.

Dr. Garcia Kutzbach has received consulting fees, speaking fees, and/or honoraria from Merck Sharp & Dohme, Novartis, Pfizer, and Eli Lilly and Company (less than \$10,000 each). Dr. Ogdie has received consulting fees from Novartis and Pfizer (less than \$10,000 each) and grant support from those companies. Dr. Scher has received consulting fees from Novartis, Janssen, and UCB (less than \$10,000 each).

Address correspondence to Jose U. Scher, MD, Division of Rheumatology and Psoriatic Arthritis Center, New York University School of Medicine and Hospital for Joint Diseases, 301 East 17th Street, Room 1608, New York, NY 10003. E-mail: Jose.Scher@nyumc.org.

Submitted for publication May 23, 2017; accepted in revised form October 19, 2017.

Methods. Adult subjects with peripheral spondyloarthritis and control subjects with preceding infections who did not develop arthritis were prospectively recruited from a geographic region with a high prevalence of ReA. Clinical variables, HLA status, and 16S ribosomal RNA gene sequencing of intestinal microbiota were analyzed.

Results. Subjects with ReA showed no significant differences from controls in gut bacterial richness or diversity. However, there was a significantly higher abundance of *Erwinia* and *Pseudomonas* and an increased prevalence of typical enteropathogens associated with ReA. Subjects with ultrasound evidence of enthesitis were enriched in *Campylobacter*, while subjects with uveitis and radiographic sacroiliitis were enriched in *Erwinia* and unclassified *Ruminococcaceae*, respectively; both were enriched in *Dialister*. Host genetics, particularly HLA-A24, were associated with differences in gut microbiota diversity irrespective of disease status. We identified several co-occurring taxa that were also predictive of HLA-A24 status.

Conclusion. This is the first culture-independent study characterizing the gut microbial community in postinfectious arthritis. Although bacterial factors correlated with disease presence and clinical features of ReA, host genetics also appeared to be a major independent driver of intestinal community composition. Understanding of these gut microbiota–host genetic relationships may further clarify the pathogenesis of postinfectious spondyloarthritis.

Reactive arthritis (ReA) is an inflammatory disorder that manifests in young adults, usually a few weeks after a gastrointestinal (GI) or genitourinary (GU) tract infection. While it is typically self-limited and resolves within months, a proportion of individuals develop persistent symptoms. ReA is classified as one of several spondyloarthritis (SpA). Symptoms include asymmetric oligoarthritis (most often of the large joints); extraarticular features, including enthesitis, tendinitis, and uveitis; and a variety of skin rashes

such as erythema nodosum, keratoderma blennorrhagicum, and circinate balanitis (1). The classic enteropathogenic bacteria associated with ReA are *Yersinia*, *Salmonella*, *Shigella*, and *Campylobacter*, while *Chlamydia* is the most common cause of ReA following GU infections (1). However, *Escherichia coli* (2) and *Clostridium difficile* (3) have also been implicated.

The mechanism of postinfectious peripheral SpA and ReA development remains elusive. HLA-B27 positivity has long been studied as a genetic risk factor for the disease (4). It is highly prevalent in Caucasian Northern Europeans, but virtually absent in other populations that develop ReA (5). In fact, several recent epidemiologic studies estimate that no more than half of individuals who develop ReA are HLA-B27 positive (6), while the presence of the allele has poor predictive value for the development of disease (7). Furthermore, cases of ReA are seldom diagnosed in the US (8), and the ones encountered are typically in immigrant populations (9). However, ReA is much more prevalent in the native population of Central America and particularly in Guatemala, where HLA-B27 positivity is low (10).

Unlike septic arthritis, which directly results from joint infection by pathogenic microorganisms, synovial fluid cultures in ReA are sterile, implying the possibility of an autoimmune phenomenon. Several models of ReA pathogenesis have been proposed. They include the persistence of causative agents that trigger an exaggerated immune response; intracellular uptake and trafficking of bacteria (or their components) into the synovium causing inflammation; biomolecular mimicry, whereby bacterial antigens have host immunologic homology but are different enough to induce an immune response in synovial fluid; Toll-like receptors (TLRs), particularly TLR-2, recognizing bacterial ligands and activating an immune cell response; and intestinal infection resulting in gut permeability, allowing luminal antigens to interact with the host immune system and cause distal joint inflammation (11,12). In support of the last model, recent investigations indicate that synovial fluid from individuals with ReA contains potentially immunogenic products, such as bacterial DNA, antigenic proteins, and lipopolysaccharides (13,14).

Another potential risk factor that has not been explored is the collection of commensals and pathogenic microorganisms residing in the gut, namely, the intestinal microbiome. Given the close relationship between gut infection and ReA, the microbiome likely plays a role in susceptibility to disease. To date, there have not been any studies looking at the intestinal microbiota as it relates to ReA or postinfectious peripheral SpA development. The

objective of this study was to characterize the gut microbiota of subjects who had previous GI or GU infections and evaluate for differences between those who developed postinfectious peripheral SpA and those who did not in a region highly prevalent for the disease. We also explored whether clinical phenotype, host genetics, and treatment strategies were associated with significant intestinal microbiota perturbations.

SUBJECTS AND METHODS

Study participants. Thirty-two subjects with ReA (postinfectious peripheral SpA) and 32 control subjects were prospectively enrolled from July to October 2014 in Guatemala City, Guatemala (an area with a high prevalence of ReA) through the Guatemala-Penn Partners Initiative (15). Subjects with ReA were recruited from 2 rheumatology clinics: Asociacion Guatemalteca Anti Enfermedades Reumaticas and Clinica Medica Especializada en Reumatologia. Controls were recruited from primary care clinics. Inclusion criteria were ages 18–55 years and preceding GI, GU, or sexually transmitted infection within 3–6 months prior to enrollment. All preceding infections and antibiotic use were subject-reported. Subjects with GI infections had preceding diarrhea, and those with GU infections had dysuria, frequency, and occasionally, hematuria. Stool or urine culture at the time of infection was not available. Exclusion criteria were an alternative diagnosis of inflammatory bowel disease (IBD), psoriasis, another inflammatory arthritis or autoimmune disease, and/or active malignancy. ReA was diagnosed by a study rheumatologist and in accordance with the Assessment of SpondyloArthritis international Society criteria for peripheral SpA (16), based on the triad of characteristic musculoskeletal findings, patient-reported history of GI/GU infections, and lack of evidence for alternative diagnosis. Although we use the term ReA throughout, our patient population can be more accurately defined under the broader category of postinfectious peripheral SpA, given the absence of confirmatory cultures/serology.

Subject evaluation and sample collection. After providing informed consent, all subjects were evaluated by a rheumatologist, who took a detailed clinical history and performed a physical and musculoskeletal examination. History of uveitis was subject-reported, although 75% of cases were diagnosed by an ophthalmologist and subsequently referred to a rheumatology clinic. Blood was obtained for standard laboratory testing and HLA typing, while fecal samples were collected for microbiota analysis around the time of study enrollment. Cultures of specific bacteria were not performed. All subjects also underwent plain radiography of the sacroiliac joints and an ultrasound of the bilateral Achilles tendons. Further details are described in Supplementary Materials, available on the *Arthritis & Rheumatology* web site at <http://onlinelibrary.wiley.com/doi/10.1002/art.40359/abstract>.

DNA extraction and sequencing. Fecal samples were stored at –80°C until processing. Bacterial DNA was extracted using a MoBio Power Soil kit and bead-beater for mechanical disruption following a previously described protocol (17). To determine gut microbiota composition, high-throughput DNA sequencing of the V4 hypervariable region of bacterial 16S ribosomal RNA (rRNA) was performed using a MiSeq Illumina platform (150-bp read length, paired-end protocol) at the New York University Genome Technology Center. Further details are

described in Supplementary Materials, <http://onlinelibrary.wiley.com/doi/10.1002/art.40359/abstract>.

Sequence analysis. The 16S rRNA sequences were analyzed using a Quantitative Insights into Microbial Ecology (QIIME) pipeline, version 1.9.1 (18), and R software, version 3.3.1 (19). Reads were demultiplexed and sequences were clustered into operational taxonomic units (OTUs) using closed-reference OTU picking based on $\geq 97\%$ similarity with the Greengenes reference database (20). Each OTU count was normalized to the total sum of counts in the sample. The QIIME pipeline and the vegan library in R were used to construct alpha diversity plots to measure the diversity within a sample by looking at species richness (number of species present) and evenness (relative abundance of different species). Weighted UniFrac was used to construct beta diversity of bacterial communities to measure the distance or dissimilarity between sample pairs (21). Beta diversity is represented by principal coordinate analysis. Further details are described in Supplementary Materials, <http://onlinelibrary.wiley.com/doi/10.1002/art.40359/abstract>.

Linear discriminant analysis (LDA) effect size (LEfSe) method. Bacterial taxa whose relative abundances were significantly different between groups were identified using the LEfSe method (22). A log LDA score of >2 was the threshold for discriminating between phenotypic groups. Given that the LEfSe method does not use multiple hypothesis testing, false discovery

rate (FDR) analysis with a threshold value of <0.2 and Bonferroni analysis with a threshold value of <0.05 were subsequently applied to identify the main differentiating taxa.

Co-occurrence network analysis. OTUs with more than one count were selected and clustered at the family level. Correlations between families were calculated using SparCC (23) with 20 iterations and 500 bootstraps. Nonsignificant correlations ($P < 0.05$, 2-sided) were then discarded. The remaining correlations were loaded into Cytoscape software, version 3.0.2 (24), to be visualized as a co-occurrence network, where each node represents a bacterial family and edges between nodes represent their correlations, with shorter edges indicating stronger correlations. The network was displayed using the edge-weighted spring-embedded metrics layout, with positive correlations in blue and negative ones in gray. We then searched for maximal cliques using the Bron-Kerbosch algorithm (25) as implemented in the NetworkX Python package (26) to identify subsets of bacteria that belong to the same clique, which may reflect synergistic cooperation among the taxa.

Statistical analysis. Statistical analyses were performed with R software and GraphPad Prism software, version 7.0b (27). For baseline characteristics, a chi-square test was used for dichotomous variables and an independent *t*-test for continuous variables. A chi-square test was also used to calculate differences in prevalence of usual intestinal enteropathogens between subjects with ReA and control subjects. The Mann-Whitney U test was used to

Table 1. Clinical and laboratory characteristics of the study population*

	Subjects with ReA (n = 32)†	Controls (n = 32)	<i>P</i> ‡
Age, mean \pm SD (range) years	39 \pm 11.5 (18–55)	36 \pm 9.9 (18–54)	0.268
Sex			0.095
Male	6 (18.8)	12 (37.5)	
Female	26 (81.3)	20 (62.5)	
Race			0.050
Caucasian (Blanca)	1 (3.1)	7 (21.9)	
Native (Indígena)	15 (46.9)	9 (28.1)	
Mixed (Mestiza)	16 (50.0)	16 (50.0)	
BMI, mean \pm SD (range) kg/m ²	25.1 \pm 4.4 (19.0–34.6)	26.0 \pm 4.3 (17.6–36.1)	0.423
Disease characteristic			
Peripheral arthritis	32 (100.0)	0 (0.0)	<0.0001
Ultrasound enthesitis	14 (43.8)	2 (6.3)	0.0005
Radiographic sacroiliitis	18 (56.3)	16 (50.0)	0.616
Uveitis	20 (62.5)	2 (6.3)	<0.0001
HLA typing			
A2 positive	14 (43.8)	16 (50.0)	0.616
A24 positive	14 (43.8)	11 (34.4)	0.442
B15 positive	2 (6.3)	2 (6.3)	§
B27 positive	2 (6.3)	2 (6.3)	§
B35 positive	19 (59.4)	15 (46.9)	0.316
C7 positive	17 (53.1)	15 (46.9)	0.617
Infection			
Gastrointestinal	23 (71.9)	29 (90.6)	0.055
Genitourinary	10 (31.3)	4 (12.5)	0.070
Treatment			
Antibiotics	20 (62.5)	15 (46.9)	0.209
Sulfasalazine	3 (9.4)	0 (0)	§

* Except where indicated otherwise, values are the number (%) of subjects. BMI = body mass index.

† The diagnosis of reactive arthritis (ReA) was based on the Assessment of SpondyloArthritis international Society criteria for postinfectious peripheral spondyloarthritis; no confirmatory cultures or serology were available to establish a definite diagnosis of ReA.

‡ By chi-square test for dichotomous variables and by independent *t*-test for continuous variables.

§ Insufficient power to detect a statistically significant difference.

calculate differences in alpha diversity and relative abundance of specific taxa that were grouped by disease/HLA status when comparisons were made between 2 variables. The Kruskal-Wallis test was used when comparisons were made among 3 variables. The Adonis (Permanova) test was used to calculate differences in beta diversity. P values less than 0.05 were considered significant.

Institutional Review Board (IRB) approval. This study was approved by the IRB of the University of Pennsylvania (approval no. 819438) and by the Ethics Committee of Universidad Francisco Marroquin. Further details are described in Supplementary Materials, <http://onlinelibrary.wiley.com/doi/10.1002/art.40359/abstract>.

RESULTS

Characteristics of the study population. Demographic characteristics of the study population are shown in Table 1. A total of 64 subjects were prospectively enrolled in the study; 32 had postinfectious peripheral SpA and 32 served as controls. All subjects reported preceding GI and/or GU infections 3–6 months prior to enrollment. None reported sexually transmitted infections. Treatment of those infections with antibiotics was reported in 62.5% of subjects with ReA and 46.9% of

controls. The majority of subjects were female and racially identified as mixed (Mestiza) or native (Indigena). Very few participants carried an HLA-B27 allele.

All subjects with ReA and no control subjects had peripheral arthritis ($P < 0.0001$); subjects with ReA had an average of 5 tender joints (predominantly large joints). Ultrasound-identified Achilles tendon enthesitis was seen in 14 subjects with ReA (43.8%; compared with 6.3% of controls [$P = 0.0005$]). The average number of tender entheses was 5, with the Achilles tendon being the most common. Radiographic sacroiliitis was demonstrated in 18 subjects with ReA (56.3%; compared with 50.0% of controls [P not significant]). This was mostly grades I and II, showing sclerosis without presence of erosions. Finally, 20 subjects with ReA reported a prior diagnosis of uveitis (62.5%; compared with 6.3% of controls [$P < 0.0001$]). Additional demographic data have been described elsewhere (28).

Gut microbiota diversity in subjects with ReA and controls. A total of 64 fecal samples were obtained from subjects with ReA and controls and sequenced. There was

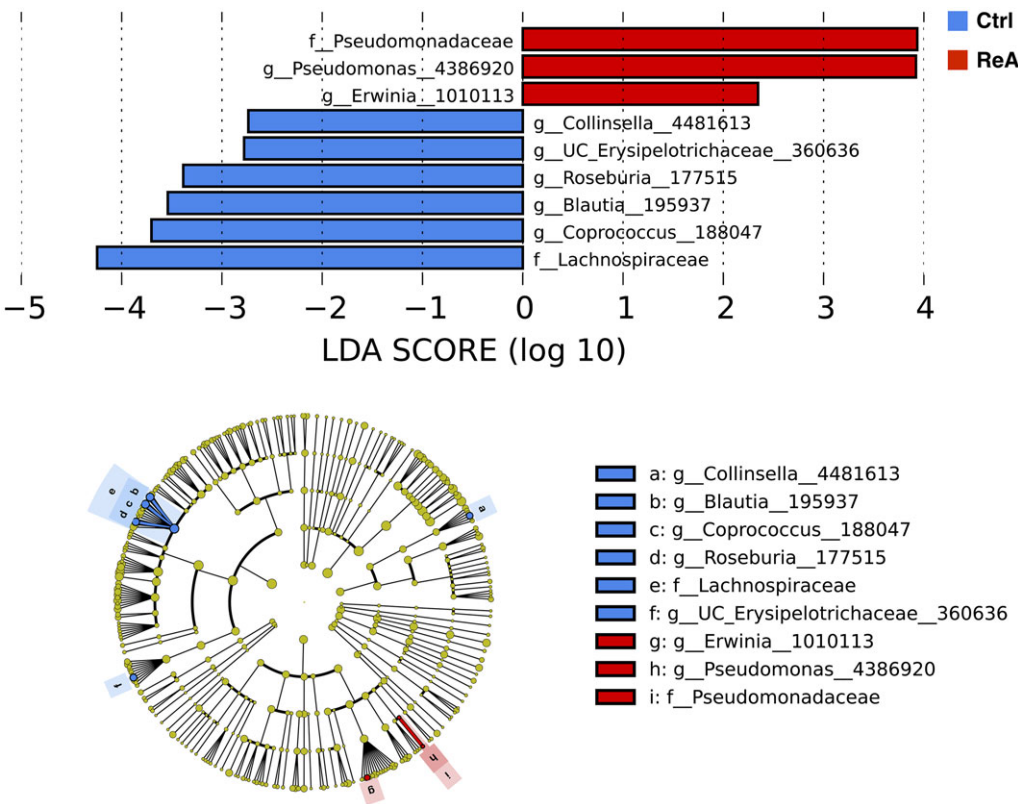


Figure 1. Linear discriminant analysis (LDA) effect size analysis of subjects with reactive arthritis (ReA) and controls (Ctrl). Top, LDA demonstrates that enteropathogens were enriched in subjects with ReA, while commensals were enriched in control subjects. Bottom, Cladogram shows the relationships among differentiating taxa between subject groups. The log LDA score was >2 for all taxa. None passed false discovery rate or Bonferroni correction thresholds. f = family; g = genus; UC = unclassified.

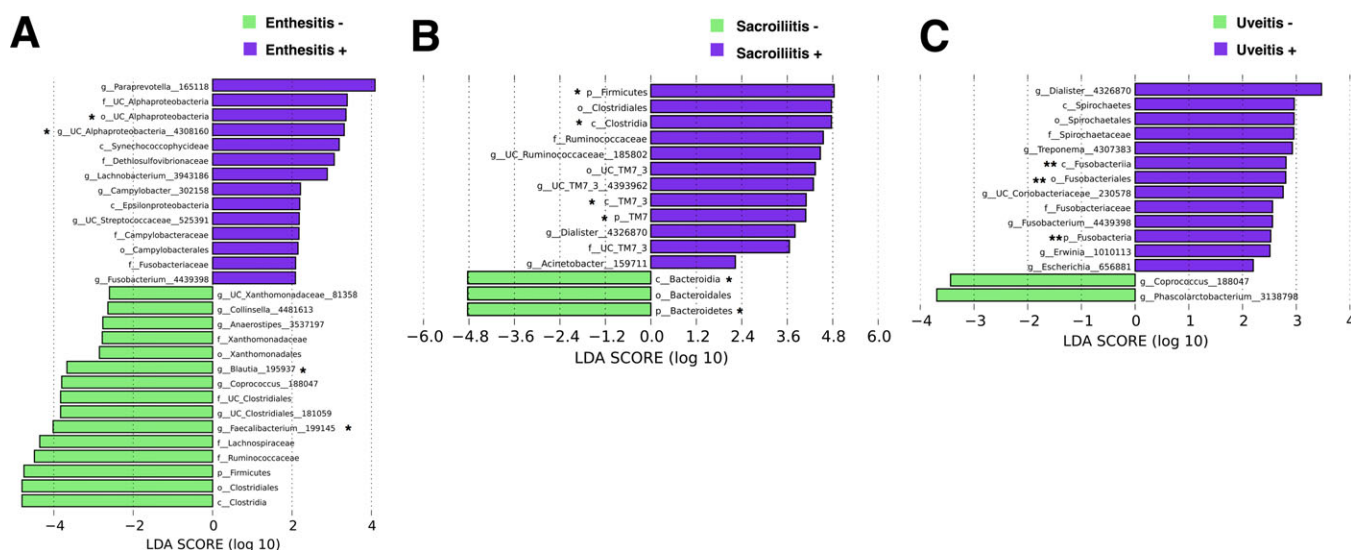


Figure 2. Linear discriminant analysis (LDA) effect size analysis for clinical and radiographic data specific to reactive arthritis. Unclassified (UC) Alphaproteobacteria (genus [g] and order [o]) were enriched in subjects with ultrasound evidence of enthesitis (A), while Clostridia (class [c]), TM7_3 (class), Firmicutes (phylum [p]), and TM7 (phylum) were enriched in subjects with radiographic sacroiliitis (B), all passing the false discovery rate (FDR) correction threshold. Fusobacteriales (order), Fusobacteria (class), and Fusobacteria (phylum) were enriched in subjects with uveitis (C), passing both FDR and Bonferroni correction thresholds. Although not achieving FDR or Bonferroni significance, *Campylobacter* was enriched in subjects with enthesitis (A), unclassified Ruminococcaceae was enriched in subjects with sacroiliitis (B), and *Erwinia* was enriched in subjects with uveitis (C). *Dialister* was independently enriched in subjects with sacroiliitis (B) and those with uveitis (C). The log LDA score was >2 for all taxa. * = passed FDR correction threshold; ** = passed FDR and Bonferroni correction thresholds. f = family.

a mean of 74,382 reads per sample after sequencing (range 46,483–122,511; median 71,233). Using a distance-based similarity of $\geq 97\%$ to define OTUs, we identified a total of 5,356 unique OTUs. There were no statistically significant differences in alpha diversity (within-subject diversity as estimated by the total number of unique OTUs, the Shannon diversity index, and Faith's Phylogenetic Diversity index) between subjects with ReA and controls (see Supplementary Figures 1A–C, <http://onlinelibrary.wiley.com/doi/10.1002/art.40359/abstract>). However, there was a trend toward overall decreased diversity in the ReA group using the Shannon index ($P = 0.069$), a finding also described in a study of psoriatic arthritis (PsA) patients (29). Evaluation of microbial similarity between subjects with ReA and controls using principal coordinate analysis based on weighted UniFrac distances showed no distinctive clustering patterns among samples (see Supplementary Figure 1D). Furthermore, there were no statistically significant differences in alpha or beta diversity when subjects were grouped by whether they had received antibiotics to treat their preceding infections (see Supplementary Figure 2A, <http://onlinelibrary.wiley.com/doi/10.1002/art.40359/abstract>). There was insufficient power to detect a difference in the case of sulfasalazine (see Supplementary Figure 2B), a frequently used medication with known antibiotic properties.

Specific intestinal taxa differentiate ReA samples and correlate with phenotypic manifestations. We applied the LefSe method to determine whether specific individual bacterial taxa were differentially enriched in subjects with ReA compared with controls (Figure 1). Subjects with ReA had a significantly higher abundance of *Erwinia* and *Pseudomonas*, 2 known intestinal enteropathogens. This finding contrasted with control individuals, in whom the relative abundance of several genera, most of them considered to be commensals, was enriched, including *Blautia*, *Coprococcus*, *Roseburia*, and *Collinsella* (log LDA score >2; none passed FDR or Bonferroni correction thresholds).

To further characterize the presence of intestinal enteropathogens typically associated with ReA, we focused our attention on sequences belonging to *Salmonella*, *Shigella*, *Campylobacter*, and *Erwinia* (a taxon that has $\geq 97\%$ identity with various species of *Salmonella*, *Shigella*, and *Yersinia* by BLAST search). Interestingly, while fewer than half of control subjects carried any of these taxa, 71.9% of subjects with disease had sequencing evidence of at least 1 such bacterium ($P = 0.042$) (see Supplementary Figure 3, <http://onlinelibrary.wiley.com/doi/10.1002/art.40359/abstract>).

Clinical and radiographic metadata showed that alpha diversity was significantly lower in subjects with

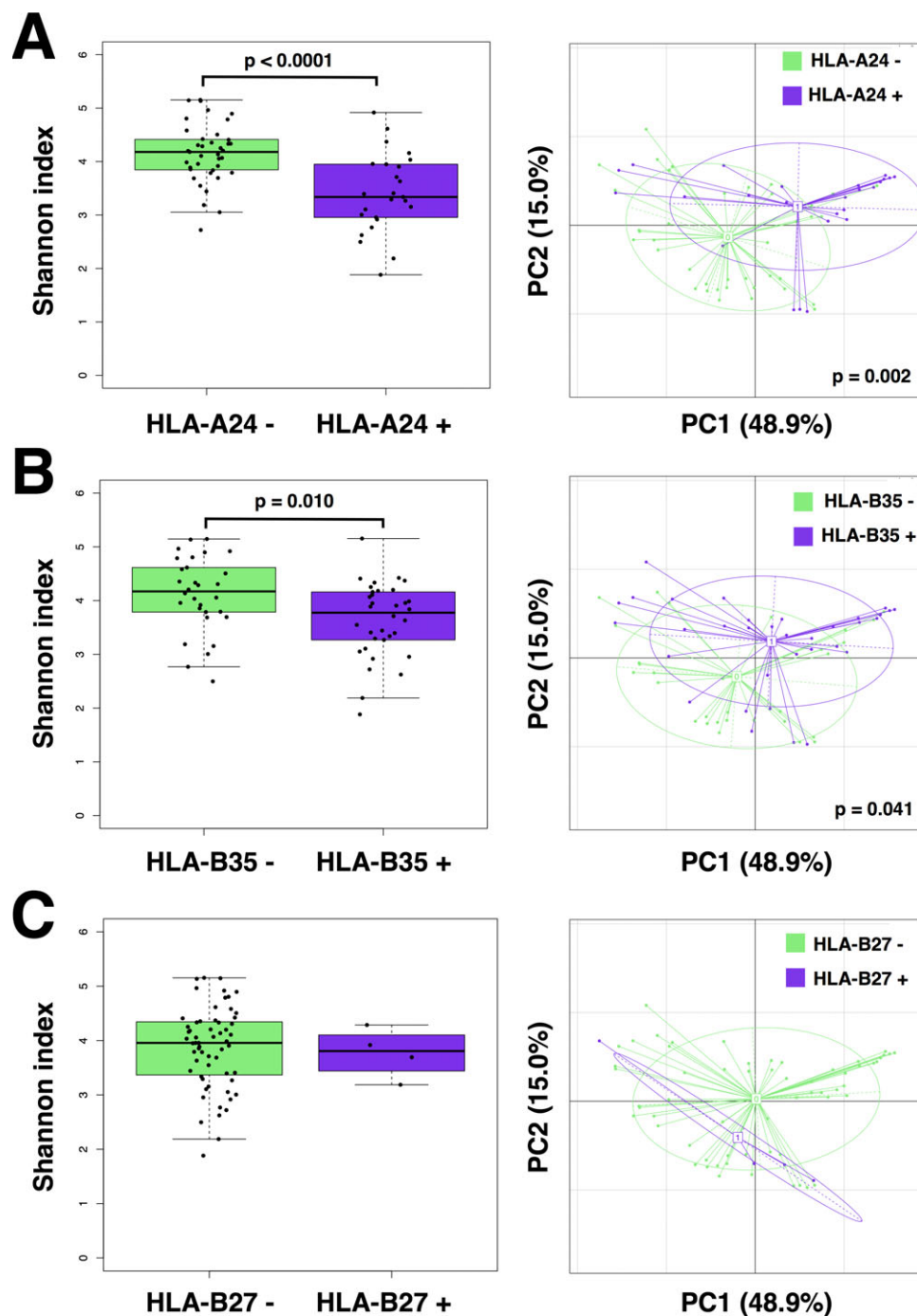


Figure 3. Alpha diversity (left) and beta diversity (right) for subjects grouped by HLA alleles. **A** and **B**, Alpha diversity was significantly lower in subjects carrying the HLA-A24 allele (**A**) and the HLA-B35 allele (**B**). Correspondingly, differences in beta diversity were also seen in subjects with HLA-A24 (**A**) and subjects with HLA-B35 (**B**). **C**, There were too few HLA-B27-positive subjects to calculate a statistical difference. Alpha diversity was determined by the Shannon diversity index. Symbols represent individual subjects. Data are shown as box plots. Each box represents the 25th to 75th percentiles. Lines inside the boxes represent the median. Lines outside the boxes (whiskers) represent the most extreme data points that do not exceed the range times the interquartile range from the box. If no points exceed that distance, then the whiskers represent the minimum and maximum values. Beta diversity, represented by principal coordinate (PC) analysis, was determined by weighted UniFrac distances. Statistical significance was calculated using the Mann-Whitney U test for alpha diversity and the Adonis (Permanova) test for beta diversity. Color figure can be viewed in the online issue, which is available at <http://onlinelibrary.wiley.com/doi/10.1002/art.40359/abstract>.

ultrasound evidence of enthesitis (see Supplementary Figure 4A, <http://onlinelibrary.wiley.com/doi/10.1002/art.40359/abstract>), and beta diversity was significantly different in subjects with radiographic evidence of sacroiliitis (see Supplementary Figure 4B). There were no diversity differences between subjects with and those without uveitis (see Supplementary Figure 4C). However, specific taxa were enriched when these manifestations were present, as shown using the LEfSe method. In particular, unclassified Alphaproteobacteria (genus and order) were enriched in subjects with enthesitis (Figure 2A), while Clostridia (class), TM7_3 (class), Firmicutes (phylum), and TM7 (phylum) were enriched in subjects with sacroiliitis (Figure 2B), all passing the FDR correction threshold. Fusobacteriales (order), Fusobacteria (class), and Fusobacteria (phylum) were enriched in subjects with uveitis, passing both FDR and Bonferroni correction thresholds (Figure 2C). Although not achieving FDR or Bonferroni significance, *Campylobacter* was overrepresented in subjects with enthesitis (Figure 2A), while unclassified Ruminococcaceae was overrepresented in subjects with sacroiliitis (Figure 2B) and *Erwinia* in subjects with uveitis (Figure 2C). Interestingly, the genus *Dialister* was independently enriched in subjects with sacroiliitis (Figure 2B) and those with uveitis (Figure 2C).

Host genes determine the intestinal microbial community composition. To investigate whether other host metadata associated with the intestinal microbiota composition, we performed correlative analyses between taxonomic communities at all hierarchical levels, patient metadata, and HLA alleles. No significant differences were observed in alpha or beta diversity when subjects were grouped by sex (see Supplementary Figure 5A, <http://onlinelibrary.wiley.com/doi/10.1002/art.40359/abstract>) or body mass index (see Supplementary Figure 5B). Although there were statistically significant differences when subjects were grouped by race (see Supplementary Figure 5C), further exploration revealed that this distinction was largely determined by HLA status.

Alpha diversity was significantly lower in those carrying the HLA-A24 allele ($P < 0.0001$) (Figure 3A), as well as in those positive for HLA-B35 ($P = 0.010$) (Figure 3B), irrespective of race and disease status. However, the presence of HLA-A2 (see Supplementary Figure 6A, <http://onlinelibrary.wiley.com/doi/10.1002/art.40359/abstract>) and HLA-C7 (see Supplementary Figure 6B) did not correlate with differences in gut microbiota diversity. Correspondingly, differences in beta diversity were also seen in subjects with HLA-A24 ($P = 0.002$) (Figure 3A) and HLA-B35 ($P = 0.041$) (Figure 3B), an effect not correlated with prior antibiotic use. Given the low prevalence of HLA-B27- and HLA-B15-positive individuals, there was

insufficient power to detect statistically significant differences in diversity for HLA-B27 (Figure 3C) or HLA-B15 (see Supplementary Figure 6C). To exclude the possibility that these changes were biased by the low number of Caucasians or by antecedent GU infections, we repeated the analysis excluding Caucasians and including only GI infections, noting similar results in both cases (see Supplementary Table 1, <http://onlinelibrary.wiley.com/doi/10.1002/art.40359/abstract>).

Interrelations of gut microbiota and metadata in ReA. To gain better insight into specific taxa driving these host-microbiome interactions, we examined the relationship between the gut community composition and HLA-A24 allele status. LEfSe analysis demonstrated a number of taxa that were distinct between the HLA-A24-positive and HLA-A24-negative groups (Figure 4). Of the genera that passed the FDR correction threshold, the relative abundance of *Prevotella* was significantly higher in subjects with an HLA-A24 allele (see Supplementary Figure 7A, <http://onlinelibrary.wiley.com/doi/10.1002/art.40359/abstract>). At the family level, Prevotellaceae was more abundant in the HLA-A24-positive group (see Supplementary Figure 7B), while Rikenellaceae and Ruminococcaceae were more abundant in the HLA-A24-negative group (see Supplementary Figures 7C and D).

To identify groups of bacteria that might be synergistically correlated with HLA-A24, we performed network analysis to determine bacteria that co-occurred with taxa identified using the LEfSe method and that were also predictive of HLA-A24 status. Representative groups (maximal cliques; see Subjects and Methods) of bacteria at the family level are shown in Figure 5. Taxa in cliques comprising Ruminococcaceae-Rikenellaceae-Coriobacteriaceae (Figure 5A) and Lachnospiraceae-Micrococcaceae-Bifidobacteriaceae (Figure 5B) were all enriched in the HLA-A24-negative cohort, and each bacterium had predictive power for HLA-A24 status. In the clique comprising Prevotellaceae-Sphingobacteriales (unclassified)-Elusimicrobiaceae (Figure 5C), only Prevotellaceae was enriched in the HLA-A24-positive cohort and had predictive power for HLA-A24 status.

DISCUSSION

In this study, we found that the prevalence of enteropathogens in subjects with ReA and postinfectious peripheral SpA was significantly increased, while several gut commensals were decreased. Intriguingly, host genetics was a major driver of microbiota richness and diversity, irrespective of disease status.

Along with IBD-related arthritis and Whipple's disease, ReA represents one of the clearest examples of

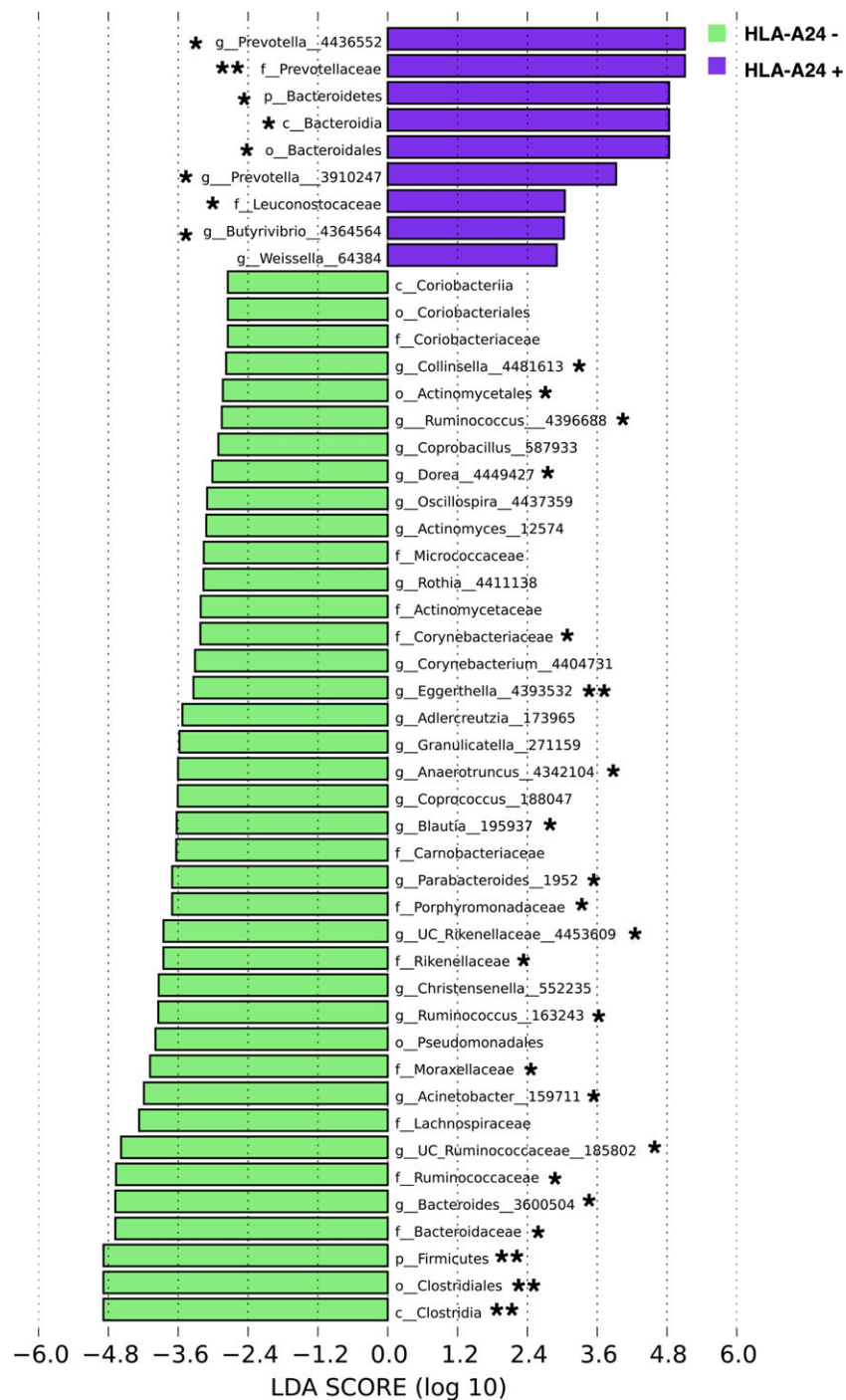


Figure 4. Linear discriminant analysis (LDA) effect size analysis of HLA-A24-positive and HLA-A24-negative subjects. LDA demonstrates that HLA-A24-negative subjects had more differentiating taxa overall compared with HLA-A24-positive subjects. A number of genera passed the false discovery rate (FDR) correction threshold. Most notably, *Prevotella* was enriched in subjects who had the HLA-A24 allele. The log LDA score was >2 for all taxa. * = passed FDR correction threshold; ** = passed FDR and Bonferroni correction thresholds. g = genus; f = family; p = phylum; c = class; o = order.

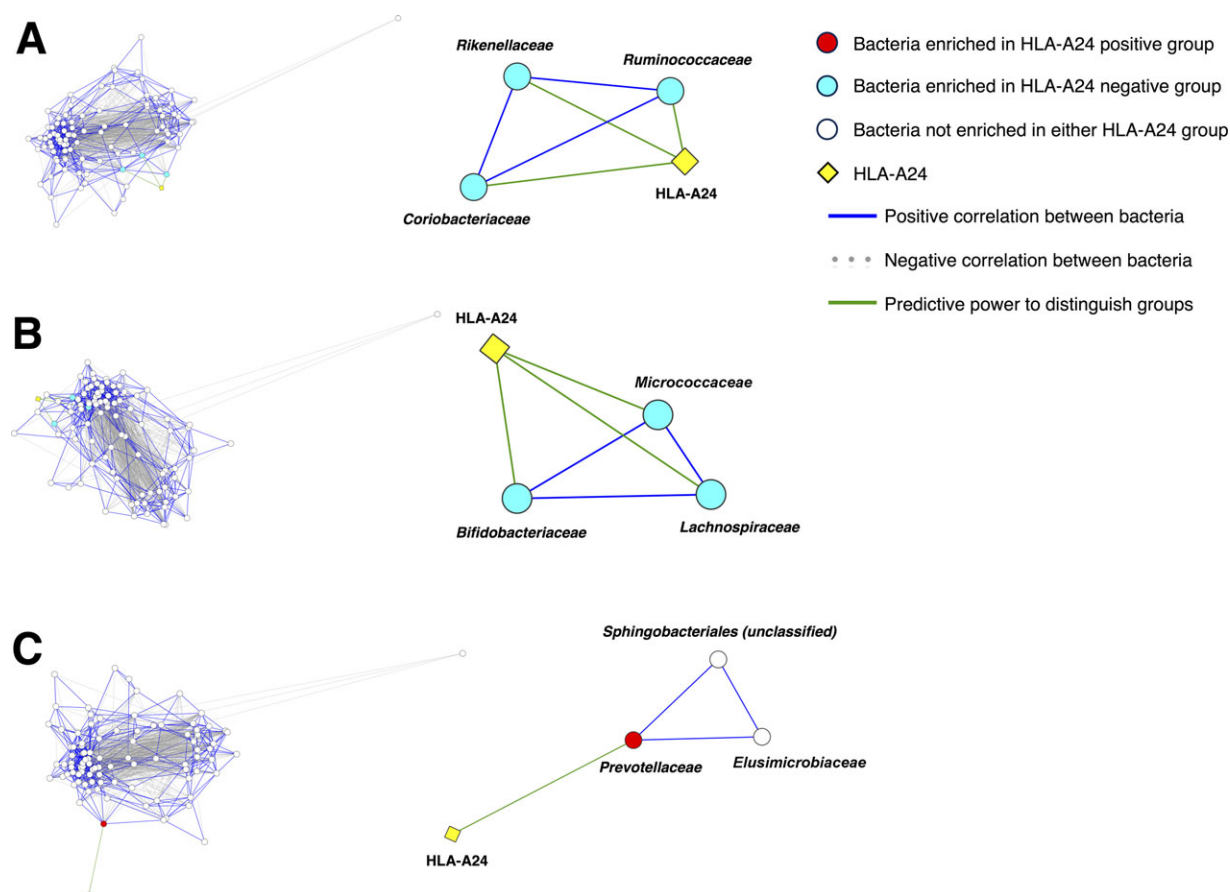


Figure 5. Co-occurrence network analysis at the family level. Left, Entire network of relationships among taxa. Right, Specific cliques of taxa in corresponding networks at left, which co-occur with one another and with at least 1 taxon in each clique having predictive power for HLA-A24 allele status. In the overall network and cliques, edge lengths are inversely proportional to the strength of the correlation or the strength of predictive power that distinguishes between HLA-A24-positive and HLA-A24-negative groups. In the case of taxa that were enriched in the HLA-A24-negative cohort, each individual taxon also had predictive power for HLA-A24 status (A and B). Only *Prevotellaceae* was enriched in the HLA-A24-positive cohort and had predictive power for HLA-A24 status (C).

the “gut-synovial” axis spectrum disorders. The pathogenesis of ReA, however, has been studied only in the context of culture-dependent microbiology methods. The overall consensus in the field is that intestinal pathogens, most notably *Yersinia*, *Salmonella*, *Shigella*, and *Campylobacter*, are triggers of systemic articular inflammation (1).

Multiple groups have linked the intestinal microbiota of animals and humans to host genetics, gut inflammatory responses, and the different clinical phenotypes of SpA (12). Two decades ago, Rath and colleagues and Taurog and colleagues determined that luminal bacteria mediated the development of arthritis and colitis in HLA-B27-transgenic rats (30,31). Since then, many studies have contributed findings corroborating this observation. Work investigating genetically susceptible animals has shown that gut dysbiosis activates a Th17-mediated immune response in the host’s intestinal lamina propria, thereby

promoting local and systemic inflammation in the form of joint disease (32,33). Clinically overt and subclinical histologic and molecular markers of gut inflammation have also been found in patients with ankylosing spondylitis (AS) (34) and in those with PsA (35). Furthermore, a recent study demonstrated that an outer membrane protein of *Salmonella typhimurium* can induce synovial fluid mononuclear cells in patients with ReA to up-regulate cytokines associated with the interleukin-23 (IL-23)/IL-17 axis (36).

This was followed by several communications describing a dysbiotic process in patients with new-onset rheumatoid arthritis (RA) (37), animal models of SpA (38,39), and cohorts of patients with SpA, including AS (40,41) and PsA (29). A summary of these findings in humans and animal models can be found in a recent review by our group (42). Consistent with these data, our

research demonstrates that subjects with ReA were characterized as having a decreased abundance of commensals in their gut microbiota compared with controls, which were enriched in the family Lachnospiraceae with associated genera—*Blautia*, *Coprococcus*, *Roseburia*, and *Collinella*. Interestingly, there was a concomitant increase in the prevalence of enteropathogens in the ReA group, particularly *Pseudomonas* and *Erwinia*, a taxon that has $\geq 97\%$ identity with the usual ReA-associated gut bacteria.

To our knowledge, this is the first culture-independent, high-throughput DNA sequencing study characterizing the overall gut community composition in postinfectious peripheral SpA. Prior efforts were directed toward only a handful of culturable organisms (1), and investigators did not report on the presence or abundance of intestinal commensals. Our findings suggest that even when the overall bacterial composition is not significantly different from that in controls, a decrease in several potentially protective bacteria could prime genetically susceptible individuals with GI or GU infections to develop ReA. This contrasts with subjects who eventually contain the immune response to the lamina propria due to the prevalence of commensals. Intriguingly, 2 of the underrepresented commensal taxa in ReA—Lachnospiraceae and *Coprococcus*—were also decreased in patients with new-onset PsA (29). Similarly, we found a positive correlation between the presence of the genus *Dialister* and the development of both uveitis and sacroiliitis. This same genus has recently been reported as a marker of disease activity in AS (41). Since ReA, AS, and PsA all belong to the SpA spectrum of diseases, it is plausible that a perturbation in the intestinal microbiota constitutes yet another common environmental risk factor among patients with these disorders. It remains to be elucidated whether the perturbations are a cause or a consequence of SpA-related inflammation.

Although the relative abundance of the usual enteropathogens associated with postinfectious peripheral SpA was expectedly low ($<1\%$ abundance for each microorganism), there was a significantly higher prevalence of such taxa in subjects with ReA compared with controls, as seen in other autoimmune conditions such as IBD (43) and further validating prior culture-dependent observations. Interestingly, the majority of ReA cases were reported in the months of April through July (28). This seasonal effect could be a determinant of disease development as it may correlate with differences in the types of pathogens that are present.

Perhaps even more remarkable is the observation that certain HLA alleles seemed to determine microbiota composition in both health and disease. These effects were independent of either disease status or prior antibiotic use. A similar finding was reported in an RA-like murine model,

where HLA-transgenic mice carrying the DRB1*0401 gene were more susceptible to collagen-induced arthritis. These mice showed gut microbiome dysbiosis and enrichment with *Clostridium*-like bacteria (44). In our study, there were significant differences in intestinal community diversity and species composition associated with HLA-A24 and, to a lesser degree, with HLA-B35. Such differences, however, were not seen with the HLA-B27 allele, which was present in only a minority of subjects. This was not surprising since prior work indicates that only 4% of Guatemalan patients with SpA are HLA-B27 positive (10). On the other hand, the frequency of the HLA-A24 allele in American Indian populations is quite elevated and estimated to be $>20\%$ (45). The presence of this allele has also been associated with a number of autoimmune diseases in non-Caucasians, including type 1 diabetes mellitus in Japan (46) and RA in a Moroccan cohort (47). Most relevant to the present study, HLA-A*2402 also correlated with AS in a Basque cohort, independently of HLA-B27 status (48). Multiple lines of evidence therefore suggest that microbial–host gene interactions conferring susceptibility to autoimmune disease can vary significantly among ethnic populations, particularly with respect to HLA alleles.

When we surveyed the microbiota composition, *Prevotella* (genus) and Prevotellaceae (family) were more abundant in subjects who were HLA-A24 positive. *Prevotella* has been implicated in the pathogenesis of RA. In particular, *Prevotella copri* correlated with disease in patients with new-onset RA, while the relative abundance of *P. copri* was lower in subjects who had the DRB1 shared epitope RA risk alleles (37). This suggests that a certain threshold for *P. copri* abundance may be necessary to overcome the lack of genetic predisposition in the case of subjects with RA. In the case of ReA, it is possible that the co-occurrence of *Prevotella* with HLA-A24 is necessary but insufficient as a triggering factor for postinfectious arthritis unless there is a concomitant reduction in beneficial, gut-protective commensals.

Interestingly, Ruminococcaceae and Rikenellaceae were more abundant in HLA-A24-negative subjects. Furthermore, Ruminococcaceae and Rikenellaceae occurred with one another, and each had predictive power for HLA-A24 status. Studies of HLA-B27-transgenic rats that exhibit many features of SpA also revealed a higher abundance of *Prevotella* and a lower abundance of Rikenellaceae (38). Moreover, terminal ileum biopsy samples from subjects with AS had a higher abundance of Ruminococcaceae and Rikenellaceae and a lower abundance of Prevotellaceae (40). Although these data could represent a true correlation with disease status, analysis with co-occurrence and host genetics was not performed since all participants with AS were HLA-B27 positive.

Taken together, our findings further support the possibility that host genetics can prime gut microbiome features to trigger autoimmunity in susceptible individuals. We propose that, moving forward, the characterization of these gene–microbiome interactions should be an integral part of any correlative human studies to avoid potential confounders that could implicate taxa in disease processes.

We acknowledge several limitations of our study. First, there was a relatively small number of participants and geographic/ethnic homogeneity, rendering the results less generalizable to other populations. However, this could also represent a strength, since this is a cohort that has not been previously evaluated, offering a new outlook on ReA pathogenesis, especially with respect to host genetics. Second, our study did not incorporate microbiota of controls without preceding GI or GU infections. Although we are not aware of any studies that have characterized the bacterial communities of the healthy native and mixed populations in Guatemala, a recent study of uncontacted American Indians in Venezuela showed a high abundance of *Prevotella* and low abundance of *Bacteroides* (49).

Another limitation relates to the lack of a timely and culture-proven diagnosis of preceding infections, which is a widely acknowledged challenge in ReA research and in most cases of ReA diagnosed in the clinical setting (50). In fact, stool cultures can occasionally confirm a preceding or concomitant infection with a classic ReA pathogen, but by the time subjects develop arthritis, their symptoms have usually resolved and the pathogens are no longer retrievable. Furthermore, serologic tests are nonspecific and are only able to demonstrate prior immunity rather than causality. For these reasons, we relied on a subject-reported history of antecedent infection, but we acknowledge that some of the infections could have been viral or secondary to other etiologies (i.e., postinfectious peripheral SpA being a more precise definition of our patient population). We also detected enteropathogens in the ReA cohort of our study, which only implies persistence of an organism's DNA, as 16S rRNA gene sequencing studies do not allow for viability determination. However, this may be of relevance since the pathogenesis of ReA is yet unknown, and some hypotheses suggest that microbial components may drive the downstream inflammatory response (12).

Uveitis was another self-reported variable, and it is possible that some of the cases were actually conjunctivitis or other related conditions. Nevertheless, 75% of the subjects were seen by an ophthalmologist, deemed to have uveitis, and subsequently referred to a rheumatology clinic, so misdiagnosis is less likely. We also note that the incidence of sacroiliitis was unexpectedly high in both the arthritis and control groups. Because most of these cases

were adjudicated as grade I sacroiliitis, it is possible that this could represent overreporting, which is also quite common in clinical practice. Unfortunately, we could not pursue further blinding or centralized readings for confirmatory purposes, and therefore, these findings should be interpreted with caution.

The use of antibiotics for the treatment of infections prior to sample collection may have also had a dysbiotic effect on the gut microbiome. However, our results were independent of antibiotic use. In the future, baseline and postarthritis characterization of microbial communities in at-risk populations may help us to discern these perturbations in a prospective manner. Complementary studies using metagenomics and metabolomics platforms will also be needed to better understand the role of gut bacterial enzymes and their byproducts in ReA pathogenesis.

In summary, the findings of this study further enhance our understanding of ReA and postinfectious peripheral SpA in a non–HLA–B27–dominated population. Using a high-throughput DNA sequencing approach, we identified several organisms that are differentially present in samples from subjects with ReA compared with those from controls. These taxa and the lack of specific commensals, as well as the associated changes in immune response, will require further research and validation in other cohorts. The effect of host genetics on shaping the human microbiome in health and disease is also intriguing and could shed light on our understanding of the symbiotic relationship between host and community diversity and composition. Furthermore, it is plausible that the combination of exposure to known pathogens, host genetics, and the makeup of commensal microorganisms could confer susceptibility to the development of ReA, postinfectious peripheral SpA, and other variants of the SpA spectrum disorders. Future mechanistic research coupled with well-designed prospective human cohorts is needed to close these knowledge gaps in the field.

ACKNOWLEDGMENTS

We would like to thank Parvathy Girija (New York University School of Medicine) for extracting DNA from fecal samples and preparing it for sequencing analysis. We would also like to thank Benjamin Wu (New York University School of Medicine) for his advice and assistance during the data analysis phase of this project.

AUTHOR CONTRIBUTIONS

All authors were involved in drafting the article or revising it critically for important intellectual content, and all authors approved the final version to be published. Dr. Scher had full access to all of

the data in the study and takes responsibility for the integrity of the data and the accuracy of the data analysis.

Study conception and design. Garcia Ferrer, Iraheta, Von Feldt, Espinoza, Garcia Kutzbach, Ogdie, Scher.

Acquisition of data. Garcia Ferrer, Garcia Kutzbach, Ogdie, Scher.

Analysis and interpretation of data. Manasson, Shen, Ubeda, Heguy, Segal, Clemente, Scher.

REFERENCES

- Hannu T. Reactive arthritis. *Best Pract Res Clin Rheumatol* 2011;25:347–57.
- Schiellerup P, Krogfelt KA, Locht H. A comparison of self-reported joint symptoms following infection with different enteric pathogens: effect of HLA-B27. *J Rheumatol* 2008;35:480–7.
- Putterman C, Rubinow A. Reactive arthritis associated with *Clostridium difficile* pseudomembranous colitis. *Semin Arthritis Rheum* 1993;22:420–6.
- Brewerton DA, Caffrey M, Nicholls A, Walters D, Oates JK, James DC. Reiter's disease and HL-A 27. *Lancet* 1973;302:996–8.
- Khan MA. HLA-B27 and its subtypes in world populations. *Curr Opin Rheumatol* 1995;7:263–9.
- Sieper J, Rudwaleit M, Braun J, van der Heijde D. Diagnosing reactive arthritis: role of clinical setting in the value of serologic and microbiologic assays. *Arthritis Rheum* 2002;46:319–27.
- Carter JD, Hudson AP. Reactive arthritis: clinical aspects and medical management. *Rheum Dis Clin North Am* 2009;35:21–44.
- Townes JM, Deodhar AA, Laine ES, Smith K, Krug HE, Barkhuizen A, et al. Reactive arthritis following culture-confirmed infections with bacterial enteric pathogens in Minnesota and Oregon: a population-based study. *Ann Rheum Dis* 2008;67:1689–96.
- Solitar BM, Lozada CJ, Tseng CE, Lowe AM, Krajewski WM, Blanchard K, et al. Reiter's syndrome among Asian shipboard immigrants: the case of The Golden Venture. *Semin Arthritis Rheum* 1998;27:293–300.
- Garcia-Kutzbach A, Montenegro A, Iraheta I, Bara C, Saenz R. Epidemiology of spondyloarthropathies in Central America. *Am J Med Sci* 2011;341:295–7.
- Tsui FW, Xi N, Rohekar S, Riarh R, Bilotta R, Tsui HW, et al. Toll-like receptor 2 variants are associated with acute reactive arthritis. *Arthritis Rheum* 2008;58:3436–8.
- Manasson J, Scher JU. Spondyloarthritis and the microbiome: new insights from an ancient hypothesis. *Curr Rheumatol Rep* 2015;17:10.
- Siala M, Gdoura R, Fourati H, Rihl M, Jaulhac B, Younes M, et al. Broad-range PCR, cloning and sequencing of the full 16S rRNA gene for detection of bacterial DNA in synovial fluid samples of Tunisian patients with reactive and undifferentiated arthritis. *Arthritis Res Ther* 2009;11:R102.
- Granfors K, Jalkanen S, Lindberg AA, Mäki-Ikola O, von Essen R, Lahesmaa-Rantala R, et al. Salmonella lipopolysaccharide in synovial cells from patients with reactive arthritis. *Lancet* 1990;335:685–8.
- Paniagua-Avila MA, Messenger E, Nelson CA, Calgua E, Barg FK, Bream KW, et al. The Guatemala-Penn Partners: an innovative inter-institutional model for scientific capacity-building, healthcare education, and public health. *Front Public Health* 2017;5:70.
- Rudwaleit M, van der Heijde D, Landewé R, Akkoc N, Brandt J, Chou CT, et al. The Assessment of SpondyloArthritis international Society classification criteria for peripheral spondyloarthritis and for spondyloarthritis in general. *Ann Rheum Dis* 2011;70:25–31.
- Scher JU, Joshua V, Artacho A, Abdollahi-Roodsaz S, Ockinger J, Kullberg S, et al. The lung microbiota in early rheumatoid arthritis and autoimmunity. *Microbiome* 2016;4:60.
- Caporaso JG, Kuczynski J, Stombaugh J, Bittinger K, Bushman FD, Costello EK, et al. QIIME allows analysis of high-throughput community sequencing data. *Nat Methods* 2010;7:335–6.
- Team RC. R: a language and environment for statistical computing. Vienna: R Foundation for Statistical Computing; 2016.
- McDonald D, Price MN, Goodrich J, Nawrocki EP, DeSantis TZ, Probst A, et al. An improved Greengenes taxonomy with explicit ranks for ecological and evolutionary analyses of bacteria and archaea. *ISME J* 2012;6:610–8.
- Lozupone C, Knight R. UniFrac: a new phylogenetic method for comparing microbial communities. *Appl Environ Microbiol* 2005;71:8228–35.
- Segata N, Izard J, Waldron L, Gevers D, Miropolsky L, Garrett WS, et al. Metagenomic biomarker discovery and explanation. *Genome Biol* 2011;12:R60.
- Friedman J, Alm EJ. Inferring correlation networks from genomic survey data. *PLoS Comput Biol* 2012;8:e1002687.
- Shannon P, Markiel A, Ozier O, Baliga NS, Wang JT, Ramage D, et al. Cytoscape: a software environment for integrated models of biomolecular interaction networks. *Genome Res* 2003;13:2498–504.
- Bron C, Kerbosch J. Finding all cliques of an undirected graph [H]. *Commun ACM* 1973;16:575–7.
- Hagberg A, Schult D, Swart P. Exploring network structure, dynamics, and function using NetworkX. In: Varoquaux G, Vaught T, Millman J, editors. 7th Python in Science conference (SciPy 2008). Pasadena (CA): 2008; pp. 11–5.
- GraphPad Prism. 7.0a for Mac ed. San Diego (CA): GraphPad Software.
- Garcia Ferrer HR, Azan A, Iraheta I, Von Feldt J, Espinoza LR, Manasson J, et al. Potential risk factors for reactive arthritis and persistence of symptoms at 2 years: a case-control study with longitudinal follow-up. *Clin Rheumatol* 2017. E-pub ahead of print.
- Scher JU, Ubeda C, Artacho A, Attur M, Isaac S, Reddy SM, et al. Decreased bacterial diversity characterizes the altered gut microbiota in patients with psoriatic arthritis, resembling dysbiosis in inflammatory bowel disease. *Arthritis Rheumatol* 2015;67:128–39.
- Rath HC, Herfarth HH, Ikeda JS, Grenther WB, Hamm TE Jr, Balish E, et al. Normal luminal bacteria, especially *Bacteroides* species, mediate chronic colitis, gastritis, and arthritis in HLA-B27/human β 2 microglobulin transgenic rats. *J Clin Invest* 1996;98:945–53.
- Taurog JD, Richardson JA, Croft JT, Simmons WA, Zhou M, Fernandez-Sueiro JL, et al. The germfree state prevents development of gut and joint inflammatory disease in HLA-B27 transgenic rats. *J Exp Med* 1994;180:2359–64.
- Wu HJ, Ivanov II, Darce J, Hattori K, Shima T, Umesaki Y, et al. Gut-residing segmented filamentous bacteria drive autoimmune arthritis via T helper 17 cells. *Immunity* 2010;32:815–27.
- Abdollahi-Roodsaz S, Joosten LA, Koenders MI, Devesa I, Roelofs MF, Radstake TR, et al. Stimulation of TLR2 and TLR4 differentially skews the balance of T cells in a mouse model of arthritis. *J Clin Invest* 2008;118:205–16.
- Mielants H, Veys EM, Cuvelier C, de Vos M, Goemaere S, de Clercq L, et al. The evolution of spondyloarthropathies in relation to gut histology. Part II. Histological aspects. *J Rheumatol* 1995;22:2273–8.
- Ciccia F, Guggino G, Ferrante A, Raimondo S, Bignone R, Rodolico V, et al. Interleukin-9 overexpression and Th9 polarization characterize the inflamed gut, the synovial tissue, and the peripheral blood of patients with psoriatic arthritis. *Arthritis Rheumatol* 2016;68:1922–31.
- Chaurasia S, Shasany AK, Aggarwal A, Misra R. Recombinant *Salmonella typhimurium* outer membrane protein A is recognized by synovial fluid CD8 cells and stimulates synovial fluid mononuclear cells to produce interleukin (IL)-17/IL-23 in patients with reactive arthritis and undifferentiated spondyloarthritis. *Clin Exp Immunol* 2016;185:210–8.

37. Scher JU, Szczesnak A, Longman RS, Segata N, Ubeda C, Bielski C, et al. Expansion of intestinal *Prevotella copri* correlates with enhanced susceptibility to arthritis. *Elife* 2013;2:e01202.
38. Lin P, Bach M, Asquith M, Lee AY, Akileswaran L, Stauffer P, et al. HLA-B27 and human β 2-microglobulin affect the gut microbiota of transgenic rats. *PLoS One* 2014;9:e105684.
39. Asquith MJ, Stauffer P, Davin S, Mitchell C, Lin P, Rosenbaum JT. Perturbed mucosal immunity and dysbiosis accompany clinical disease in a rat model of spondyloarthritis. *Arthritis Rheumatol* 2016;68:2151–62.
40. Costello ME, Ciccio F, Willner D, Warrington N, Robinson PC, Gardiner B, et al. Intestinal dysbiosis in ankylosing spondylitis. *Arthritis Rheumatol* 2015;67:686–91.
41. Tito RY, Cypers H, Joossens M, Varkas G, van Praet L, Glorieux E, et al. *Dialister* as a microbial marker of disease activity in spondyloarthritis. *Arthritis Rheumatol* 2017;69:114–21.
42. Scher JU, Littman DR, Abramson SB. Microbiome in inflammatory arthritis and human rheumatic diseases. *Arthritis Rheumatol* 2016;68:35–45.
43. Martinez-Medina M, Garcia-Gil LJ. *Escherichia coli* in chronic inflammatory bowel diseases: an update on adherent invasive *Escherichia coli* pathogenicity. *World J Gastrointest Pathophysiol* 2014;5:213–27.
44. Gomez A, Luckey D, Yeoman CJ, Marietta EV, Berg Miller ME, Murray JA, et al. Loss of sex and age driven differences in the gut microbiome characterize arthritis-susceptible 0401 mice but not arthritis-resistant 0402 mice. *PLoS One* 2012;7:e36095.
45. Gonzalez-Galarza FF, Takeshita LY, Santos EJ, Kempson F, Maia MH, Da Silva AL, et al. Allele frequency net 2015 update: new features for HLA epitopes, KIR and disease and HLA adverse drug reaction associations. *Nucleic Acids Res* 2015;43(Database issue):D784–8.
46. Nakanishi K, Inoko H. Combination of HLA-A24, -DQA1*03, and -DR9 contributes to acute-onset and early complete β -cell destruction in type 1 diabetes: longitudinal study of residual β -cell function. *Diabetes* 2006;55:1862–8.
47. Atouf O, Benbouazza K, Brick C, Bzami F, Bennani N, Amine B, et al. HLA polymorphism and early rheumatoid arthritis in the Moroccan population. *Joint Bone Spine* 2008;75:554–8.
48. De Juan MD, Reta A, Belzunegui J, Figueroa M, Maruri N, Cuadrado E. HLA-A*2402 and a microsatellite (D6S248) are secondary independent susceptibility markers to ankylosing spondylitis in Basque patients. *Hum Immunol* 2004;65:175–80.
49. Clemente JC, Pehrsson EC, Blaser MJ, Sandhu K, Gao Z, Wang B, et al. The microbiome of uncontacted Amerindians. *Sci Adv* 2015;1:e1500183.
50. Hannu T, Inman R, Granfors K, Leirisalo-Repo M. Reactive arthritis or post-infectious arthritis? *Best Pract Res Clin Rheumatol* 2006;20:419–33.

Genetic Variants in *ERAP1* and *ERAP2* Associated With Immune-Mediated Diseases Influence Protein Expression and the Isoform Profile

Aimee L. Hanson,¹ Thomas Cuddihy,¹ Katelin Haynes,¹ Dorothy Loo,¹ Craig J. Morton,² Udo Oppermann,³ Paul Leo,⁴ Gethin P. Thomas,⁵ Kim-Anh Lê Cao,¹ Tony J. Kenna,⁴ and Matthew A. Brown⁴

Objective. Endoplasmic reticulum aminopeptidase 1 (ERAP-1) and ERAP-2, encoded on chromosome 5q15, trim endogenous peptides for HLA-mediated presentation to the immune system. Polymorphisms in *ERAP1* and/or *ERAP2* are strongly associated with several immune-mediated diseases with specific HLA backgrounds, implicating altered peptide handling and presentation as prerequisites for autoreactivity against an arthritogenic peptide. Given the thorough characterization of disease risk-associated polymorphisms that alter ERAP activity, this study aimed instead to interrogate the expression effect of chromosome 5q15 polymorphisms to determine their effect on ERAP isoform and protein expression.

Methods. RNA sequencing and genotyping across chromosome 5q15 were performed to detect genetic variants in *ERAP1* and *ERAP2* associated with altered total gene and isoform-specific expression. The functional implication of a putative messenger RNA

splice-altering variant on ERAP-1 protein levels was validated using mass spectrometry.

Results. Polymorphisms associated with ankylosing spondylitis (AS) significantly influenced the transcript and protein expression of ERAP-1 and ERAP-2. Disease risk-associated polymorphisms in and around both genes were also associated with increased gene expression. Furthermore, key risk-associated *ERAP1* variants were associated with altered transcript splicing, leading to allele-dependent alternate expression of 2 distinct isoforms and significant differences in the type of ERAP-1 protein produced.

Conclusion. In accordance with studies demonstrating that polymorphisms that increase aminopeptidase activity predispose to immune disease, the increased risk also attributed to increased expression of *ERAP1* and *ERAP2* supports the notion of using aminopeptidase inhibition to treat AS and other ERAP-associated conditions.

Supported by the Queensland Government Premier's Fellowship for Science and the NHMRC (Senior Principal Research Fellowship grant APP1024879 to Dr. Brown). Dr. Oppermann's work was supported by Arthritis Research UK (grant 20522).

¹Aimee L. Hanson, BSc (Hons), Thomas Cuddihy, MSc, Katelin Haynes, PhD, Dorothy Loo, MSc, Kim-Anh Lê Cao, PhD: University of Queensland, Princess Alexandra Hospital, Brisbane, Queensland, Australia; ²Craig J. Morton, PhD: St. Vincent's Institute of Medical Research, Fitzroy, Victoria, Australia; ³Udo Oppermann, PhD: University of Oxford, Oxford, UK; ⁴Paul Leo, PhD, Tony J. Kenna, PhD, Matthew A. Brown, MBBS, MD, FRACP, FAHMS, FAA: Queensland University of Technology and Princess Alexandra Hospital, Brisbane, Queensland, Australia; ⁵Gethin P. Thomas, PhD: University of Queensland, Princess Alexandra Hospital, Brisbane, Queensland, Australia, and Charles Sturt University, Wagga Wagga, New South Wales, Australia.

Drs. Kenna and Brown contributed equally to this work.

Address correspondence to Matthew A. Brown, MBBS, MD, Queensland University of Technology, Translational Research Institute, 37 Kent Street, Woolloongabba, Queensland 4102, Australia. E-mail: matt.brown@qut.edu.au.

Submitted for publication April 28, 2017; accepted in revised form October 26, 2017.

HLA-mediated presentation of endogenous peptides to CD8⁺ T cells educates the immune system to differentiate between self-derived and foreign antigens. Consequently, aberrations in peptide presentation pathways may evoke misinformed immune cell reactivity against host tissue, leading to pathology. Aminopeptidases function in the processing of peptide precursors to generate molecules of optimal length and composition for HLA loading. Disease risk-associated polymorphisms in the endoplasmic reticulum aminopeptidase genes *ERAP1* and/or *ERAP2* are seen in several immune-mediated diseases, including ankylosing spondylitis (AS) (1,2), psoriasis (3), Crohn's disease (4), and Behçet's disease (5).

Robust genetic interactions exist between *ERAP1* and the HLA class I alleles HLA-B27 and HLA-B40 in AS (1,6), HLA-Cw6 in psoriasis (3), and HLA-B51 in Behçet's disease (5). Synergism between HLA class I loci

and *ERAP1* is most pronounced in AS, with risk-associated polymorphisms in the gene contributing to strong disease risk (lead single-nucleotide polymorphism [SNP] rs30187; $P = 4.4 \times 10^{-45}$, odds ratio [OR] 1.29) (7) in HLA-B27 carriers alone (1). Although 80–95% of AS patients carry the major genetic risk factor HLA-B27, this allele contributes only ~20% of the genetic risk for the disease, and >113 additional genetic loci have confirmed disease associations (1,2,7–10). Evidence points to the involvement of altered peptide handling in disease pathogenesis (11–13), potentially driving production of an immunogenic HLA-B27-specific peptide repertoire that misinforms the immune response and/or impedes the folding, stability, and function of HLA-B27.

In AS, the *ERAP1* locus contains 2 independent association signals (1). The stronger is tagged by SNP rs30187 (K528R; OR 1.29, $P = 4.4 \times 10^{-45}$) (7), the protective allele at which a ~40% decrease in enzymatic activity is conferred (1). Conversely, the rs30187 risk allele alters the HLA-B27-bound peptidome by causing both elevated production and destruction of different HLA-B27 epitopes (11,14–16). The second association signal is tagged by rs10050860 (D575N; $P = 9.28 \times 10^{-36}$). This SNP has previously been shown not to be functional in both recombinant protein and cellular assays (1,17), and the functional mechanism driving disease association at this signal has not been determined. In vitro studies have demonstrated that protective *ERAP1* variants, as well as *ERAP1* silencing or inhibition, reduce surface expression of HLA-B27 free heavy chains (18), although this finding has not been universal (19). HLA-B27 free heavy chain expression on the cell surface has been shown to induce the expansion of Th17 cells and secretion of the proinflammatory cytokine interleukin-17A (20).

Homozygous deletion of *ERAP1* in the HLA-B27-transgenic rat model of AS does not alter levels of folded HLA-B27 or HLA-B27 heavy-chain dimers on the surface of peripheral blood mononuclear cells (PBMCs) and does not prevent the development of spondyloarthritis (SpA) in these rats (21). The relevance of this in human SpA is, however, unclear. Rats lack ERAP-2, which in humans is thought to interact with ERAP-1 to influence peptide presentation. Because the transgenic rats involved have at least 20 copies of the HLA-B27 transgene per cell, as opposed to 1 or 2 copies in human HLA-B27-positive AS, they may develop SpA as a result of a pathogenic process different from that in human disease. Evidence suggests that disease-associated polymorphisms in *ERAP1* also exert an expression effect (12), with the risk genotype being correlated with increased gene expression (22).

At *ERAP2*, the AS-associated nonsense mutation rs2248374 is an expression quantitative trait locus (eQTL)

at which the protective G allele results in complete loss of gene expression due to nonsense-mediated decay of an alternatively spliced transcript (23). The presence of ERAP-2 influences the HLA-B27 peptide pool, decreasing the abundance of peptides with N-terminal basic residues and increasing the percentage of 9-mer peptides presented (24), lowering the affinity of the HLA-B27 peptidome (16–25). Given the intricate role of both aminopeptidases in shaping the HLA-B27 peptidome, it is possible that variants increasing aminopeptidase expression may act concordantly to increase AS risk in individuals carrying disease-associated active variants of *ERAP1* and *ERAP2*.

In the current study, we used RNA-Seq to identify *ERAP1* and *ERAP2* polymorphisms associated with varied gene and isoform expression in patients with AS and healthy controls. RNA-Seq allows interrogation of the transcriptional landscape of a gene, enabling identification of splice-altering variants (splicing QTLs [sQTLs]) that may drive the production of distinct isoforms with phenotypic consequences. Despite extensive characterization of alternate *ERAP2* transcripts that radically transform the global expression of this gene (23), alternate isoforms of *ERAP1* have been infrequently studied in the broader literature. We demonstrate that AS risk-associated single-nucleotide polymorphisms (SNPs) in *ERAP1* and *ERAP2* are associated with substantial eQTL effects at both the transcript and protein levels and show that risk-associated variants in *ERAP1* are associated with altered splicing of the encoded gene transcript. This indicates that the disease-associated SNPs in *ERAP1* and *ERAP2* influence disease risk through effects on transcription and splice variation in addition to the functional effects of coding variants in *ERAP1*.

PATIENTS AND METHODS

Human research ethics. Human ethics approval was granted by Princess Alexandra Hospital and University of Queensland Ethics Committees (approval nos. Metro South HREC/05/QPAH/221 and UQ 2006000102). Written informed consent was received from all participants prior to inclusion in the study.

Sample selection. Fifty-four patients with AS diagnosed according to the modified New York criteria (26) and 70 healthy controls were included in this study. Peripheral venous blood was collected from AS patients at the Princess Alexandra Hospital Ankylosing Spondylitis Clinic, and PBMCs from patients and controls were collected as described previously (7).

Genotyping, imputation, and disease association analysis. Genotyping was conducted during the 2013 ImmunoChip study of 9,049 AS patients and 13,607 healthy control subjects (7). *P* values for SNP disease associations upon conditioning with rs30187 were derived using logistic regression on the complete ImmunoChip data set in Plink (<http://pngu.mgh.harvard>).

edu/purcell/plink/ (27), with inclusion of the rs30187 genotype as a covariate. Imputation of SNPs within an R^2 window value of 0.1 with rs30187 (*ERAP1*) or rs2910686 (*ERAP2*) was conducted using the 1000 Genomes phase 1 reference panel for the subset of 124 individuals included in this study. Phasing was conducted using SHAPEIT (28), and imputation was conducted using IMPUTE2 (29), with the “info” metric used to remove poorly imputed SNPs (info < 0.5). A total of 1,221 SNPs spanning *ERAP1* and *ERAP2* were used in the final analysis.

RNA sequencing. RNA was reverse transcribed, prepared for sequencing using an Illumina TruSeq Stranded Total RNA Library Prep Kit, and sequenced using an Illumina HiSeq 2000 system. Reads were mapped to the human genome Ensembl Genome Reference Consortium Build 37, release 75 (GRCh37.75) using TopHat version 2.0.6 employing the Bowtie 2 version 2.0.2 aligner (30,31). Aligned reads were supplied to HTSeq (32) to generate counts per gene. Isoform-specific reads were generated using the Cufflinks suite (33) and assembled into a reference transcriptome. RSEM (34) was used to align reads to generate isoform counts of known and novel transcripts. Gene and isoform counts were normalized using DESeq2 (35).

Statistical analysis. *Expression QTL detection.* All statistical analyses were performed using R statistical software (36). A generalized linear mixed-effects model (GLMM) with a negative binomial distribution and logarithmic link was fitted using the lme4 package (37) to test for the effect of genotype on gene or isoform expression, correcting for the fixed effect of patient sex and random effect of sequencing batch, according to the following equation:

$$\text{glmer}(\text{expression} \sim \text{genotype} + \text{sex} + (1|\text{batch}), \\ \text{family} = \text{neg.bin})$$

The change in gene or isoform expression attributed to the addition of a minor allele was quantified as the exponentiated regression coefficient for the genotype term (referred to here as the incidence rate ratio [IRR]), with IRR^2 interpretable as the fold change in expression in those homozygous for the minor allele relative to those homozygous for the major allele at a given SNP. *P* values were adjusted for multiple testing using Benjamini and Hochberg false discovery rate correction (38).

Significant SNPs were cross-referenced to the set of significant disease-associated SNPs previously identified at this locus (7), and the direction of the effect of the disease risk allele was inferred. Pairwise conditioning was conducted by adding each significant eQTL individually as a covariate into the GLMM and assessing the genotype effect on expression at each remaining SNP, according to the following equation:

$$\text{glmer}(\text{expression} \sim \text{genotype} + \text{sex} + \text{conditional SNP genotype} \\ + (1|\text{batch}), \text{family} = \text{neg.bin})$$

Wilcoxon's test was used to test for differences in gene expression between patients and controls.

Splicing QTL detection. Splicing QTLs were found for 2 highly expressed isoforms of *ERAP1*, herein termed isoform 19E and isoform 20E. The isoform 19E proportion for each individual was calculated from isoform counts as follows: isoform 19E/(isoform 19E + 20E). A 2-sample *t*-test was used to assess the difference in isoform proportion between patients and controls. A linear model was applied to test for the effect

of genotype on isoform proportion while correcting for any disease status effect, according to the following equation:

$$\text{lm}(\text{isoform 19E proportion} \sim \text{genotype} + \text{status})$$

SNPs that were determined to be significant eQTLs for both transcripts, and significant sQTLs with an effect on isoform proportion, were cross-referenced to the set of significant disease-associated SNPs previously identified at this locus (7), and the direction of the effect of the disease risk allele was inferred. Wilcoxon's test was used to test for differences in isoform expression between patients and controls.

Haplotype data. A chi-square test was performed to assess the disease association of a haplotype containing the *ERAP1* activity-altering SNP rs30187 and splice-altering SNP rs7063, using the European cohort of 9,069 AS patients and 13,578 healthy controls genotyped in the Immunochip investigation (7).

Mass spectrometry (MS) for quantification of ERAP-1 isoform and total protein expression. PBMCs from 39 samples obtained from both patients and controls (15 homozygous for the risk [major] allele at rs7063; 15 heterozygous and 9 homozygous for the protective allele) (see Supplementary Table 5, available on the *Arthritis & Rheumatology* web site at <http://onlinelibrary.wiley.com/doi/10.1002/art.40369/abstract>) were prepared for MS (see Supplementary Methods, available on the *Arthritis & Rheumatology* web site at <http://onlinelibrary.wiley.com/doi/10.1002/art.40369/abstract>). The following peptides were targeted for detection and quantification in samples using an Agilent 1260 Chip HPLC/6490 Triple Quadrupole mass spectrometer (for details, see Supplementary Table 6, available on the *Arthritis & Rheumatology* web site at <http://onlinelibrary.wiley.com/doi/10.1002/art.40369/abstract>): for ERAP1 isoform 19E, VWLQSEKLER; for ERAP1 isoform 20E, VWLQSEKLEHDPEADATG; for ERAP1 common peptide, NPVGYPALWQFLR.

Samples were spiked with 0.5 fmoles weighted peptide mix standard for quantification, and 8 μL ($\sim 2 \mu\text{g}$) was subjected to MS. A standard curve was generated by injecting 1 μL of peptide mix standards at 0.1 fmoles/ μL , 0.2 fmoles/ μL , 0.4 fmoles/ μL , 0.6 fmoles/ μL , and 0.8 fmoles/ μL .

Statistical analysis of MS data. Mass chromatograms were analyzed using Skyline (39) to determine ERAP-1 isoform 19E, isoform 20E, and total protein concentrations in each sample. A linear model was used to test for the effect of the rs7063 genotype on protein expression for each isoform and total protein, correcting for the effect of disease status and HLA-B27 status. A *t*-test was used to test for differences in isoform or total ERAP-1 expression between patients and controls.

Protein modeling of ERAP-1 isoform 20E. The sequence of human ERAP-1 isoform 20E was obtained from UniProt sequence entry Q9NZ08-2. The sequence was submitted to the online modeling server Phyre2 (40) in intensive mode. A set of 4 templates was used by the server to generate the final model, with 92% of the sequence modeled at >90% confidence. A total of 80 residues (residues 1–45, 487–513, and 941–948) were built ab initio, including residues in the C-terminal extension caused by the additional exon 20.

Data access. The RNA sequencing data used for transcript expression analysis have been submitted to the NCBI Sequence Read Archive (project no. SRP100652, experiment no. SRX2586069), with all sample metadata included within BioProject (accession no. PRJNA376610).

RESULTS

Disease risk SNPs in *ERAP1* and *ERAP2* are associated with increased total gene expression. Total gene expression information (normalized transcript counts) was tested for an association with genotype at 1,221 genotyped and imputed SNPs across chromosome 5q15. There were 113 disease risk-associated SNPs identified as eQTLs significantly influencing total *ERAP1* expression (see Supplementary Table 1, available on the *Arthritis & Rheumatology* web site at <http://onlinelibrary.wiley.com/doi/10.1002/art.40369/abstract>). At every SNP, the disease risk allele was associated with an increase in gene expression over the

corresponding protective allele. Pairwise conditioning identified 38 SNPs as variants controlling the expression effect at this locus (see Supplementary Table 1); conditioning with any of these 38 SNPs abolished the significance of all 113 original eQTLs. The 38 variants span a region from the nineteenth intron of the gene to ~50 kb upstream of the first exon (Figure 1A). All 38 SNPs lost their disease association but retained their expression association upon conditioning on rs30187, which itself displayed a modest eQTL effect (IRR^2 1.185, $P = 2.4 \times 10^{-3}$). Imputed SNP rs39840 (linked with genotyped SNPs rs27038 and rs27041; AS disease associations $P = 5.7 \times 10^{-19}$ and $P = 4.9 \times 10^{-19}$, respectively) was the most significant eQTL

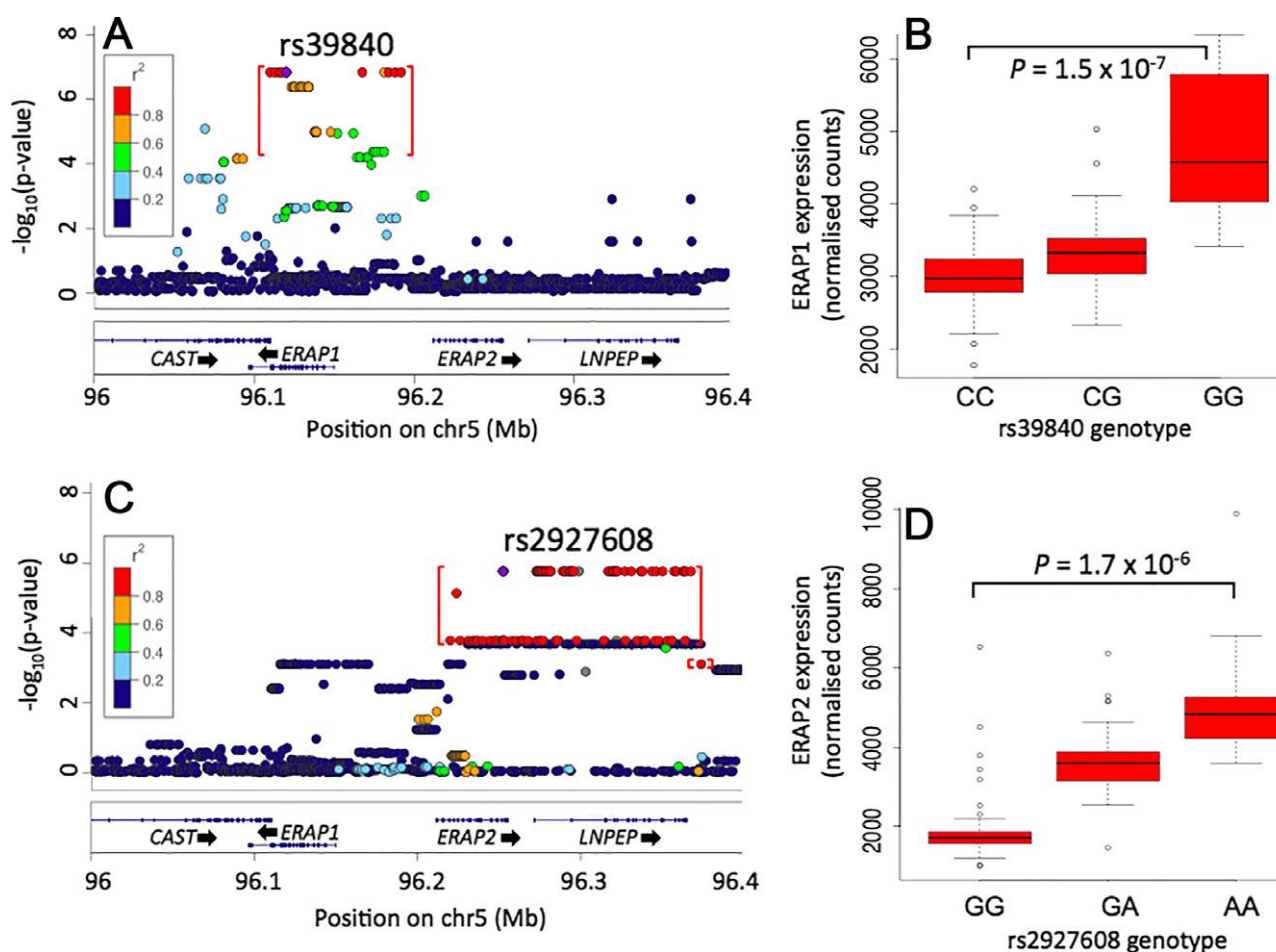


Figure 1. Correlation of genotypes across chromosome (Chr.) 5q15 locus single-nucleotide polymorphisms (SNPs) with endoplasmic reticulum aminopeptidase 1 (ERAP-1) and ERAP-2 gene expression. **A** and **C**, LocusZoom plots of P values for the effect of chromosome 5q15 locus SNPs on expression of *ERAP1* (**A**) and *ERAP2* (**C**) plotted against the genomic region. Expression quantitative trait loci (eQTLs) controlling for the expression effect are shown within the red brackets. Lead eQTLs are shown in purple. Boxed areas show SNPs colored according to linkage disequilibrium between these variants and according to the color key. **B** and **D**, Box plots of the lead *ERAP1* eQTL rs39840 (risk allele G) genotype (**B**) and the lead representative *ERAP2* SNP rs2927608 (risk allele A) genotype (**D**) versus total transcript expression of the corresponding gene. P values were derived from a generalized linear mixed-effects model testing for an effect of genotype on gene expression taken from normalized RNA sequencing counts. Each box represents the 25th to 75th percentiles. Lines inside the boxes represent the median. Lines outside the boxes represent the 10th and 90th percentiles. Circles indicate outliers. In **B**, $n = 79$ in the CC genotype group, $n = 39$ in the CG group, and $n = 6$ in the GG group. In **D**, $n = 44$ in the GG genotype group, $n = 54$ in the GA group, and $n = 26$ in the AA group.

identified (IRR^2 1.343, $P = 1.5 \times 10^{-7}$). Homozygosity for the risk allele at this SNP conferred a 34.3% increase in *ERAP1* expression compared with the protective homozygous genotype (Figure 1B and Supplementary Table 1). There was no significant difference in mean *ERAP1* expression between AS patients and healthy controls.

ERAP2 expression has a bimodal distribution due to the effects of the rs2248374 nonsense mutation found at ~50% frequency in the population (23). To generate an expression distribution amenable to modeling, 38 individuals homozygous for the rs2248374 G allele, expressing very low to no *ERAP2* transcript, were removed, and we corrected for the rs2248374 genotype to ablate the expression effect of this SNP in heterozygotes. One hundred fifty-six SNPs exhibited a significant association with *ERAP2* expression. Pairwise conditioning identified 94 SNPs that controlled for the *ERAP2* expression association of all other eQTLs (Supplementary Table 2, available on the *Arthritis & Rheumatology* web site at <http://onlinelibrary.wiley.com/doi/10.1002/art.40369/abstract>). Tight linkage disequilibrium (LD) between SNPs across the entire *ERAP2* locus (Figure 1C) made it difficult to pinpoint a position for the eQTL signal. As at the *ERAP1* locus, disease risk genotypes were consistently associated with increased gene expression at all expression-controlling SNPs within and around the *ERAP2* gene, with the risk genotype at the most significant eQTLs resulting in a 148% elevation in expression (IRR^2 2.476, $P = 1.7 \times 10^{-6}$) (Figure 1D). There was no significant difference in mean *ERAP2* expression between AS patients and healthy control subjects; this study had low power to detect such a difference given the small sample size (38 patients and 48 controls) upon

removal of rs2248374 homozygotes and the need to control for rs2248374 (which is disease associated) in the analysis.

Alternate expression of 2 *ERAP1* isoforms is governed by genotype and associated with disease. Eleven unique *ERAP1* isoforms were assembled from RNA-Seq data (Supplementary Figure 1A, available on the *Arthritis & Rheumatology* web site at <http://onlinelibrary.wiley.com/doi/10.1002/art.40369/abstract>). Only 2 transcripts, differing in the inclusion of the C-terminal exon 20 (RM [STOP] → HDPEADATG[STOP]), Ensembl ID ENST00000443439 (941 amino acids, 19 exons; 19E) and Ensembl ID ENST00000296754 (948 amino acids, 20 exons; 20E) (Figure 2; see also Supplementary Table 3, available on the *Arthritis & Rheumatology* web site at <http://onlinelibrary.wiley.com/doi/10.1002/art.40369/abstract>), were highly expressed in all individuals (see Supplementary Figure 1B). We identified 158 disease-associated SNPs as significant eQTLs for both isoforms when tested independently for an expression effect on each (see Supplementary Table 4, available on the *Arthritis & Rheumatology* web site at <http://onlinelibrary.wiley.com/doi/10.1002/art.40369/abstract>). At every SNP, the disease risk variant was associated with a significant increase in expression of isoform 19E and a significant decrease in expression of isoform 20E. The proportion of isoform 19E transcripts expressed by an individual was significantly associated with disease status ($P = 0.047$ by *t*-test), with patients expressing a significantly greater proportion of the 19-exon isoform (66.1%) compared with controls (61.9%).

Genotyping of the same 158 disease-associated SNPs (henceforth called sQTLs) had significant effects on

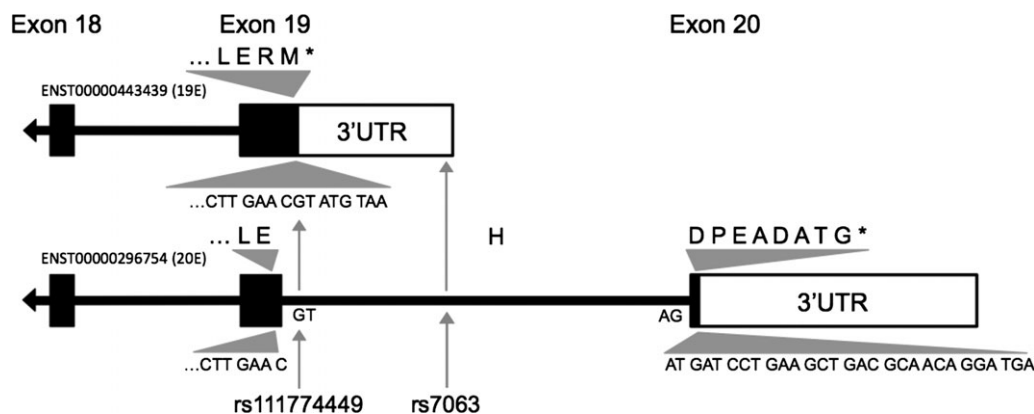


Figure 2. Schematic representation of the 3' end of 2 *ERAP1* transcripts demonstrated to be highly expressed in peripheral blood mononuclear cells. Isoform ENST00000443439 has 19 exons (19E), and isoform ENST00000296754 has 20 exons (20E) with an alternate 3'-untranslated region (3'-UTR) sequence. Codons and corresponding amino acids are shown for exon 19 of 19E and exons 19 and 20 of 20E, beginning 2 amino acids before the first point of variation between the transcripts (RM*→HDPEADATG*). The codon for amino acid H in isoform 20E spans a splice junction. **Shaded arrows** indicate the locations of 2 putative splice-interfering single-nucleotide polymorphisms (rs111774449 [G/A variant; Arg→His]) at the exon–intron 19 interface and rs7063 [A/T variant]) falling within the transcription termination motif in the 3'-UTR of isoform 19E, identified as the most significant *ERAP1* slicing quantitative trait locus from the statistical analyses using RNA-Seq data.

ERAP1 isoform proportions. Pairwise conditioning identified 9 SNPs that controlled for the sQTL effect; conditioning with any of these 9 SNPs ablated the effect of all other SNPs on the expression of isoform 20E and thus their effect on the isoform proportion (see Supplementary Table 4, available on the *Arthritis & Rheumatology* web site at <http://onlinelibrary.wiley.com/doi/10.1002/art.40369/abstract>). The SNP rs7063 (disease association OR 1.34, $P = 1.3 \times 10^{-41}$), situated between exon 19 and exon 20 (Figure 2), exhibited the most significant effect on isoform proportion (OR 1.16, $P = 1.2 \times 10^{-23}$), at which individuals homozygous for the risk (major) allele expressed 105% more (IRR² = 2.05, $P = 8.7 \times 10^{-12}$) and 47% less (IRR² 0.53, $P = 1.0 \times 10^{-17}$) of the 19-exon and 20-exon isoforms, respectively, than those homozygous for the protective allele (Figures 3A and B). Individuals heterozygous for rs7063 expressed similar amounts of both transcripts (for isoform 19E, 56%; for isoform 20E, 44%), whereas

individuals homozygous for the risk allele expressed predominantly isoform 19E (average 71%), and those homozygous for the protective allele expressed predominantly isoform 20E (average 59%) (Figure 3D).

None of the 58 most significant sQTLs exhibited significant eQTL effects on total *ERAP1* expression, and all retained a significant disease association upon correction for rs30187 (Supplementary Table 4) but lost this association upon correction for both rs30187 and rs10050860. These SNPs clustered within and around the C-terminus–encoding exons 19 and 20 (Figure 3C). Upon correction for rs10050860 alone, rs7063 retained a genome-wide significant disease association ($P = 1.4 \times 10^{-10}$). Conversely, a far weaker association remained for rs10050860 ($P = 2.6 \times 10^{-5}$) following correction for rs7063. LD between rs7063 and rs10050860 ($R^2 = 0.55$) was considerably stronger than that between rs7063 and rs30187 ($R^2 = 0.21$).

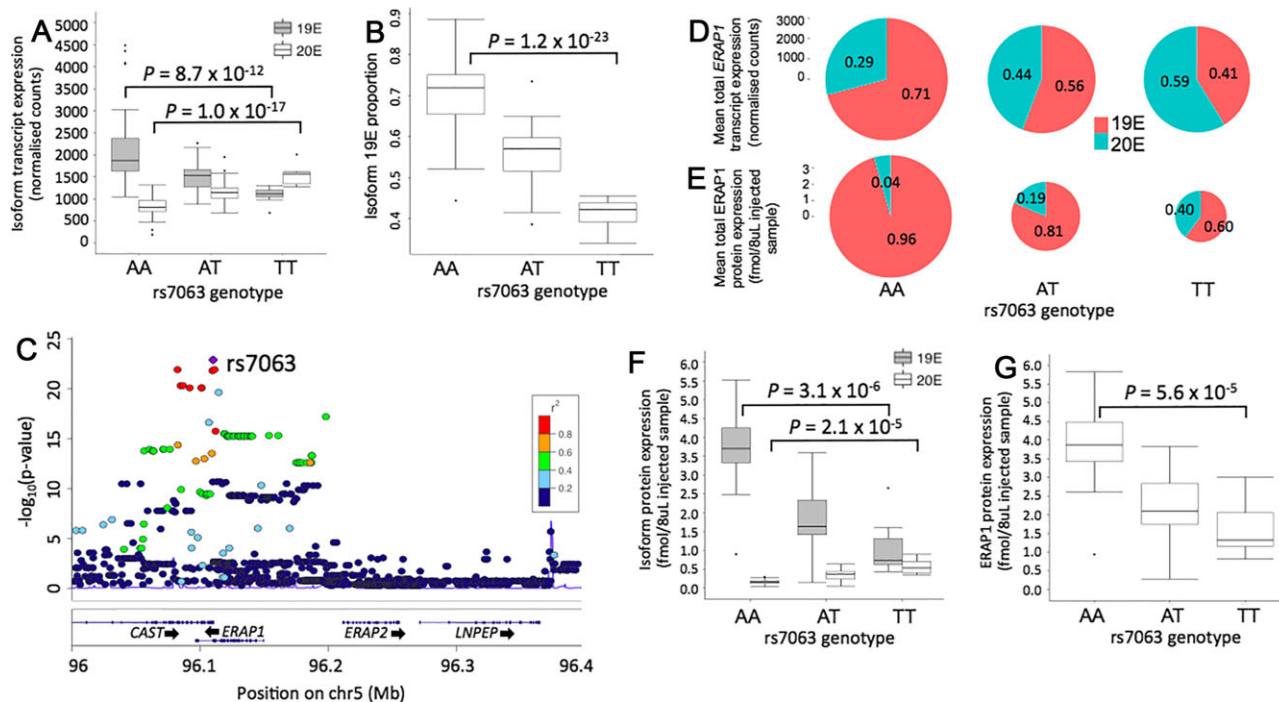


Figure 3. Correlation of genotypes across chromosome 5q15 locus SNPs with expression of 2 *ERAP1* isoforms. **A**, Transcript expression of *ERAP1* isoforms 19E and 20E, split according to genotype at splicing QTL (sQTL) rs7063 (risk allele A). **B**, *ERAP1* isoform 19E proportion split according to rs7063 genotype. **C**, Locus plot showing P values for the effect of chromosome 5q15 locus SNPs on the *ERAP1* isoform 19E proportion, plotted against the genomic region. The most significant sQTL rs7063 is shown in purple. Boxed area shows SNPs colored according to linkage disequilibrium between these variants and according to the color key. **D** and **E**, Pie graphs showing the proportional contribution of the 19E and 20E isoforms to total *ERAP1* transcript expression (**D**) and protein levels (**E**), measured using RNASeq and mass spectrometry, respectively, in individuals categorized according to rs7063 genotype. The radius of each graph denotes the mean total *ERAP1* expression at the transcript or protein level. **F**, Protein expression of *ERAP1* isoforms 19E and 20E split according to rs7063 genotype. **G**, Total *ERAP1* protein expression split by genotype at rs7063. Data in **A**, **B**, **F**, and **G** are shown as box plots. Each box represents the 25th to 75th percentiles. Lines inside the boxes represent the median. Lines outside the boxes represent the 10th and 90th percentiles. Circles indicate outliers. In **A** and **B**, $n = 73$ in the AA genotype group, $n = 43$ in the AT group, and $n = 8$ in the TT group. In **D** and **E**, $n = 124$ in the RNA-Seq cohort and $n = 39$ in the mass spectrometry cohort. In **F** and **G**, $n = 15$ in the AA genotype group, $n = 15$ in the AT group, and $n = 9$ in the TT group. See Figure 1 for other definitions. Color figure can be viewed in the online issue, which is available at <http://onlinelibrary.wiley.com/doi/10.1002/art.40369/abstract>.

Table 1. Significant association of ankylosing spondylitis with *ERAP1* haplotypes containing rs7063 risk allele A and rs30187 risk allele T*

Haplotype	Haplotype frequency	Frequency in controls (n = 13,578)	Frequency in patients (n = 9,069)	P
rs7063T/rs30187T	0.0458	0.0429	0.0501	3.2×10^{-4}
rs7063T/rs30187C	0.2360	0.2630	0.1955	1.1×10^{-61}
rs7063A/rs30187T	0.3194	0.2956	0.3552	1.7×10^{-40}
rs7063A/rs30187C	0.3988	0.3985	0.3992	0.89

* Associations were determined by chi-square test.

A strong disease-protective haplotype results from co-occurrence of the protective alleles at rs30187 and the sQTL rs7063. The protective haplotype, rs30187C/rs7063T (low *ERAP1* enzyme activity/decreased expression of *ERAP1* isoform 19E, increased expression of isoform 20E) showed a disease association of $P = 1.1 \times 10^{-61}$ (Table 1) in 9,069 genotyped AS patients and 13,578 healthy controls. This haplotype association exceeded the individual disease association of both SNPs in isolation (for rs30187, $P = 4.4 \times 10^{-45}$; for rs7063, $P = 1.3 \times 10^{-41}$).

Genotype at *ERAP1* sQTL rs7063 is strongly associated with alternate expression of 2 *ERAP1* isoforms at the protein level. Protein derived from both isoform 19E and isoform 20E of the *ERAP1* transcript was detected using MS. The SNP genotype at rs7063 was significantly associated with protein expression of both isoforms

independently and total *ERAP1* expression (the sum of the expression of both isoforms) (Figures 3F and G). Individuals homozygous for the risk allele at rs7063 expressed 3.52 times more isoform 19E ($P = 3.1 \times 10^{-6}$) and 0.29 times less isoform 20E ($P = 2.1 \times 10^{-5}$), and expressed 2.37 times more total *ERAP1* protein overall ($P = 5.6 \times 10^{-5}$) than those homozygous for the protective allele. At the protein level, isoform 19E was the predominantly expressed form of *ERAP1* in all 3 genotype groups (Figure 3E), and expression was significantly higher, on average, than expression of isoform 20E ($P = 1.4 \times 10^{-10}$). There was no significant difference in the mean expression of either isoform at the protein level, or total *ERAP1* protein levels, between AS patients and healthy controls.

In silico analysis of *ERAP1* isoform 20E predicts folding nature of the alternate protein. Ab initio protein structure modeling of the *ERAP1* 20E isoform suggested that the unique additional residues on the C-terminal end of the protein fold back across the surface of domain 4 of *ERAP1*, potentially forming salt bridge interactions with residues Arg⁷⁵⁰ and Arg⁷⁰⁸ (Figure 4).

DISCUSSION

The genetic association of variants in *ERAP1* and *ERAP2* with several immune-mediated diseases makes

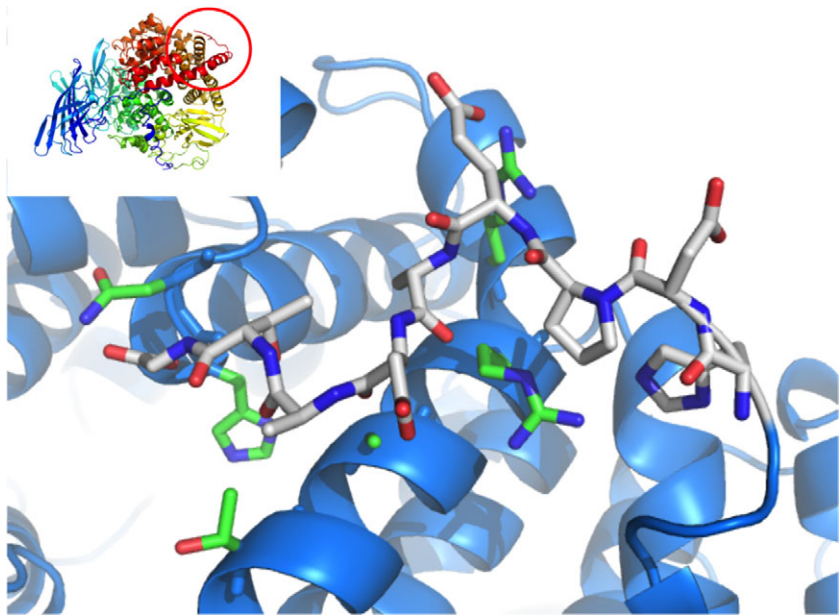


Figure 4. Modeled structure of endoplasmic reticulum aminopeptidase 1 (*ERAP1*) isoform 20E. The protein is shown in blue. Residues of the 20E extension are shown as bonds colored according to atom type, with carbon atoms shown in white. Residues in the body of the protein that are within contact with the modeled 20E extension are shown as bonds colored according to atom type, with carbon atoms shown in green. The model suggests that the 20E extension residues sit across the surface of domain 4 of *ERAP1* and are unlikely to interfere with protein function. **Inset,** Overview of the model, with the protein shown in a rainbow color gradient from the N-terminus (blue) to the C-terminus (red). **Encircled area,** Region that is shown expanded in the main figure.

these enzymes important targets for functional investigation. The current study shows that AS risk-associated variants in these genes consistently demonstrated an eQTL effect that increases aminopeptidase expression. Indeed, the protective influence of the nonsense mutation rs2248374 (23) in *ERAP2* implies that some aspect of the functional role of the enzyme in peptide presentation is linked to pathology in a way that can be ablated with loss of expression. It is expected that this is also the case in *ERAP1*, at which increased expression may be exacerbating the pathogenic effect of co-occurring missense mutations shown to alter enzymatic activity and peptide handling (11,12). It has been previously shown that *ERAP1* messenger RNA (mRNA) and protein expression is increased in lymphoid cell lines carrying disease susceptibility variants across *ERAP1* haplotypes (15,22). Our results validate the influence of genetic variants across *ERAP1* and *ERAP2* on transcript and protein expression levels.

Previous fine-mapping and haplotype evolution studies indicate that the *ERAP1* association with AS is driven by 2 independent association signals, the first tagged by the coding variant rs30187 (K528R), which is likely the causative SNP, and the second tagged by the coding variant rs10050860 (D575N) (1,6). Further studies using recombinant ERAP-1 and cell lines carrying ERAP-1 variants have shown that rs30187 has a substantial effect on peptide cleavage and peptides presented by HLA class I antigens (1,17,41). It has been suggested that *ERAP1* variants act in haplotype combinations (42,43). However, many of the variants and haplotypes observed in these studies have been found at frequencies that are markedly different from those reported in the literature and likely represent an experimental artifact (44,45). In the current study, we sought to investigate the functional mechanisms by which *ERAP1* and *ERAP2* variants operate, to explain the known genetic association of these genes with AS and other diseases.

The major finding of the current study suggests complex regulation of *ERAP1* expression by 2 independently acting variants, 1 in moderate LD with rs30187, which influences global *ERAP1* expression, and the second in moderate LD with rs10050860, which influences alternate splicing of 2 distinct transcripts. Our results suggest that the differences between these 2 forms of the *ERAP1* transcript, and encoded protein, are critically important and influence the levels of functional enzymes in cells. Given the cross-disease-concordant action of *ERAP1* and *ERAP2* polymorphisms in conditions such as psoriasis and Crohn's disease (46), these findings have relevance far beyond AS alone.

Harvey et al (12) demonstrated a strong positive correlation between the strength of AS disease association

for variants in *ERAP1* and their effect on *ERAP1* expression ($r = 0.75$) (47). Similarly, we observed that the most significant *ERAP1* eQTLs are strongly associated with AS. Although linked within the haplotype containing the key functional variant rs30187, these SNPs retained a significant expression effect upon correction for rs30187. This implies that, in addition to the effects of rs30187 on ERAP-1 activity, there are ≥ 1 variants in moderate LD with rs30187 driving altered enzyme expression. Joint inheritance of these alleles would mean that any alterations in the HLA-B27 peptidome due to ERAP-1 hyperactivity would be exacerbated by enzyme overexpression. This could potentially flood HLA-B27 with an immunogenic repertoire stimulating the CD8-mediated immune response (48) or lead to destruction of peptides that protect (in some manner) against the immunologic processes that lead to AS (49). Concordantly, increased transcript expression in individuals expressing *ERAP2* and carrying *ERAP2* disease risk-associated polymorphisms supports the significance of increased aminopeptidase expression in disease pathology. The identification of disease-associated expression-influencing variants at this locus, independent of the rs2248374-null mutant, implies that the patients who express ERAP-2 have varied expression phenotypes and thus disease susceptibility.

Of great interest was the finding that 2 expressed isoforms of *ERAP1*, the alternate expression of which correlated with genotype at strong disease risk-associated SNPs, may play a substantial role in disease. These 2 transcripts, encoding different versions of the ERAP-1 protein, have been previously identified (50,51) and annotated as ENST00000443439 (19 exons, 18 coding; 19E) and ENST00000296754 (20 exons, 19 coding; 20E) in the Ensembl database (52). Isoform quantification at the transcript level revealed that isoforms 19E and 20E are transcribed forms of *ERAP1*, expressed in all 124 individuals and at levels high enough to potentially contribute to the functional output of the enzyme.

We demonstrate here that alternate expression of these 2 isoforms is likely modulated by a genetic splice-interfering variant rather than by the common mechanism of alternate splicing, and that this variant is strongly associated with AS. The observation that the disease risk-associated allele at all significant *ERAP1* sQTLs correlated with increased expression of the 19E transcript and decreased expression of the 20E transcript suggests that there may be some disease-protective feature of the 20E isoform specifically. SNPs exhibiting the most significant sQTL effect were localized around the exon/intron 19 boundary, around the first point of sequence variation between the 2 isoforms, and it has been previously noted that a number of the strongest disease-associated variants

in *ERAP1* fall in this location, with a potential involvement in splicing (12).

The most significant sQTLs retained a strong disease association upon correction for rs30187, implying that they are situated within the rs10050860-tagged haplotype; perhaps a splice site variant governing *ERAP1* isoform expression is of greatest functional importance at this position. Our data suggest that the rs10050860 association is driven by the sQTL rs7063, but we cannot formally exclude effects due to other polymorphisms in strong LD with it, noting that rs10050860 itself has been shown not to affect ERAP-1 peptide cleavage (1,17).

MS quantification of isoform expression showed that both the 19E and 20E isoforms of the ERAP-1 protein were present at detectable levels in all 39 assayed samples. Similarly, observed differences in the molecular mass of ERAP-1 isolated from various human cell lines confirms the co-occurrence of the 2 forms of the full-length protein (53). One putative mRNA splice-altering mutation (rs7063) in *ERAP1* contributed to marked variability in the type of ERAP-1 protein expressed. This variant has an association with AS of $P = 1.3 \times 10^{-41}$ and an association of $P = 2.5 \times 10^{-17}$ upon correction for rs30187. The observation that a far stronger association of rs7063 with AS remained after correction for rs10050860 ($P = 1.4 \times 10^{-10}$) compared with the rs10050860 association upon correction for rs7063 ($P = 2.6 \times 10^{-5}$) supports the notion that rs7063, or a marker in tight LD with it, is the more important variant at the second independent *ERAP1* disease-associated haplotype.

SNP rs7063 falls in the middle of the conserved transcription termination sequence (AATAAA) in the 3'-UTR of isoform 19E, a motif recognized by cleavage and polyadenylation-specific factors involved in 3'-end transcription termination in mammals (54). The risk allele (major allele T on the reverse strand in the motif AATAAA, allele A on the forward strand) would be expected to promote correct termination of the 19-exon form of the transcript, whereas the protective allele may result in loss of termination sequence recognition, producing the 20-exon form of the transcript. Variant rs111774449, falling in the splice donor sequence at the 3'-end of exon 19 (55), may also be a candidate for isoform switching but is rare (minor allele frequency of <0.01 in the ExAC data set) and was not genotyped or imputed in this study.

The strong disease-protective haplotype that arises from co-occurrence of rs30187 and rs7063 protective alleles is evidence that *ERAP1* expression dynamics contribute to the pathogenicity afforded by increased enzyme activity. The enhanced genetic contribution of SNP haplotypes at 5q15 has been previously noted, with carriage of both disease-associated haplotypes increasing the risk by

~4 fold, a far greater risk than the additive effects of either variant alone (1.2–1.3-fold for either variant in isolation) (1). The current study provides a potential functional mechanism to explain this observation.

Quantification of ERAP-1 protein isoforms in individuals with different rs7063 genotypes implied differences in the dynamics of translation from mRNA to protein. Despite approximately equal levels of the 19E and 20E transcripts in individuals heterozygous for rs7063, 81% of the ERAP-1 protein detected in these individuals was of the 19E isoform. This raises the question of whether loss of isoform 20E posttranscription due to sequence or structural variation between the 2 isoforms (gain of a C-terminal exon) perhaps contributes to less efficient translation of isoform 20E, or misfolding and degradation of the protein, with subsequent lack of function. If this is the case, the mechanism of protection conferred by the disease-protective genotype at splice-site SNPs may arise due to skewed expression toward the 20E transcript, subsequent loss of this isoform at the protein level, and thus a decrease in the overall level of functional ERAP-1 available to the cell.

Ab initio modeling of the additional amino acid residues of isoform 20E was required to explore the role of the exon 20 residues in the structure of ERAP-1. The area of ERAP-1 domain 4 with which the exon 20-derived residues are predicted to interact (Figure 4) is effectively invariant structurally between the open and closed forms of ERAP-1, implying that the presence of the isoform 20E C-terminal extension is unlikely to alter the open- to closed-form dynamics believed to be required for substrate binding and release (56,57). Tertiary structure modeling, however, could not predict whether these residues interfere with folding of the mature protein. The UCSC Genome Browser 100 vertebrate conservation track (58) shows very low sequence conservation in exon 20 relative to the other 19 exons of *ERAP1* and, indeed, other coding exons in general. This suggests that 19-exon ERAP-1 is the predominant functional form of the enzyme, and that the appended 7 amino acids in isoform 20E are irrelevant to the mature enzyme, which is thus tolerant of substituting mutations, or that the protein itself is removed from the cell before it can actively contribute to peptide trimming.

To date, differential gene expression studies in AS have shown no evidence for significant changes in the expression of genes encoding disease-associated aminopeptidases in patients relative to healthy controls (59,60). Here, we demonstrate the ability of eQTL studies to identify genotype-driven altered gene expression in disease, which would go unnoticed by differential expression studies that pool samples of different genotypes. Importantly, it must be acknowledged that dynamic changes in the

isoforms derived from a transcriptional unit can be far more insightful than measures of total gene expression, adding layers of complexity to the functional output of a gene. It appears that increased aminopeptidase expression governed by altered transcript dynamics at both *ERAP1* and *ERAP2* is a key mechanism driving the degree to which these enzymes contribute to immune-mediated disease. These findings support ERAP inhibition as a therapeutic approach to treating diseases including AS and psoriasis, in which protective genetic variants lead to loss of both ERAP levels and ERAP function.

ACKNOWLEDGMENTS

We thank L. Bradbury and K. Hollis for assistance with ascertainment of participant samples and all participants who provided samples and clinical details for this project. We also thank B. Gautier for assistance with statistical model design and testing.

AUTHOR CONTRIBUTIONS

All authors were involved in drafting the article or revising it critically for important intellectual content, and all authors approved the final version to be published. Dr. Brown had full access to all of the data in the study and takes responsibility for the integrity of the data and the accuracy of the data analysis.

Study conception and design. Thomas, Kenna, Brown.

Acquisition of data. Hanson, Cuddihy, Haynes, Loo, Morton, Oppermann, Leo.

Analysis and interpretation of data. Hanson, Leo, Thomas, Cao, Kenna, Brown.

REFERENCES

- Evans DM, Spencer CC, Pointon JJ, Su Z, Harvey D, Kochan G, et al. Interaction between ERAP1 and HLA-B27 in ankylosing spondylitis implicates peptide handling in the mechanism for HLA-B27 in disease susceptibility. *Nat Genet* 2011;43:761–7.
- Wellcome Trust Case Control Consortium, Australo-Anglo-American Spondylitis Consortium, Burton PR, Clayton DG, Cardon LR, Craddock N, et al. Association scan of 14,500 nonsynonymous SNPs in four diseases identifies autoimmunity variants. *Nat Genet* 2007;39:1329–37.
- Strange A, Capon F, Spencer CC, Knight J, Weale ME, Allen MH, et al. A genome-wide association study identifies new psoriasis susceptibility loci and an interaction between HLA-C and ERAP1. *Nat Genet* 2010;42:985–90.
- Franke A, McGovern DP, Barrett JC, Wang K, Radford-Smith GL, Ahmad T, et al. Genome-wide meta-analysis increases to 71 the number of confirmed Crohn's disease susceptibility loci. *Nat Genet* 2010;42:1118–25.
- Kirino Y, Bertsias G, Ishigatsubo Y, Mizuki N, Tugal-Tutkun I, Seyahi E, et al. Genome-wide association analysis identifies new susceptibility loci for Behcet's disease and epistasis between HLA-B*51 and ERAP1. *Nat Genet* 2013;45:202–7.
- Cortes A, Pulit SL, Leo PJ, Pointon JJ, Robinson PC, Weisman MH, et al. Major histocompatibility complex associations of ankylosing spondylitis are complex and involve further epistasis with ERAP1. *Nat Commun* 2015;6:7146.
- International Genetics of Ankylosing Spondylitis Consortium, Cortes A, Hadler J, Pointon JP, Robinson PC, Karaderi T, et al. Identification of multiple risk variants for ankylosing spondylitis through high-density genotyping of immune-related loci. *Nat Genet* 2013;45:730–8.
- Australo-Anglo-American Spondyloarthritis Consortium, Reveille JD, Sims AM, Danoy P, Evans DM, Leo P, et al. Genome-wide association study of ankylosing spondylitis identifies non-MHC susceptibility loci. *Nat Genet* 2010;42:123–7.
- Ellinghaus D, Jostins L, Spain SL, Cortes A, Bethune J, Han B, et al. Analysis of five chronic inflammatory diseases identifies 27 new associations and highlights disease-specific patterns at shared loci. *Nat Genet* 2016;48:510–8.
- Danoy P, Pryce K, Hadler J, Bradbury LA, Farrar C, Pointon J, et al. Association of variants at 1q32 and STAT3 with ankylosing spondylitis suggests genetic overlap with Crohn's disease. *PLoS Genet* 2010;6:e1001195.
- Seregin SS, Rastall DP, Evnouchidou I, Aylsworth CF, Quiroga D, Kamal RP, et al. Endoplasmic reticulum aminopeptidase-1 alleles associated with increased risk of ankylosing spondylitis reduce HLA-B27 mediated presentation of multiple antigens. *Autoimmunity* 2013;46:497–508.
- Harvey D, Pointon JJ, Evans DM, Karaderi T, Farrar C, Appleton LH, et al. Investigating the genetic association between ERAP1 and ankylosing spondylitis. *Hum Mol Genet* 2009;18:4204–12.
- Benjamin RJ, Abrams JR, Parnes JR, Madrigal JA, Parham P. Polymorphic specificity of Q1/28, a monoclonal antibody that preferentially reacts with free class I heavy chains. *Immunogenetics* 1992;37:73–6.
- Evnouchidou I, Birtley J, Seregin S, Papakyriakou A, Zervoudi E, Samiotaki M, et al. A common single nucleotide polymorphism in endoplasmic reticulum aminopeptidase 2 induces a specificity switch that leads to altered antigen processing. *J Immunol* 2012;189:2383–92.
- Sanz-Bravo A, Campos J, Mazariegos MS, López de Castro JA. Dominant role of the ERAP1 polymorphism R528K in shaping the HLA-B27 peptidome through differential processing determined by multiple peptide residues. *Arthritis Rheumatol* 2015;67:692–701.
- Martin-Esteban A, Sanz-Bravo A, Guasp P, Barnea E, Admon A, Lopez de Castro JA. Separate effects of the ankylosing spondylitis associated ERAP1 and ERAP2 aminopeptidases determine the influence of their combined phenotype on the HLA-B*27 peptidome. *J Autoimmun* 2017;79:28–38.
- Garcia-Medel N, Sanz-Bravo A, van Nguyen D, Galocha B, Gomez-Molina P, Martin-Esteban A, et al. Functional interaction of the ankylosing spondylitis-associated endoplasmic reticulum aminopeptidase 1 polymorphism and HLA-B27 in vivo. *Mol Cell Proteomics* 2012;11:1416–29.
- Chen L, Ridley A, Hammitzsch A, Al-Mossawi MH, Bunting H, Georgiadis D, et al. Silencing or inhibition of endoplasmic reticulum aminopeptidase 1 (ERAP1) suppresses free heavy chain expression and Th17 responses in ankylosing spondylitis. *Ann Rheum Dis* 2016;75:916–23.
- Haroon N, Tsui FW, Uchanska-Ziegler B, Ziegler A, Inman RD. Endoplasmic reticulum aminopeptidase 1 (ERAP1) exhibits functionally significant interaction with HLA-B27 and relates to subtype specificity in ankylosing spondylitis. *Ann Rheum Dis* 2012;71:589–95.
- Bowness P, Ridley A, Shaw J, Chan AT, Wong-Baeza I, Fleming M, et al. Th17 cells expressing KIR3DL2+ and responsive to HLA-B27 homodimers are increased in ankylosing spondylitis. *J Immunol* 2011;186:2672–80.
- Barnea E, Melamed Kadosh D, Haimovich Y, Satumtira N, Dorris ML, Nguyen MT, et al. The human leukocyte antigen (HLA)-B27 peptidome in vivo, in spondyloarthritis-susceptible HLA-B27 transgenic rats and the effect of Erp1 deletion. *Mol Cell Proteomics* 2017;16:642–62.

22. Costantino F, Talpin A, Evnouchidou I, Kadi A, Leboime A, Said-Nahal R, et al. ERAP1 gene expression is influenced by nonsynonymous polymorphisms associated with predisposition to spondyloarthritis. *Arthritis Rheumatol* 2015;67:1525–34.
23. Andres AM, Dennis MY, Kretschmar WW, Cannons JL, Lee-Lin SQ, Hurle B, et al. Balancing selection maintains a form of ERAP2 that undergoes nonsense-mediated decay and affects antigen presentation. *PLoS Genet* 2010;6:e1001157.
24. Martin-Esteban A, Guasp P, Barnea E, Admon A, López de Castro JA. Functional interaction of the ankylosing spondylitis-associated endoplasmic reticulum aminopeptidase 2 with the HLA-B*27 peptide in human cells. *Arthritis Rheumatol* 2016;68:2466–75.
25. Garcia-Medel N, Sanz-Bravo A, Alvarez-Navarro C, Gomez-Molina P, Barnea E, Marcilla M, et al. Peptide handling by HLA-B27 subtypes influences their biological behavior, association with ankylosing spondylitis and susceptibility to endoplasmic reticulum aminopeptidase 1 (ERAP1). *Mol Cell Proteomics* 2014;13:3367–80.
26. Van der Linden S, Valkenberg HA, Cats A. Evaluation of diagnostic criteria for ankylosing spondylitis: a proposal for modification of the New York criteria. *Arthritis Rheum* 1984;27:361–8.
27. Purcell S, Neale B, Todd-Brown K, Thomas L, Ferreira MA, Bender D, et al. PLINK: a tool set for whole-genome association and population-based linkage analyses. *Am J Hum Genet* 2007;81:559–75.
28. Delaneau O, Marchini J, Zagury JF. A linear complexity phasing method for thousands of genomes. *Nat Methods* 2012;9:179–81.
29. Howie BN, Donnelly P, Marchini J. A flexible and accurate genotype imputation method for the next generation of genome-wide association studies. *PLoS Genet* 2009;5:e1000529.
30. Kim D, Pertea G, Trapnell C, Pimentel H, Kelley R, Salzberg SL. TopHat2: accurate alignment of transcriptomes in the presence of insertions, deletions and gene fusions. *Genome Biol* 2013;14:R36.
31. Langmead B, Salzberg SL. Fast gapped-read alignment with Bowtie 2. *Nat Methods* 2012;9:357–9.
32. Anders S, Pyl PT, Huber W. HTSeq: a Python framework to work with high-throughput sequencing data. *Bioinformatics* 2015;31:166–9.
33. Trapnell C, Williams BA, Pertea G, Mortazavi A, Kwan G, van Baren MJ, et al. Transcript assembly and quantification by RNA-Seq reveals unannotated transcripts and isoform switching during cell differentiation. *Nat Biotechnol* 2010;28:511–5.
34. Li B, Dewey CN. RSEM: accurate transcript quantification from RNA-Seq data with or without a reference genome. *BMC Bioinformatics* 2011;12:323.
35. Love MI, Huber W, Anders S. Moderated estimation of fold change and dispersion for RNA-Seq data with DESeq2. *Genome Biol* 2014;15:550.
36. Team RC. R: a language and environment for statistical computing. Vienna, Austria: R Foundation for Statistical Computing; 2015.
37. Bates D, Maechler M, Bolker B, Walker S. lme4: linear mixed-effects models using Eigen and S4. R package version 1.1-8. 2015.
38. Benjamini Y, Hochberg Y. Controlling the false discovery rate: a practical and powerful approach to multiple testing. *J Royal Stat Soc* 1995;57:289–300.
39. MacLean B, Tomazela DM, Shulman N, Chambers M, Finney GL, Frewen B, et al. Skyline: an open source document editor for creating and analyzing targeted proteomics experiments. *Bioinformatics* 2010;26:966–8.
40. Kelley LA, Mezulis S, Yates CM, Wass MN, Sternberg MJ. The Phyre2 web portal for protein modeling, prediction and analysis. *Nat Protoc* 2015;10:845–58.
41. Chen L, Fischer R, Peng Y, Reeves E, McHugh K, Ternette N, et al. Critical role of endoplasmic reticulum aminopeptidase 1 in determining the length and sequence of peptides bound and presented by HLA-B27. *Arthritis Rheumatol* 2014;66:284–94.
42. Reeves E, Colebatch-Bourn A, Elliott T, Edwards CJ, James E. Functionally distinct ERAP1 allotype combinations distinguish individuals with ankylosing spondylitis. *Proc Natl Acad Sci U S A* 2014;111:17594–9.
43. Reeves E, Elliott T, Edwards CJ, James E. Both rare and common ERAP1 allotypes have distinct functionality defined by polymorphic context and are important in AS association. *Proc Natl Acad Sci U S A* 2017;114:E1575–6.
44. Roberts AR, Appleton LH, Cortes A, Vecellio M, Lau J, Watts L, et al. ERAP1 association with ankylosing spondylitis is attributable to common genotypes rather than rare haplotype combinations. *Proc Natl Acad Sci U S A* 2017;114:558–61.
45. Robinson PC, Brown MA. ERAP1 biology and assessment in ankylosing spondylitis. *Proc Natl Acad Sci U S A* 2015;112:E1816.
46. Parkes M, Cortes A, van Heel DA, Brown MA. Genetic insights into common pathways and complex relationships among immune-mediated diseases. *Nat Rev Genet* 2013;14:661–73.
47. Dixon AL, Liang L, Moffatt MF, Chen W, Heath S, Wong KC, et al. A genome-wide association study of global gene expression. *Nat Genet* 2007;39:1202–7.
48. Benjamin R, Parham P. HLA-B27 and disease: a consequence of inadvertent antigen presentation? *Rheum Dis Clin North Am* 1992;18:11–21.
49. Kenna TJ, Brown MA. Immunopathogenesis of ankylosing spondylitis. *Int J Clin Rheumatol* 2013;8:265–74.
50. Hattori A, Matsumoto H, Mizutani S, Tsujimoto M. Molecular cloning of A-LAP highly related to placental leucine aminopeptidase/oxytocinase. *J Biochem* 1999;125:931–8.
51. Hattori A, Matsumoto K, Mizutani S, Tsujimoto M. Genomic organization of the human adipocyte-derived leucine aminopeptidase gene and its relationship to the placental leucine aminopeptidase/oxytocinase gene. *J Biochem* 2001;130:235–41.
52. Yates A, Akanni W, Amode MR, Barrell D, Billis K, Carvalho-Silva D, et al. Ensembl 2016. *Nucleic Acids Res* 2016;44:D710–6.
53. Yousaf N, Low WY, Onipinla A, Mein C, Caulfield M, Munroe PB, et al. Differences between disease-associated endoplasmic reticulum aminopeptidase 1 (ERAP1) isoforms in cellular expression, interactions with tumour necrosis factor receptor 1 (TNF-R1) and regulation by cytokines. *Clin Exp Immunol* 2015;180:289–304.
54. Richard P, Manley JL. Transcription termination by nuclear RNA polymerases. *Genes Dev* 2009;23:1247–69.
55. National Center for Biotechnology Information. NCBI Human Genome Browser. US National Library of Medicine; 2015.
56. Kochan G, Krojer T, Harvey D, Fischer R, Chen L, Vollmar M, et al. Crystal structures of the endoplasmic reticulum aminopeptidase-1 (ERAP1) reveal the molecular basis for N-terminal peptide trimming. *Proc Natl Acad Sci U S A* 2011;108:7745–50.
57. Nguyen TT, Chang SC, Evnouchidou I, York IA, Zikos C, Rock KL, et al. Structural basis for antigenic peptide precursor processing by the endoplasmic reticulum aminopeptidase ERAP1. *Nat Struct Mol Biol* 2011;18:604–13.
58. University of California Santa Cruz (UCSC). UCSC Genome Browser: Vertebrate Multiz Alignment & Conservation (100 Species). 2015.
59. Duan R, Leo P, Bradbury L, Brown MA, Thomas G. Gene expression profiling reveals a downregulation in immune-associated genes in patients with AS. *Ann Rheum Dis* 2010;69:1724–9.
60. Assassi S, Reveille JD, Arnett FC, Weisman MH, Ward MM, Agarwal SK, et al. Whole-blood gene expression profiling in ankylosing spondylitis shows upregulation of toll-like receptor 4 and 5. *J Rheumatol* 2011;38:87–98.

Efficacy and Safety of Atacicept in Patients With Systemic Lupus Erythematosus

Results of a Twenty-Four-Week, Multicenter, Randomized, Double-Blind, Placebo-Controlled, Parallel-Arm, Phase IIb Study

Joan T. Merrill,¹ Daniel J. Wallace,² Stephen Wax,³ Amy Kao,³ Patricia A. Fraser,³ Peter Chang,³ and David Isenberg,⁴ on behalf of the ADDRESS II Investigators

Objective. To evaluate the efficacy and safety of atacicept, an antagonist of B lymphocyte stimulator/APRIL-mediated B cell activation, in patients with systemic lupus erythematosus (SLE).

Methods. ADDRESS II is a 24-week, multicenter, randomized, double-blind, placebo-controlled, parallel-arm, phase IIb study evaluating the safety and efficacy of atacicept in patients with SLE (ClinicalTrials.gov identifier NCT01972568). Patients with active, autoantibody-positive SLE receiving standard therapy were randomized (1:1:1) to receive atacicept (75 mg or 150 mg) or placebo for 24 weeks. The primary end point was the SLE responder index 4 (SRI-4) at week 24.

Results. The intent-to-treat (ITT) population included 306 patients. There was a trend toward an improved SRI-4 response rate with atacicept 75 mg (57.8%; adjusted odds ratio [OR] 1.78, $P = 0.045$) and

150 mg (53.8%; adjusted OR 1.56, $P = 0.121$) at week 24 as compared with placebo (44.0%) (primary analysis; using the screening visit as baseline). In a prespecified sensitivity analysis using study day 1 as baseline, a significantly larger proportion of patients receiving atacicept 75 mg and 150 mg achieved an SRI-4 response at week 24 compared with placebo. In predefined subpopulations with high levels of disease activity (HDA) at baseline, serologically active disease, or both, statistically significant improvements in the SRI-4 and SRI-6 response rates were seen with atacicept versus placebo. A severe risk of disease flare was reduced with atacicept therapy in both the ITT and the HDA populations. The risks of serious adverse events and serious or severe infection were not increased with atacicept as compared with placebo.

Conclusion. Atacicept treatment showed evidence of efficacy in SLE, particularly in HDA and serologically active patients. Reductions in disease activity and severe flare were observed with atacicept treatment, with an acceptable safety profile.

Systemic lupus erythematosus (SLE) is a multisystem autoimmune disease with a fluctuating disease course characterized by sporadic, unpredictable disease flares (1–3). Standard treatments include antimalarial, corticosteroid, and immunosuppressive drugs (4). Despite improved understanding of the disease process, there remains a significant unmet need for new treatment because of the continued high risk of death and progressive organ damage (5–7). The long-term burden of disease symptoms and toxic effects of immunosuppressive therapies also significantly affects quality of life (8–10).

Elevated serum levels of the cytokines B lymphocyte stimulator (BLyS) and APRIL in SLE patients

ClinicalTrials.gov identifier: NCT01972568.

Supported by EMD Serono, Inc., a division of Merck KGaA, Darmstadt, Germany.

¹Joan T. Merrill, MD: University of Oklahoma Health Sciences Center, Oklahoma City; ²Daniel J. Wallace, MD: Cedars-Sinai Medical Center, David Geffen School of Medicine, University of California, Los Angeles; ³Stephen Wax, MD, PhD, Amy Kao, MD, MPH, MS, Patricia A. Fraser, MD, MPH, SM (current address: Sanofi Genzyme, Cambridge, Massachusetts), Peter Chang, PhD: EMD Serono Research and Development Institute, Billerica, Massachusetts; ⁴David Isenberg, MD: University College London, London, UK.

Dr. Merrill has received consulting fees from EMD Serono, Anthera Pharmaceuticals, GlaxoSmithKline, and Eli Lilly (less than \$10,000 each). Dr. Wallace has received consulting fees from EMD Serono (less than \$10,000). Drs. Wax, Kao, Fraser, and Chang have long-term incentives from EMD Serono. Dr. Isenberg has received consulting fees from EMD Serono (less than \$10,000); fees provided to Dr. Isenberg are passed on to a local arthritis charity.

Address correspondence to Joan T. Merrill, MD, University of Oklahoma Health Sciences Center, 2929 NW 19th Street, Oklahoma City, OK 73107. E-mail: JTMmail@aol.com.

Submitted for publication March 7, 2017; accepted in revised form October 19, 2017.

correlate with both disease activity (11,12) and autoantibody production (13–16). These factors are therefore promising targets for new investigational therapies. The BLYS inhibitor belimumab has demonstrated efficacy and safety in phase III studies in SLE (17,18) and is approved for treating patients with active disease. Efficacy of atacicept, the dual APRIL/BLYS inhibitor, was suggested by the APRIL SLE study, which also confirmed its biologic activity in reducing total B cell, plasma cell, and serum immunoglobulin levels in SLE patients (19,20).

We report herein the findings of ADDRESS II, a randomized, placebo-controlled phase IIb study of weekly doses of atacicept (75 or 150 mg) versus placebo in patients with active, autoantibody-positive SLE receiving standard therapy (ClinicalTrials.gov identifier NCT01972568).

PATIENTS AND METHODS

Study design. In this 24-week, multicenter, randomized, double-blind, placebo-controlled, parallel-arm, phase IIb study, patients with SLE receiving standard therapy were assigned to once-weekly subcutaneous injections of placebo or atacicept, 75 or 150 mg. The study included a screening period of up to 4 weeks, a treatment period of 24 weeks (reported herein), and a safety follow-up period of 24 weeks (see Supplementary Figure 1, available on the *Arthritis & Rheumatology* web site at <http://onlinelibrary.wiley.com/doi/10.1002/art.40360/abstract>). A long-term extension was offered as part of a separate protocol (see Supplementary Figure 2, available at <http://onlinelibrary.wiley.com/doi/10.1002/art.40360/abstract>). The data reported herein were generated by the ADDRESS II study investigators in Latin America, Asia, South Africa, Europe, UK, and the US.

Prednisone-equivalent corticosteroid dosages could be adjusted during screening (up to 40 mg/day) but had to be ≤ 30 mg/day and no more than the dosage at the screening visit by week 4, except that patients receiving < 7.5 mg/day at screening could be taking as much as 7.5 mg/day at week 4. Dosage tapering was encouraged during weeks 5–16. One corticosteroid rescue with ≤ 30 mg/day was allowed, but the dosage had to be reduced to the dosage at week 4 within 7 days. The dosage at week 16 remained stable during weeks 17–24.

Single immunosuppressive or immunomodulatory drugs and/or an antimalarial drug were permitted. We excluded patients who had received treatment with other investigational agents within the previous 3 months, within a period of 5 half-lives of that drug from the screening visit, or per the washout requirement from the previous protocol, whichever was longest. Patients who had received belimumab (or other anti-BLYS therapy), rituximab, ocrelizumab, or other B cell-directed biologic drug within 1 year before the screening visit were excluded. Background therapy had to remain stable during the screening and treatment periods. Use of nonpermitted medicines or therapies required discontinuation of atacicept and was considered a treatment failure (for details, see Supplementary Text 1, available at <http://onlinelibrary.wiley.com/doi/10.1002/art.40360/abstract>).

Baseline was defined as the screening visit for assessments of disease activity and as treatment day 1 for all other assessments. Interim safety and disease activity data were regularly monitored by an independent Data Safety Monitoring Board.

Eligibility criteria. Eligible patients were age ≥ 18 years with at least moderately active SLE, as defined by an SLE Disease Activity Index 2000 (SLEDAI-2K) score of ≥ 6 , met at least 4 of the American College of Rheumatology revised classification criteria for SLE (21,22), had a disease duration of ≥ 6 months, and were positive for antinuclear antibody (titer $\geq 1:80$ on HEp-2 cell substrate) and/or anti-double-stranded DNA (anti-dsDNA) antibody (≥ 30 IU/ml) at screening. Up-to-date vaccinations against *Streptococcus pneumoniae* and influenza virus were required (could be given during screening). Patients with severe glomerulonephritis (urine protein-to-creatinine ratio > 2.0 mg/mg and/or estimated glomerular filtration rate < 40 ml/minute/1.73 m²) and those with major central nervous system manifestations were excluded. (For further eligibility criteria, see Supplementary Text 2, available at <http://onlinelibrary.wiley.com/doi/10.1002/art.40360/abstract>.)

All patients provided written informed consent. The study was performed in accordance with the Declaration of Helsinki, the International Conference on Harmonisation Note for Guidance on Good Clinical Practice (ICH Topic E6, 1996), and applicable regulatory requirements. All study sites received approval for the study from their local ethics board.

Randomization. An interactive web response system was used to randomize the patients 1:1:1 to either of 3 study arms. Randomization was stratified according to the SLEDAI-2K total score (6–9 versus ≥ 10), race (black/African American versus other), and use of mycophenolate mofetil at screening.

Assessment of end points. The primary end point was the SLE Responder Index 4 (SRI-4) (17,18) without clinically significant use of nonpermitted medication or treatment at week 24 compared with the screening visit. The SRI-4 is a composite end point that includes SLEDAI-2K score ≥ 4 point reduction; $< 10\%$ increase in physician's global assessment; no new organ with British Isles Lupus Assessment Group (BILAG) [2004] A (severe) disease, and no more than 1 new BILAG B (moderate) organ score.

Key secondary end points were corticosteroid dosage reduction and patient's global assessment of change at 24 weeks. (For complete details, see Supplementary Text 3, available at <http://onlinelibrary.wiley.com/doi/10.1002/art.40360/abstract>.) Other disease activity end points were severe flares, as assessed by the Safety of Estrogens in Lupus Erythematosus National Assessment (SELENA) version of the SLEDAI (the SELENA-SLEDAI flare index [SFI]) or by a new BILAG A (severe) manifestation (23). An evaluation of the SRI-6 in the predefined high disease activity (HDA) subpopulation (SLEDAI-2K score ≥ 10 at screening) was performed.

Assessment of biomarkers. Biomarker assessments included serum concentrations of IgG, IgM, and IgA, complement C3 and C4 (measured using Tina-Quant complement C4 and C3c tests; Roche Diagnostics), and anti-dsDNA antibodies (measured by enzyme-linked immunosorbent assay; Phadia).

Assessment of safety. Safety was assessed according to the findings on the physical examination, vital signs measurements, electrocardiograms, and clinical laboratory tests. Reports of adverse events (AEs) and serious AEs were also evaluated.

Statistical analysis. Assuming a 30% response rate with placebo and a 2-sided alpha value of 0.05, a total of 93 patients per arm would provide 80% power to detect a 20% absolute difference in the proportion of patients achieving an SRI-4 response for each of the 2 active drug groups versus placebo. With the 1:1:1 randomization ratio, the planned total sample size was therefore 279.

Data analysis was planned for the following populations: intent-to-treat (ITT; all randomized patients), modified ITT (all randomized patients who received at least 1 dose of study medication, whether atacept or placebo), safety (all

randomized patients who received at least 1 dose of study medication, whether atacept or placebo, and were analyzed according to actual treatment received), and HDA (a subgroup of the modified ITT population with a SLEDAI-2K score of ≥ 10 at screening). The primary efficacy analysis was performed using the modified ITT population. Step-down sequential testing was used to control for multiplicity in testing the 2 atacept doses. The atacept 150-mg arm was to be first compared with placebo (primary analysis; 2-sided $\alpha = 0.05$) and, if statistically significant, the atacept 75-mg arm was compared with placebo. Prespecified sensitivity analyses

Table 1. Demographic features and clinical characteristics at screening (intent-to-treat population)*

	Placebo (n = 100)	Atacept	
		75 mg (n = 102)	150 mg (n = 104)
Age, mean \pm SD years	40 \pm 13.0	37 \pm 11.2	39 \pm 11.6
Sex, no. (%)			
Female	90 (90)	93 (91.2)	97 (93.3)
Male	10 (10)	9 (8.8)	7 (6.7)
Race, no. (%)			
White	78 (78.0)	72 (70.6)	66 (63.5)
Black/African American	5 (5.0)	6 (5.9)	9 (8.7)
Asian	7 (7.0)	15 (14.7)	14 (13.5)
Native American or Alaska Native	4 (4.0)	3 (2.9)	4 (3.8)
Native Hawaiian or other Pacific Islander	1 (1.0)	0 (0.0)	0 (0.0)
Other	5 (5.0)	6 (5.9)	11 (10.6)
Hispanic or Latino ethnicity, no. (%)	57 (57.0)	51 (50.0)	45 (43.3)
Geographic region			
Europe	26 (26.0)	23 (22.5)	30 (28.8)
Asia	5 (5.0)	12 (11.8)	10 (9.6)
North America	22 (22.0)	21 (20.6)	20 (19.2)
Central and South America	47 (47.0)	46 (45.1)	44 (42.3)
Disease duration, mean \pm SD years	6.79 \pm 7.648	6.77 \pm 6.854	6.93 \pm 6.954
SLEDAI-2K			
Mean \pm SD score	10 \pm 2.8	10 \pm 3.3	10 \pm 3.0
No. (%) with score of ≥ 10	52 (52.0)	54 (52.9)	51 (49.0)
Physician's global assessment score, mean \pm SD	1.50 \pm 0.452	1.42 \pm 0.532	1.46 \pm 0.460
BILAG 2004 1A or 2B score, no. (%)	60 (60.0)	57 (55.9)	72 (69.2)
Serologically active disease†	29 (29.0)	29 (28.4)	26 (25.0)
Medications			
Corticosteroid (prednisone equivalent)			
Mean \pm SD dose, mg/day	9.40 \pm 7.503	10.18 \pm 8.898	9.41 \pm 7.417
No. (%) taking >7.5 mg/day	54 (54.0)	56 (54.9)	55 (52.9)
Antimalarial drug, no. (%)	78 (78.0)	75 (73.5)	80 (76.9)
Immunosuppressive drug, no. (%)			
Azathioprine	20 (20.0)	20 (19.6)	21 (20.2)
Methotrexate	18 (18.0)	12 (11.8)	13 (12.5)
Mycophenolate mofetil	16 (16.0)	16 (15.7)	18 (17.3)
Other‡	0 (0.0)	1 (1.0)	3 (2.9)
Serum biomarkers			
ANA titer $\geq 1:80$, no. (%)	96 (96.0)	99 (97.1)	98 (94.2)
Anti-dsDNA ≥ 15 IU/ml, no. (%)	47 (47.0)	51 (50.0)	49 (47.1)
Complement, no. (%) under LLN			
C3 <0.9 gm/liter	32 (32.0)	36 (35.3)	33 (31.7)
C4 <0.1 gm/liter	19 (19.0)	16 (15.7)	21 (20.2)
IgG, mean \pm SD gm/liter	14.2 \pm 4.64	13.9 \pm 4.66	15.0 \pm 5.52

* The intent-to-treat population consisted of all patients randomized into the study who received at least 1 dose of study medication. SLEDAI-2K = Systemic Lupus Erythematosus Disease Activity Index 2000; BILAG = British Isles Lupus Assessment Group; ANA = antinuclear antibody; LLN = lower limit of normal.

† Anti-double-stranded DNA (anti-dsDNA) antibody positivity (≥ 15 IU/ml) and low levels of complement (<0.9 gm/liter of C3 and/or <0.1 gm/liter of C4).

‡ Other immunosuppressive drugs were cyclosporine and leflunomide.

for the primary end point were conducted as follows: 1) using treatment day 1 as baseline (rather than the screening visit), 2) in the HDA subpopulation, and 3) in patient subgroups with serologically active disease (anti-dsDNA antibody level ≥ 15 IU/ml and low levels of complement [C3 < 0.9 gm/liter and/or C4 < 0.1 gm/liter]).

Analyses of key secondary end points (corticosteroid dosage reduction and patient's global assessment of change at week 24) were performed in a hierarchical manner (first, the 150-mg dose versus placebo, then, the 75-mg dose versus placebo) to control for overall Type I error (2-sided $\alpha = 0.05$) but became exploratory if the primary end point was not met for either atacicept dose. All other secondary end points were analyzed descriptively using appropriate summary statistics.

All treatment effect tests were conducted at a 2-sided alpha level of 0.05. *P* values and 2-sided 95% confidence intervals (95% CIs) are presented where applicable. Binary end points were analyzed using logistic regression, adjusted for randomization stratification factors. Continuous end points were analyzed using analysis of covariance, adjusted for the baseline value and randomization stratification factors. Time to severe SLE flares was defined according to the BILAG and SFI flare indices separately, and analyzed using a Cox proportional hazard regression model adjusted for baseline stratification factors. Patients not experiencing severe flare were censored at time of last treatment.

RESULTS

Study population. A total of 306 patients were randomized to receive either placebo ($n = 100$), atacicept 75 mg ($n = 102$), or atacicept 150 mg ($n = 104$). Disposition of the study patients is shown in Supplementary Figure 3 (available at <http://onlinelibrary.wiley.com/doi/10.1002/art.40360/abstract>). All randomized patients ($n = 306$, the ITT population) received at least 1 dose of atacicept or placebo and were included in the modified ITT and safety analyses. Forty-four patients (14.4%) discontinued treatment prematurely after randomization (16.0% of the placebo group, 15.7% of the atacicept 75-mg group, and 11.5% of the atacicept 150-mg group). The main reasons for discontinuation were AEs (16 patients [36.4%]) or the patient's decision to withdraw ($n = 16$ patients [36.4%]). One patient was lost to follow-up.

The demographic features, disease characteristics and severity, and background medications at baseline were similar between groups, except that more patients in the atacicept 150-mg group than in the 75-mg group had BILAG 2004 1A or 2B scores at screening (Table 1). BILAG A and B organ system manifestations were mainly mucocutaneous and musculoskeletal (Supplementary Table 1, available at <http://onlinelibrary.wiley.com/doi/10.1002/art.40360/abstract>), and the most common SLEDAI-2K disease manifestations included arthritis, rash, and low levels of complement (Supplementary Table 2, available at <http://onlinelibrary.wiley.com/doi/10.1002/art.40360/abstract>).

In the ITT population, 84 patients (27.5%) had serologically active disease.

The HDA subpopulation included 158 patients (51.6%). Baseline BILAG A and B organ system and SLEDAI-2K manifestations were mainly balanced across treatment arms, although more patients in the atacicept 150-mg group than the 75-mg group experienced BILAG B mucocutaneous (76.5% versus 58.2%) and musculoskeletal (66.7% versus 56.4%) manifestations (Supplementary Table 1). Other clinical features of SLE in the HDA subpopulation were comparable to those in the ITT population, except for the following SLEDAI-2K manifestations, which were more frequent in HDA patients: low complement levels (50.0% versus 35.6%), anti-dsDNA antibody positivity (67.7% versus 48.0%), and proteinuria (14.6% versus 8.2%) (Supplementary Tables 1 and 2). Daily doses of corticosteroids at screening were similar in the ITT and HDA populations (Supplementary Table 3, available at <http://onlinelibrary.wiley.com/doi/10.1002/art.40360/abstract>).

SRI responses. *SRI-4 response.* In the primary efficacy analysis, there was a trend toward an improved SRI-4 response rate at week 24 with atacicept 75 mg (57.8%; adjusted odds ratio [OR] 1.78 [95% CI 1.01–3.12], $P = 0.045$) and atacicept 150 mg (53.8%; adjusted OR 1.56 [95% CI 0.89–2.72], $P = 0.121$) versus placebo (44.0%) (Table 2). Differences in treatment response versus placebo were observed from around week 16 (Figure 1A).

Since the primary end point was not met, all other analyses are considered exploratory. In a prespecified sensitivity analysis using day 1 as baseline, both atacicept doses improved SRI-4 response rates at week 24 in the ITT population ($P < 0.05$ for each comparison) (Supplementary Figure 4, available at <http://onlinelibrary.wiley.com/doi/10.1002/art.40360/abstract>). The serologically active patient subgroup achieved significantly higher SRI-4 response rates with both 75 mg (62.1% [adjusted OR 5.96 (95% CI 1.85–19.15)], $P = 0.003$) and 150 mg (61.5% [adjusted OR 7.49 (95% CI 2.12–26.44)], $P = 0.002$) of atacicept versus placebo (24.1%) at week 24 (Table 2). Furthermore, dose-dependent improvements in SRI-4 response rates were seen in the HDA subpopulation, with atacicept 150 mg improvement (62.7%) being significantly higher than placebo (42.3%) at week 24 (adjusted OR 2.44 [95% CI 1.09–5.44], $P = 0.029$) (Table 2). Improvement in treatment response was observed from week 4, and this increased to the end of treatment (Figure 1B).

SRI-6 response. In the HDA subpopulation, an SRI-6 response at week 24 occurred more frequently with atacicept 150 mg (54.9% [adjusted OR 3.31 (95% CI 1.44–7.61)], $P = 0.005$) versus placebo (28.8%) (Table 2).

Table 2. SRI responder rates at week 24*

Population	Response rate, no. (%)			Atacicept 75 mg versus placebo response			Atacicept 150 mg versus placebo response		
	Placebo	Atacicept 75 mg	Atacicept 150 mg	Treatment effect size, %	Adjusted OR (95% CI)	P	Treatment effect size, %	Adjusted OR (95% CI)	P
ITT population†									
No. of patients	100	102	104						
SRI-4 score	44 (44.0)	59 (57.8)	56 (53.8)	13.8	1.78 (1.01–3.12)	0.045	9.8	1.56 (0.89–2.72)	0.121
SRI-6 score	30 (30.0)	32 (31.4)	38 (36.5)	1.4	1.08 (0.59–1.98)	0.810	6.5	1.44 (0.79–2.62)	0.230
No. serologically active	29	29	26						
SRI-4 score	7 (24.1)	18 (62.1)	16 (61.5)	37.9	5.96 (1.85–19.15)	0.003	37.4	7.49 (2.12–26.44)	0.002
SRI-6 score	4 (13.8)	13 (44.8)	12 (46.2)	31.0	5.48 (1.49–20.13)	0.010	32.4	6.45 (1.66–25.06)	0.007
HDA population‡									
No. of patients	52	55	51						
SRI-4 score	22 (42.3)	33 (60.0)	32 (62.7)	17.7	2.11 (0.97–4.59)	0.060	20.4	2.44 (1.09–5.44)	0.029
SRI-6 score	15 (28.8)	24 (43.6)	28 (54.9)	14.8	1.98 (0.88–4.46)	0.098	26.1	3.31 (1.44–7.61)	0.005
No. serologically active	24	25	20						
SRI-4 score	6 (25.0)	16 (64.0)	13 (65.0)	39.0	5.97 (1.70–21.02)	0.005	40.0	7.72 (1.88–31.67)	0.005
SRI-6 score	4 (16.7)	12 (48.0)	11 (55.0)	31.3	4.88 (1.28–18.64)	0.020	38.3	7.31 (1.71–31.28)	0.007

* The Systemic Lupus Erythematosus Responder Index 4 (SRI-4) score represents a ≥ 4 -point reduction, and the SRI-6 score represents a ≥ 6 -point reduction, in the score on the Safety of Estrogens in Lupus Erythematosus National Assessment (SELENA) version of the SLEDAI, with no new BILAG domain score or no more than 1 new BILAG B domain score, and no deterioration from baseline of >0.3 points in the physician's global assessment. Serologically active was defined as the anti-dsDNA antibody positivity (≥ 15 IU/ml) and low levels of complement (<0.9 gm/liter of C3 and/or <0.1 gm/liter of C4). Adjusted odds ratios (ORs), 95% confidence intervals (95% CIs), and *P* values were estimated from a logistic regression model and adjusted for prespecified covariates. See Table 1 for other definitions.

† The intent-to-treat (ITT) population consisted of all patients randomized into the study who received at least 1 dose of study medication.

‡ The high disease activity (HDA) population consisted of all patients with a SLEDAI-2K score of ≥ 10 at screening.

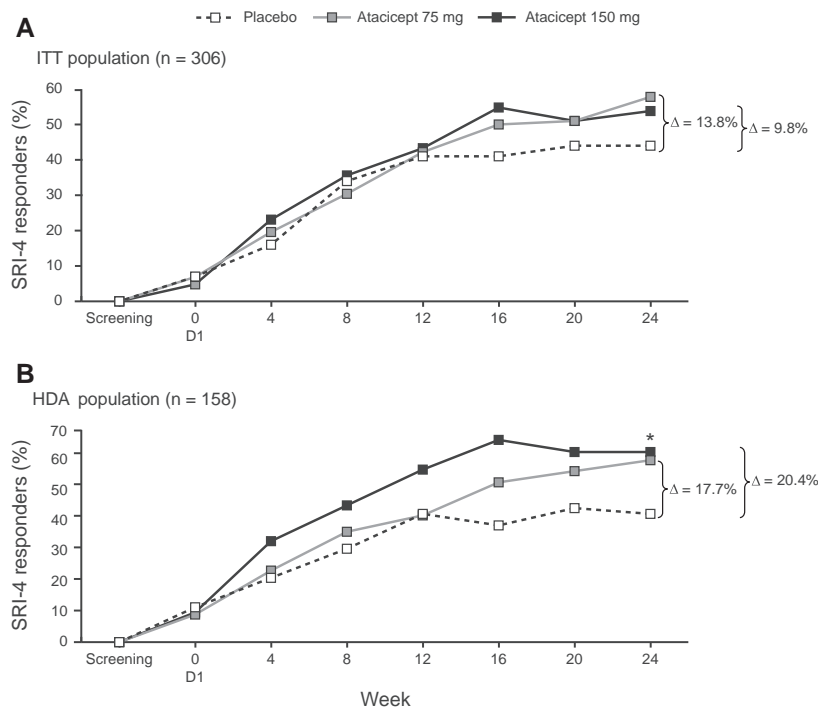


Figure 1. Effect of atacicept on the disease response of patients with systemic lupus erythematosus (SLE), as determined by the SLE Responder Index 4 (SRI-4). **A**, Proportion of SRI-4 responders in the intent-to-treat (ITT) population. **B**, Proportion of SRI-4 responders in the high disease activity (HDA) subpopulation. Values at the right are the effect size (Δ) for the indicated treatment groups. * = $P < 0.05$ versus placebo. D1 = treatment day 1.

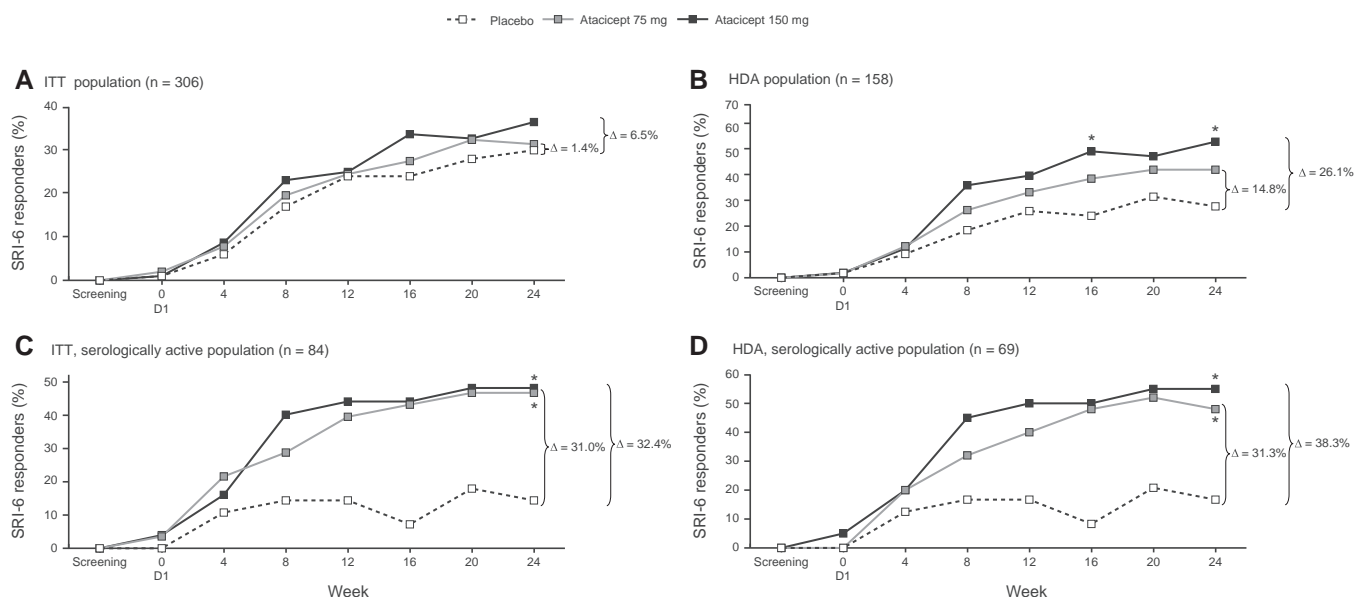


Figure 2. Effect of atacept on the disease response of patients with systemic lupus erythematosus (SLE), as determined by the SLE Responder Index 6 (SRI-6). **A**, Proportion of SRI-6 responders in the intent-to-treat (ITT) population. **B**, Proportion of SRI-6 responders in the high disease activity (HDA) subpopulation. **C**, Proportion of SRI-6 responders in the serologically active subgroup (anti-double-stranded DNA [anti-dsDNA] antibody positive [≥ 15 IU/ml] and low levels of complement) of the ITT population. **D**, Proportion of SRI-6 responders in the serologically active subgroup (anti-dsDNA antibody positive and low levels of complement) of the HDA subpopulation. * = $P < 0.05$ versus placebo. D1 = treatment day 1.

Separation of treatment effects was observed as early as week 8 and attained a significant difference by week 16 (Figure 2B). The effect was not significant at week 24 in the ITT population (Figure 2A). The treatment effect size was pronounced in the patients with serologically active disease, both in the ITT population and in the HDA population (Table 2 and Figures 2C and D). Similarly, a subgroup of patients within the HDA subpopulation who were positive for anti-dsDNA antibody, had low complement levels, or both at baseline achieved a 30.6% increase in the SRI-6 response rate with atacept 150 mg treatment versus placebo.

Modified SRI-4 and SRI-6 response rates excluding anti-dsDNA antibodies and complement levels. Although the treatment effect size (Δ) for atacept versus placebo was lower after these SLEDAI serologic parameters were excluded from the calculation of improvement in the SLEDAI-2K score, differences between atacept 150 mg and placebo were still apparent in the HDA subpopulation. For the modified SRI-4, the values ranged from $\Delta 16.5\%$ in HDA patients to $\Delta 23.2\%$ in HDA patients who had anti-dsDNA antibodies or low complement levels at screening. For the modified SRI-6, the values ranged from $\Delta 18.2\%$ in HDA patients to $\Delta 21.8\%$ in HDA patients who had anti-dsDNA antibodies or low complement levels at screening (Supplementary Table 4, available at <http://onlinelibrary.wiley.com/doi/10.1002/art.40360/abstract>).

Severe disease flares. In the ITT population, the incidence of severe disease flares was reduced with atacept 75 mg according to the incidence of new BILAG A manifestation (Figure 3A) and with atacept 150 mg according to the SFI (2.9% versus 14.0% with placebo; hazard ratio (HR) 0.18 [95% CI 0.05–0.62], $P = 0.002$). The impact on disease flare was more pronounced in the HDA subpopulation: both atacept doses led to reductions in severe flares according to both the incidence of a new BILAG A manifestation (Figure 3B) and the SFI (with 150 mg, HR 0.19 [95% CI 0.05–0.68], $P = 0.004$; with 75 mg, HR 0.33 [95% CI 0.12–0.94], $P = 0.029$) versus placebo (25.0%).

Findings of key secondary end points. Atacept 75 mg or 150 mg did not significantly increase the proportion of patients achieving a corticosteroid dosage reduction to ≤ 7.5 mg/day at week 24 versus placebo (17.9%, 11.3%, and 18.9%, respectively) in patients whose corticosteroid dosage was ≥ 10 mg/day at screening. Similarly, with atacept versus placebo, no difference was observed in the proportion of patients reporting the following 7 categories of change in the patient's global assessment: very much improved, much improved, minimally improved, no change, minimally worse, much worse, or very much worse at week 24 since beginning the treatment (data not shown).

Levels of biomarkers. In patients with low levels of serum complement C3 ($n = 101$) or C4 ($n = 56$) at

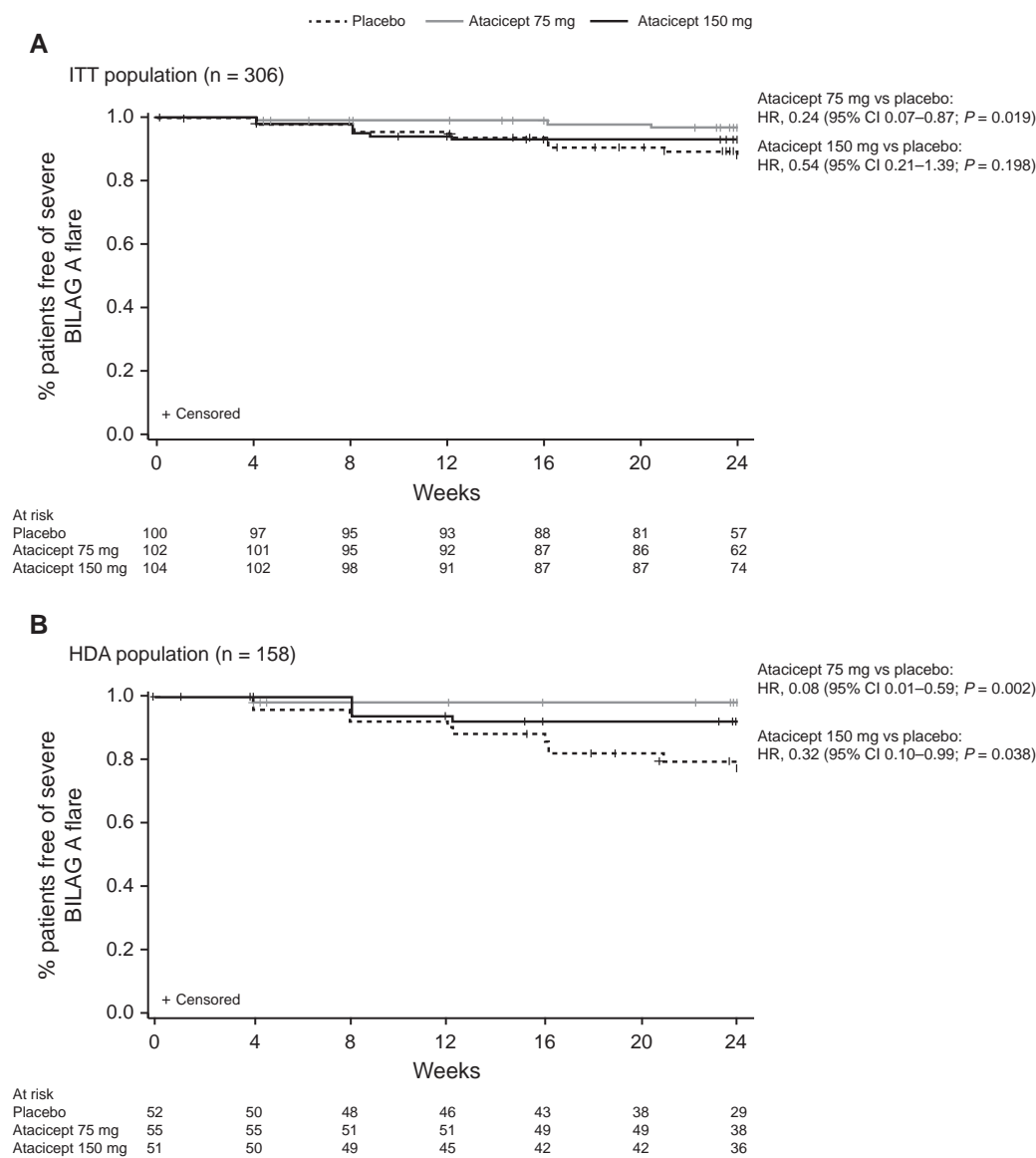


Figure 3. Kaplan-Meier analysis of time to first severe flare according to scores on the British Isles Lupus Assessment Group (BILAG) A grade manifestations. **A**, Intent-to-treat (ITT) population. **B**, High disease activity (HDA) subpopulation. Numbers across the bottom of the x-axes are the numbers of patients at the indicated time points. HR = hazard ratio; 95% CI = 95% confidence interval.

baseline, atacicept at either dosage led to a steady increase in serum C3 or C4 levels, respectively, from week 4 until week 24, but in the placebo group, the levels remained similar to baseline throughout the treatment period. At week 24, the median percentage increase in the serum C3 levels compared with baseline (treatment day 1) was 5.3% with atacicept 75 mg and 22.1% with atacicept 150 mg versus 1.5% with placebo. The median percentage increase in the serum C4 level was 64.5% with atacicept 75 mg and 128.6% with atacicept 150 mg (Figures 4A and B). In patients with a low C3 and/or C4 level

at baseline (n = 109), a normalized C3 and C4 level at week 24 was achieved in 52.6% and 30.6% taking atacicept 150 mg and 75 mg, respectively, versus 17.1% taking placebo.

In patients with anti-dsDNA antibodies at baseline (n = 147), both atacicept dosages reduced anti-dsDNA antibody levels over time. At week 24, the median percentage change versus baseline was –23.6% with atacicept 75 mg and –28.2% with atacicept 150 mg. Anti-dsDNA antibody levels increased by a median of 16.0% with placebo treatment (Figure 4C). Treatment with atacicept 150 mg

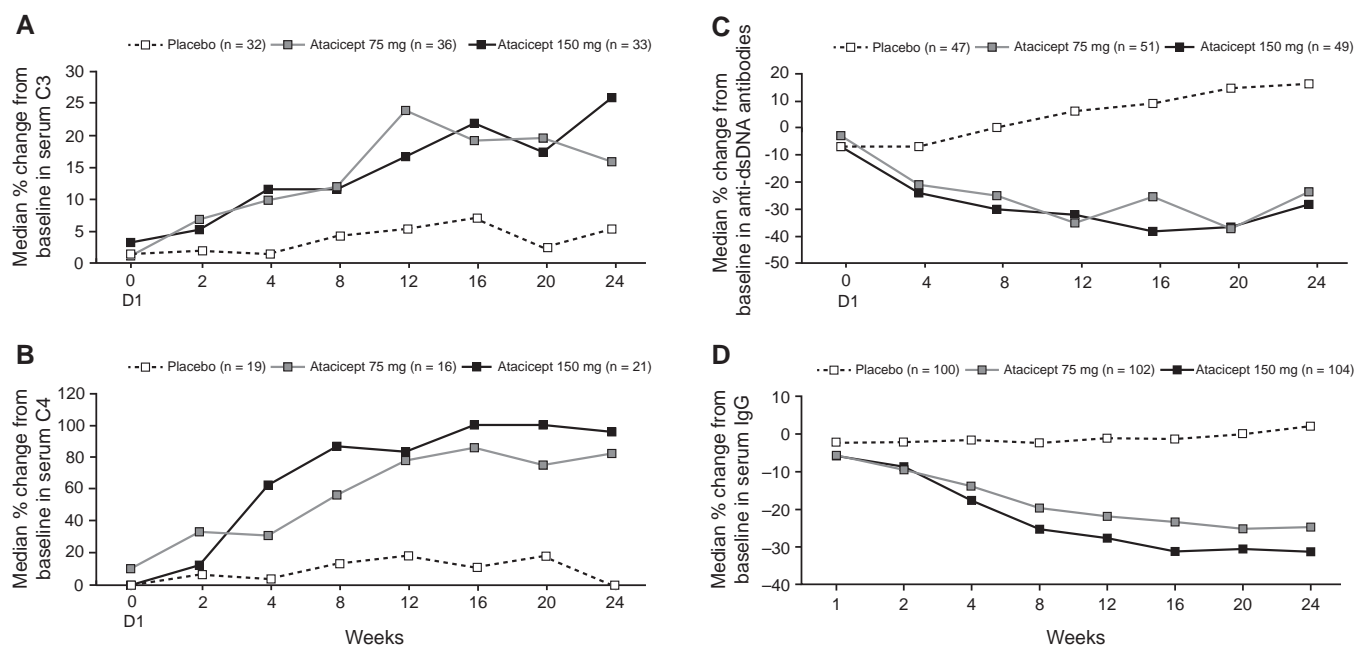


Figure 4. Changes in serum biomarkers over time. The median percentage change from baseline over 24 weeks is shown for **A**, serum complement C3 levels (C3-low patients), **B**, serum complement C4 levels (C4-low patients), **C**, anti-double-stranded DNA (anti-dsDNA) antibody levels (anti-dsDNA antibody-positive patients), and **D**, serum IgG levels.

and 75 mg increased the likelihood of not having a positive anti-dsDNA antibody result at week 24 as compared with placebo (30.6%, 19.6%, and 2.1%, respectively).

At week 24, serum IgG levels were reduced from baseline by ~30% and 25% with atacicept 150 and 75 mg, respectively (Figure 4D and Supplementary Figure 5, available at <http://onlinelibrary.wiley.com/doi/10.1002/art.40360/abstract>). There were no incidents of severe hypogammaglobulinemia (serum IgG <3 gm/liter). The median percentage reduction in the serum levels of IgA (~50% with 150 mg and ~45% with 75 mg) and IgM (~70% with 150 mg and ~60% with 75 mg) compared with baseline were of greater magnitude than the median percentage reduction in the serum level of IgG (Supplementary Figure 6, available at <http://onlinelibrary.wiley.com/doi/10.1002/art.40360/abstract>).

Safety. Rates of treatment-emergent AEs (TEAEs) were higher with atacicept 75 mg and 150 mg versus placebo (81.4%, 80.8%, and 72.0%, respectively). The most commonly reported AEs across treatment arms were injection site reactions, injection site pain, urinary tract infections, upper respiratory tract infections, and diarrhea (Supplementary Table 5, available at <http://onlinelibrary.wiley.com/doi/10.1002/art.40360/abstract>). Incidence rates of TEAEs were similar with atacicept 75 and 150 mg and placebo, except for upper respiratory tract infections (9.8%, 12.5%, and 3.0%, respectively) and diarrhea (6.9%, 11.5%, and 5.0%), which were more common with atacicept, and

urinary tract infections (11.8%, 11.5%, and 17.0%), which were more common with placebo. Other commonly reported infections with atacicept 75 and 150 mg included nasopharyngitis (4.9% and 6.7%), bronchitis (1.0% and 3.8%), and influenza (2.9% and 2.9%). Pneumonia occurred in 1 patient (1.0%) in each atacicept group. There were fewer serious TEAEs with atacicept 75 and 150 mg than with placebo (5.8%, 8.8%, and 12.0%, respectively). One patient treated with atacicept 150 mg (1%) reported a serious infection, compared with 5.9% treated with atacicept 75 mg and 5.0% treated with placebo.

The incidence of TEAEs leading to treatment discontinuation was comparable between study arms. Severe treatment-emergent injection site reactions were infrequent, occurring in 1 patient (1.0%) receiving atacicept 75 mg and 1 patient (1.0%) receiving placebo. There were no notable differences in clinical laboratory parameters (i.e., hematology, liver function tests) between either of the atacicept groups and placebo. No deaths occurred during the study. Immunogenicity was assessed predose and postdose: 7 patients in the atacicept 75-mg group and 1 patient in the atacicept 150-mg group had measurable antibodies to atacicept at week 24.

DISCUSSION

ADDRESS II compared the efficacy and safety of 2 doses of atacicept (75 and 150 mg) with placebo in

patients with active, autoantibody-positive SLE receiving standard treatment. The primary end point of an SRI-4 response at week 24 was not met in the ITT population, although there was a trend toward increased response rates with atacept. A more robust increase in the SRI-4 response rates for both atacept doses was observed in the sensitivity analysis in which day 1 was used as baseline. The treatment effect size according to the SRI-4 in the ITT population observed with atacept 150 mg versus placebo ($\Delta 9.8\%$ [adjusted OR 1.56] and $\Delta 14.8\%$ [adjusted OR 1.96] in the primary and sensitivity analyses, respectively) was similar to that observed with the highest dose of belimumab (10 mg/kg) in the 52-week BLISS-52 and BLISS-76 studies ($\Delta 14.0\%$ and $\Delta 9.7\%$, respectively) (17,18). Similar to the much larger BLISS studies, this trial was conducted on a background of standard care and included some adjustments in the steroid dosage, which protects the safety of the sickest subpopulations, but supports high SRI-4 response rates in the placebo group among patients with moderate disease, a tradeoff that may limit the effect size if there is a ceiling of response rates for targeted treatments in a heterogeneous disease.

We analyzed response in the stratified subpopulation of patients with HDA (SLEDAI-2K of ≥ 10 at baseline). Major treatment effects were observed with atacept 150 mg versus placebo according to both the SRI-4 ($\Delta 20.4\%$), a measure of clinically meaningful response, and the SRI-6 ($\Delta 26.1\%$), an end point that requires a greater response. Even with the greater threshold for an SRI-6 response in patients with severe disease, the response rate with atacept 150 mg remained high (54.9%). These findings are consistent with the findings of subgroup analyses in blisibimod and belimumab studies that demonstrated an increased treatment effect in patients with HDA (24,25). These data suggest that when the target population is patients with HDA, there is a greater likelihood of discriminating an effective treatment from placebo, and this may have implications for future trial designs.

Serologic activity also defined a subpopulation with increased responsiveness to belimumab (18,24). We observed increased treatment effect sizes for SRI-4 and SRI-6 with atacept in patients with serologically active disease, both in the ITT and HDA populations, consistent with the roles played by BLyS in B cell proliferation and maturation, autoantibody production, and thus, disease pathogenesis (16,26–28). Since serologic normalization can lead to a potential 4-point improvement in the SLEDAI score (potentially accounting for achievement of an SRI-4 response without clinical improvement), the extent to which serologic effects contributed to SRI response rates in these populations was examined by excluding serologic data from the SRI assessment.

Despite reductions in treatment effect sizes, response differences were still pronounced, confirming that atacept treatment led to both clinical and serologic improvements.

Consistent with the post hoc analysis of the APRIL-SLE study, in which flare rates were reduced with atacept 150 mg (29), we observed reductions in the incidence of new, severe BILAG A scores and SFI severe flares with atacept versus placebo in both the ITT population and the HDA subpopulation. Atacept has therefore demonstrated consistent flare reduction in 2 studies.

The biomarker results were comparable with those previously observed in studies of atacept, including the APRIL-SLE study (29–31). Reduced serum immunoglobulin and anti-dsDNA autoantibody levels and increased complement levels were apparent soon after administration of atacept and continued to the end of treatment. The magnitude of changes appeared to be greater than those reported for agents targeting BLyS alone (17,18,25,32). This is consistent with the role of APRIL in plasma cell survival (33,34), antibody production, and potentially, associated complement consumption.

The safety profile of atacept was acceptable. Compared with placebo, there was no increase in the overall frequency of serious AEs or in the subset of serious infections associated with active treatment. Reassuringly, there were no cases of severe hypogammaglobulinemia and no deaths. The atacept 150 mg treatment arm of the APRIL-SLE study was prematurely terminated as a cautionary measure, as recommended by the Independent Data Monitoring Committee, following 2 deaths from pulmonary infections complicated by pulmonary alveolar hemorrhage. Although most large clinical trials of new therapy in SLE report similar small numbers of deaths (17,18,24,25,32), several additional risk-mitigation measures were established for the ADDRESS II study in response to these fatal infection outcomes. These included requirements for medical monitor review of the patients' screening data to confirm eligibility as well as up-to-date vaccinations against pneumococcus and seasonal influenza (could be administered during the screening period up to 2 weeks prior to randomization). These measures may have minimized the risk of serious infections in this study population.

Potential limitations of the study include the low proportion of black/African American patients enrolled and the 24-week duration. Future studies will be needed to evaluate responses in patients from populations with renal and/or central nervous system disease and populations known to be at high risk of developing lupus and experiencing poor outcomes. More prolonged atacept treatment may have provided more reliable efficacy discrimination, and it will be important to assess the safety of

longer-term treatment with atacicept. Completers of this 24-week study were offered enrollment in a long-term extension study, the results of which will be reported as soon as they are available.

In summary, although this phase IIb study did not meet its primary end point, there was robust discrimination between atacicept and placebo treatments in multiple end points, particularly in subpopulations with serologic activity and/or high levels of disease activity. There was no increase in the risk of serious AEs, including serious infections, in patients treated with atacicept. These results support further clinical evaluation of atacicept in SLE.

ACKNOWLEDGMENTS

The authors thank the patients and their families, as well as the ADDRESS II study team, for their participation.

AUTHOR CONTRIBUTIONS

All authors were involved in drafting the article or revising it critically for important intellectual content, and all authors approved the final version to be published. Dr. Merrill had full access to all of the data in the study and takes responsibility for the integrity of the data and the accuracy of the data analysis.

Study conception and design. Merrill, Fraser, Isenberg.

Acquisition of data. Merrill, Kao, Fraser.

Analysis and interpretation of data. Merrill, Wallace, Wax, Kao, Fraser, Chang, Isenberg.

ROLE OF THE STUDY SPONSOR

EMD Serono, Inc., a division of Merck KGaA (Darmstadt, Germany), was involved in the study design, the collection, analysis, and interpretation of the data, and the writing of the manuscript. EMD Serono (including EMD Serono authors) and all other authors approved the final version of the manuscript and were involved in the final decision to submit the manuscript for publication. Writing assistance was provided by the Bioscript Group (Macclesfield, UK, a scientific communications group) and was directed and supported by EMD Serono, Inc.

REFERENCES

1. Rekvig OP, Van der Vlag J. The pathogenesis and diagnosis of systemic lupus erythematosus: still not resolved. *Semin Immunopathol* 2014;36:301–11.
2. Bertsias G, Cervera R, Boumpas D. Systemic lupus erythematosus: pathogenesis and clinical features. 2012. URL: http://www.eular.org/myuploaddata/files/sample%20chapter20_mod%2017.pdf.
3. Lisnevskaja L, Murphy G, Isenberg D. Systemic lupus erythematosus. *Lancet* 2014;384:1878–88.
4. Bertsias G, Ioannidis JP, Boletis J, Bombardieri S, Cervera R, Dostal C, et al. EULAR recommendations for the management of systemic lupus erythematosus: report of a task force of the EULAR Standing Committee for International Clinical Studies Including Therapeutics. *Ann Rheum Dis* 2008;67:195–205.
5. Bernatsky S, Boivin JF, Joseph L, Manzi S, Ginzler E, Gladman DD, et al. Mortality in systemic lupus erythematosus. *Arthritis Rheum* 2006;54:2550–7.
6. Cervera R, Khamashta MA, Font J, Sebastiani GD, Gil A, Lavilla P, et al. Morbidity and mortality in systemic lupus erythematosus during a 10-year period: a comparison of early and late manifestations in a cohort of 1,000 patients. *Medicine (Baltimore)* 2003;82:299–308.
7. Lateef A, Petri M. Unmet medical needs in systemic lupus erythematosus. *Arthritis Res Ther* 2012;14 Suppl 4:S4.
8. Schmeding A, Schneider M. Fatigue, health-related quality of life and other patient-reported outcomes in systemic lupus erythematosus. *Best Pract Res Clin Rheumatol* 2013;27:363–75.
9. Gordon C, Isenberg D, Lerstrom K, Norton Y, Nikai E, Pushparajah DS, et al. The substantial burden of systemic lupus erythematosus on the productivity and careers of patients: a European patient-driven online survey. *Rheumatology (Oxford)* 2013;52:2292–301.
10. Thamer M, Hernan MA, Zhang Y, Cotter D, Petri M. Prednisone, lupus activity, and permanent organ damage. *J Rheumatol* 2009;36:560–4.
11. Salazar-Camarena DC, Ortiz-Lazareno PC, Cruz A, Oregon-Romero E, Machado-Contreras JR, Munoz-Valle JF, et al. Association of BAFF, APRIL serum levels, BAFF-R, TACI and BCMA expression on peripheral B-cell subsets with clinical manifestations in systemic lupus erythematosus. *Lupus* 2016;25:582–92.
12. Hegazy M, Darwish H, Darweesh H, El-Shehaby A, Emad Y. Raised serum level of APRIL in patients with systemic lupus erythematosus: correlations with disease activity indices. *Clin Immunol* 2010;135:118–24.
13. McCarthy EM, Lee RZ, Ni Gabhann J, Smith S, Cunnane G, Doran MF, et al. Elevated B lymphocyte stimulator levels are associated with increased damage in an Irish systemic lupus erythematosus cohort. *Rheumatology (Oxford)* 2013;52:1279–84.
14. Zhang J, Roschke V, Baker KP, Wang Z, Alarcon GS, Fessler BJ, et al. Cutting edge: a role for B lymphocyte stimulator in systemic lupus erythematosus. *J Immunol* 2001;166:6–10.
15. Stohl W, Metyas S, Tan SM, Cheema GS, Oamar B, Roschke V, et al. Inverse association between circulating APRIL levels and serological and clinical disease activity in patients with systemic lupus erythematosus. *Ann Rheum Dis* 2004;63:1096–103.
16. Koyama T, Tsukamoto H, Miyagi Y, Himeji D, Otsuka J, Miyagawa H, et al. Raised serum APRIL levels in patients with systemic lupus erythematosus. *Ann Rheum Dis* 2005;64:1065–7.
17. Navarra SV, Guzmán RM, Gallacher AE, Hall S, Levy RA, Jimenez RE, et al, for the BLISS-52 Study Group. Efficacy and safety of belimumab in patients with active systemic lupus erythematosus: a randomised, placebo-controlled, phase 3 trial. *Lancet* 2011;377:721–31.
18. Furie R, Petri M, Zamani O, Cervera R, Wallace DJ, Tegzová D, et al. A phase III, randomized, placebo-controlled study of belimumab, a monoclonal antibody that inhibits B lymphocyte stimulator, in patients with systemic lupus erythematosus. *Arthritis Rheum* 2011;63:3918–30.
19. Dall'Era M, Chakravarty E, Wallace D, Genovese M, Weisman M, Kavanaugh A, et al. Reduced B lymphocyte and immunoglobulin levels after atacicept treatment in patients with systemic lupus erythematosus: results of a multicenter, phase Ib, double-blind, placebo-controlled, dose-escalating trial. *Arthritis Rheum* 2007;56:4142–50.
20. Pena-Rossi C, Nasonov E, Stanislav M, Yakusevich V, Ershova O, Lomareva N, et al. An exploratory dose-escalating study investigating the safety, tolerability, pharmacokinetics and pharmacodynamics of intravenous atacicept in patients with systemic lupus erythematosus. *Lupus* 2009;18:547–55.
21. Tan EM, Cohen AS, Fries JF, Masi AT, McShane DJ, Rothfield NF, et al. The 1982 revised criteria for the classification of systemic lupus erythematosus. *Arthritis Rheum* 1982;25:1271–7.
22. Hochberg MC. Updating the American College of Rheumatology revised criteria for the classification of systemic lupus erythematosus. *Arthritis Rheum* 1997;40:1725.

23. Isenberg DA, Rahman A, Allen E, Farewell V, Akil M, Bruce IN, et al. BILAG 2004: development and initial validation of an updated version of the British Isles Lupus Assessment Group's disease activity index for patients with systemic lupus erythematosus. *Rheumatology (Oxford)* 2005;44:902–6.
24. Van Vollenhoven RF, Petri MA, Cervera R, Roth DA, Ji BN, Kleoudis CS, et al. Belimumab in the treatment of systemic lupus erythematosus: high disease activity predictors of response. *Ann Rheum Dis* 2012;71:1343–9.
25. Furie RA, Leon G, Thomas M, Petri MA, Chu AD, Hislop C, et al. A phase 2, randomised, placebo-controlled clinical trial of blisibimod, an inhibitor of B cell activating factor, in patients with moderate-to-severe systemic lupus erythematosus, the PEARL-SC study. *Ann Rheum Dis* 2015;74:1667–75.
26. Ota M, Duong BH, Torkamani A, Doyle CM, Gavin AL, Ota T, et al. Regulation of the B cell receptor repertoire and self-reactivity by BAFF. *J Immunol* 2010;185:4128–36.
27. Yu G, Boone T, Delaney J, Hawkins N, Kelley M, Ramakrishnan M, et al. APRIL and TALL-I and receptors BCMA and TACI: system for regulating humoral immunity. *Nat Immunol* 2000;1:252–6.
28. Ju S, Zhang D, Wang Y, Ni H, Kong X, Zhong R. Correlation of the expression levels of BLyS and its receptors mRNA in patients with systemic lupus erythematosus. *Clin Biochem* 2006;39:1131–7.
29. Isenberg D, Gordon C, Licu D, Copt S, Rossi CP, Wofsy D. Efficacy and safety of atacicept for prevention of flares in patients with moderate-to-severe systemic lupus erythematosus (SLE): 52-week data (APRIL-SLE randomised trial). *Ann Rheum Dis* 2015;74:2006–15.
30. Van Vollenhoven RF, Kinnman N, Vincent E, Wax S, Bathon J. Atacicept in patients with rheumatoid arthritis and an inadequate response to methotrexate: results of a phase II, randomized, placebo-controlled trial. *Arthritis Rheum* 2011;63:1782–92.
31. Van Vollenhoven RF, Wax S, Li Y, Tak PP. Safety and efficacy of atacicept in combination with rituximab for reducing the signs and symptoms of rheumatoid arthritis: a phase II, randomized, double-blind, placebo-controlled pilot trial. *Arthritis Rheumatol* 2015;67:2828–36.
32. Isenberg DA, Petri M, Kalunian K, Tanaka Y, Urowitz MB, Hoffman RW, et al. Efficacy and safety of subcutaneous tabalumab in patients with systemic lupus erythematosus: results from ILLUMINATE-1, a 52-week, phase III, multicentre, randomised, double-blind, placebo-controlled study. *Ann Rheum Dis* 2016;75:323–31.
33. Benson MJ, Dillon SR, Castigli E, Geha RS, Xu S, Lam KP, et al. Cutting edge: the dependence of plasma cells and independence of memory B cells on BAFF and APRIL. *J Immunol* 2008;180:3655–9.
34. Belnoue E, Pihlgren M, McGaha TL, Tougne C, Rochat AF, Bossen C, et al. APRIL is critical for plasmablast survival in the bone marrow and poorly expressed by early-life bone marrow stromal cells. *Blood* 2008;111:2755–64.

Understanding the Antibody Repertoire in Neuropsychiatric Systemic Lupus Erythematosus and Neuromyelitis Optica Spectrum Disorder

Do They Share Common Targets?

Simone Mader,¹ Venkatesh Jeganathan,¹ Yoshiyuki Arinuma,² Yuichiro Fujieda,³ Irena Dujmovic,⁴ Jelena Drulovic,⁴ Yuka Shimizu,⁵ Yuko Sakuma,⁶ Joel N. H. Stern,⁷ Cynthia Aranow,¹ Meggan Mackay,¹ Shinsuke Yasuda,⁵ Tatsuya Atsumi,⁵ Shunsei Hirohata,⁶ and Betty Diamond¹

Objective. IgG anti-DWEYS antibodies cross-reactive with DNA and the *N*-methyl-D-aspartate receptor subunits GluN2A and GluN2B are known to be associated with neuropsychiatric systemic lupus erythematosus (NPSLE). IgG anti-DWEYS have not been investigated in demyelinating NPSLE or in another demyelinating disorder, neuromyelitis optica spectrum disorder (NMOSD), which is a disease also found mainly in young women and associated with aquaporin 4 (AQP-4) or myelin oligodendrocyte glycoprotein (MOG) antibodies. This study was undertaken to investigate the frequency of all of these brain-reactive antibodies in patients with NPSLE, those with demyelinating NPSLE, and those with NMOSD.

Supported by the NIH (grant P01-AI-073693 to Dr. Diamond) and the SLE Lupus Foundation (PhD Basic Science grant to Dr. Mader).

¹Simone Mader, PhD, Venkatesh Jeganathan, PhD, Cynthia Aranow, MD, Meggan Mackay, MD, Betty Diamond, MD: The Feinstein Institute for Medical Research, Manhasset, New York; ²Yoshiyuki Arinuma, MD: The Feinstein Institute for Medical Research, Manhasset, New York, and Kitasato University School of Medicine, Kanagawa, Japan; ³Yuichiro Fujieda, MD: The Feinstein Institute for Medical Research, Manhasset, New York, and Hokkaido University, Hokkaido, Japan; ⁴Irena Dujmovic, MD, Jelena Drulovic, MD: Clinical Center of Serbia University School of Medicine, Belgrade, Serbia; ⁵Yuka Shimizu, MD, Shinsuke Yasuda, MD, PhD, Tatsuya Atsumi: Hokkaido University, Hokkaido, Japan; ⁶Yuko Sakuma, Shunsei Hirohata, MD: Kitasato University School of Medicine, Kanagawa, Japan; ⁷Joel N. H. Stern, PhD: The Feinstein Institute for Medical Research, Manhasset, New York, and Hofstra Northwell School of Medicine, Hempstead, New York.

Drs. Mader and Jeganathan contributed equally to this work.

Address correspondence to Betty Diamond, MD, The Center of Autoimmune, Musculoskeletal and Hematopoietic Diseases, The Feinstein Institute for Medical Research, 350 Community Drive, Manhasset, NY 11030. E-mail: bdiamond@nshs.edu.

Submitted for publication July 7, 2017; accepted in revised form October 17, 2017.

Methods. Serum samples from patients with NPSLE (n = 108), patients with SLE without neuropsychiatric manifestations (n = 38), patients with NMOSD (n = 33), and healthy controls (n = 106) were assessed for the frequency of IgG anti-brain antibodies as well as IgG antibodies to AQP-4, MOG, GluN2A/GluN2B, and double-stranded DNA (dsDNA).

Results. Sera were positive for IgG anti-AQP-4 antibodies in 27 (82%) of 33 patients with NMOSD and 3 (27%) of 11 patients with demyelinating NPSLE, whereas all sera from patients with non-demyelinating NPSLE, patients with SLE, and healthy controls were negative for IgG anti-AQP-4. IgG anti-MOG were detected at high titers in 3 (50%) of 6 patients with NMOSD who were negative for IgG anti-AQP-4, and at low titers in 2 (18%) of 11 patients with demyelinating NPSLE and 1 (1%) of 97 patients with non-demyelinating NPSLE. IgG antibodies to dsDNA were present in 11 (33%) of 33 patients with NMOSD. Only 4 (12%) of 33 patients with NMOSD were positive for IgG anti-DWEYS, compared to 11 (29%) of 38 patients with SLE and 59 (55%) of 108 patients with NPSLE. IgG anti-DWEYS antibodies were present in 56 (58%) of 97 patients with non-demyelinating NPSLE and 3 (27%) of 11 patients with demyelinating NPSLE. Serum IgG brain-reactive antibodies were present at a similar frequency in patients with non-demyelinating NPSLE (72 [75%] of 96), those with demyelinating NPSLE (9 [82%] of 11), and those with SLE (32 [84%] of 38), but were less frequent in patients with NMOSD (20 [61%] of 33).

Conclusion. Patients with demyelinating NPSLE should be tested for IgG antibodies to AQP-4, MOG, and DWEYS. IgG anti-AQP-4 can be considered diagnostic

for NMOSD, whereas none of these antibodies appear to be diagnostic for demyelinating NPSLE. Moreover, IgG anti-dsDNA are present in patients with NMOSD but are not cross-reactive with IgG anti-DWEYS, indicating that the antigenic stimulus and mechanisms of tissue damage are potentially different between demyelinating NPSLE and NMOSD.

Systemic lupus erythematosus (SLE) is a chronic inflammatory disease that is characterized by the presence of various autoantibodies. Neuropsychiatric manifestations of SLE (NPSLE) can be very severe, and the diagnosis remains challenging. There are a variety of clinical presentations that include neurologic and psychiatric symptoms. Both an increased frequency of mortality and a diminished quality of life, in comparison to SLE patients without neuropsychiatric manifestations, are features that are associated with NPSLE (1). NPSLE is characterized by 19 neuropsychiatric syndromes, as defined by the American College of Rheumatology (ACR) 1999 nomenclature (2). The frequency of these neuropsychiatric symptoms among SLE patients can be challenging to evaluate, and the frequencies vary widely in different patient studies, ranging from an incidence of neuropsychiatric symptoms in as few as 10% of SLE patients to as many as 90% (3).

Attribution of symptoms to SLE is also complicated because specific biomarkers for NPSLE have yet to be identified. Many of the neuropsychiatric syndromes classified by the ACR are not unique to NPSLE and are also present in other autoimmune diseases. For example, demyelination syndrome in patients with NPSLE can result in clinical and imaging features similar to those found in multiple sclerosis (4). Thus, the diagnosis of NPSLE is based on a combination of psychiatric and neurologic testing, magnetic resonance imaging (MRI), electroencephalography, nerve conduction studies, and cerebrospinal fluid analysis (5). Postmortem brain studies in patients with NPSLE are rare, and the findings have suggested that there are a variety of different neuropathologic manifestations that can occur in patients with NPSLE, such as hemorrhage, cortical and subcortical atrophy, microinfarcts, and demyelination (6).

Results of previous studies have suggested that certain antibodies, such as anti-ribosomal P protein or antiphospholipid antibodies, anti-Sm antibodies, complement components, and immune complexes, may be responsible for emergence of some of the focal or diffuse neuropsychiatric symptoms observed in NPSLE (7–10). To date, more than 100 different antibodies have been reported in patients with SLE or NPSLE (11), of which some might be directly associated with the disease. The identification of specific antibodies showing a potential

association with discrete manifestations of NPSLE not only would facilitate early diagnosis and treatment, but also could result in increased understanding of disease pathogenesis and the development of therapeutic approaches with less severe immunosuppression.

Previously, investigators in our group demonstrated that antibodies against the amino acid sequence DWEYS, a consensus sequence in the extracellular domain of the GluN2A/GluN2B subunits of the neuronal *N*-methyl-D-aspartate (NMDA) receptor, can induce apoptosis of hippocampal neurons through excitotoxicity and have been linked to cognitive impairment in a mouse model (12). IgG anti-DWEYS antibodies in patients with SLE display cross-reactivity with double-stranded DNA (dsDNA) (13). Elevated titers of IgG anti-DWEYS are more frequently detected in patients with NPSLE than in healthy controls, and their presence is linked to spatial cognitive impairment (14,15). So far, there are no data addressing whether IgG anti-DWEYS have a role in demyelinating NPSLE, and it remains unknown whether these antibodies are also found in other neurologic diseases, such as neuromyelitis optica spectrum disorder (NMOSD), which is also a disease that mainly affects young women and which has characteristics that can overlap with those of demyelinating NPSLE (16). In addition, some patients with NMOSD have been shown to develop SLE, or vice versa.

NMOSD is an autoimmune disease characterized by damage to the central nervous system (CNS), directed primarily to astrocytes, and the presence of serum antibodies that bind to the astrocytic water channel protein aquaporin 4 (AQP-4) (17). Antibodies recognizing conformation-dependent epitopes of myelin oligodendrocyte glycoprotein (MOG) are found in a subgroup of patients with NMOSD who are negative for IgG anti-AQP-4 (18,19). NMOSD most commonly affects areas with high levels of AQP-4 expression, such as the brain, optic nerve, and spinal cord, often resulting in long-spanning, demyelinating spinal cord lesions and/or optic neuritis. Demyelination, particularly optic neuritis and myelitis, are also part of the spectrum of symptoms in NPSLE (2,20,21). Although demyelination can be related to SLE activity, it can sometimes be difficult to distinguish NPSLE from NMOSD. Case reports suggest that some patients with NMOSD develop SLE, and vice versa (2,16,22,23), raising the possibility of an overlap between the 2 diseases and making it difficult to distinguish whether the demyelination is part of SLE or NMOSD, or possibly both diseases.

In addition, IgG anti-dsDNA and IgG antinuclear antibodies (ANAs), both of which are diagnostic hallmarks of SLE, can also be found in NMOSD (24), although data on their frequency and role in NMOSD are

sparse. Unlike in SLE, it is not known whether anti-dsDNA antibodies in NMOSD are cross-reactive with the NMDA receptor and whether they are also linked to the cognitive impairment often observed in patients with NMOSD (25).

The purpose of this study was to understand the antibody repertoire in NPSLE, especially in patients with demyelinating NPSLE and patients with NMOSD, and to investigate the frequency of all brain-reactive antibodies that have been associated with both diseases. We also wanted to establish the frequency of antibodies that have been shown to be associated with NPSLE, such as dsDNA antibodies and ANAs as well as IgG anti-DWEYS antibodies, in patients with NMOSD. The frequency and staining patterns of these brain-reactive antibodies were assessed in comparison to patients with SLE without neuropsychiatric manifestations and healthy controls.

PATIENTS AND METHODS

Patients. Patients with NMOSD were recruited from the Clinic of Neurology, Clinical Center of Serbia in Belgrade ($n = 31$) and the Northwell Health System in New York ($n = 2$). All patients with NMOSD met the revised diagnostic criteria for NMOSD (26), and only patients without any clinical evidence of other autoimmune diseases were included in this study. Patients with SLE ($n = 38$) were recruited from the Feinstein Institute for Medical Research (FIMR) in New York or the Kitasato University School of Medicine in Japan ($n = 1$). All patients with SLE fulfilled the ACR revised classification criteria for SLE (27,28). Patients with active NPSLE or those with a history of NPSLE or other CNS events were excluded from the SLE group.

All patients with NPSLE were recruited in Japan, from the Kitasato University School of Medicine ($n = 60$) or at the Hokkaido University Graduate School of Medicine ($n = 31$), or were recruited from the Clinic of Neurology, Clinical Center of Serbia ($n = 17$). Patients with NPSLE fulfilled the ACR 1999 criteria for NPSLE (2). Demyelination in NPSLE was identified on the basis of MRI findings. All patients with demyelinating NPSLE met the ACR 1999 criteria for demyelination (2), and all had either transverse myelitis occurring at 2 different time points or transverse myelitis with white matter demyelination or optic neuropathy occurring at 2 different time points.

In addition, 106 healthy control subjects from the FIMR ($n = 7$), the Clinic of Neurology, Clinical Center of Serbia ($n = 23$), or the Bioreclamation/IVT bank ($n = 76$) were included in the analyses. The present study was approved by the Northwell Health Institutional Review Board. Blood samples were collected from patients with NMOSD, patients with SLE, and healthy controls according to protocols approved by the appropriate institutional review boards at each of the participating institutions.

All serum samples were stored at -20°C and thawed only once, to prevent freeze-thawing effects. Individuals provided informed consent through the appropriate institutional review boards. The investigators were blinded with regard to each patient's clinical information.

Cell-based assay for testing antibodies to AQP-4 and MOG. Antibodies to AQP-4 and MOG in the serum of all patients

and controls were assessed using live cell-based assays, as previously described (18,29). All serum samples were analyzed at $20\times$ and $40\times$ screening dilutions, using human HEK 293T cells transfected with AQP-4 (M23 AQP-4 isoform) or MOG. Non-transfected cells were used as negative controls, to exclude non-specific binding to HEK 293T cells. Antibody-positive samples were serially diluted, and the titers of each antibody were determined. High-titer IgG anti-MOG antibodies were defined as those with a titer of ≥ 80 times the mean value in healthy control serum.

For the detection of IgG anti-AQP-4 antibodies, cells transfected with the M23 isoform of AQP-4 were stained 72 hours following transfection. Briefly, cells were blocked with phosphate buffered saline (PBS)–10% fetal bovine serum (FBS), and then incubated with serum samples diluted in PBS–10% FBS for 1 hour at 4°C . Following washing steps with PBS–10% FBS, cells were incubated with Alexa 594–conjugated goat anti-human IgG (Life Technologies) diluted in PBS–10% FBS ($400\times$ dilution) for 30 minutes at room temperature. Following washing with PBS–10% FBS, the cells were stained with DAPI and analyzed using a fluorescence microscope. Nontransfected cells were used as a negative control, and dead cells were excluded from the analysis. For the detection of IgG anti-MOG antibodies, we performed the same protocol as for IgG anti-AQP-4, but analyzed the samples 24 hours after transfection.

Determination of dsDNA antibodies in serum samples. Serum IgG anti-dsDNA antibodies in patients and healthy controls were determined as described previously, with some modifications (13,14). Briefly, half-well plates (Costar) were dry-coated with calf thymus DNA ($400\text{ }\mu\text{g/ml}$; Sigma). In order to produce dsDNA, the sonicated calf thymus DNA was filtered through a $0.45\text{ }\mu\text{m}$ nitrocellulose Millex HA syringe filter (Millipore). The plates were blocked with 3% FBS and subsequently incubated with serum in $50\times$ and $100\times$ dilutions, followed by incubation with alkaline phosphatase (AP)–conjugated goat anti-human IgG ($1,000\times$ dilution; Southern Biotechnology). The plates were then developed with AP substrate (Sigma), and the optical density at an absorbance of 405 nm was read using an automated plate reader (Victor3; PerkinElmer). Positive and negative controls were included in each plate. Cutoff values were calculated as the mean plus 4 times the SD of values in healthy control serum; the mean plus 2 SD was used to define antibody-positive serum.

Determination of DWEYS peptide-reactive antibodies in serum samples. Serum IgG anti-DWEYS antibodies in patients and healthy controls were determined by enzyme-linked immunosorbent assay (ELISA), as previously described (13,14). Briefly, half-well ELISA plates (Costar) were coated with streptavidin ($2.5\text{ }\mu\text{g/ml}$; Southern Biotechnology) in bicarbonate buffer (pH 8.6) overnight at 4°C . The plates were blocked with 2% bovine serum albumin (BSA) in PBS for 1 hour at room temperature, followed by incubation with biotinylated DWEYS peptide ($5\text{ }\mu\text{g/ml}$; Anaspec) in 0.2% BSA. The plates were then incubated with the serum samples ($100\times$ dilution), followed by incubation with goat anti-human IgG conjugated to AP, diluted in 0.2% BSA ($1,000\times$ dilution), for 1 hour. Subsequently, the plates were developed with AP substrate (Sigma), and the optical density at an absorbance of 405 nm was read using an automated plate reader (Victor 3; PerkinElmer). As a quality control, the same serum samples, either positive or negative for IgG anti-DWEYS, were assayed in each plate. All samples were assayed in triplicate. Cutoff values were calculated as the mean

plus 4 times the SD of values in healthy control serum; the mean plus 2 SD was used to define antibody-positive serum.

Determination of ANAs in serum samples. ANAs in the serum from patients and healthy controls were determined using a QuantaLite ANA ELISA (Inova Diagnostics) following the manufacturer's instructions, with use of relevant positive and negative controls supplied by the kit. Briefly, the plates were blocked with 3% FBS–PBS and incubated with serum at 41× dilution, followed by incubation with AP-labeled IgG and subsequently with horseradish peroxidase substrate (included in the kit). The optical density, measured as the absorbance at 405 nm (expressed in arbitrary units, following the conversion specified by the manufacturer), was determined using an automated plate reader (Victor3; PerkinElmer). Cutoff values were calculated as the mean plus 4 times the SD of values in healthy control serum; the mean plus 2 SD was the cutoff used to define antibody-positive serum.

Determination of IgG anti-brain antibodies in serum samples. IgG anti-brain antibodies were analyzed in the same manner as previously described (30). Briefly, 12-week-old, unmanipulated C57BL/6 mice (Jackson Laboratories) were anesthetized with isoflurane. The mouse brains were isolated after perfusion with 4% paraformaldehyde (PFA), using cardiac perfusion. Each extracted brain was postfixed overnight in 4% PFA and then incubated with 30% sucrose for 48 hours at 4°C. The brains were transferred to OCT embedding medium on dry ice and frozen at –80°C. Sagittal sections (12 µm) of mouse brain were cut on a cryostat and frozen at –80°C. IgG anti-brain antibodies were analyzed in the serum of patients using a 100× dilution. Sections of the brain were washed 2 times with PBS and blocked with 3% BSA–4% goat serum diluted in PBS–0.1% Triton for 1 hour at room temperature. Subsequently, the sections were incubated with serum samples

using a 100× dilution for 1 hour at room temperature. Following 3 washing steps with PBS–Tween (10 minutes each), the slides were incubated with anti-human secondary antibodies, labeled with Alexa 488, for 1 hour at room temperature. Following washing, the slides were mounted with Dako mounting solution. As a quality control, we used the same positive and negative serum in each round of staining. In addition, a secondary antibody staining omitting the serum was included. All procedures in animals were approved by the FIMR Institutional Animal Care and Use Committee.

Statistical analysis. Statistical analyses of mean and SD values, median (range) values, and significance of group differences, as well as linear regression analyses were performed using GraphPad Prism version 5. Between-group comparisons were performed with the Kruskal-Wallis test, using Dunn's post hoc test for multiple comparisons, the Mann-Whitney *U* test, and the chi-square test. Statistical significance was defined as a 2-sided *P* value of less than or equal to 0.05, and Bonferroni corrections for multiple comparisons were applied when appropriate.

RESULTS

Specificity of IgG anti-AQP-4 antibodies for NMOSD, and detection in only a few patients with demyelinating NPSLE. IgG anti-AQP-4 antibodies were analyzed in patients with SLE, patients with NPSLE, patients with NMOSD, and a large set of healthy controls, using a live cell-based assay (29) (results in patients with demyelinating NPSLE are shown in Figure 1). All patients and healthy controls analyzed in this study were matched for sex

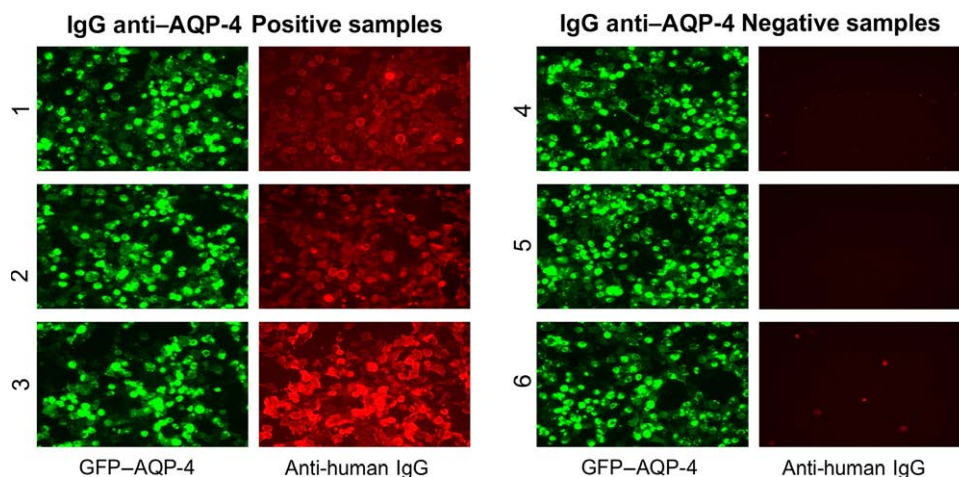


Figure 1. Cell-based assay for the detection of IgG anti-aquaporin 4 (anti-AQP-4) antibodies in patients with demyelinating neuropsychiatric systemic lupus erythematosus (NPSLE). Representative images of live cell-based assays show the detection of IgG anti-AQP-4 antibodies in the serum of 3 patients with demyelinating NPSLE (patients 1, 2, and 3), whereas no IgG anti-AQP-4 reactivity was seen in the serum of 3 other patients with demyelinating NPSLE (patients 4, 5, and 6). HEK 293T cells were transfected to express AQP-4 fused to green fluorescent protein (GFP) on the cell surface (GFP-AQP-4; green). Serum from patients with demyelinating NPSLE was added to the HEK 293T cells overexpressing GFP-AQP-4. Antibody testing was performed at serum dilutions of 1:20 and 1:40. Anti-human IgG was detected using an anti-human IgG secondary antibody (Alexa Fluor 594; red). IgG anti-AQP-4-negative serum samples show no costaining of anti-human IgG to the GFP-AQP-4-transfected cells. Dead cells were excluded by DAPI staining, and positive samples were also added to nontransfected cells, in which no antibody binding was observed (results not shown). IgG anti-AQP-4 antibody titers were determined by serial dilution of antibody-positive samples. Original magnification × 40.

Table 1. IgG anti-AQP-4 antibody serum status and titers in patients with NPSLE, patients with NMOSD, patients with SLE, and healthy controls*

	NPSLE			NMOSD (n = 33)	SLE (n = 38)	Healthy controls (n = 106)	P†
	All (n = 108)	Without demyelination (n = 97)	With demyelination (n = 11)				
IgG anti-AQP-4 positive, no. (%)	3 (3)	0 (0)	3 (27)	27 (82)	0 (0)	0 (0)	0.0056
IgG anti-AQP-4 titer, median (min-max)	320 (160-10,240)	—	320 (160-10,240)	1,280 (40-20,480)	—	—	—

* A live cell-based assay was used to detect antibodies recognizing conformation-dependent epitopes of the astrocyte water channel protein aquaporin 4 (AQP-4). IgG anti-AQP-4 serum status is presented as the number (%) of subjects with serum positivity for IgG anti-AQP-4 within each patient group (patients with neuropsychiatric systemic lupus erythematosus [NPSLE], in total and stratified by demyelination status, patients with neuromyelitis optica spectrum disorder [NMOSD], and patients with SLE without neuropsychiatric manifestations) and healthy controls. Titers of IgG anti-AQP-4 are presented as the median (minimum [min]–maximum [max]) in all IgG anti-AQP-4-positive groups.

† By chi-square test.

and age (details on the demographic characteristics of all subjects are available upon request from the corresponding author).

IgG anti-AQP-4 were found in the serum of 27 (82%) of 33 patients with NMOSD. In contrast, IgG anti-AQP-4 were detected in only 3 (3%) of 108 patients with NPSLE (Table 1). When we divided patients with NPSLE into those with and those without demyelination, IgG anti-AQP-4 were found in 3 (27%) of the 11 patients with demyelinating NPSLE (Table 1 and Figure 1), whereas none of the 97 patients with non-demyelinating NPSLE were positive for IgG anti-AQP-4. In addition, no IgG anti-AQP-4 antibodies were found in the 38 patients with SLE without neuropsychiatric manifestations or in the 106 healthy controls.

Serum anti-MOG antibodies detected in IgG anti-AQP-4-negative patients with NMOSD but rarely found in patients with NPSLE. A live cell-based assay (18) was used to detect antibodies recognizing conformation-dependent epitopes of MOG (Table 2) (further details available upon request from the corresponding author).

High-titer IgG anti-MOG antibodies (titer range 80–20,480) were detected only in patients with NMOSD who were negative for IgG anti-AQP-4 (3 [50%] of 6 patients). IgG anti-MOG antibodies expressed at lower titers (titer levels <80) were found in 2 (18%) of 11 patients with demyelinating NPSLE and in 1 (1%) of 97 patients with non-demyelinating NPSLE. In addition, 5 (5%) of 106 healthy controls exhibited low titers of IgG anti-MOG antibodies (median titer level 20).

Specificity of anti-NMDAR (GluN2A/GluN2B) antibodies for SLE and NPSLE, with none detected in patients with NMOSD or healthy controls. We investigated the presence of IgG anti-DWEYS antibodies by ELISA in the serum of patients and healthy controls (Figures 2A and B). There were no significant differences in the expression of IgG anti-DWEYS between healthy controls and patients with NMOSD. However, both in patients with SLE and in patients with NPSLE, significantly higher titers of IgG anti-DWEYS were observed (Figure 2A). There was no significant difference in the titers of IgG anti-DWEYS antibodies

Table 2. IgG anti-MOG antibody serum status and titers in patients with NPSLE, patients with NMOSD, patients with SLE, and healthy controls*

	NPSLE			NMOSD		SLE (n = 38)	Healthy controls (n = 106)	P†
	All (n = 108)	Without demyelination (n = 97)	With demyelination (n = 11)	IgG anti-AQP-4 negative (n = 6)	IgG anti-AQP-4 positive (n = 27)			
IgG anti-MOG positive, no. (%)	3 (3)	1 (1)	2 (18)	3 (50)	0 (0)	0 (0)	5 (5)	<0.0001
IgG anti-MOG titer, median (min-max)	20 (20-40)	40 (40)	20 (20)	1,280 (80-20,480)	—	—	20 (20)	—

* A live cell-based assay was used to detect antibodies recognizing conformation-dependent epitopes of myelin oligodendrocyte glycoprotein (MOG). IgG anti-MOG serum status is presented as the number (%) of subjects with serum positivity for IgG anti-MOG antibodies in patients with NPSLE (in total and stratified by demyelination status), patients with NMOSD (stratified by IgG anti-AQP-4 status), patients with SLE, and healthy controls. Titers of IgG anti-MOG are presented as the median (minimum–maximum) in all IgG anti-MOG-positive groups. See Table 1 for other definitions.

† By chi-square test.

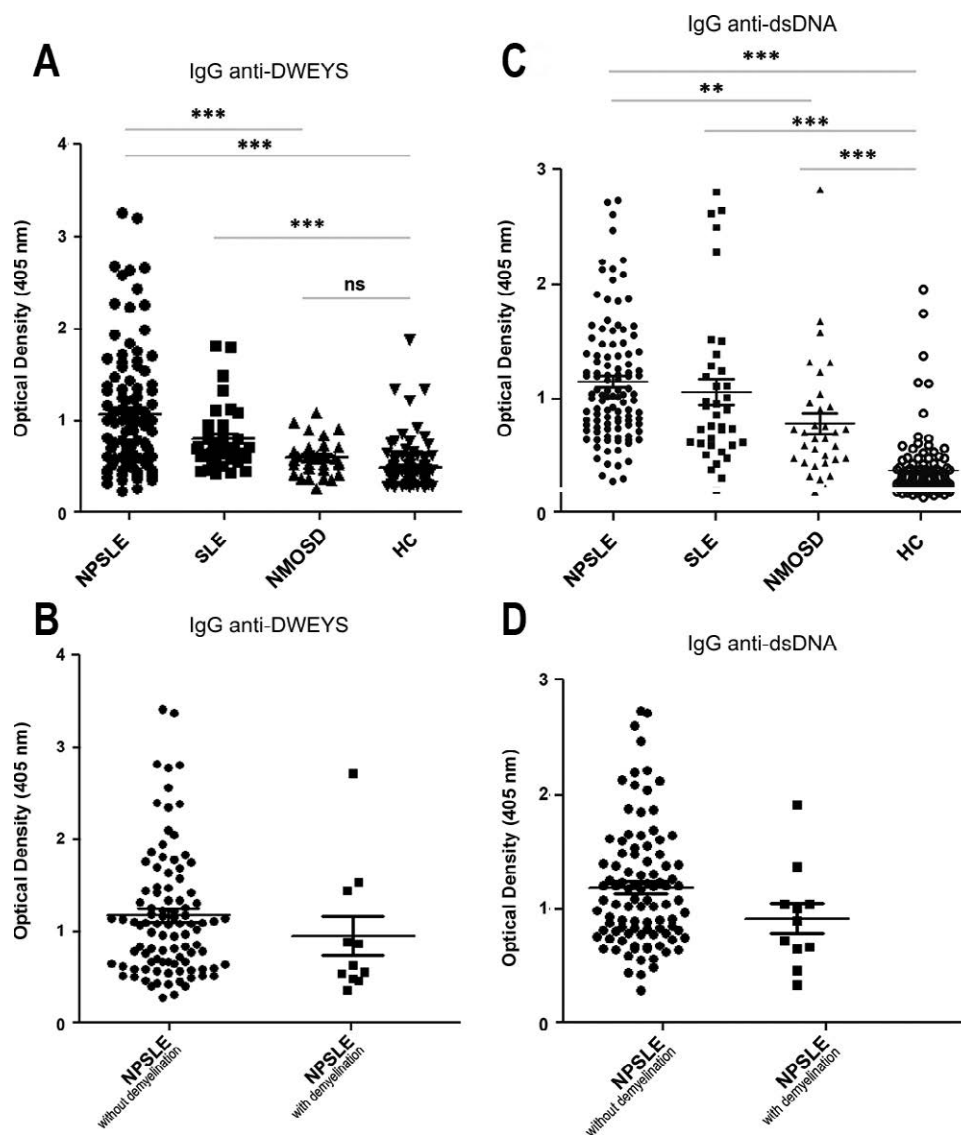


Figure 2. Expression of antibodies to GluN2A/GluN2B (IgG anti-DWEYS) and IgG double-stranded DNA (anti-dsDNA) in the serum of patients with neuropsychiatric systemic lupus erythematosus (NPSLE), patients with SLE without neuropsychiatric manifestations, patients with neuromyelitis optica spectrum disorder (NMOSD), and healthy controls (HC) (A and C). Patients with NPSLE were also analyzed for serum IgG anti-DWEYS and anti-dsDNA antibodies according to their demyelination status (those without and those with demyelination) (B and D). Data in all patient groups and healthy controls are presented as the absorbance at an optical density of 405 nm. Symbols represent individual subjects; horizontal lines with bars indicate the mean \pm SEM. Groups were compared by Mann-Whitney U test or Kruskal-Wallis test with Dunn's correction for multiple comparisons where appropriate. ** = $P = 0.001$ to 0.01 ; *** = $P < 0.001$. NS = not significant.

between patients with demyelinating NPSLE and patients with non-demyelinating NPSLE (Figure 2B).

IgG anti-DWEYS antibodies were present in 59 (55%) of 108 patients with NPSLE and 11 (29%) of 38 patients with SLE (Table 3). In contrast, only 4 (4%) of 106 healthy controls and 4 (12%) of 33 patients with NMOSD had IgG anti-DWEYS reactivity. When we divided patients with NPSLE according to their demyelination status, 56 (58%) of 97 patients with non-demyelinating

NPSLE exhibited IgG DWEYS antibodies, compared to 3 (27%) of 11 patients with demyelinating NPSLE, suggesting that these antibodies are not associated with demyelinating symptoms in NPSLE.

Differences in frequencies and staining patterns of IgG anti-brain antibodies in patients with SLE and patients with NPSLE compared to patients with NMOSD. Serum samples from patients and healthy controls were analyzed for IgG anti-brain antibodies in experiments using

Table 3. Frequency of DWEYS, dsDNA, and IgG anti-brain antibodies in the serum of patients with NPSLE, patients with SLE, patients with NMOSD, and healthy controls*

	NPSLE			SLE (n = 38)	NMOSD (n = 33)	Healthy controls (n = 106)	P†
	All (n = 108)	Without demyelination (n = 97)	With demyelination (n = 11)				
IgG anti-DWEYS	59 (55)	56 (58)	3 (27)	11 (29)	4 (12)	4 (4)	<0.0001
IgG anti-dsDNA	83 (77)	77 (79)	6 (55)	20 (53)	11 (33)	6 (6)	<0.0001
IgG anti-brain	81 (75)	72 (75)‡	9 (82)	32 (84)	20 (61)	13 (13)§	<0.0001

* Values are the number (%) of patients and healthy controls with serum positivity for IgG anti-DWEYS, IgG anti-double-stranded DNA (anti-dsDNA), and IgG anti-brain antibodies. See Table 1 for other definitions.

† P values for a significant trend between groups were determined using the chi-square test.

‡ Data were available from 96 patients.

§ Data were available from 104 control subjects.

PFA-fixed rodent brain sections, which allowed us to observe whether there was a difference in the frequency (Table 3) and staining patterns (Figure 3) of these antibodies between the groups. Overall, 72 (75%) of 96 patients with non-demyelinating NPSLE had IgG anti-brain antibodies. The frequency was strikingly similar between

patients with demyelinating NPSLE (9 [82%] of 11) and patients with SLE (32 [84%] of 38). In contrast, the percentage of patients with NMOSD who were positive for IgG anti-brain antibodies was lower (20 [61%] of 33), likely attributable to the fact that the propensity of IgG anti-AQP-4 antibodies to bind to a conformational epitope of the AQP-4 protein may be disrupted by PFA fixation. In addition, usage of mouse brain tissue, rather than human tissue, in these experiments may have contributed to the lower sensitivity and specificity of the IgG anti-brain antibody frequencies in the serum of patients with NMOSD, as has been demonstrated previously (17). Only 13 (13%) of 104 healthy controls had IgG anti-brain antibodies.

Staining of the serum from patients with SLE as well as patients with NPSLE revealed a neuronal staining pattern (Figure 3). In contrast, IgG anti-brain antibodies in the serum of patients with NMOSD mostly showed a pattern of vasculature staining, sometimes accompanied by neuronal staining. Only 1 NPSLE serum sample, which harbored IgG anti-AQP-4 antibodies, showed staining of the vasculature. Two NPSLE serum samples, which were positive for low titers of IgG anti-AQP-4, did not show vasculature staining, but did exhibit neuronal staining.

Elevated levels of IgG anti-dsDNA in patients with SLE, patients with NPSLE, and patients with NMOSD compared to healthy controls. We next assessed the frequency of IgG anti-dsDNA antibodies in all patients and healthy controls (Table 3). We used an ELISA that is designed to detect IgG anti-dsDNA, and not single-stranded DNA (ssDNA) antibodies, since ssDNA antibodies are removed by binding to a nitrocellulose filter. IgG anti-dsDNA were present in 20 (53%) of 38 patients with SLE and 83 (77%) of 108 patients with NPSLE, compared to 11 (33%) of 33 patients with NMOSD and 6 (6%) of 106 healthy controls. When stratified by demyelination status, 6 (55%) of 11 patients with demyelinating NPSLE and 77 (79%) of 97 patients with non-demyelinating NPSLE exhibited elevated titers of IgG anti-dsDNA.

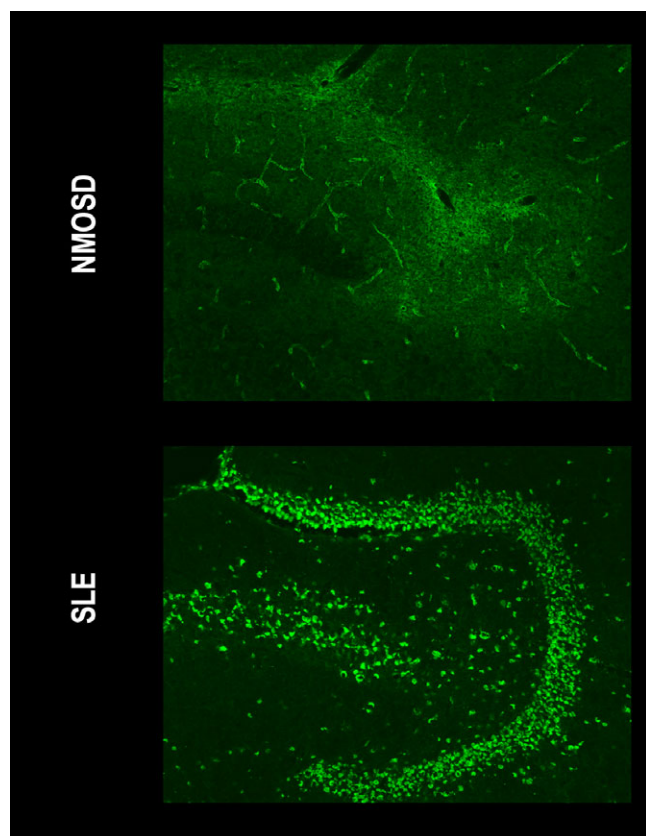


Figure 3. Staining patterns of serum IgG anti-brain antibodies. Representative results show immunostaining for serum IgG anti-brain antibodies in mouse brain tissue from the hippocampus region incubated with serum from a patient with neuromyelitis optica spectrum disorder (NMOSD) and serum from a patient with systemic lupus erythematosus (SLE). Original magnification $\times 40$.

Patients with NMOSD had significantly higher levels of IgG anti-dsDNA compared to healthy controls (Figure 2C). However, the levels were significantly lower in patients with NMOSD than in patients with NPSLE. Since most patients with NMOSD are negative for IgG anti-DWEYS, dsDNA antibodies in patients with NMOSD are not cross-reactive with GluN2A/GluN2B, unlike that observed in patients with SLE and patients with NPSLE.

Patients with non-demyelinating NPSLE had IgG anti-dsDNA titers that were comparable to those in patients with demyelinating NPSLE (Figure 2D). There was no significant difference in IgG anti-dsDNA reactivity between patients with demyelinating NPSLE and patients with NMOSD (Figures 2C and D).

Elevated levels of IgG ANAs in patients with SLE, patients with NPSLE, and patients with NMOSD compared to healthy controls. IgG ANAs were analyzed using a commercially available ANA ELISA plate. A substantial percentage of patients with NPSLE (96 [89%] of 108) and patients with SLE (34 [89%] of 38) had raised levels of IgG ANAs as compared to healthy controls (5 [5%] of 106) and patients with NMOSD (11 [33%] of 33). However, levels of ANAs were also significantly elevated in patients with NMOSD when compared to healthy controls. The frequency of positivity for IgG ANAs was lower in patients with demyelinating NPSLE (8 [73%] of 11) compared to patients with non-demyelinating NPSLE (88 [91%] of 97). There was no difference in the frequency of IgG ANA-positive serum between patients with demyelinating NPSLE and patients with non-demyelinating NPSLE (results available in Supplementary Figures 1A and B, on the *Arthritis & Rheumatology* web site at <http://onlinelibrary.wiley.com/doi/10.1002/art.40356/abstract>).

DISCUSSION

In this study, we analyzed the frequency of brain-reactive antibodies in a large number of patients with NPSLE as compared to patients with SLE without neuropsychiatric manifestations. Our results showed no difference in the frequency of serum IgG anti-brain antibodies or in the neuronal staining pattern of these antibodies between patients with SLE and patients with NPSLE. This confirms the observations made in previous studies in animal models, showing that circulating autoantibodies directed against brain components are not sufficient to cause neuropathologic symptoms, and that a second insult is required to breach the blood-brain barrier and allow IgG anti-brain antibodies to access the CNS and thereby initiate disease pathogenesis. The route of entry of antibodies may contribute to differences in the

clinical presentation of patients. In our study, we observed that the majority of patients with SLE and patients with NPSLE (~80% in each group) exhibited a neuronal staining pattern upon incubation of their serum with mouse brain tissue. Thus, serum antibodies both from patients with SLE and from patients with NPSLE appeared to be binding to neuronal antigens expressed particularly in the hippocampal and cortical areas of the rodent brain tissue. This region-specific binding could contribute to cognitive impairment, which is one of the most common symptoms in NPSLE (31).

Identification of specific target antigens, such as the NMDA receptor, which is highly expressed within these areas, and associations with clinical symptoms are of central importance in future studies. Investigators in our group have previously recognized that anti-dsDNA antibodies, a hallmark finding in SLE, that cross-react with the GluN2A/GluN2B subunits of the neuronal NMDA receptor can cause neuronal damage upon breach of the blood-brain barrier, as assessed in a mouse model (13). Presence of these antibodies is correlated with impairment of spatial cognition in rodents and humans (14,32) and psychiatric manifestations in patients with NPSLE (33). The frequency of GluN2A/GluN2B antibodies (IgG anti-DWEYS) was elevated both in patients with SLE and in patients with NPSLE compared to healthy controls, as has been previously shown (33). Our results confirm these findings, showing a higher frequency of IgG anti-DWEYS in patients with NPSLE compared to patients with SLE. It remains questionable whether anti-dsDNA-anti-GluN2A/GluN2B cross-reactive antibodies are able to breach the blood-brain barrier by themselves. It has been suggested that they can bind to and activate endothelial cells to cause blood-brain barrier impairment alternately (34); however, they might require a secondary insult to breach the blood-brain barrier, such as activation of cytokines or chemokines, complement activation, or anti-endothelial antibodies (35).

The frequency of IgG anti-dsDNA and IgG anti-DWEYS antibodies has not been tested in patients with demyelinating NPSLE, nor have they been tested in patients with NMOSD, which is another demyelinating disorder in young women that has been reported to overlap with SLE or share neurologic features with NPSLE. Since autoantibodies directed against the NMDA receptor possess pathogenic potential, it is important to know whether IgG anti-dsDNA antibodies in another CNS autoimmune disease cross-react with the NMDA receptor, or whether this specificity is specific to SLE.

We therefore investigated the frequency of IgG anti-dsDNA and IgG anti-DWEYS in the serum of patients with NMOSD, an inflammatory and demyelinating

disease in which patients have recently been reported to harbor IgG anti-dsDNA antibodies (36). The significance and pathogenicity of dsDNA antibodies in the course of NMOSD remains unknown. NMOSD is a disease of great interest for researchers, due to the discovery in 2005 of highly specific IgG anti-AQP-4 antibodies in the serum of patients (17), which resulted in the classification of NMOSD as its own disease rather than being defined as a severe variant of multiple sclerosis (37). IgG anti-AQP-4 are predictive of NMOSD (26). Antibodies recognizing conformation-dependent epitopes of MOG (a protein expressed on the outer surface of the myelin sheath), which are found in a subgroup of IgG anti-AQP-4-negative patients with NMOSD (18,38), may also contribute to demyelination. The processes of demyelination, particularly myelitis and optic neuritis, are also observed in some patients with NPSLE and are one of the least understood symptoms in NPSLE.

Recently reported findings indicate that patients with NMOSD develop other autoimmune diseases at a high frequency (36). An increasing number of case studies have described patients with SLE who develop NMOSD, or vice versa (16,23). Precise data on the frequency of NMOSD as a comorbidity of SLE is still mainly based on small studies and case reports, and needs further investigation (16). Due to similar patterns of demyelination in some of the patients with NPSLE and patients with NMOSD, it can be difficult to distinguish whether the demyelination, particularly myelitis and/or optic neuritis, is part of the activity of SLE or part of the activity of NMOSD, or both (39). NMOSD shares many typical features with NPSLE, such as a strikingly high preponderance in women and a beneficial response to immunosuppressive therapeutic approaches. In addition, serum IgG anti-dsDNA and IgG ANAs can be found in both patient groups.

In our study, we analyzed brain-reactive antibodies, including antibodies to DWEYS, MOG, and AQP-4. In addition, we analyzed dsDNA antibodies in a large cohort of patients with NPSLE, patients with SLE, and patients with NMOSD without any other autoimmune diseases. A large set of healthy controls was also included. Our results confirm that IgG anti-AQP-4 are present in the vast majority of patients with NMOSD, and we also show that these antibodies can also be found in a small number of patients with demyelinating NPSLE. The presence of IgG anti-AQP-4 in 3 of 11 patients with demyelinating NPSLE suggests that NPSLE patients with demyelination should be routinely tested for IgG anti-AQP-4. In that case, the diagnostic criteria for comorbid NMOSD would be met. In contrast, we did not find IgG anti-AQP-4 antibodies in patients with non-demyelinating NPSLE. Since IgG anti-AQP-4-negative patients with

demyelinating NPSLE showed serum positivity for brain-reactive antibodies, it is likely that additional antibodies play a role in the disease pathogenesis. Although ~80% of patients with SLE or NPSLE had antibodies reactive to mouse brain tissue, with a neuronal staining pattern, particularly of the cortex and hippocampus, serum from only 61% of patients with NMOSD showed staining on rodent brain tissue. This finding may reflect the fact that PFA fixation can alter the conformational epitope dependency of IgG anti-AQP-4 antibodies. In addition, some studies have shown that IgG anti-AQP-4 antibodies preferentially bind to human brain tissue, rather than rodent brain. Another explanation could be that IgG anti-AQP-4 antibodies have to reach a certain titer to produce clear staining on rodent brain tissue.

Our finding that IgG anti-DWEYS were present in the serum of 58% of patients with non-demyelinating NPSLE and in 27% of patients with demyelinating NPSLE suggests that other antibodies or non-antibody-mediated mechanisms may be associated with demyelination. Despite the presence of dsDNA antibodies in 33% of patients with NMOSD, IgG anti-DWEYS were found in only 12% of these patients. IgG anti-dsDNA antibodies in NMOSD are not cross-reactive with DWEYS, indicating that there is a different trigger for their production, and potentially different mechanisms of tissue damage in this disease. It remains to be investigated whether IgG anti-dsDNA antibodies in patients with NMOSD cross-react with an antigen other than the NMDA receptor subunits GluN2A and GluN2B. Moreover, since predictive biomarkers are currently lacking, it would be important to investigate whether IgG anti-DWEYS positivity might be predictive of the development of NPSLE in patients with NMOSD.

ACKNOWLEDGMENT

The plasmids for AQP-4 and MOG were a kind gift from Prof. Markus Reindl (Medical University of Innsbruck, Austria).

AUTHOR CONTRIBUTIONS

All authors were involved in drafting the article or revising it critically for important intellectual content, and all authors approved the final version to be published. Dr. Diamond had full access to all of the data in the study and takes responsibility for the integrity of the data and the accuracy of the data analysis.

Study conception and design. Mader, Jeganathan, Arinuma, Fujieda, Dujmovic, Drulovic, Shimizu, Sakuma, Stern, Aranow, Mackay, Yasuda, Atsumi, Hirohata, Diamond.

Acquisition of data. Mader, Jeganathan, Arinuma, Fujieda, Dujmovic, Drulovic, Shimizu, Sakuma, Stern, Aranow, Mackay, Yasuda, Atsumi, Hirohata, Diamond.

Analysis and interpretation of data. Mader, Jeganathan, Arinuma, Fujieda, Dujmovic, Drulovic, Shimizu, Sakuma, Stern, Aranow, Mackay, Yasuda, Atsumi, Hirohata, Diamond.

REFERENCES

- Hanly JG, Urowitz MB, Su L, Bae SC, Gordon C, Wallace DJ, et al. Prospective analysis of neuropsychiatric events in an international disease inception cohort of patients with systemic lupus erythematosus. *Ann Rheum Dis* 2010;69:529–35.
- ACR Ad Hoc Committee on Neuropsychiatric Lupus Nomenclature. The American College of Rheumatology nomenclature and case definitions for neuropsychiatric lupus syndromes. *Arthritis Rheum* 1999;42:599–608.
- Hanly JG. Diagnosis and management of neuropsychiatric SLE. *Nat Rev Rheumatol* 2014;10:338–47.
- Jeltsch-David H, Muller S. Neuropsychiatric systemic lupus erythematosus: pathogenesis and biomarkers. *Nat Rev Neurol* 2014;10:579–96.
- Hanly JG. New insights into central nervous system lupus: a clinical perspective. *Curr Rheumatol Rep* 2007;9:116–24.
- Hanly JG, Walsh NM, Sangalang V. Brain pathology in systemic lupus erythematosus. *J Rheumatol* 1992;19:732–41.
- Arnett FC, Reveille JD, Moutsopoulos HM, Georgescu L, Elkon KB. Ribosomal P autoantibodies in systemic lupus erythematosus: frequencies in different ethnic groups and clinical and immunogenetic associations. *Arthritis Rheum* 1996;39:1833–9.
- Isshi K, Hirohata S. Differential roles of the anti-ribosomal P antibody and antineuronal antibody in the pathogenesis of central nervous system involvement in systemic lupus erythematosus. *Arthritis Rheum* 1998;41:1819–27.
- Hirohata S, Sakuma Y, Yanagida T, Yoshio T. Association of cerebrospinal fluid anti-Sm antibodies with acute confusional state in systemic lupus erythematosus. *Arthritis Res Ther* 2014;16:450.
- Sanna G, Bertolaccini ML, Cuadrado MJ, Laing H, Khamashta MA, Mathieu A, et al. Neuropsychiatric manifestations in systemic lupus erythematosus: prevalence and association with antiphospholipid antibodies. *J Rheumatol* 2003;30:985–92.
- Sherer Y, Gorstein A, Fritzler MJ, Shoenfeld Y. Autoantibody explosion in systemic lupus erythematosus: more than 100 different antibodies found in SLE patients. *Semin Arthritis Rheum* 2004;34:501–37.
- Faust TW, Chang EH, Kowal C, Berlin R, Gazaryan IG, Bertini E, et al. Neurotoxic lupus autoantibodies alter brain function through two distinct mechanisms. *Proc Natl Acad Sci U S A* 2010;107:18569–74.
- DeGiorgio LA, Konstantinov KN, Lee SC, Hardin JA, Volpe BT, Diamond B. A subset of lupus anti-DNA antibodies cross-reacts with the NR2 glutamate receptor in systemic lupus erythematosus. *Nat Med* 2001;7:1189–93.
- Kowal C, DeGiorgio LA, Lee JY, Edgar MA, Huerta PT, Volpe BT, et al. Human lupus autoantibodies against NMDA receptors mediate cognitive impairment. *Proc Natl Acad Sci U S A* 2006;103:19854–9.
- Diamond B, Volpe BT. A model for lupus brain disease. *Immunol Rev* 2012;248:56–67.
- Pittock SJ, Lennon VA, de Seze J, Vermersch P, Homburger HA, Wingerchuk DM, et al. Neuromyelitis optica and non organ-specific autoimmunity. *Arch Neurol* 2008;65:78–83.
- Lennon VA, Kryzer TJ, Pittock SJ, Verkman AS, Hinson SR. IgG marker of optic-spinal multiple sclerosis binds to the aquaporin-4 water channel. *J Exp Med* 2005;202:473–7.
- Mader S, Gredler V, Schanda K, Rostasy K, Dujmovic I, Pfaller K, et al. Complement activating antibodies to myelin oligodendrocyte glycoprotein in neuromyelitis optica and related disorders. *J Neuroinflammation* 2011;8:184.
- Probstel AK, Rudolf G, Dornmair K, Collongues N, Chanson JB, Sanderson NS, et al. Anti-MOG antibodies are present in a subgroup of patients with a neuromyelitis optica phenotype. *J Neuroinflammation* 2015;12:46.
- Theodoridou A, Settas L. Demyelination in rheumatic diseases. *J Neurol Neurosurg Psychiatry* 2006;77:290–5.
- Bertsias GK, Ioannidis JP, Aringer M, Bollen E, Bombardieri S, Bruce IN, et al. EULAR recommendations for the management of systemic lupus erythematosus with neuropsychiatric manifestations: report of a task force of the EULAR standing committee for clinical affairs. *Ann Rheum Dis* 2010;69:2074–82.
- Jacobi C, Stinge K, Kretz R, Hartmann M, Storch-Hagenlocher B, Breitbart A, et al. Neuromyelitis optica (Devic's syndrome) as first manifestation of systemic lupus erythematosus. *Lupus* 2006;15:107–9.
- Adawi M, Bisharat B, Bowirrat A. Systemic Lupus Erythematosus (SLE) complicated by neuromyelitis optica (NMO – Devic's disease): clinic-pathological report and review of the literature. *Clin Med Insights Case Rep* 2014;7:41–7.
- Monson N. Antinuclear antibodies in neuromyelitis optica: guardians of the brain? *Eur J Neurol* 2016;23:223–4.
- Saji E, Arakawa M, Yanagawa K, Toyoshima Y, Yokoseki A, Okamoto K, et al. Cognitive impairment and cortical degeneration in neuromyelitis optica. *Ann Neurol* 2013;73:65–76.
- Wingerchuk DM, Banwell B, Bennett JL, Cabre P, Carroll W, Chitnis T, et al. International consensus diagnostic criteria for neuromyelitis optica spectrum disorders. *Neurology* 2015;85:177–89.
- Hochberg MC. Updating the American College of Rheumatology revised criteria for the classification of systemic lupus erythematosus. *Arthritis Rheum* 1997;40:1725.
- Tan EM, Cohen AS, Fries JF, Masi AT, McShane DJ, Rothfield NF, et al. The 1982 revised criteria for the classification of systemic lupus erythematosus. *Arthritis Rheum* 1982;25:1271–7.
- Mader S, Lutterotti A, Di Pauli F, Kuenz B, Schanda K, Aboul-Enein F, et al. Patterns of antibody binding to aquaporin-4 isoforms in neuromyelitis optica. *PLoS One* 2010;5:e10455.
- Brimberg L, Sadiq A, Gregersen PK, Diamond B. Brain-reactive IgG correlates with autoimmunity in mothers of a child with an autism spectrum disorder. *Mol Psychiatry* 2013;18:1171–7.
- Hanly JG, Robichaud J, Fisk JD. Anti-NR2 glutamate receptor antibodies and cognitive function in systemic lupus erythematosus. *J Rheumatol* 2006;33:1553–8.
- Chang EH, Volpe BT, Mackay M, Aranow C, Watson P, Kowal C, et al. Selective impairment of spatial cognition caused by autoantibodies to the N-methyl-D-aspartate receptor. *EBioMedicine* 2015;2:755–64.
- Arinuma Y, Yanagida T, Hirohata S. Association of cerebrospinal fluid anti-NR2 glutamate receptor antibodies with diffuse neuropsychiatric systemic lupus erythematosus. *Arthritis Rheum* 2008;58:1130–5.
- Yoshio T, Okamoto H, Hirohata S, Minota S. IgG anti-NR2 glutamate receptor autoantibodies from patients with systemic lupus erythematosus activate endothelial cells. *Arthritis Rheum* 2013;65:457–63.
- Stock AD, Wen J, Putterman C. Neuropsychiatric lupus, the blood brain barrier, and the TWEAK/Fn14 pathway. *Front Immunol* 2013;4:484.
- Pereira WL, Reiche EM, Kallaur AP, Oliveira SR, Simao AN, Lozovoy MA, et al. Frequency of autoimmune disorders and autoantibodies in patients with neuromyelitis optica. *Acta Neuropsychiatr* 2017;29:170–8.
- Weinshenker BG. Neuromyelitis optica is distinct from multiple sclerosis. *Arch Neurol* 2007;64:899–901.
- Jarius S, Rupprecht K, Kleiter I, Borisow N, Asgari N, Pitarokoli K, et al. MOG-IgG in NMO and related disorders: a multicenter study of 50 patients. Part 1. Frequency, syndrome specificity, influence of disease activity, long-term course, association with AQP4-IgG, and origin. *J Neuroinflammation* 2016;13:279.
- Birnbaum J, Petri M, Thompson R, Izbudak I, Kerr D. Distinct subtypes of myelitis in systemic lupus erythematosus. *Arthritis Rheum* 2009;60:3378–87.

A Rare Variant (rs933717) at *FBXO31-MAP1LC3B* in Chinese Is Associated With Systemic Lupus Erythematosus

Yuan-yuan Qi,¹ Xu-jie Zhou,¹ Swapan K. Nath,² Celi Sun,² Yan-na Wang,¹ Ping Hou,¹ Rong Mu,³ Chun Li,³ Jian-ping Guo,³ Zhan-guo Li,³ Geng Wang,⁴ Hu-ji Xu,⁴ Yan-jie Hao,¹ Zhuo-li Zhang,¹ Wei-hua Yue,⁵ Huoru Zhang,⁶ Ming-hui Zhao,¹ and Hong Zhang¹

Objective. Recent evidence from genetic, cell biology, and animal model studies has suggested a pivotal role of autophagy in mediating systemic lupus erythematosus (SLE). However, the genetic basis has not yet been thoroughly examined. Therefore, the aim of the present study was to identify additional susceptibility variants in autophagy-related genes along with their functional significance.

Methods. First, we performed a gene family-based genetic association analysis in SLE patients with the use of ImmunoChip arrays, and then we selected the most strongly associated polymorphisms for replication in additional cohorts. To identify regulatory clues, we analyzed publicly available blood expression quantitative trait locus data and Encyclopedia of DNA Elements data on transcription factor binding sites and cell type-specific differential expression. Functional effects were

tested by luciferase reporter assays, electrophoretic mobility shift assays, and differential gene expression assays.

Results. In 14,474 samples, we observed that the rare Chinese variant rs933717T was associated with susceptibility to SLE (0.11% in cases versus 0.87% in controls; $P = 2.36 \times 10^{-10}$, odds ratio 0.13). The rs933717 risk allele C correlated with increased *MAP1LC3B* expression; increased *MAP1LC3B* messenger RNA was observed in SLE patients and in lupus-prone mice. In reporter gene constructs, the risk allele increased luciferase activity up to 2.7–3.8-fold in both HEK 293T and Jurkat cell lines, and the binding of HEK 293T and Jurkat cell nuclear extracts to the risk allele was also increased.

Conclusion. We observed a likely genetic association between light chain 3B, a widely used marker for autophagy, and susceptibility to SLE.

Supported by the National Science Foundation of China (grant 81570629), the National Key Research and Development Program of China (grant 2016YFC0904102), the Training Program of the Major Research Plan of the National Natural Science Foundation of China (grant 91642120), the Natural Science Foundation for Innovation Research Group of China (grant 81321064), the Capital of Clinical Characteristics and the Applied Research Fund (grant Z14110-7002514037), the Beijing Natural Science Foundation (grants 7152148 and 7131016), the Chinese Society of Nephrology (grant 15020030-591), the Beijing Nova Program (grant 2017019), and the NIH (grants AR-060366 and MD-007909).

¹Yuan-yuan Qi, PhD, Xu-jie Zhou, MD, PhD, Yan-na Wang, MD, Ping Hou, MD, Yan-jie Hao, MD, Zhuo-li Zhang, MD, PhD, Ming-hui Zhao, MD, PhD, Hong Zhang, MD, PhD: Peking University First Hospital, Beijing, China; ²Swapan K. Nath, PhD, Celi Sun, PhD: Oklahoma Medical Research Foundation, Oklahoma City; ³Rong Mu, MD, Chun Li, MD, Jian-ping Guo, PhD, Zhan-guo Li, MD, PhD: Peking University People's Hospital, Beijing, China; ⁴Geng Wang, MD, Hu-ji Xu, MD, PhD: Changzheng Hospital, Naval Medical University, Shanghai, China; ⁵Wei-hua Yue, MD, PhD: Peking University Sixth Hospital, Beijing, China; ⁶Huoru Zhang, PhD: University of Hong Kong, Hong Kong, China.

Address correspondence to Xu-jie Zhou, MD, PhD, Renal Division, Peking University First Hospital, Number 8 Xishiku Street, Xicheng District, Beijing 100034, China. E-mail: zhouxujie@bjmu.edu.cn.

Submitted for publication April 11, 2017; accepted in revised form October 10, 2017.

Systemic lupus erythematosus (SLE) is a complex autoimmune disease with diverse clinical phenotypes and outcomes (1). Although the exact pathogenesis of SLE remains unclear, genetic factors are known to play key roles. To date, hypothesis-free genome-wide association studies (GWAS) have identified >80 susceptibility loci (2). However, all of these variants account for no more than 30% of the total genetic risk in SLE, and our knowledge of the genetic background is still limited (2). Further pathway testing analysis might help to improve our understanding of the pathogenic processes implicated in SLE.

Autophagy is an evolutionarily conserved homeostatic process by which cytoplasmic materials are delivered to lysosomes for degradation (3). The autophagic process is implemented by autophagy-related proteins that also play a part in regulating immune responses, including the direct elimination of microorganisms, inflammation, antigen presentation, lymphocyte homeostasis, and secretion of immune mediators (4). Recent studies suggest that autophagy is deregulated in peripheral T and B cells in lupus-

prone mice and SLE patients (5–7). Strikingly, the number of autophagosomes in CD19+ B cells from NZB/NZW mice increased significantly before the disease had developed (7). In addition, more recent data indicated that a related process, light chain 3 (LC3)–associated phagocytosis, controlled immune responses to dying cells; its inhibition led to development of an SLE-like disease (8–10). Inhibition of autophagy is likely to ameliorate murine lupus via reduction of proinflammatory cytokines. All of these studies suggest that autophagy plays a highly important role in SLE (11). Thus, it would be useful to discover the extent to which disease-associated genetic variants in LC3-associated phagocytosis–related genes affect autophagy in humans.

Genetic data derived from GWAS and follow-up studies indicated variants in genes related to autophagy, including *ATG5*, *ATG7*, *IRGM*, *DRAM1*, *CDKN1B*, *APOL1*, *MTMR3*, *CLEC16A*, *LRRK2*, and *ATG16L2*, especially in Asian populations (12–20). Most of these genetic associations (*ATG5*, *ATG7*, *IRGM*, *MTMR3*, *LRRK2*, and *ATG16L2*) could be replicated in our previous studies (2,13,14,20). However, only a few of these genetic associations were reported in Caucasians (*ATG5*, *IRGM*, and *CLEC16A*) or Africans (*APOL1*). This could suggest a genetic heterogeneity, and that the autophagy gene has a major genetic impact in Asian populations (18,21). Thus, there is a need for a systematic evaluation of genetic associations in SLE patients from a pathway perspective, especially in Asians. In addition, the question remains as to whether the associated variant might have functional significance.

To find additional autophagy gene variants in Chinese SLE patients, in the present study we included genes involved in the autophagic process according to the HGNC. We then conducted a genetic association study in >10,000 Han Chinese using a 4-stage strategy (Figure 1), including genetic discovery, genetic replication, bioinformatic analysis, and experimental validation.

PATIENTS AND METHODS

Sample description. The discovery cohort consisted of 500 healthy donors (mean \pm SD age 32.0 ± 8.6 years; female:male ratio 3:1) and 500 SLE patients (Northern Han Chinese) (mean \pm SD age 31.9 ± 11.2 years; female:male ratio 6:1). Replication cohort 1 consisted of 7,180 healthy donors (mean \pm SD age 37.6 ± 15.3 years; female:male ratio 4:1) and 2,666 SLE patients (mean \pm SD age 34.6 ± 13.4 years; female:male ratio 9:1) (all Northern Han Chinese). To further replicate our genetic finding, 1,366 SLE patients and 2,279 controls (replication cohort 2) were enrolled (all Southern Han Chinese). In all patients, SLE was diagnosed by local rheumatologists, and the diagnosis met the American College of Rheumatology revised criteria (22) as updated in 1997 (23). The study was approved by the Medical Ethics Committee of Peking University, and all

participants provided informed consent (Institutional Review Board approval no. 2016[1139]).

Genes and single-nucleotide polymorphism (SNP) selection. A total of 46 autophagy-related genes were found by searching the HGNC database (www.genenames.org). As shown in Figure 1, 5 genes were excluded because they were pseudogenes (*BECN1P1*, *ATG3P1*, *ATG12P1*, *ATG12P2*, and *ATG4AP1*), and 9 genes were not covered by ImmunoChip (*MAP1LC3C*, *ATG4B*, *SNX4*, *WIPI2*, *RB1CC1*, *ATG2A*, *DRAM1*, *ATG2B*, and *GABARAPL2*). This left a total of 32 genes for further analysis: *ATG4C*, *DRAM2*, *ATG9A*, *ATG16L1*, *ATG7*, *ATG3*, *ATG10*, *ATG12*, *ATG5*, *ATG9B*, *SNX30*, *AMBRA1*, *ATG13*, *ATG16L2*, *EI24*, *GABARAPL1*, *ATG101*, *MAP1LC3B2*, *ULK1*, *ATG14*, *MAP1LC3B*, *GABARAP*, *ULK2*, *BECN1*, *VMP1*, *WIPI1*, *EPG5*, *ATG4D*, *MAP1LC3A*, *SOGA1*, *ATG4A*, and *VMA21*. SNPs in autophagy-related genes were included, along with a 20-kb segment upstream and a 20-kb segment downstream. The results for 6 genes (*ATG9A*, *ATG3*, *ATG13*, *GABARAP*, *BECN1*, and *SOGA1*) should be interpreted with caution due to single variant involvement in ImmunoChip (24) (Figure 1). We analyzed a total of 342 SNPs, mapped to 26 loci associated with autophagy-related genes (>2 SNPs per gene).

Genotyping and quality control. During the discovery stage, 1,000 participants (500 SLE patients and 500 healthy controls) were genotyped using ImmunoChip, and quality control was undertaken as previously reported (24). Of these, 10 SLE patients and 7 healthy controls were excluded due to a low call rate, relatedness, or the presence of outliers (Figure 1). During the replication stage, genotyping was performed by TaqMan allele discrimination assays (replication cohort 1) using a TaqMan Universal PCR Master Mix and a predesigned SNP genotyping assay mix. These mixes contained polymerase chain reaction (PCR) primers and probes purchased from Applied Biosystems. Genotyping was performed using a 7500 Sequence Detection System (Applied Biosystems), or genotype data were directly extracted from a HumanOmniZhongHua-8 BeadChip (replication cohort 2) (Huoru Zhang, et al: unpublished observations).

Bioinformatic analysis. Variants were annotated using Encyclopedia of DNA Elements (ENCODE) data and blood expression quantitative trait locus (eQTL) data. Regulatory features were annotated using the following databases: rVarBase (<http://rv.psych.ac.cn>), Ensemble (<http://asia.ensembl.org/index.html>), rSNPBase (<http://rsnp.psych.ac.cn>), SNiPA (<http://snipa.helmholtz-muenchen.de/snipa/index.php>), Regulome DB (<http://regulome.stanford.edu>), and HaploReg v4.1 (<http://archive.broadinstitute.org/mammals/haploreg>). Genetic signatures of natural selection in the human genome were analyzed using the Human Genome Diversity Project Selection Browser (<http://hgdp.uchicago.edu>).

Allele-dependent gene expression regulations/eQTLs were queried using the Gene Expression Variation (GENEVAR) database (<http://www.sanger.ac.uk/humgen/genevar>) and the Genome-Wide Repository of Associations between SNPs and Phenotypes database (<https://grasp.nihbi.nih.gov/overview.aspx>). Differential messenger RNA (mRNA) expression data were obtained from ArrayExpress (<http://www.ebi.ac.uk/arrayexpress>).

Luciferase reporter assay. Sequences of 101 bp flanking rs933717 were synthesized and subcloned into pGL4.23 (engineered firefly luciferase gene luc2/minimal promoter [luc2/minP]; Promega) using the *Kpn* I and *Bgl* II restriction sites (sequences are shown in Supplementary Table 1, available on the *Arthritis &*

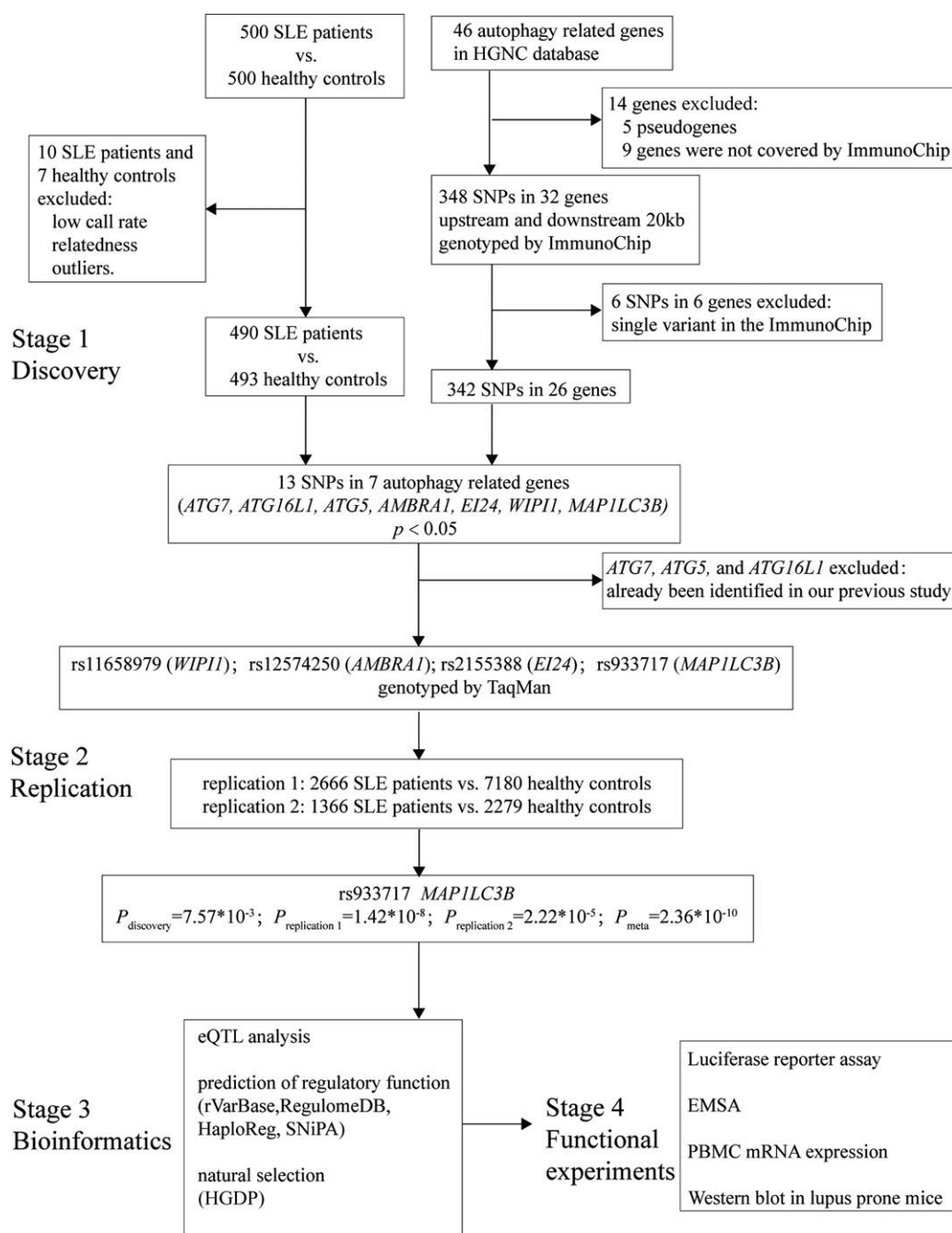


Figure 1. Flow chart of the study design. In stage 1, autophagy-related genes were systematically selected and a tentative genetic discovery study was conducted using ImmunoChip arrays. Stage 2 was performed to replicate in independent populations novel loci discovered in stage 1. After combined analysis with the discovery and replication 1 cohorts, single-nucleotide polymorphisms (SNPs) with significance at $P < 2.6 \times 10^{-7}$ were further replicated using the replication 2 cohort. After the 2-stage genetic association analysis, bioinformatic analysis was performed to annotate the susceptibility loci in stage 3. Given the possible functional annotations for the novel loci from stage 3, in-house experimental validations were performed in vitro in stage 4. SLE = systemic lupus erythematosus; eQTL = expression quantitative trait locus; HGDP = Human Genome Diversity Project; EMSA = electrophoretic mobility shift assay; PBMC = peripheral blood mononuclear cell.

Rheumatology web site at <http://onlinelibrary.wiley.com/doi/10.1002/art.40353/abstract>. HEK 293T cells (1.5×10^5 /well) and Jurkat cells (2×10^5 /well) were transfected with 0.8 μ g pGL4.23 DNA containing rs933717 and 0.08 μ g pRL-TK vector (as

transfection control) using Lipofectamine 2000 (Thermo Fisher Scientific). After 48 hours, cells were lysed and analyzed for luciferase activity using a Dual-Luciferase Assay System (Promega). Each experiment was repeated 3 times.

Electrophoretic mobility shift assay (EMSA). Nuclear proteins from HEK 293T and Jurkat cells were extracted using NE-PER Nuclear and Cytoplasmic Extraction Reagents (Thermo Fisher Scientific). EMSA was performed according to instructions for a DIG Gel Shift Kit (catalog no. 335 3591910; Roche). The single-stranded oligonucleotides used to synthesize the double-stranded ones are shown in Supplementary Table 2, <http://onlinelibrary.wiley.com/doi/10.1002/art.40353/abstract>. For supershift assays, 10 μ l of anti-EBF-1 (catalog no. H00001879-D01P; Novus Biologicals), anti-ROAZ (catalog no. ab169096; Abcam), or anti-ZIC4 (catalog no. sc-101202; Santa Cruz Biotechnology) antibody was incubated with nuclear proteins from HEK 293T or Jurkat cells for 1 hour before adding the relevant labeled probe. Electrophoresis took place in 5% polyacrylamide gels (in 0.5 \times Tris-borate-EDTA [TBE] buffer), and the dye was run two-thirds of the way to the bottom of the plate in 0.5 \times TBE buffer at 50V. The gel was then transferred to nylon membranes (catalog no. LC2003; Thermo Fisher Scientific) at 200 mA for 30 minutes and cross-linked at 120 \times 100 μ J/cm². After incubation for 30 minutes in blocking solution, the membrane was incubated with antibody solution for 1 hour and washed twice in washing buffer for 15 minutes. The membrane was then exposed and scanned using an LAS-3000 Imaging System (GE Healthcare Bioscience). The experiments were carried out in triplicate.

LC3B-II Western blotting in MRL-*lpr/lpr* and C57BL mice. Lymph nodes from 10 MRL-*lpr/lpr* mice (mean \pm SD weight 23.1 \pm 0.8 gm) and 10 C57BL mice (mean \pm SD weight 22.4 \pm 0.9 gm) were obtained for Western blotting. The antibodies used were specific for β -actin (catalog no. 8457; Cell Signaling Technology) and LC3 (catalog no. L7543; Sigma-Aldrich). Tissue proteins from the inguinal lymph nodes were extracted and lysed in radioimmunoprecipitation assay buffer (100 mM Tris HCl [pH 8], 150 mM NaCl, 1% Triton X-100, 1 mM MgCl₂, and 25 mM Na₃VO₄) in the presence of complete protease inhibitor mixture (catalog no. P8340; Sigma-Aldrich). The proteins were separated by 15% sodium dodecyl sulfate-polyacrylamide gel electrophoresis and then transferred to a PVDF membrane (Millipore). The antibody dilutions were 1:1,000 for both anti-LC3 and anti- β -actin. The signal was detected using enhanced chemiluminescence detection reagents, and images were visualized using an LAS-3000 Imaging System. LC3B-II levels were

normalized by densitometry to β -actin levels using ImageJ software (National Institutes of Health).

All mice were purchased from the Model Animal Research Center of Nanjing University and maintained in pathogen-free housing conditions. Assay procedures were performed according to the criteria outlined in the Guide for the Care and Use of Laboratory Animals (Ministry of Health, People's Republic of China, 1998). The study was approved by the Ethics Committee of Peking University.

Statistical analysis. Allelic and genotypic associations were assessed using Plink (<https://www.cog-genomics.org/plink>) to give the odds ratio with a 95% confidence interval. Quantitative variables with a normal distribution were expressed as the mean \pm SD, and Student's *t*-test was performed. In eQTL analysis, Spearman's coefficient was calculated. Statistical analysis was performed with SPSS 13.0 software.

RESULTS

Novel genetic associations of *MAP1LC3B* rs933717 in SLE. The discovery stage of the genetic analysis found 13 SNPs in 7 autophagy-related genes (*ATG7*, *ATG16L1*, *ATG5*, *AMBRA1*, *EI24*, *WIP1*, and *MAP1LC3B*) with *P* < 0.05. Of these genes, *ATG5* showed the most associations, consistent with previous reports on GWAS and candidate genes (12,13) (see Supplementary Table 3, <http://onlinelibrary.wiley.com/doi/10.1002/art.40353/abstract>).

Since the aim was to identify novel gene associations, we excluded *ATG7*, *ATG5*, and *ATG16L1* from further study because they had been associated in our previous study (13). We therefore studied 4 other SNPs in promising loci in an additional replication cohort (replication cohort 1). From these, we identified 2 novel loci that were significantly associated with SLE (*P* < 0.05); the strongest signal was from rs933717 of *MAP1LC3B* (*P*_{discovery} = 7.57×10^{-3} , *P*_{replication1} = 1.42×10^{-8}), which approached genome-wide significance (*P* < 5×10^{-8}) (Table 1).

Table 1. Association of *MAP1LC3B* rs933717 with susceptibility to systemic lupus erythematosus in a Chinese population*

SNP	Chr.	Minor allele	Stage (no. of cases/no. of controls)	MAF, case/control	<i>P</i> †	OR (95% CI)
rs933717	16	T	Discovery (490/493)	0.20/1.22	7.57×10^{-3}	0.17 (0.04–0.74)
			Replication 1 (2,666/7,180)	0.13/0.88	1.42×10^{-8}	0.15 (0.07–0.32)
			Replication 2 (1,366/2,279)	0.02/0.75	2.22×10^{-5}	0.05 (0.01–0.36)
			Combined (4,522/9,952)	0.11/0.87	2.36×10^{-10}	0.13 (0.07–0.24)
rs12574250	11	A	Discovery (490/493)	5.20/7.71	2.39×10^{-2}	0.66 (0.46–0.95)
			Replication 1 (2,666/7,180)	5.95/7.49	1.94×10^{-4}	0.78 (0.69–0.89)
			Combined (3,156/7,673)	5.83/7.51	2.24×10^{-5}	0.77 (0.68–0.87)
rs11658979	17	G	Discovery (490/493)	10.82/14.20	2.34×10^{-2}	0.73 (0.56–0.96)
			Replication 1 (2,666/7,180)	11.74/12.22	0.36	0.96 (0.87–1.05)
			Combined (3,156/7,673)	11.60/12.35	0.10	0.93 (0.85–1.02)
rs2155388	11	A	Discovery (490/493)	7.55/10.75	1.39×10^{-2}	0.68 (0.50–0.93)
			Replication 1 (2,666/7,180)	8.08/8.67	0.19	0.93 (0.83–1.04)
			Combined (3,156/7,673)	8.00/8.80	0.04	0.89 (0.80–0.99)

* SNP = single-nucleotide polymorphism; Chr. = chromosome; MAF = minor allele frequency; OR = odds ratio; 95% CI = 95% confidence interval.

† Combined from Cochran-Mantel-Haenszel statistics. A test for Hardy-Weinberg equilibrium was performed in the controls at all 3 stages. For ImmunoChip analysis, the *P* value threshold with Bonferroni correction was less than 2.6×10^{-7} when considering 192,194 variants.

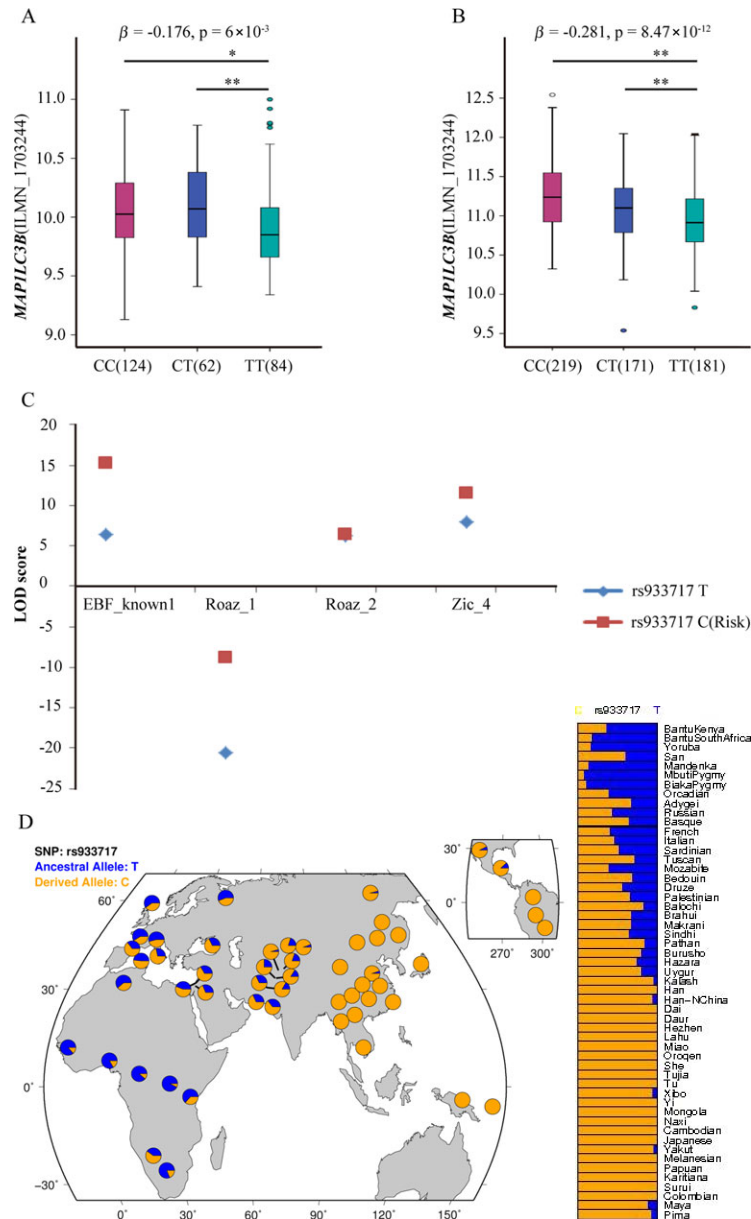


Figure 2. Series of bioinformatics analyses supporting the functional role of *MAPILC3B* rs933717. **A**, Expression quantitative trait locus (QTL) analysis in the Gene Expression Variation database. The expression data in transformed B cell lines were a pool of 4 populations from healthy HapMap samples including Utah residents with ancestry from northern and western Europe (CEU), Han Chinese in Beijing, China (CHB), Yoruba in Ibadan, Nigeria (YRI), and Japanese in Tokyo, Japan (JPT). **B**, Expression QTL analysis in HapMap3 individuals. The lymphoblast expression data consisted of a pool of 618 individuals from 7 HapMap3 populations including 80 CHB, 82 JPT, 108 YRI, 82 Gujarati Indians in Houston, Texas (GIH), 83 Luhya in Webuye, Kenya (LWK), 45 Mexican ancestry in Los Angeles, California (MXL), and 138 Masai in Kinyawa, Kenya (MKK). A total of 47 individuals were not successfully genotyped at rs933717, leaving 571 individuals for further analysis. In **A** and **B**, data are shown as box plots. Y-axes denote *MAPILC3B* expression in gene expression chips. ILMN_1703244 denotes the probe in the gene expression chip (Illumina). Numbers in parentheses in x-axis labels denote the sample size of persons with the genotype. β = partial regression coefficient. Each box represents the 25th to 75th percentiles. Lines inside the boxes represent the median. Lines outside the boxes represent the 10th and 90th percentiles. Circles indicate outliers. * = $P < 0.01$; ** = $P < 0.001$. **C**, Prediction of transcription factors. Altering the rs933717 allele from T to C increased the binding affinity for transcription factors EBF_known1, Roaz_1, Roaz_2, and Zic_4. LOD = logarithm of odds. **D**, Genetic signatures of natural selection in the human genome. Shown is the detailed global allele frequency distribution of the single-nucleotide polymorphism (SNP) rs933717 in 53 world populations.

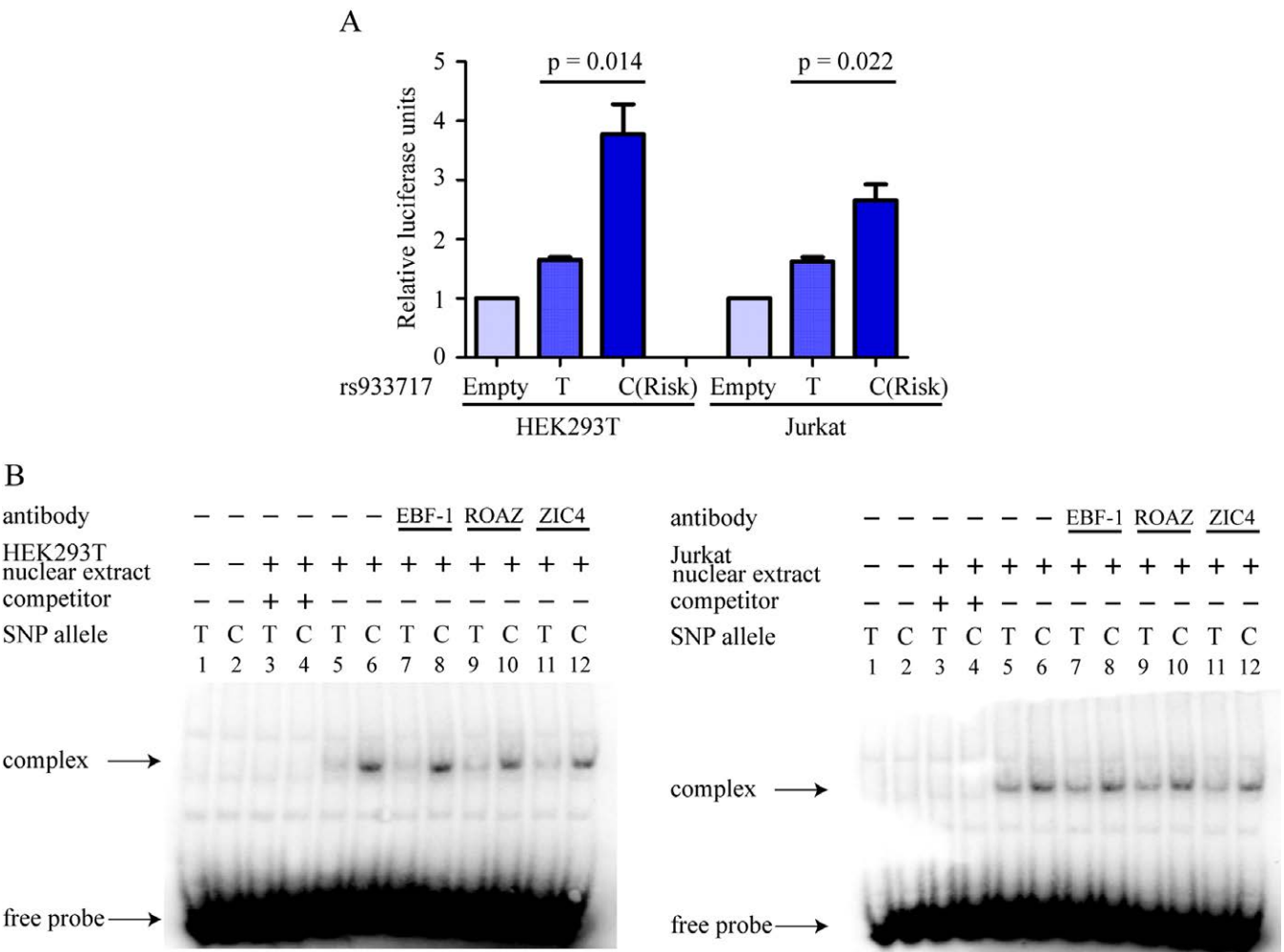


Figure 3. Experimental validation of bioinformatic analysis findings. **A**, Luciferase reporter assay. Shown are luciferase reporter assays of the transcriptional activity of rs933717 in HEK 293T and Jurkat cell lines. Values are the mean \pm SEM. The luciferase activity of rs933717C was significantly greater than that of the rs933717T protective allele in both cell lines. **B**, Electrophoretic mobility shift assay (EMSA). Alleles of rs933717 showed different binding affinities for HEK 293T (left) and Jurkat (right) cell lines. EMSA showed complex formation after addition of HEK 293T and Jurkat cell nuclear extract (lanes 5 and 6). After competition with a 200-fold excess of unlabeled probes, the complex was eliminated (lanes 3 and 4). ROAZ-, EBF-1-, and ZIC4-specific antibodies were not observed to supershift the complex formation using either the C or T probe (lanes 7–12). The digoxigenin-labeled C probe showed a higher affinity for nuclear protein–DNA complex (lanes 6, 8, 10, and 12). Lanes 1 and 2 were negative controls. SNP = single-nucleotide polymorphism.

Therefore, rs933717 was replicated in a second independent cohort ($P_{\text{replication2}} = 2.22 \times 10^{-5}$) and reached genome-wide significance when the cohorts were combined ($P = 2.36 \times 10^{-10}$) (Table 1).

Bioinformatic functional annotations of *MAP1LC3B* rs933717 eQTL analysis. *MAP1LC3B* rs933717 was annotated to be expression SNPs in ENCODE data, as it showed that rs933717CC (risk) correlated with increased *MAP1LC3B* expression ($P = 6 \times 10^{-3}$) in Epstein-Barr virus-transformed lymphoblastoid cell lines from 270 HapMap samples in the GENEVAR database (Figure 2A).

With a larger sample size, this association may be even stronger, as shown by array quantification of 618 individuals from 7 HapMap3 populations ($P = 8.47 \times 10^{-12}$) (Figure 2B), the Genotype-Tissue Expression pilot analysis ($P = 1.55 \times 10^{-7}$) (25), and a genome-wide eQTL analysis in whole peripheral blood from 1,469 unrelated individuals ($P = 9.7 \times 10^{-9}$) (26). In addition, risk genotypes of rs933717 correlated significantly with higher expression of several autophagy-related genes, suggesting *trans*-eQTL effects (see Supplementary Table 4, <http://onlinelibrary.wiley.com/doi/10.1002/art.40353/abstract>).

Prediction of regulatory function. The in silico bioinformatic analysis with ENCODE data demonstrated that rs933717 resided in a transcription factor (TF) binding region. Four binding site motifs span the rs933717 region for binding by the following TFs: EBF_known1, Roaz_1, Roaz_2, and Zic_4. The differences between the logarithm of odds scores for the alleles T and C (risk) were 8.8, 11.9, 0.2, and 3.7 for EBF_known1, Roaz_1, Roaz_2, and Zic_4, respectively (Figure 2C). The data showed that rs933717 could affect transcriptional enhancer activity, suggesting that rs933717 might reside in an important region for gene transcriptional regulation (see Supplementary Tables 5–7, <http://onlinelibrary.wiley.com/doi/10.1002/art.40353/abstract>).

Genetic signatures of natural selection in the human genome. We further investigated the detailed global allele frequency distribution of rs933717 in 53 populations. Intriguingly, the risk allele rs933717C showed regional enrichment; the highest frequencies (~100%) were found in East Asia, South Asia, and Southeast Asia, followed by the Middle East and Europe, and the lowest were found in Africa (Figure 2D). Population selection analysis indicated that standardized integrated haplotype scores were 1.781 in Utah residents with ancestry from northern and western Europe (CEU) and 1.477 in Yoruba in Ibadan, Nigeria (YRI), and Fay and Wu's H^+ was -13.663 in CEU and -3.449 in YRI. Neither the standardized integrated haplotype scores nor Fay and Wu's H^+ were available in an East Asian population (27,28).

Increased reporter gene activity in risk allele C of rs933717. The effects of the variant-containing sequences on gene expression were assessed by luciferase reporter assay, in which sequences of 101 bp flanking rs933717 were synthesized and subcloned into minimal promoter-driven firefly luciferase vector pGL4.23 (luc2/minP) reporter vectors and transfected into HEK 293T and Jurkat cells. We observed that the presence of the risk allele C of rs933717 significantly increased luciferase activity from 1.7-fold to 3.8-fold ($P = 0.014$) in HEK 293T cells and from 1.6-fold to 2.7-fold ($P = 0.022$) in Jurkat cells (Figure 3A).

Differential binding of nuclear extract at rs933717. Evidence of enhancer activity was provided by EMSA; oligonucleotides containing risk allele C of rs933717 showed a greater affinity for nuclear protein–DNA complex with HEK 293T and Jurkat cell nuclear extract than did oligonucleotides containing protective allele T of rs933717 (Figure 3B). The nuclear protein–DNA complex was abolished by addition of excessive unlabeled competitor probes (Figure 3B). In silico analysis using the JASPAR, TransFac, and MAPPER databases predicted binding at the transcription factor binding sites for ROAZ, EBF-1, and ZIC4. However, in the supershift assay, ROAZ-, EBF-

1-, and ZIC4-specific antibodies were not observed to supershift the complex formation with either an rs933717 C probe or an rs933717 T probe (Figure 3B). In contrast, in the same 2 EMSA experiments performed with HEK 293T cell- and Jurkat cell-derived nuclear samples, the digoxigenin-labeled C probe showed a higher affinity for the nuclear protein–DNA complex (Figure 3B). This also indicated that rs933717C differed from rs933717T in formation of the nuclear protein–DNA complex.

Increased autophagy in SLE patients and in lymph nodes of lupus-prone mice. Consistent with the observation that risk alleles are associated with higher levels of gene expression, increased *MAP1LC3B* expression was also observed in patients with SLE. We used mRNA expression data from a comparatively large project focusing on the gene expression profiling of peripheral blood mononuclear cells (project E-GEOD-20864; ArrayExpress) from 21 SLE patients compared with 45 healthy individuals in a GEO database. That study found significantly elevated levels of *MAP1LC3B* expression in SLE patients compared to normal controls ($P = 1.28 \times 10^{-9}$) (Figure 4A). The result was successfully replicated (in an independent cohort enrolled in our own center) by expression microarray conducted using an Illumina HT-12 v4 Expression BeadChip. Compared with 12 healthy controls, the level of *MAP1LC3B* expression was significantly higher in 13 SLE patients ($P = 2.00 \times 10^{-2}$) (Figure 4B).

Using LC3 immunoblotting, autophagy was quantified in lymph nodes obtained from MRL-*lpr/lpr* lupus-prone mice and C57BL healthy control mice. The cellular autophagy response was assessed using LC3B-II normalized to β -actin, the most widely used index. The level of autophagy was significantly higher in lymph nodes from MRL-*lpr/lpr* mice than in those from healthy control mice ($P = 0.013$) (Figure 4C).

DISCUSSION

In the current study, we conducted various analyses. First, we carried out a gene family-based genetic association analysis involving 26 autophagy-related genes. Although ImmunoChip was designed for dense mapping of immune-related genes instead of autophagy pathway analysis, an increasing number of studies highlighted its power for detecting previously overlooked susceptibility loci (24). Also, the ImmunoChip design included several rare variants considered to have significant functional effects that might have been previously overlooked.

We observed that rs933717 (*MAP1LC3B*) was associated, with genome-wide significance, with susceptibility to SLE in >10,000 Chinese individuals. Of special note, rs933717 was found to be associated with susceptibility to

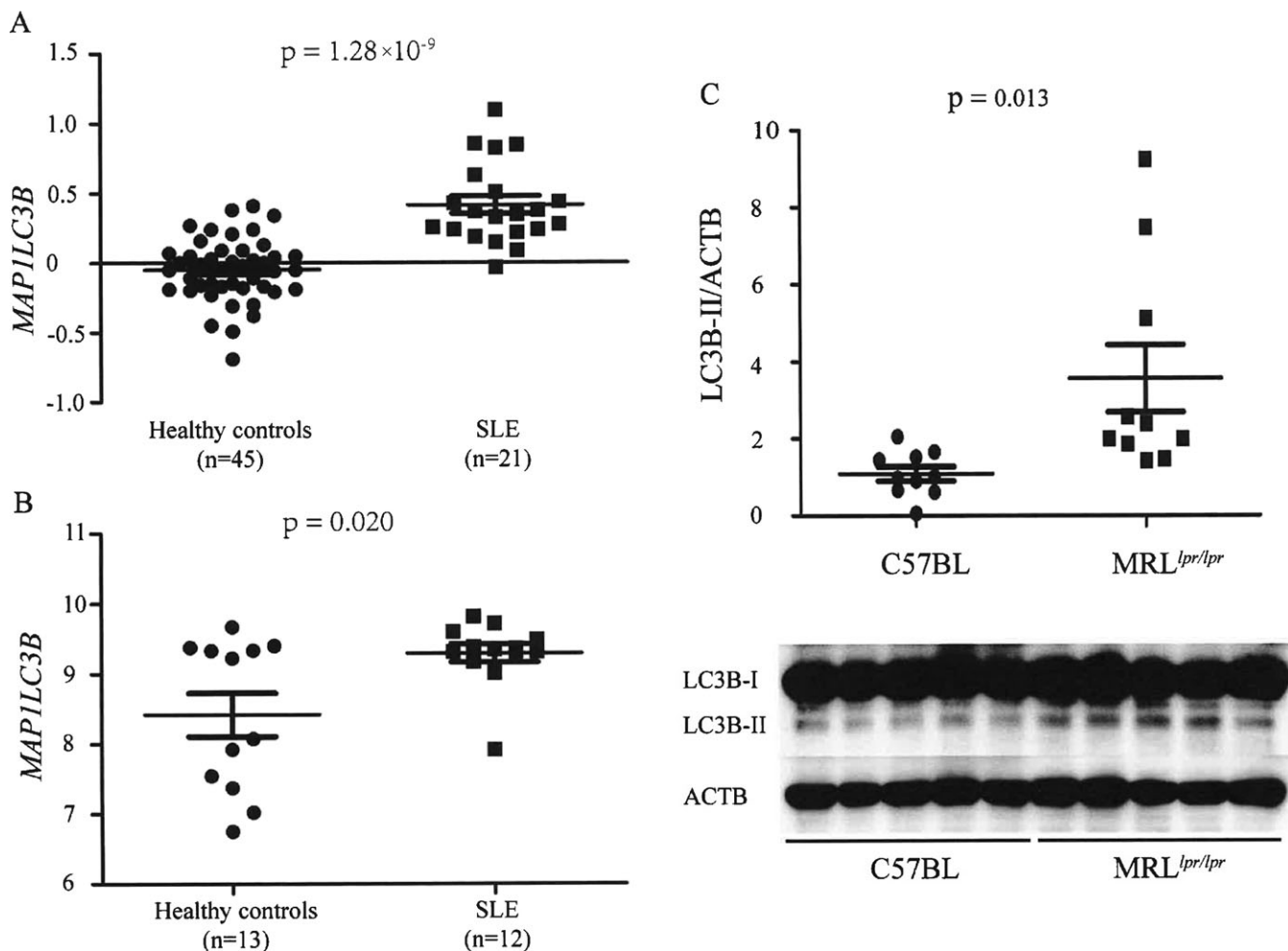


Figure 4. Autophagy was increased in patients with systemic lupus erythematosus (SLE) and in lymph nodes from MRL-*lpr/lpr* mice. **A**, *MAP1LC3B* expression was significantly greater in SLE patients according to the GEO data. *MAP1LC3B* mRNA expression in peripheral blood mononuclear cells (PBMCs) from SLE patients and healthy individuals was analyzed based on project E-GEOD-20864 obtained from ArrayExpress. E-GEOD-20864 is a comparatively large project focusing on gene expression profiling of PBMCs from SLE patients and healthy individuals. **B**, *MAP1LC3B* expression was significantly greater in SLE patients in our own cohort. Expression microarray analysis was conducted using an Illumina HT-12 v4 Expression BeadChip in healthy controls and SLE patients. **C**, Autophagy was significantly greater in lymph nodes from MRL-*lpr/lpr* mice. Bottom, Blots shown are representative of independent experiments performed in 10 C57BL mice and 10 MRL-*lpr/lpr* mice. Top, Scatterplot shows results of densitometry of light chain 3B-II (LC3B-II) levels relative to ACTB/ β -actin. Symbols represent individual subjects (**A** and **B**) or mice (**C**); bars show the mean \pm SEM (**A** and **B**) or the median and interquartile range (**C**). Levels of LC3B-II were significantly greater in lymph nodes from MRL-*lpr/lpr* mice than in those from C57BL control mice.

age-related cataracts in a GWAS using 530,101 SNPs from the Illumina Human660W-Quad BeadChip array in a total of 7,397 individuals in an Electronic Medical Records and Genomics Network study. However, the P value was 0.000041, suggesting that a large sample size may be critically necessary. We found data to suggest that the T allele has a protective function, consistent with that previous report (29). In contrast, expression analysis suggested a likely pathogenic role of increased *MAP1LC3B* expression in SLE patients, which might be because of an allele-dependent effect of risk allele rs933717C. To identify

possible molecular mechanisms, functional annotations were performed using ENCODE data, which supported a likely regulatory feature of these variants. To confirm these bioinformatic clues, an in-house functional luciferase reporter assay and an EMSA were carried out. Both supported an enhancer role of the rs933717 region, and LC3B-II levels were higher in lupus-prone mice than in control mice. Taken together, the results from genetic association, expression association, and functional validation tests strongly suggest that *MAP1LC3B* rs933717 is involved in SLE etiology.

Microtubule-associated protein LC3B is encoded by the *MAP1LC3B* gene. LC3B is a central protein in autophagy since it is involved in cargo recruitment into autophagosomes and in biogenesis and maturation of autophagosomes. More importantly, LC3B is the most widely used autophagosome marker (30). In the present study, expression analysis suggested a likely pathogenic role of increased LC3B in SLE patients. Further experiments also showed that LC3B levels were higher in lupus-prone mice than in healthy control mice, corroborating the current observation that higher levels of LC3B were consistently observed in lupus-prone mouse models and SLE patients (5–7). Following these observations, it was further suggested that autophagy is genetically associated with SLE. Our data suggested that rs933717 of *MAP1LC3B* could increase the expression of LC3B in immune cells by both *cis*- and *trans*-eQTL effects. Genetic association, expression association, and functional validation highlight the likely important role of rs933717 in Chinese SLE patients. However, the associations were not able to determine whether rs933717 was the single causal variant or whether it was just in linkage disequilibrium with a nearby variant. Thus, further fine-mapping analysis is needed.

SLE is an autoimmune disease and is characterized as an abnormality of the immune system that includes antigen presentation by antigen-presenting cells as well as the survival of autoreactive T and B cells that leads to the production of large amounts of autoantibodies. Recent studies indicated that autophagy was involved in the presentation of intracellular antigens to major histocompatibility complex (MHC) class II molecules (31,32). Higher rates of autophagy led to a more active MHC presentation process, which might lead to the breakdown of immune tolerance and an increase of the immune response. In addition, increased autophagy would promote the survival of autoimmune T and B cells, which in turn would lead to high levels of autoantibody and cytokine production and multiple organ/system involvement (33–40). Thus, high levels of autophagy might promote the initiation of autoimmunity in SLE by influencing multiple aspects of the immune system. More importantly, it was recently reported that LC3-associated phagocytosis controls immune responses to dying cells and that its inhibition leads to the development of SLE-like disease (9). Our data reinforced the notion that LC3 might be genetically involved in SLE (9).

We included SNP mapping to autophagy-related genes along with regions 20 kb upstream and downstream. Although rs933717 was annotated to be an intronic variant of *FBXO31*, its associated regulatory SNP-related genes included *MAP1LC3B* (proximal transcriptional regulation) and *FBXO31* (distal transcriptional regulation and RNA

binding protein-mediated regulation) (Ensembl [<http://asia.ensembl.org/index.html>] and rSNPBase [<http://rsnp.psych.ac.cn/>]). It is difficult to determine the exact causal variant and gene in this type of strategy of forward genetic association. In most cases, GWAS implicated disease susceptibility loci rather than directly identifying disease-associated genes. This is because many of the disease-associated SNPs were located in an intergenic region with the susceptibility gene, or the functional locus was located within a region near the SNP, which often contained multiple genes. We thus also analyzed the differential expression of *FBXO31* between SLE patients and healthy controls using data from GEO and from our own cohort. We found no significant difference in expression of *FBXO31* ($P = 0.092$ for data from GEO accession no. GSE20864; $P = 0.343$ for data from our center). Thus, rs933717 was more likely to be involved in the pathogenesis of SLE by influencing *MAP1LC3B*. F-box proteins, in conjunction with Skp1, Cul1, and Rbx1, generate F-box containing complex (or SCF complex) that is responsible for the ubiquitination of proteins, leading to their activation or degradation. The F-box protein *FBXO31* is required for normal mitotic progression and genome stability due to its role in regulating FOXM1 levels during the G₂/M transition. Therefore, future study targeting *FBXO31* is also of interest.

Genetic associations between autophagy gene variants were pronounced in Asian populations, as most autophagy genetic associations could be replicated in our previous studies (2,13,14,20). However, few of these genetic associations were reported in Caucasians or Africans, suggesting genetic heterogeneity and that the autophagy gene has a major impact in Asian populations (18,21). The rs933717 variant is seen in Asians but is more common in Caucasians, which might be because of natural selection. However, the mechanisms by which this kind of natural selection affects autophagy and SLE epidemiology need to be further investigated, including independent replications observed in other populations (24).

In the current study, differential effects of nuclear protein binding with the rs933717 C/T allele were observed, which may support the notion that rs933717 influences the expression of *MAP1LC3B*. However, the exact transcription factor was not clearly determined, as it was not validated by anti-ROAZ or anti-EBF-1 antibody-specific supershift assay. Further exploration to seek the binding factor, such as chromatin immunoprecipitation and promoter microarray analysis or ChIP-Seq, or in other cell lines, is still warranted.

In summary, we systemically evaluated genes involved in autophagy in a large sample using a 4-stage strategy, including genetic discovery, genetic replication,

bioinformatic analysis, and experimental validation. We observed likely novel genetic associations between LC3B (encoded by *MAP1LC3B*), an excellent marker for autophagic structures, and susceptibility to SLE. Our work was committed to providing a more complete understanding of SLE pathogenesis, especially focusing on autophagy. A deeper knowledge of the relationship between autophagy and SLE is likely to lead to the discovery of new therapeutic targets.

ACKNOWLEDGMENTS

We thank all members of our laboratory for their technical assistance. We also thank the patients and their families and the healthy donors for their cooperation and for giving consent to participate in this study.

AUTHOR CONTRIBUTIONS

All authors were involved in drafting the article or revising it critically for important intellectual content, and all authors approved the final version to be published. Dr. Zhou had full access to all of the data in the study and takes responsibility for the integrity of the data and the accuracy of the data analysis.

Study conception and design. Zhou, Nath, Hong Zhang.

Acquisition of data. Qi, Zhou, Nath, Sun, Y. Wang, Hou, Mu, C. Li, Guo, Z. Li, G. Wang, Xu, Hao, Z. Zhang, Yue, Huoru Zhang, Zhao, Hong Zhang.

Analysis and interpretation of data. Qi, Zhou, Hong Zhang.

REFERENCES

- Rahman A, Isenberg DA. Systemic lupus erythematosus. *N Engl J Med* 2008;358:929–39.
- Moliner J, Yang W, Zhou XJ, Sun C, Okada Y, Zhang H, et al. Confirmation of five novel susceptibility loci for systemic lupus erythematosus (SLE) and integrated network analysis of 82 SLE susceptibility loci. *Hum Mol Genet* 2017;26:1205–16.
- Levine B, Mizushima N, Virgin HW. Autophagy in immunity and inflammation. *Nature* 2011;469:323–35.
- Deretic V, Saitoh T, Akira S. Autophagy in infection, inflammation and immunity. *Nat Rev Immunol* 2013;13:722–37.
- Alessandri C, Barbati C, Vacirca D, Piscopo P, Confaloni A, Sanchez M, et al. T lymphocytes from patients with systemic lupus erythematosus are resistant to induction of autophagy. *FASEB J* 2012;26:4722–32.
- Gros F, Arnold J, Page N, Decossas M, Korganow AS, Martin T, et al. Macroautophagy is deregulated in murine and human lupus T lymphocytes. *Autophagy* 2012;8:1113–23.
- Clarke AJ, Ellinghaus U, Cortini A, Stranks A, Simon AK, Botto M, et al. Autophagy is activated in systemic lupus erythematosus and required for plasmablast development. *Ann Rheum Dis* 2015;74:912–20.
- Bandyopadhyay U, Overholtzer M. LAP: the protector against autoimmunity. *Cell Res* 2016;26:865–6.
- Martinez J, Cunha LD, Park S, Yang M, Lu Q, Orchard R, et al. Noncanonical autophagy inhibits the autoinflammatory, lupus-like response to dying cells. *Nature* 2016;533:115–9.
- Martinez J, Almendinger J, Oberst A, Ness R, Dillon CP, Fitzgerald P, et al. Microtubule-associated protein 1 light chain 3 α (LC3)-associated phagocytosis is required for the efficient clearance of dead cells. *Proc Natl Acad Sci U S A* 2011;108:17396–401.
- Li B, Yue Y, Dong C, Shi Y, Xiong S. Blockade of macrophage autophagy ameliorates activated lymphocytes-derived DNA induced murine lupus possibly via inhibition of proinflammatory cytokine production. *Clin Exp Rheumatol* 2014;32:705–14.
- International Consortium for Systemic Lupus Erythematosus Genetics, Harley JB, Alarcon-Riquelme ME, Criswell LA, Jacob CO, Kimberly RP, et al. Genome-wide association scan in women with systemic lupus erythematosus identifies susceptibility variants in ITGAM, PXX, KIAA1542 and other loci. *Nat Genet* 2008;40:204–10.
- Zhou XJ, Lu XL, Lv JC, Yang HZ, Qin LX, Zhao MH, et al. Genetic association of PRDM1-ATG5 intergenic region and autophagy with systemic lupus erythematosus in a Chinese population. *Ann Rheum Dis* 2011;70:1330–7.
- Zhou XJ, Nath SK, Qi YY, Cheng FJ, Yang HZ, Zhang Y, et al. Identification of MTMR3 as a novel susceptibility gene for lupus nephritis in northern Han Chinese by shared-gene analysis with IgA nephropathy. *Arthritis Rheumatol* 2014;66:2842–8.
- Zhang YM, Cheng FJ, Zhou XJ, Qi YY, Zhao MH, Zhang H. Rare variants of ATG5 are likely to be associated with Chinese patients with systemic lupus erythematosus. *Medicine (Baltimore)* 2015;94:e939.
- Yang W, Tang H, Zhang Y, Tang X, Zhang J, Sun L, et al. Meta-analysis followed by replication identifies loci in or near CDKN1B, TET3, CD80, DRAM1, and ARID5B as associated with systemic lupus erythematosus in Asians. *Am J Hum Genet* 2013;92:41–51.
- Parkes M, Barrett JC, Prescott NJ, Tremelling M, Anderson CA, Fisher SA, et al. Sequence variants in the autophagy gene IRGM and multiple other replicating loci contribute to Crohn's disease susceptibility. *Nat Genet* 2007;39:830–2.
- Freedman BI, Langefeld CD, Andringa KK, Croker JA, Williams AH, Garner NE, et al. End-stage renal disease in African Americans with lupus nephritis is associated with APOL1. *Arthritis Rheumatol* 2014;66:390–6.
- Schuster C, Gerold KD, Schober K, Probst L, Boerner K, Kim MJ, et al. The autoimmunity-associated gene CLEC16A modulates thymic epithelial cell autophagy and alters T cell selection. *Immunity* 2015;42:942–52.
- Zhang YM, Zhou XJ, Cheng FJ, Qi YY, Hou P, Zhao MH, et al. Autophagy-related gene LRRK2 is likely a susceptibility gene for systemic lupus erythematosus in northern Han Chinese. *Oncotarget* 2017;8:13754–61.
- Gateva V, Sandling JK, Hom G, Taylor KE, Chung SA, Sun X, et al. A large-scale replication study identifies TNIP1, PRDM1, JAZF1, UHRF1BP1 and IL10 as risk loci for systemic lupus erythematosus. *Nat Genet* 2009;41:1228–33.
- Tan EM, Cohen AS, Fries JF, Masi AT, McShane DJ, Rothfield NF, et al. The 1982 revised criteria for the classification of systemic lupus erythematosus. *Arthritis Rheum* 1982;25:1271–7.
- Hochberg MC. Updating the American College of Rheumatology revised criteria for the classification of systemic lupus erythematosus [letter]. *Arthritis Rheum* 1997;40:1725.
- Sun C, Moliner J, Looger LL, Zhou XJ, Kim K, Okada Y, et al. High-density genotyping of immune-related loci identifies new SLE risk variants in individuals with Asian ancestry. *Nat Genet* 2016;48:323–30.
- GTEx Consortium. Human genomics: the Genotype-Tissue Expression (GTEx) pilot analysis: multitissue gene regulation in humans. *Science* 2015;348:648–60.
- Fehrmann RS, Jansen RC, Veldink JH, Westra HJ, Arends D, Bonder MJ, et al. Trans-eQTLs reveal that independent genetic variants associated with a complex phenotype converge on intermediate genes, with a major role for the HLA. *PLoS Genet* 2011;7:e1002197.
- Voight BF, Kudaravalli S, Wen X, Pritchard JK. A map of recent positive selection in the human genome. *PLoS Biol* 2006;4:e72.
- Willer CJ, Scott LJ, Bonnycastle LL, Jackson AU, Chines P, Pruim R, et al. Tag SNP selection for Finnish individuals based on the CEPH Utah HapMap database. *Genet Epidemiol* 2006;30:180–90.
- Ritchie MD, Verma SS, Hall MA, Goodloe RJ, Berg RL, Carrell DS, et al. Electronic medical records and genomics (eMERGE)

- network exploration in cataract: several new potential susceptibility loci. *Mol Vis* 2014;20:1281–95.
30. Klionsky DJ, Abdelmohsen K, Abe A, Abedin MJ, Abeliovich H, Acevedo Arozena A, et al. Guidelines for the use and interpretation of assays for monitoring autophagy (3rd edition). *Autophagy* 2016;12:1–222.
 31. Zwart W, Griekspoor A, Kuijl C, Marsman M, van Rheeën J, Janssen H, et al. Spatial separation of HLA-DM/HLA-DR interactions within MHC and phagosome-induced immune escape. *Immunity* 2005;22:221–33.
 32. Nimmerjahn F, Milosevic S, Behrends U, Jaffee EM, Pardoll DM, Bornkamm GW, et al. Major histocompatibility complex class II-restricted presentation of a cytosolic antigen by autophagy. *Eur J Immunol* 2003;33:1250–9.
 33. Zhou XJ, Zhang H. Autophagy in immunity: implications in etiology of autoimmune/autoinflammatory diseases. *Autophagy* 2012;8:1286–99.
 34. Zhou XJ, Cheng FJ, Zhang H. Emerging view of autophagy in systemic lupus erythematosus. *Int Rev Immunol* 2015;34:280–92.
 35. Pua HH, Dzhalgalov I, Chuck M, Mizushima N, He YW. A critical role for the autophagy gene Atg5 in T cell survival and proliferation. *J Exp Med* 2007;204:25–31.
 36. Arsov I, Li X, Matthews G, Coradin J, Hartmann B, Simon AK, et al. BAC-mediated transgenic expression of fluorescent autophagic protein Beclin 1 reveals a role for Beclin 1 in lymphocyte development. *Cell Death Differ* 2008;15:1385–95.
 37. Pua HH, He YW. Maintaining T lymphocyte homeostasis: another duty of autophagy. *Autophagy* 2007;3:266–7.
 38. Pua HH, Guo J, Komatsu M, He YW. Autophagy is essential for mitochondrial clearance in mature T lymphocytes. *J Immunol* 2009;182:4046–55.
 39. Arsov I, Adebayo A, Kucerova-Levisohn M, Haye J, MacNeil M, Papavasiliou FN, et al. A role for autophagic protein Beclin 1 early in lymphocyte development. *J Immunol* 2011;186:2201–9.
 40. Henault J, Martinez J, Riggs JM, Tian J, Mehta P, Clarke L, et al. Noncanonical autophagy is required for type I interferon secretion in response to DNA-immune complexes. *Immunity* 2012;37:986–97.

DOI: 10.1002/art.40341

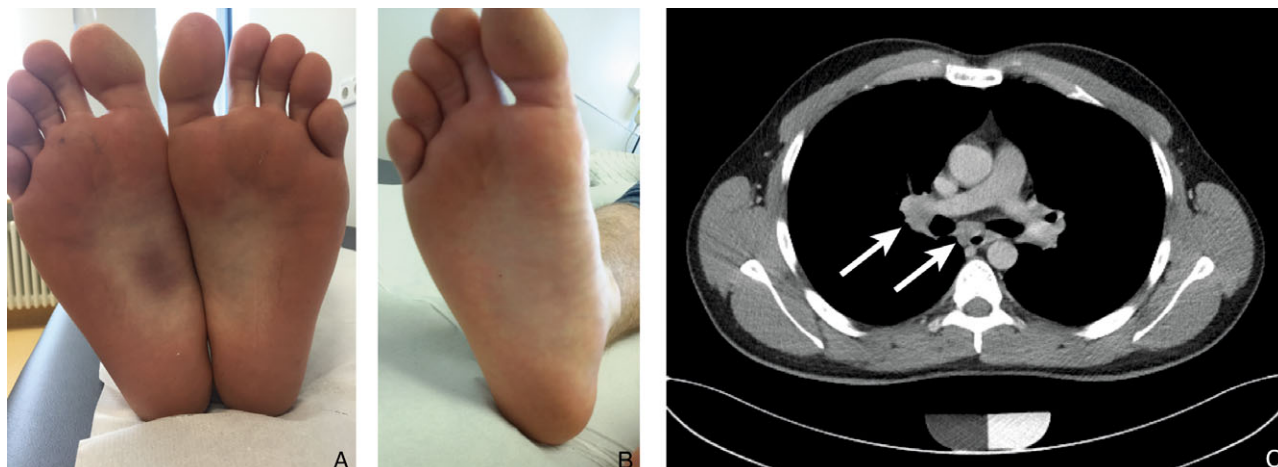
Clinical Images: Unilateral plantar erythema nodosum in sarcoidosis

The patient, a 32-year-old man, presented with mild exertional dyspnea, pain and swelling of both ankles, and general malaise. Physical examination revealed symmetric arthritis in both ankles and a vivid nodular erythema on the sole of the right foot (A), accompanied by slight pain with pressure. Treatment with ibuprofen had not improved the symptoms. The erythrocyte sedimentation rate and C-reactive protein level were elevated (73 mm/hour and 30 mg/liter, respectively), but all other parameters, including levels of angiotensin-converting enzyme and soluble interleukin-2 receptor, were within normal range. Computed tomography of the chest showed enlarged mediastinal lymph nodes (C) (arrows) compatible with a diagnosis of Lofgren's syndrome. Based on this hypothesis, glucocorticosteroid treatment (starting dosage 40 mg/day) was initiated, after which the arthritis, dyspnea, and malaise resolved, and the levels of inflammation markers normalized within 2 weeks. The erythema nodosum improved and resolved after 2 months (B). A literature search revealed that unilateral plantar erythema nodosum is rare but is seen occasionally in children with infections (dermatophytes, *Streptococcus*, *Yersinia enterocolitica*, or *Mycoplasma*). In adults, only 3 cases have been reported. Plantar erythema nodosum was associated with Crohn's disease in 1 case (1) and with granulomatous mastitis in another (2); in the third, it appeared to be idiopathic (3). The patient described here represents the first reported case of unilateral plantar erythema nodosum with sarcoidosis.

1. Châtillon F, Chizzolini C, Kaya G, Borradori L, Hauser C. Plantar erythema nodosum in a patient with Crohn's disease. *Dermatology* 1999;199:190.
2. Polat M, Kaya H. Plantar erythema nodosum associated with granulomatous mastitis. *Indian J Dermatol Venereol Leprol* 2016;82:202–4.
3. Ohtake N, Kawamura T, Akiyama C, Furue M, Tamaki K. Unilateral plantar erythema nodosum. *J Am Acad Dermatol* 1994;30:654–5.

Axel J. Hueber, MD, PhD
 Georg Schett, MD
 Bernhard Manger, MD
 Friedrich-Alexander University Erlangen-Nürnberg
 and Universitätsklinikum Erlangen
 Erlangen, Germany

Clinical Images: Unilateral plantar erythema nodosum in sarcoidosis



The patient, a 32-year-old man, presented with mild exertional dyspnea, pain and swelling of both ankles, and general malaise. Physical examination revealed symmetric arthritis in both ankles and a vivid nodular erythema on the sole of the right foot (A), accompanied by slight pain with pressure. Treatment with ibuprofen had not improved the symptoms. The erythrocyte sedimentation rate and C-reactive protein level were elevated (73 mm/hour and 30 mg/liter, respectively), but all other parameters, including levels of angiotensin-converting enzyme and soluble interleukin-2 receptor, were within normal range. Computed tomography of the chest showed enlarged mediastinal lymph nodes (C) (arrows) compatible with a diagnosis of Lofgren's syndrome. Based on this hypothesis, glucocorticosteroid treatment (starting dosage 40 mg/day) was initiated, after which the arthritis, dyspnea, and malaise resolved, and the levels of inflammation markers normalized within 2 weeks. The erythema nodosum improved and resolved after 2 months (B). A literature search revealed that unilateral plantar erythema nodosum is rare but is seen occasionally in children with infections (dermatophytes, *Streptococcus*, *Yersinia enterocolitica*, or *Mycoplasma*). In adults, only 3 cases have been reported. Plantar erythema nodosum was associated with Crohn's disease in 1 case (1) and with granulomatous mastitis in another (2); in the third, it appeared to be idiopathic (3). The patient described here represents the first reported case of unilateral plantar erythema nodosum with sarcoidosis.

1. Châtillon F, Chizzolini C, Kaya G, Borradori L, Hauser C. Plantar erythema nodosum in a patient with Crohn's disease. *Dermatology* 1999;199:190.
2. Polat M, Kaya H. Plantar erythema nodosum associated with granulomatous mastitis. *Indian J Dermatol Venereol Leprol* 2016;82:202-4.
3. Ohtake N, Kawamura T, Akiyama C, Furue M, Tamaki K. Unilateral plantar erythema nodosum. *J Am Acad Dermatol* 1994;30:654-5.

Axel J. Hueber, MD, PhD
Georg Schett, MD
Bernhard Manger, MD
*Friedrich-Alexander University Erlangen-Nürnberg
and Universitätsklinikum Erlangen
Erlangen, Germany*

Accumulation of Antigen-Driven Lymphoproliferations in Complement Receptor 2/CD21^{−/low} B Cells From Patients With Sjögren's Syndrome

Salomé Glauzy,¹ Marco Boccitto,¹ Jason M. Bannock,¹ Fabien R. Delmotte,¹
David Saadoun,² Patrice Cacoub,² John A. Ice,³ Kathy L. Sivils,⁴ Judith A. James,⁴
Sandra L. Wolin,¹ and Eric Meffre¹

Objective. Patients with Sjögren's syndrome (SS) are prone to develop malignant lymphomas, and a correlation has been established between the lymphoproliferations occurring in these disorders and the presence in patients' blood of an unusual B cell population that down-regulates complement receptor 2/CD21. This study was undertaken to identify the B cell compartment from which these lymphoproliferations emerge and determine the mechanisms that promote clonal B cell expansion in patients with SS.

Methods. The reactivity of antibodies expressed by CD19+CD10−CD27−IgM+CD21^{−/low} cells isolated from the blood of patients with SS was tested using a polymerase chain reaction–based approach that allows us to clone and express, in vitro, recombinant antibodies produced by single B cells.

Results. Clonal expansions were identified in CD21^{−/low} B cells isolated from the peripheral blood of 3 patients with SS. These lymphoproliferations expressed B cell receptors (BCRs) that displayed somatic hypermutation lineage trees characteristic of a strong selection by antigens; one of these antigens was identified as a ribosomal self antigen. When the mutated BCR sequences expressed by the expanded CD21^{−/low} B cell clones from patients with SS were reverted in vitro to their germline counterparts, one clone remained autoreactive.

Conclusion. Clonal lymphoproliferations in patients with SS preferentially accumulate in the autoreactive CD21^{−/low} B cell compartment often expanded in these subjects, and recognition of self antigens may drive the clonal B cell expansion while further refining BCR self-reactivity.

Supported by the NIH (National Institute of Allergy and Infectious Diseases [NIAID] grants AI-061093, AI-071087, and AI-082713 [to Dr. Meffre], NIAID and National Institute of Arthritis and Musculoskeletal and Skin Diseases grants U19-AI-082714 and P30-AR-053483 [to Drs. Sivils and James], National Institute of General Medical Sciences grant R01-GM-073863 [to Dr. Wolin], and Ruth L. Kirschstein National Service Award F32-ES-026227 [to Dr. Boccitto]).

¹Salomé Glauzy, PhD, Marco Boccitto, PhD, Jason M. Bannock, Fabien R. Delmotte, Sandra L. Wolin, MD, PhD, Eric Meffre, PhD: Yale University School of Medicine, New Haven, Connecticut; ²David Saadoun, MD, PhD, Patrice Cacoub, MD: Sorbonne Universités, UPMC Université Paris 06, UMR 7211, Inflammation-Immunopathology-Biotherapy Department, INSERM, UMR_S 959, CNRS, FRE3632, and AP-HP, Groupe Hospitalier Pitié-Salpêtrière, Department of Internal Medicine and Clinical Immunology, National Reference Center for Autoimmune and Autoinflammatory Diseases, Paris, France; ³John A. Ice, MD: Oklahoma Medical Research Foundation, Oklahoma City; ⁴Kathy L. Sivils, PhD, Judith A. James, MD, PhD: Oklahoma Medical Research Foundation and University of Oklahoma Health Sciences Center, Oklahoma City.

Address correspondence to Eric Meffre, PhD, Yale University School of Medicine, 300 George Street, Room 353F, New Haven, CT 06511. E-mail: Eric.meffre@yale.edu.

Submitted for publication November 10, 2016; accepted in revised form October 10, 2017.

Sjögren's syndrome (SS) is an autoimmune disease characterized by lymphocytic infiltration of the exocrine glands. The frequency of non-Hodgkin's B cell lymphoma is 15–20-fold higher in patients with SS than in the general population (1). The appearance of lymphoma correlates with an increased proportion of circulating CD19+CD10−CD27−IgM+CD21^{−/low} cells, referred to hereinafter as CD21^{−/low} B cells, suggesting that these B cells may represent the initial reservoir for transformed clones (2). Consistent with this hypothesis, increased numbers of circulating CD21^{−/low} B cells have been observed in patients with other autoimmune diseases, including rheumatoid arthritis (RA), and such patients are also prone to develop lymphomas, although at a lower frequency than in patients with SS, further supporting a correlation between CD21^{−/low} B cells and the emergence of transformed clones (3). However, monoclonal expansions in the CD21^{−/low} B cell compartment in patients with SS have not yet been reported.

Table 1. Characteristics of the patients with Sjögren's syndrome (SS)*

	Patient SS01	Patient SS1003	Patient SS201	Patient SS202	Patient SS53	Patient SS03	Patient SS204	Patient SS59
Sex	Female	Female	Female	Female	Female	Female	Female	Male
Age at study entry, years	28	69	45	67	56	71	57	76
PTPN22 genotype†	CC	CC	CT	CT	CC	CC	CC	CC
ANAs	1:1,280	+	+	+	+	+	+	1:120, nuclear speckled
Anti-Ro/anti-La	Both	Anti-Ro	None	Anti-Ro	Anti-Ro	Both	Anti-Ro	None
Rheumatoid factor	+	+	—	—	—	+	+	—
Monoclonal Ig	+	+	—	—	NA	+	+	NA
Cryoglobulin	+	+	—	—	NA	+	+	NA
Lymphocytic infiltrate‡	Chisholm grade 4	Chisholm grade 4	Chisholm grade 4	Chisholm grade 4	Focus score of 4.0; focal lymphocytic sialadenitis	Chisholm grade 4	Chisholm grade 4	Focus score of 1.1; focal lymphocytic sialadenitis
Lymphoma type	—	MALT lymphoma	MALT lymphoma	—	—	MZ lymphoma	Lymphocytic lymphoma	—
Site of lymphoma	—	Parotid gland	Orbit	—	—	Bone marrow	Lymph node	—
Medication	Steroids, HCQ	Rituximab	Rituximab	None	None	HCQ	Rituximab	None

* ANAs = antinuclear antibodies; NA = not available; MALT = mucosa-associated lymphoid tissue; MZ = marginal zone; HCQ = hydroxychloroquine.

† The CC genotype indicates a patient who did not carry the protein tyrosine phosphatase N22 (PTPN22) risk allele. The CT genotype indicates a patient who carried 1 PTPN22 risk allele.

‡ Grade 4 on the Chisholm and Mason scale for assessing labial salivary gland biopsy tissues (27) indicates the presence of >1 lymphocyte focus/4 mm² of tissue. A focus is an aggregate of ≥50 lymphocytes and histiocytes. Grades 3 and 4 (≥1 focus) are considered positive for a diagnosis of Sjögren's syndrome.

In the present study, we identified 3 patients with SS whose peripheral blood exhibited a monoclonal expansion in their CD21^{-low} B cells. In 2 of the SS samples, the lymphoproliferations expressed autoreactive antibodies.

PATIENTS AND METHODS

Patients. We recruited 8 patients with primary SS diagnosed according to the American–European Consensus Group criteria (4) (Table 1). Patients provided their signed informed consent prior to the collection of blood samples, in accordance with study protocols approved by the institutional review board.

Single-cell sorting. Mononuclear cells from the blood of healthy donors and patients with SS were enriched for B cells by magnetic separation with CD20 microbeads (Miltenyi Biotec). Prior to purification, the cells were stained with Pacific Blue–conjugated anti-human CD19, PerCP–Cy5.5–conjugated anti-human CD27, phycoerythrin–Cy7–conjugated anti-human CD10, allophycocyanin–conjugated anti-human CD21, and fluorescein isothiocyanate–conjugated anti-human IgM (all from BioLegend). Single cells were sorted on a FACSaria (BD Biosciences) in 96-well polymerase chain reaction (PCR) plates, into CD19+CD21^{low} CD10+IgM^{high}CD27– new emigrant/transitional B cells, CD19+CD21+CD10–IgM+CD27– mature naive B cells, and CD19^{high}CD21^{-low}CD10–CD27– B cells (the subset hereinafter referred to as CD21^{-low} B cells). The sorted cells were immediately frozen on dry ice.

Synthesis of complementary DNA, amplification of Ig genes, and production and purification of antibodies. RNA from single cells was reverse-transcribed in the original 96-well plates in 12.5- μ l reactions containing 100 units of Superscript II reverse transcriptase (RT) (Gibco BRL) for 45 minutes at 42°C. The RT-PCRs, primer sequences, cloning strategy, expression vectors, and methods used for in vitro antibody production and purification have been described previously (5).

Enzyme-linked immunosorbent assays (ELISAs) and indirect immunofluorescence assays. Analyses of antibody reactivity were performed as described previously, using a highly polyreactive antibody, ED38, as the positive control for assays of HEp-2 cell reactivity and polyreactivity, whereas mnUNGdef05 λ 50 and mnUNGdef05 κ 69, which were previously cloned from single mature naive B cells from a patient with uracil N-glycosylase (UNG) deficiency, were used as weak HEp-2-reactive and polyreactive control antibodies (5,6). Antibodies were considered polyreactive when they recognized all 3 distinct antigens: double-stranded DNA (dsDNA), insulin, and lipopolysaccharide (LPS). In addition, reactivity to Ro 52 and reactivity to rheumatoid factor were each assessed by a specific ELISA, in which the plates were coated with 1 μ g/ml Ro 52 (Sigma-Aldrich) or 1 μ g/ml rabbit IgG revealed by peroxidase-conjugated rabbit anti-human IgG (Jackson ImmunoResearch).

For indirect immunofluorescence assays, HEp-2 cell-coated slides (Bion Enterprises) were incubated in a moist chamber at room temperature with purified recombinant antibodies at 50–100 μ g/ml, in accordance with the manufacturer's instructions.

Strategy for reverting mutated antibodies to their unmutated counterpart. Using a multitemplate PCR strategy, germline V_H and J_H templates were first amplified with overlapping, reverted third complementarity-determining region (CDR3) primers combined with primers annealing with either

upstream germline V_H genes or downstream J_H segments. A second PCR fused the 2 overlapping V_H and J_H PCR fragments, thus generating germline revertant antibody sequences (7).

Immunoprecipitation and end-labeling of associated RNAs. Five micrograms of each monoclonal antibody was coupled to SureBeads protein G magnetic beads (Bio-Rad) for 30 minutes in phosphate buffered saline (PBS) at room temperature, with rotation. Beads were washed once in PBS, pH 7.4, and then equilibrated in NET-2 lysis buffer (50 mM Tris HCl [pH 7.4], 150 mM NaCl, 1 mM MgCl₂, 0.5% Nonidet P40). Cell lysates, prepared in NET-2 containing 1 \times complete protease inhibitors (Roche), 100 μ M phenylmethylsulfonyl fluoride, and 200 units/ml RNase OUT (Invitrogen), were added to the beads and incubated for 30 minutes. The beads were then washed 3 times in 750 μ l of NET-2, transferred to new microcentrifuge tubes, and washed an additional 3 times. Beads were then resuspended in 350 μ l NET-2, 2 μ l glycogen, 5 μ l 20% sodium dodecyl sulfate, and 40 μ l NaOAc. The resuspended beads were then extracted twice with acid phenol:chloroform:isoamyl alcohol (25:24:1, volume/volume), and the nucleic acids were precipitated from the aqueous phase with a 2.5 volume of ethanol. T4 RNA ligase was used to end-label the precipitated RNA with [³²P]-cytidine-3',5'-bisphosphate, overnight at 4°C. Labeled RNAs were then resolved on a 5% polyacrylamide–7M urea gel. Gels were dried, exposed on Fujifilm imaging plates, and visualized with a Typhoon imager system (GE Healthcare).

Statistical analysis. Statistical analysis was performed using GraphPad Prism software (version 5.0). Differences between groups were analyzed for statistical significance using a nonparametric Mann-Whitney test. *P* values less than or equal to 0.05 were considered significant.

RESULTS

Accumulation of monoclonal expansions in CD21^{-low} B cells from patients with SS. To determine the B cell compartment from which clonal lymphoproliferations either originated or colonized in the peripheral blood of patients with SS, we analyzed samples from 4 patients with SS in addition to 4 samples from a previously reported cohort of patients with SS (2,5) to amplify the expression of Ig genes in CD21^{-low} B cells and CD19+CD10–CD27–IgM+CD21+ mature naive B cells (Table 1). Samples from 5 of the patients with SS (identified as patients SS01, SS201, SS03, SS204, and SS59 in Table 1) showed enhanced frequencies of peripheral CD21^{-low} B cells, whereas only a few peripheral CD21^{-low} B cells were found in the blood of healthy donors (3) (Figure 1A).

Analyses of Ig sequences revealed the presence of monoclonal expansions in CD21^{-low} B cells from 3 of the 5 patients. In patients SS204 and SS59, clonal sequences accounted for 98% and 85% of the isolated CD21^{-low} B cells, respectively, whereas in patient SS03, all of the CD21^{-low} B cells corresponded to an expanded clone (Figure 1B; see also Supplementary Tables 1–3, available on the *Arthritis & Rheumatology* web site at <http://onlinelibrary.wiley.com/doi/10.1002/art.40352/abstract>). In patients SS03 and SS204, the

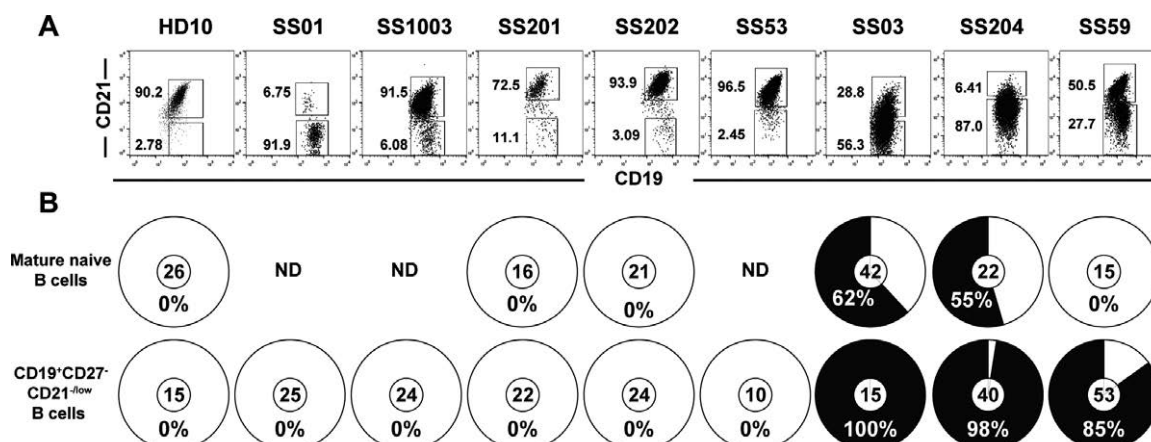


Figure 1. Accumulation of monoclonal expansions in CD21^{-low} B cells from patients with Sjögren's syndrome (SS). **A**, Dot plots represent the expression of CD19 and CD21 on CD19+CD27⁻ gated B cells from a representative healthy donor (HD) and 8 patients with SS. Values beside the boxes indicate the percentage of positive cells. **B**, Frequencies of monoclonal expansions (indicated as percentages and black-shaded portions of the pie charts) are summarized for the subsets of mature naive B cells and CD19+CD27⁻CD21^{-low} B cells. Values in the center circles are the number of sequences analyzed. ND = not done.

frequencies of clonal expansions were lower in mature naive B cells than in CD21^{-low} B cells (Figure 1B and Supplementary Tables 4 and 5 [http://onlinelibrary.wiley.com/doi/10.1002/art.40352/abstract]). Moreover, in patient SS03, clonal expansions were not detected in CD19+CD10+CD27⁻IgM^{high}CD21^{-low} new emigrant/transitional B cells (Supplementary Table 6 [http://onlinelibrary.wiley.com/doi/10.1002/art.40352/abstract]). These findings indicate that the origin of lymphoproliferations in SS could not be attributed to bone marrow. In sample SS59, from a patient with SS who did not develop lymphoma, monoclonal expansions were not identified in mature naive B cells (Figure 1B and Supplementary Table 7 [http://onlinelibrary.wiley.com/doi/10.1002/art.40352/abstract]), suggesting that the clonal expansions may have originated from CD21^{-low} B cells.

Strong antigen-specific selection revealed by the monoclonal expansion Ig sequences. We then analyzed the characteristics of the antibodies expressed by the monoclonal expansions of B cells from the blood of patients with SS. The expanded clones from all 3 SS samples expressed antibodies with mutated heavy-chain and light-chain genes, revealing that they originated from antigen-stimulated B cells (Figures 2 and 3). The preferential accumulation of replacement mutations in heavy-chain CDR regions of the expanded clonal B cells (CDR2 in sample SS03 and CDR1 in sample SS204) further supports the notion that antigenic selection pressure is occurring during these expansions (Figures 2A and B). In addition, the identification of related heavy-chain gene sequences with different numbers of mutations in the 3 clonal expansions also suggests that antigenic selection is ongoing

(Figures 2A and B). This was especially evident in the clonal expansion of B cells from patient SS03, in which clone H16 from the mature naive B cell compartment displayed only 8 mutations in its heavy chain, all of which were shared by the related clones that contained 12 additional mutations (Figures 2A and B). Of note, the expanded clone from patient SS59 contained the lowest numbers of mutations in both heavy-chain and light-chain genes, and this correlated with a modestly expanded CD21^{-low} B cell population (Figures 2A and B), suggesting that the lymphoproliferation and expansion began more recently in this patient than in the other 2 patients with SS.

Lineage tree analysis of the heavy chains expressed during SS clonal expansions revealed linear and poorly branched mutation acquisition patterns, suggesting that strong antigen-specific selection occurs (8) (Figure 2B). The κ -chains in the expanded clones from patients SS03 and SS204 also displayed intraclonal diversification with poorly branched lineage trees (Figures 3A and B). Strong antigenic selection was further evidenced by elevations in the replacement-to-silence mutation ratios in the CDRs, and sometimes in the framework regions, of the heavy chains and κ -chains expressed by these lymphoproliferations (Figures 2C and 3C). These findings support the conclusion that clonal expansions in patients with SS appear to be driven by strong antigenic stimulation.

Expression of potentially autoreactive antibodies by the monoclonal expansion of B cells in patients with SS. To determine the nature of the antigens that may drive lymphoproliferation, we tested the reactivity of the antibodies expressed by the monoclonal expansions of B cells in patients with SS. Since CD21^{-low} B cells are enriched in

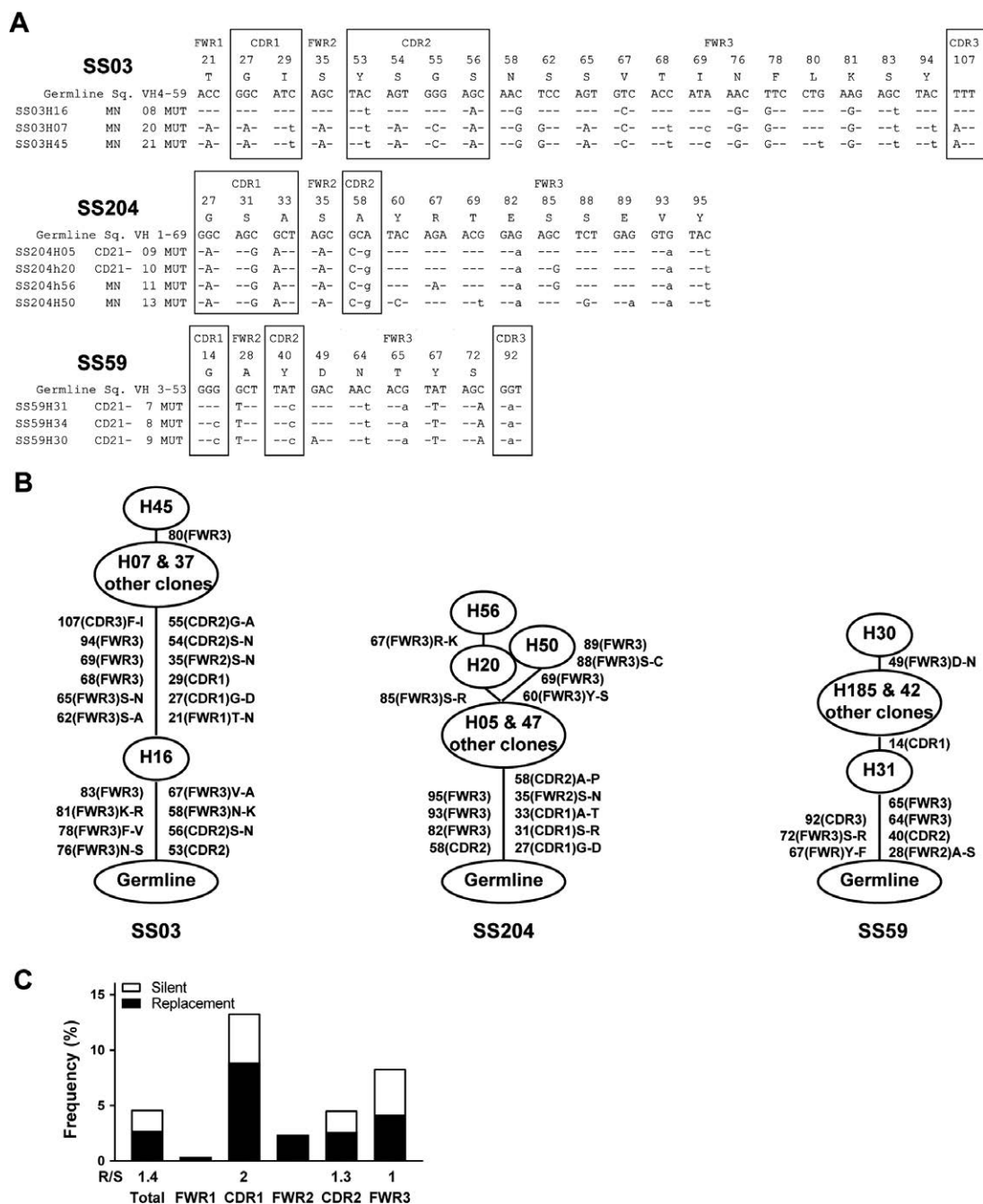


Figure 2. Clonal expansions in B cells from patients with Sjögren's syndrome (SS) are driven by antigenic stimulation. **A**, Alignments of Ig heavy-chain gene sequences (Sq.) of the monoclonal expansions from 3 patients with SS. Replacement amino acids are indicated in upper case, and silent mutations are shown in lower case. Codon positions within framework regions (FWRs) 1–3 and complementarity-determining regions (CDRs) 1–3 are indicated. **B**, Clonal trees of the monoclonal expansions from 3 patients with SS. Mutations and their codon position are indicated on the sides of the branches, with affected regions in parentheses and amino acid changes also shown. **C**, Frequencies of mutations in the V_H genes from combined lymphoproliferations, in total and for each FWR and CDR. Frequencies are calculated from the number of replacement (R) and silent (S) nucleotide exchanges per basepair. The R/S mutation ratio for each region is indicated when the number of silent mutations is not zero. MN = mature naive (B cells); MUT = mutations; CD21- = CD21^{-low} (B cells).

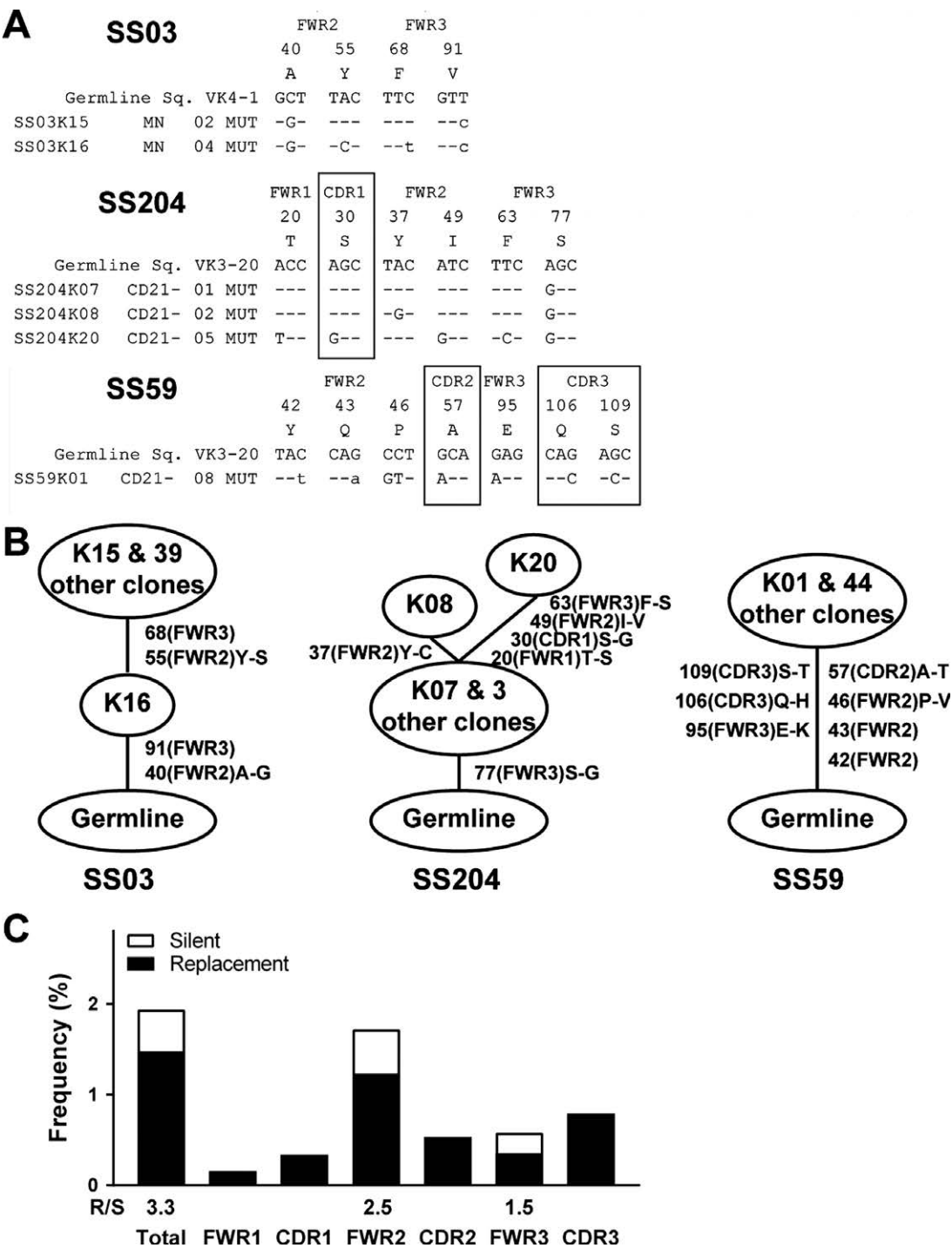


Figure 3. Intraclonal diversification, with poorly branched lineage trees, displayed by κ -chains in expanded B cell clones from patients with SS. **A**, Alignments of Ig κ -chain gene sequences of the monoclonal expansions from 3 patients with SS. Replacement amino acids are indicated in upper case, and silent mutations are shown in lower case. Codon positions within the FWRs and CDRs are indicated. **B**, Clonal trees of the monoclonal expansions from 3 patients with SS. Mutations and their codon position are indicated on the sides of the branches, with affected regions in parentheses and amino acid changes also shown. **C**, Frequencies of mutations in V_{κ} genes from combined lymphoproliferations, in total and for each FWR and CDR. Frequencies are calculated from the number of replacement and silent nucleotide exchanges per basepair. The R/S mutation ratio for each region is indicated when the number of silent mutations is not zero. See Figure 2 for definitions.

autoreactive clones (2), we performed ELISAs to assess their reactivity toward human HEP-2 cells and their potential multispecificity/polyreactivity (5). We found that in 2 of the 3 SS blood samples in which lymphoproliferations were evident, mutated recombinant antibodies cloned from samples SS59 and SS03 were autoreactive (Figure 4A). SS59 clones were highly HEP-2-reactive and polyreactive and recognized nuclear antigens (Figures 4A–C). Mutated antibodies arising from the SS03 clonal expansion were weakly HEP-2-reactive and polyreactive, as validated by comparisons with mnUNGdef05 λ 50, a low HEP-2-positive control antibody, and mnUNGdef05 κ 69, a low polyreactive-positive control antibody, respectively (6) (Figures 4A and C). Antibodies from the SS204 sample were not HEP-2-reactive or polyreactive, although some weak reactivity below the values for the low-positive control was detected for dsDNA and LPS antigens (Figures 4A and C).

Since Ro 52 is a major self antigen in SS, and anti-IgG rheumatoid factor reactivity has been suggested to be associated with lymphomas (9), we tested the SS lymphoproliferations for reactivity to these antigens (Figure 4D). Consistent with their aforementioned polyreactivity, SS59 clones and, to a lesser extent, SS03 clones displayed reactivity to Ro 52 and rheumatoid factor, while SS204 clones did not bind these self antigens (Figure 4D).

Because some prominent autoantigens in patients with SS, such as Ro 60, La, Sm, and RNP, consist of proteins complexed with small noncoding RNAs (10), we explored whether the self antigens recognized by SS lymphoproliferations included these RNAs. To determine this, we performed immunoprecipitations on human keratinocytes with these recombinant antibodies and examined the RNAs present in the immunoprecipitates. Although we did not detect the characteristic noncoding RNAs associated with these autoantigens, antinuclear antibodies from SS59 mutated clones recognized an antigen associated with 5S and 5.8S ribosomal RNAs (rRNAs), revealing that these antibodies may harbor antiribosomal reactivity (Figure 5). Antibodies from the SS03 and SS204 clones did not immunoprecipitate small RNAs (Figure 5). Taken together, these findings indicate that in 2 of the 3 SS samples displaying lymphoproliferations, autoreactive antibodies that cross-react with Ro 52 were expressed and rheumatoid factor reactivity was a shared feature. Furthermore, in 1 of the SS samples, a ribosomal antigen associated with 5S and 5.8S rRNAs was recognized.

Autoreactive B cell origin of the lymphoproliferations in patients with SS. To determine whether the autoreactive monoclonal B cell expansions in patients with SS were derived from unmutated self-reactive clones that

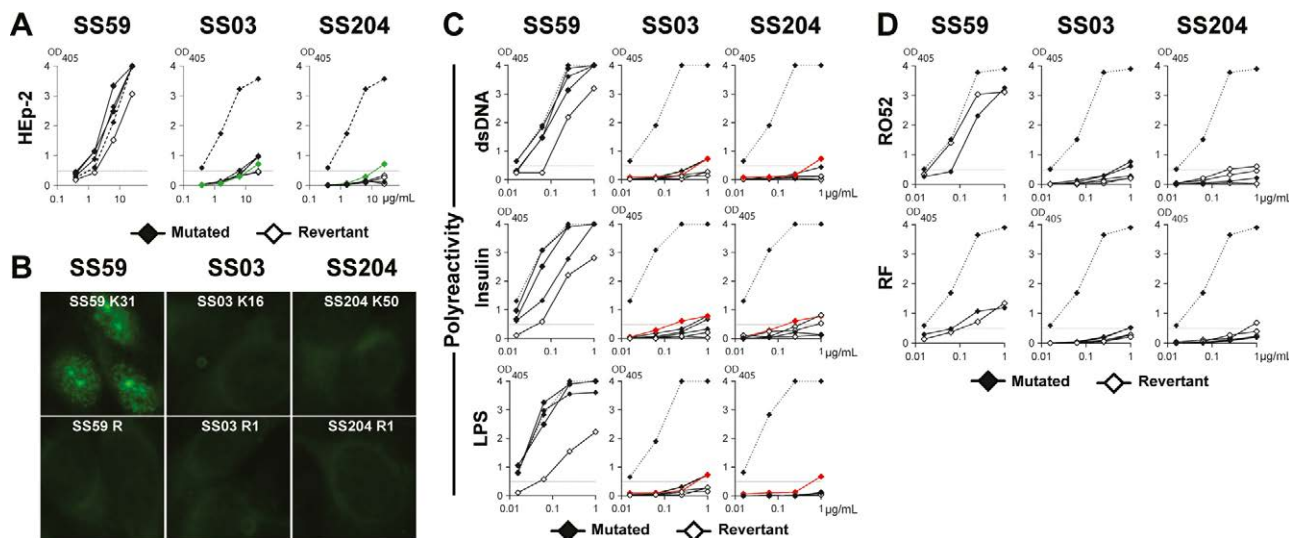


Figure 4. Expression of autoreactive antibodies by monoclonal B cell expansions in patients with Sjögren's syndrome (SS). **A**, Antibodies from mutated and revertant clones of B cells from patients with SS were tested by enzyme-linked immunosorbent assay (ELISA) for reactivity against HEP-2 cell lysates. The reactivity of the ED38-positive control (black solid diamonds with dotted lines) and that of the mnUNGdef05 λ 50 low-positive control (green solid diamonds with solid lines) are also shown. **B**, Immunofluorescence assays show that the recombinant mutated antibody from sample SS59 displays antinuclear reactivity, whereas no antibody reactivity is evident in samples SS03 and SS204. **C**, Antibodies from mutated and revertant clones of B cells from patients with SS were tested by ELISA for polyreactivity against double-stranded DNA (dsDNA), insulin, and lipopolysaccharide (LPS) antigens. The polyreactivity of the ED38-positive control (black solid diamonds with dotted lines) and that of the mnUNGdef05 κ 69 low-positive control (red solid diamonds with solid lines) are also shown. **D**, The reactivity of mutated and revertant antibodies from patients with SS to Ro 52 and rheumatoid factor (RF) was assessed by ELISA. Solid diamonds with dotted lines in **D** show the positive control. The horizontal lines in **A**, **C**, and **D** show the cutoff for positive reactivity at an optical density (OD) of 405 nm.

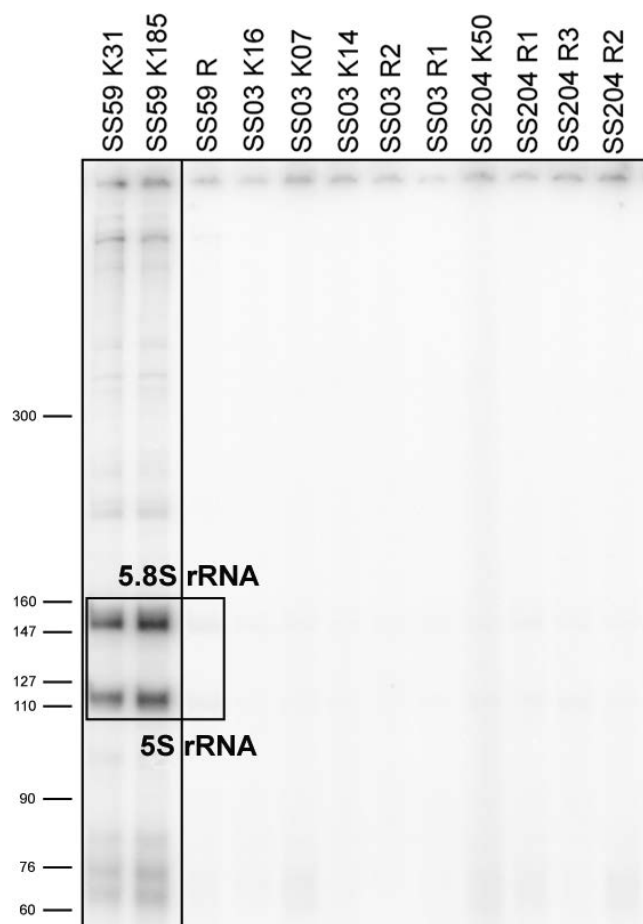


Figure 5. Binding of ribosomal components from the B cell lymphoproliferations in a patient with Sjögren's syndrome (SS). Antibodies from mutated clones (K) and revertant clones (R) of B cells from 3 patients with SS were used to carry out immunoprecipitations from human keratinocyte lysates. RNAs within the immunoprecipitates were end-labeled with [³²P]-cytidine-3',5'-bisphosphate. The boxed region denotes the 5S and 5.8S ribosomal RNAs (rRNAs) enriched after immunoprecipitation with recombinant mutated B cell clones from patient SS59.

acquired somatic hypermutation (SHM), we reverted in vitro-mutated antibody heavy-chain and light-chain genes to their original unmutated sequences (see Supplementary Figure 1, available on the *Arthritis & Rheumatology* web site at <http://onlinelibrary.wiley.com/doi/10.1002/art.40352/abstract>) (7). Because Ig heavy-chain CDR3 regions play an essential role in conferring antibody polyreactivity and, potentially, autoreactivity (11), we designed primers to revert CDR3 sequences, referred to hereinafter as revertants, thereby allowing for conservative, and sometimes more extended, reversion scenarios for these antibodies (see Supplementary Figure 1). We then tested the revertant reactivities by ELISA and immunofluorescence assays, and compared their

reactivities to those of their mutated counterparts (Figure 4). The reverted antibody from SS59 monoclonal expansions retained HEp-2 reactivity (Figure 4A), suggesting that this lymphoproliferation may originate from an intrinsically self-reactive B cell.

Consistent with this hypothesis, the SS59 revertant also remained polyreactive and retained Ro 52 and rheumatoid factor reactivity, although this unmutated antibody bound dsDNA, insulin, and LPS with decreased affinity (Figures 4C and D). However, we found that SHM was responsible for the antinuclear reactivity of sample SS59, because the SS59 revertant did not stain nuclear structures and did not enrich for 5S and 5.8S rRNAs in immunoprecipitations (Figures 4B and 5). Revertants from samples SS03 and SS204 showed weak reactivity against some of the tested antigens. SS03 revertants were borderline HEp-2-reactive but were not polyreactive and did not bind Ro 52 or IgG (Figure 4). Although SS204 revertants were not HEp-2-reactive, some of them displayed weak reactivity for insulin, Ro 52, and rheumatoid factor (Figure 4). We conclude that lymphoproliferations in CD21^{-low} B cells from patients with SS often express autoreactive antibodies, and these may originate from B cell clones activated by self antigens. This process may promote the proliferation of B cells and the acquisition of SHM, thereby enhancing the B cell receptor (BCR) affinity for self.

DISCUSSION

We showed that the lymphoproliferations occurring in the peripheral blood of patients with SS accumulate in the CD21^{-low} B cell compartment and are often characterized by the expression of autoreactive antibodies. Non-Hodgkin's B cell lymphoma occurs frequently in patients with SS, and its occurrence is reportedly correlated with the proportion of CD21^{-low} B cells in the patient's blood (2,12,13). In addition, patients with other autoimmune diseases, including RA and systemic lupus erythematosus, or those with chronic infections are also prone to develop lymphomas, although at a lower frequency than in SS, and display increased numbers of CD21^{-low} B cells in their blood, further supporting the notion of a correlation between CD21^{-low} B cells and the emergence of transformed clones (3,9,14).

By studying samples from patients with SS in which the frequency of CD21^{-low} B cells was at least 30% in the CD19+CD27⁻ peripheral B cell compartment, we identified 3 patients who displayed monoclonal expansions in their blood. All 3 patients with SS showed the highest frequency of expanded clones in their CD21^{-low} B cells, suggesting that the monoclonal expansions may originate from this compartment. Consistent with this hypothesis,

the lymphoproliferation occurring in 1 of the SS samples was restricted to CD21^{-low} B cells and was not detected in other B cell compartments, including new emigrant/transitional and mature naive B cells. Of note, samples SS1003 and SS201, both of which were from patients with mucosa-associated lymphoid tissue lymphoma, displayed only a modest increase in the frequency of CD21^{-low} B cells. However, both of these patients had been treated with rituximab, a medication that depletes B cells; therefore, their treatment likely led to alterations in the frequency of CD21^{-low} B cells in their blood. Since CD21^{-low} B cells from patients with SS and patients with RA often express autoreactive antibodies, it is likely that these cells may contain self-reactive precursors of lymphoproliferation (2,3).

However, the detection of monoclonal expansions in mature naive B cells from 2 of the patients with SS may challenge this scenario. Our findings suggest that lymphoproliferations could emerge from this peripheral B cell compartment, which is also enriched in autoreactive clones (15). Consistent with this hypothesis, a precursor clone (H16) was identified in mature naive B cells that displayed a heavy chain with only 8 mutations, whereas all other related clones from mature naive and CD21^{-low} B cells harbored 12 additional mutations. Therefore, lymphoproliferative clones may originate from activated mature naive B cells and then preferentially develop and accumulate in the CD21^{-low} B cell compartment. However, we cannot exclude the possibility that the detection of expanded clones in mature naive B cells might be attributed to the suboptimal gating strategies that were utilized to distinguish CD21^{-low} B cells from CD21⁺ mature naive B cells, since all other cell surface markers used to identify these 2 B cell subpopulations are the same. Indeed, the overwhelming expansion of transformed clones expressing low levels of surface CD21 may contribute to their detection in CD21-expressing mature naive B cells. Additional studies are therefore warranted to determine whether B cell lymphomas in patients with SS originate either from mature naive B cells or from CD21^{-low} B cells, both of which are enriched in autoreactive clones.

An interesting line of inquiry is to determine what mechanisms preside over the emergence of B cell lymphomas accumulating in the CD21^{-low} B cell compartment. Intrinsic and extrinsic B cell mechanisms likely contribute to the development of lymphomas in patients with SS. Long-term stimulation of BCRs by self antigens may favor the malignant transformation of CD21^{-low} B cells (5,8). Consistent with this hypothesis, we found that expanded B cell clones from 2 of the 3 patients with SS expressed mutated autoreactive BCRs, whereas antibodies expressed by expanded B cells from patient SS204 did

not appear to be autoreactive. The poorly branched trees, reflecting the linear SHM acquisition history of the lymphoproliferations identified in all 3 patients with SS, suggest a strong antigen-specific selection in which rare SHM events that increase BCR self-reactivity are highly selected (8). The putative unmutated germline clones from which the 3 mutated SS B cell expansions originated displayed either decreased or no self-reactivity in comparison to their mutated counterparts, suggesting that SHM did increase self-reactivity in both lymphoproliferations in which autoreactive BCRs were expressed.

BCR self-reactivity seems to be a common feature shared by many B cell lymphomas, including chronic lymphocytic lymphomas and diffuse large B cell lymphomas (7,16). In diffuse large B cell lymphomas, BCRs have been reported to recognize dying cells or DNA (16–18). BCR self-reactivity is critical for the survival and maintenance of transformed B cell clones, because replacement by nonautoreactive BCRs induced clonal death (16). BCR self-reactivity is also associated with the emergence of chronic lymphocytic lymphomas, being characterized by the emergence of clones that retain strong self-reactive BCR features and that are associated with worse prognoses in patients (7). The recognition of nuclear antigens, such as ribosomal structures, as observed herein in the B cell expansions in patient SS59, may facilitate the activation and proliferation of B cells, because these self antigens contain RNAs that provide BCR costimulatory signals through binding of Toll-like receptor 7 (TLR-7) (19).

Similarly, rheumatoid factor reactivity, which has been identified in salivary gland lymphomas or inferred on the basis of CDR3 homology, may also be a factor contributing to the TLR-7–driven activation of clonally expanded B cells in patients with SS, since a common feature in the serum of patients with SS is the binding of the clonally expanded BCRs to IgG immune complexes that contain small noncoding RNAs (20,21). TLR-7/BCR coligation induces the expression of Axl in B cells, which may favor the formation or recruitment of these activated B cells in tertiary lymphoid structures (22). Lymphomas in patients with SS, usually found in the mucosal tissue, may initially develop in a salivary gland from a cluster of proliferating B cells that seed tertiary lymphoid structures, thereby offering a favorable environment for B cell expansion by providing T cell help and BAFF (9,23,24).

Indeed, BAFF is important for B cell survival, and its concentration is elevated in the serum and salivary glands of patients with SS (25). Since CD21^{-low} B cells are dependent on BAFF for their survival, anti-BAFF therapy may be beneficial in patients with SS, by affecting the survival of proliferating B cells (26). Alternatively, and despite the heterogeneous efficacy of anti-B cell therapy

in patients with SS, anti-CD20 therapy may be considered, since it has the capacity to eliminate CD21^{-low} B cells, including potentially premalignant clonal B cell expansions that display high expression of CD20. Additional analyses could clarify which regimen may be more beneficial to thwart autoimmune features and eliminate clonal B cell lymphoproliferations in patients with SS.

ACKNOWLEDGMENTS

We thank Dr. Nancy Ruddle for her insightful comments on the manuscript, and Dr. L. Devine and C. Wang for performing the cell sorting.

AUTHOR CONTRIBUTIONS

All authors were involved in drafting the article or revising it critically for important intellectual content, and all authors approved the final version to be published. Dr. Meffre had full access to all of the data in the study and takes responsibility for the integrity of the data and the accuracy of the data analysis.

Study conception and design. Meffre.

Acquisition of data. Glauzy, Boccitto, Bannock, Delmotte, Saadoun, Cacoub, Ice, Sivils, James, Meffre.

Analysis and interpretation of data. Glauzy, Boccitto, Wolin, Meffre.

REFERENCES

- Ioannidis JP, Vassiliou VA, Moutsopoulos HM. Long-term risk of mortality and lymphoproliferative disease and predictive classification of primary Sjögren's syndrome. *Arthritis Rheum* 2002;46:741–7.
- Saadoun D, Terrier B, Bannock J, Vazquez T, Massad C, Kang I, et al. Expansion of autoreactive unresponsive CD21^{-low} B cells in Sjögren's syndrome-associated lymphoproliferation. *Arthritis Rheum* 2013;65:1085–96.
- Isnardi I, Ng YS, Menard L, Meyers G, Saadoun D, Srdanovic I, et al. Complement receptor 2/CD21- human naive B cells contain mostly autoreactive unresponsive clones. *Blood* 2010;115:5026–36.
- Vitali C, Bombardieri S, Jonsson R, Moutsopoulos HM, Alexander EL, Carsons SE, et al. Classification criteria for Sjögren's syndrome: a revised version of the European criteria proposed by the American-European Consensus Group. *Ann Rheum Dis* 2002;61:554–8.
- Wardemann H, Yurasov S, Schaefer A, Young JW, Meffre E, Nussenzweig MC. Predominant autoantibody production by early human B cell precursors. *Science* 2003;301:1374–7.
- Cantaert T, Schickel JN, Bannock JM, Ng YS, Massad C, Delmotte FR, et al. Decreased somatic hypermutation induces an impaired peripheral B cell tolerance checkpoint. *J Clin Invest* 2016;126:4289–302.
- Hervé M, Xu K, Ng YS, Wardemann H, Albesiano E, Messmer BT, et al. Unmutated and mutated chronic lymphocytic leukemias derive from self-reactive B cell precursors despite expressing different antibody reactivity. *J Clin Invest* 2005;115:1636–43.
- William J, Euler C, Primarolo N, Shlomchik MJ. B cell tolerance checkpoints that restrict pathways of antigen-driven differentiation. *J Immunol* 2006;176:2142–51.
- Nocturne G, Virone A, Ng WF, le Guern V, Hachulla E, Cornec D, et al. Rheumatoid factor and disease activity are independent predictors of lymphoma in primary Sjögren's syndrome. *Arthritis Rheumatol* 2016;68:977–85.
- Hardin JA, Rahn DR, Shen C, Lerner MR, Wolin SL, Rosa MD, et al. Antibodies from patients with connective tissue diseases bind specific subsets of cellular RNA-protein particles. *J Clin Invest* 1982;70:141–7.
- Ichiyoshi Y, Casali P. Analysis of the structural correlates for antibody polyreactivity by multiple reassortments of chimeric human immunoglobulin heavy and light chain V segments. *J Exp Med* 1994;180:885–95.
- Zintzaras E, Voulgarelis M, Moutsopoulos HM. The risk of lymphoma development in autoimmune diseases: a meta-analysis. *Arch Intern Med* 2005;165:2337–44.
- Theander E, Henriksson G, Ljungberg O, Mandl T, Manthorpe R, Jacobsson LT. Lymphoma and other malignancies in primary Sjögren's syndrome: a cohort study on cancer incidence and lymphoma predictors. *Ann Rheum Dis* 2006;65:796–803.
- Charles ED, Brunetti C, Marukian S, Ritola KD, Talal AH, Marks K, et al. Clonal B cells in patients with hepatitis C virus-associated mixed cryoglobulinemia contain an expanded anergic CD21^{low} B-cell subset. *Blood* 2011;117:5425–37.
- Glauzy S, Sng J, Bannock J, Gottenberg JE, Korganow AS, Cacoub P, et al. Defective early B cell tolerance checkpoints in Sjögren's syndrome patients. *Arthritis Rheumatol* 2017;69:2203–08.
- Young RM, Wu T, Schmitz R, Dawood M, Xiao W, Phelan JD, et al. Survival of human lymphoma cells requires B-cell receptor engagement by self-antigens. *Proc Natl Acad Sci U S A* 2015;112:13447–54.
- Catera R, Silverman GJ, Hatzi K, Seiler T, Didier S, Zhang L, et al. Chronic lymphocytic leukemia cells recognize conserved epitopes associated with apoptosis and oxidation. *Mol Med* 2008;14:665–74.
- Chu CC, Catera R, Zhang L, Didier S, Agagnina BM, Damle RN, et al. Many chronic lymphocytic leukemia antibodies recognize apoptotic cells with exposed nonmuscle myosin heavy chain IIA: implications for patient outcome and cell of origin. *Blood* 2010;115:3907–15.
- Lau CM, Broughton C, Tabor AS, Akira S, Flavell RA, Mamula MJ, et al. RNA-associated autoantigens activate B cells by combined B cell antigen receptor/Toll-like receptor 7 engagement. *J Exp Med* 2005;202:1171–7.
- Martin T, Weber JC, Levallois H, Labouret N, Soley A, Koenig S, et al. Salivary gland lymphomas in patients with Sjögren's syndrome may frequently develop from rheumatoid factor B cells. *Arthritis Rheum* 2000;43:908–16.
- Bende RJ, Aarts WM, Riedl RG, de Jong D, Pals ST, van Noesel CJ. Among B cell non-Hodgkin's lymphomas, MALT lymphomas express a unique antibody repertoire with frequent rheumatoid factor reactivity. *J Exp Med* 2005;201:1229–41.
- Nündel K, Green NM, Shaffer AL, Moody KL, Busto P, Eilat D, et al. Cell-intrinsic expression of TLR9 in autoreactive B cells constrains BCR/TLR7-dependent responses. *J Immunol* 2015;194:2504–12.
- Mariette X. Lymphomas complicating Sjögren's syndrome and hepatitis C virus infection may share a common pathogenesis: chronic stimulation of rheumatoid factor B cells. *Ann Rheum Dis* 2001;60:1007–10.
- Stott DI, Hiepe F, Hummel M, Steinhauser G, Berek C. Antigen-driven clonal proliferation of B cells within the target tissue of an autoimmune disease: the salivary glands of patients with Sjögren's syndrome. *J Clin Invest* 1998;102:938–46.
- Groom J, Kalled SL, Cutler AH, Olson C, Woodcock SA, Schneider P, et al. Association of BAFF/BLyS overexpression and altered B cell differentiation with Sjögren's syndrome. *J Clin Invest* 2002;109:59–68.
- Jacobi AM, Huang W, Wang T, Freimuth W, Sanz I, Furie R, et al. Effect of long-term belimumab treatment on B cells in systemic lupus erythematosus. *Arthritis Rheum* 2010;62:201–10.
- Chisholm DM, Mason DK. Labial salivary gland biopsy in Sjögren's disease. *J Clin Pathol* 1968;21:656–60.

Belimumab for the Treatment of Early Diffuse Systemic Sclerosis

Results of a Randomized, Double-Blind, Placebo-Controlled, Pilot Trial

Jessica K. Gordon¹, Viktor Martyanov,² Jennifer M. Franks,² Elana J. Bernstein,³ Jackie Szymonifka,³ Cynthia Magro,⁴ Horatio F. Wildman,⁴ Tammara A. Wood,² Michael L. Whitfield,² and Robert F. Spiera¹

Objective. To assess the safety and efficacy of treatment with belimumab in patients with early diffuse cutaneous systemic sclerosis (dcSSc) treated with background mycophenolate mofetil (MMF).

Methods. In this 52-week, investigator-initiated, single-center, double-blind, placebo-controlled, pilot study, 20 patients with dcSSc recently started on MMF were randomized 1:1 to additionally receive belimumab at 10 mg/kg intravenously or placebo. We assessed safety, efficacy, and differential gene expression.

Results. In the belimumab group, the median modified Rodnan skin thickness score (MRSS) decreased from 27 (interquartile range [IQR] 26.5, 31) to 18 (IQR 11, 23) ($P = 0.039$). In the placebo group, the median MRSS decreased from 28 (IQR 22, 28) to 21 (IQR 14, 25) ($P = 0.023$). The median change in MRSS was -10 (IQR -13 , -9) in the belimumab group and -3.0 (IQR -15 , -1) in the placebo group ($P = 0.411$). There were no significant differences between the groups in the number of

adverse events (AEs). A significant decrease in expression of B cell signaling and profibrotic genes and pathways was observed in patients with improved MRSS in the belimumab group but not in the placebo group.

Conclusion. Patients in both treatment groups experienced significant improvements in MRSS. The median difference was greater in the belimumab group but did not achieve statistical significance in this small pilot study. AEs were similar between the groups. Changes in gene expression were consistent with mechanism of action and showed that clinical response to treatment with belimumab is associated with a significant decrease in profibrotic genes and pathways. Additional studies are needed to determine the role of belimumab in the treatment of dcSSc.

Systemic sclerosis (SSc) is a multisystem connective tissue disease characterized by autoimmunity, fibrosis, and vasculopathy (1). Immune dysregulation in SSc is manifested by the presence of autoantibodies and alterations in phenotype and activation levels of B cells, T cells, cytokines, and other components of the immune system (2). Current treatment paradigms for SSc depend on the organ system involved and include immunosuppressive regimens such as methotrexate, mycophenolate mofetil (MMF), cyclophosphamide, and autologous stem cell transplantation for severe and rapidly progressive disease with poor prognostic features (3). Although these treatments are effective, improved therapies for SSc are needed (4).

Abnormalities in B cell function and homeostasis have been observed in SSc. Skin and lung samples from SSc patients show B cell infiltrates (5,6). Gene expression studies performed on SSc skin show high expression of immunoglobulin genes in patients from an inflammatory intrinsic molecular gene expression subset (7). B cell homeostasis is disrupted in SSc, with greater numbers of

ClinicalTrials.gov identifier: NCT01670565.

Supported by GlaxoSmithKline.

¹Jessica K. Gordon, MD, MSc, Robert F. Spiera, MD: Hospital for Special Surgery, New York, New York; ²Viktor Martyanov, PhD, Jennifer M. Franks, BS, Tammara A. Wood, MS, Michael L. Whitfield, PhD: Geisel School of Medicine at Dartmouth, Hanover, New Hampshire; ³Elana J. Bernstein, MD, MSc, Jackie Szymonifka, MA: New York Presbyterian Hospital, Columbia University, New York, New York; ⁴Cynthia Magro, MD, Horatio F. Wildman, MD: Weill Cornell Medical College, New York, New York.

Dr. Whitfield has received consulting fees from Bristol-Myers Squibb, GlaxoSmithKline, Biogen, and Shire (less than \$10,000 each) and from UCB and Celdara Medical (more than \$10,000 each). Dr. Spiera has received consulting fees from GlaxoSmithKline (less than \$10,000).

Address correspondence to Jessica K. Gordon, MD, MSc, Hospital for Special Surgery, Department of Rheumatology, 535 East 70th Street, New York, NY 10021. E-mail: gordonj@hss.edu.

Submitted for publication May 19, 2017; accepted in revised form October 19, 2017.

transitional and naive B cells and fewer memory B cells as well as altered expression of molecules involved in B cell regulation compared with healthy controls (8). Although reduced in number, memory B cells in SSc are hyperreactive, leading to increased antibody formation (9). BAFF, also known as B lymphocyte stimulator (BLyS), is increased in the serum of patients with SSc and correlates with the extent of skin fibrosis (10). Serum levels of APRIL, a homolog of BAFF, are also elevated in SSc patients and have been associated with an increased incidence of pulmonary fibrosis (11).

Anti-B cell strategies using rituximab, a monoclonal antibody directed against the CD20 antigen, have been studied for use in SSc in observational studies and small trials. In a retrospective study from the European League Against Rheumatism (EULAR) Scleroderma Trial and Research group, patients with diffuse cutaneous SSc (dcSSc) who were treated with rituximab had a greater decrease in modified Rodnan skin thickness score (MRSS) (12) and a smaller decline in forced vital capacity (FVC) compared with matched controls (13). Prospective studies have shown mixed results—some with benefit (14) and others without significant change (5).

Belimumab (Benlysta; GlaxoSmithKline) is a recombinant, fully human monoclonal antibody which is approved by the US Food and Drug Administration for the treatment of systemic lupus erythematosus (15). Belimumab binds to soluble human BLyS and inhibits its biologic activity, leading to apoptosis of B lymphocytes and decreased autoantibody production (16). We report the first investigation of the use of belimumab in SSc.

PATIENTS AND METHODS

Study design and participants. This was an investigator-initiated, industry-supported, single-center, randomized, double-blind, placebo-controlled, pilot study. Patients fulfilled both the American College of Rheumatology (ACR) preliminary criteria for SSc (17) and the ACR/EULAR 2013 criteria for SSc (18) and had dcSSc (19). Patients were included if they were age >18 years, had disease duration of <3 years since the first SSc-related symptom other than Raynaud's phenomenon (RP), and had a baseline MRSS of ≥ 16 . Patients were excluded if their diffusing capacity for carbon monoxide (DLco) was <30% predicted, if their ejection fraction was <50%, if they had been receiving MMF for >3 months, if they had previously received rituximab or belimumab, or if they required prednisone at >10 mg/day (full inclusion criteria are available in Supplementary File 1, available on the *Arthritis & Rheumatology* web site at <http://onlinelibrary.wiley.com/doi/10.1002/art.40358/abstract>). The protocol was approved by the Institutional Review Board at Hospital for Special Surgery. Patients provided written informed consent before enrollment, and the study was performed in accordance with the Declaration of Helsinki and Good Clinical Practice Guidelines. An

independent data and safety monitoring board regularly reviewed safety data.

The primary objective was to assess the safety and tolerability of belimumab in patients with dcSSc receiving background MMF therapy, as assessed by the number of adverse events (AEs) and serious AEs (SAEs). The primary efficacy end point was the difference in the median change in MRSS after 52 weeks of treatment. Secondary efficacy end points included change in MRSS at 6 months as well as change at 52 weeks in FVC and DLco on pulmonary function testing (PFT) and change at 52 weeks in the Short Form 36 (SF-36) health survey mental component summary (MCS) score and physical component summary (PCS) score (20), the Scleroderma Health Assessment Questionnaire disability index (SHAQ DI) score (21), and, post hoc, the ACR composite response index in dcSSc (CRISS) score (22). Skin biopsy samples were assessed using histopathology, immunohistochemistry, and differential gene expression analysis to evaluate change with treatment and to explore the biologic basis of the clinical changes observed. Serum BLyS levels were assessed at baseline using a custom enzyme-linked immunosorbent assay (ELISA) (see Supplementary File 2, <http://onlinelibrary.wiley.com/doi/10.1002/art.40358/abstract>).

Patients were assessed at monthly visits for AE ascertainment, interval history, physical examination, and clinical laboratory testing. AEs were listed according to the National Cancer Institute's common terminology (23). The MRSS was measured at screening, baseline, and every 3 months by the same physician (JKG or RFS). PFTs with measurement of FVC and DLco were performed at baseline and after 6 and 12 months.

Dosing and visits. At baseline, 14 patients were naive to MMF and the other 6 had been receiving MMF at <2,000 mg/day for <3 months. The MMF-naive group was started on MMF at their first baseline visit, and this dose was up-titrated over the course of 2 weeks to 1,000 mg twice daily by mouth with weekly complete blood counts. All patients continued to receive MMF monotherapy for 3 months to ensure individual tolerability of MMF. MMF was chosen so that background therapy would be uniform and not a further source of variability in this small study. Our preference is to use MMF over methotrexate in patients with interstitial lung disease (ILD), and such patients were included. Two patients withdrew during the wash-in period due to disease progression. After this wash-in period, patients were randomized to receive belimumab or identical placebo at the second baseline visit. Belimumab at 10 mg/kg or identical placebo (normal saline) was given intravenously at 2-week intervals for the first 3 doses and then at 4-week intervals until week 48 as patients maintained background MMF at 1,000 mg twice daily. The final assessment occurred 4 weeks following the final belimumab infusion at week 52. Adherence to MMF was assessed by pill count.

Randomization and blinding. Patients were randomly assigned (1:1) using block randomization performed by personnel in biostatistics and pharmacy. Investigators, patients, and study personnel were masked to treatment assignment.

Dermatopathology. Two 3-mm punch biopsies of lesional forearm skin were performed at the first baseline visit and at 52 weeks. The posttreatment biopsy samples were obtained 1-cm adjacent to baseline biopsy samples. At each time point, one specimen was formalin-fixed and paraffin-embedded, and the other was stored in RNAlater. Sections for histopathology were stained with hematoxylin and eosin (H&E), anti- α -smooth muscle actin (anti- α -SMA), CD34, procollagen, CD3, and CD79 using standard techniques. A dermatopathologist (CM) who was blinded with regard

to treatment status compared each case. Slides were scored semi-quantitatively based on collagen density and degree of infiltrate on H&E staining as well as intensity of staining. Skin thickness was measured from the epidermis to the subcutis by a micrometer. Eccrine coils and hair follicles were counted per section.

Statistical analysis. This pilot trial was conducted to obtain initial safety and efficacy data in order to perform a power calculation for a larger study, so formal power calculation was not done to determine sample size. The efficacy analyses were performed using a modified intent-to-treat population, including all randomly assigned patients who received at least 1 dose of study drug and had at least 1 follow-up MRSS. This included 9 patients in each group. Comparative safety analyses included all patients who were randomized and received at least 1 infusion ($n = 20$). For subanalyses, we classified patients as clinical improvers if they individually demonstrated a 20% decrease in the MRSS, as in previous studies (24).

Comparisons were performed using Mann-Whitney U tests and Wilcoxon signed rank tests, as appropriate. All analyses were performed using SAS software version 9.3 for Windows (SAS Institute) with a significance level of 0.05. Since this was a pilot trial, adjustment for multiple comparisons was not performed for the clinical outcomes.

Gene expression analyses by DNA microarray. Tissue samples stored in RNAlater were homogenized, and RNA was purified as previously described (25). Baseline and posttreatment biopsy samples from 18 patients were used for analyses. Expression data were imputed for missing values and collapsed to unique genes using GenePattern (26), median-centered in Cluster 3.0 (27), and visualized in Java TreeView (28). Data from this study are available from the NCBI GEO (accession no. GSE97248).

Differentially expressed genes (DEGs) were identified via Significance Analysis of Microarrays (29). DEGs with a false discovery rate (FDR) of $\leq 10\%$ were treated as significant and were evaluated for significant functional enrichment via g:Profiler (30) ($P \leq 0.05$ corrected for multiple testing via default Gene Set Counts and Sizes method). We performed gene set enrichment analysis (GSEA) (31,32) in GenePattern. GSEA was run against Canonical Pathways database version 5.2. Pathways with a GSEA FDR of $\leq 5\%$ were treated as significant.

Intrinsic subset assignment. Expression data and subset labels collected from GEO accession nos. GSE9285, GSE32413, and GSE45485 were used to train and test a multinomial elastic net (25,33,34). The glmnet (35) and caret (36) packages implemented in R (www.r-project.org) were used with repeated cross-validation ($10\times$, 3-fold) to train the classifier and assess robustness (37). The inflammatory subset score was quantified as the probability of being assigned to the inflammatory molecular subset from the multinomial elastic net.

RESULTS

Primary and secondary efficacy analyses. Patients were recruited from August 17, 2012 until September 12, 2014. Of 25 patients screened, 22 patients enrolled in the MMF wash-in period (see Supplementary File 3, <http://onlinelibrary.wiley.com/doi/10.1002/art.40358/abstract>). Two

patients withdrew prior to randomization—1 due to scleroderma renal crisis and 1 due to progressive myopathy. Twenty patients were randomized 1:1, and 9 patients in each group completed 52 weeks of treatment. One patient in the placebo group withdrew due to progressive cardiomyopathy, and 1 in the belimumab group withdrew due to progressive ILD after receiving 2 infusions. Both patients withdrew prior to the 12-week MRSS assessment. Baseline characteristics of randomized patients were balanced between groups with 2 exceptions. The baseline SHAQ DI score and RP score on a visual analog scale (VAS) were significantly worse in the belimumab group (Table 1).

Patients in both groups experienced significant improvements in the MRSS. In the belimumab group, the median MRSS decreased from 27 (interquartile range [IQR] 26.5, 31) to 18 (IQR 11, 23) ($P = 0.039$), while in the placebo group, the median MRSS decreased from 28 (IQR 22, 28) to 21 (IQR 14, 25) ($P = 0.023$) (Figure 1A). The MRSS changed by a median of -10 (IQR -13 , -9) in the

Table 1. Characteristics of the patients at baseline*

	Belimumab	Placebo
Age, mean \pm SD years	56.7 \pm 10.26	53 \pm 12.1
Disease duration, mean \pm SD months	11.7 \pm 7.82	9 \pm 4.03
Female, %	80	70
Caucasian, %	90	70
Hispanic, %	30	10
ILD, %	10	20
Anti-Scl-70 positive, %	20	30
Anti-RNA polymerase III positive, %	70	30
MRSS, 0–51	27 (26.5, 31)	28 (22, 28)
SHAQ DI score, 0–3	1.38 (1.13, 1.75) [†]	0.38 (0.13, 0.63)
VAS pain score, 0–150 mm	45.0 (42.0, 55.0)	30.0 (4.0, 49.0)
VAS RP score, 0–150 mm	63.0 (43.0, 74.0) [‡]	8.0 (0.0, 12.0)
VAS ulcers score, 0–150 mm	0.0 (0.0, 66.0)	0.0 (0.0, 3.0)
VAS breathing score, 0–150 mm	1.0 (0.0, 11.0)	0.0 (0.0, 19.0)
VAS overall score, 0–150 mm	48.0 (33.0, 72.0)	47.0 (28.0, 53.0)
SF-36 MCS score, 0–100	66 (44, 77)	62 (34, 68)
SF-36 PCS score, 0–100	38 (31, 44)	45 (38, 66)
PGA, 0–10	6.3 (4.9, 7.3)	4.8 (4.2, 5.7)
FVC, % predicted	88 (81, 100)	95 (88, 101)
DLco, % predicted§	85 (67, 94)	81 (81, 87)

* Values for age, disease duration, percent female, percent Caucasian, percent Hispanic, presence of interstitial lung disease (ILD), and autoantibody status are given for all patients randomized ($n = 10$ per group). All other values are given for treated patients ($n = 9$ per group). Except where indicated otherwise, values are the median (interquartile range). MRSS = modified Rodnan skin thickness score; SHAQ DI = Scleroderma Health Assessment Questionnaire disability index; VAS = visual analog scale; RP = Raynaud's phenomenon; SF-36 = Short Form 36 health survey; MCS = mental component summary; PCS = physical component summary; PGA = physician's global assessment; FVC = forced vital capacity; DLco = diffusing capacity for carbon monoxide.

[†] $P = 0.021$ versus placebo.

[‡] $P = 0.004$ versus placebo.

[§] Adjusted for hemoglobin level.

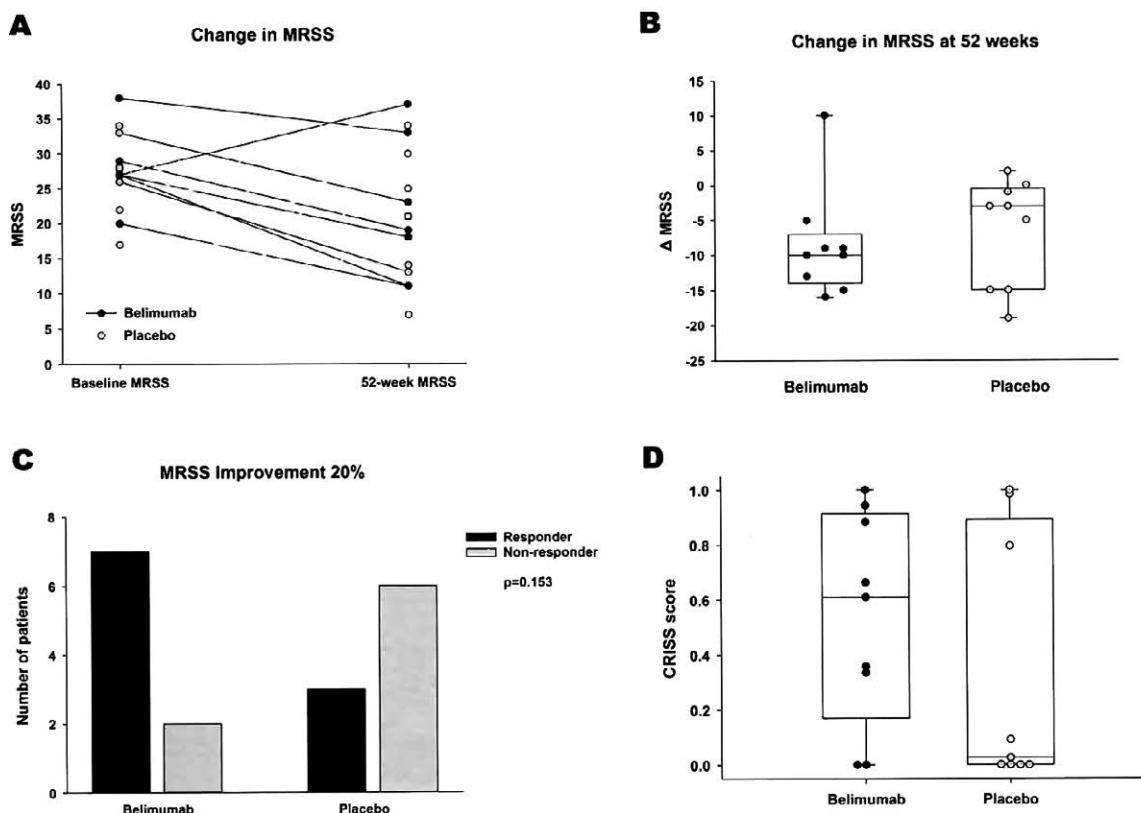


Figure 1. Changes in modified Rodnan skin thickness score (MRSS) and composite response index in diffuse cutaneous systemic sclerosis (CRISS) score. **A**, MRSS at baseline and at week 52 in patients treated with belimumab and those treated with placebo. The median MRSS decreased from 27 (interquartile range [IQR] 26.5, 31) to 18 (IQR 11, 23) in the belimumab group ($P = 0.039$) and from 28 (IQR 22, 28) to 21 (IQR 14, 25) in the placebo group ($P = 0.023$). **B**, Median change in MRSS. The MRSS changed by a median of -10 (IQR -13 , -9) in the belimumab group and by a median of -3.0 (IQR -15 , -1) in the placebo group ($P = 0.411$). **C**, Proportion of patients achieving MRSS improvement of at least 20%. **D**, CRISS score at 52 weeks. The median CRISS score was 0.61 (IQR 0.34, 0.88) in the belimumab group and 0.03 (IQR 0, 0.80) in the placebo group ($P = 0.345$). Although CRISS scores in the belimumab group tended to be higher, statistical significance was not reached due to small sample size and distribution of placebo values. In **B** and **D**, data are presented as box plots, where the boxes represent the 25th to 75th percentiles, the lines within the boxes represent the median, and the lines outside the boxes represent minimum and maximum values. Circles represent individual patients.

belimumab group and by a median of -3.0 (IQR -15 , -1) in the placebo group ($P = 0.411$) (Figure 1B). Because there was no statistically significant difference between the groups in the median change in MRSS, the primary efficacy end point was not met. In the belimumab group, 7 of 9 patients were clinical improvers compared to 3 of 9 patients in the placebo group ($P = 0.153$) (Figure 1C). FVC and DLco remained stable during treatment (Table 2).

Multiple secondary outcome measures were assessed (Table 2). Significantly greater improvements were observed in the belimumab group for the SHAQ DI score and the VAS RP score. There were no significant differences seen in VAS pain score, VAS ulcers score, VAS breathing score, VAS overall score, physician's global assessment, SF-36 MCS score, or SF-36 PCS score. In a

post hoc analysis, we assessed the CRISS score at baseline compared to 52 weeks. The median CRISS score at 52 weeks was 0.61 (IQR 0.34, 0.88) in the belimumab group and 0.03 (IQR 0, 0.80) in the placebo group ($P = 0.345$) (Figure 1D).

AEs. There was no difference between the groups in the total number of AEs (53 in the belimumab group and 56 in the placebo group; $P = 0.868$). There was no difference between the groups in the total number of infectious AEs (18 in the belimumab group and 16 in the placebo group; $P = 0.818$). There were 3 SAEs postrandomization, all of which occurred in the placebo group (Table 3). One patient was hospitalized with an anxiety attack. The 2 other SAEs were hospitalizations due to chest pain and dyspnea related to progression of SSc-related

Table 2. Change in primary and secondary end points at 52 weeks*

	Belimumab + MMF (n = 9)	Placebo + MMF (n = 9)
MRSS, 0–51	–10 (–13, –9)	–3.0 (–15, –1)
SHAQ DI score, 0–3	–0.25 (–0.38, –0.25)†	0.00 (–0.13, 0.13)
VAS pain score, 0–150 mm	–10.5 (–40.5, 6.5)	–1.0 (–32.0, 0.0)
VAS RP score, 0–150 mm	–30.0 (–40.0, –14.0)‡	0.0 (–7.0, 22.0)
VAS ulcers score, 0–150 mm	–12.0 (–38.0, 1.0)	0.0 (–7.5, 4.0)
VAS breathing score, 0–150 mm	2.0 (0.0, 7.0)	0.0 (–7.0, 3.0)
VAS overall score, 0–150 mm	–14.0 (–29.0, –9.00)	–10.0 (–40.0, –6.0)
SF-36 MCS score, 0–100	7.50 (2.50, 18.50)	3.00 (0.00, 10.00)
SF-36 PCS score, 0–100	8.00 (–3.50, 19.00)	–3.00 (–3.00, 27.00)
PGA, 0–10	–4.43 (–8.05, –0.90)	–1.67 (–2.87, –0.90)
FVC, % predicted	5.00 (0.00, 8.00)	–2.00 (–6.00, 4.00)
DLco, % predicted§	2.00 (–7.00, 7.00)	0.00 (–6.00, 7.00)
CRIS score	0.61 (0.34, 0.88)	0.03 (<0.001, 0.80)

* Values are the median (interquartile range). MMF = mycophenolate mofetil; CRIS = composite response index in diffuse cutaneous systemic sclerosis (see Table 1 for other definitions).

† $P = 0.042$ versus placebo + MMF.

‡ $P = 0.029$ versus placebo + MMF.

§ Adjusted for hemoglobin level.

cardiomyopathy, both of which occurred in 1 patient. This patient was withdrawn from the study to receive treatment off protocol. Two SAEs occurred during the wash-in phase prior to randomization in 1 patient who experienced scleroderma hypertensive crisis resulting in 2 hospitalizations. No deaths occurred during the study period. All AEs occurring more than once are shown in Supplementary File 4 (<http://onlinelibrary.wiley.com/doi/10.1002/art.40358/abstract>).

Dermatopathology findings. The majority of biopsy samples from both groups demonstrated an overall improvement in microscopic morphology with a qualitative decrease in degree of sclerosis, hyalinization of collagen, thickness of collagen fiber bundles, and dermal thickness. There were no significant differences between the groups in skin thickness, collagen density, degree of infiltrate on H&E staining, number of follicles and eccrine structures, and staining intensity of α -SMA, trichrome, CD34, procollagen, CD3, or CD79. This complete

Table 3. Adverse events (AEs) in each treatment group*

	Belimumab + MMF (n = 10)	Placebo + MMF (n = 10)
Total AEs	53	56
Total infectious AEs	18	16
Serious AEs	0	3

* There were no significant differences between the groups. MMF = mycophenolate mofetil.

analysis is included as Supplementary File 5 (<http://onlinelibrary.wiley.com/doi/10.1002/art.40358/abstract>).

BLyS levels. Baseline BLyS levels in our patients were higher than those in healthy controls, consistent with previous findings (10). The median BLyS level was 1.46 ng/ml (IQR 1.25, 2.05) in 15 patients versus 0.67 ng/ml (IQR 0.59, 0.87) in 50 healthy controls ($P < 0.001$). There was no difference between improvers and nonimprovers in baseline BLyS levels (median 1.48 ng/ml [IQR 1.23, 1.95] versus 1.74 ng/ml [IQR 1.27, 2.08], respectively; $P = 0.66$).

Differential gene expression and intrinsic subset assignment. Differential expression analysis demonstrated that there were 43 significant DEGs that decreased post-treatment in the belimumab arm (Figure 2A; also see Supplementary File 6, <http://onlinelibrary.wiley.com/doi/10.1002/art.40358/abstract>). These genes were significantly enriched in immune system signaling including defense response, inflammatory response, and complement activation (see Supplementary File 7, <http://onlinelibrary.wiley.com/doi/10.1002/art.40358/abstract>). Significantly down-regulated pathways included B cell receptor activation and Toll-like receptor signaling as well as integrin signaling pathways (Figure 2B; also see Supplementary File 8, <http://onlinelibrary.wiley.com/doi/10.1002/art.40358/abstract>). In contrast, there were no significant DEGs in the placebo group; therefore, presentation of differential expression is limited to the belimumab arm.

We then examined DEGs specifically in belimumab improvers. There were 76 significant DEGs whose levels were decreased posttreatment (Figure 2C; also see Supplementary File 9, <http://onlinelibrary.wiley.com/doi/10.1002/art.40358/abstract>). These genes were enriched in immune and fibrotic signaling (e.g., extracellular matrix [ECM] organization, vasculature development, and collagen metabolic process) (see Supplementary File 10, <http://onlinelibrary.wiley.com/doi/10.1002/art.40358/abstract>). Down-regulated pathways included both fibrotic signaling (transforming growth factor β [TGF β]/TGF β receptor [TGF β R] signaling and ECM regulators) and B cell signaling (B cell antigen receptor and B cell receptor signaling) (Figure 2D; also see Supplementary File 11, <http://onlinelibrary.wiley.com/doi/10.1002/art.40358/abstract>).

Finally, we examined the baseline differences between belimumab improvers and nonimprovers. There were 19 genes with higher expression in improvers (see Supplementary File 12 and Supplementary Figure 1A, <http://onlinelibrary.wiley.com/doi/10.1002/art.40358/abstract>) enriched in collagen metabolic process and ECM organization. Pathways enriched in improvers included ECM–receptor interaction and other ECM-related gene sets as well as TGF β R signaling (see Supplementary File 13 and Supplementary Figure 1B, <http://onlinelibrary.wiley.com/doi/10.1002/art.40358/abstract>).

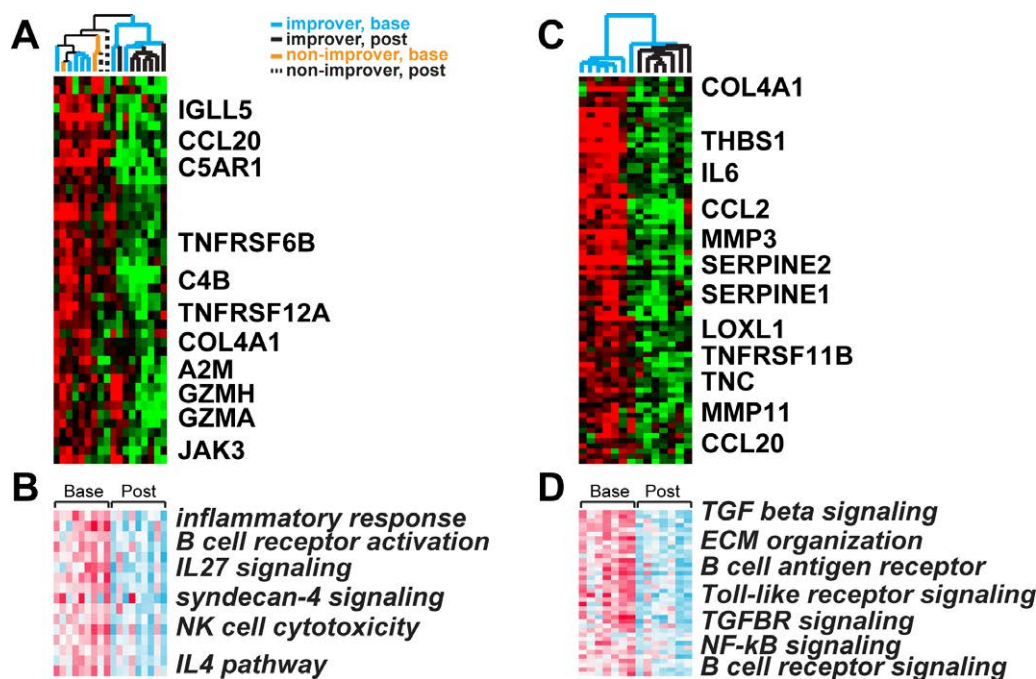


Figure 2. Gene expression changes in the belimumab arm and in belimumab improvers (patients who individually demonstrated a 20% decrease in the modified Rodnan skin thickness score). **A**, Sample genes that were significantly down-regulated (false discovery rate [FDR] $\leq 10\%$) posttreatment in the belimumab arm. **B**, Sample pathways that were significantly down-regulated (FDR $\leq 5\%$) posttreatment in the belimumab arm. **C**, Sample genes that were significantly down-regulated posttreatment in belimumab improvers. **D**, Sample pathways that were significantly down-regulated posttreatment in belimumab improvers. Base = baseline; IL-27 = interleukin-27; NK = natural killer; TGF = transforming growth factor; ECM = extracellular matrix; TGF β R = TGF β receptor.

40358/abstract). There were no significant DEGs in placebo improvers, although this could be attributed to sample size.

There was no difference between treatment groups in baseline frequency of intrinsic gene expression subsets. Molecular subset at baseline was not associated with clinical improvement in the belimumab arm (Figure 3A), the placebo arm (Figure 3B), or the pooled treatment arms ($P > 0.05$ by Fisher's exact test; data not shown). Fifteen patients were assigned to either an inflammatory or a proliferative molecular subset at baseline. In a pooled analysis, 9 of these patients (60%) changed their subset to normal-like, and this was accompanied by a decrease in MRSS for all 9 patients. Furthermore, 8 of 10 improvers were assigned to a normal-like molecular subset posttreatment.

We quantified an inflammatory subset score and tracked this change over the course of treatment. The change in inflammatory subset score correlated with the change in MRSS (Pearson's $r = 0.51$, $P = 0.03$), particularly for patients assigned to the inflammatory molecular subset at baseline (Pearson's $r = 0.81$, $P = 0.008$) (Figure 3C). These findings suggest that an overall reduction in inflammatory gene expression and

movement toward the normal-like subset was associated with improvement in MRSS.

DISCUSSION

This is the first double-blind, randomized controlled trial of belimumab for the treatment of early dcSSc. We observed clinically and statistically significant improvement in MRSS in both treatment groups. Although the median difference in MRSS was greater in the belimumab group, the difference was not statistically significant in this small pilot study. A larger proportion of patients in the belimumab group were clinical improvers, although this did not reach statistical significance. The CRIS score, evaluated post hoc, favored the belimumab group, but the difference was not statistically significant. The SHAQ DI score and VAS RP score showed significantly greater improvements in the belimumab group. However, given that the baseline values for these measures were worse in the belimumab group, this may represent regression to the mean. There were no significant differences for the other secondary outcome measures.

Using differential gene expression analysis, we were able to detect differences between the groups. We

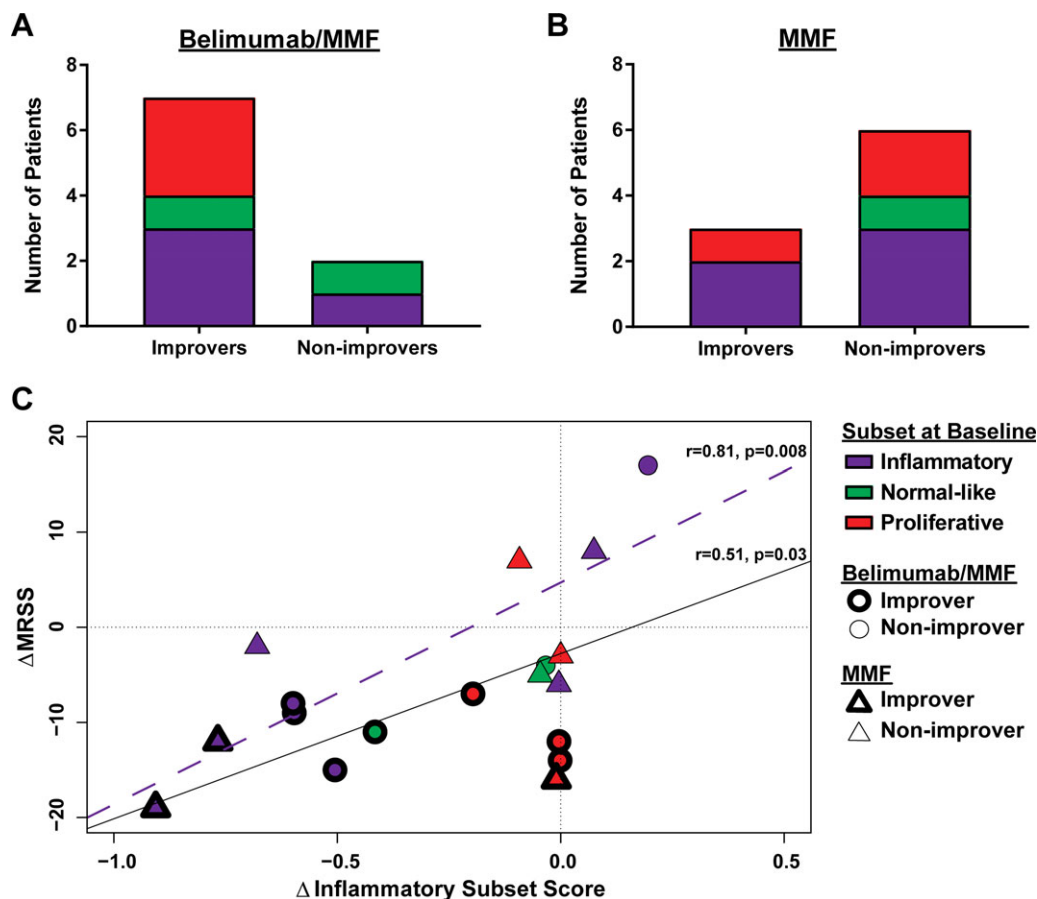


Figure 3. Patients were assigned to one of the intrinsic molecular subsets based on gene expression signatures at baseline: inflammatory (purple), normal-like (green), or proliferative (red). **A**, In the belimumab/mycophenolate mofetil (MMF) treatment arm, improvers (patients who individually demonstrated a 20% decrease in the modified Rodnan skin thickness score [MRSS]) spanned all 3 subsets, while nonimprovers were assigned to an inflammatory or normal-like molecular subset. **B**, In the MMF treatment arm, improvers were assigned to either an inflammatory or a proliferative molecular subset, while nonimprovers spanned all 3 subsets. **C**, We used the inflammatory gene expression signature to quantify an inflammatory subset score for each patient at baseline and at 12 months, and we correlated changes in this score with changes in MRSS. Symbols represent individual patients. Regression lines are shown for all patients (solid) and for only those patients assigned to the inflammatory molecular subset (dashed).

observed significant changes in gene expression only in the belimumab arm, driven largely by the improvers. There were no significant DEGs in nonimprovers or in the placebo arm, despite the fact that the placebo patients were treated with MMF. The clinical improvers treated with belimumab and background MMF showed significant decrease of B cell signaling consistent with the mechanism of action of belimumab. This group also displayed high baseline levels and posttreatment down-regulation of fibrotic genes and pathways including collagens, ECM, and TGF β /TGF β R signaling. The role of B cells in stimulating collagen synthesis and contributing to fibrosis in SSc via multiple mechanisms (including generation of interleukin-6 and CCL2, which were down-regulated in belimumab improvers in this trial) has been described (38–41). A recent study (42) demonstrated induction of

collagen secretion and profibrotic cytokines in skin fibroblasts by B cells and particularly by BAFF. Our findings suggest that clinical response to belimumab is associated with a decrease in profibrotic genes and pathways. However, the use of MMF can also impact gene expression as well as intrinsic subset assignment (43). We found no association between baseline intrinsic subsets and clinical response. However, improvers were more likely to be assigned to a normal-like molecular subset following treatment, and decrease in inflammatory gene expression signatures accompanied decrease in MRSS.

Although our investigation has several strengths which will enable planning for future studies, there are limitations to the conclusions that can be drawn from this pilot study. As a pilot trial the sample size was small, and the study was underpowered to detect modest differences

between treatment groups. Our use of MMF as an active comparator likely blunted our ability to detect a difference between the groups with regard to impact of belimumab on clinical outcomes. However, most patients with early progressive dcSSc are treated with immunosuppressive therapies, and data suggest that such patients have improved survival (4). The use of an active comparator therefore not only provides an answer to a more clinically relevant question, but also improves recruitment and ability to carry out a trial. Future studies should include patients treated only with belimumab to assess direct effects of belimumab. Larger clinical trials will be needed to determine the role of belimumab in the treatment of early dcSSc, and this report suggests that such studies are warranted.

ACKNOWLEDGMENTS

We would like to recognize the assistance of our research coordinators in carrying out this study: Kamini Doobay, Eliza Pelrine, and Annel Fernandez.

AUTHOR CONTRIBUTIONS

All authors were involved in drafting the article or revising it critically for important intellectual content, and all authors approved the final version to be published. Dr. Gordon had full access to all of the data in the study and takes responsibility for the integrity of the data and the accuracy of the data analysis.

Study conception and design. Gordon, Spiera.

Acquisition of data. Gordon, Bernstein, Magro, Wildman, Wood, Whitfield, Spiera.

Analysis and interpretation of data. Gordon, Martynov, Franks, Szymonifka, Whitfield, Spiera.

ROLE OF THE STUDY SPONSOR

This work was supported as an investigator-initiated study by a research grant from GlaxoSmithKline. Except for running the custom BLyS level ELISA tests described, GlaxoSmithKline had no role in the study design or in the collection, analysis, or interpretation of the data, the writing of the manuscript, or the decision to submit the manuscript for publication. Publication of this article was not contingent upon approval by GlaxoSmithKline.

REFERENCES

1. Medsger TA. Natural history of systemic sclerosis and the assessment of disease activity, severity, functional status, and psychologic well-being. *Rheum Dis Clin North Am* 2003;29:255–73.
2. Pattanaik D, Brown M, Postlethwaite BC, Postlethwaite AE. Pathogenesis of systemic sclerosis. *Front Immunol* 2015;6:272.
3. Nagaraja V, Denton CP, Khanna D. Old medications and new targeted therapies in systemic sclerosis. *Rheumatology (Oxford)* 2015;54:1944–53.
4. Herrick AL, Pan X, Peytrignet S, Lunt M, Hesselstrand R, Mouthon L, et al. Treatment outcome in early diffuse cutaneous systemic sclerosis: the European Scleroderma Observational Study (ESOS). *Ann Rheum Dis* 2017;76:1207–18.
5. Lafyatis R, Kissin E, York M, Farina G, Viger K, Fritzler MJ, et al. B cell depletion with rituximab in patients with diffuse cutaneous systemic sclerosis. *Arthritis Rheum* 2009;60:578–83.
6. Lafyatis R, O'Hara C, Feghali-Bostwick CA, Matteson E. B cell infiltration in systemic sclerosis-associated interstitial lung disease. *Arthritis Rheum* 2007;56:3167–8.
7. Milano A, Pendergrass SA, Sargent JL, George LK, McCalmont TH, Connolly MK, et al. Molecular subsets in the gene expression signatures of scleroderma skin. *PLoS One* 2008;3:e2696.
8. Soto L, Ferrier A, Aravena O, Fonseca E, Berendsen J, Biere A, et al. Systemic sclerosis patients present alterations in the expression of molecules involved in B-cell regulation. *Front Immunol* 2015;6:496.
9. Sato S, Fujimoto M, Hasegawa M, Takehara K. Altered blood B lymphocyte homeostasis in systemic sclerosis: expanded naive B cells and diminished but activated memory B cells. *Arthritis Rheum* 2004;50:1918–27.
10. Matsushita T, Hasegawa M, Yanaba K, Kodaera M, Takehara K, Sato S. Elevated serum BAFF levels in patients with systemic sclerosis: enhanced BAFF signaling in systemic sclerosis B lymphocytes. *Arthritis Rheum* 2006;54:192–201.
11. Matsushita T, Fujimoto M, Hasegawa M, Tanaka C, Kumada S, Ogawa F, et al. Elevated serum APRIL levels in patients with systemic sclerosis: distinct profiles of systemic sclerosis categorized by APRIL and BAFF. *J Rheumatol* 2007;15:2056–62.
12. Clements P, Lachenbruch P, Seibold J, White B, Weiner S, Martin R, et al. Inter and intraobserver variability of total skin thickness score (modified Rodnan TSS) in systemic sclerosis. *J Rheumatol* 1995;22:1281–5.
13. Jordan S, Distler JH, Maurer B, Huscher D, van Laar JM, Allanore Y, et al. Effects and safety of rituximab in systemic sclerosis: an analysis from the European scleroderma trial and research (EUSTAR) group. *Ann Rheum Dis* 2015;74:1188–94.
14. Daoussis D, Melissaropoulos K, Sakellaropoulos G, Antonopoulos I, Markatseli TE, Simopoulou T, et al. A multicenter, open-label, comparative study of B-cell depletion therapy with rituximab for systemic sclerosis-associated interstitial lung disease. *Semin Arthritis Rheum* 2017;46:625–31.
15. Benlysta (belimumab) prescribing information. Rockville (MD): Human Genome Sciences; 2011.
16. Baker KP, Edwards BM, Main SH, Choi GH, Wager RE, Halpern WG, et al. Generation and characterization of LymphoStat-B, a human monoclonal antibody that antagonizes the bioactivities of B lymphocyte stimulator. *Arthritis Rheum* 2003;48:3253–65.
17. Subcommittee for Scleroderma Criteria of the American Rheumatism Association Diagnostic and Therapeutic Criteria Committee. Preliminary criteria for the classification of systemic sclerosis (scleroderma). *Arthritis Rheum* 1980;23:581–90.
18. Van den Hoogen F, Khanna D, Fransen J, Johnson SR, Baron M, Tyndall A, et al. 2013 classification criteria for systemic sclerosis: an American College of Rheumatology/European League Against Rheumatism collaborative initiative. *Arthritis Rheum* 2013;65:2737–47.
19. LeRoy EC, Medsger TA Jr. Criteria for the classification of early systemic sclerosis. *J Rheumatol* 2001;28:1573–6.
20. Ware JE Jr, Snow KK, Kosinski M, Gandek B. SF-36 health survey: manual and interpretation guide. Boston: The Health Institute, New England Medical Center; 1993.
21. Steen VD, Medsger TA Jr. The value of the Health Assessment Questionnaire and special patient-generated scales to demonstrate change in systemic sclerosis patients over time. *Arthritis Rheum* 1997;40:1984–91.
22. Khanna D, Berrocal VJ, Giannini EH, Seibold JR, Merkel PA, Mayes MD, et al. The American College of Rheumatology provisional composite response index for clinical trials in early diffuse cutaneous systemic sclerosis. *Arthritis Rheumatol* 2016;68:299–311.
23. Trotti A, Colevas AD, Setser A, Rusch V, Jaques D, Budach V, et al. CTCAE v3.0: development of a comprehensive grading system for the adverse effects of cancer treatment. *Semin Radiat Oncol* 2003;13:176–81.

24. Gordon JK, Martyanov V, Magro C, Wildman HF, Wood TA, Huang WT, et al. Nilotinib (Tasigna™) in the treatment of early diffuse systemic sclerosis: an open-label, pilot clinical trial. *Arthritis Res Ther* 2015;17:213.
25. Hinchcliff M, Huang CC, Wood TA, Matthew Mahoney J, Martyanov V, Bhattacharyya S, et al. Molecular signatures in skin associated with clinical improvement during mycophenolate treatment in systemic sclerosis. *J Invest Dermatol* 2013;133:1979–89.
26. Reich M, Liefeld T, Gould J, Lerner J, Tamayo P, Mesirov JP. GenePattern 2.0. *Nat Genet* 2006;38:500–1.
27. De Hoon MJ, Imoto S, Nolan J, Miyano S. Open source clustering software. *Bioinformatics* 2004;20:1453–4.
28. Saldanha AJ. Java Treeview: extensible visualization of microarray data. *Bioinformatics* 2004;20:3246–8.
29. Tusher VG, Tibshirani R, Chu G. Significance analysis of microarrays applied to the ionizing radiation response. *Proc Natl Acad Sci U S A* 2001;98:5116–21.
30. Reimand J, Kull M, Peterson H, Hansen J, Vilo J. g:Profiler: a web-based toolset for functional profiling of gene lists from large-scale experiments. *Nucleic Acids Res* 2007;35(Web Server issue):W193–200.
31. Subramanian A, Tamayo P, Mootha VK, Mukherjee S, Ebert BL, Gillette MA, et al. Gene set enrichment analysis: a knowledge-based approach for interpreting genome-wide expression profiles. *Proc Natl Acad Sci U S A* 2005;102:15545–50.
32. Mootha VK, Lindgren CM, Eriksson KF, Subramanian A, Sihag S, Lehar J, et al. PGC-1 α -responsive genes involved in oxidative phosphorylation are coordinately downregulated in human diabetes. *Nat Genet* 2003;34:267–73.
33. Milano A, Pendergrass SA, Sargent JL, George LK, McCalmont TH, Connolly MK, et al. Molecular subsets in the gene expression signatures of scleroderma skin. *PLoS One* 2008;3:e2696.
34. Pendergrass SA, Lemaire R, Francis IP, Mahoney JM, Lafyatis R, Whitfield ML. Intrinsic gene expression subsets of diffuse cutaneous systemic sclerosis are stable in serial skin biopsies. *J Invest Dermatol* 2012;132:1363–73.
35. Friedman J, Hastie T, Tibshirani R. Regularization paths for generalized linear models via coordinate descent. *J Stat Softw* 2010;33:1–22.
36. Kuhn M. Building predictive models in R using the caret package. *J Stat Softw* 2008;28:1–26.
37. Franks J, Martyanov V, Cai G, Whitfield ML. Novel machine learning classifier accurately predicts intrinsic molecular subsets for patients with systemic sclerosis [abstract]. *Arthritis Rheumatol* 2017;69 Suppl 10. URL: <http://acrabstracts.org/abstract/novel-machine-learning-classifier-accurately-predicts-intrinsic-molecular-subsets-for-patients-with-systemic-sclerosis/>.
38. Kraaij MD, van Laar JM. The role of B cells in systemic sclerosis. *Biologics* 2008;2:389–95.
39. Daoussis D, Liossis SN. B cells tell scleroderma fibroblasts to produce collagen. *Arthritis Res Ther* 2013;15:125.
40. Wu M, Mohan C. B-cells in systemic sclerosis: emerging evidence from genetics to phenotypes. *Curr Opin Rheumatol* 2015;27:537–41.
41. Sakkas LI, Bogdanos DP. Systemic sclerosis: new evidence reinforces the role of B cells. *Autoimmun Rev* 2016;15:155–61.
42. François A, Chatelus E, Wachsmann D, Sibilia J, Bahram S, Alsaleh G, et al. B lymphocytes and B-cell activating factor promote collagen and profibrotic markers expression by dermal fibroblasts in systemic sclerosis. *Arthritis Res Ther* 2013;15:R168.
43. Toledo D, Hinchcliff M, Taroni J, Wood TA, Franks J, Shah S, et al. Longitudinal analysis of MMF Clinical, Molecular, and Immunohistochemistry (IHC) responses shows SSc patients lose their inflammatory signature and rebound upon treatment cessation [abstract]. *Arthritis Rheumatol* 2016;68 Suppl 10. URL: <http://acrabstracts.org/abstract/longitudinal-analysis-of-mmfc-clinical-molecular-and-immunohistochemistry-ihc-responses-shows-sscpatients-lose-their-inflammatory-signature-and-rebound-upon-treatment-cessation/>.

LETTERS

DOI 10.1002/art.40365

Implications of elevated C-reactive protein and serum amyloid A levels in IgG4-related disease: comment on the article by Perugino et al

To the Editor:

We read with great interest the article by Perugino et al (1), which provides an excellent overview of IgG4-related disease (IgG4-RD). However, the authors did not discuss the prognostic/diagnostic implications of increased C-reactive protein (CRP) levels in IgG4-RD or the potential secondary complications of such increased levels. Therefore, we want to highlight the clinical relevance of elevated CRP in IgG4-RD.

In patients with IgG4-RD, levels of CRP may be elevated (2). Serum amyloid A (SAA) is an acute-phase protein that is also often elevated during inflammation. Sustained high levels of SAA can lead to deposition of AA amyloid fibrils in the tissues, leading to AA amyloidosis (3). Several infectious autoimmune and rheumatic diseases have been associated with secondary AA amyloidosis (4). This association has also recently been demonstrated by our group in a patient with IgG4-RD (5).

In our cohort of IgG4-RD patients, we have now prospectively established simultaneous levels of erythrocyte sedimentation

rate (ESR), CRP, SAA, and serum IgG4. In 9 of 28 patients (32%), SAA was elevated (ranging from 5 to 350 mg/liter; normal <4 mg/liter) and was significantly correlated with levels of CRP ($r = 0.816$, $P = 0.001$) (Figure 1C). No significant correlation between SAA and serum IgG4 levels was found ($P = 0.642$) (Figure 1A), and a weak correlation between SAA levels and the ESR was observed ($r = 0.382$, $P = 0.0145$) (Figure 1B). Furthermore, no correlation was seen between SAA levels and disease activity (IgG4-RD Responder Index) (6) at the time these inflammation parameters were measured ($P = 0.881$) (Figure 1D).

AA amyloidosis is a very serious clinical complication with an increased risk of mortality, that predominantly affects the kidneys (3). AA amyloidosis may be an overlooked, rare complication of IgG4-RD because the majority of patients with IgG4-RD have normal levels of CRP (2) and because IgG4-RD is often treated after the diagnosis has been established, leading to normalization of CRP and SAA levels. In the current study, the elevated levels of SAA correlated with elevated levels of CRP, but not with levels of serum IgG4. Furthermore, no correlation was found between the SAA levels and scores on the IgG4-RD Responder Index. Thus, patients with IgG4-RD may have an increased risk of developing unnoticed secondary amyloidosis. We therefore recommend that both CRP and SAA be routinely measured in patients with IgG4-RD, with prompt treatment if levels are elevated.

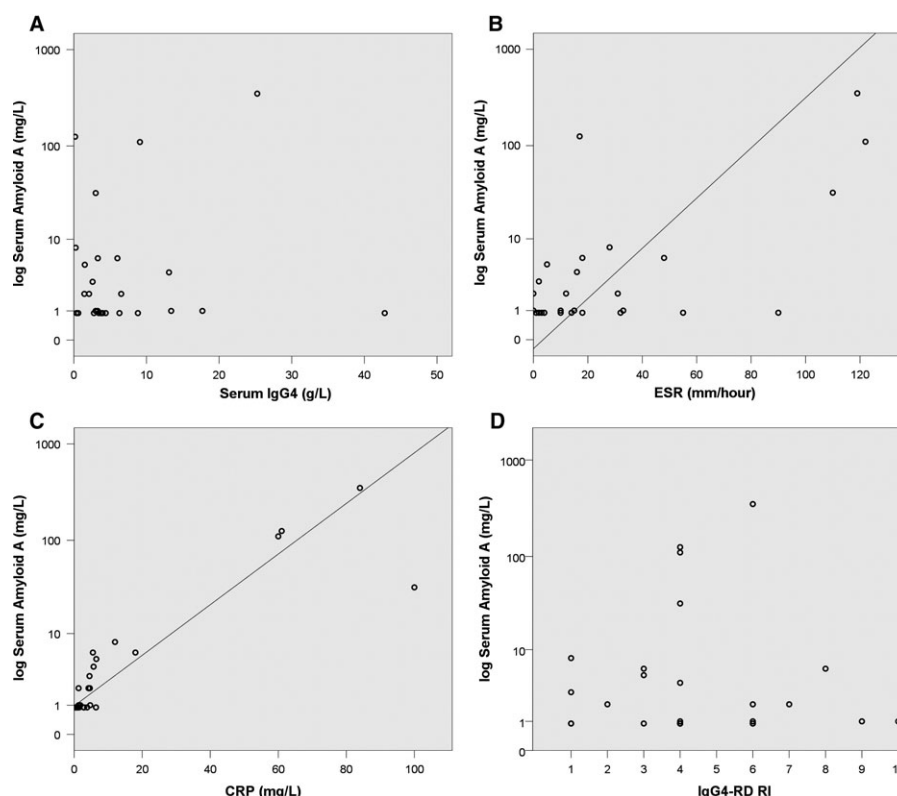


Figure 1. Correlation between serum amyloid A (SAA) levels and serum IgG4 levels (A), the erythrocyte sedimentation rate (ESR) (B), C-reactive protein (CRP) levels (C), and the IgG4-related disease (IgG4-RD) Responder Index (RI) (D) in 28 patients with IgG4-RD.

A. Faiz Karim, MD
 Laura E. M. Eurelings, BS
 P. Martin van Hagen, MD, PhD
 Jan A. M. van Laar, MD, PhD
*Erasmus Medical Center
 Rotterdam, The Netherlands*

1. Perugino CA, Mattoo H, Mahajan VS, Maehara T, Wallace ZS, Pillai S, et al. IgG4-related disease: insights into human immunology and targeted therapies. *Arthritis Rheumatol* 2017;69:1722–32.
2. Wallace ZS, Deshpande V, Mattoo H, Mahajan VS, Kulikova M, Pillai S, et al. IgG4-related disease: clinical and laboratory features in one hundred twenty-five patients. *Arthritis Rheumatol* 2015;67:2466–75.
3. Lachmann HJ, Goodman HJ, Gilbertson JA, Gallimore JR, Sabin CA, Gillmore JD, et al. Natural history and outcome in systemic AA amyloidosis. *N Engl J Med* 2007;356:2361–71.
4. Bunker D, Gorevic P. AA amyloidosis: Mount Sinai experience, 1997–2012. *Mt Sinai J Med* 2012;79:749–56.
5. Karim F, Clahsen-van Groningen M, van Laar JA. AA amyloidosis and IgG4-related disease. *N Engl J Med* 2017;376:599–600.
6. Carruthers MN, Stone JH, Deshpande V, Khosroshahi A. Development of an IgG4-RD Responder Index. *Int J Rheumatol* 2012; 2012:259408.

DOI 10.1002/art.40362

Reply

To the Editor:

We thank Dr. Karim and colleagues for their thoughtful comments on our article, including their mention of a patient with longstanding IgG4-RD who developed secondary (AA) amyloidosis, presumably as a consequence of well-established, untreated inflammation (Karim F, Clahsen-van Groningen M, van Laar JA. AA amyloidosis and IgG4-related disease. *N Engl J Med* 2017;376:599–600). We completely agree with Karim et al regarding the destructive nature of IgG4-RD that goes undiagnosed, particularly its ability to cause both endocrine and exocrine failure of the pancreas, end-stage liver disease from the effects of biliary tract disease, chronic renal failure from the effects of tubulointerstitial nephritis, vision loss and deleterious cosmetic issues from orbital disease, chronic pain from retroperitoneal fibrosis, and so on.

Indeed, because IgG4-RD has been recognized as a unique disease entity for less than 15 years, the full toll from this condition in terms of damage from both the disease itself and its therapy is still being described. We note that IgG4-RD patients with elevated levels of serum CRP are the exception rather than the rule (Wallace ZS, Deshpande V, Mattoo H, Mahajan VS, Kulikova M, Pillai S, et al. IgG4-related disease: clinical and laboratory features in one hundred twenty-five patients. *Arthritis Rheumatol* 2015;67:2466–75). The more common scenario is the finding of an extremely high ESR—the effect of hypergammaglobulinemia of both IgG4 and IgG1 (and sometimes all 4 IgG subclasses)—in the setting of normal CRP levels.

Because any indolent and chronic inflammatory state can result in secondary amyloidosis, we agree that IgG4-RD in the case reported by Karim and colleagues was likely related to the subsequent development of amyloidosis. The current rarity of secondary amyloidosis and the growing, but still inadequate,

awareness of IgG4-RD may partially explain why this was the first published connection between these entities. To our knowledge, serum amyloid A concentrations have not been measured systematically in other cohorts, including in our own. The case reported by Karim and colleagues underscores the importance of early recognition of IgG4-RD and control of the associated inflammation as early and as effectively as possible. The utility of serum amyloid A as a biomarker of interest in IgG4-RD requires further investigation.

Cory A. Perugino, DO
 John H. Stone, MD, MPH
*Massachusetts General Hospital
 Boston, MA*

DOI 10.1002/art.40363

Varicella zoster virus–specific T cell responses in untreated giant cell arteritis: comment on the article by England et al

To the Editor:

Giant cell arteritis (GCA) is a large vessel vasculitis of unknown cause. Although infections have long been suspected to be potential disease triggers, a disease-causing pathogen has not been identified to date (1). Recently, investigators in several studies reported varicella zoster virus (VZV) particles in artery biopsy specimens (2). Similar to other herpesviruses, VZV has a very high prevalence and remains dormant in a latent stage controlled by the immune system. Loss of T cell–mediated virus control results in herpes zoster (shingles).

The study by England et al (3) now provides epidemiologic evidence for a potential association between VZV and GCA. The authors used 2 independent health care provider data sets (Medicare and MarketScan). In these databases, prior herpes zoster events were associated with a diagnosis of GCA (hazard ratios 2.16 and 1.99 in the 2 data sets, respectively) (3). Use of antiviral drugs or vaccination did not alter the risk of GCA.

T cells are important in the pathogenesis of GCA (4). Genetic association studies and strict tissue tropism suggest that it is an antigen-driven disease (4,5). The antigen could be either a self antigen or a pathogen-derived antigen that is expressed only in the large arteries. The immunopathology and epidemiologic data implicate VZV as a potential immune target. We hypothesized that cross-reactive VZV-specific T cell immunity may contribute to the pathogenesis of GCA. If our hypothesis were shown to be true, we expected the number of VZV-reactive T cells to be increased in patients with GCA compared to control patients.

We compared the frequency of VZV-specific peripheral blood T cells in 32 patients, all of whom provided informed consent to participate in our prospective GCA cohort study. These patients included the following: 15 patients with newly diagnosed GCA (all of whom had received prednisone treatment for < 5 days at the time of sample collection [median 0 days, mean 1 day]), 60% with biopsy-proven GCA, mean age 74.4 years), 10 control patients with inflammatory disease (5 with polymyalgia rheumatica, 2 with autoinflammatory disease, 1 with aortitis, 1 with myelodysplastic syndrome, and 1 with antineutrophil cytoplasmic antibody–associated vasculitis (mean age 66.5 years), and 7 control

A. Faiz Karim, MD
 Laura E. M. Eurelings, BS
 P. Martin van Hagen, MD, PhD
 Jan A. M. van Laar, MD, PhD
*Erasmus Medical Center
 Rotterdam, The Netherlands*

1. Perugino CA, Mattoo H, Mahajan VS, Maehara T, Wallace ZS, Pillai S, et al. IgG4-related disease: insights into human immunology and targeted therapies. *Arthritis Rheumatol* 2017;69:1722–32.
2. Wallace ZS, Deshpande V, Mattoo H, Mahajan VS, Kulikova M, Pillai S, et al. IgG4-related disease: clinical and laboratory features in one hundred twenty-five patients. *Arthritis Rheumatol* 2015;67:2466–75.
3. Lachmann HJ, Goodman HJ, Gilbertson JA, Gallimore JR, Sabin CA, Gillmore JD, et al. Natural history and outcome in systemic AA amyloidosis. *N Engl J Med* 2007;356:2361–71.
4. Bunker D, Gorevic P. AA amyloidosis: Mount Sinai experience, 1997–2012. *Mt Sinai J Med* 2012;79:749–56.
5. Karim F, Clahsen-van Groningen M, van Laar JA. AA amyloidosis and IgG4-related disease. *N Engl J Med* 2017;376:599–600.
6. Carruthers MN, Stone JH, Deshpande V, Khosroshahi A. Development of an IgG4-RD Responder Index. *Int J Rheumatol* 2012; 2012:259408.

DOI 10.1002/art.40362

Reply

To the Editor:

We thank Dr. Karim and colleagues for their thoughtful comments on our article, including their mention of a patient with longstanding IgG4-RD who developed secondary (AA) amyloidosis, presumably as a consequence of well-established, untreated inflammation (Karim F, Clahsen-van Groningen M, van Laar JA. AA amyloidosis and IgG4-related disease. *N Engl J Med* 2017;376:599–600). We completely agree with Karim et al regarding the destructive nature of IgG4-RD that goes undiagnosed, particularly its ability to cause both endocrine and exocrine failure of the pancreas, end-stage liver disease from the effects of biliary tract disease, chronic renal failure from the effects of tubulointerstitial nephritis, vision loss and deleterious cosmetic issues from orbital disease, chronic pain from retroperitoneal fibrosis, and so on.

Indeed, because IgG4-RD has been recognized as a unique disease entity for less than 15 years, the full toll from this condition in terms of damage from both the disease itself and its therapy is still being described. We note that IgG4-RD patients with elevated levels of serum CRP are the exception rather than the rule (Wallace ZS, Deshpande V, Mattoo H, Mahajan VS, Kulikova M, Pillai S, et al. IgG4-related disease: clinical and laboratory features in one hundred twenty-five patients. *Arthritis Rheumatol* 2015;67:2466–75). The more common scenario is the finding of an extremely high ESR—the effect of hypergammaglobulinemia of both IgG4 and IgG1 (and sometimes all 4 IgG subclasses)—in the setting of normal CRP levels.

Because any indolent and chronic inflammatory state can result in secondary amyloidosis, we agree that IgG4-RD in the case reported by Karim and colleagues was likely related to the subsequent development of amyloidosis. The current rarity of secondary amyloidosis and the growing, but still inadequate,

awareness of IgG4-RD may partially explain why this was the first published connection between these entities. To our knowledge, serum amyloid A concentrations have not been measured systematically in other cohorts, including in our own. The case reported by Karim and colleagues underscores the importance of early recognition of IgG4-RD and control of the associated inflammation as early and as effectively as possible. The utility of serum amyloid A as a biomarker of interest in IgG4-RD requires further investigation.

Cory A. Perugino, DO
 John H. Stone, MD, MPH
*Massachusetts General Hospital
 Boston, MA*

DOI 10.1002/art.40363

Varicella zoster virus–specific T cell responses in untreated giant cell arteritis: comment on the article by England et al

To the Editor:

Giant cell arteritis (GCA) is a large vessel vasculitis of unknown cause. Although infections have long been suspected to be potential disease triggers, a disease-causing pathogen has not been identified to date (1). Recently, investigators in several studies reported varicella zoster virus (VZV) particles in artery biopsy specimens (2). Similar to other herpesviruses, VZV has a very high prevalence and remains dormant in a latent stage controlled by the immune system. Loss of T cell–mediated virus control results in herpes zoster (shingles).

The study by England et al (3) now provides epidemiologic evidence for a potential association between VZV and GCA. The authors used 2 independent health care provider data sets (Medicare and MarketScan). In these databases, prior herpes zoster events were associated with a diagnosis of GCA (hazard ratios 2.16 and 1.99 in the 2 data sets, respectively) (3). Use of antiviral drugs or vaccination did not alter the risk of GCA.

T cells are important in the pathogenesis of GCA (4). Genetic association studies and strict tissue tropism suggest that it is an antigen-driven disease (4,5). The antigen could be either a self antigen or a pathogen-derived antigen that is expressed only in the large arteries. The immunopathology and epidemiologic data implicate VZV as a potential immune target. We hypothesized that cross-reactive VZV-specific T cell immunity may contribute to the pathogenesis of GCA. If our hypothesis were shown to be true, we expected the number of VZV-reactive T cells to be increased in patients with GCA compared to control patients.

We compared the frequency of VZV-specific peripheral blood T cells in 32 patients, all of whom provided informed consent to participate in our prospective GCA cohort study. These patients included the following: 15 patients with newly diagnosed GCA (all of whom had received prednisone treatment for < 5 days at the time of sample collection [median 0 days, mean 1 day]), 60% with biopsy-proven GCA, mean age 74.4 years), 10 control patients with inflammatory disease (5 with polymyalgia rheumatica, 2 with autoinflammatory disease, 1 with aortitis, 1 with myelodysplastic syndrome, and 1 with antineutrophil cytoplasmic antibody–associated vasculitis (mean age 66.5 years), and 7 control

patients with noninflammatory disease (mean age 72.0 years). We quantified antigen-specific T cells using an interferon- γ (IFN γ) enzyme-linked immunospot (ELISpot) assay. Live attenuated varicella vaccine (200 plaque-forming units/ml) and the immunodominant glycoprotein E (1 μ g/ml) were used as VZV antigens (6).

Additionally, we stimulated T cells with an aortic explant-derived protein extract from a patient with GCA. This represented a source for potential self and/or VZV antigens. Aortic wall proteins were fractionated in phosphate buffered saline by size-exclusion chromatography (Superdex 200 column; GE Healthcare) into 5 pools (P1–P5), each of which was separately added to the cells (range >500 kD [P1] to <10 kD [P5]; 10 μ g/ml). Influenza vaccine antigen (0.4 μ g/ml) was used as an unrelated comparator. Staphylococcal enterotoxin B (0.5 μ g/ml)-treated wells served as a positive control. Preliminary experiments indicated high reactivity with the aortic wall protein extracts. To exclude nonspecific stimulation, we adapted the standard IFN γ ELISpot protocol (7) as follows: peripheral blood mononuclear cells (PBMCs) (75,000/well) were preincubated with the antigen overnight. On day 2, we added autologous PBMCs (50,000/well), followed by incubation for 36 hours on the ELISpot plates. This procedure reduced nonspecific IFN γ production. The response against viral antigens was not affected (data not shown).

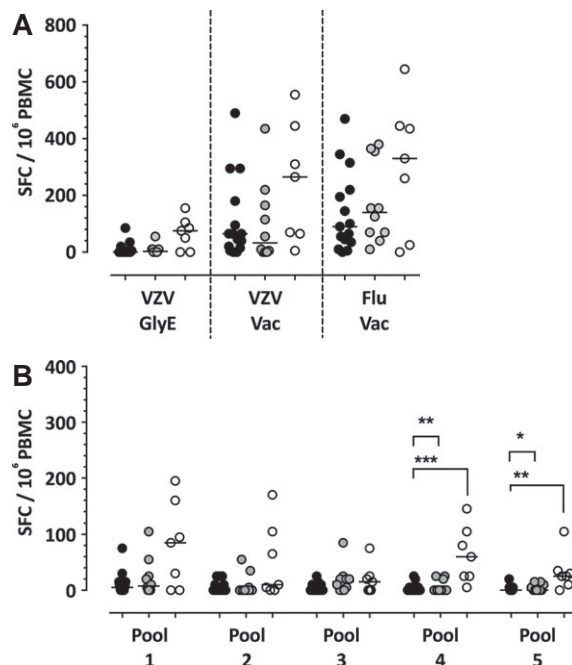


Figure 1. Varicella zoster virus (VZV) T cell reactivity in patients with giant cell arteritis (solid circles), control patients with inflammatory disease (shaded circles), and control patients with noninflammatory disease (open circles). **A**, T cell reactivity against VZV and influenza vaccine, assessed by interferon- γ enzyme-linked immunospot assay. **B**, T cell responses to aortic wall proteins. Aortic wall proteins were fractionated into 5 pools, and each pool was added separately to the cells. Cells treated with medium alone were used for background correction. Each data point represents a single patient. Horizontal lines show the median. * = $P < 0.05$; ** = $P < 0.01$; *** = $P < 0.001$. SFC = spot-forming cell; PBMC = peripheral blood mononuclear cell; GlyE = glycoprotein E; Flu = influenza vaccine (vac) antigen.

The median VZV (glycoprotein E, vaccine) and Flu-TIV T cell reactivity was higher in patients with noninflammatory disease compared to those with GCA, with no statistically significant differences (Figure 1A). Control patients with noninflammatory disease had stronger T cell responses to aortic extract ($P = 0.0006$ and 0.0036 for pools 4 and 5, respectively) (Figure 1B). Such reduced peripheral T cell reactivity could reflect immunosenescence or exhaustion, which may result in loss of VZV control. The responses in control patients with inflammatory disease were, however, comparable to those in GCA patients. This suggested that systemic inflammation might blunt the reactivity. However, strong antigen-independent T cell stimulation with phorbol myristate acetate resulted in comparable IFN γ and interleukin-17 effector functions in all 3 study groups (data not shown).

In conclusion, we observed no GCA-specific alterations in VZV- or aortic protein-specific T cell reactivity. Our results provide evidence against involvement of VZV-specific (or cross-reactive) effector T cells in the pathogenesis of GCA. We focused only on IFN γ -producing T cells; other effector cells might be present at different frequencies. It is further possible that VZV- or aortic tissue-specific T cells concentrate at the site of inflammation. Thus, assessment of the peripheral blood compartment may miss these cells. This would, however, not explain the comparable VZV- and aortic protein-reactive T cell frequencies in GCA and other inflammatory conditions.

In the study by England et al, only a minority (<6%) of the GCA patients had a herpes zoster event in the year prior to GCA diagnosis. Such patients may show T cell reactivity profiles distinct from those observed in our study population but the differences might have been missed due to our small sample size. However, based on the studies showing the presence of VZV in almost all GCA biopsy specimens, we expected to observe a signal even when studying a small patient population. Notably, several other groups of investigators observed no VZV, antigen, or genome in temporal arteries (8–10). The truth probably lies somewhere in between, and as stated in the England article, VZV (and other viruses) may be a trigger for GCA but is not the only one.

Supported by the Swiss National Science Foundation (SNSF) (grant PZ00P3-173517 to Dr. Berger). Dr. Recher's work is supported by SNSF grant PP00P3_144863. Dr. Mehling's work is supported by SNSF grant PZ00P3_154733.

Marc B. Bigler, MSc
Julia R. Hirsiger, BSc
Mike Recher, MD
Matthias Mehling, MD
Thomas Daikeler, MD
University Hospital Basel
Christoph T. Berger, MD 
University of Basel
and University Hospital Basel
Basel, Switzerland

1. Van Timmeren MM, Heeringa P, Kallenberg CG. Infectious triggers for vasculitis. *Curr Opin Rheumatol* 2014;26:416–23.
2. Gilden D, Nagel MA. Varicella zoster virus triggers the immunopathology of giant cell arteritis. *Curr Opin Rheumatol* 2016;28:376–82.
3. England BR, Mikuls TR, Xie F, Yang S, Chen L, Curtis JR. Herpes zoster as a risk factor for incident giant cell arteritis. *Arthritis Rheumatol* 2017;69:2351–8.

4. Weyand CM, Goronzy JJ. Immune mechanisms in medium and large-vessel vasculitis. *Nat Rev Rheumatol* 2013;9:731–40.
5. Carmona FD, Vaglio A, Mackie SL, Hernandez-Rodriguez J, Monach PA, Castaneda S, et al. A genome-wide association study identifies risk alleles in plasminogen and P4HA2 associated with giant cell arteritis. *Am J Hum Genet* 2017;100:64–74.
6. Malavive GN, Jones L, Black AP, Ogg GS. Rapid effector function of varicella-zoster virus glycoprotein I-specific CD4+ T cells many decades after primary infection. *J Infect Dis* 2007; 195:660–4.
7. Berger CT, Carlson JM, Brumme CJ, Hartman KL, Brumme ZL, Henry LM, et al. Viral adaptation to immune selection pressure by HLA class I-restricted CTL responses targeting epitopes in HIV frameshift sequences. *J Exp Med* 2010;207:61–75.
8. Alvarez-Lafuente R, Fernandez-Gutierrez B, Jover JA, Judez E, Loza E, Clemente D, et al. Human parvovirus B19, varicella zoster virus, and human herpes virus 6 in temporal artery biopsy specimens of patients with giant cell arteritis: analysis with quantitative real time polymerase chain reaction. *Ann Rheum Dis* 2005; 64:780–2.
9. Procop GW, Eng C, Clifford A, Villa-Forte A, Calabrese LH, Roselli E, et al. Varicella zoster virus and large vessel vasculitis, the absence of an association. *Pathog Immun* 2017;2:228–38.
10. Muratore F, Croci S, Tamagnini I, Zerbini A, Bellafiore S, Belloni L, et al. No detection of varicella-zoster virus in temporal arteries of patients with giant cell arteritis. *Semin Arthritis Rheum* 2017. E-pub ahead of print.

DOI 10.1002/art.40370



Reply

To the Editor:

We thank Dr. Bigler and his colleagues for their interest in our study and for sharing the results from their laboratory. The authors proposed evaluating a biologic mechanism linking VZV to GCA through assessment of cross-reactive VZV-specific T cell immunity, hypothesizing that the number of VZV-reactive T cells would be increased in GCA patients relative to controls. Using a small sample of GCA and control patients (with inflammatory or noninflammatory disease), the authors tested this hypothesis through the quantification of VZV-specific T cells and T cell reactivity (in response to stimulation with a protein extract from an aortic tissue specimen obtained from a single GCA patient) in vitro, finding no significant differences between GCA and control patients.

In our study, prior herpes zoster reactivation was observed in only a minority of GCA patients, which led to our interpretation that despite our finding of a significant association between GCA and herpes zoster, there was a low population-attributable risk. Thus, one possible explanation for the null findings by Bigler et al is that the protein extract from the single GCA patient did not contain VZV or VZV cross-reactive antigens.

As Bigler and colleagues point out (and we acknowledged in our article), there have been conflicting reports on the presence of VZV in the temporal arteries of GCA patients. Given the epidemiologic associations observed in our study, we look forward to additional translational research studies investigating potential mechanistic links between VZV and GCA.

Bryant R. England, MD 
 Ted R. Mikuls, MD, MSPH
*University of Nebraska Medical Center
 and Veterans Affairs Nebraska–
 Western Iowa Health Care System
 Omaha, NE*
 Jeffrey R. Curtis, MD, MS, MPH 
University of Alabama at Birmingham

DOI 10.1002/art.40332

Single-strain versus multistrain probiotic supplementation treatment strategy for rheumatoid arthritis: comment on the article by Marietta et al

To the Editor:

We read with interest the recent article by Marietta et al on gut microbial dysbiosis as a key factor in the pathogenesis of inflammatory diseases such as rheumatoid arthritis (RA) (1). Altered microbiota, well described in RA patients, seem associated with perturbation of certain metabolic pathways, and the therapies addressed to correct gut microbiome dysbiosis could help in the maintenance of immune homeostasis of the host (1).

In particular, the authors discussed the ability of *Prevotella histicola* to modulate the systemic and mucosal immune response (by suppression of antigen-specific Th17 responses and increased transcription of interleukin-10) in an animal model. On this basis, they suggested a possible role of this human gut commensal in treatment strategies for RA (1).

According to the authors, a “single bacterium” is what seems to make the “difference” in the balance of microbiota; in our opinion, however, this should be a subject of discussion. In fact, what they observed could just be the “readjustment of the microbiota,” and the concept of *Prevotella* “monotherapy” is potentially misleading, since the administration of this microorganism as well as others could be just a way to induce a shift in the balance of flora from proinflammatory to antiinflammatory. In fact, even in the different setting of HIV disease, but notably in human subjects, it has been shown that supplementing antiretroviral therapy with *Prevotella*-free multistrain probiotics (*Streptococcus faecium* and *Streptococcus salivarius* subspecies *thermophilus*; bifidobacteria—represented by *Bifidobacterium breve*, *Bifidobacterium infantis*, and *Bifidobacterium longum*; *Lactobacillus acidophilus*, *Lactobacillus plantarum*, *Lactobacillus casei*, and *Lactobacillus delbrueckii* subspecies *bulgaricus* [Alfa-sigma]) reduces the levels of immune activation on CD4+ T lymphocytes for both of the markers CD38 and HLA-DR and their simultaneous expression, with plasma levels of lipopolysaccharide binding protein and high-sensitivity C-reactive protein normalizing to values comparable to those in controls (2). Multistrain probiotic supplementation (*L. plantarum* [De Simone Formulation {DSM} 24730], *S. salivarius* subspecies *thermophilus* [DSM 24731], *B. breve* [DSM 24732], *Lactobacillus paracasei* [DSM 24733], *L. delbrueckii* subspecies *bulgaricus* [DSM 24734], *L. acidophilus* [DSM 24735], *B. longum* [DSM 24736], *B. infantis* [DSM 24737] [DuPont]) is also associated with a reduction of enterocyte apoptosis and density of intraepithelial lymphocytes,

an improvement of mitochondrial morphology, and a recovery of the integrity of the gut epithelial barrier (3–6). The analogy between RA and HIV (2 different and seemingly unrelated diseases) is that both pathologies have a common state of generalized inflammation and dysbiosis.

In conclusion, the recent article by Marietta et al succeeds in drawing attention to the relationships between the microbiota and inflammatory diseases but at the same time opens the debate on how to correct intestinal dysbiosis. We believe that the microbiome should be considered a complex anatomic system in which interactions between all of its components allow proper functioning. In this sense, based on our experience, the therapeutic approach with multistrain probiotics seems to be potentially more suitable to reduce systemic inflammation and immune activation in RA, as in the setting of HIV.

Giancarlo Ceccarelli, MD, PhD, MSC
Vincenzo Vullo, MD
Gabiella d'Ettorre, MD, PhD
University of Rome Sapienza
Rome, Italy

1. Marietta EV, Murray JA, Luckey DH, Jeraldo PR, Lamba A, Patel R, et al. Suppression of inflammatory arthritis by human gut-derived *Prevotella histicola* in humanized mice. *Arthritis Rheumatol* 2016;68:2878–88.
2. D'Ettorre G, Ceccarelli G, Giustini N, Serafino S, Calantone N, de Girolamo G, et al. Probiotics reduce inflammation in antiretroviral treated, HIV-infected individuals: results of the “Probio-HIV” clinical trial. *PLoS One* 2015;10:e0137200.
3. D'Ettorre G, Rossi G, Scagnolari C, Andreotti M, Giustini N, Serafino S, et al. Probiotic supplementation promotes a reduction in T-cell activation, an increase in Th17 frequencies, and a recovery of intestinal epithelium integrity and mitochondrial morphology in ART-treated HIV-1-positive patients. *Immun Inflamm Dis* 2017;5:244–60.
4. Ceccarelli G, Fratino M, Selvaggi C, Giustini N, Serafino S, Schietroma I, et al. A pilot study on the effects of probiotic supplementation on neuropsychological performance and microRNA-29a-c levels in antiretroviral-treated HIV-1-infected patients. *Brain Behav* 2017;7:e00756.
5. Scagnolari C, Corano Scheri G, Selvaggi C, Schietroma I, Najafi Fard S, Mastrangelo A, et al. Probiotics differently affect gut-associated lymphoid tissue indoleamine-2,3-dioxygenase mRNA and cerebrospinal fluid neopterin levels in antiretroviral-treated HIV-1 infected patients: a pilot study. *Int J Mol Sci* 2016;17. pii: E1639.
6. Scheri GC, Fard SN, Schietroma I, Mastrangelo A, Pinacchio C, Giustini N, et al. Modulation of tryptophan/serotonin pathway by probiotic supplementation in human immunodeficiency virus-positive patients: preliminary results of a new study approach. *Int J Tryptophan Res* 2017;10:1178646917710668.

DOI 10.1002/art.40331

Reply

To the Editor:

We thank Dr. Ceccarelli and colleagues for their comments on our recent article on the use of gut-derived commensals as a treatment option for autoimmune diseases like RA. Dysbiosis in RA patients has been well established (1,2).

We believe that reduced abundance of certain taxa might lead to an expansion of opportunist pathogens or perhaps loss of the homeostatic effects of those microbes. Decreased levels of *Prevotella* in RA patients compared to healthy individuals have been demonstrated previously in another study (3). In our recent article in *Arthritis & Rheumatology*, we report that treatment with *Prevotella histicola* can protect against arthritis in mice via differentiation of T cells and dendritic cells to regulatory cells. Moreover, we have clearly shown that immune response locally in the gut is modulated in the small intestine. Thus, our approach has a direct effect via the small intestine rather than via an indirect modification of the microbiome of the colon.

In our study, we did not correlate the protection provided by *P histicola* with a shift in the composition of the microbiome. It is likely that *P histicola* treatment does shift the microbiome toward a composition similar to that found in a healthy phenotype, as supported by our recent data in the experimental autoimmune encephalomyelitis model (4). However, the ability of *P histicola* to suppress disease in mice depleted of gut flora by antibiotics suggests that *P histicola* itself has immunomodulating properties. It should be noted that other groups have shown similar results with a single bacterial strain. For example, arthritis phenotype could be driven by treating germ-free mice with gut-resident segmented filamentous bacteria (5).

As noted by Ceccarelli et al, supplementation with multistrain probiotics down-regulates immune activation, which supports the hypothesis that commensals can be used for treating diseases. However, HIV is a disease of immunodeficiency, while RA and other autoimmune diseases are immune “competent”; therefore, requirements for treating the 2 different types of diseases will more than likely be different. One can speculate that an immunodeficiency disease like HIV may have many more abnormalities in the immune system and may require a multiprobiotic approach. In fact, we believe that monotherapy is advantageous if the correct bacterial strain is used, as a mixture of probiotics can lead to an expansion of microbes at different rates in individuals and may have unintended consequences. Mixtures may also be more difficult to maintain and administer. The *P histicola* strain described in our report was isolated from the human upper gut and may therefore have a much more significant impact on the intestinal immune system, as well as on extraintestinal diseases that are influenced by the immune responses occurring in the gut.

Supported by Department of Defense grant W81XWH-10-1-0257 to Dr. Taneja.

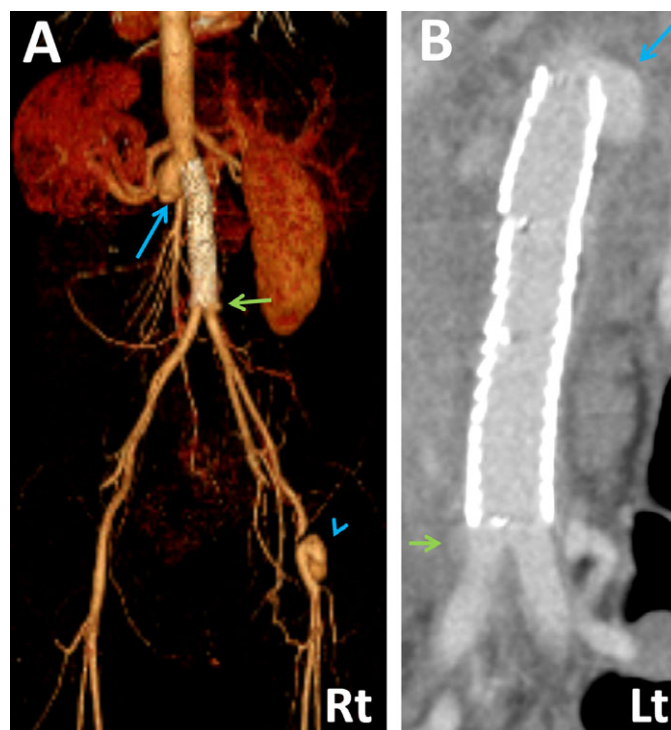
Eric Marietta, PhD
Ashutosh Mangalam, PhD
Joseph Murray, MD
Veena Taneja, PhD
Mayo Clinic
Rochester, MN

1. Chen J, Wright K, Davis JM, Jeraldo P, Marietta EV, Murray J, et al. An expansion of rare lineage intestinal microbes characterizes rheumatoid arthritis. *Genome Med* 2016;8:43.
2. Zhang X, Zhang D, Jia H, Feng Q, Wang D, Liang D, et al. The oral and gut microbiomes are perturbed in rheumatoid arthritis and partly normalized after treatment. *Nat Med* 2015;21:895–905.

3. Vahtovuo J, Munukka E, Korkeamäki M, Luukkainen R, Toivanen P. Fecal microbiota in early rheumatoid arthritis. *J Rheumatol* 2008;35:1500–5.
4. Mangalam A, Shahi SK, Luckey D, Karau M, Marietta E, Luo N, et al. Human gut-derived commensal bacteria suppress CNS inflammatory and demyelinating disease. *Cell Rep* 2017;20:1269–77.
5. Wu HJ, Ivanov II, Darce J, Hattori K, Shima T, Umesaki Y, et al. Gut-residing segmented filamentous bacteria drive autoimmune arthritis via T helper 17 cells. *Immunity* 2010;32:815–27.

DOI: 10.1002/art.40337

Clinical Images: Aneurysm formation after stent grafting in vascular Behçet's disease



The patient, a 40-year-old man with a history of oral and ileocecal ulcers, acneiform lesions, erythema nodosum, and deep vein thrombosis, presented with fever, abdominal pain, and a pulsatile mass in the right groin. Two months previously, he had undergone stent grafting via the right femoral artery for an abdominal aortic aneurysm. Enhanced computed tomography showed aneurysms at both ends of the stent (**A** and **B**) (arrows) and at the right femoral puncture site (arrowhead). Vascular Behçet's disease was diagnosed based on the history of mucocutaneous, skin, and vascular lesions. A second stent grafting and vein-graft replacement were performed to treat the aneurysms. High-dose methylprednisolone treatment was started immediately after the second surgery. Subsequently, treatment with methotrexate and infliximab was initiated, along with oral corticosteroids in a tapering dosage. With continuation of this treatment regimen, the patient has had no recurrence of aneurysms to date (8 months after the second stent grafting). It is impossible to know whether the aneurysms formed due to preexisting inflammation or to the induction of inflammation in a previously normal artery in a pathergy-like reaction. Either way, it seems likely that treatment with antiinflammatory and immunosuppressive agents prevented aneurysm formation after the second procedure.

Suguru Honda, MD
Fumio Hirano, MD, PhD
Mariko Mouri, MD
Hisanori Hasegawa, MD, PhD
Hitoshi Kohsaka, MD, PhD
Tokyo Medical and Dental University
Tokyo, Japan

ACR ANNOUNCEMENTS

AMERICAN COLLEGE OF RHEUMATOLOGY
2200 Lake Boulevard NE, Atlanta, Georgia 30319-5312
www.rheumatology.org

ACR Meetings

Annual Meetings

October 19–24, 2018, Chicago

November 8–13, 2019, Atlanta

State-of-the-Art Clinical Symposium

April 13–15, 2018, Chicago

For additional information, contact the ACR office.

ACR State-of-the-Art Clinical Symposium

The 2018 State-of-the-Art Clinical Symposium (SOTA), to be held April 13–15 in Chicago, Illinois, offers high-impact rheumatology education over the course of a single weekend. The symposium will provide up to 12 hours of nonconcurrent sessions with an emphasis on clinical application to rheumatology practice. Attendees will hear key opinion leaders speak on a range of content in areas such as therapeutic developments, recent research findings, and scientific advances. The program will include breakfast and lunch roundtable discussions to allow for personal interactions with experts. The Fellows-in-Training (FIT) Educational Session at SOTA will be offered as a presymposium session encouraging FITs to explore career opportunities and participate in hands-on workshops designed to further their understanding of essential rheumatologic areas. (FIT travel scholarship recipients are required to attend this session.) In addition, the presymposium program E/M Documentation Trends and Best Practices Training will provide guidance from expert coders on the changes to the 2018 payment policies and insight into difficult E&M coding situations. Be sure to register by the

early-bird deadline of February 14 and book your hotel room by March 23. For additional information and to register, visit www.rheumatology.org/Learning-Center/Educational-Activities.

Education Programs

Fourteenth International Sjögren's Symposium. April 18–21, 2018, Capital Hilton Hotel, Washington, DC. The International Sjögren's Symposium is designed to facilitate precision medicine practices in all aspects of clinical care, including patient diagnosis, prognosis, therapeutic responses, and prevention. Specifically, the symposium is meant to bring together leaders from the Sjögren's syndrome/autoimmunity research community to enhance translation of novel discoveries into clinical practice. Presented by the Johns Hopkins University School of Medicine and the NIH. To register or for additional information, visit the web site <http://tinyurl.com/ISSS2018DC>.

Eleventh International Congress on Autoimmunity. May 16–20, 2018, Lisbon, Portugal. The International Congress on Autoimmunity encompasses the most up-to-date clinical and basic research findings on more than 80 autoimmune diseases, with courses and lectures by some of the world's most distinguished experts. The official language will be English. Registration fees are €620 (early; until March 6), €720 (March 7–May 8), and €820 (May 9–onsite) for full participants, and €380 (early; until March 6), €430 (March 7–May 8), and €480 (May 9–onsite) for trainees (students/fellows/residents) and nurses. Optional courses and functions are available for additional fees. For additional information, e-mail reg_autoimmunity18@kenes.com, phone +41 22 908 0488, or visit the web site <http://autoimmunity.kenes.com/2018>.